EMERGING MECHANISMS FOR SKELETAL MUSCLE MASS REGULATION

EDITED BY: Yuji Ogura, Shuichi Sato, Yann Simon Gallot and Susan Tsivitse Arthur

PUBLISHED IN: Frontiers in Cell and Developmental Biology

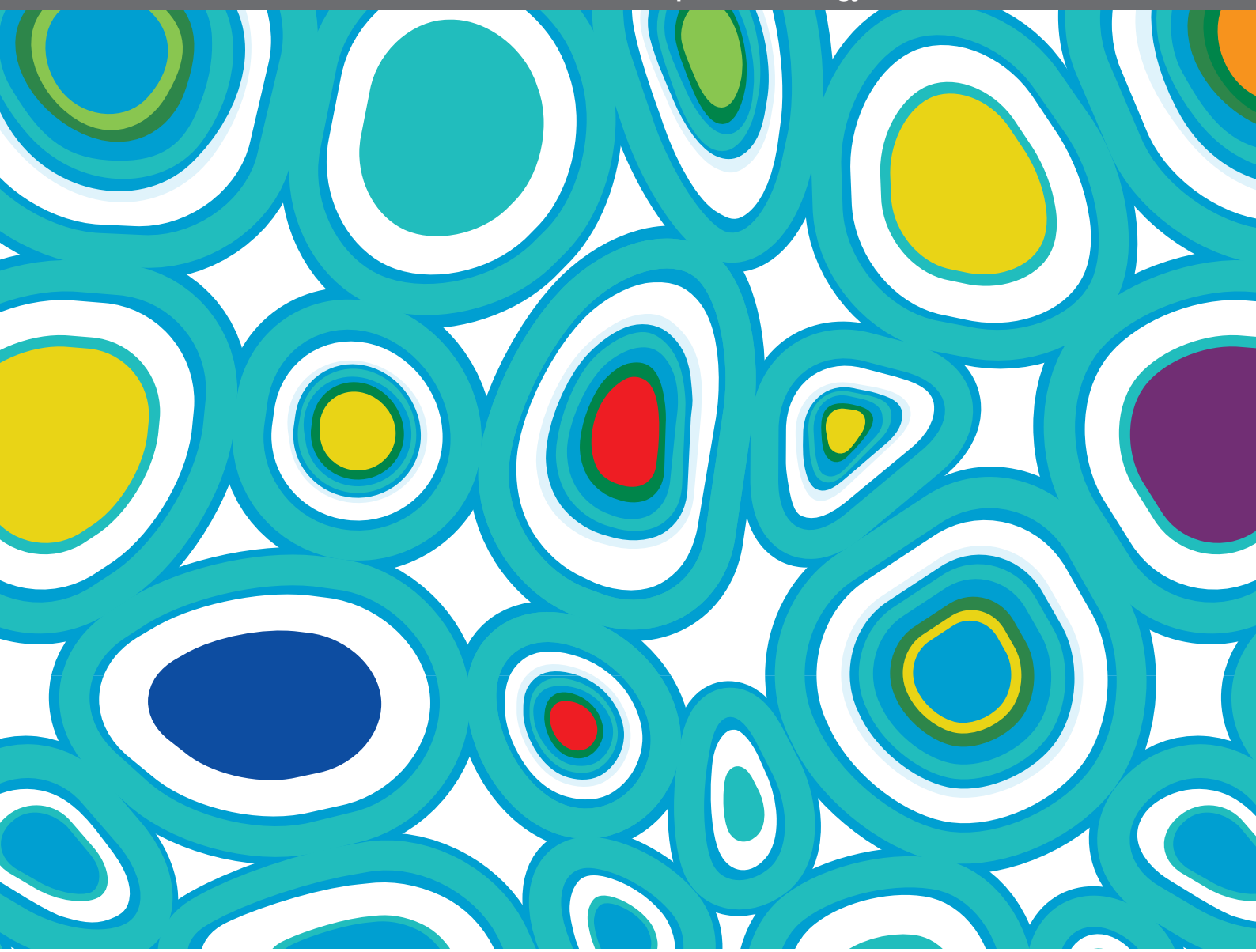

frontiers Research Topics

frontiers

ISSN 1664-8714
ISBN 978-2-88971-639-5
DOI 10.3389/978-2-88971-639-5

About Frontiers

Frontiers is more than just an open-access publisher of scholarly articles: it is a pioneering approach to the world of academia, radically improving the way scholarly research is managed. The grand vision of Frontiers is a world where all people have an equal opportunity to seek, share and generate knowledge. Frontiers provides immediate and permanent online open access to all its publications, but this alone is not enough to realize our grand goals.

Frontiers Journal Series

The Frontiers Journal Series is a multi-tier and interdisciplinary set of open-access, online journals, promising a paradigm shift from the current review, selection and dissemination processes in academic publishing. All Frontiers journals are driven by researchers for researchers; therefore, they constitute a service to the scholarly community. At the same time, the Frontiers Journal Series operates on a revolutionary invention, the tiered publishing system, initially addressing specific communities of scholars, and gradually climbing up to broader public understanding, thus serving the interests of the lay society, too.

Dedication to Quality

Each Frontiers article is a landmark of the highest quality, thanks to genuinely collaborative interactions between authors and review editors, who include some of the world's best academicians. Research must be certified by peers before entering a stream of knowledge that may eventually reach the public - and shape society; therefore, Frontiers only applies the most rigorous and unbiased reviews.
Frontiers revolutionizes research publishing by freely delivering the most outstanding research, evaluated with no bias from both the academic and social point of view. By applying the most advanced information technologies, Frontiers is catapulting scholarly publishing into a new generation.

What are Frontiers Research Topics?

Frontiers Research Topics are very popular trademarks of the Frontiers Journals Series: they are collections of at least ten articles, all centered on a particular subject. With their unique mix of varied contributions from Original Research to Review Articles, Frontiers Research Topics unify the most influential researchers, the latest key findings and historical advances in a hot research area! Find out more on how to host your own Frontiers Research Topic or contribute to one as an author by contacting the Frontiers Editorial Office: frontiersin.org/about/contact

EMERGING MECHANISMS FOR SKELETAL MUSCLE MASS REGULATION

Topic Editors:
Yuji Ogura, St. Marianna University School of Medicine, Japan
Shuichi Sato, University of Louisiana at Lafayette, United States
Yann Simon Gallot, University of Évry Val d'Essonne, France
Susan Tsivitse Arthur, University of North Carolina at Charlotte, United States

Citation: Ogura, Y., Sato, S., Gallot, Y. S., Arthur, S. T., eds. (2021). Emerging Mechanisms for Skeletal Muscle Mass Regulation. Lausanne: Frontiers Media SA. doi: 10.3389/978-2-88971-639-5

Table of Contents

frontiers in Cell and Developmental Biology

EDITORIAL
published: 27 September 2021
doi: 10.3389/fcell.2021.764095

Editorial: Emerging Mechanisms for Skeletal Muscle Mass Regulation

Yuji Ogura[1]*, *Shuichi Sato*[2], *Yann S. Gallot*[3] and *Susan Tsivitse Arthur*[4]

[1] Department of Physiology, St. Marianna University School of Medicine, Kawasaki, Japan, [2] School of Kinesiology, University of Louisiana at Lafayette, Lafayette, LA, United States, [3] LBEPS, Univ Evry, IRBA, Université Paris Saclay, Evry, France, [4] Department of Applied Physiology, Health and Clinical Sciences University of North Carolina at Charlotte, Charlotte, NC, United States

Keywords: myocyte, signaling, cancer, homeostasis, myogenesis

Editorial on the Research Topic

Emerging Mechanisms for Skeletal Muscle Mass Regulation

Skeletal muscle is considered an essential tissue involved in many physiological functions such as metabolism, thermoregulation, respiration, and locomotion. It has become clear that genetic and environmental factors are intricately involved in regulating skeletal muscle volume or myofiber size. The complexity of the orchestration of the signaling pathways that regulate these factors is intriguing. Muscle biologists strive to elucidate the myriad of signaling interactions critical for muscle volume and homeostasis. In this topic, we aimed to gain new insights into the basis of muscle volumetric and homeostatic regulation. We collected nine papers that embody novel or important concepts to skeletal myology. The three main areas compose the manuscripts: adult myogenesis, skeletal muscle mass regulation, and cancer-induced muscle weakness.

Adult myogenesis is a critical process to establish proper myofiber. The first article examined the role of hypoxia-inducible factor 1α (HIF-1α) in myogenesis by Cirillo et al. The authors have previously reported that hypoxia-preconditioning upregulated both HIF-1α and Wnt7a followed by enhanced hypertrophy (Cirillo et al., 2017). In this study, the authors showed that HIF-1α directly binds to the Wnt7a promotor region and stimulates its expression under hypoxic conditions. Activation of HIF-1α is sufficient to improve muscle regeneration via activation of Wnt7a signaling in mice. These results provide novel evidence of the cooperation of HIF-1α and Wnt7a in myogenic machinery.

The unfolded protein response (UPR), an evolutionarily conserved intracellular signaling mechanism, is an important event involved in adult myogenesis (Bohnert et al., 2018). The article by Tan et al. demonstrates that the knockdown of RNA-dependent protein kinase-like ER eukaryotic translation initiation factor 2 alpha kinase (PERK), one of the three UPR signaling branches, exaggerated myotube formation through perturbing micro RNA (miRNA) networks in the immortalized mouse skeletal myoblast cell line C2C12 culture. While *in vivo* confirmation is required, the results propose the unique relationship between UPR and miRNA in the context of myogenic differentiation.

Myod family inhibitor (Mdfi or I-mfa) is a myogenic repressor (Chen et al., 1996). However, the inhibitory role of Mdfi is controversial. Using CRISPR/Cas9-engineered Mdfi-overexpressing C2C12 cells, Huang et al. found that Mdfi promoted several myogenic regulatory factors and fast-to-slow transition of myosin heavy chain (MyHC) isoforms expression. Thus, the results suggest that Mdfi plays a positive role in myogenic differentiation under a culture setting.

Requirements volumetric muscle gain with resistance training is a practical research area with universal implications. Using genetically-modified mice, Joanne et al. report in their original research study that a lack of desmin, an intermediate filament protein of skeletal muscle, caused

Edited and reviewed by:
Ana Cuenda,
Consejo Superior de Investigaciones Científicas (CSIC), Spain

***Correspondence:**
Yuji Ogura
yuji_ogura@marianna-u.ac.jp

Specialty section:
This article was submitted to Signaling, a section of the journal Frontiers in Cell and Developmental Biology

Received: *25 August 2021*
Accepted: *01 September 2021*
Published: *27 September 2021*

Citation:
Ogura Y, Sato S, Gallot YS and Arthur ST (2021) Editorial: Emerging Mechanisms for Skeletal Muscle Mass Regulation. Front. Cell Dev. Biol. 9:764095. doi: 10.3389/fcell.2021.764095

disruption of sarcomere integrity and mitochondrial abnormalities. Four weeks of mechanical overload revealed a functional decline in overloaded plantaris muscle in the desmin-knockout mice, associated with a disrupted autophagy system. These data demonstrated that desmin is necessary for overload-induced muscle adaptation.

This Research Topic includes two comprehensive review articles discussing skeletal muscle homeostasis. White provides a compelling discussion on the relationship of pathways for muscle protein synthesis and metabolism including how metabolic signaling such as AMP-activated protein kinase (AMPK) affects anabolism and catabolism processes including mechanistic target of rapamycin (mTOR) signaling. Considerable effort has focused on the role of branched-chain amino acids (BCAAs) trafficking in coordinating protein turnover.

The second review article discusses transduction of mechanical signals to the nucleus. This research area has recently received attention in skeletal myology. A mechanical network in the nucleoskeleton and cytoskeleton is a crucial element to understand cellular mechanobiology. Proper mechanotransduction to the nucleus can initiate appropriate response and adaptation of muscle cells to local environmental changes. van Ingen and Kirby summarized the current concept and topic of nuclear mechanobiology related to skeletal muscle homeostasis and function.

Cancer biology is now an important field of skeletal myology because cancer development causes substantial volumetric reduction of skeletal muscle in patients. There are three articles in this collection that examine the crosstalk of skeletal muscle with cancer. Straughn et al. demonstrated that the anti-tumorigenic compound Withaferin A (WFA), purified from the plant *Withania somnifera*, directly acts to the skeletal muscle to induce hypertrophic adaptation under ovarian cancer environment. Thus, WFA could be a potential therapeutic means to ameliorate both ovarian cancer and cancer-related muscle wasting.

Colon-26 (C26) tumor cells-derived factor inhibits myotube growth signals. Since passive stretch has been identified to increase protein synthesis and muscle volume, Halle et al. demonstrated that passive stretch in C2C12 myotubes could prevent diminished protein synthesis signaling and fast-type myosin expression induced by C26 tumor-derived factors in a cultured setting. This study provides initial evidence that mechanical stimulus could counteract cancer-induced muscle deconditioning.

Finally, Mallard et al. reviewed the research to understand the alterations in skeletal muscle in breast cancer patients, particularly as a consequence of chemotherapy, and then prospectively described potential mechanisms based on multiple types of cancer-related conditions. This review article also includes information regarding the fundamental signaling pathways that regulate skeletal muscle volume.

We hope that our Research Topic is informative to advance the field of skeletal muscle research. Lastly, we thank the authors for their contributions to this collection.

AUTHOR CONTRIBUTIONS

YO wrote the first draft of the manuscript. YO, SS, YSG, and STA wrote the manuscript. All authors contributed to manuscript revision, read, and approved the submitted version.

FUNDING

SS was supported by Louisiana Board of Regents Support Fund (LEQSF (2017-20)-RD-A-22).

REFERENCES

Bohnert, K. R., McMillan, J. D., and Kumar, A. (2018). Emerging roles of ER stress and unfolded protein response pathways in skeletal muscle health and disease. *J. Cell Physiol.* 233, 67–78. doi: 10.1002/jcp.25852

Chen, C. M., Kraut, N., Groudine, M., and Weintraub, H. (1996). I-mf, a novel myogenic repressor, interacts with members of the MyoD family. *Cell* 86, 731–741. doi: 10.1016/s0092-8674(00)80148-8

Cirillo, F., Resmini, G., Ghiroldi, A., Piccoli, M., Bergante, S., Tettamanti, G., et al. (2017). Activation of the hypoxia-inducible factor 1alpha promotes myogenesis through the noncanonical Wnt pathway, leading to hypertrophic myotubes. *FASEB J.* 31, 2146–2156. doi: 10.1096/fj.201600878R

Conflict of Interest: The authors declare that the research was conducted in the absence of any commercial or financial relationships that could be construed as a potential conflict of interest.

frontiers in Cell and Developmental Biology

ORIGINAL RESEARCH
published: 11 November 2020
doi: 10.3389/fcell.2020.593508

HIF-1α Directly Controls WNT7A Expression During Myogenesis

*Federica Cirillo[1], Giulia Resmini[1], Elia Angelino[2], Michele Ferrara[3], Adriana Tarantino[1,4], Marco Piccoli[1], Paola Rota[1,5], Andrea Ghiroldi[1], Michelle M. Monasky[4], Giuseppe Ciconte[4], Carlo Pappone[4,6], Andrea Graziani[2] and Luigi Anastasia[1,6]**

[1] Laboratory of Stem Cells for Tissue Engineering, IRCCS Policlinico San Donato, San Donato Milanese, Italy, [2] Department of Molecular Biotechnology and Health Sciences, University of Turin, Turin, Italy, [3] Division of Genetics and Cell Biology, Chromatin Dynamics Unit, IRCCS San Raffaele Scientific Institute, Milan, Italy, [4] Arrhythmology Department, IRCCS Policlinico San Donato, Milan, Italy, [5] Department of Biomedical, Surgical and Dental Sciences, University of Milan, Milan, Italy, [6] Vita-Salute San Raffaele University, Faculty of Medicine, Milan, Italy

OPEN ACCESS

Edited by:
Susan Tsivitse Arthur,
University of North Carolina at Charlotte, United States

Reviewed by:
Eoin P. Cummins,
University College Dublin, Ireland
Sivareddy Kotla,
University of Texas MD Anderson Cancer Center, United States
Colin E. Evans,
Northwestern University, United States

***Correspondence:**
Luigi Anastasia
anastasia.luigi@hsr.it

Specialty section:
This article was submitted to Signaling, a section of the journal Frontiers in Cell and Developmental Biology

Received: 10 August 2020
Accepted: 20 October 2020
Published: 11 November 2020

Citation:
Cirillo F, Resmini G, Angelino E, Ferrara M, Tarantino A, Piccoli M, Rota P, Ghiroldi A, Monasky MM, Ciconte G, Pappone C, Graziani A and Anastasia L (2020) HIF-1α Directly Controls WNT7A Expression During Myogenesis. Front. Cell Dev. Biol. 8:593508. doi: 10.3389/fcell.2020.593508

Herein we unveil that Hypoxia-inducible factor-1α (HIF-1α) directly regulates *WNT7A* expression during myogenesis. In fact, chromatin immunoprecipitation (ChiP) and site-directed mutagenesis experiments revealed two distinct hypoxia response elements (HREs) that are specific HIF-1α binding sites on the *WNT7A* promoter. Remarkably, a pharmacological activation of HIF-1α induced *WNT7A* expression and enhanced muscle differentiation. On the other hand, silencing of *WNT7A* using CRISPR/Cas9 genome editing blocked the effects of HIF-1α activation on myogenesis. Finally, treatment with prolyl hydroxylases (PHDs) inhibitors improved muscle regeneration *in vitro* and *in vivo* in a cardiotoxin (CTX)-induced muscle injury mouse model, paving the way for further studies to test its efficacy on acute and chronic muscular pathologies.

Keywords: Hypoxia-inducible factor-1α, WNT7a, myogenesis, hypertrophy, Prolyl-hydroxylases, FG-4592

INTRODUCTION

Skeletal muscle regeneration is a complex process which occurs throughout the lifespan thanks to an adult stem cell reservoir present in the adult muscle. In particular, satellite cells (about 1% of the muscle cell population) consist of roughly a 9:1 mixture of both $Pax7^{+}/Myf5^{+}$ muscle-committed progenitors, which can be triggered to differentiate and regenerate the tissue, and $Pax7^{+}/Myf5^{-}$ uncommitted *bona fide* adult stem cells, which keep replenishing the committed pool (Kuang et al., 2007). Many factors, including aging, can reduce or damage this stem cell population, thus altering muscle homeostasis and causing degeneration (Garcia-Prat et al., 2013). Unfortunately, previous attempts to increase regeneration by inducing muscle differentiation were unsuccessful, as they triggered a rapid depletion of the stem cell reservoir (Ambrosio et al., 2009). On the other hand, the cell-secreted factor Wnt7a has been shown to stimulate symmetric satellite stem cell division, dramatically enhancing muscle regeneration, whereas its depletion caused a marked reduction in the number of satellite cells following muscle healing (Le Grand et al., 2009). In fact, Wnt7a is a member of the Wnt signaling pathway, which is crucial during embryonic development and tissue homeostasis (Gough, 2012). In particular, Wnt7a has been shown to be essential for muscle differentiation and it promotes skeletal muscle hypertrophy (Tanaka et al., 2011). Indeed, Wnt7a overexpression, or treatment with a Wnt7a recombinant protein, has been shown to stimulate myoblasts to form hypertrophic myotubes (Tanaka et al., 2011; von Maltzahn et al., 2011; Bentzinger et al., 2014). Moreover, treatment with exogenous Wnt7a can affect myogenesis,

as it increases satellite cells motility and engraftment, resulting in an enhancement of muscle strength (Bentzinger et al., 2014). However, people have struggled to therapeutically exploit Wnt7a and, to date, little is known about its upstream regulators to possibly envision other strategies to activate myogenesis (von Maltzahn et al., 2011). However, in this context, we previously reported that subjecting murine skeletal myoblasts C2C12 to a hypoxic pre-conditioning (1% O_2 for 24 h) induced the upregulation of the hypoxia-inducible factor-1α (HIF-1α) as well as an activation of the non-canonical WNT-pathway, including Wnt7a, eventually leading to an activation of myogenesis and the formation of hypertrophic myotubes (Cirillo et al., 2017). However, we failed to recognize the mechanism of the observed effects.

Thus, in this study, we investigated the possible mechanistic link between the HIF-1α and *WNT7A*. In particular, chromatin immunoprecipitation (ChiP) and site-directed mutagenesis experiments revealed that HIF-1α specifically binds to two distinct, and previously unreported, hypoxia response elements (HREs) on the *WNT7A* promoter, eventually activating its transcription and inducing myogenesis.

MATERIALS AND METHODS

Cell Cultures

C2C12 murine myoblasts (Merck), HIF-1α-silenced C2C12 murine myoblasts (shHIF-1α), and *WNT7A-KO* silenced C2C12 murine myoblasts, which were obtained in our previous study (Cirillo et al., 2017), were cultured in growth medium (GM) made of Dulbecco's modified Eagle's medium (DMEM, Merck) with high glucose concentration (4.5 g/L) supplemented with 10% (v/v) fetal bovine serum (FBS, Merck), 2 mM glutamine (Merck), penicillin/streptomycin 1X (Euroclone; GM) at 37°C in a 5% CO_2 and 95% air-humidified atmosphere. Cells were treated for 24 h under hypoxic culture conditions (1% O_2) or with prolyl-hydroxylases (PHDs) inhibitors (IOX2 or FG-4592) at 37°C in a 5% CO_2/21% O_2 atmosphere. In order to induce muscle differentiation, 75×10^3 C2C12 murine myoblasts were seeded in 35 mm culture plates, cultured in GM for 24 h, and then switched to a differentiation medium (DM) containing DMEM supplemented with 2% (v/v) horse serum (HS; Merck; Scaringi et al., 2013). The DM was changed every day for 7 days. Cells were analyzed at 24 h post-treatment (PT) and at the third and seventh days of skeletal muscle differentiation. These cells were tested and found to be negative for mycoplasma contamination before the experiments.

WNT7A Plasmid Construct Preparation

Genomic DNA was extracted from C2C12 murine myoblasts and used as the template for *WNT7A* promoter amplification. The PCR reaction was prepared using a Phusion High-Fidelity kit (New England Biolabs) and employing the following primers: forward 5′-GGGGTACCCCGGAAGCTATCACAGGCTT-3′, containing *Kpn*I enzymatic site, and reverse 5′-GGGT TCGAACCCTAGCATCCTTCGCTAACT-3′, containing the *Hin*dIII enzymatic site. The PCR fragment and the vector pNL1.1(Nluc; Promega) were digested with KnpI and *Hin*dIII (Promega) restriction enzymes for 2 h at 37°C, and then they were purified from agarose gel using Wizard® SV Gel and PCR Clean-Up System (Promega). The fragment was inserted into the multiple cloning site of pNL1.1 vector using T4 Ligase Fast (Promega), and the reaction was incubated for 1 h at room temperature. The presence of the insert in the plasmid was finally verified by DNA sequencing.

Nano-Glo Luciferase Reporter Assays

The regulation of the *WNT7A* promoter mediated by HIF-1α was evaluated with the Nano-Glo® Dual-Luciferase® Assay System kit (Promega), which enables a high-throughput analysis of mammalian cells containing the following reporter genes: (a) Nanoluc (pNL1.1empty and pNL1.1WNT7A_promoter) and (b) pGL4.54(luc2/TK), containing the reporter gene Firefly as internal control. Briefly, cells were seeded in a 96-well plate at a concentration of 5×10^3 cells per well, transfected with the pNL1.1 or pNL1.1WNT7A_promoter (90 ng) plasmids and pGL4.54(luc2/TK; 10 ng) plasmid as internal control, according to ViaFect Transfection Reagent® protocol (Promega), and then incubated for 24 h. After transfection, cells were exposed for 24 h to hypoxic culture conditions (1% O_2) or to the PHDs inhibitors, IOX2 (Merck) or FG-4592 (Roxadustat, Selleckchem), at their respective IC_{50} working concentrations. Then, an equal volume of ONE-Glo™ EX Luciferase Assay Reagent was added to each well, incubated for 30 min, and then the luminescence was analyzed with a Varioskan™ LUX Multimode Microplate Reader (Thermo Fisher Scientific). To turn off the luminescence of the Firefly luciferase and provide the substrate for the Nanoluc, an equal volume of NanoDLR™ Stop&Glo® Reagent was added to the mixture and incubated for 30 min before analysis.

Chromatin Immunoprecipitation Assays

The identification of the binding sequence of the HIF-1α protein on the *WNT7A* promoter was obtained with a ChIP using a SimpleChIP® Enzymatic Chromatin IP Kit (Magnetic Beads, Cell Signaling Technology) according to the manufacturer's instructions. Briefly, 1×10^7 C2C12 cells were seeded in GM and cultured for 24 h under hypoxic (1% O_2) or normoxic (21% O_2) culture conditions. Then, cells were harvested by scraping and the genomic DNA was cross-linked with bound proteins with 1% formaldehyde for 10 min at room temperature. Then, the genomic DNA was digested with Micrococcal Nuclease for 20 min at 37°C to achieve DNA sizes ranging from 150 to 900 bp, and then subjected to sonication (Branson Sonifier 150). The immunoprecipitation was achieved using: (a) rabbit monoclonal anti-HIF-1α, 1:1,000 dilution (clone D2U3T, Cell Signaling Technologies), (b) rabbit monoclonal anti-Histone-H3 as technical positive control, 1:50 dilution (D2B12, Cell Signaling Technologies), and (c) IgG rabbit, 5 μg, as the negative control. The mixture was then incubated at 4°C overnight under rotation. The immuno-complexes were collected with ChIP Grade Protein G Magnetic Beads and incubated for 2 h at 4°C under rotation. The elutes were digested with Proteinase K at 65°C for 4 h, and the precipitated DNA was recovered using DNA Purification Spin Columns. Finally, the purified DNA

was amplified by Real-Time PCR using the following ChIP primers designed on the *WNT7A* promoter and on the known *VEGF-HRE*: WNT7A1 forward 5′-GGAAGCTATCACAGGCT-3′ and reverse 5′-ACCGTGGATTCAAGGA-3′; WNT7A2 forward 5′- TGTCAGCATGGCTGGCGC-3′and reverse 5′-AGTTCTTCATGCATAC-3′; WNT7A3 forward 5′-GCAGTCT GGAAGGCTAAGC-3′ and reverse 5′-GTCAAACTCAAAGTC AC-3′; WNT7A4 forward 5′-TTCACCTCCTCAGTTTCTCCA-3′ and reverse 5′-AGCCCAATGACCAGTAGCAG-3′; WNT-7A5 forward 5′-TCCAGTCCAATTCCAAGTC-3′ and reverse 5′-GTCTGTGCGAGGGGCTGA-3′; WNT7A6 forward 5′-GAG GGTGAGGAGAGAATG-3′ and reverse 5′-CCTTGTTAGAG CTCTGTCA-3′; WNT7A7 forward 5′-CGTGAGGGTTCTG AAATG-3′ and reverse 5′-GGAATCCTGCCTGCCTAG-3′; VEGF-HRE forward 5′-GAACAAGGGCCTCTGTCT-3′ and reverse 5′-CACCAAATTTGTGGCACT-3′.

Site-Directed Mutagenesis

The identification of HIF-1α binding sites on the *WNT7A* promoter was performed by site-directed mutagenesis experiments followed by luciferase assays. Each HRE sequence, which was identified as a putative binding site for HIF-1α on the *WNT7A* promoter, was deleted using the QuickChange Lightning Site-Directed Mutagenesis kit (Agilent). Briefly, in order to generate a mutant plasmid containing a single HRE deletion, a thermal cycling reaction mix was performed using pNL1.1WNT7A_promoter as the template, together with two synthetic mutagenic primers suitably designed to insert the desired deletion. Following the temperature cycling, the product was treated with Dnp I endonuclease, which recognized both methylated and hemimethylated DNA, to digest the parental DNA template and to select the mutant DNA. The vector DNA containing the deletion was then transformed into XL10-Gold ultracompetent cells. Each mutant plasmid was subjected to DNA sequencing to confirm the correct deletion.

Determination of the IC_{50} for the PHDs Inhibitors IOX2 and FG-4592

The IC_{50} was calculated using a Dual-Glo® Luciferase Assay System kit (Promega) that enables a high-throughput analysis of mammalian cells containing the Firefly [Luciferase-pcDNA3, oxygen dependent domain (ODD)-Luciferase-pcDNA3] and Renilla pRenilla-Cytomegalovirus (pRL-CMV) luciferase reporters. Briefly, 5×10^3 cells per well were seeded in a 96-well plate, and then transfected for 24 h with a Luciferase-pcDNA3 or an ODD-Luciferase-pcDNA3 (80 ng), containing the firefly gene reporter. A co-transfection with pRL-CMV (8 ng), containing the Renilla gene reporter, was performed as an internal control, according to the ViaFect Transfection Reagent® protocol (Promega). After transfection, cells were treated with 10, 25, 50, and 100 μM IOX2 or FG-4592 (Roxadustat) for 24 h, and then an equal volume of Dual-Glo Luciferase Reagent was added to each well, incubated at room temperature for 30 min, and then analyzed with a Varioskan™ LUX Multimode Microplate Reader (Thermo Fisher Scientific). Then, an equal volume of Dual-Glo® Stop & Glo® Reagent was added to each well in order to quench the luminescence from the firefly reaction and to provide the substrate for the Renilla luciferase. The mixture was incubated for 30 min before analysis. The IC_{50} values were calculated by linear regression.

Cell Viability Assays

RealTime-Glo™ kits MT Cell Viability Assay (Promega) was used to investigate the effects of PHDs treatment or *WNT7A* silencing on cell viability. Briefly, 2×10^3 C2C12 and *WNT7A*-KO murine myoblasts, treated with 50 μM IOX2 or 40 μM FG-4592, were seeded in a 96-well plate and incubated for 3, 6, 24, and 48 h (T0) with MT Cell Viability Substrate (1:1,000 dilution) and NanoLuc® Enzyme (1:1,000 dilution). The luminescence signal was measured by Varioskan™ Lux Multimode Microplate Reader.

Cell Toxicity Assays

To assess the cytotoxicity of the PHDs inhibitors, 5×10^3 C2C12 murine myoblasts were seeded in a 96-well plate and treated with 50 μM IOX2 or 40 μM FG-4592 for 24 h before analysis with a CellTox™ Cytotoxicity Assay (Promega). Briefly, 100 μl of CellTox Buffer containing CellTox Green Dye (1:500 dilution) was added to each well and incubated at room temperature for 15 min. The fluorescence analysis (excitation wavelength of 485-500 nm and emission filter of 520-530 nm) was measured by Varioskan™ Lux Multimode Microplate Reader.

RNA Extraction and Gene Expression by Real-Time Quantitative PCR (qPCR)

Total RNA was isolated using ReliaPrep™ RNA Miniprep Systems (Promega), and reverse transcribed to cDNA using the iScript cDNA synthesis kit (BioRad), according to the manufacturer's instructions. Real-Time Quantitative PCR was performed on 10 ng of cDNA template, 0.2 μM primers, and GoTaq® qPCR Master Mix (Promega) in 20 μl final volume using a StepOnePlus® Real-Time PCR System (Applied Biosystem). The following primers were used: VEGF forward 5′-AAAAACGAAAGCGCA-3′ and reverse 5′-TTTCTCCGCTCTGAA-3′; PHD2 forward 5′-CTGT GGAACAGCCCTTTTT-3′ and reverse 5′- CGAGTCTCTCTG CGAATCCT-3′; MYOG forward 5′-AGCCACACTGAGGGA-3′ and reverse 5′-GTTGAGGGAGCTGAG-3′; myosin heavy chain (MHC) forward 5′-TGGAGCAGGAGGAATACAAG-3′ and reverse 5′-GCATAGTGGATGAGGGAGAA-3′; WNT1 forward 5′-AACCTTCACAACAACGAG-3′ and reverse 5′-GTTGCTGCCTCGGTTG-3′; WNT3A forward 5′-CTTAGTG CTCTGCAGCCTGA-3′ AND REVERSE 5′-GAGTGCTCAGA GAGGAGTACTGG-3′; WNT4 forward 5′-GGGTGGAGTGCA AGTGTCA-3′ and reverse 5′-CACGCCAGCACGTCTTTAC-3′; WNT7A forward 5′-ACTGTGGCTGCGACAAG-3′ and reverse 5′-CTTCATGTTCTCCTCCAG-3′; WNT9a forward 5′-TCGTGGGTGTGAAGGTGATA-3′ and reverse 5′-CAGG AGCCAGACACACCAT-3′; WNT11 forward 5′-CAGGATCCC AAGCCAATAAA3′ and reverse 5′-TCCAGGGAGGCACGT AGA-3′; MYOR forward 5′-GCCCAGCGACATTTCTTC-3′ and reverse 5′-CGCTTCCTCTTGCATCCT-3′; RPL13

forward 5′- CTCGGCCGTTCCTGTAT-3′ and reverse 5′-GTGGAAGTGGGGCTTCAGTA-3′. RPL13 was used as the housekeeping gene. The amplification program consisted of an initial denaturation at 95°C for three min, followed by 40 cycles of 5 s each at 95°C and 30 s at 57°C; WNT7A was amplified at 53°C. Relative quantification of target genes was performed in triplicate and calculated by the equation $2^{-\Delta\Delta Ct}$.

Total Protein Extraction and Isolation of the Nucleus Compartment

For total protein extraction, 7.5×10^4 cells were seeded and harvested at the seventh day of skeletal muscle differentiation, as previously described. Cells were collected after enzymatic digestion with trypsin (Merck), lysed by sonication, and centrifuged at 800 × for 10 min. Supernatant was used to determine total protein content with the bicinchoninic acid (BCA) Protein Assay Kit (Pierce), according to the manufacturer's instructions.

For nuclei separation, 5×10^6 cells were collected after enzymatic digestion with trypsin (Merck), centrifuged at the maximum speed, resuspended in 400 μl of Buffer A (10 mM KCl, 0.1 mM Ethylenediaminetetraacetic acid (EDTA), 1 mM Dithiothreitol (DTT), 10 mM Hepes, pH 7.9), containing protease and phosphatase inhibitors cocktail (Merck), and incubated on ice for 20 min. Then, 10% NP40 was added to the cell suspension, mixed for 40 s, and centrifuged 40 s at the maximum speed. After centrifugation, the pellet was resuspended in 80 μl of Buffer C (0.4 M NaCl, 1 mM EDTA, 1 mM DTT, 20 mM Hepes, pH 7.9), containing a protease and phosphatase inhibitors cocktail, and then mixed for 30 min at 4°C at the maximum speed. Finally, the nuclear suspension was centrifuged for 5 min at 4°C at the maximum speed, collected and transferred to a new tube. The total protein content was determined with the BCA Protein Assay Kit (Pierce), according to the manufacturer's instructions.

Western Blot Analyses

Proteins were denatured by boiling for 10 min in sample buffer (0.6 g/100 mL Tris, 2 g/100 mL SDS, 10% glycerol, 1% 2-mercaptoethanol, pH 6.8) and loaded into a 10% SDS–PAGE gel, then transferred onto a nitrocellulose membrane (Trans-blot, Bio-Rad Laboratories) by electroblotting. Nitrocellulose membranes were incubated with a blocking solution containing 5% (w/v) non-fat dry milk or 5% (w/v) BSA (Merck) in Tris-buffer saline with 0.1% Tween® 20 (TBS-T) for 1 h. Blots were incubated for 2 h at room temperature with the following primary antibodies: rabbit monoclonal anti-HIF-1α, 1:1,000 dilution (clone D2U3T, Cell Signaling Technology), rabbit monoclonal anti-HIF2α, 1:250 dilution (clone D9E3, Cell Signaling Technology) goat polyclonal anti-Lamin A/C, 1:1,000 dilution (clone N-18, Santa Cruz Biotechnology), mouse monoclonal anti-MyoD1, 1:1,000 dilution (clone 5.2F, Abcam), mouse monoclonal anti-myosin (skeletal, fast), 1:1,000 dilution (clone MY-32, Merck), rabbit polyclonal anti-Wnt7a, 1:1,000 dilution (abcam) and rabbit polyclonal anti-EE1a, 1:1,000 dilution (Cell Signaling Technology). The total amount of transferred proteins was used to normalize mice proteins using the REVERT Total Protein Stain kit (LI-COR Biotechnology), following manufacturer's instructions. Membranes were washed three times for 10 min with TBS-T, and then incubated with the appropriate anti-mouse, anti-rabbit, or anti-goat HRP-conjugated secondary antibodies (Dako, Agilent Technologies), 1:2,000 dilution, for 1 h at room temperature. After three washes for 10 min with TBS-T, the immunoreactive bands were visualized using the enhanced chemiluminescence detection kit reagents (ECL Advance, GeHealthcare), according to the manufacturer's instructions.

Immunofluorescence Staining

After differentiation for 7 days in DM, cells were washed with phosphate saline buffer (PBS) and fixed for 15 min in 4% (w/v) paraformaldehyde at room temperature. For permeabilization and blocking, cells were incubated for 1 h in the presence of PBS 0.1% (v/v) Triton X-100 (TX-100, Merck) and 5% (w/v) FBS (Merck) at room temperature. Then, cells were incubated for 2 h at room temperature with mouse monoclonal anti-Myosin (Skeletal, fast; clone MY-32, Merck), diluted 1:200 in PBS 0.1% (v/v) Triton X-100 (TX-100) and 5% (w/v) FBS. After incubation, cells were washed three times in PBS and incubated for 1 h at room temperature with an anti-mouse FITC-conjugated secondary antibody (Jackson ImmunoResearch), diluted 1:200. Cell nuclei were counterstained with Hoechst 33,342 (1:500 dilution, Merck). Myogenesis was assessed by measuring the myotube area and the number of myonuclei per myotube using a fluorescent microscope (Olympus TH4-200) equipped with an acquisition camera. To quantify both differentiation and fusion indexes, 10 fields were chosen randomly and, for each field, a minimum of one hundred myosin-positive myotubes with more than two myonuclei were measured using the ImageJ v1.49o software. The area and the number of nuclei per myotube was the mean of ten measurements averaged from three different experiments. The negative control of MHC was performed using proliferating wild-type- and *WNT7A*-KO-silenced murine myoblasts.

CRISPR/Cas9 Mediated Knockout of the *WNT7A* Gene in C2C12 Murine Myoblasts

The knockout of the *WNT7A* gene was obtained performing CRISPR/Cas9 genome editing. In particular, crRNAs and tracrRNA were obtained from TrueGuide™ Synthetic gRNA kit (Thermo Fisher Scientific), and they were reconstituted and annealed following the manufacturer's instructions. In particular, the target sequence 5′-GGGCATAGTCTACCTCCGGATCGG-3′ was selected as the crRNA of the *WNT7A* gene, while the target sequence 5′-AAAUGUGAGAUCAGAGUAAU-3′, which doesn't recognize any sequence in the human genome (Thermo Fisher Scientific), was used as the negative control. Briefly, they were re-suspended using 1X Tris-EDTA buffer pH 8.0 to prepare a 100 μM stock solution. Then, gRNAs were generated preparing a mix composed of 10 μL crRNA, 10 μL tracrRNA, 10 μL annealing buffer, and 20 μL nuclease-free water. The mixture was incubated at 95°C for 5 min followed by 10 min on 78°C, and then 25°C for 5 min.

The transfection was performed seeding 5×10^5 C2C12 murine myoblasts in a 24-well plate. Two different mixtures were prepared:

- 1,250 ng of TrueCut™ Cas9 Protein v2 (Thermo Fisher Scientific), 2.5 μl of Lipofectamine™ Cas9 Plus™ Reagent, 240 ng of gRNA, and 25 μl of Opti-MEM I Medium.
- 1.5 μl Lipofectamine™ CRISPRMAX™ reagent (ThermoFisher Scientific) and 25 μl of Opti-MEM I Medium.

The diluted Lipofectamine™ CRISPRMAX™ reagent in Opti-MEM I Medium was incubated for 1 min at room temperature, then added to gRNA/Opti-MEM I solution for 15 min. Then, the mixture was added to murine myoblasts and incubated at 37°C for 2 days. After the incubation, single-cell clones were isolated using a limiting dilution cloning in 96-well plates, following the manufacturer's instructions. The efficiency of *WNT7A* knockout (*WNT7A*-KO) was verified by sequencing.

Genomic DNA Extraction and Amplification by PCR

Genomic DNA was isolated using Wizard® Genomic DNA Purification kit (Promega), according to the manufacturer's instructions, and used to amplify the *WNT7A* and *RPL13* genes using the following primers: *WNT7A* forward 5′-CTTGTTGCGCTTGTTCTCC-3′ and reverse 5′-CGCAATTCCACAGACTCG-3′; *RPLI* 5′-CTCGGCCGTTC CTGTAT-3′ and reverse 5′-GTGGAAGTGGGGCTTCAGTA-3′. The amplification program consisted of an initial denaturation at 98°C for 30 s, followed by 30 cycles of 10 s each at 98°C, 15 s at 57°C, and 30 s at 72°C. The amplification was concluded by a final extension step at 72°C for 10 min.

Animals

The procedure involving mice was performed according to the animal protocol guidelines described by the Institutional Animal Care and Use Committee (IACUC) authorization no. 89-2018-PR at San Raffaele Scientific Institute (Milan, Italy). All mice were housed for two weeks in individual cages with a 12-h light/dark cycle, allowing free access to food and water. All efforts were made to minimize animal suffering and to reduce the number of mice used, in accordance with the European Communities Council Directive of November 24, 1986 (86/609/EEC). The number of mice estimated sufficient to detect a difference between two means as large as one SD unit with 80% power and a significance level of 95% at Student's *t*-test were calculated with the program by R.V. Lenth[1] and no formal randomization procedure was used. The investigators conducting the experiments were blind to the experimental group assessed. The investigators quantifying the experimental outcomes continued to be blinded to the animal group or intervention. Finally, the statistical evaluation of the experimental data was performed by another investigator who was not directly involved in data collection and parameter measurement.

Cardiotoxin-Induced Muscle Regeneration and Exogenous FG-4592 Administration

Experiments on muscle regeneration were conducted on 8–10-week-old male C57Bl/6N mice, matched for weight, purchased from Charles River Laboratories (Calco, Italy). Cardiotoxin (CTX, from Naja mossambica mossambica, Latoxan, Portes-les-Valence, France[2]) was dissolved in sterile saline to a final concentration of 10 μM. Mice were anesthetized by isoflurane inhalation, and hindlimbs were shaved and cleaned with alcohol. Tibialis anterior (TA) muscles were injected with 45 μl of CTX with a 30-gauge needle, with 15 micro-injections of 3 μl CTX each in the mid-belly of the muscle to induce homogeneous damage. The TA muscles of the contralateral hindlimbs were injected with a saline solution. A 50 mg/ml of FG-4592 stock solution was first prepared in DMSO, then further diluted in sterile PBS to 1 mg/ml and stored aliquoted at −20°C. FG-4592 was administrated 24 h before CTX injury by i.p. injection using 31-gauge needles at a dose of 10 mg/kg (Hoppe et al., 2016; Xuan et al., 2018). DMSO, diluted at 2% in saline solution, was inoculated by i.p. injection to control mice. The experiments were conducted using seven mice for each group, although one mouse of the FG-4592 group died spontaneously during the procedure. Mice were sacrificed 7 days after CTX treatment.

Histological Analyses

Histological analysis was performed as previously reported (Reano et al., 2017). Briefly, TA muscles were frozen in liquid nitrogen-cooled isopentane and mounted in Killik embedding medium (Bio-optica). Transverse muscle sections (7 μm) were cryosectioned from the mid-belly of each muscle. Sections were stained with Hematoxylin (Bio-optica)/Eosin (Merck) to reveal general muscle architecture. For immunofluorescence, after fixing in PFA 4% for 10 min, slices were permeabilized with 0.2% Triton X-100 in 1% BSA for 15 min and blocked with 4% BSA for 1 h. The primary antibodies anti-laminin (1:200; Dako, Agilent Technologies) and anti-CD31 (1:100; Space srl) were incubated overnight at 4°C, while the incubation with the secondary antibody (1:450, anti-rabbit, Alexa Fluor™ Antibodies) was performed at room temperature for 1 h. Finally, the slices were incubated with Hoechst 33342 (Merck) for 15 min. Images were acquired using Axio Lab.A1 (Zeiss) and quantified with ImageJ v1.49o software.

Statistical Analyses

All assays were performed from three up to eleven replicates, and the quantitative data are displayed as mean ± standard deviation. The statistical analysis was performed with GraphPad Prism 7.0 (GraphPad Software, United States). The Student's *t*-test or One-Way ANOVA and Dunnett test for multiple comparisons were used to determine the significance values. *P* values of less than 0.05 were considered to be significant. All *P* values were calculated from data obtained from at least three independent

[1] www.stat.uiowa.edu/~rlenth/Power/index.html

[2] http://www.latoxan.net/

experiments. Statistical significance was assumed for $^{*}p < 0.05$. All error bars represent the standard deviation of the mean.

RESULTS

HIF-1α Binding on the *WNT7A* Promoter

To test whether HIF-1α activation was directly responsible for *WNT7A* transcriptional induction, HIF-1α-silenced (kd-HIF-1α) and control (HIF-1α) murine myoblasts were seeded to set up a luciferase assay. They were transiently co-transfected with plasmid pNL1.1WNT7A_promoter, containing the luciferase gene under the control of the *WNT7A* promoter (**Figure 1A**), and with plasmid pGL4.54 (luc2/TK), containing the luciferase gene under the TK promoter activity as the internal control. After transfection, cells were switched to hypoxic culture conditions (1% O_2) for 24 h, then tested for *WNT7A* promoter activation by luciferase assay. Results revealed a 2.5-fold luminescence increase in WT myoblasts upon the hypoxic treatment, as compared to normoxic controls, which was consistent with an enhancement of the *WNT7A* promoter activity under hypoxia (**Figure 1B**). On the other hand, a 40% silencing of HIF-1α nuclear translocation, tested by WB, (**Supplementary Figures S1A,B**) caused a significant reduction (-40% luminescence) in *WNT7A* promoter activation under hypoxia, as compared to WT myoblasts (**Supplementary Figures S1C, D**). Next, quantitative ChIP (qChIP) assays were performed to identify any binding regions of HIF-1α on the *WNT7A* promoter, by dividing it into seven putative binding sequences from −1,000 to −197 bp, each containing at least one Hypoxia Responsive Element (HRE; 5′-CGTG-3′; **Figure 1C**). ChIP for HIF-1α binding to the *VEGF-HRE* was included as a positive control (**Supplementary Figure S2A**). After qChIP with the HIF-1α antibody, the *VEGF-HRE* and each sequence of *WNT7A* promoters were amplified by qPCR with specific primers. Results confirmed the specificity of HIF-1α binding on *VEGF-HRE* upon hypoxia pre-conditioning (**Supplementary Figure S2B**). Moreover, while no significant binding on *WNT7A* promoter was observed under normoxia, results showed that, under hypoxia, HIF-1α bound to Seq.1 (−1,000 −843 bp) and Seq.4 (−653 −489 bp; **Figure 1D** and **Supplementary Figure S3**), which contain one and three HRE sequences, respectively **(Figure 1E)**. To further discriminate among these four HRE sites, which were responsible for HIF-1α binding, site-directed mutagenesis experiments were performed to generate four mutants of the *WNT7A* promoter (1.1, 4.1, 4.2, and 4.3), each carrying a single HRE deletion **(Figure 1E)**. C2C12 murine myoblasts were transiently co-transfected with plasmid pNL1.1-WNT7A (Wild Type or one of the mutants) and with plasmid pGL4.54(luc2/TK), as the internal control, and then cultured under hypoxic conditions (1% O_2) for 24 h. Luciferase assays revealed a 40% decrease in luminescence for deletion 1.1 and 4.2, while no significant differences could be observed for mutants 4.1 and 4.3, compared to WT. This data supports the hypothesis that only HREs 1.1 and 4.2, localized on sequence 1 and 4, respectively, were responsible for HIF-1α binding on the *WNT7A* promoter (**Figure 1F**). Then, to assess the time course of Wnt7a protein accumulation, murine myoblasts were cultured for 3, 6, 12, and 24 h under normoxic or hypoxic culture conditions. Results revealed no significant changes in Wnt7a protein under normoxia, but a significant increase of 1.6 and 1.7 folds at 12 and 24 h, respectively, under hypoxia (**Supplementary Figures S4A,B**). Finally, to exclude HIF-2α involvement in the activation of *WNT7A* promoter, its nuclear translocation was evaluated in murine myoblasts pre-treated under hypoxia (1% O_2) for 24 h. Results showed no significant alterations in HIF-2α accumulation into the nuclei (**Supplementary Figures S5A,B**).

The Pharmacological Activation of HIF-1α Induces *WNT7A* Transcription

Since HIF-1α can directly activate *WNT7A* transcription, it was assessed whether the induction of *WNT7A* could be also obtained through the pharmacological stabilization of HIF-1α using the two PHDs inhibitors, IOX2 and FG-4592 (Maxwell and Eckardt, 2016). For this purpose, the IC_{50} of both compounds was determined by transiently co-transfecting C2C12 myoblasts with the ODD-luciferase-pcDNA3 plasmid, containing the oxygen dependent domain (ODD) of HIF-1α, and with the pRL-CMV plasmid, as the internal control **(Figure 2A)**. Then, transfected cells were treated for 24 h with IOX2 or FG-4592 at different concentrations (10, 25, 50, and 100 μM) under normoxic conditions, and the emitted luminescence was collated to untreated controls. Results showed an IC_{50} of 50 μM and 40 μM for IOX2 or FG-4592, respectively **(Figure 2B)**. Next, murine myoblasts were cultured with IOX2 and FG-4592 at their IC_{50} concentration for 3, 6, 12, 24, and 48 h and the effects on proliferation rate were analyzed. Results revealed that pre-treatment with the PHDs inhibitors did not significantly modify the cell growth (**Supplementary Figure S6A**). Furthermore, a 24 h pre-conditioning with the drugs did not induce any toxic effect on murine myoblast (**Supplementary Figure S6B**). To assess the activation of HIF-1α pathway, its nuclear translocation and the expression of its main target genes were evaluated. Unlike the untreated control, both IOX2 and FG-4592 treatments induced HIF-1α nuclear translocation, with an 8.8- and 15-fold protein increase, respectively **(Figure 2C)**. Moreover, qPCR analyses of HIF-1α target genes demonstrated that IOX2 treatment induced a 1.6- and 4.4-fold increase in the expression of *VEGF* and *PHD2*, respectively, while FG-4592 promoted a 2.1- and 4.8-fold increase of the same genes, as compared to untreated controls **(Figure 2D)**. Successively, the activation of the *WNT7A* promoter was investigated by luciferase assay, revealing that IOX2 and FG-4592 treatments induced a 1.4- and 1.3-fold luminescence increase, respectively **(Figures 2E,F)**. To further confirm the activation of the *WNT7A* promoter upon pharmacological hypoxia, the time course of Wnt7a protein expression was analyzed. Data revealed that IOX2 pre-treatment induced a 1.4-, 1.7-, and 2-fold increase at 6, 12, and 24 h (**Supplementary Figure 7A**). Along this line, murine myoblasts pre-treated with FG-4592 showed a 1.55- and 1.7-fold increase at 12 and 24 h, respectively (**Supplementary Figure 7B**). Based on these results, the accumulation of Wnt7a protein induced by the pharmacological hypoxia was investigated at 24 h as compared to the untreated cells, revealing a 1.5-

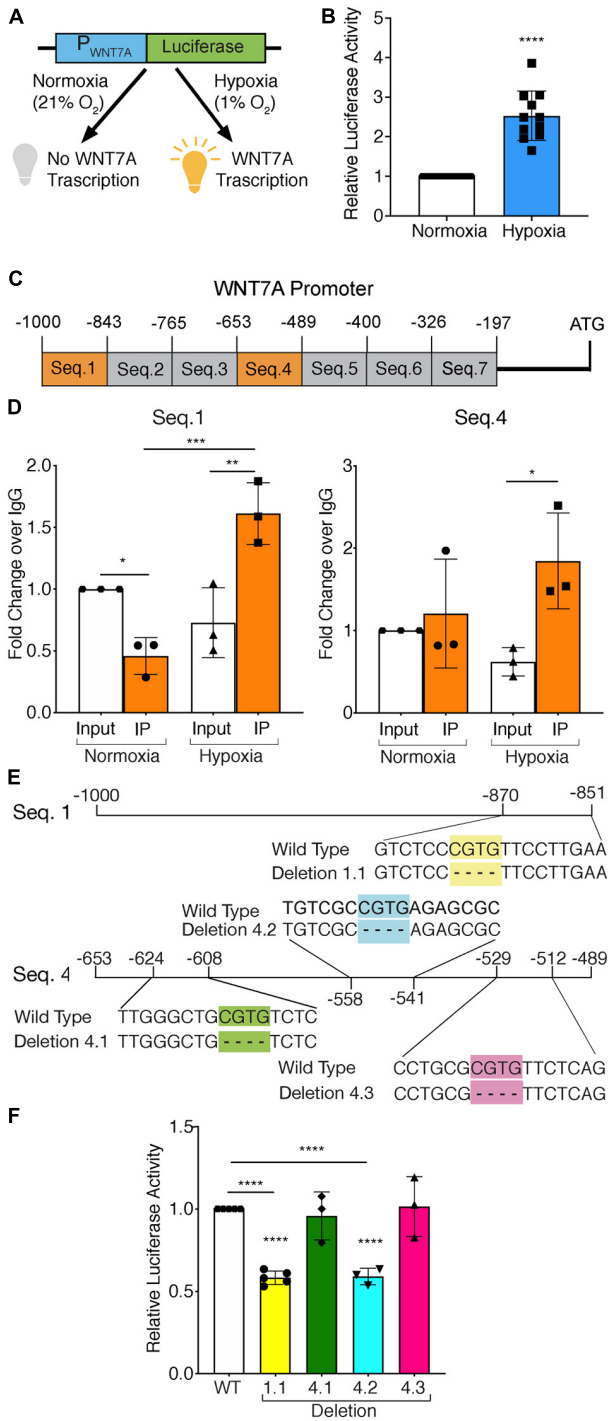

FIGURE 1 | Assessment of hypoxia inducible factor-1α (HIF-1α) binding to the *WNT7A* promoter after 24h at 1% O_2. **(A)** Schematic representation of pNL1.1 plasmid containing the *WNT7A* promoter upstream of the luciferase gene reporter. Under normoxia, HIF-1α is degraded and cannot bind the HRE sequences on the *WNT7A* promoter, inhibiting the luminescence signal; under hypoxia, HIF-1α is stabilized and can bind the *WNT7A* promoter, inducing the expression of the luciferase gene. **(B)** Quantification of pNL1.1-*WNT7A* promoter activity by luciferase assay in murine myoblasts under normoxia and hypoxia (1% O_2; $n = 11$). **(C)** Schematic representation of the seven

(Continued)

FIGURE 1 | Continued
binding sequences designed within the *WNT7A* promoter and used for qPCR analysis after chromatin immunoprecipitation (ChiP). **(D)** qPCR analysis of HIF-1α binding on Seq.1 and Seq.4 of the *WNT7A* promoter ($n = 3$). **(E)** Schematic representation of the deletions of the HRE binding sequences identified in Seq. 1 (Deletion 1.1) and Seq. 4 (Deletion 4.1, 4.2, and 4.3) inserted in the pNL1.1-*WNT7A* promoter construct using site-directed mutagenesis experiments. **(F)** Quantification of mutated pNL1.1-*WNT7A* promoter activity by luciferase assay ($n = 5$ for mutation 1.1, $n = 3$ for mutation 4.1, 4.2 and 4.3). Data information: all data represent mean ± SD. $^*p < 0.05$, $^{**}p < 0.01$, $^{***}p < 0.001$, $^{****}p < 0.0001$ (Ordinary one-way ANOVA).

and 1.3-fold increase in murine myoblasts pre-treated with IOX2 and FG-4592, respectively (**Figure 2G**). To exclude that other Wnt proteins were induced by IOX2 and FG-4592 pre-treatment, *WNT1*, *WNT3a*, *WNT4*, *WNT9a*, and *WNT11* gene expressions were determined. Results revealed that murine myoblasts did not express the isoforms *WNT1* and *WNT3a*, and that pre-treatment with PHDs inhibitors did not induce any alterations in the gene expression of *WNT4*, *WNT9a*, and *WNT11* (**Supplementary Figure 8**).

Treatment With PHDs Inhibitors Induces Myogenesis

To assess whether a pharmacological activation of HIF-1α would affect myogenesis, C2C12 murine myoblasts were pre-treated with IOX2 or FG-4592 in GM for 24 h, and then induced to differentiate for 7 days by switching them to DM without the PHDs inhibitors. At the end of the differentiation process, an extensive formation of MHC-positive myotubes was sighted in both pre-treated and untreated cells, whereas no signal was detected in the negative controls (**Figure 3A**). Quantitative evaluation of the differentiation parameters revealed no significant changes in the fusion indexes, whereas a 1.5- and 1.3-fold increase in the differentiation indexes could be observed in IOX2 and FG-4592 pre-treated myoblasts, respectively, as compared to untreated controls (**Figure 3B**). Next, the alterations of MyoD, Myogenin, and MHC, which are, respectively, the early, intermediate, and late myogenic differentiation markers, were investigated (**Figure 4A**). Protein expression analyses revealed that IOX2 and FG-4592 induced a 1.6- and 1.5-fold increase, respectively, of the nuclear localization of the early differentiation marker, MyoD (**Figure 4B**). Along this line, IOX2 and FG-4592 down-regulated the mRNA level of the main MyoD corepressor, *MYOR*, by 2.2- and 2.6-fold, respectively, compared to controls (**Figure 4C**). Finally, gene expression analyses showed a 2.0- and 1.4-fold increase of *MYOGENIN* at day 3 of differentiation, and a 2.2- and 2.3-fold enhancement of *MHC* at day 7 of differentiation, in IOX2 and FG-4592 pre-treated myoblasts, respectively (**Figures 4D,E**).

WNT7A Silencing Counteracts the Effects of HIF-1α Activation on Myogenesis

To further elucidate the direct involvement of Wnt7a in mediating HIF-1α effects on myogenesis, *WNT7A* silencing

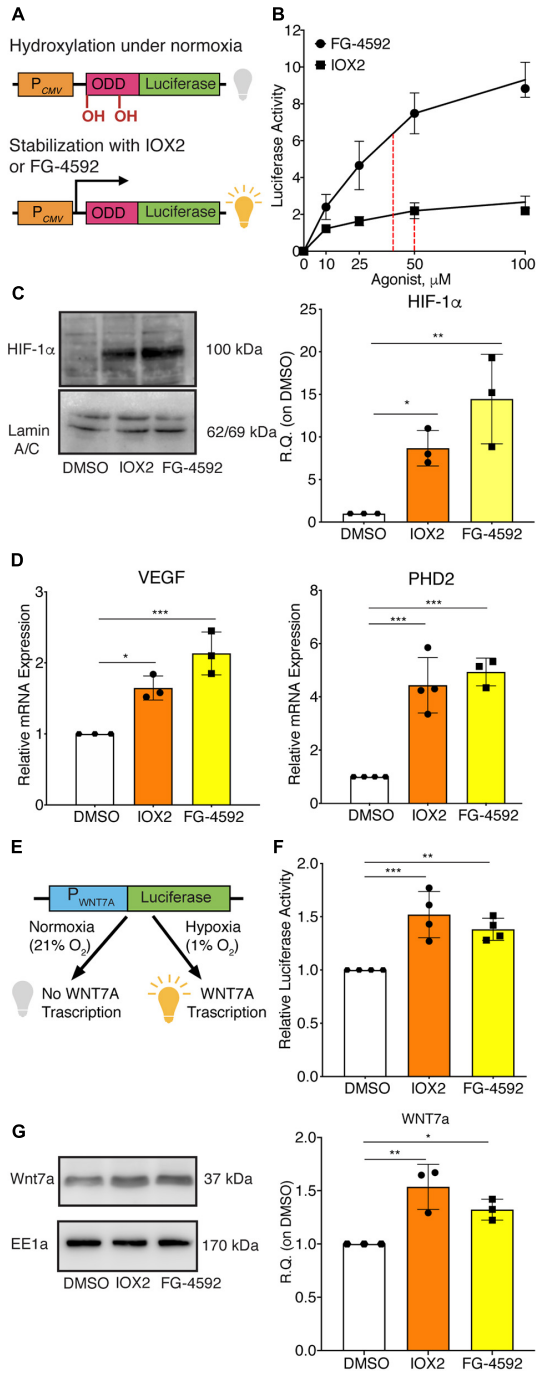

FIGURE 2 | Pharmacological activation of hypoxia inducible factor-1α (HIF-1α) with prolyl-hydroxylases (PHDs) inhibitors and its effects on *WNT7A* regulation. **(A)** Schematic representation of the pcDNA3 construct containing the oxygen dependent domain (ODD)-luciferase reporter gene. Under normoxia, the proline residues on the ODD sequence are hydroxylated by the PHDs, and the complex degraded by the proteasome, eventually inhibiting the generation of the luminescence signal; the pharmacological inhibition of the PHDs causes the stabilization of the ODD, inducing the production of luminescence. **(B)** IC_{50} quantification of IOX2 or FG-4592 by luciferase assay with the ODD-pcDNA3 construct ($n = 3$). **(C)** Western blot analysis and relative quantification of HIF-1α nuclear localization in murine myoblasts treated with *(Continued)*

FIGURE 2 | Continued
IOX2 or FG-4592 for 24 h. The nuclear marker Lamin A/C was used as the housekeeper ($n = 3$). **(D)** qPCR analysis of HIF-1α target genes, *VEGF* and *PHD2*, upon PHDs inhibition with IOX2 or FG-4592 ($n = 3$). **(E)** Schematic representation of pNL1.1 plasmid containing the *WNT7A* promoter upstream of the luciferase gene reporter under normoxia and upon IOX2 or FG-4592 treatment. **(F)** Quantification of pNL1.1-*WNT7A* promoter activity by luciferase assay of murine myoblasts treated with IOX2 or FG-4592 ($n = 4$). **(G)** Western blot analysis and relative quantification of Wnt7a accumulation in murine myoblasts treated with IOX2 or FG-4592 for 24 h. EE1a was used as the housekeeper ($n = 3$). Data information: all data represent mean ± SD. $^{*}p < 0.05$, $^{**}p < 0.01$, $^{***}p < 0.001$ (Ordinary one-way ANOVA).

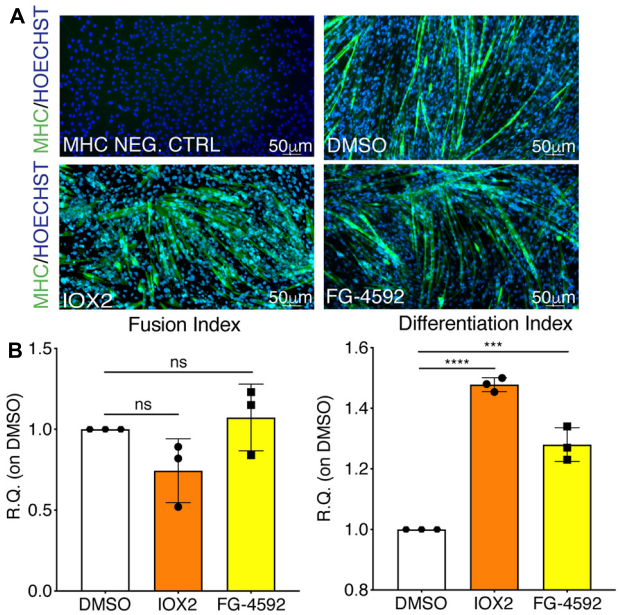

FIGURE 3 | Effects of hypoxia inducible factor-1α (HIF-1α) pharmacological activation on skeletal muscle differentiation. **(A)** Immunofluorescence staining of myosin heavy chain (MHC; green) in proliferating (MHC NEG. CTRL) and differentiated murine myoblasts treated with IOX2 or FG-4592 for 24 h in growth medium (GM) and then switched to differentiation medium (DM) without the prolyl-hydroxylases (PHDs) inhibitors for 7 days. Nuclei were stained with Hoechst 33342. Magnification is 200×. **(B)** Quantification of the fusion index, as the ratio between MHC-positive nuclei and the total number of nuclei, and of the differentiation index, as the ratio between myotubes area and MHC-positive nuclei at the end of differentiation ($n = 3$). Data information: all data represent mean ± SD. $^{***}p < 0.001$, $^{****}p < 0.0001$ (Ordinary one-way ANOVA).

was performed using the CRISPR/Cas9 genome editing in C2C12 murine myoblasts. To this purpose, a gRNA sequence targeted into exon 1, of the four present in the *WNT7A* gene, was selected (**Figure 5A**). A non-targeting gRNA sequence, which is unable to recognize any sequence in the human genome, was used as a negative control. PCR products of the *WNT7A*-targeted genomic region were analyzed by Sanger sequencing, confirming the introduction of a frameshift in the gene (**Figure 5B**). To quantify *WNT7A* silencing, quantitative PCR and Western Blot analysis were performed on wild-type and *WNT7A*-KO myoblasts. In particular, results demonstrated

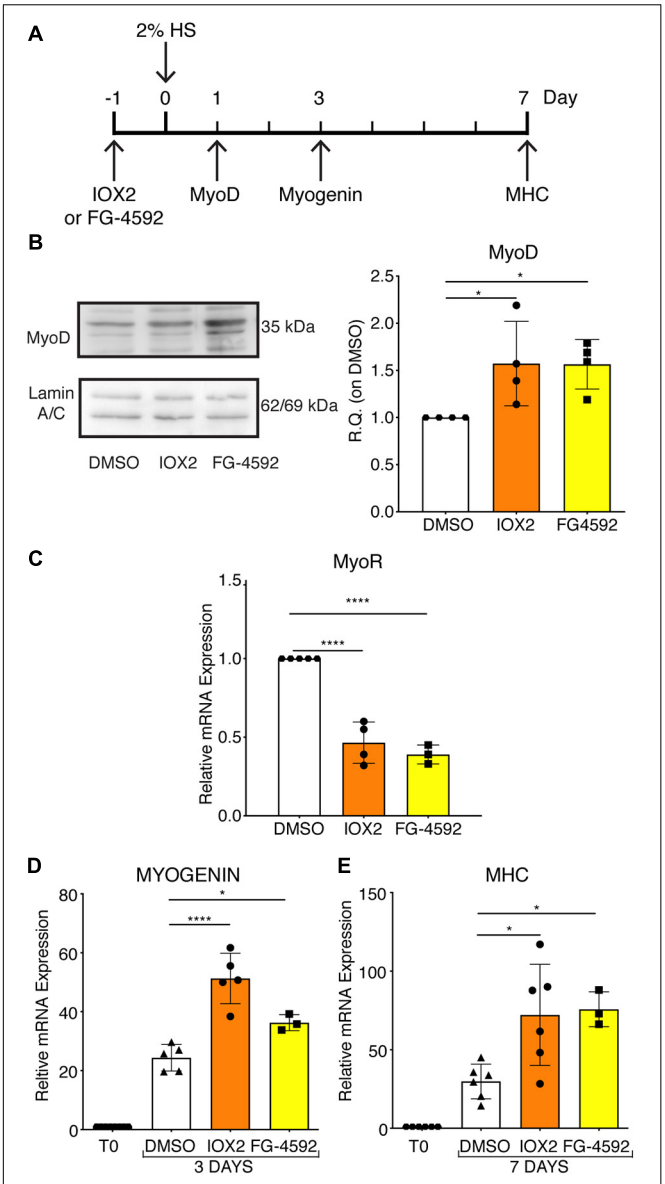

FIGURE 4 | Modulation of myogenic differentiation markers upon pharmacological hypoxia. **(A)** Schematic representation of myogenic marker during skeletal muscle differentiation. **(B)** Western blot analysis and relative quantification of MyoD nuclear localization of murine myoblasts treated for 24 h with IOX2 or FG-4592. The nuclear marker Lamin A/C was used as the housekeeper ($n = 4$). **(C)** qPCR analysis of MyoR upon prolyl-hydroxylases (PHDs) inhibitors treatment ($n = 4$ for IOX2 and $n = 3$ for FG-4592). **(D,E)** qPCR analyses of MYOGENIN at 3 days (**D**, $n = 5$ for IOX2 and $n = 3$ for FG-4592) and of myosin heavy chain (MHC) at 7 days of differentiation (**E**, $n = 6$ for IOX2 and $n = 3$ for FG-4592), in murine myoblasts pre-treated with IOX2 or FG-4592. Data information: all data represent mean ± SD. $^{*}p < 0.05$, $^{****}p < 0.0001$ (Ordinary one-way ANOVA).

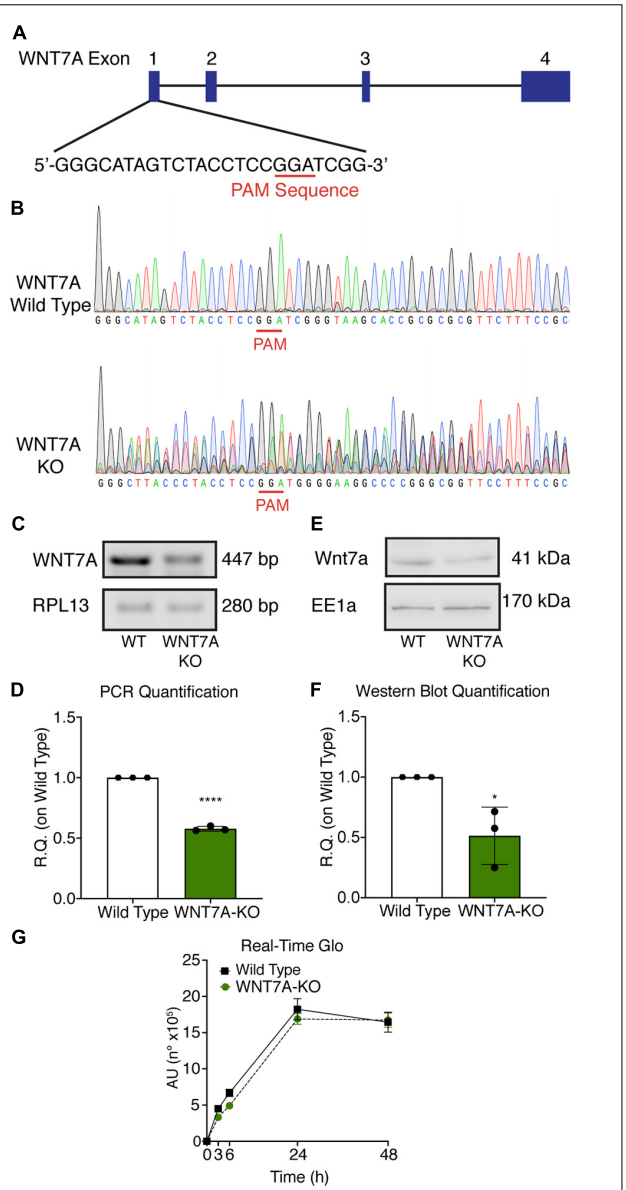

FIGURE 5 | Characterization of *WNT7A* inhibition using CRISPR/Cas9 model in C2C12. **(A)** Graphical representation of the mouse *WNT7A*-targeted locus. Boxes and lines indicate exons and introns, respectively. The oligo represents sgRNA target sequence and Protospacer Adjacent Motifs (PAM) site is marked in red. **(B)** Sanger DNA sequencing were conducted on PCR products amplified from the genomic *WNT7A* loci of C2C12. **(C,D)** Genomic PCR analysis **(C)** and quantification of *WNT7A* inhibition **(D)**. RPLI was used as the housekeeper ($n = 3$). **(E,F)** Western Blot analysis **(E)** and quantification **(F)** of *WNT7A* expression in wild type (WT) and *WNT7A*-silenced murine myoblasts (*WNT7A*-KO; $n = 3$). **(G)** Cell viability analyzed by RealTime-Glo™ kits MT Cell Viability Assay of wild type and *WNT7A*-silenced murine myoblasts ($n = 3$). Data information: all data represent mean ± SD. $^{*}p < 0.05$, $^{****}p < 0.0001$ (Student's *t*-test).

that *WNT7A*-KO cells exhibited a 44% decrease in *WNT7A* genomic expression **(Figures 5C,D)** and a 49% reduction of Wnt7a total protein **(Figures 5E,F)**, as compared to wild-type cells. After confirming the *WNT7A* silencing, the analysis of cell proliferation was performed revealing that *WNT7A*-KO cells did not exhibit significant modifications in cell growth rate, as compared to the wild type cells **(Figure 5G)**. Next, the effects of *WNT7A* silencing on the activation of the HIF-1α pathway, upon physical or pharmacological hypoxia, were

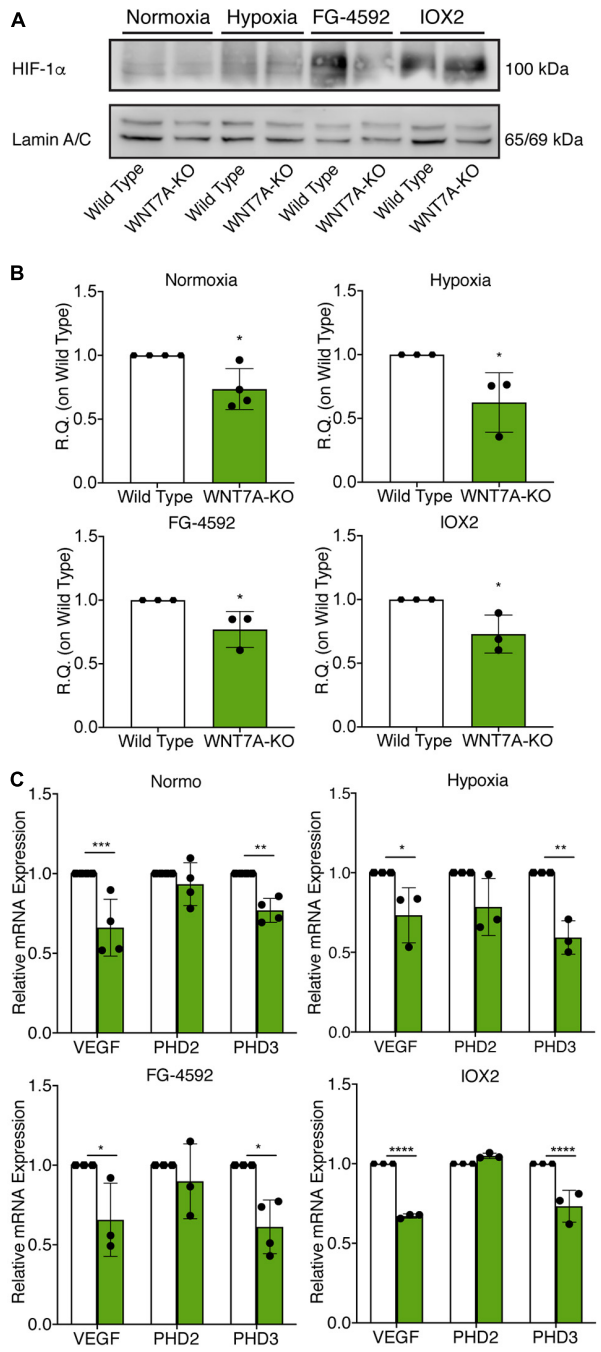

FIGURE 6 | Modulation of hypoxia inducible factor-1α (HIF-1α) pathway induced by *WNT7A* silencing upon physical and pharmacological hypoxia. **(A,B)** Western blot analysis (A) and relative quantification (B) of HIF-1α nuclear localization in wild type (WT) and *WNT7A*-silenced murine myoblasts (*WNT7A*-KO) treated under normoxia, hypoxia, FG-4592 or IOX2. The nuclear marker Lamin A/C was used as the housekeeper ($n = 4$ for Normoxia, $n = 3$ for Hypoxia, IOX2 and FG-4592). **(C)** qPCR analysis of HIF-1α target genes, *VEGF*, *PHD2,* and *PHD3* in WT and WNT7A-silenced murine myoblasts (WNT7A-KO) upon physical and pharmacological hypoxia ($n = 4$ for Normoxia, $n = 3$ for Hypoxia, IOX2 and FG-4592). Data information: all data represent mean ± SD. For western blot analysis of HIF-1α $^{*}p < 0.05$ (Student's *t*-test). For qPCR analysis of HIF-1α target genes $^{*}p < 0.05$, $^{**}p < 0.01$, $^{***}p < 0.001$, $^{****}p < 0.0001$ (ordinary one-way ANOVA).

investigated **(Figure 6A)**. In particular, *WNT7A-KO* cells showed a 27% reduction of HIF-1α nuclear localization under normoxia (**Figure 6B**). The decrease of HIF-1α into the nuclei was also confirmed following physical and pharmacological hypoxia. Indeed, *WNT7A*-KO cells showed a 38%, 24%, and 28% decrease in HIF-1α nuclear localization when *WNT7A*-KO cells were cultured under hypoxia (1% oxygen) or with IOX2 and FG-4592, respectively **(Figure 6B)**. Moreover, reduction of HIF-1α into the nuclei reflected a significant down-regulation of its main target genes. In particular, *WNT7A*-KO cells showed a 36% and 24% decrease in *VEGF* and *PHD3* gene expression, whereas no statistical significance was observed in the gene expression of *PHD2* under normoxia culture condition **(Figure 6C)**. Similarly, silencing of *WNT7A* induced a 27% and 41% reduction in the gene expression of *VEGF* and *PHD3*, respectively, under physical hypoxia **(Figure 6C)**. Similarly, pre-treatment with FG-4592 and IOX2 reduced by 39% and 27% the gene expression of *PHD3*, respectively, and by 33% that of *VEGF* **(Figure 6C)**. Then, the effects of *WNT7A* silencing were assessed on myogenesis at the end of the differentiation process, ultimately evaluating the formation of MHC-positive myotubes, which was undetectable in the negative control of wild type and *WNT7A*-KO cells (**Figures 7A,B**). Then, *WNT7A*-KO cells were then induced to differentiate under normoxic conditions for 7 days showing a 56% and a 15% reduction in the fusion and differentiation indexes as compared to wild-type controls, respectively **(Figures 7C,D)**. Then, we assessed whether *WNT7A* silencing would hamper the beneficial effects on myogenesis of HIF-1α induced-activation. To this purpose, *WNT7A*-KO cells were subjected to hypoxic (1% oxygen) conditions or incubated with PHDs inhibitors FG-4592 or IOX2 to induce HIF-1α activation before differentiation under normoxia. Results showed that *WNT7A*-KO cells exhibited a 46% and 20% reduction in the fusion and differentiation indexes, respectively, when subjected to a pre-treatment under physical hypoxia **(Figures 7E,F)**. Similarly, *WNT7A*-KO cells showed a 63% and 67% decrease in the fusion indexes upon FG-4592 and IOX2 pre-treatment, respectively **(Figures 7G–J)**. Moreover, a 15% reduction in the differentiation index was induced by FG-4592 pre-treatment, while no significant changes were observed with IOX2 **(Figures 7G–J)**. To further assess whether *WNT7A* silencing would hinder the effects of HIF-1α activation, MyoD and MHC protein expression was determined. Results showed that MyoD nuclear localization decreased by 29%, 13%, and 42% under normoxia, hypoxia, and FG-4592 pre-treatment conditions, respectively, while no significant changes were observed with IOX2, as compared to WT cells **(Figures 8A,B)**. Similarly, *WNT7A*-KO cells exhibited a marked down-regulation of MHC expression at the end of the differentiation process, as MHC decreased by 80%, 34%, 36%, and 18% under normoxic, hypoxic, FG-4592, and IOX2 pre-treatment conditions, respectively **(Figures 8C,D)**.

Effects of FG-4592 Injection on Skeletal Muscle Regeneration *in vivo*

To assess whether a pharmacological activation of HIF-1α would affect skeletal muscle regeneration *in vivo*, C57Bl/6N

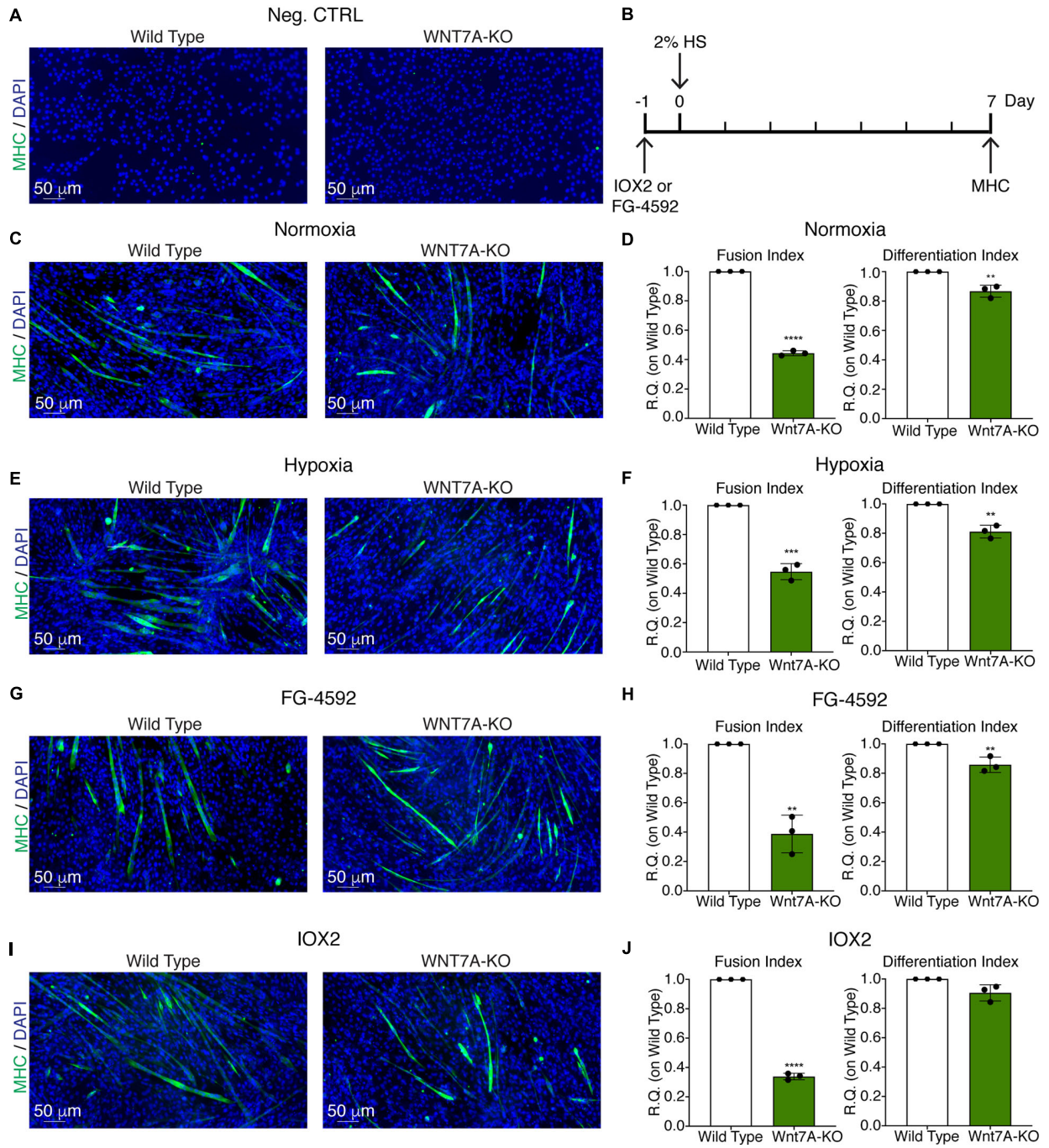

FIGURE 7 | Effects of *WNT7A* inhibition on skeletal muscle differentiation upon physical and pharmacological hypoxia. **(A)** Negative control of myosin heavy chain (MHC) staining in proliferation wild type (WT) and *WNT7A*-silenced murine myoblasts (*WNT7A*-KO)**. (B)** Schematic representation of MHC staining at 7 days of the differentiation process. **(C,E,G, I)** Immunofluorescence staining of MHC (green) in WT and *WNT7A*-silenced murine myoblasts (*WNT7A*-KO) treated under normoxia **(C)**, hypoxia **(E)**, FG-4592 **(G),** or IOX2 **(I)** for 24 h in GM and then switched to differentiation medium (DM) without the prolyl-hydroxylases (PHDs) inhibitors for 7 days. Nuclei were stained with Hoechst 33342. Magnification is 200× ($n = 3$). **(D,F,H,J)** Quantification of the fusion index, as the ratio between MHC-positive nuclei and the total number of nuclei, and of the differentiation index, as the ratio between myotubes area and MHC-positive nuclei at the end of differentiation ($n = 3$). Data information: all data represent mean ± SD. $^{**}p < 0.01$, $^{***}p < 0.001$, $^{****}p < 0.0001$ (Student's *t*-test).

mice were pre-treated with a single intraperitoneal injection of saline solutions or FG-4592 (10 mg/kg, as previously reported as optimal to induce HIF-1α activation in mice, and comparable to a 40–50 μM concentration in the *in vitro* experiments), 1 day before CTX-induced degeneration of the TA muscles (**Figure 9A**; Xuan et al., 2018). FG-4592

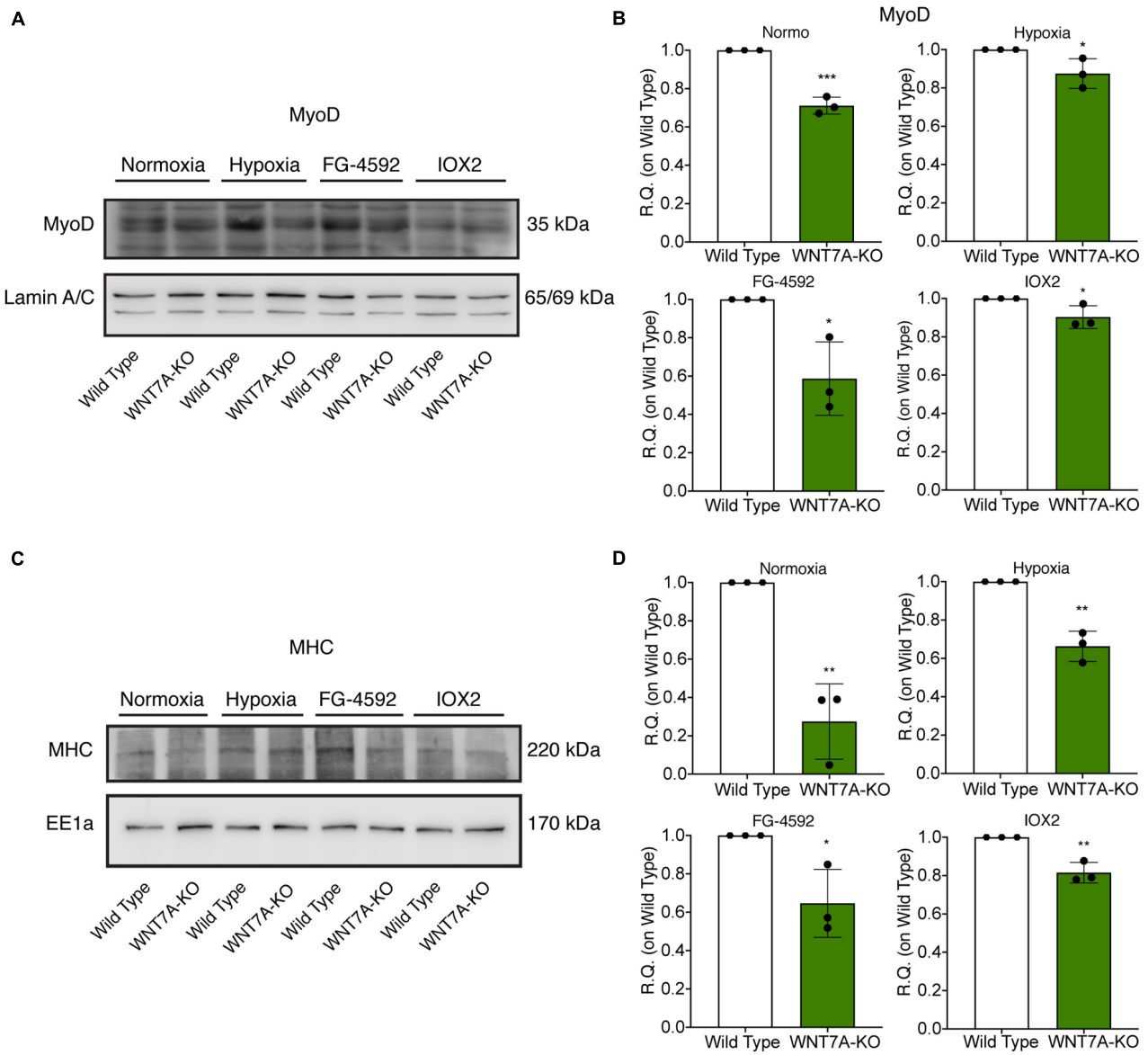

FIGURE 8 | Modulation of MyoD nuclear translocation and myosin heavy chain (MHC) expression in wild type (WT) and *WNT7A*-silenced murine myoblasts upon physical and pharmacological hypoxia. **(A,B)** Western blot analysis **(A)** and relative quantification **(B)** of MyoD nuclear localization were tested after 24 h preconditioning under physical or chemical hypoxia in WT and *WNT7A*-KO. The nuclear marker Lamin A/C was used as the housekeeper ($n = 3$). **(C,D)** Western blot analysis **(C)** and relative quantification **(D)** of MHC were measured at the end of the skeletal muscle differentiation in WT and *WNT7A*-KO. The early endosomal antigen 1a (EE1a) was used as the housekeeper ($n = 3$). Data information: all data represent mean ± SD. $^{*}p < 0.05$, $^{**}p < 0.01$, $^{****}p < 0.0001$ (Student's *t*-test).

pre-treated mice were sacrificed 7 days after injury and, while Hematoxylin/Eosin analyses revealed no macroscopic difference between FG-4592-injected and control muscles **(Figure 9B)**, laminin staining showed a 25% enhancement of cross-sectional area (CSA) and an 8% increase of minimal Feret's diameter of regenerating myofibers, characterized by centrally located nuclei **(Figures 9C–E)**. These results were also confirmed by CSA and minimal Feret's diameter distribution analyses, proving that FG-4592 injection induced a shift of a frequency distribution toward larger fibers **(Figures 9F,G)**. Then, to confirm that pre-treatment with FG-4592 promoted muscle regeneration by the activation of HIF-1α pathway, the total amount of HIF-1α and Wnt7a proteins were analyzed revealing a 2.2- and a 2.4-fold increase, respectively **(Figures 10A,B)**. Finally, to exclude the possibility that the effects on muscle regeneration could be due to the activation of angiogenesis induced by FG-4592, CD31 staining was performed on the muscle sections **(Figure 10C)**. Results indicated that FG-4592 treatment did not significantly modify the number of regenerating fibers nor the density of capillaries at 7 days after the muscle injury, compared to control mice **(Figures 10D,E)**, supporting the hypothesis that

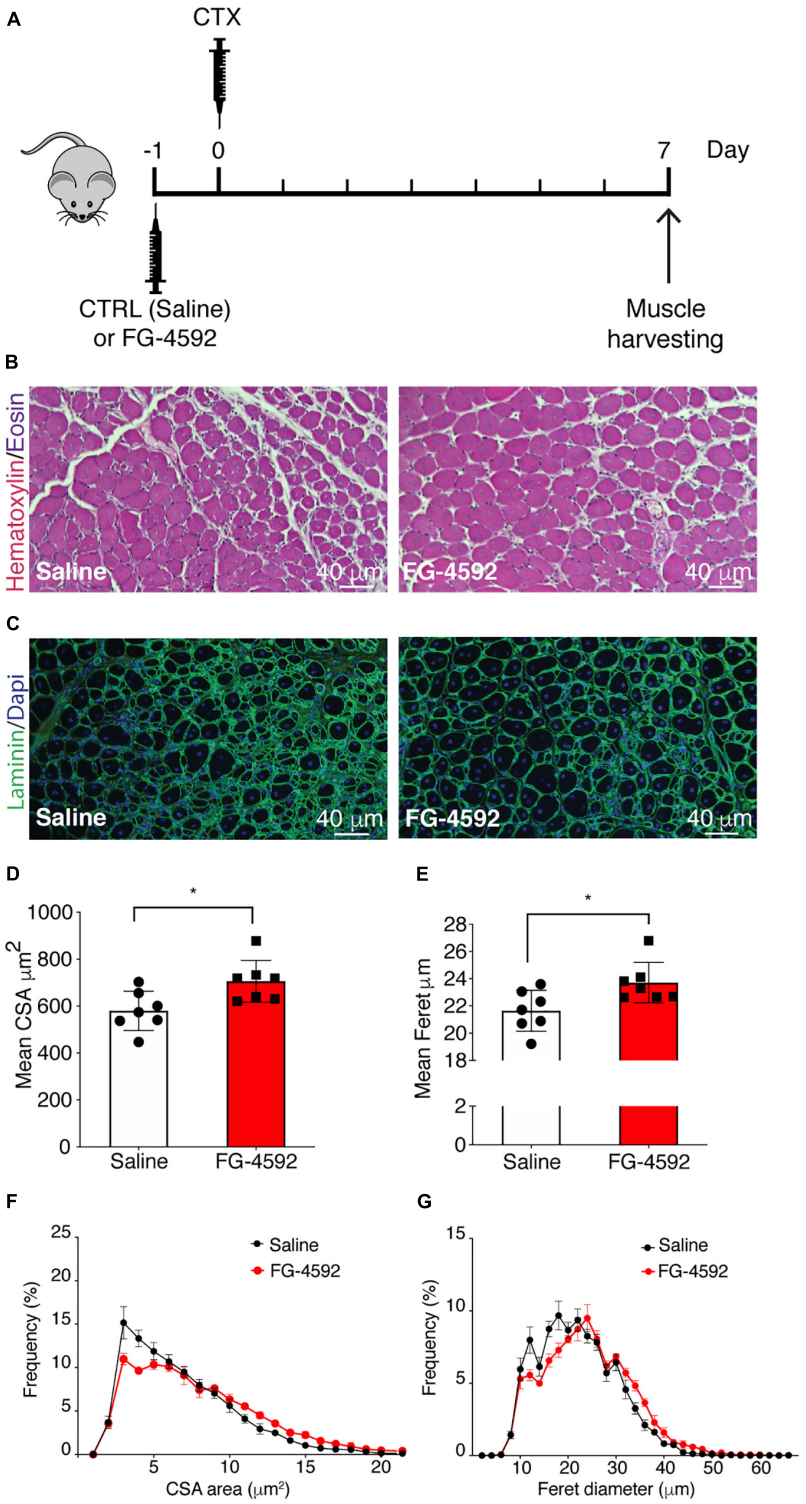

FIGURE 9 | Effects of FG-4592 treatment on muscle regeneration. **(A)** Schematic illustration of the experimental procedure: 24 h before cardiotoxin (CTX) injury of tibialis anterior (TA) muscle, mice were injected by i.p. with FG-4592 (10 mg/kg). Mice were sacrificed 7 days after CTX-induced injury, and TA muscles were collected. **(B)** Immunohistochemical detection of hematoxylin/eosin in FG-4592 pre-treated mice, compared to controls. Scale bars = 40 μM (n = 7 mice for each group). **(C)** Immunofluorescence staining of laminin (green) in saline and FG-4,592 pre-treated mice. Nuclei were stained with Hoechst 33,342. Scale bars = 40 μM (n = 7 mice for each group). **(D,E)** Quantification of CSA **(D)** and minimal Feret diameter **(E)** averages in FG-4592 or saline pre-treated mice. **(F,G)** Representation of CSA **(F)** and minimal Feret diameter **(G)** distribution in saline or FG-4592 pre-treated mice. Data information: all data represent mean ± SD. *$p < 0.05$ (Student's t-test).

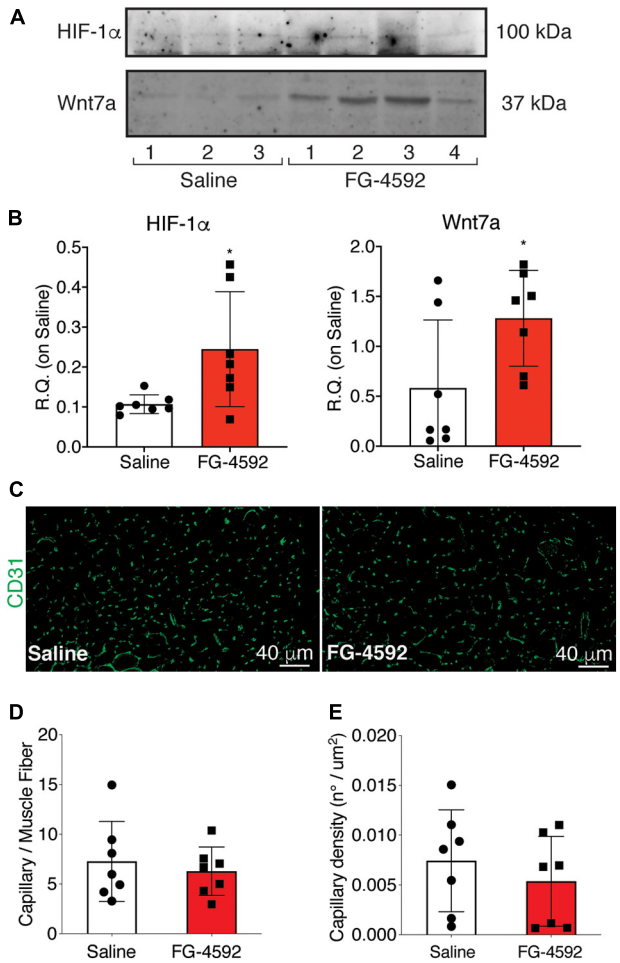

FIGURE 10 | Assessment of activation of hypoxia inducible factor-1α (HIF-1α) pathway in FG-4,592 or saline treated mice upon cardiotoxin CTX-induced muscle injury. **(A,B)** Western blot analysis (A) and relative quantification (B) of HIF-1α and Wnt7a accumulation in saline and FG-4592 pre-treated mice 7 days after CTX-induced muscle injury ($n = 7$). **(C)** Immunofluorescence staining of CD31 (green) on tibial anterior muscle sections of saline and FG-4592 pre-treated mice 7 days after CTX-induced muscle injury (Scale bars = 40 μM). **(D** and **E)** Quantification of the total number of capillaries (D), normalized for the total number of muscle fibers, and the density of capillaries (E), calculated as the total number of capillaries on the area of the fibers, in saline or FG-4592 pre-treated mice ($n = 7$ for each group). Data information: all data represent mean ± SD. $p > 0.05$, n.s., $^*p < 0.05$ (Student's *t*-test).

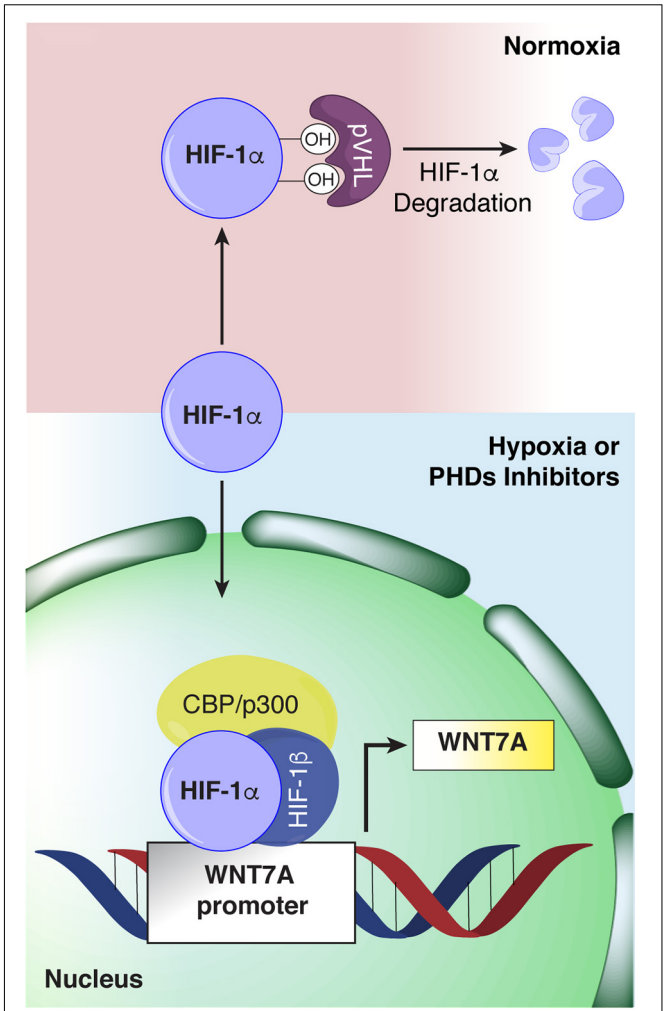

FIGURE 11 | Schematic representation of hypoxia inducible factor-1α (HIF-1α) binding to the *WNT7A* promoter. Under normoxia, HIF-1α is hydroxylated by the active prolyl-hydroxylases (PHDs) and sent to proteasomal degradation. Under hypoxia or upon PHDs inhibition, HIF-1α cannot be hydroxylated, and it translocates to the cell nucleus, where it forms a transcriptional complex with its α-subunit and CBP/p300, and binds to specific HRE sequences on the *WNT7A* promoter region.

FG-4592 promotes muscle regeneration independently from angiogenesis activation.

DISCUSSION

The discovery that HIF-1α regulates *WNT7A* gene expression in skeletal muscle cells by directly binding to its promoter **(Figure 11)** unveils a novel mechanism in the complex myogenic machinery. Remarkably, this could lead to the development of new therapeutic approaches for muscular diseases. While the key role of Wnt7a in muscle regeneration has been established, attempts to therapeutically exploit it have faced the drawback of the high hydrophobicity of its protein (von Maltzahn et al., 2013). On the other hand, a pharmacological activation of HIF-1α has been shown to be feasible, also in humans, and several clinical trials for non-muscular pathologies, including renal anemia, are currently in advanced phases (von Maltzahn et al., 2013; Maxwell and Eckardt, 2016). In particular, HIF is a transcription factor constituted by HIF-1β which is constitutively expressed, and HIF-1α or HIF-2α, which are the oxygen-sensitive subunits (Wang et al., 1995). At high oxygen concentration, the α-subunit is recognized and hydroxylated by the PHDs, which use oxygen and 2-oxoglutarate (2-OG) as co-substrates, promoting its proteasomal degradation (Kim and Kaelin, 2003). Otherwise at low oxygen levels, the PHDs are inhibited, and HIF-1α can translocate to the nuclei and induce the expression

of its target genes (Kim and Kaelin, 2003). In this contest, we also reported a novel, PHD independent, activation of HIF-1α by sialidase NEU3, which may also be further exploited in the future (Scaringi et al., 2013; Piccoli et al., 2017). HIF-1α activation has been shown to promote neo-angiogenesis and cell survival in several pathologies, including cancer (Krock et al., 2011; Hubbi and Semenza, 2015). However, none of the previous studies recognized its direct contribution to the myogenic machinery and even created the misconception that HIF-1α activation would primarily impair the process (Di Carlo et al., 2004; Majmundar et al., 2015). Ultimately, the current notion is that the HIFs, which are induced under the hypoxic conditions typical of satellite cell niches, contribute to preserving muscle progenitor cells in a quiescent, undifferentiated state (Di Carlo et al., 2004; Gustafsson et al., 2005; Clarke and van der Kooy, 2009; Eliasson and Jonsson, 2010; Mohyeldin et al., 2010). Along this line, Di Carlo et al. (2004) reported the first evidence that exposure to prolonged hypoxia blocks myogenesis, and inhibited MyoD, Myf5, and MYOGENIN expression. More recently, it was shown that hypoxic culture conditions favor the quiescence of satellite cell-derived primary myoblasts by upregulating Pax7, a key regulator of satellite cell self-renewal, and downregulating MyoD and Myogenin (Liu et al., 2012). Overall, these and other studies corroborated the notion that hypoxia is detrimental for muscle differentiation, and HIFs activation was acknowledged to inhibit the process (Majmundar et al., 2015). Actually, the role of each of the three different HIFs (HIF-1α, HIF-2α, and HIF-3α) has been shown to be distinct, and their activation is dependent on the degree and the duration of oxygen deprivation (Wang et al., 1995; Dengler et al., 2014; Yang et al., 2017). In particular, it was established that, among all the different HIFs, only HIF-2α is responsible for maintaining satellite cells in a quiescent state (Xie et al., 2018). HIF-2α is activated under mild hypoxia (1.3%, consistent with the oxygen tension of the stem cell niche), whereas HIF-1α appears to be induced only under extreme hypoxia (below 1% O_2), such as in the case of an ischemic event that causes muscle damage followed by regeneration (Yang et al., 2017; Xie et al., 2018). In this context, our study unveils that a 24 h pre-conditioning under hypoxia (1% oxygen) did not induce the activation of HIF-2α, although we cannot rule out its involvement at longer exposure times, whereas it promoted the nuclear translocation of HIF-1α, which in turn activated myogenesis. In particular, we discovered that HIF-1α directly binds two HREs on the *WNT7A* promoter, ultimately activating muscle regeneration. At this stage, we cannot exclude that *WNT7A* could be a general target of HIF-1α also in other cells, as the binding was also observed in a model of oligodendrocytes (Yuen et al., 2014).

Based on these results, we investigated the possibility of pharmacologically induce *WNT7A*, and ultimately myogenesis, by administering some PHDs inhibitors, which are known as HIF-1α activators. In particular, we assessed the effects of IOX2 and FG-4592 (the latter also known as Roxadustat®), two commercially available PHDs inhibitors, which present higher selectivity for PHD2 as compared to other 2-OG dioxygenases (Chiang Chan et al., 2015; Yeh et al., 2017). Remarkably, both compounds induced myogenesis *in vitro* and promoted myotube hypertrophy. Interestingly, treatment of skeletal myoblasts with PHDs inhibitors activated MyoD nuclear translocation even before subjecting cells to differentiation, supporting the hypothesis that the drug increased their commitment to myogenesis. The treatment also caused an early and increased expression of the differentiation markers Myogenin and MHC, similarly to what it was previously observed with Wnt7a induction or supplementation (von Maltzahn et al., 2011). These effects were reverted by *WNT7A* silencing *via* CRISPR/Cas9 genome editing. Actually, we could only obtain a 44% reduction of *WNT7A*, possibly due to the presence of a contamination of untransfected cells. Nonetheless, this reduction was sufficient to significantly impair myogenesis.

Overall, these results support the critical role played by Wnt7a in the activation of myogenesis upon a hypoxic stimulus. In particular, the HRE binding sequences on the *WNT7*A promoter suggest that the activation of HIF-1α, which has been observed after a hypoxic damage in a muscle, is instrumental for activating myoblasts to regenerate the tissue. Thus, we tested this hypothesis also *in vivo* in a mouse model of CTX-induced injury. Mice were pre-treated with a single intraperitoneal injection of 10mg/kg FG-4592, which has already been shown to activate the HIF-1α pathway without evident toxic effects in mice models and is comparable to the dose used for the *in vitro* assays (Xuan et al., 2018). Results showed that FG-4592 treatment induced the accumulation of HIF-1α and Wnt7a in the TA muscles, eventually improving muscle regeneration after CTX-induced muscle injury and leading to the formation of significantly larger fibers. Notably, we demonstrated that the effects were independent from an activation of angiogenesis, which could also be induced by HIF-1α, as no changes in the endothelial marker CD31 expression could be observed (Razban et al., 2012). Based on these results, a post-conditioning model of muscle injury could unveil the potential of this (or other) PHDs inhibitors in counteracting several skeletal muscle diseases and in developing of a new therapeutic approach characterized by multiple injections or by other routes of drug administration. Along this line, it is reasonable to hypothesize a possible role of HIF-1α in skeletal muscle atrophy in the elderly. Indeed, aging is a physiological condition which shows a metabolic shift of myofibers from glycolytic to oxidative metabolism (Ohlendieck, 2011). The increase of the oxidative myofibers could be due to a reduction of HIF-1α activation and the expression of its target genes (Higashimura et al., 2011). Based on these premises, it would be interesting to test the effects of these PHDs inhibitors in pathologies characterized by skeletal muscle atrophy as primary or secondary effects, such as cancer, Acquired Immunodeficiency Syndrome (AIDS), diabetes, and heart failure. Studies in this direction are ongoing in our laboratory.

DATA AVAILABILITY STATEMENT

All datasets generated in this study are included in the article/**Supplementary Material Table 1**.

ETHICS STATEMENT

The animal study was reviewed and approved by Italian Ministry of Health.

AUTHOR CONTRIBUTIONS

LA and FC conceived the study and designed and analyzed all the experiments. LA, FC, MF, CP, EA, MM, GC, and AGr wrote the manuscript. FC, GR, AT, PR, MP, and AGh performed all the *in vitro* experiments. MF and EA performed all the *in vivo* study. LA, FC, and MP prepared the figures. All authors reviewed the results and approved the final version of the manuscript.

FUNDING

This work was partially supported by Ricerca Corrente funding from the Italian Ministry of Health to IRCCS Policlinico San Donato.

SUPPLEMENTARY MATERIAL

The Supplementary Material for this article can be found online at: https://www.frontiersin.org/articles/10.3389/fcell.2020.593508/full#supplementary-material

REFERENCES

Ambrosio, F., Kadi, F., Lexell, J., Fitzgerald, G. K., Boninger, M. L., and Huard, J. (2009). The effect of muscle loading on skeletal muscle regenerative potential: an update of current research findings relating to aging and neuromuscular pathology. *Am. J. Phys. Med. Rehabil.* 88, 145–155. doi: 10.1097/phm.0b013e3181951fc5

Bentzinger, C. F., Von Maltzahn, J., Dumont, N. A., Stark, D. A., Wang, Y. X., Nhan, K., et al. (2014). Wnt7a stimulates myogenic stem cell motility and engraftment resulting in improved muscle strength. *J. Cell Biol.* 205, 97–111. doi: 10.1083/jcb.201310035

Chiang Chan, M., Atasoylu, O., Hodson, E., Tumber, A., Leung, I. K. H., Chowdhury, R., et al. (2015). Potent and selective triazole-based inhibitors of the hypoxia-inducible factor prolyl-hydroxylases with activity in the murine brain. *PLoS One* 10:e0132004. doi: 10.1371/journal.pone.0132004

Cirillo, F., Resmini, G., Ghiroldi, A., Piccoli, M., Bergante, S., Tettamanti, G., et al. (2017). Activation of the hypoxia-inducible factor 1alpha promotes myogenesis through the noncanonical Wnt pathway, leading to hypertrophic myotubes. *FASEB J.* 31, 2146–2156. doi: 10.1096/fj.201600878r

Clarke, L., and van der Kooy, D. (2009). Low oxygen enhances primitive and definitive neural stem cell colony formation by inhibiting distinct cell death pathways. *Stem Cells* 27, 1879–1886. doi: 10.1002/stem.96

Dengler, V. L., Galbraith, M., and Espinosa, J. M. (2014). Transcriptional regulation by hypoxia inducible factors. *Crit. Rev. Biochem. Mol. Biol.* 49, 1–15. doi: 10.3109/10409238.2013.838205

Di Carlo, A., De Mori, R., Martelli, F., Pompilio, G., Capogrossi, M. C., and Germani, A. (2004). Hypoxia inhibits myogenic differentiation through accelerated MyoD degradation. *J. Biol. Chem.* 279, 16332–16338. doi: 10.1074/jbc.m313931200

Eliasson, P., and Jonsson, J. I. (2010). The hematopoietic stem cell niche: low in oxygen but a nice place to be. *J. Cell Physiol.* 222, 17–22. doi: 10.1002/jcp.21908

Garcia-Prat, L., Sousa-Victor, P., and Munoz-Canoves, P. (2013). Functional dysregulation of stem cells during aging: a focus on skeletal muscle stem cells. *FEBS J.* 280, 4051–4062. doi: 10.1111/febs.12221

Gough, N. R. (2012). Focus issue: wnt and beta-catenin signaling in development and disease. *Sci. Signal.* 5:eg2. doi: 10.1126/scisignal.2002806

Gustafsson, M. V., Zheng, X., Pereira, T., Gradin, K., Jin, S., Lundkvist, J., et al. (2005). Hypoxia requires notch signaling to maintain the undifferentiated cell state. *Dev. Cell* 9, 617–628. doi: 10.1016/j.devcel.2005.09.010

Higashimura, Y., Nakajima, Y., Yamaji, R., Harada, N., Shibasaki, F., Nakano, Y., et al. (2011). Up-regulation of glyceraldehyde-3-phosphate dehydrogenase gene expression by HIF-1 activity depending on Sp1 in hypoxic breast cancer cells. *Arch. Biochem. Biophys.* 509, 1–8. doi: 10.1016/j.abb.2011.02.011

Hoppe, G., Yoon, S., Gopalan, B., Savage, A. R., Brown, R., Case, K., et al. (2016). Comparative systems pharmacology of HIF stabilization in the prevention of retinopathy of prematurity. *Proc. Natl. Acad. Sci. U.S.A.* 113, E2516–E2525. doi: 10.1007/978-1-4612-2808-0_1

Hubbi, M. E., and Semenza, G. L. (2015). Regulation of cell proliferation by hypoxia-inducible factors. *Am. J. Physiol. Cell Physiol.* 309, C775–C782.

Kim, W., and Kaelin, W. G. Jr. (2003). The von Hippel-Lindau tumor suppressor protein: new insights into oxygen sensing and cancer. *Curr. Opin. Genet. Dev.* 13, 55–60. doi: 10.1016/s0959-437x(02)00010-2

Krock, B. L., Skuli, N., and Simon, M. C. (2011). Hypoxia-induced angiogenesis: good and evil. *Genes Cancer* 2, 1117–1133. doi: 10.1177/1947601911423654

Kuang, S., Kuroda, K., Le Grand, F., and Rudnicki, M. A. (2007). Asymmetric self-renewal and commitment of satellite stem cells in muscle. *Cell* 129, 999–1010. doi: 10.1016/j.cell.2007.03.044

Le Grand, F., Jones, A. E., Seale, V., Scime, A., and Rudnicki, M. A. (2009). Wnt7a activates the planar cell polarity pathway to drive the symmetric expansion of satellite stem cells. *Cell Stem Cell* 4, 535–547. doi: 10.1016/j.stem.2009.03.013

Liu, W., Wen, Y., Bi, P., Lai, X., Liu, X. S., Liu, X., et al. (2012). Hypoxia promotes satellite cell self-renewal and enhances the efficiency of myoblast transplantation. *Development* 139, 2857–2865. doi: 10.1242/dev.079665

Majmundar, A. J., Lee, D. S., Skuli, N., Mesquita, R. C., Kim, M. N., Yodh, A. G., et al. (2015). HIF modulation of Wnt signaling regulates skeletal myogenesis in vivo. *Development* 142, 2405–2412. doi: 10.1242/dev.123026

Maxwell, P. H., and Eckardt, K. U. (2016). HIF prolyl hydroxylase inhibitors for the treatment of renal anaemia and beyond. *Nat. Rev. Nephrol.* 12, 157–168. doi: 10.1038/nrneph.2015.193

Mohyeldin, A., Garzon-Muvdi, T., and Quinones-Hinojosa, A. (2010). Oxygen in stem cell biology: a critical component of the stem cell niche. *Cell Stem Cell* 7, 150–161. doi: 10.1016/j.stem.2010.07.007

Ohlendieck, K. (2011). Proteomic profiling of fast-to-slow muscle transitions during aging. *Front. Physiol.* 2:105. doi: 10.3389/fphys.2011.00105

Piccoli, M., Conforti, E., Varrica, E., Ghiroldi, A., Cirillo, F., Resmini, G., et al. (2017). NEU3 sialidase role in activating HIF-1α in response to chronic hypoxia in cyanotic congenital heart patients. *Int. J. Cardiol.* 230, 6–13. doi: 10.1016/j.ijcard.2016.12.123

Razban, V., Lotfi, A. S., Soleimani, M., Ahmadi, H., Massumi, M., Khajeh, S., et al. (2012). HIF-1alpha overexpression induces angiogenesis in mesenchymal stem cells. *Biores Open Access.* 1, 174–183. doi: 10.1089/biores.2012.9905

Reano, S., Angelino, E., Ferrara, M., Malacarne, V., Sustova, H., Sabry, O., et al. (2017). Unacylated ghrelin enhances satellite cell function and relieves the dystrophic phenotype in duchenne muscular Dystrophy mdx model. *Stem Cells* 35, 1733–1746. doi: 10.1002/stem.2632

Scaringi, R., Piccoli, M., Papini, N., Cirillo, F., Conforti, E., Bergante, S., et al. (2013). NEU3 sialidase is activated under hypoxia and protects skeletal muscle cells from apoptosis through the activation of the epidermal growth factor receptor signaling pathway and the hypoxia-inducible factor (HIF)-1alpha. *J. Biol. Chem.* 288, 3153–3162. doi: 10.1074/jbc.m112.404327

Tanaka, S., Terada, K., and Nohno, T. (2011). Canonical Wnt signaling is involved in switching from cell proliferation to myogenic differentiation of mouse myoblast cells. *J. Mol. Signal.* 6:12. doi: 10.1186/1750-2187-6-12

von Maltzahn, J., Bentzinger, C. F., and Rudnicki, M. A. (2011). Wnt7a-Fzd7 signalling directly activates the Akt/mTOR anabolic growth pathway in skeletal muscle. *Nat. Cell Biol.* 14, 186–191. doi: 10.1038/ncb2404

von Maltzahn, J., Zinoviev, R., Chang, N. C., Bentzinger, C. F., and Rudnicki, M. A. (2013). A truncated Wnt7a retains full biological activity in skeletal muscle. *Nat. Commun.* 4:2869.

Wang, G. L., Jiang, B. H., Rue, E. A., and Semenza, G. L. (1995). Hypoxia-inducible factor 1 is a basic-helix-loop-helix-PAS heterodimer regulated by cellular O2 tension. *Proc. Natl. Acad. Sci. U.S.A.* 92, 5510–5514. doi: 10.1073/pnas.92.12.5510

Xie, L., Yin, A., Nichenko, A. S., Beedle, A. M., Call, J. A., and Yin, H. (2018). Transient HIF2A inhibition promotes satellite cell proliferation and muscle regeneration. *J. Clin. Invest.* 128, 2339–2355. doi: 10.1172/jci96208

Xuan, L., Xin-Xin, C., Ya-Jing, C., Ting-Ting, W., Huaxi, X., Huiyong, Y., et al. (2018). Therapeutic potential of a prolyl hydroxylase inhibitor FG-4592 for Parkinson's Diseases in vitro and in vivo: regulation of redox biology and mitochondrial function. *Front. Aging Neurosci.* 10:121. doi: 10.3389/fnagi.2018.00121

Yang, X., Yang, S., Wang, C., and Kuang, S. (2017). The hypoxia-inducible factors HIF1alpha and HIF2alpha are dispensable for embryonic muscle development but essential for postnatal muscle regeneration. *J. Biol. Chem.* 292, 5981–5991. doi: 10.1074/jbc.m116.756312

Yeh, T., Leissing, M. T., Abboud, I. M., Thinnes, C. C., Atasoylu, O., Holt-Martyn, J. P., et al. (2017). Molecular and cellular mechanisms of HIF prolyl hydroxylase inhibitors in clinical trials. *Chem. Sci.* 8, 7651–7668. doi: 10.1039/c7sc02103h

Yuen, T. J., Silbereis, J. C., Griveau, A., Chang, S. M., Daneman, R., Fancy, S. P. J., et al. (2014). Oligodendrocyte-encoded HIF function couples postnatal myelination and white matter angiogenesis. *Cell* 158, 383–396. doi: 10.1016/j.cell.2014.04.052

Conflict of Interest: The authors declare that the research was conducted in the absence of any commercial or financial relationships that could be construed as a potential conflict of interest.

frontiers in Cell and Developmental Biology

ORIGINAL RESEARCH
published: 22 January 2021
doi: 10.3389/fcell.2021.605875

Mdfi Promotes C2C12 Cell Differentiation and Positively Modulates Fast-to-Slow-Twitch Muscle Fiber Transformation

Bo Huang[1†], Yiren Jiao[1†], Yifan Zhu[1], Zuocheng Ning[1], Zijian Ye[1], Qing X. Li[2], Chingyuan Hu[3] and Chong Wang[1]*

[1] National Engineering Research Center for Breeding Swine Industry, Guangdong Provincial Key Lab of Agro-Animal Genomics and Molecular Breeding, Guangdong Laboratory for Lingnan Modern Agriculture, College of Animal Science, South China Agricultural University, Guangzhou, China, [2] Department of Molecular Biosciences and Bioengineering, University of Hawai'i at Mānoa, Honolulu, HI, United States, [3] Department of Human Nutrition, Food and Animal Sciences, University of Hawai'i at Mānoa, Honolulu, HI, United States

OPEN ACCESS

Edited by:
Yuji Ogura, St. Marianna University School of Medicine, Japan

Reviewed by:
Jamal Bouitbir, University Hospital of Basel, Switzerland
Stephan Krähenbühl, University of Basel, Switzerland
Mohamed A. A. Mahdy, South Valley University, Egypt

***Correspondence:**
Chong Wang
betty@scau.edu.cn

[†] *These authors have contributed equally to this work*

Specialty section:
This article was submitted to Signaling, a section of the journal Frontiers in Cell and Developmental Biology

Received: *14 September 2020*
Accepted: *04 January 2021*
Published: *22 January 2021*

Citation:
Huang B, Jiao Y, Zhu Y, Ning Z, Ye Z, Li QX, Hu C and Wang C (2021) Mdfi Promotes C2C12 Cell Differentiation and Positively Modulates Fast-to-Slow-Twitch Muscle Fiber Transformation. Front. Cell Dev. Biol. 9:605875. doi: 10.3389/fcell.2021.605875

Muscle development requires myoblast differentiation and muscle fiber formation. Myod family inhibitor (Mdfi) inhibits myogenic regulatory factors in NIH3T3 cells, but how Mdfi regulates myoblast myogenic development is still unclear. In the present study, we constructed an Mdfi-overexpression (Mdfi-OE) C2C12 cell line by the CRISPR/Cas9 system and performed RNA-seq on Mdfi-OE and wild-type (WT) C2C12 cells. The RNA-seq results showed that the calcium signaling pathway was the most significant. We also established the regulatory networks of Mdfi-OE on C2C12 cell differentiation and muscle fiber type transformation and identified hub genes. Further, both RNA-seq and experimental verification demonstrated that Mdfi promoted C2C12 cell differentiation by upregulating the expression of Myod, Myog, and Myosin. We also found that the positive regulation of Mdfi on fast-to-slow-twitch muscle fiber transformation is mediated by *Myod*, *Camk2b*, and its downstream genes, such as *Pgc1a*, *Pdk4*, *Cs*, *Cox4*, *Acadm*, *Acox1*, *Cycs*, and *Atp5a1*. In conclusion, our results demonstrated that Mdfi promotes C2C12 cell differentiation and positively modulates fast-to-slow-twitch muscle fiber transformation. These findings further our understanding of the regulatory mechanisms of Mdfi in myogenic development and muscle fiber type transformation. Our results suggest potential therapeutic targets for muscle- and metabolic-related diseases.

Keywords: Mdfi, C2C12 cells, CRISPR/Cas9 system, RNA-seq, differentiation, muscle fiber type transformation

INTRODUCTION

Skeletal muscle accounts for about 45% of the human body weight (Turner and Badylak, 2012). Skeletal muscle development plays a crucial role in maintaining the muscle loss caused by disease, injury, and aging. Thus, it is of considerable significance to understand the mechanism of muscle myogenic development for preventing adverse effects on human health.

The skeletal muscle tissue maintains homeostasis through skeletal muscle satellites self-renewal and differentiation when suffered from pathological change or injury (Fry et al., 2015). When stimulated by injury or growth signals, skeletal muscle satellite cells are activated and proliferate to form myoblasts (Abou-Khalil et al., 2009). Subsequently, myoblasts exit the cell cycle, and

the myogenic regulator factor (MRF) family, including myogenic factor 5 (Myf5), myogenic differentiation 1 (MyoD), myogenin (Myog), and myogenic factor 6 (Myf6), gradually expresses (Hernandez-Hernandez et al., 2017b). Myf5 is first expressed when satellite cells are activated. Previous studies have found that Myf5 transforms many non-muscle cells into muscle cells (Delfini et al., 2000). MyoD began to express at the proliferation phase of myoblasts and mainly maintains its early differentiation (Zammit et al., 2004). Myog is not expressed in the proliferation phase of myoblasts, but its expression is significantly upregulated when the cells entered the differentiation phase (Bentzinger et al., 2012). Myf6 mainly regulates the terminal differentiation of myoblasts and is highly expressed in mature muscle fibers (Bentzinger et al., 2012). As a result, these myoblasts undergo differentiation to either repair damaged muscle fibers or fuse into multi-nuclear myotubes to form new myofibers (Mashinchian et al., 2018). Myogenic differentiation is, therefore, an essential process in muscle development which determines myoblast fate, muscle formation, and regeneration. Elucidating the mechanism of muscle cell differentiation is critical for understanding skeletal muscle development.

Skeletal muscles are composed of multi-nucleated cells that have numerous myofibers (Bassel-Duby and Olson, 2006). Based on myosin heavy chains (MyHC), mature mammalian skeletal muscle fibers can be classified as type I (MyHC I), type IIa (MyHC IIa), type IIx (MyHC IIx), and type IIb (MyHC IIb) (Schiaffino and Reggiani, 2011). Slow-twitch muscle is mainly composed of type I and type IIa muscle fibers, which are rich in myoglobin and mitochondria, have a strong fatigue resistance. Type IIb muscle fibers mainly exist in fast-twitch muscles, displaying low myoglobin and mitochondrial content, and have weak resistance to fatigue resistance (Chen et al., 2018). Skeletal muscle fiber type transformation is directly correlated with some human muscular and metabolic diseases. For example, muscle atrophy leads to an increase in the proportion of slow-twitch muscle fibers and a decrease in the proportion of fast-twitch muscle fibers (Wang and Pessin, 2013). In the skeletal muscles of patients with type 2 diabetes, the proportion of slow oxidative fibers is decreased, which leads to a decrease in oxidative enzyme activity (Oberbach et al., 2006). Chronic liver disease (CLD) led to the transformation of muscle fibers from type IIb to type I (Aguirre et al., 2020). Chronic obstructive pulmonary disease (COPD) significantly increases the expression of tumor necrosis factor (TNF)-like weak inducer of apoptosis (TWEAK), then increases the proportion of type 1 muscle fibers and decreases the proportion of type 2 muscle fibers (Lu et al., 2017). Therefore, elucidating the mechanism of muscle fiber type transformation is essential for preventing adverse health effects.

Myod family inhibitor (Mdfi, also known as I-mfa) is a class of novel myogenic repressor. The yeast two-hybrid experiments showed that Mdfi inhibits the Myod family's transactivation activity and leads to repressing the myogenic differentiation of NIH-3T3 cells (Chen et al., 1996). However, Huang et al. (2019) found that in chicken primary myoblasts overexpression of the MyoD family inhibitor domain-containing protein (MDFIC) promotes myotubes' formation, while it shows opposite results after the knockdown of MDFIC (Huang et al., 2019). MDFIC shares a high degree homology C-terminal domain with Mdfi (Thebault and Mesnard, 2001). In addition, miR-27b inhibits Mdfi to regulate the development of pig muscle satellite cells (PSCs) *in vitro* (Hou et al., 2018). Conflicting reports on the function of Mdfi exist. We, therefore, explored the regulatory mechanisms of Mdfi in muscle development in the present study.

In this study, we constructed a Mdfi-overexpressing C2C12 cell line by the CRISPR/Cas9 system and performed RNA-seq on Mdfi overexpression (Mdfi-OE) and wild-type (WT) C2C12 cells. Real-time quantitative polymerase chain reaction (qPCR), Western blot, immunofluorescence, and RNA-seq analyses demonstrated that Mdfi promotes C2C12 cell differentiation by upregulating the expression of Myod and myogenin and positively modulates muscle fiber transformation, and successfully established the regulatory network. This study furthers our understanding of the regulatory mechanisms of Mdfi in myogenic differentiation and muscle fiber type transformation. Our results help develop new strategies for treating muscle- and metabolic-related diseases.

MATERIALS AND METHODS

C2C12 Cell Culture, Transfection, and Differentiation

The C2C12 cell line (ATCC® , CRL-1772™) used in this study was purchased from American Type Culture Collection (ATCC, VA, United States). The pX330-U6-Chimeric_BB-CBh-hSpCas9 (pX330, #42230) was purchased from Addgene (Cambridge, MA, United States). C2C12 cells were cultured in Dulbecco's Modified Eagle Medium (DMEM)/High Glucose (Catalog No. SH30243.01, Hyclone, GE Healthcare Bio-Sciences, Pittsburgh, PA, United States) with 10% Fetal Bovine Serum (FBS) (Catalog No. FBS10099-141, Gibco, Grand Island, NY, United States). C2C12 cells were seeded in 6-well plates (2×10^5 cells per well). When plates reached 80–90% confluence, the cells were cultured by myogenic differentiation induction medium. C2C12 cells transfected with pX330, pX330-sgRNA plasmid, or co-transfected with pEGFP by Lipofectamine 2000 (Invitrogen, Carlsbad, CA, United States), according to the manufacturer's instructions. The medium was replaced with fresh growth medium 6 h later.

Construction of a Mdfi-Overexpressing Cell Line by CRISPR/Cas9

We constructed a Mdfi-overexpressing C2C12 cell line by inserting a Mdfi transgene cassette into the genome ROSA26 locus using the CRISPR/Cas9 system. The Genome-CRISPR™ mouse ROSA26 safe harbor gene knock-in kit was purchased from GeneCopoeia Inc (Catalog No. SH-ROS-K200, GeneCopoeia Inc., Rockville, MD, United States). We transfected the MCP-ROSA26-CG01 vector into C2C12 cells with DC-DON-SH02, Mdfi donor, and DC-RFP-SH02. After transfection for 24 h, puromycin (2 μg/mL) was used to screen Mdfi-overexpressing monoclonal cells. After puromycin screening for 72 h, we obtained Mdfi-overexpressing monoclonal cells using limiting dilution assay.

RNA Extraction and qPCR Analysis

The methods used for the RNA extraction and PCR analysis have been described previously (Hou et al., 2017). Briefly, total RNAs were extracted from C2C12 cells using TRIzol reagent (Invitrogen) according to the manufacturer's instructions. After DNase I (Takara Bio Inc., Japan) digestion, total RNAs (500 ng) were reverse transcribed to cDNA using PrimeScript^{TM} RT Master Mix (TaKaRa, Otsu, Shiga, Japan). SYBR Green Real-time PCR Master Mix reagents (Toyobo Co., Ltd., Osaka, Japan) were used for qPCR. The PCR reactions were carried out on a CFX96^{TM} Optical Reaction Module (Bio-Rad, Hercules, CA, United States). The relative expression of mRNAs was normalized with β-actin levels using the $\Delta\Delta$Ct method. Primers used for qPCR are shown in **Supplementary Table 1**.

Immunofluorescent Assay

Wild-type and Mdfi-OE C2C12 cells were seeded in the 48-well at a density of 5×10^{4}/mL and maintained in the growth medium. When cells reached 90% confluence, we changed the growth medium to the differentiation medium (2% house serum) for induction differentiation. At differentiation for 1, 3, 5, and 7 days, we removed the old medium and washed the C2C12 cells three times by PBS. The C2C12 cells were fixed for 20 minutes by 80% acetone, permeabilized for 10 min by 0.5% Triton^{TM} X-100 (Sigma-Aldrich, St. Louis, MO, United States). We used the BCA protein assay kit (Dingguo, China) to block for 1 h, followed by incubating the C2C12 cells with the primary myosin antibody for 1 h. We incubated the C2C12 cells with secondary antibody for 30 min. Finally, we incubated the C2C12 cells with DAPI. The myosin-positive C2C12 cells were observed and recorded using a Nikon TE2000-U inverted microscope (Nikon Instruments, Tokyo, Japan). More than six fields of view were captured in each cell well. The percentage of myosin-positive C2C12 cells, calculated as the number of nuclei present in multi-nucleic myotubes (myosin-positive and containing at least three nuclei) in comparison with the total number of nuclei. The percentage of MyHC-positive C2C12 cells was calculated as the number of nuclei present in multi-nucleic myotubes (MyHC I, MyHC IIa, and MyHC IIb -positive, and containing at least three nuclei) relative the total number of nuclei. Data were counted with Image J software (National Institutes of Health, Bethesda, MD, United States). They were analyzed with the GraphPad Prism (GraphPad Software, La Jolla, CA, United States). The data were expressed as the mean ± standard error of the mean (SEM) with SPSS software (SPSS, Inc., Chicago, IL, United States).

Immunoprecipitation

C2C12 cells were washed twice with precooled PBS, PBS was finally drained, and a 1mL precooled modified RIPA Buffer was added to the petri dish. The cell suspension was transferred to a 1.5 mL centrifuge tube at 4°C for 15 min. After standing, centrifuge at 14,000*g* for 15 min, and transfer the supernatant to a new centrifuge tube. The protein A agarose beads was washed twice with PBS and then prepared into 50% concentration with PBS. About 100 μL 50% protein A agarose beads was added to every 1 mL total protein and incubated at 4°C for 10 min. The supernatant was centrifuged at 4°C, 14,000 rpm for 15 min, and the supernatant was transferred to a new centrifuge tube to remove the protein A beads. The total protein was diluted at least 1:10 times, diluted to about 1 μg/μL with PBS, and incubated overnight at 4°C. An aliquot of 100 μL protein A agarose beads was then added into the centrifuge tube to capture the antigen-antibody complex. The mixture was shaken for 24 h at 4°C. After centrifugation at 14,000 rpm for 5 s, the agarose beads antigen-antibody complex was collected and the supernatant was removed. The agarose beads were washed with precooled NP-40 lysate three times. After washing, an aliquot of 60 mL of 2 × SDS-PAGE buffer was added in the centrifuge tube, mixed gently, add boiled with boiling water for 5 min. After centrifugation, the supernatant was transferred to a new centrifuge tube for subsequent electrophoresis and the remaining agarose beads were collected.

Luciferase Reporter Assay (Promoter Activity Detection)

The genomic DNA of C2C12 cells was isolated for the PCR amplification template. The promoter of the *Camk2b* gene was amplified by PCR using PrimerSTAR® (TaKaRa, Dalian, Liaoning, China). Then, we cloned the promoter of the *Camk2b* gene into the eukaryotic expression vector pGL3-Basic (named as pGL3-Basic-Camk2b). Similarly, we amplified the full length of the *Myod* gene and cloned it into the pcDNA3.1 plasmid (pcDNA3.1-Myod). According to Promega's dual luciferase reporter assay kit (Promega, Madison, WI, United States), we transfected the pGL3-Basic, pGL3-Basic-Camk2b and pcDNA3.1, pGL3-Basic-Camk2b and pcDNA3.1-Myod into C2C12 cell by Lipofectamine^{TM} 3000 Transfection Reagent (Thermo Fisher Scientific, MA, United States). At last, we identified the double-luciferase activity by BioTek Synergy 2 multifunctional microplate reader (BioTek, Winooski, VT, United States). The ratio of the expression of firefly luciferase to renilla luciferase was the promoter activity. The PCR primer pairs were listed in **Supplementary Table 1**.

Chromatin Immunofluorescent Assay

The chromatin immunoprecipitation (ChIP)-IT® Express Magnetic ChIP kit & sonication shearing kit (Catalog number 53008) was purchased from Active Motif (Carlsbad, CA, United States). For the ChIP assay, the DNA was immunoprecipitated with the Myod or Camk2b antibody, and ChIP analysis was performed according to the manufacturer's protocol. DNA samples prior to immunoprecipitation were used as a template for input control. Primers used for ChIP assay are shown in **Supplementary Table 1**. The antibodies used for ChIP assay are shown in **Supplementary Table 1**.

Western Blot Assay

Methods used for Western blot assay have been described previously (Hou et al., 2017). C2C12 cells lysed in RIPA buffer containing 1 μM phenylmethanesulfonyl fluoride (PMSF). About 30 μg protein lysates were separated using SDS-PAGE and then electroblotted onto polyvinylidene fluoride

membranes (Bio-Rad). The membranes were blocked with 6% skim milk buffer for 2 h at room temperature and incubated with different diluted antibodies at 4°C overnight. Finally, the polyvinylidene fluoride membranes were incubated with horseradish peroxidase-conjugated secondary antibodies at room temperature for 1 h. The antibodies used in this study are listed in **Supplementary Table 2**. The band intensities were quantified with Image J and normalized to those of β-actin. Data were analyzed using the GraphPad Prism and were expressed as change in fold relative to the control.

Mitochondrial DNA Copy Number

Total cellular DNA was extracted from WT and Mdfi-OE C2C12 cells with DNAzol reagent (Invitrogen). Mitochondrial 16S ribosomal RNA (mito-16sRNA) was used as the internal reference gene of mitochondrial DNA, and the hexokinase gene (Mito-HEXO) was used as the internal reference gene of nuclear DNA. The expression level of mito-16sRNA relative to Mito-HEXO was quantified, and the expression of mito-16sRNA reflected the copy number of mitochondrial DNA.

RNA-seq Analysis

Wild-type and Mdfi-OE C2C12 cell samples were sequenced using 150 bp paired-end mRNA sequencing methods based on the Illumina HiSeq platform (Caporaso et al., 2012). We used FastQC software to check Pass Filter Data quality. Cutadapt (version 1.9.1), a second-generation software of sequencing data quality statistics, was used to remove the adapter and low-quality sequences from the raw data and obtain clean data (clean reads). After quality control, clean reads were mapped to the mouse reference genome (*Mus musculus* 10.fa) using Hisat2 with one mismatch tolerance. We acquired expression levels based on the read counts using Subread (Liao et al., 2019). Differential expression analysis was performed on DESeq2 software. $p < 0.05$ and $|\log2\text{FoldChange}| > 1$ was set as the cutoff criteria for differentially expressed analysis. Kyoto Encyclopedia of Genes and Genomes (KEGG) enrichment analyses of genes were conducted using KOBAS 3.0 (kobas.cbi.pku.edu.cn) (Xie et al., 2011). The KEGG database analysis was used to analyze the enriched pathways for the differentially expressed genes (DEGs). The Benjamini-Hochberg procedure was applied to control the false discovery rate ($p < 0.05$). String database v10.5 (string-db.org) was used to establish the protein–protein interactions (PPI) of DEGs between the Mdfi-OE and WT groups with the criterion of medium confidence (0.700) (Szklarczyk et al., 2019). Moreover, we applied Cytoscape 3.6 (Shannon et al., 2003) to visualize the network and highlight the most representative gene.

Statistical Analysis

All data are expressed as the mean ± SEM. There were three replicates in each group. The assumptions of normality of data and homogeneity of variances between the groups were analyzed by SPSS. The dual-luciferase reporter system data were analyzed by one-way ANOVA (SPSS 18.0, Chicago, IL, United States). Significant differences between the control and the treatment groups were determined using the Student's *t*-test. We considered $p < 0.05$ to be statistically significant. * is $p < 0.05$ and ** is $p < 0.01$.

RESULTS

The Expression Profile of Mdfi During C2C12 Cell Differentiation

Myod family inhibitor is expressed mainly in the cytoplasm of C2C12 cells, which have been fused into myotube (**Figure 1A**). The Mdfi and myosin co-immunofluorescent assay results showed that Mdfi expressed mainly in the cytoplasm of myosin positive C2C12 cells (**Figure 1B**). Meanwhile, we identified the mRNA and protein level of Mdfi in the differentiation phase of C2C12 cells by qPCR and Western blot. The qPCR results showed that the mRNA level of *Mdfi* was increased at day 3 ($p < 0.05$), day 5 ($p < 0.001$), and day 7 ($p < 0.01$) compared to day 1 (**Figure 1C**). The Western blot results are consistent with the qPCR results. The protein level of Mdfi was higher on day 5 ($p < 0.05$) and day 7 ($p < 0.05$) than day 1 in the differentiation phase (**Figure 1D**). Although the protein level of Mdfi was not increased significantly at day 3 ($p > 0.05$) compared to day 1, there was still an increasing trend. These results indicated that the expression of Mdfi was significantly increased during myoblast differentiation.

Construction of a Mdfi-OE C2C12 Cell Line by CRISPR/Cas9

To explore the function of Mdfi in C2C12 myogenic development, we used the CRISPR/Cas9 system to construct a stable Mdfi-overexpressing (Mdfi-OE) C2C12 cell line. Immunofluorescent assay results showed that we have successfully inserted Mdfi into C2C12 cells at ROSA26 locus, which provided candidate Mdfi-OE monoclonal cells (**Figure 2A**). The PCR amplification results showed that the left and right homologous arms were successfully recombined, indicating the correct integration of the Mdfi donor at the ROSA26 locus (**Figure 2B**). Results of PCR amplification showed that the non-insertion fragment in the Mdfi-OE monoclonal cells could not be amplified (**Figure 2C**). These results indicated that monoclonal C2C12 cells represent a heterozygous C2C12 Mdfi-OE cell line. The qPCR results showed that the mRNA level of *Mdfi* was significantly upregulated compared with the WT ($p < 0.01$) (**Figure 2D**). The Western blot results showed that the Mdfi protein level of monoclonal cells was significantly increased compared to WT ($p < 0.01$), indicating that Mdfi successfully overexpressed in monoclonal cells (**Figures 2E,F**). These results indicated that we have successfully constructed a Mdfi-OE C2C12 cell line to explore the function of Mdfi in C2C12 myogenic development.

Characteristics of Differentiation and Muscle Fiber Types in C2C12 Cells With Mdfi-OE

To further investigate the potential role of Mdfi in the differentiation of C2C12 cells, we induced the WT and Mdfi-OE

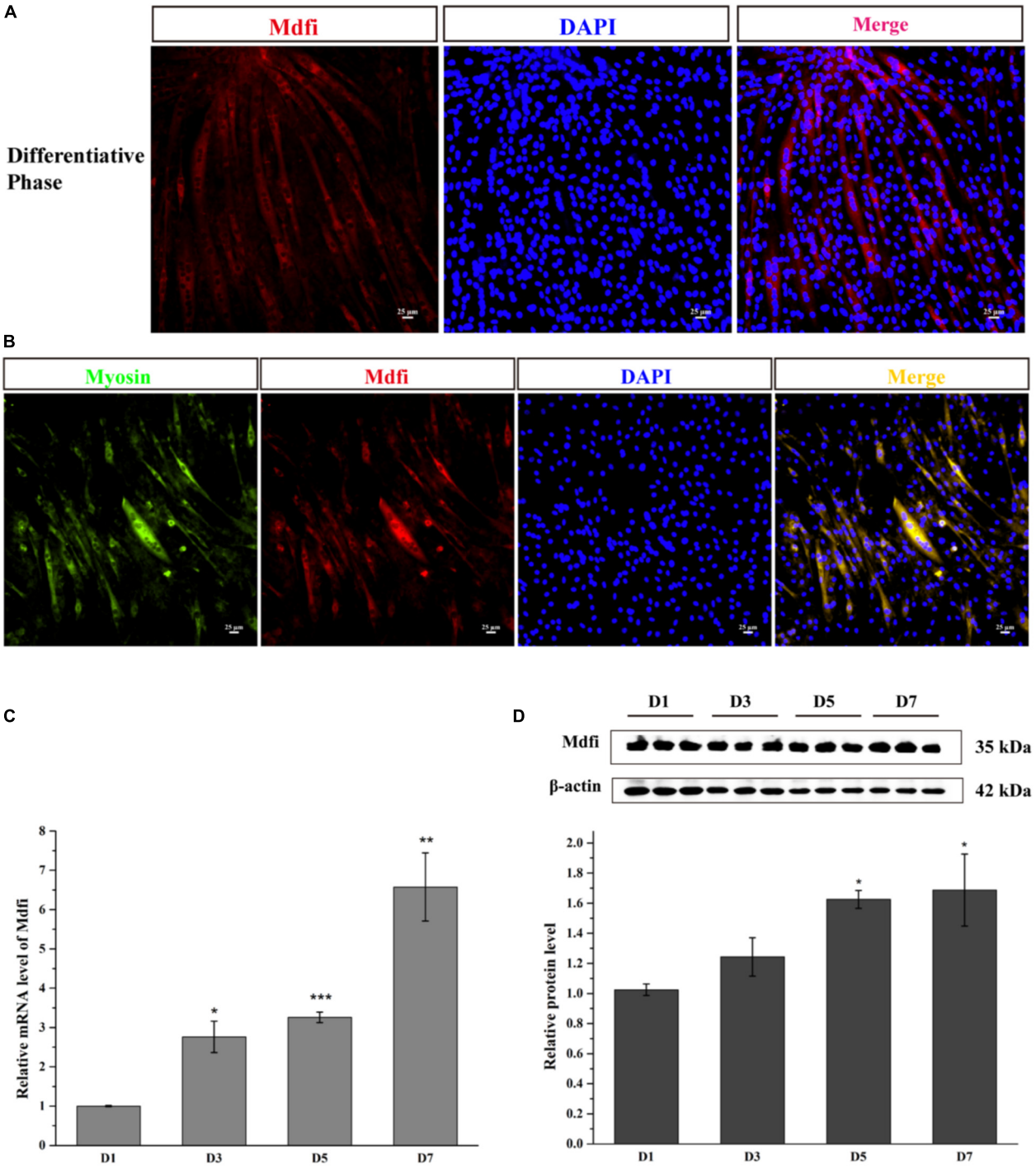

FIGURE 1 | Mdfi-expression profile during C2C12 cell development. **(A)** Mdfi immunofluorescence of C2C12 cells in differentiative phase. **(B)** Mdfi and myosin co-immunofluorescence of C2C12 cells in differentiative phase. Myosin: green, a molecular marker of myogenesis; Mdfi: red; DAPI: blue, cell nuclei; Merge: C2C12 cells fused into multi-nucleic myotubes. **(C)** qPCR identified Mdfi mRNA level on days 1, 3, 5, and 7 after differentiation induction. **(D)** Western blot identified Mdfi protein level on days 1, 3, 5, and 7 after differentiation induction. $^{*}p < 0.05$; $^{**}p < 0.01$; $^{***}p < 0.001$. The results are presented as Mean ± SEM of three replicates for each group. Magnification 200×. The scale bar on the photomicrographs represents 25 μm.

C2C12 cells in the differentiated medium at D1, 3, 5, and 7. Under white light, we observed that Mdfi-OE C2C12 cells fused into thicker myotubes than the WT group (**Supplementary Figure 1**). Myosin immunofluorescent staining results showed that Mdfi significantly increased the percentage of the myosin-positive cells at D5 ($p < 0.001$) and D7 ($p < 0.001$) (**Figures 3A,B**). In

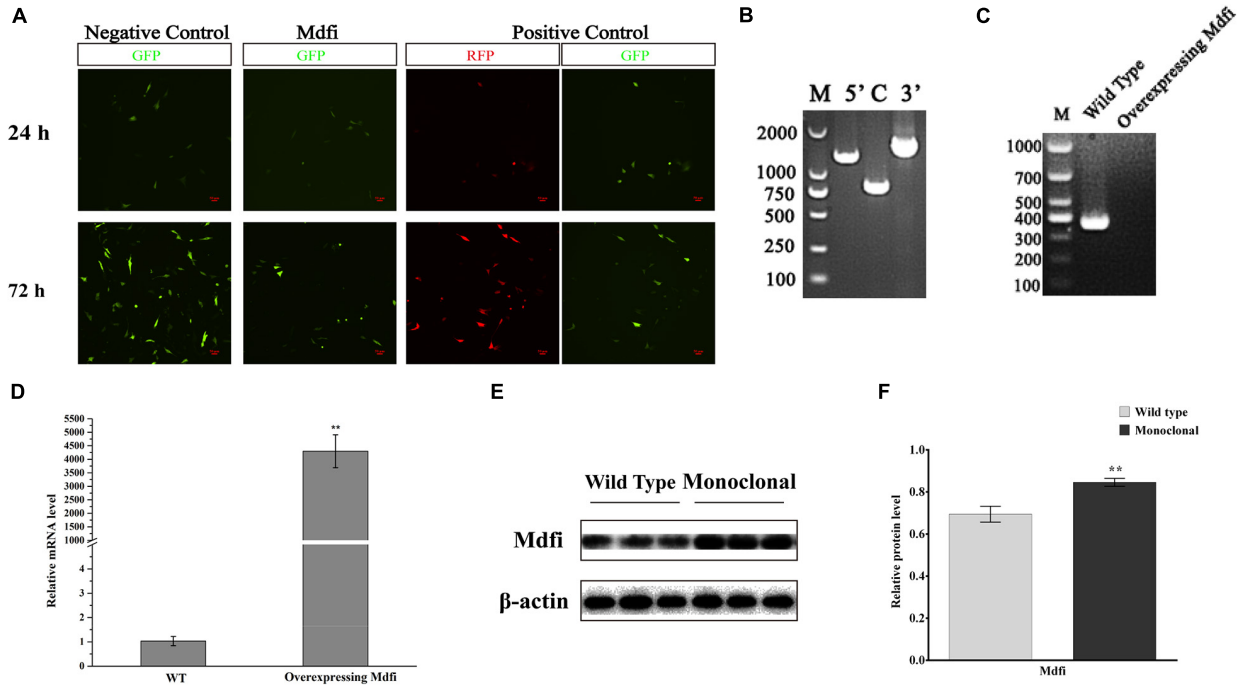

FIGURE 2 | Construction of a Mdfi-overexpressing C2C12 cell line. **(A)** Inverted fluorescence microscopy was used to investigate the expression of GFP and RFP protein in the C2C12 cell after puromycin screening for 24 and 72 h after transfected with Rosa26 + Donor, Rosa26 + Donor-Mdfi, and Rosa26+ Donor-RFP, respectively. **(B)** The homologous recombination status of left and right homologous arms and the insertion of the Mdfi gene in the monoclonal clone was confirmed. **(C)** Single or double allele insertion of Mdfi in monoclonal clone was confirmed through PCR amplification. **(D)** qPCR measured the mRNA level of Mdfi. **(E)** Western blot measured the protein level of Mdfi. **(F)** The relative protein levels obtained through Western blot band gray scanning analysis. ***$p < 0.001$. The results are presented as Mean ± SEM of three replicates for each group.

addition, we performed immunofluorescent staining on different subtypes of MyHC. The results showed that overexpression of Mdfi significantly increased the percentage of MyHC I ($p < 0.05$) and MyHC IIa ($p < 0.01$) positive C2C12 cells (**Figure 3C**). In contrast, overexpression of Mdfi decreased the percentage of MyHC IIb ($p < 0.05$) positive C2C12 cells (**Figures 3C,D**).

RNA-seq Analysis in Mdfi-OE vs WT C2C12 Cells

To further investigate the function of Mdfi in C2C12 myoblast differentiation, we performed RNA-Seq to profile genes expressed. The mRNA profiles were generated by sequencing six C2C12 cell samples (three each from Mdfi-OE and WT). Sample's length, clean reads, Q30 quality scores, GC content, and unique mapped rate were summarized in **Table 1**. A total of 254 million clean reads were retrieved from the mRNA profiles. The length of the clean reads ranged from 147.69 to 148.30 nt. Q30 quality scores of the six samples were above 92%. The GC content of the samples ranged from 49 to 50%. The unique mapped rate was above 83%. Based on the criteria of $p < 0.05$ and $|\text{Log2FoldChange}| > 1$, we identified 1,522 DEGs between Mdfi-OE and WT groups (**Supplementary Table 3**). Among these DEGs, 434 genes were upregulated, and 1,088 genes were downregulated in Mdfi-OE vs. WT (**Figure 4A**). *Mdfi* was markedly upregulated by 64-fold. Based on the KEGG analysis, 94 pathways were significantly enriched with a $p < 0.05$ (**Supplementary Table 4**). The first 20 KEGG pathways were shown in **Figure 4B**. The "calcium signaling pathway" was the most enriched. Furthermore, we established a PPI network composed of 1,522 DEGs, 287 nodes, and 1,024 edges (**Figure 4C**). High degreed-nodes in the regulatory network are also known as hub genes. We identified nine hub genes in the gene network, including six upregulated genes and three downregulated genes. These genes all play the key roles in the differentiation of the C2C12 cells with overexpressing Mdfi, which warrants further investigations. To validate the results of RNA-seq, we used qPCR to validate changes in expression levels of C2C12 cells overexpressed with Mdfi with induced differentiation. The qPCR results for all the DEGs were consistent with the results of the RNA-seq data ($p < 0.01$) (**Figures 4D,E**).

As expected, our RNA-seq analysis results showed that the IIa muscle fiber marker gene, myosin heavy chain 2 (*Myh2*) (about 1.33-fold), and myoglobin (*Mb*) (about 1.60-fold) were upregulated. In contrast, the IIb muscle fiber marker gene, myosin heavy chain 4 (*Myh4*) (about 2.46-fold), was downregulated. Furthermore, we identified six pathways involved in muscle fiber transformation in our RNA-seq results, such as "calcium signaling pathway," "PI3K-Akt signaling pathway", and "mTOR signaling pathway" (**Table 2**). In addition, we analyzed the intersection of genes in these pathways. The more

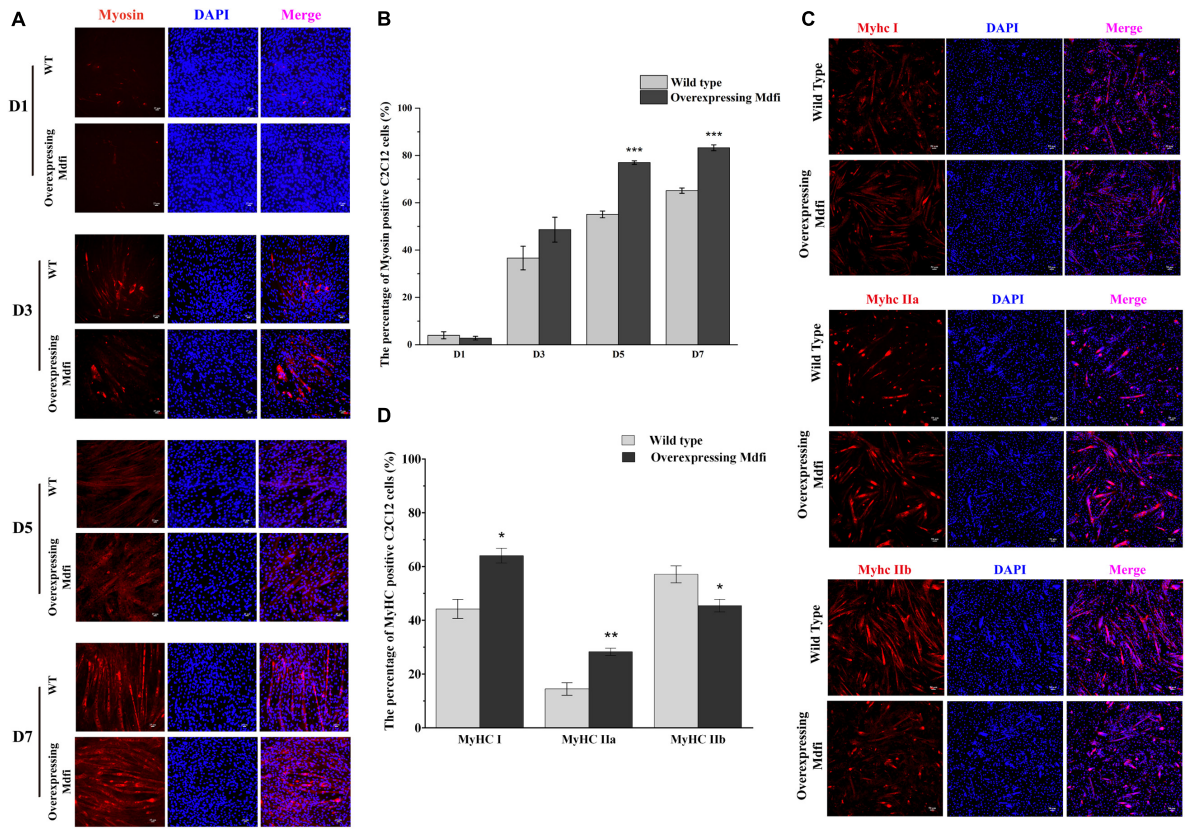

FIGURE 3 | Characteristics of differentiation and muscle fiber types in C2C12 cells with Mdfi overexpression. **(A)** Representative images of differentiating wild-type and overexpressing Mdfi C2C12 cells on days 1, 3, 5, and 7 in white light or myosin immunofluorescent staining. Myosin: red, a molecular marker of myogenesis; DAPI: blue, cell nuclei; Merge: the C2C12 cells fused into primary myotubes are shown in the insets. **(B)** Quantitative diagram of the percentage of myosin-positive C2C12 cells. **(C)** MyHC I, MyHC IIa, and MyHC IIb immunofluorescence staining in WT and Mdfi-OE C2C12 cells, respectively. **(D)** Quantitative diagram of the percentage of MyHC I, MyHC IIa, and MyHC IIb-positive C2C12 cells. The results are presented as Mean ± SEM of three replicates for each group. Magnification 200×. The scale bar on the photomicrographs represents 25 μm.

TABLE 1 | Overview of mRNA sequencing data.

Samples	ID	Length	Clean reads	Q30 (%)	GC (%)	Unique mapped reads (%)
Wild-Type 1	DC1	148.29	42843674	92.47	50.40	50.40
Wild-Type 2	DC2	148.29	41911008	92.10	49.85	49.85
Wild-Type 3	DC3	148.30	47325970	92.39	49.69	49.69
Mdfi-OE 1	DE1	147.85	39635016	92.06	49.15	49.15
Mdfi-OE 2	DE2	147.69	40636938	92.11	49.11	49.11
Mdfi-OE 3	DE3	148.07	41973956	92.71	49.52	49.52

Samples: Wild-Type 1/2/3 represent normal C2C12 cells. Mdfi-OE 1/2/3 represent overexpression of Mdfi in C2C12 cells. ID represents sample serial numbers. Length represents the length of sequencing reads. Clean reads were done after removing impurity reads for raw reads. Q30% represents the percentage of bases with mass values greater than or equal to 30. GC Content is the G and C base content. Unique mapped reads are the percentage of each sample aligned to the mouse reference genome.

pathways the gene is involved in, the more likely it is engaged in Mdfi regulating the transformation of muscle fiber types. As shown in the gene Venn diagram, calcium/calmodulin-dependent protein kinase II beta (*Camk2b*) was enriched in three pathways (**Figure 4F**). We then selected genes enriched in the above pathways to establish a regulatory network (**Figure 4G**); we found that most of the genes, especially *Camk2b*, ATPase sarcoplasmic/endoplasmic reticulum calcium ion transporting 2 (*Atp2a2*), and myoglobin (*Mb*), were related to calcium-induced muscle fiber type transformation. Particularly, *Camk2b* was the most degree hub gene in the gene network.

Mdfi-OE Promoted C2C12 Cells Myogenic Differentiation

To further validate the regulatory mechanism of Mdfi on C2C12 cell differentiation, we performed additional experiments. The qPCR results showed that overexpression of Mdfi significantly

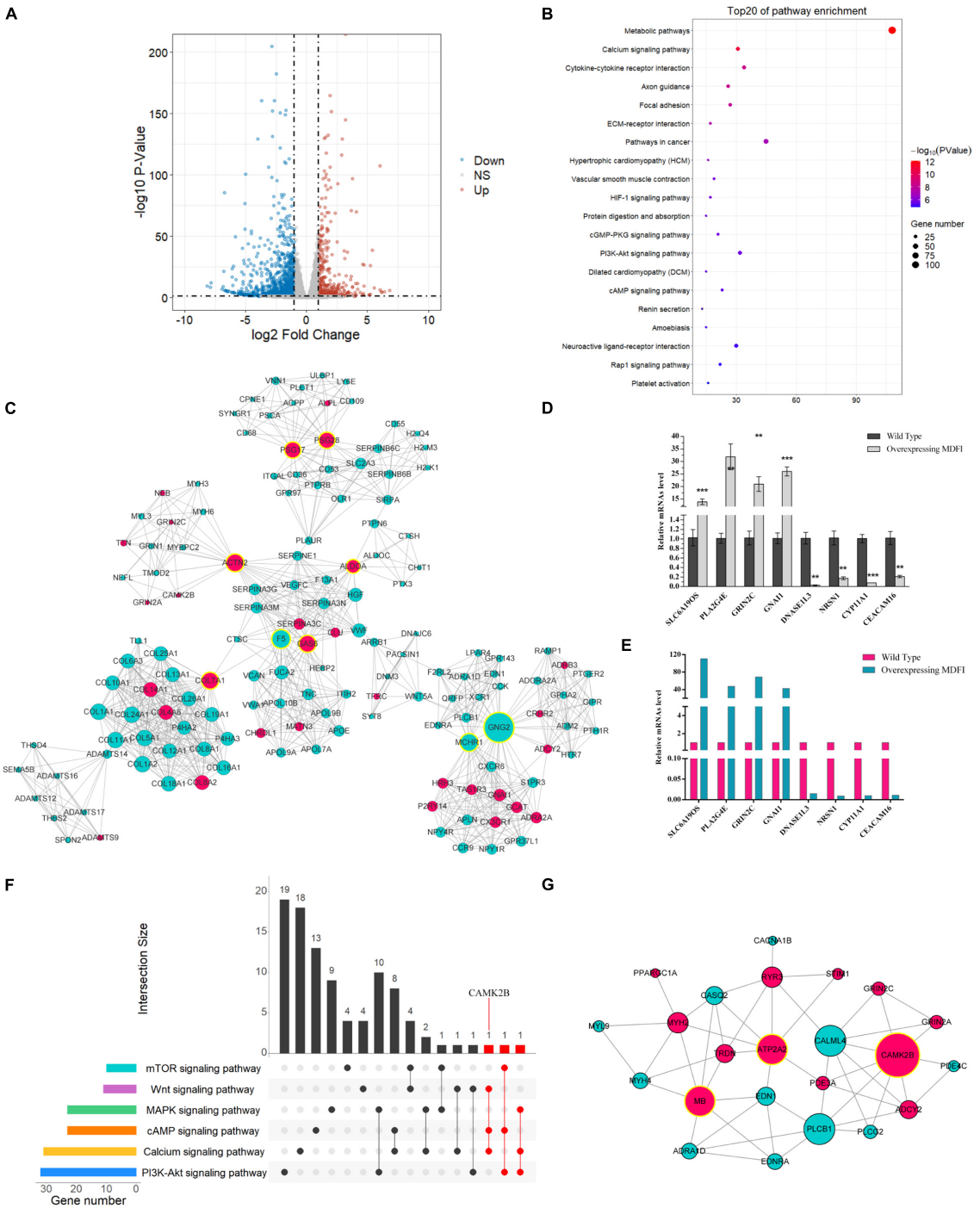

FIGURE 4 | RNA-seq analysis in Mdfi-OE vs. WT C2C12 cells. **(A)** The Volcano plot displays an overview of the DEGs. The X-axis represents the log-transformed *P*-value, and the Y-axis indicates the multiple of the DEGs. The gray dots represent DEGs that are not differentially expressed, the red dots represent the upregulated DEGs, and the blue dots represent the downregulated DEGs. |Log2FoldChange| > 1 and $p < 0.05$ were set as the criteria. **(B)** The first twenty pathways of the DEGs. The X-axis represents the number of DEGs enriched in the pathway. **(C)** PPI network in Mdfi-OE vs. WT. The network displays gene interactions. Nodes represent genes, and edges represent gene interactions. The upregulated genes are shown in red, downregulated genes are shown in green, and hub genes are shown in yellow. **(D)** qPCR validated of DEGs. **(E)** Expression levels of DEGs in RNA-seq. $^{**}p < 0.01$, $^{***}p < 0.001$. **(F)** The upset plot of the intersection of each pathway. The transverse bar graph at the bottom left shows the number of genes enriched in each pathway. The black points in the dot matrix at the bottom left and in the bar graph at the top indicate genes included in the pathways. The bars above represent the number of genes corresponding to each intersection. The red bars represent the number of intersection genes enriched in three or more pathways ($n \geq 3$). **(G)** The gene network displayed the gene interactions and was generated by Cytoscape (version 3.6). Nodes represent genes, and edges represent gene interactions. The upregulated genes are shown in red, downregulated genes are shown in green, and hub genes are shown in yellow.

TABLE 2 | The significantly enriched pathways related to muscle fiber type transformation.

Term	Count	*p*-Value
Calcium signaling pathway	31	1.41E-11
PI3K-Akt signaling pathway	32	1.99E-06
cAMP signaling pathway	23	3.26E-06
mTOR signaling pathway	10	0.043912
Wnt signaling pathway	11	0.026485
MAPK signaling pathway	23	0.000322

increased the mRNA level of *Myod* ($p > 0.001$), *Myog* ($p > 0.01$), and *Myosin* ($p > 0.001$) mainly at D3 and D5 (**Figure 5A**). There was no significant difference in mRNA levels of Myod, *Myog*, and *Myosin* between Mdfi-OE and WT at D1 (**Figure 5A**). The Western blot results showed that Mdfi significantly increased the Myod protein level in D3 and D5, Myog protein level in D1, D3, and D5, and Myosin protein level in D3, D5, and D7 (**Figures 5B,C**). Although the Myod and Myosin protein level of Mdfi-OE was not increased significantly at D1 compared to WT, there was still an increasing trend (**Figures 5B,C**). There was no significant difference in protein levels of Myod and Myog between Mdfi-OE and WT at D7 (**Figures 5B,C**). Furthermore, the Co-IP results showed that Mdfi interacted with both Myod and Myog (**Figure 5D**). These results indicated that Mdfi promotes C2C12 myogenic differentiation by upregulating the expression of Myod, Myog, and Myosin.

Mdfi Promotes the Muscle Fiber Type From the Fast-Twitch Muscle Fiber to the Slow-Twitch Muscle Fiber

To further examine the regulation mechanism of Mdfi on the transformation of muscle fiber types, we performed additional experiments. The qPCR results showed that overexpression of Mdfi increased the mRNA level of *Tnni1*, *MyHC I*, *MyHC IIa*, and *Mb* but decreased the mRNA level of *MyHC IIb* (**Figure 6A**). Furthermore, we used qPCR to identify the mitochondrial DNA copy number, and the results showed that overexpression of Mdfi increased the mitochondrial DNA copy number in C2C12 cells (**Figure 6B**). We also detected the expression level of *Camk2b* and its downstream cellular energy metabolism and mitochondrial oxidative phosphorylation-related genes. The qPCR results showed that overexpression of Mdfi increased the mRNA level of *Camk2b*, PPARG coactivator 1 alpha (*Pgc1a*), pyruvate dehydrogenase kinase (*Pdk4*), citrate synthase (*Cs*), cytochrome c oxidase subunit 4 (*Cox4*), acyl-Coenzyme A dehydrogenase medium-chain (*Acadm*), acyl-Coenzyme A oxidase 1 (*Acox1*), cytochrome c (*Cycs*) and ATP synthase H^+ transporting mitochondrial F1 complex alpha subunit 1 (*Atp5a1*) (**Figure 6C**). The Ch-IP results showed that Myod bound to the promoter region of *Camk2b* (**Figure 6D**). Overexpression of *Myod* increased the expression of *Camk2b* (**Figure 6E**). Dual-luciferase reporter system results showed that overexpressing *Myod* increased the promoter activity of *Camk2b* (**Figure 6F**). Combined with the above findings, Mdfi promoted the expression of *Myod*, thus upregulating the expression of *Camk2b*. Subsequently, *Camk2b* promoted the expression of downstream genes, such as *Pgc1a*, *Pdk4*, *Cs*, *Cox4*, *Acadm*, *Acox1*, *Cycs*, and *Atp5a1*. These results suggested that overexpression of Mdfi positively regulated the transformation of muscle fiber types from fast-twitch muscle to slow-twitch muscle.

DISCUSSION

In myoblast development, Mdfi blocked the myogenic differentiation of non-muscle-derived stem cells by inhibiting exogenous MRFs expression (Chen et al., 1996). However, Huang et al. (2019) found that MDFIC, which has the same domain as Mdfi, promoted the myogenic differentiation of muscle-derived stem cells. Its regulatory mechanism has not been studied in the muscle-derived stem cells. These opposite regulation functions of myogenic differentiation may be caused by the difference between species and cell types. Similarly, the function and regulatory mechanism of Mdfi on muscle fiber type transformation are also unclear. Therefore, we aimed to reveal the regulatory mechanism of Mdfi on myogenic cell differentiation and muscle fiber type transformation. In the present study, we successfully constructed a Mdfi-OE C2C12 cell line and found that overexpression of Mdfi promotes C2C12 cell differentiation and positively modulates fast-to-slow-twitch muscle fibers transformation.

Mdfi-OE Promoted C2C12 Cells Myogenic Differentiation by Upregulating the Expression of Myod, Myogenin, and Myosin

As myoblasts differentiated and fused into myotubes, myosin began to express (Crow and Stockdale, 1986; D'Albis et al., 1989). Therefore, myosin was considered as a marker of muscle differentiation and maturation in the study of muscle development (Pizon et al., 2005; Zhao et al., 2014). In the present study, we selected myosin as a marker of myoblast differentiation and the immunofluorescent staining of myosin showed that overexpression of Mdfi significantly increased the percentage of myosin-positive C2C12 cells. In the process of myogenic differentiation, the dynamically temporal and spatial expression of MRFs family proteins control the determination and differentiation of myoblasts (Hernandez-Hernandez et al., 2017a). Previous studies have shown that Di-(2-ethylhexyl)-phthalate (DEHP) inhibited C2C12 cell differentiation by repressing the expression of Myod and Myog, resulting in decreased myotube formation and MyHC expression (Chen et al., 2013). In our study, the qPCR and Western blot results showed that Mdfi-OE significantly increases the expression of Myod, Myog, and Myosin in C2C12 cells, mainly in the middle and late stages of differentiation (D3 and D5). Meanwhile, the expression of Mdfi is dynamic in the process of myogenic differentiation. Therefore, we speculate that Mdfi plays an important role in the middle and late stage of C2C12 cell differentiation. Furthermore, the Co-IP results showed that

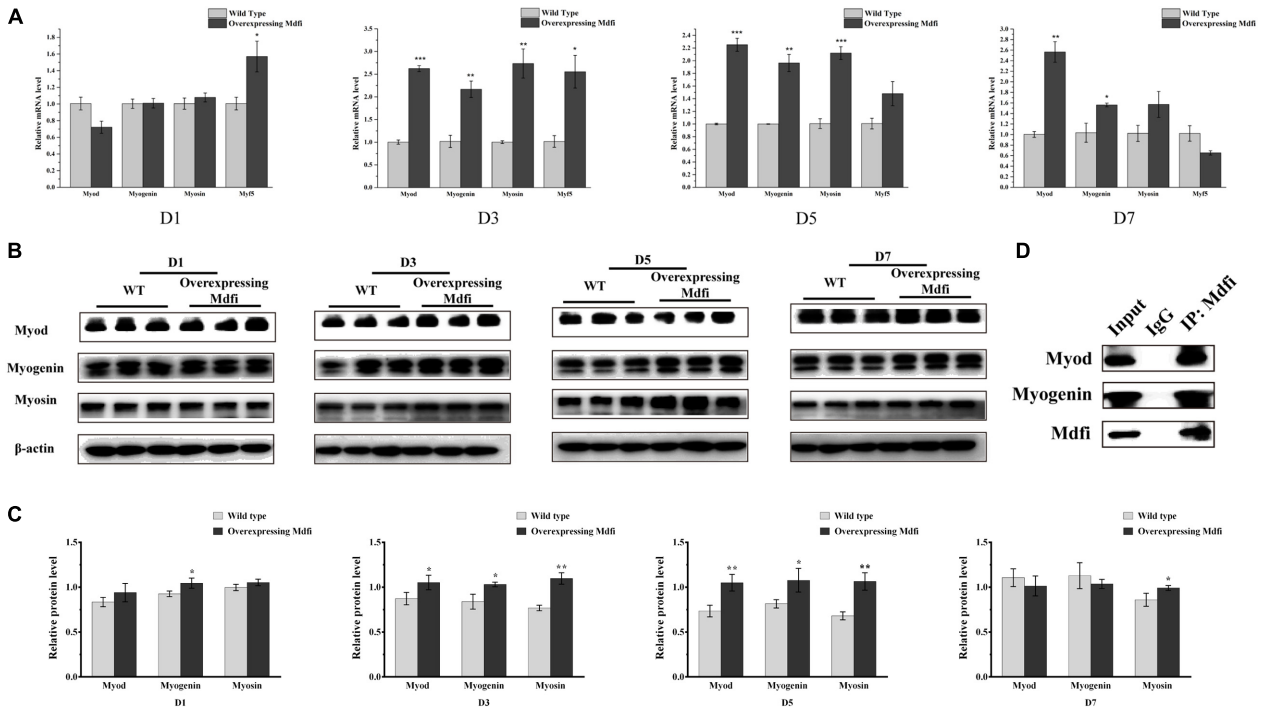

FIGURE 5 | Mdfi promotes the differentiation of C2C12 cells. **(A)** qPCR detection of myogenic marker genes on days 1, 3, 5, and 7 in both WT and Mdfi-OE C2C12 cells. **(B)** Western blot identified the protein of myogenic marker genes on days 1, 3, 5, and 7 after differentiation induction in both WT and Mdfi-OE C2C12 cells. **(C)** The relative protein levels were obtained through Western blot band gray scanning analysis. **(D)** Co-IP identified the interaction of Mdfi with Myod and Myog, respectively. $^{*}p < 0.05$; $^{**}p < 0.01$; $^{***}p < 0.001$. The results are presented as Mean ± SEM of three replicates for each group.

Mdfi interacted with both Myod and Myog. Therefore, we concluded that Mdfi regulates the differentiation and maturation of C2C12 cells by dynamically regulating Myod, Myog, and Myosin (**Figure 7**).

Pathway Enrichment and Gene Network Construction in RNA-seq Analysis

In our RNA-Seq analysis results, the "calcium signaling pathway" was the most enriched. The high intracellular calcium concentration induced myogenic differentiation and promoted the transformation of muscle fibers from fast-twitch to slow-twitch (Tu et al., 2016; Ravel-Chapuis et al., 2017). Numerous upregulated DEGs were enriched in the calcium signaling pathway, such as purinergic receptor P2X ligand-gated ion channel 5 (*P2rx5*), ryanodine receptor 3 (*Ryr3*), stromal interaction molecule 1 (*Stim1*), *Atp2a2*, and *Camk2b*, were involved in the process of myogenic differentiation. P2rx5, a ligand-gated ion channel, caused calcium to flow through the plasma membrane and promoted the terminal differentiation of myoblasts (Ryten et al., 2002). Ryr3 is a sarcoplasmic reticulum calcium release channel in skeletal muscle (Protasi et al., 2000). Stim1 is a sarcoplasmic reticulum membrane protein that can sense the change of calcium content. Overexpression of Stim1 promoted C2C12 cell differentiation and enhanced myotube formation, whereas *Stim1*-knockdown resulted in the opposite effects (Phuong et al., 2013). Atp2a2, also known as SERCA2, is a calcium transport ATPase, which functions as the reuptake of calcium from the cytoplasm to the sarcoplasmic reticulum (Harrer et al., 1995). Atp2a2 previously has been shown to express primarily in the slow-twitch skeletal muscle, and the knockdown of *Atp2a2* in C2C12 cells inhibited the expression of slow-twitch muscle marker genes (Wei et al., 2015). Camk2b, a calcium-dependent kinase, promoted mitochondrial biogenesis and involved in muscle fiber type transformation (Al-Shanti and Stewart, 2009). These genes were significantly upregulated in our RNA-Seq results and involved in regulating the formation of muscle fibers through calcium-transport. This result suggests that Mdfi-OE may promote C2C12 cell differentiation by regulating the calcium signaling pathway.

We also successfully established a PPI network and identified nine hub genes. Six upregulated hub genes are actinin alpha 2 (*Actn2*), growth arrest-specific 6 (*Gas6*), pregnancy-specific glycoprotein family members (*Psg17*, *Psg28*), collagen type VII alpha 1 (*Col7a1*), and aldolase A fructose-bisphosphate (*Aldoa*). Actn2, a muscle-specific actin-binding protein, bound explicitly disintegrin and metallopeptidase domain 12 (Adam12) to promote myoblast fusion (Galliano et al., 2000). Gas6 was increasingly secreted during C2C12 cell differentiation, and it has the same expression trend during the regeneration of muscle injury (Chikazawa et al., 2020). Psg17 and Psg28 are the members of the pregnancy-specific glycoprotein family. Psg17 bound CD9 protein to regulate the pregnancy process of the mouse (Wynne et al., 2006). To our knowledge, there are no published reports

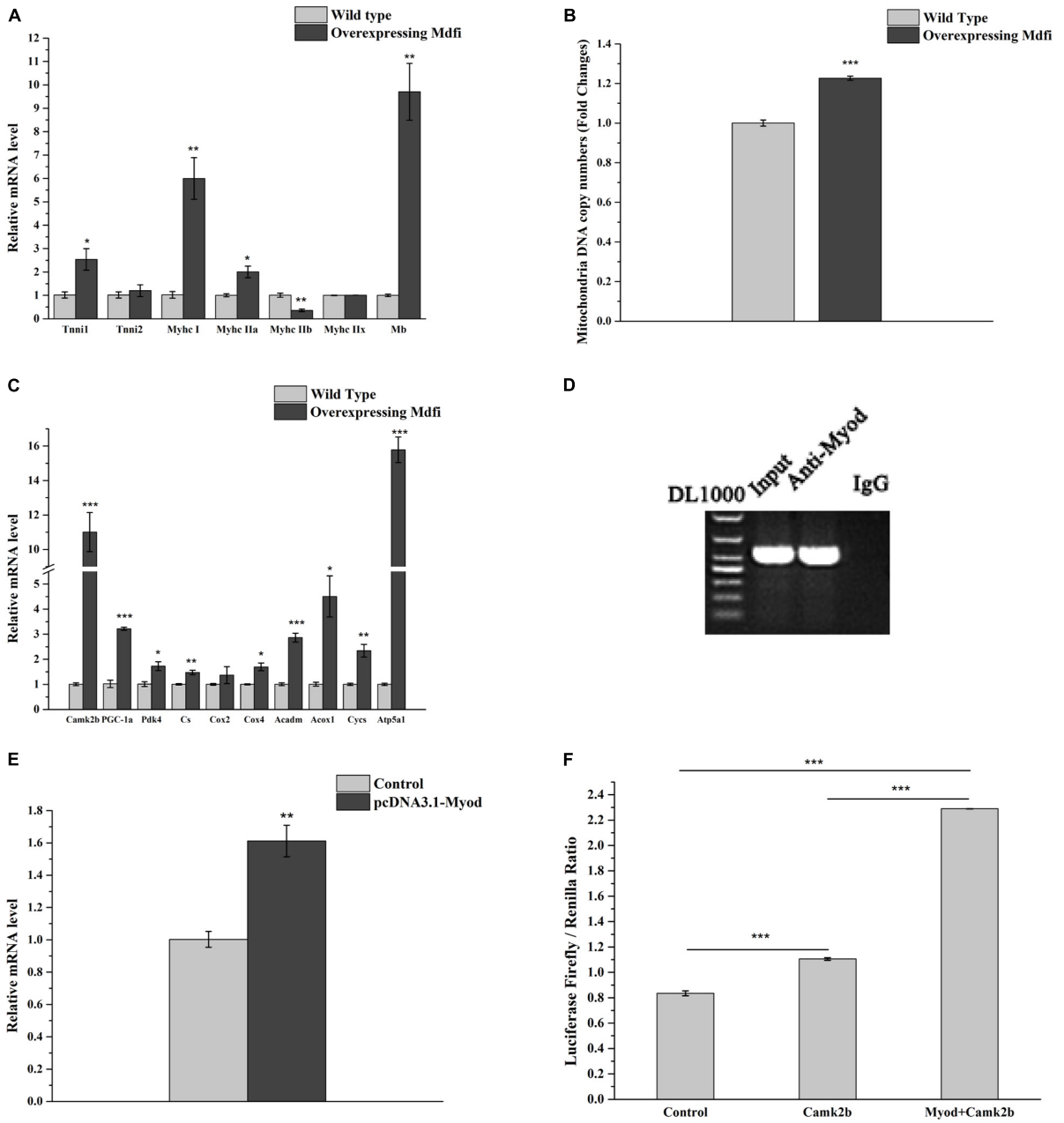

FIGURE 6 | Mdfi positively regulated the transformation of muscle fiber types from fast-twitch muscle to slow-twitch muscle in C2C12 cells. **(A)** qPCR identified the mRNA level of marker genes of different muscle fiber types in WT and Mdfi-OE C2C12 cells, respectively. **(B)** qPCR identified the relative copy number of mitochondrial DNA in WT and Mdfi-OE C2C12 cells, respectively. **(C)** qPCR identified the mRNA levels of energy metabolism-related genes in WT and Mdfi-OE C2C12 cells, respectively. **(D)** ChIP assay identified the binding of Myod to the Camk2b promoter region. **(E)** qPCR detection of the mRNA level of the *Camk2b* gene in C2C12 cells after Myod overexpressing. **(F)** The dual-luciferase reporter system identified the promoter activity of Camk2b after Myod overexpressing. $^{*}p < 0.05$; $^{**}p < 0.01$; $^{***}p < 0.001$. The results are presented as Mean ± S.E.M. of three replicates for each group.

on Psg28. Col7a1, one of the extracellular matrix components, had different expression patterns in various types of muscle fibers (Zhu et al., 2016). Aldoa interacts with RYR to promote calcium release from the sarcoplasmic reticulum into the cytoplasm (Kramerova et al., 2008). Meanwhile, three downregulated hub genes are G protein subunit gamma 2 (*Gng2*), coagulation factor V (*F5*), and melanin-concentrating hormone receptor 1 (*Mchr1*). Gng2 is a member of guanine nucleotide-binding protein (G protein), which plays an essential role in various transmembrane signaling systems, mainly by binding G Protein-Coupled Receptors (GPCR; Liang et al., 2016). F5 is a critical factor in the blood coagulation process, primarily promoting

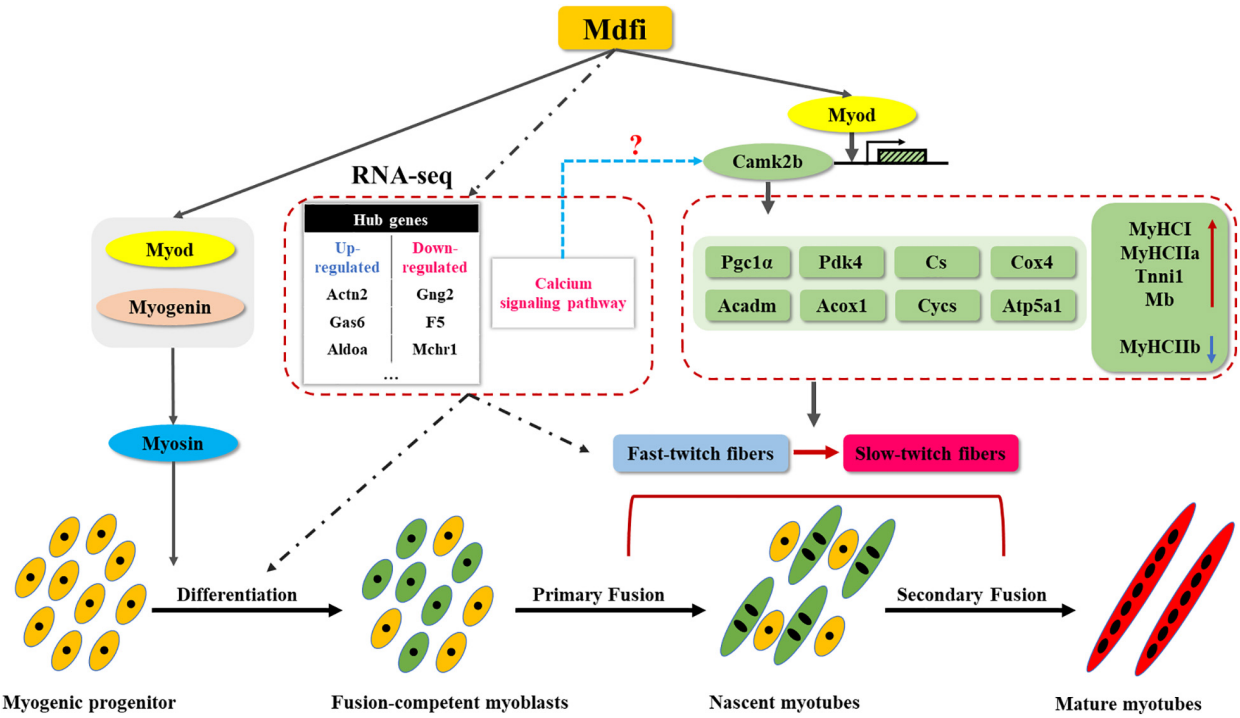

FIGURE 7 | Mdfi overexpression promoted C2C12 cell differentiation and positively modulated fast-to-slow-twitch muscle fibers transformation. We constructed a Mdfi-overexpressing C2C12 cell line by the CRISPR/Cas9 system. During C2C12 myogenic development, Mdfi promotes the differentiation of C2C12 cells by upregulating the expression of Myod, Myog, and Myosin. Mdfi positively modulated fast-to-slow-twitch muscle fibers transformation by upregulating the mRNA levels of *Myod*, *Camk2b*, and its downstream genes, such as *Pgc1a*, *Pdk4*, *Cs*, *Cox4*, *Acadm*, *Acox1*, *Cycs*, and *Atp5a1*. In addition, the calcium signaling pathway was the most significant in C2C12 cells with Mdfi-OE. We also systematically established regulatory networks and identified hub genes in them. Their regulation mechanism in Mdfi regulation of C2C12 cell differentiation and the muscle fiber type transformation warrants further investigations.

the conversion of prothrombin to thrombin (Rodgers et al., 1987). Mchr1 is a GPCR mainly expressed in the brain and also expressed in muscle tissue (Saito et al., 2013). Some of these hub genes are involved in muscle formation and regeneration of muscle injury, while others were novel genes not involved in muscle development. All the above hub genes are significantly changed in our RNA-Seq results. The role of these genes in the process of Mdfi regulating C2C12 cell differentiation warrants further investigations.

Mdfi-OE Positively Modulates Fast-to-Slow-Twitch Muscle Fibers Transformation

Skeletal muscle is a dynamically changing system with high plasticity. Skeletal muscle responds to external environmental stimuli, nutrient levels, mechanical training, and age, and adjusts the content of different MyHC subtypes in muscle fibers. In addition, the transformation of muscle fiber types occurs due to the changes in intracellular signal pathways caused by internal physiological changes, pathological stimulation, and stress (Grange et al., 2001; Pette, 2002). In the present study, we performed immunofluorescent staining to examine different subtypes of MyHC and found that overexpression of Mdfi increased the percentage of MyHC I and MyHC IIa positive C2C12 cells. In contrast, overexpression of Mdfi decreased the percentage of MyHC IIb positive C2C12 cells.

As expected, in the RNA-seq results, we found that *Myh4*, *Myh2*, and *Mb* expressed differently between WT and Mdfi-OE C2C12 cells. Moreover, the qPCR results showed that Mdfi overexpression increased the expression of MyHC I (*Myh7*), MyHC IIa (*Myh2*), *Tnni 1*, and *Mb*, while decreased the expression of MyHC IIb (*Myh4*). These qPCR results were consistent with the results of the RNA-seq data. This evidence indicated that the overexpression of Mdfi promotes the transformation of muscle fibers from type IIb to type IIa and type I. Furthermore, we explored the regulatory mechanism of Mdfi in regulating the transformation of muscle fiber types. In the qPCR results, we found that *Camk2b* was upregulated, enriched in three pathways related to the transformation of muscle fiber types, and identified as the hub genes in the network. The gene *Camk2b*, a downstream dependent kinase of the calcium signaling pathway, promoted mitochondrial biogenesis and participated in the transformation of muscle fiber types from fast-twitch muscle to slow-twitch muscle (Al-Shanti and Stewart, 2009). In mouse muscle development, *Camk2* regulated the oxidative metabolism of mouse muscle mediating by AMPK signaling (Raney and Turcotte, 2008). Therefore, we examined the expression of *Camk2b*, and the qPCR results demonstrated that overexpression of Mdfi significantly increased its expression.

Furthermore, we detected the expression level of downstream cellular energy metabolism and mitochondrial oxidative phosphorylation-related genes of *Camk2b*, such as *Pgc1a*, *Pdk4*, *Cs*, *Cox4*, *Acadm*, *Acox1*, *Cycs*, and *Atp5a1*. The knockin of *Pgc1a* in mice increased the distribution of red oxidized fibers and promoted the transformation of muscle fibers from type IIx to type I. Conversely, the knockout of *Pgc1a* in skeletal muscle induced the transformation of muscle fibers from type I and IIa to type IIx and IIb (Arany et al., 2007). *Pdk4* was activated by the co-expression of *Pgc1a* and estrogen-related receptor alpha (*Erra*) and played an important role in glucose oxidative phosphorylation (Sugden and Holness, 2003). In rat liver mitochondria, the inhibition of *Cox2* induced mitochondrial toxicity by inhibiting oxidative phosphorylation (Syed et al., 2016). During the development of porcine skeletal muscle, the addition of niacin supplementation promoted genes involved in mitochondrial fatty acid catabolism, citric acid cycle, and oxidative phosphorylation, such as *Cact*, *Sdha*, *Cox4*, and *Cox6a1*. Their expression induced the transformation of muscle fibers from type II to type I (Khan et al., 2013). The genes *Acadm*, *Acox1*, *Cycs*, and *Atp5a1* were marker genes of mitochondrial fatty acid oxidation and oxidative phosphorylation in the muscle (Kitamura et al., 2020). The qPCR results showed an increase in expression of these genes. In addition, the Ch-IP results demonstrated that Myod binds to the promoter of *Camk2b* to regulate the transcriptional activation of *Camk2b*.

All the above results indicated that Mdfi promotes the transcriptional activation of *Camk2b* by binding to Myod, increasing the expression of downstream *Pgc1a*, *Pdk4*, *Cs*, *Cox4*, *Acadm*, *Acox1*, *Cycs*, and *Atp5a1*, and ultimately promoting the transformation of muscle fibers from type IIb to type IIa and type I (**Figure 7**). In addition, whether Mdfi activates *Camk2b* through the calcium signaling pathway to regulate muscle fiber type transformation needs to be further explored.

CONCLUSION

In conclusion, our findings have further characterized the regulatory function of Mdfi in C2C12 cell differentiation and muscle fiber type transformation. Mdfi-OE promoted the differentiation of C2C12 cells by upregulating the expression of Myod, Myog, and Myosin. Meanwhile, Mdfi-OE promoted the expression of *Camk2b* by binding to Myod. *Camk2b*, in turn, upregulated the expression of downstream genes, such as *Pgc1a*, *Pdk4*, *Cs*, *Cox4*, *Acadm*, *Acox1*, *Cycs*, and *Atp5a1*, and ultimately promoting the transformation of muscle fibers from the fast-twitch to the slow-twitch. In addition, combined with RNA-seq results, we found that the calcium signaling pathway was the most significant in C2C12 cells with Mdfi-OE. Its regulation mechanism in Mdfi regulation of C2C12 cell differentiation and the muscle fiber type transformation warrants further investigations. We also systematically established the regulatory networks of Mdfi-OE on C2C12 cell differentiation and muscle fiber type transformation and identified hub genes. These results led us to propose a regulatory mechanism model of how Mdfi regulates muscle development. Mdfi may be a therapeutic target for muscle- and metabolic-related diseases treatment.

DATA AVAILABILITY STATEMENT

The datasets presented in this study can be found in online repositories. The names of the repository/repositories and accession number(s) can be found below: http://www.ncbi.nlm.nih.gov/bioproject/679162.

AUTHOR CONTRIBUTIONS

CW, BH, and YJ designed the research. YJ and YZ performed the research and developed the methods. BH, ZN, and ZY analyzed the data. BH, QL, CH, and CW wrote the manuscript. All authors made contributions to this study and read and approved the final manuscript.

FUNDING

This work was supported by the South China Agricultural University Major Project for International Science and Technology Cooperation Cultivation (2019SCAUGH01), the Guangdong Provincial Key Area Research and Development Program (2018B020203002), the Provincial Agricultural Science Innovation and Promotion Project (2020KJ106), the China Postdoctoral Science Foundation (2018M640789), and the USDA (HAW05020-H).

SUPPLEMENTARY MATERIAL

The Supplementary Material for this article can be found online at: https://www.frontiersin.org/articles/10.3389/fcell.2021.605875/full#supplementary-material

Supplementary Figure 1 | Cell fusion observation under white light.

Supplementary Table 1 | All the primers used in this study.

Supplementary Table 2 | Antibodies used in the study.

Supplementary Table 3 | The DEGs in Mdfi-OE vs. WT.

Supplementary Table 4 | The KEGG pathways were enriched by DEGs.

REFERENCES

Abou-Khalil, R., Le Grand, F., Pallafacchina, G., Valable, S., Authier, F. J., Rudnicki, M. A., et al. (2009). Autocrine and paracrine angiopoietin 1/Tie-2 signaling promotes muscle satellite cell self-renewal. *Cell Stem Cell* 5, 298–309. doi: 10.1016/j.stem.2009.06.001

Aguirre, F., Abrigo, J., Gonzalez, F., Gonzalez, A., Simon, F., and Cabello-Verrugio, C. (2020). Protective Effect of Angiotensin 1-7 on Sarcopenia Induced by Chronic Liver Disease in Mice. *Int. J. Mol. Sci.* 21:21113891. doi: 10.3390/ijms21113891

Al-Shanti, N., and Stewart, C. E. (2009). Ca2+/calmodulin-dependent transcriptional pathways: potential mediators of skeletal muscle

growth and development. *Biol. Rev. Camb. Philos. Soc.* 84, 637–652. doi: 10.1111/j.1469-185X.2009.00090.x

Arany, Z., Lebrasseur, N., Morris, C., Smith, E., Yang, W. L., Ma, Y. H., et al. (2007). The transcriptional coactivator PGC-1 beta drives the formation of oxidative type IIX fibers in skeletal muscle. *Cell Metab.* 5, 35–46. doi: 10.1016/j.cmet.2006.12.003

Bassel-Duby, R., and Olson, E. N. (2006). Signaling pathways in skeletal muscle remodeling. *Ann. Rev. Biochem.* 75, 19–37. doi: 10.1146/annurev.biochem.75.103004.142622

Bentzinger, C. F., Wang, Y. X., and Rudnicki, M. A. (2012). Building muscle: molecular regulation of myogenesis. *Cold Spr. Harb Perspect. Biol.* 4:a008342. doi: 10.1101/cshperspect.a008342

Caporaso, J. G., Lauber, C. L., Walters, W. A., Berg-Lyons, D., Huntley, J., Fierer, N., et al. (2012). Ultra-high-throughput microbial community analysis on the Illumina HiSeq and MiSeq platforms. *ISME J.* 6, 1621–1624. doi: 10.1038/ismej.2012.8

Chen, C. M., Kraut, N., Groudine, M., and Weintraub, H. (1996). I-mf, a novel myogenic repressor, interacts with members of the MyoD family. *Cell* 86, 731–741. doi: 10.1016/s0092-8674(00)80148-8

Chen, S. S., Hung, H. T., Chen, T. J., Hung, H. S., and Wang, D. C. (2013). Di-(2-ethylhexyl)-phthalate reduces MyoD and myogenin expression and inhibits myogenic differentiation in C2C12 cells. *J. Toxicol. Sci.* 38, 783–791.

Chen, X., Guo, Y., Jia, G., Liu, G., Zhao, H., and Huang, Z. (2018). Arginine promotes skeletal muscle fiber type transformation from fast-twitch to slow-twitch via Sirt1/AMPK pathway. *J. Nutr. Biochem.* 61, 155–162. doi: 10.1016/j.jnutbio.2018.08.007

Chikazawa, M., Shimizu, M., Yamauchi, Y., and Sato, R. (2020). Bridging molecules are secreted from the skeletal muscle and potentially regulate muscle differentiation. *Biochem. Biophys. Res. Commun.* 522, 113–120. doi: 10.1016/j.bbrc.2019.11.010

Crow, M. T., and Stockdale, F. E. (1986). Myosin expression and specialization among the earliest muscle fibers of the developing avian limb. *Dev. Biol.* 113, 238–254.

D'Albis, A., Couteaux, R., Janmot, C., and Roulet, A. (1989). Specific programs of myosin expression in the postnatal development of rat muscles. *Eur. J. Biochem.* 183, 583–590. doi: 10.1111/j.1432-1033.1989.tb21087.x

Delfini, M. C., Hirsinger, E., Pourquie, O., and Duprez, D. (2000). Delta 1-activated notch inhibits muscle differentiation without affecting Myf5 and Pax3 expression in chick limb myogenesis. *Development* 127, 5213–5224.

Fry, C. S., Lee, J. D., Mula, J., Kirby, T. J., Jackson, J. R., Liu, F., et al. (2015). Inducible depletion of satellite cells in adult, sedentary mice impairs muscle regenerative capacity without affecting sarcopenia. *Nat. Med.* 21, 76–80. doi: 10.1038/nm.3710

Galliano, M. F., Huet, C., Frygelius, J., Polgren, A., Wewer, U. M., and Engvall, E. (2000). Binding of ADAM12, a marker of skeletal muscle regeneration, to the muscle-specific actin-binding protein, alpha -actinin-2, is required for myoblast fusion. *J. Biol. Chem.* 275, 13933–13939. doi: 10.1074/jbc.275.18.13933

Grange, R. W., Meeson, A., Chin, E., Lau, K. S., Stull, J. T., Shelton, J. M., et al. (2001). Functional and molecular adaptations in skeletal muscle of myoglobin-mutant mice. *Am. J. Phys. Cell Phys.* 281, C1487–C1494. doi: 10.1152/ajpcell.2001.281.5.C1487

Harrer, J. M., Ponniah, S., Ferguson, D. G., and Kranias, E. G. (1995). Expression of phospholamban in C2C12 cells and regulation of endogenous SERCA1 activity. *Mol. Cell Biochem.* 146, 13–21. doi: 10.1007/bf00926876

Hernandez-Hernandez, J. M., Garcia-Gonzalez, E. G., Brun, C. E., and Rudnicki, M. A. (2017a). The myogenic regulatory factors, determinants of muscle development, cell identity and regeneration. *Semin. Cell Dev. Biol.* 72, 10–18. doi: 10.1016/j.semcdb.2017.11.010

Hernandez-Hernandez, M., Garcia-Gonzalez, E. G., Brun, C. E., and Rudnicki, M. A. (2017b). The myogenic regulatory factors, determinants of muscle development, cell identity and regeneration. *Sem.Cell Dev. Biol.* 72, 10–18.

Hou, L., Xu, J., Jiao, Y., Li, H., Pan, Z., Duan, J., et al. (2018). MiR-27b Promotes Muscle Development by Inhibiting MDFI Expression. *Cell Physiol. Biochem.* 46, 2271–2283. doi: 10.1159/000489595

Hou, L., Xu, J., Li, H., Ou, J., Jiao, Y., Hu, C., et al. (2017). MiR-34c represses muscle development by forming a regulatory loop with Notch1. *Sci. Rep.* 7:9346. doi: 10.1038/s41598-017-09688-y

Huang, W., Guo, L., Zhao, M., Zhang, D., Xu, H., and Nie, Q. (2019). The Inhibition on MDFIC and PI3K/AKT Pathway Caused by miR-146b-3p Triggers Suppression of Myoblast Proliferation and Differentiation and Promotion of Apoptosis. *Cells* 8:8070656. doi: 10.3390/cells8070656

Khan, M., Ringseis, R., Mooren, F. C., Kruger, K., Most, E., and Eder, K. (2013). Niacin supplementation increases the number of oxidative type I fibers in skeletal muscle of growing pigs. *BMC Vet. Res.* 9:177. doi: 10.1186/1746-6148-9-177

Kitamura, K., Erlangga, J. S., Tsukamoto, S., Sakamoto, Y., Mabashi-Asazuma, H., and Iida, K. (2020). Daidzein promotes the expression of oxidative phosphorylation- and fatty acid oxidation-related genes via an estrogen-related receptor alpha pathway to decrease lipid accumulation in muscle cells. *J. Nutr. Biochem.* 77:108315. doi: 10.1016/j.jnutbio.2019.108315

Kramerova, I., Kudryashova, E., Wu, B., Ottenheijm, C., Granzier, H., and Spencer, M. J. (2008). Novel role of calpain-3 in the triad-associated protein complex regulating calcium release in skeletal muscle. *Hum. Mol. Genet.* 17, 3271–3280. doi: 10.1093/hmg/ddn223

Liang, B., Li, C., and Zhao, J. (2016). Identification of key pathways and genes in colorectal cancer using bioinformatics analysis. *Med. Oncol.* 33:111. doi: 10.1007/s12032-016-0829-6

Liao, Y., Smyth, G. K., and Shi, W. (2019). The R package Rsubread is easier, faster, cheaper and better for alignment and quantification of RNA sequencing reads. *Nucleic Acids Res.* 47, e4710.1093. doi: ARTN e4710.1093/nar/gkz114

Lu, J. J., Wang, Q., Xie, L. H., Zhang, Q., and Sun, S. H. (2017). Tumor necrosis factor-like weak inducer of apoptosis regulates quadriceps muscle atrophy and fiber-type alteration in a rat model of chronic obstructive pulmonary disease. *Tob. Induc. Dis.* 15:43. doi: 10.1186/s12971-017-0148-5

Mashinchian, O., Pisconti, A., Le Moal, E., and Bentzinger, C. F. (2018). The Muscle Stem Cell Niche in Health and Disease. *Curr. Top Dev. Biol.* 126, 23–65. doi: 10.1016/bs.ctdb.2017.08.003

Oberbach, A., Bossenz, Y., Lehmann, S., Niebauer, J., Adams, V., Paschke, R., et al. (2006). Altered fiber distribution and fiber-specific glycolytic and oxidative enzyme activity in skeletal muscle of patients with type 2 diabetes. *Diabetes Care* 29, 895–900. doi: 10.2337/diacare.29.04.06.dc05-1854

Pette, D. (2002). The adaptive potential of skeletal muscle fibers. *Can. J. Appl. Physiol.* 27, 423–448.

Phuong, T. T., Yun, Y. H., Kim, S. J., and Kang, T. M. (2013). Positive feedback control between STIM1 and NFATc3 is required for C2C12 myoblast differentiation. *Biochem. Biophys. Res. Commun.* 430, 722–728. doi: 10.1016/j.bbrc.2012.11.082

Pizon, V., Gerbal, F., Diaz, C. C., and Karsenti, E. (2005). Microtubule-dependent transport and organization of sarcomeric myosin during skeletal muscle differentiation. *EMBO J.* 24, 3781–3792. doi: 10.1038/sj.emboj.7600842

Protasi, F., Takekura, H., Wang, Y., Chen, S. R., Meissner, G., Allen, P. D., et al. (2000). RYR1 and RYR3 have different roles in the assembly of calcium release units of skeletal muscle. *Biophys. J.* 79, 2494–2508. doi: 10.1016/S0006-3495(00)76491-5

Raney, M. A., and Turcotte, L. P. (2008). Evidence for the involvement of CaMKII and AMPK in Ca2+-dependent signaling pathways regulating FA uptake and oxidation in contracting rodent muscle. *J. Appl. Physiol.* 104, 1366–1373. doi: 10.1152/japplphysiol.01282.2007

Ravel-Chapuis, A., Belanger, G., Cote, J., Michel, R. N., and Jasmin, B. J. (2017). Misregulation of calcium-handling proteins promotes hyperactivation of calcineurin-NFAT signaling in skeletal muscle of DM1 mice. *Hum. Mol. Genet.* 26, 2192–2206. doi: 10.1093/hmg/ddx109

Rodgers, G. M., Cong, J. Y., Goll, D. E., and Kane, W. H. (1987). Activation of coagulation factor V by calcium-dependent proteinase. *Biochim. Biophys. Acta* 929, 263–270. doi: 10.1016/0167-4889(87)90252-7

Ryten, M., Dunn, P. M., Neary, J. T., and Burnstock, G. (2002). ATP regulates the differentiation of mammalian skeletal muscle by activation of a P2X5 receptor on satellite cells. *J. Cell Biol.* 158, 345–355. doi: 10.1083/jcb.200202025

Saito, Y., Hamamoto, A., and Kobayashi, Y. (2013). Regulated Control of Melanin-Concentrating Hormone Receptor 1 through Posttranslational Modifications. *Front. Endocrinol.* 4:154. doi: 10.3389/fendo.2013.00154

Schiaffino, S., and Reggiani, C. (2011). Fiber types in mammalian skeletal muscles. *Physiol. Rev.* 91, 1447–1531. doi: 10.1152/physrev.00031.2010

Shannon, P., Markiel, A., Ozier, O., Baliga, N. S., Wang, J. T., Ramage, D., et al. (2003). Cytoscape: a software environment for integrated models of

biomolecular interaction networks. *Genome Res.* 13, 2498–2504. doi: 10.1101/gr.1239303

Sugden, M. C., and Holness, M. J. (2003). Recent advances in mechanisms regulating glucose oxidation at the level of the pyruvate dehydrogenase complex by PDKs. *Am. J. Physiol. Endocrinol. Metab.* 284, E855–E862. doi: 10.1152/ajpendo.00526.2002

Syed, M., Skonberg, C., and Hansen, S. H. (2016). Mitochondrial toxicity of selective COX-2 inhibitors via inhibition of oxidative phosphorylation (ATP synthesis) in rat liver mitochondria. *Toxicol. Vitro* 32, 26–40. doi: 10.1016/j.tiv.2015.12.003

Szklarczyk, D., Gable, A. L., Lyon, D., Junge, A., Wyder, S., Huerta-Cepas, J., et al. (2019). STRING v11: protein-protein association networks with increased coverage, supporting functional discovery in genome-wide experimental datasets. *Nucleic Acids Res.* 47, D607–D613. doi: 10.1093/nar/gky1131

Thebault, S., and Mesnard, J. M. (2001). How the sequestration of a protein interferes with its mechanism of action: example of a new family of proteins characterized by a particular cysteine-rich carboxy-terminal domain involved in gene expression regulation. *Curr. Protein Pept. Sci.* 2, 155–167. doi: 10.2174/1389203013381143

Tu, M. K., Levin, J. B., Hamilton, A. M., and Borodinsky, L. N. (2016). Calcium signaling in skeletal muscle development, maintenance and regeneration. *Cell Calcium* 59, 91–97. doi: 10.1016/j.ceca.2016.02.005

Turner, N. J., and Badylak, S. F. (2012). Regeneration of skeletal muscle. *Cell Tissue Res.* 347, 759–774. doi: 10.1007/s00441-011-1185-7

Wang, Y., and Pessin, J. E. (2013). Mechanisms for fiber-type specificity of skeletal muscle atrophy. *Curr. Opin. Clin. Nutr. Metab. Care* 16, 243–250. doi: 10.1097/MCO.0b013e328360272d

Wei, H., Li, Z., Wang, X., Wang, J., Pang, W., Yang, G., et al. (2015). microRNA-151-3p regulates slow muscle gene expression by targeting ATP2a2 in skeletal muscle cells. *J. Cell Physiol.* 230, 1003–1012. doi: 10.1002/jcp.24793

Wynne, F., Ball, M., McLellan, A. S., Dockery, P., Zimmermann, W., and Moore, T. (2006). Mouse pregnancy-specific glycoproteins: tissue-specific expression and evidence of association with maternal vasculature. *Reproduction* 131, 721–732. doi: 10.1530/rep.1.00869

Xie, C., Mao, X., Huang, J., Ding, Y., Wu, J., Dong, S., et al. (2011). KOBAS 2.0: a web server for annotation and identification of enriched pathways and diseases. *Nucleic Acids Res.* 39, W316–W322. doi: 10.1093/nar/gkr483

Zammit, P. S., Golding, J. P., Nagata, Y., Hudon, V., Partridge, T. A., and Beauchamp, J. R. (2004). Muscle satellite cells adopt divergent fates: a mechanism for self-renewal? *J. Cell Biol.* 166, 347–357. doi: 10.1083/jcb.200312007

Zhao, C., Farruggio, A. P., Bjornson, C. R., Chavez, C. L., Geisinger, J. M., Neal, T. L., et al. (2014). Recombinase-mediated reprogramming and dystrophin gene addition in mdx mouse induced pluripotent stem cells. *PLoS One.* 9:e96279. doi: 10.1371/journal.pone.0096279

Zhu, J., Shi, X., Lu, H., Xia, B., Li, Y., Li, X., et al. (2016). RNA-seq transcriptome analysis of extensor digitorum longus and soleus muscles in large white pigs. *Mol. Genet. Genomics* 291, 687–701. doi: 10.1007/s00438-015-1138-z

Conflict of Interest: The authors declare that the research was conducted in the absence of any commercial or financial relationships that could be construed as a potential conflict of interest.

frontiers in Cell and Developmental Biology

ORIGINAL RESEARCH
published: 25 February 2021
doi: 10.3389/fcell.2021.636498

Withaferin A and Ovarian Cancer Antagonistically Regulate Skeletal Muscle Mass

*Alex R. Straughn[1], Natia Q. Kelm[1] and Sham S. Kakar[1,2]**

[1] James Graham Brown Cancer Center, University of Louisville, Louisville, KY, United States, [2] Department of Physiology, University of Louisville, Louisville, KY, United States

Cachexia is a complex wasting syndrome that overwhelmingly affects the majority of late-stage cancer patients. Additionally, there are currently no efficacious therapeutic agents to treat the muscle atrophy induced by the cancer. While several preclinical studies have investigated the molecular signals orchestrating cachexia, very little information exists pertaining to ovarian cancer and the associated cachexia. Work from our lab has recently demonstrated that the steroidal lactone Withaferin A (WFA) is capable of attenuating the atrophying effects of ovarian cancer in a preclinical mouse model. However, it remained to be determined whether WFA's effect was in response to its anti-tumorigenic properties, or if it was capable of targeting skeletal muscle directly. The purpose of this study was to uncover whether WFA was capable of regulating muscle mass under tumor-free and tumor-bearing conditions. Treatment with WFA led to an improvement in functional muscle strength and mass under tumor-bearing and naïve conditions. WFA and ovarian cancer were observed to act antagonistically upon critical skeletal muscle regulatory systems, notably myogenic progenitors and proteolytic degradation pathways. Our results demonstrated for the first time that, while WFA has anti-tumorigenic properties, it also exerts hypertrophying effects on skeletal muscle mass, suggesting that it could be an anti-cachectic agent in the settings of ovarian cancer.

Keywords: atrophy, cachexia, satellite cells, catabolism, ovary

OPEN ACCESS

Edited by:
Yann Simon Gallot, University of Évry Val d'Essonne, France

Reviewed by:
Andrea Bonetto, Indiana University, United States
James A. Carson, University of Tennessee Health Science Center (UTHSC), United States
Aditi Arun Narsale, San Diego Biomedical Research Institute, United States

***Correspondence:**
Sham S. Kakar
sham.kakar@louisville.edu

Specialty section:
This article was submitted to Signaling, a section of the journal Frontiers in Cell and Developmental Biology

Received: *01 December 2020*
Accepted: *05 February 2021*
Published: *25 February 2021*

Citation:
Straughn AR, Kelm NQ and Kakar SS (2021) Withaferin A and Ovarian Cancer Antagonistically Regulate Skeletal Muscle Mass. Front. Cell Dev. Biol. 9:636498. doi: 10.3389/fcell.2021.636498

INTRODUCTION

Late-stage cancer patients frequently exhibit the complex metabolic syndrome cachexia (Gadducci et al., 2001). Cachexia is primarily marked by a loss of muscle strength and mass (Fearon et al., 2011; Fearon et al., 2012). This sequela of cancer is observed in up to 80% of cancer patients and is the direct cause of mortality in up to 30% of cancer patients, contingent upon the oncological setting (Fearon et al., 2011; Fearon et al., 2012). However, until recently, very few reports have examined cachexia in the settings of ovarian cancer. Ovarian cancer is the most lethal gynecological malignancy and the fifth leading cause of cancer-related deaths amongst women in the United States (Siegel et al., 2019). A recent meta-analysis reported that cachexia is observed in 11–54% of ovarian cancer patients, although it was noted that this wide range could be attributable to different cut-off points for assessing the induction of sarcopenia in patients (Ubachs et al., 2019).

The development of a cachectic state in cancer patients is highly correlated with a decrease in quality of life, tumor resurgence, and the development of resistance to chemotherapeutic agents (Fearon et al., 2011; Fearon et al., 2012; Johns et al., 2013). Indeed, in the settings of ovarian cancer, cachexia usually accompanies the onset of chemotherapeutic resistance and the development of ascites (Barreto et al., 2016). Current first-line therapy for ovarian cancer patients (cytoreductive surgery followed by treatment with a platinum-based antineoplastic agent) initially shows a high response rate, but approximately 70% of patients will relapse and develop resistance to platinum therapy (Cannistra, 2004; Ozols et al., 2003). Both primary debulking surgery and treatment with chemotherapeutic agents (such as cisplatin) are independently associated with the induction of cachexia and are associated with a decline in ovarian cancer patient survival (Huang et al., 2020). To date, no clinically efficacious treatment is available for the treatment of cachexia.

Three recent preclinical reports have examined cachexia in the settings of ovarian cancer, one of which was from our laboratory (Pettersen et al., 2020; Pin et al., 2018; Straughn and Kakar, 2019). While different ovarian cancer cell lines were utilized in the studies, interleukin-6 (IL-6) was examined to varying degrees in all three studies, likely due to its known roles in ovarian cancer progression (Dijkgraaf et al., 2012) and its association with the induction of cachexia (Bonetto et al., 2012). Quite interestingly, the report from Pettersen et al. demonstrated that intra-tumoral Activin A signaling promotes the secretion of IL-6 from ovarian cancer cells, and that inhibiting this signaling axis can reduce the ability of cancer cells to accelerate autophagy and impede the induction of cachexia (Pettersen et al., 2020). Along similar lines, work from our laboratory demonstrated that treatment of tumor-bearing mice with Withaferin A (WFA) at one concentration results in both the reduction in various proinflammatory cytokines and an improvement in muscle strength (Straughn and Kakar, 2019). The works by Pin et al. (2018) and Straughn and Kakar (2019) suggest that preservation of muscle mass could result in improvements in patient quality of life and survival and conclude that further research into the mechanisms responsible for muscle wasting in the settings of ovarian cancer is of the utmost clinical importance.

Skeletal muscle mass is primarily regulated by (1) myogenic progenitors, (2) the rate of protein degradation, and (3) the rate of protein synthesis (Schiaffino et al., 2013). Satellite cells are the primary myogenic progenitors responsible for the majority of skeletal muscle regeneration (Kuang et al., 2007; Relaix and Zammit, 2012), and have been shown to be spuriously activated in an NF-κB-dependent manner in multiple models of cancer-induced cachexia (He et al., 2013). While an increase in proliferating satellite cells has been evidenced in the settings of cancer-induced cachexia, it was simultaneously demonstrated that they are functionally inactivated (i.e., did not differentiate/fuse with muscle to repair injury) through a Pax7-dependent downregulation of MyoD, leading to a failure in muscle repair (He et al., 2013).

Additionally, cancer-induced cachexia has been reported to upregulate various branches of the unfolded protein response (UPR), exerting deleterious effects on muscle mass (Bohnert et al., 2016; Bohnert et al., 2018). The protein kinase R-like endoplasmic reticulum kinase (PERK) arm of the UPR is required for both the survival and differentiation of satellite cells to facilitate proper muscle repair (Xiong et al., 2017). However, overactivation of the UPR is known to result in skeletal muscle atrophy through activation of proteolytic systems (Afroze and Kumar, 2019). Upregulation of both the ubiquitin proteasome system (UPS) and autophagy-lysosomal system (ALS) have been observed in skeletal muscle in the settings of cancer-induced cachexia, facilitating proteolytic degradation of proteins culminating in the atrophy of muscle (Sandri, 2010; Sandri, 2016). In addition to protein degradation modalities, the UPR also acts to limit the rate of protein synthesis through an inhibition in translation and regulation of the Akt/mTOR pathway, attenuating muscle mass (Qin et al., 2010).

In our efforts to identify a potential therapeutic agent to treat cachexia, we explored the possibility of WFA as a drug to target cachexia. WFA is a steroidal lactone that is purified from the plant *Withania somnifera*, and is not currently known to have an anabolic effect on skeletal muscle. WFA is known for its inhibitory effects on the proliferation and survival of various cancer cells (Chandrasekaran et al., 2018; Chang et al., 2017; Kyakulaga et al., 2018; Royston et al., 2018; Xia et al., 2018; Zhang and Zhang, 2017), including ovarian cancer (Fong et al., 2012; Kakar et al., 2012, 2014, 2016, 2017). WFA has been shown to induce apoptosis of both ovarian cancer cells and cancer stem cells (Kakar et al., 2017), at least in part due to a rampant increase in the production of reactive oxygen species and subsequent DNA damage (Fong et al., 2012). Interestingly, a recent report has shown in multiple breast cancer cell lines that WFA activates autophagy in the cancer cells in a UPR-dependent manner (Ghosh et al., 2017). Notably missing from this report is the effect that WFA has on UPR signaling and autophagy in non-tumorigenic cells/tissues. Recent work from our group has shown that WFA is capable of attenuating the cachectic phenotype induced by a xenograft model of ovarian cancer using the A2780 cell line (Straughn and Kakar, 2019), which is genetically similar to endometrioid-type ovarian cancer (Domcke et al., 2013; Hernandez et al., 2016).

In the present study, we sought to corroborate our prior findings that WFA treatment attenuates the atrophying and weakening effects of a xenograft model of ovarian cancer, elucidate the mechanisms by which ovarian cancer induces a cachectic phenotype, and investigate if WFA would improve functional muscle strength or size in a tumor-free setting. Further, we assessed the effect of WFA on select critical regulators of skeletal muscle, namely satellite cells and signaling to the UPS and ALS through the UPR. Promisingly, WFA treatment led to significant improvements in muscle grip strength, myofibrillar cross-sectional area (CSA), and the minimal Feret's diameter in both tumor-free and tumor-bearing mice. Similar to published reports (He et al., 2013), our xenograft model of ovarian cancer led to a robust activation of satellite cells without improvements in myofibrillar size or muscle strength in female NSG mice, underlying a common assault to myogenic progenitors. Interestingly, WFA was found to be a more

potent activator of satellite cells than the A2780 ovarian cancer xenografts. Further, we report that WFA treatment and our xenograft model differentially regulate the UPR pathways in skeletal muscle. WFA appears to produces an adaptive UPR through slight elevation in global UPR activation and robust activation of the IRE1α arm, whereas the A2780 xenografts resulted in muscle atrophy through an activation of the UPS and ALS, due to the induction of a maladaptive UPR. Summarily, WFA is a novel regulator of skeletal muscle mass that attenuates the effects of ovarian cancer-induced cachexia.

MATERIALS AND METHODS

Cell Line

The A2780 ovarian cancer cell line was maintained in Roswell Park Memorial Institute (RPMI) Medium-1640 supplemented with: 10% Fetal Bovine Serum (FBS, Hyclone), 100 U/ml Penicillin, and 10 μg/ml Streptomycin. Cells were cultured in a humidified atmosphere of 5% CO_2 at 37°C, and the medium was changed every 48 h as described previously (Kakar et al., 2017). The A2780 ovarian cancer cell line is of human origin, necessitating the utilization of immune-deficient mice.

Generation of Tumor in Mice

As described previously (Kelm et al., 2020; Straughn and Kakar, 2019), six-week-old female NOD.Cg-*Prkdc*^{scid} *Il2rg*^{TM1Wjl}/SzJ (NSG, Jackson Lab Strain #005557) immunodeficient mice were initially randomly assigned to a tumor-free or tumor-bearing group (30 mice/group). Tumor-bearing groups received an intraperitoneal (i.p.) injection of 8.0×10^5 low passage A2780 cells suspended in 100 μl sterile PBS. Control group received i.p. injection of 100 μl sterile PBS alone. After an initial refractory period of 8 days, mice in both the tumor-free and tumor-bearing groups were stratified into a group that would receive vehicle injections (10% dimethyl sulfoxide, 90% glycerol trioctanoate) or one of two concentrations of WFA (2 or 4 mg/kg) via i.p. injection (10 mice/group). Injections were performed once every 3 days until the culmination of the study. Post-euthanization, several tissues were collected, weighed, snap frozen in liquid nitrogen, and then stored at −80°C for further analysis. While alive, the mice were housed in a 12-h light–dark cycle and given water and food *ad libitum*. The Institutional Animal Care and Use Committee (IACUC, protocol # 15405) and Institutional Biosafety Committee (IBC, protocol # 18-208) of the University of Louisville approved all experimental protocols in mice in advance. None of the data in these experiments include data/samples from our initial publication discussing cachexia in the context of ovarian cancer (Straughn and Kakar, 2019).

Grip Strength Measurements

Protocol used for the measurement of grip strength was essentially similar to as described previously (Gallot et al., 2018; Straughn and Kakar, 2019). Before assessment, mice were weighed on a commercially available digital scale. Forepaw and total grip strength of mice were measured using a digital grip strength meter (Columbus Instruments, Columbus, OH, United States) and then normalized by total body weight. Before the beginning of the test, the mice were acclimatized for five minutes. The mouse was allowed to grasp the total paw pull-bar assembly, and in a separate experiment the forepaw pull-bar assembly. The mouse was then gently drawn with constant force in a straight line away from the device until the mouse could no longer grasp the bar. Force at time of release was recorded as the peak tension. Each mouse was tested five times with a delay of 20–40 s between each testing. The mean peak tension was calculated from the recordings normalized by total body weight at time of recording. Forelimb and total limb grip strength were assessed on a weekly basis to balance elucidating functional muscle changes in response to tumor burden and WFA treatment, while simultaneously avoiding habituation to the grip strength analyses.

Total RNA Extraction and qPCR

Isolation of total RNA from the gastrocnemius (GA) was performed using an RNeasy Fibrous Tissue Mini Kit (Qiagen Catalog # 74704) according to the manufacturer's instructions. Skeletal muscle RNA was treated with an RNase-free DNase kit (RNase-Free DNase Set, Qiagen Catalog # 79254) in column according to the manufacturer's instructions. First strand cDNA was synthesized using 1 μg of purified RNA and a commercially available kit (iScript^{TM} cDNA synthesis, Bio-Rad Catalog # 170-8891). Quantification of mRNA expression was performed similar to as previously described (Hindi and Kumar, 2016; Fong et al., 2012) using the SYBR Green dye method on a 7300 Real-Time PCR system (Applied Biosystems) using gene-specific primers, detailed in **Supplementary Table 1**.

Histology and Morphometric Analysis of Skeletal Muscle

Select muscles of the lower limb of the mice were isolated, flash frozen in liquid nitrogen, mounted in optimal cutting temperature (OCT) embedding medium, and then sectioned using a microtome cryostat. To assess tissue morphology, 10 μm thick transverse sections were cut from the mid-belly of the tibialis anterior (TA) and then subjected to Hematoxylin and Eosin (H&E) staining. Images of H&E-stained TA muscle sections were quantified using Fiji software (National Institute of Health software) to measure myofiber CSA. Skeletal myofiber CSA was calculated by analyzing ∼500–700 myofibers per muscle as previously described (Kakar et al., 2012).

Immunohistochemical Staining of Skeletal Muscle for the Detection of Satellite Cells and Quantification

To detect changes in the number and myogenic status of satellite cells, 8 μm thick transverse sections were cut from the mid-belly of the TA. Slides were fixed in freshly prepared 3.7% Formalin solution for 5 min. Slides were subsequently washed in 0.3 M Glycine in PBS for 10 min. Slides were then briefly washed in 0.1% Triton in PBS. Slides were then incubated for 10 min in 0.1% Triton in PBS. Slides were then subjected to an antigen retrieval step. Briefly, slides were incubated in Coplin staining jars

containing 0.01 M citrate buffer and placed inside of a pressure cooker. Slides were incubated on "High Pressure" for 10 min. Slides were cooled and then washed in PBS. Slides were then blocked in a PBS solution containing 3% bovine serum albumin, 2% horse serum, and Mouse-on-Mouse blocking reagent (1 drop per 1.25 ml of blocking solution) for 60 min in a humidified chamber. Slides were then incubated overnight at 4°C in blocking solution containing primary antibodies against Pax7, MyoD, and Laminin proteins. The next day, slides were washed three times with PBS. Following, slides were incubated for 60 min in blocking solution containing appropriate secondary antibodies conjugated to fluorophores with minimally overlapping spectral emissions. Slides were subsequently washed three times using PBS for 5 min. Slides were then incubated for 5 min in DAPI resuspended in PBS (1:5,000). Slides were subsequently washed three times using PBS for 5 min. Refer to **Supplementary Table 2** for a complete list of antibodies utilized. Four images from distinct areas of the muscle were captured for each animal. Imaging and quantification were performed by two separate people to allow for blinding of group identity through the use of an alphanumeric identifier. Group identities were unmasked after all data was quantified and submitted to the principal investigator, such that group-wise comparisons could be performed. For the analysis, the number of Laminin + myofibers was first counted, such that the data could eventually be normalized between images to account for differences in the size/area imaged. Next, distinct puncta in the Texas Red channel (corresponding to the secondary antibody employed for Pax7) were annotated on the image using Fiji software. These marks were then compared with the DAPI channel. When the mark for the Texas Red channel did not overlap with nuclear staining on the DAPI channel, the prospective satellite cell was ruled as a false positive and the identifying mark on the image was deleted. After deletion of false positives from the cell count feature, the number of satellite cells for the respective image was recorded. The frequency of Pax7+ cells per laminin + myofiber was then calculated for each image and then averaged. Next, the marks from the Texas Red channel were compared against the YFP channel (corresponding to the secondary antibody employed for MyoD). Two additional cell counts were initialized such that we could count cells that also exhibited YFP overlap (i.e., satellite cells that were Pax7+/MyoD+) vs. cells that did not have a YFP spectral emission (i.e., satellite cells that were Pax7+/MyoD-). The proportion of differentiating satellite cells and the proportion of satellite cells that were proliferating/quiescent was calculated for each of the four images and then averaged. This process was repeated for all 60 mice (totaling 240 RGBY images).

Imaging

Slides were mounted using Eukitt Quick-hardening mounting medium (Sigma-Aldrich) and visualized at −0.4°C on a Nikon TiE 3000 inverted microscope (Nikon) equipped with a digital camera (DS-U2/L2-Ri1 digital microscope camera (Nikon) for light microscopy or DXM-1200C coded digital camera (Nikon) for fluorescent microscopy), and Nikon NIS Elements AR software (Nikon). Exposure times were consistent for each staining type. Image levels were equally adjusted using Adobe Photoshop CS6 software (Adobe) to remove non-specific background staining. Margins of cropped images are indicated by a dashed red border or a solid black line.

Protein Extraction and Western Blotting

Quadriceps femoris (QF) samples were homogenized in chilled RIPA buffer (Sigma) supplemented with a Complete Mini Protease Inhibitor tablet (Roche Molecular Biochemicals, Indianapolis, IN, United States). Tissue lysates were centrifuged at 10,000 RPM and the supernatants were collected. Protein concentration for each sample was determined using the Bradford reagent method (Bio-Rad), according to manufacturer's instructions. Protein lysates (50 μg) were separated on 10% SDS-PAGE gels at 100 V for 2 h. The proteins were transferred to nitrocellulose membranes at 100 V for 90 min. The membranes were blocked with 5% non-fat milk in Tris Buffered Saline supplemented with Tween-20 (0.05%; TBS-T) for 30–60 min. The membranes were then washed three times with TBS-T for 5 min. The membranes were then incubated with primary antibody at 4°C overnight. The membranes were washed three times with TBS-T for 5 min each followed by incubation in TBS-T containing horseradish peroxidase conjugated secondary antibody (1:3,000 dilution) for 1 h. The membranes were rinsed three times with TBS-T for 5 min each. Visualization of immunoreactive bands was enhanced using chemiluminescence reagents (Sigma). The membranes were stripped off using Restore™ Western Blot Stripping Buffer (Thermo Scientific Catalog # 21059) for 15 min, blocked, and re-probed with horseradish peroxidase-conjugated β-Actin or GAPDH as a control to normalize loading variation. Refer to **Supplementary Table 2** for a complete list of antibodies utilized.

Graphical Display and Statistical Analysis

For the sake of transparency, the majority of the results were expressed as box-and-whisker plots with the box comprised of the first, second, and third quartiles, and the lower and upper whiskers corresponding to the minimum and maximum values, respectively, to display the entire range of data. Individual data points are depicted as black circles. Cropping of images is indicated by a dashed red border or a solid black line around the field of view. Statistical analysis of the data was performed using an unpaired two-tailed *t*-test with Welch's correction for simple two group comparisons, a one-way analysis of variance (ANOVA) followed by Tukey's Honestly Significant Difference Test (HSDT) *post hoc* analysis for comparisons between 3 or more groups with one experimental factor, or a two-way ANOVA followed by Tukey's multiple comparison test *post hoc* analysis for comparisons between 4 or more groups containing two experimental factors to determine statistically significant differences between groups with GraphPad Prism 8.3.0 software for Mac (La Jolla, CA, United States). ANOVA summaries and the results of the multiple comparison tests are presented in **Supplementary Material**. Welch-corrected or Tukey-corrected *p*-value of <0.05 was considered statistically significant, unless otherwise specified.

Ethics Statement

All procedures involving the usage of mice were carried out in strict accordance to the standards of the National Institute of Health guide for the care and use of laboratory animals. The Institutional Animal Care and Use Committee (IACUC, protocol # 15405) and Institutional Biosafety Committee (IBC, protocol # 18-208) of the University of Louisville approved all experimental protocols in mice in advance. No human data or tissue was used in this study.

RESULTS

Withaferin A Improves Basal Grip Strength and Attenuates the Effects of Ovarian Cancer on Skeletal Muscle

Recent work from our lab has demonstrated that the A2780 ovarian cancer cell line is capable of inducing a skeletal muscle cachectic phenotype and that WFA attenuates these changes (Straughn and Kakar, 2019). In the present study, we attempted to elucidate whether WFA has an effect on functional muscle strength and the size of muscle in tumor-free mice, and to corroborate our prior results in tumor-bearing mice using the same lower dosage of WFA (2 mg/kg), but a different upper dosage of WFA (4 mg/kg) due to the deleterious effects previously observed with 6 mg/kg of WFA. Additionally, due to the previously reported tumor-associated mortality, the amount of xenografted cells was reduced from 1×10^6 to 8×10^5. A parallel report to this study from our lab examining gross body changes, tumor burden, and the effect on cardiac muscle in response to the xenografting of the A2780 ovarian cancer cell line and WFA treatment has recently been discussed in the work by Kelm et al. (2020). Information pertinent to this manuscript can be found in Figure 1, Supplementary Figure 1 and Supplementary Table 1 of the aforementioned manuscript. Before the mice received i.p. xenografts of the A2780 ovarian cancer cells, we performed forelimb and total grip strength analyses to ensure no significant differences within the groups stratified to become tumor-free or tumor-bearing existed at the start of the study (**Supplementary Figures 1A,B**). As expected, no significant differences were found in the baseline forelimb (tumor-free: 0.051 ± 0.004 N/g; "tumor-bearing": 0.052 ± 0.004 N/g) or total grip strength (tumor-free: 0.094 ± 0.006 N/g; "tumor-bearing": 0.092 ± 0.007 N/g) in the groups that were initially stratified to become tumor-free or tumor-bearing animals, as determined by an unpaired two-tailed Welch-corrected *t*-test [forelimb: $t(57.63) = 0.74$, $p = 0.47$; total limb: $t(54.92) = 1.27$, $p = 0.21$] (**Supplementary Figures 1A,B**). Subsequently, mice were examined for changes in grip strength once per week until the culmination of the study. Based upon the mortality rate observed in our previous study (Straughn and Kakar, 2019), the endpoint of this study was set at week 4 post-xenografting of the ovarian cancer cells. One-week post-xenografting, before WFA treatment was initiated, we observed a significant reduction in the forelimb (tumor-free: 0.056 ± 0.003 N/g; tumor-bearing: 0.049 ± 0.003 N/g) and total grip strengths (tumor-free: 0.096 ± 0.004 N/g; tumor-bearing: 0.088 ± 0.006 N/g) of the tumor-bearing mice compared to the tumor-free control group [forelimb: $t(56.62) = 8.02$; total limb: $t(52.64) = 6.03$; $p < 0.0001$ for both comparisons], suggesting a rapid onset of muscle decline (**Supplementary Figures 1C,D**).

At the terminal week of the study, we observed that treatment with WFA at 2 and 4 mg/kg significantly improved the forelimb grip strength of tumor-free mice (**Figure 1A**), and that the higher dosage of WFA had significantly improved the total grip strength of the tumor-free mice (**Figure 1B**) compared to the tumor-free vehicle-treated group as determined by a two-way ANOVA followed by Tukey's multiple comparison test *post hoc* analysis (forelimb – WFA 2 mg/kg: $p = 0.02$; WFA 4 mg/kg: $p < 0.0001$; total limb – WFA 2 mg/kg: $p = 0.30$; WFA 4 mg/kg: $p = 0.0005$), suggesting that WFA treatment improves basal grip strength. Similar to our recently reported study (Straughn and Kakar, 2019), the forelimb and total limb grip strength of the tumor-bearing vehicle-treated group was significantly reduced compared to the tumor-free groups ($p < 0.0001$ for all comparisons) (**Figures 1A,B**). The tumor-bearing WFA-treated groups displayed forelimb and total grip strengths that were significantly increased compared to the tumor-bearing vehicle-treated ($p < 0.0001$ for all comparisons), but not significantly different than the tumor-free vehicle-treated group, corroborating our prior report that WFA ameliorates the weakening effects on skeletal muscle in our xenograft model of ovarian cancer-induced cachexia (**Figures 1A,B**). Grip strength analyses for week 2 and week 3 post-xenografting are presented in **Supplementary Figures 1E–H**. These intermediate timepoints demonstrate similar trends and p-values as the terminal week of the study.

Post-mortem, we collected select muscles of the lower extremities (TA, GA, and QF) and weighed them to detect changes in muscle mass (**Figure 1C**). Muscle weights were normalized by the initial body weight (IBW) to account for differences in the size of the mouse/muscle at baseline, while excluding the confounding effect of tumor burden on body weight. A reduction in the normalized weight of the TA, GA, and QF muscles was observed in the tumor-bearing vehicle-treated group compared to the tumor-free vehicle-treated group ($p < 0.05$ for all comparisons) (**Figure 1C**). Within the tumor-free groups, the WFA 4 mg/kg group displayed a significant increase in normalized weight of the TA, GA, and QF muscles compared to the vehicle-treated group ($p < 0.05$ for all comparisons) (**Figure 1C**). Within the tumor-bearing groups, treatment with both concentrations of WFA led to a statistically significant increase in normalized wet weight of the TA and GA muscles compared to the vehicle-treated group (**Figure 1C**). Curiously, these results are in contrast with those from our prior publication, where we did not observe significant differences in muscle mass (Straughn and Kakar, 2019). Experimental differences between the two studies, such as the initial cancer cell xenograft volume and duration of treatment could account for the seemingly discrepant results. It is also possible that the relatively small sample size in the first study did not allow us to observe small differences in muscle mass.

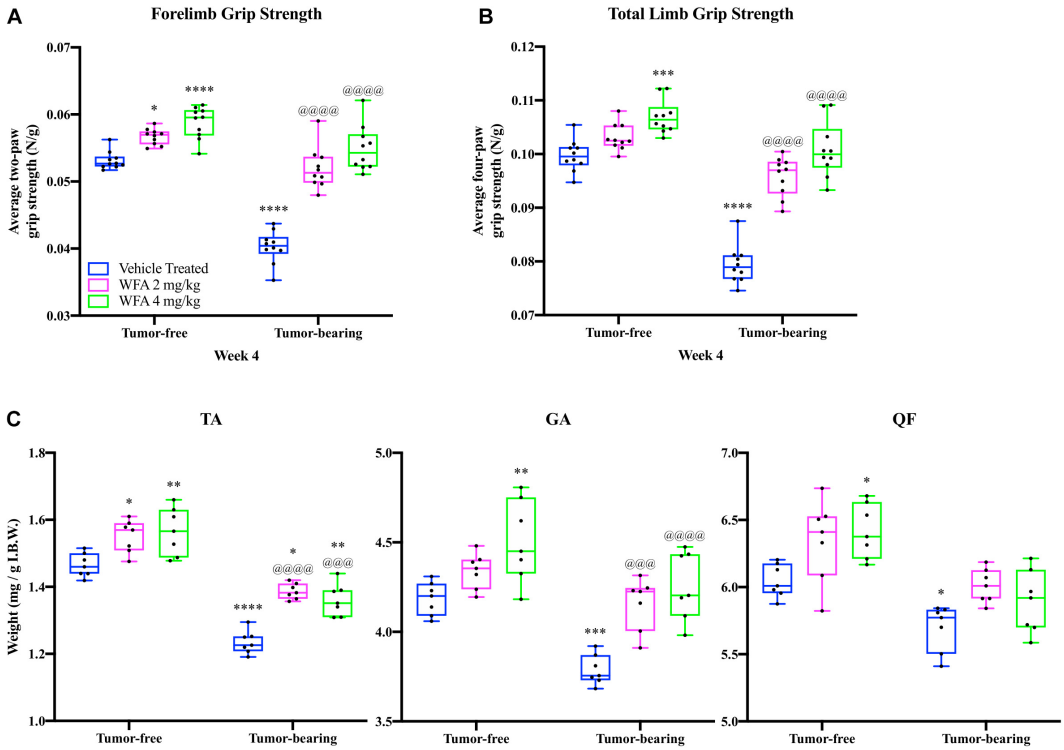

FIGURE 1 | Withaferin A increases the grip strength and myofiber size of female NSG mice. Quantification of mean **(A)** forelimb and **(B)** total limb grip strength normalized to body weight in tumor-free and tumor-bearing vehicle-treated, WFA 2 mg/kg, and WFA 4 mg/kg groups at week four post-xenografting of A2780 cells. $N = 10$ in each group. **(C)** Quantification of tibialis anterior (TA), gastrocnemius (GA), and quadriceps femoris (QF) muscle wet weight normalized by initial body weight. $N = 7$ in each group. $^{*}p < 0.05$; $^{**}p < 0.01$; $^{***}p < 0.001$; $^{****}p < 0.0001$, value significantly different from corresponding value of tumor-free vehicle-treated group by two-way ANOVA followed by Tukey's multiple comparison test *post hoc* analysis. $^{@}p < 0.05$, value significantly different from corresponding value of tumor-bearing vehicle-treated group.

In an attempt to corroborate the changes in muscle strength and weight in response to WFA treatment and the ovarian cancer cells, changes in myofibrillar size in the TA muscle were examined via H&E staining (**Figure 2A**). Similar to the changes in grip strength observed, both concentrations of WFA led to a significant increase in the average myofibrillar CSA in the TA muscle of the tumor-free WFA-treated groups (WFA 2 mg/kg: 1,916.39 ± 85.72 μm^2; WFA 4 mg/kg: 1,904.98 ± 80.50 μm^2) compared to the tumor-free vehicle-treated group (1,652.48 ± 46.13 μm^2) ($p < 0.0001$ for both comparisons) (**Figure 2B**). The average CSA of the tumor-bearing vehicle-treated group (1,097.28 ± 74.60 μm^2) was significantly decreased compared to all tumor-free groups ($p < 0.0001$ for all comparisons) (**Figure 2B**). Within the tumor-bearing groups, both dosages of WFA led to a complete rescue in myofibrillar CSA (WFA 2 mg/kg: 1,629.72 ± 94.96 μm^2; WFA 4 mg/kg: 1,748.13 ± 68.90 μm^2) compared to the tumor-bearing vehicle-treated group ($p < 0.0001$ for both comparisons) (**Figure 2B**). The average myofibrillar CSA of the tumor-bearing WFA-treated groups was not significantly different from that of the tumor-free vehicle-treated group (WFA 2 mg/kg: $p = 0.99$; WFA 4 mg/kg: $p = 0.07$) (**Figure 2B**). To confirm accurate measurement of the CSA, the minimal Feret's diameter was measured in conjunction with the CSA (**Figure 2C**). Nearly identical trends and levels of significance in the minimal Feret's diameter were observed compared to the CSA, indicating the validity of our histological assessment (**Figure 2C**). While we observed changes in myofiber size, muscle mass, and grip strength, it cannot be stated definitively that these are linked. Indeed, whether or not a correlation between muscle size and muscle functions exists is currently unresolved and under intense debate within the current literature (Loenneke et al., 2019; Taber et al., 2019).

Withaferin A Modulates Satellite Cell Activation and Differentiation

Dysregulation of NF-κB signaling has been shown to spuriously activate satellite cells and lead to an impairment of skeletal muscle repair (He et al., 2013; Straughn et al., 2019). Previous work from our lab demonstrated that WFA treatment results in a reduction in activation/nuclear translocation of the canonical NF-κB signaling pathway component p65 within the xenografted tumor (Straughn and Kakar, 2019). However, we did not assess changes in NF-κB signaling within skeletal muscle in our prior study. Thus, we performed western blotting against phospho- and total levels of p65 in protein extracts from the QF muscle (**Supplementary Figures 2A,B**). We observed a significant

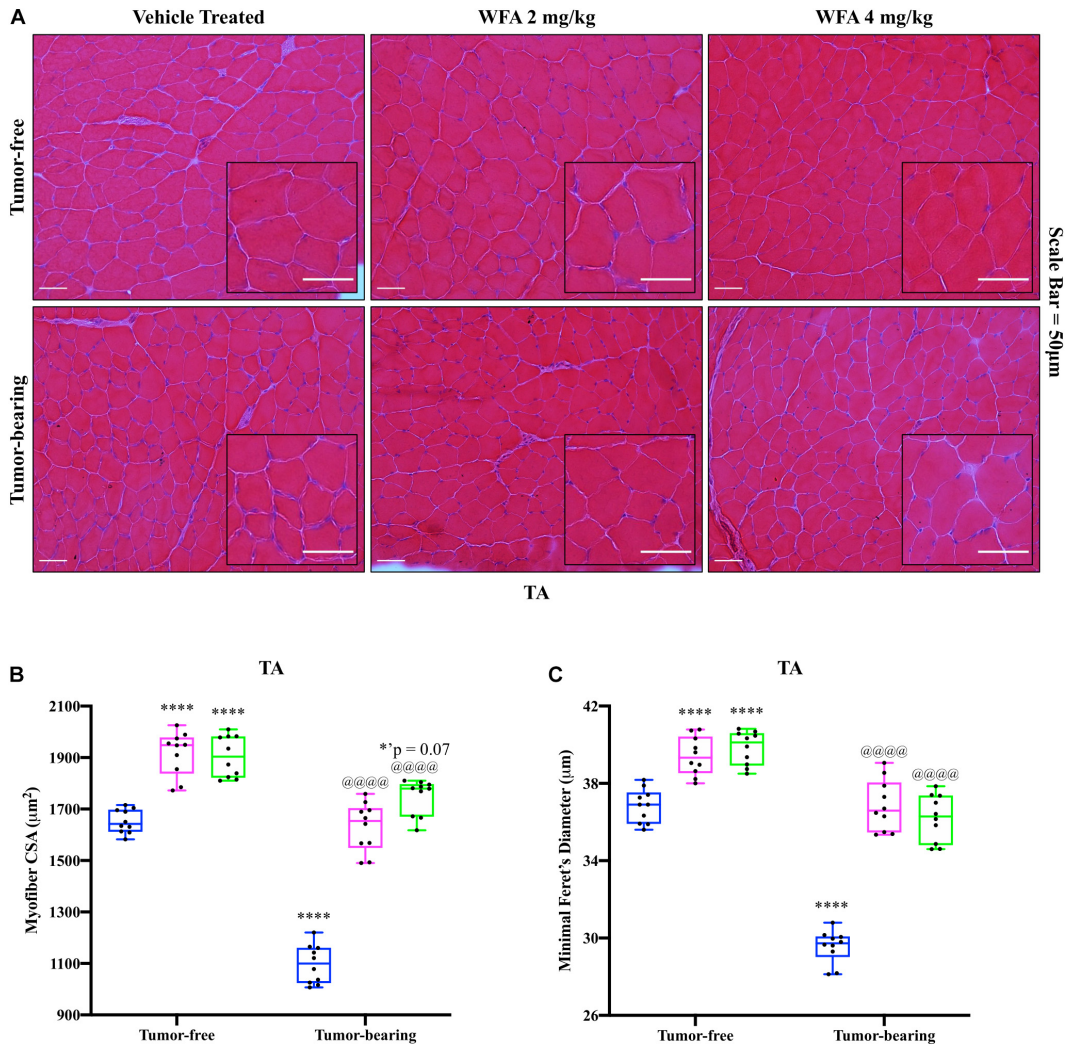

FIGURE 2 | Withaferin A rescues skeletal muscle at the structural level. **(A)** Representative images of H&E-stained transverse TA muscle sections. Scale bar = 50 μm. Inset images magnified from whole image. Quantification of average **(B)** myofiber cross-sectional area (CSA) and **(C)** minimal Feret's diameter in TA muscle. $N = 10$ in all groups. $^{*}p < 0.05$; $^{**}p < 0.01$; $^{***}p < 0.001$; $^{****}p < 0.0001$, value significantly different from corresponding value of tumor-free vehicle-treated group by two-way ANOVA followed by Tukey's multiple comparison test *post hoc* analysis. $^{@}p < 0.05$, value significantly different from corresponding value of tumor-bearing vehicle-treated group.

increase in the ratio of phosphorylated p65 to total p65 protein in the tumor-bearing vehicle-treated group (**Supplementary Figure 2B**). This increase in NF-κB activation was ameliorated upon treatment with WFA group (**Supplementary Figure 2B**). Next, we assessed for changes in the IKK complex and RelA at a transcriptional level in the GA muscle (**Supplementary Figure 2C**). The relative transcript levels of *RelA* and *IKK*β were significantly increased in the tumor-bearing vehicle-treated group compared to the tumor-free vehicle-treated group (**Supplementary Figure 2C**). As expected, WFA treatment in both tumor-free and tumor-bearing animals led to a significant reduction in relative transcript levels of *RelA* and *IKK*β compared to their vehicle-treated controls (**Supplementary Figure 2C**). Due to WFA's known role in inhibiting canonical NF-κB signaling (Heyninck et al., 2014; Kaileh et al., 2007), and the effect ovarian cancer has on this signaling pathway (Chen et al., 2008), we investigated if WFA or our xenograft model induced the activation of satellite cells.

The TA muscle was subjected to immunofluorescent immunohistochemical (IHC) staining for Pax7 (a marker of satellite cells), MyoD (a marker of myogenic differentiation), and Laminin (a marker of the basal lamina) (**Figure 3A**). As accurate IHC detection of satellite cells can be challenging, individual color channels were compared against negative control slides to optimize visualization of satellite cells, minimize non-specific background staining, and rule out false positives ($Pax7^{+}/DAPI^{-}$ cells) (Feng et al., 2018). Initially, the number of satellite cells per field (normalized by the number of $Laminin^{+}$ myofibers) was quantified to assess whether our model of ovarian cancer or WFA treatment affected the satellite cell

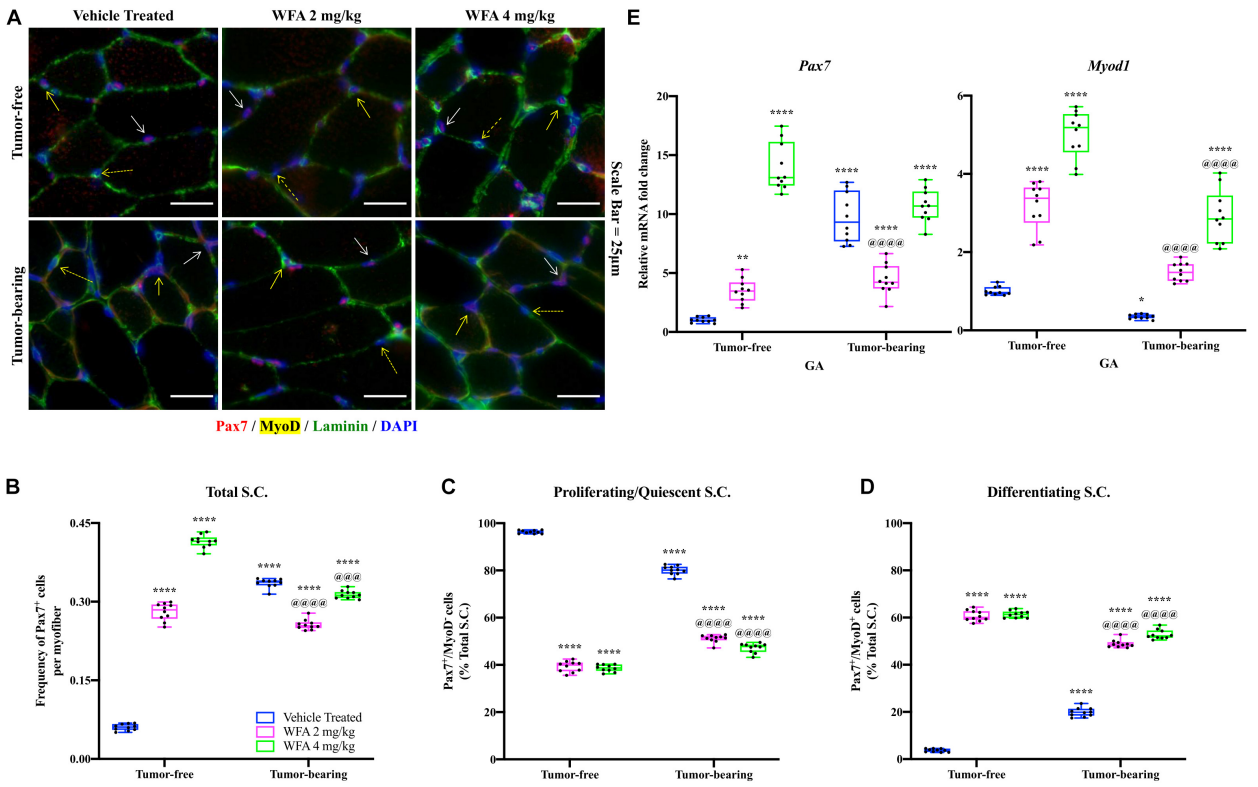

FIGURE 3 | Withaferin A is a potent activator of satellite cells. **(A)** Representative images of transverse TA muscle sections after immunostaining for Pax7 (red color), MyoD (yellow color), and Laminin (green color) proteins in tumor-free and tumor-bearing groups. Nuclei were identified by counterstaining with DAPI (blue color). Scale bar = 25 μm. Quantification of **(B)** the total number of $Pax7^+$ cells per $Laminin^+$ myofiber, **(C)** the proportion of $Pax7^+/MyoD^-$ cells, and **(D)** the proportion of $Pax7^+/MyoD^+$ cells. $N = 10$ in all groups. Solid white arrow denotes $Pax7^+/MyoD^-$ cells. Solid yellow arrow denotes $Pax7^+/MyoD^+$ cells. Dashed yellow arrow denotes $Pax7^-/MyoD^+$ cells. **(E)** Relative mRNA levels of *Pax7* and *Myod1* in GA muscle. $N = 10$ in all groups. $^*p < 0.05$; $^{**}p < 0.01$; $^{***}p < 0.001$; $^{****}p < 0.0001$, value significantly different from corresponding value of tumor-free vehicle-treated group by two-way ANOVA followed by Tukey's multiple comparison test *post hoc* analysis. $^{@}p < 0.05$, value significantly different from corresponding value of tumor-bearing vehicle-treated group.

population at large (**Figure 3B**). Within the tumor-free groups, WFA treatment significantly increased the normalized amount of $Pax7^+$ cells (WFA 2 mg/kg: 0.28 ± 0.02; WFA 4 mg/kg: 0.42 ± 0.01) compared to the tumor-free vehicle-treated group (0.06 ± 0.01) ($p < 0.0001$ for both comparisons) (**Figure 3B**). There was also a significant increase in the amount of $Pax7^+$ cells in the tumor-bearing vehicle-treated group (0.34 ± 0.01) compared to the tumor-free vehicle-treated group ($p < 0.0001$) (**Figure 3B**). Interestingly, within the tumor-bearing groups, the WFA 2 mg/kg group displayed a significant reduction in $Pax7^+$ cells (0.26 ± 0.01) compared to the vehicle-treated and WFA 4 mg/kg groups (0.31 ± 0.01) ($p < 0.0001$ for both comparisons) (**Figure 3B**). No definitive reason for this experimental observation has currently been elucidated. A small, but statistically significant decrease in the tumor-bearing WFA 4 mg/kg group was observed compared to the tumor-bearing vehicle-treated group ($p = 0.0004$) (**Figure 2B**). The tumor-free WFA 4 mg/kg group displayed the highest proportion of $Pax7^+$ cells, suggesting that WFA is a potent activator of satellite cells.

After assessing changes in the gross number of satellite cells, we investigated their myogenic status to determine if the satellite cells were functionally activated. Satellite cells that are $Pax7^+/MyoD^-$ are self-renewing or returning to quiescence, whereas satellite cells that are $Pax7^+/MyoD^+$ have committed to the myogenic lineage and will facilitate in muscle repair (Kuang and Rudnicki, 2008; Kuang et al., 2007). Similar to published reports (Didier et al., 2012), the vast majority of nuclei within and outside of myofibers were found to be $Pax7^-/MyoD^+$, and as such were not considered myogenic progenitors. It was not feasible to enumerate the population of $Pax7^-/MyoD^+$ cells in response to the xenografted cancer or WFA treatment due to experimental limitations. However, distinct populations of $Pax7^+/MyoD^-$ and $Pax7^+/MyoD^+$ cells were present (**Figures 3C,D**). Consistent with published reports (Yoshida et al., 1998), the majority of the satellite cells in the tumor-free vehicle-treated group were $Pax7^+/MyoD^-$ (96.29 ± 0.69%) and a small population was found to be $Pax7^+/MyoD^+$ (3.71 ± 0.69%) (**Figures 3C,D**). The proportion of proliferating satellite cells in the tumor-bearing vehicle-treated group (80.10 ± 1.88%) was significantly decreased, and the proportion of differentiating satellite cells (19.90 ± 1.88%) was significantly increased compared to the tumor-free vehicle-treated group (**Figures 3C,D**). In the tumor-free groups, there was a significant decrease in the proportion

of proliferating satellite cells (WFA 2 mg/kg: 39.27 ± 2.28%; WFA 4 mg/kg: 38.63 ± 1.49%) and a significant increase in differentiating satellite cells (WFA 2 mg/kg: 60.73 ± 2.28%; WFA 4 mg/kg: 61.37 ± 1.49%) in the WFA-treated groups compared to the vehicle-treated group ($p < 0.0001$ for all comparisons) (**Figures 3C,D**). In the tumor-bearing groups, there was a significant decrease in the proportion of proliferating satellite cells (WFA 2 mg/kg: 51.15 ± 1.63%; WFA 4 mg/kg: 47.21 ± 1.99%) and a significant increase in differentiating satellite cells (WFA 2 mg/kg: 48.85 ± 1.63%; WFA 4 mg/kg: 52.79 ± 1.99%) in the WFA-treated groups compared to the tumor-free and tumor-bearing vehicle-treated groups ($p < 0.0001$ for all comparisons) (**Figures 3C,D**).

To corroborate our IHC data, we performed qPCR on GA muscle extracts to assess relative transcript levels of *Pax7* and *Myod1* (**Figure 3E**). Similar to the IHC data, the tumor-bearing vehicle-treated group displayed a significant increase in relative transcript levels of *Pax7* and a significant decrease in *Myod1* compared to the tumor-free vehicle-treated group (**Figure 3E**). The tumor-free and tumor-bearing WFA-treated groups displayed significant increases in *Pax7* compared to the tumor-free vehicle-treated group and a significant increase in *Myod1* compared to both vehicle-treated groups (**Figure 3E**). While both WFA treatment and xenografting of ovarian cancer into mice led to an increase in satellite cell proliferation, WFA appears to signal for the differentiation of satellite cells through a mechanism not presently known.

Withaferin A Induces an Adaptive Unfolded Protein Response

It has been demonstrated in the Lewis lung carcinoma and $Apc^{Min/+}$ models of cancer-induced cachexia that several markers of the UPR are upregulated compared to tumor-free hosts as a byproduct of increased endoplasmic reticulum (ER) stress (Bohnert et al., 2016). Due to the UPR's role in regulating muscle mass and common perturbations associated with cancer-induced cachexia, we investigated if components of the UPR are augmented in response to WFA treatment or xenografting of the A2780 ovarian cancer cell line. Overall, both WFA and the xenografted ovarian cancer cell line led to activation of various components of the UPR in skeletal muscle, with the A2780 ovarian cancer cell line leading to a higher degree of activation than WFA treatment (**Figure 4**).

The relative transcript levels of *Eif2ak3* [encoding the protein PERK (Hayes et al., 1999)], *Atf4* [encoding the protein ATF4 (Karpinski et al., 1992)], *Ddit3* [encoding the protein CHOP (Marola et al., 2019)], *Ppp1r15a* [encoding the protein GADD34 (Clavarino et al., 2012)], *Hspa5* [encoding the protein GRP78 (Elfiky et al., 2020)], *Hsp90B1* [encoding the protein GRP94 (Chen et al., 2005)], and *Tnfrsf10B* [encoding death receptor 5 (DR5; Dittmann et al., 2020)] were significantly increased in the GA muscle of the tumor-bearing vehicle-treated group compared to the tumor-free vehicle-treated group ($p < 0.0001$ for all comparisons) (**Figure 4**). Curiously, relative transcript levels of *Ern1* [encoding inositol requiring enzyme 1α (IRE1α; Tirasophon et al., 1998)] were significantly reduced in the tumor-bearing vehicle-treated group compared to the tumor-free vehicle-treated group ($p = 0.001$) (**Figure 4**).

In the tumor-free mice, we observed: (1) transcriptional upregulation of *Eif2ak3*, *Ddit3*, *Ppp1r15a*, and *Ern1*, (2) downregulation of *Hspa5* and *Hsp90B1*, and (3) no change in transcript levels of *Atf4* and *Tnfrsf10B* in the WFA-treated groups compared to the vehicle-treated group ($p < 0.001$ or 0.0001 for most comparisons) (**Figure 4**). In the tumor-bearing mice, the WFA treatments produced a mixture of (dis)similar results. In the tumor-bearing WFA 2 mg/kg group, we observed: (1) an upregulation of relative transcript levels of *Ddit3* ($p < 0.01$), (2) a reduction in *Eif2ak3*, *Atf4*, *Ppp1r15a*, *Hspa5*, *Hsp90B1*, and *Tnfrsf10B* ($p < 0.0001$ for all comparisons), and (3) no significant difference in relative transcript levels of *Ern1* ($p = 0.9016$) compared to the tumor-bearing vehicle-treated group (**Figure 4**). In the tumor-bearing WFA 4 mg/kg group, we observed: (1) a significant increase in relative transcript levels of *Ddit3* and *Ern1* ($p < 0.0001$ for both comparisons) and (2) a decrease in relative transcript levels of *Eif2ak3*, *Atf4*, *Ppp1r15a*, *Hspa5*, *Hsp90B1*, and *Tnfrsf10B* (*Eif2ak3*: $p = 0.0085$; $p < 0.001$ for all other comparisons) compared to the tumor-bearing vehicle-treated group (**Figure 4**). The expression of *Atf6* was not detectable in a sufficient number of samples within the tumor-free or tumor-bearing groups, therefore no conclusions were drawn for this branch of the UPR (Data not shown).

Subsequently, activation of the PERK and IRE1α arms of the UPR were assessed by Western blotting for both the phosphorylated and total protein levels of PERK and IRE1α in an attempt to corroborate the changes observed at the transcriptional level (**Figures 5A,B**). The ratio of phosphorylated PERK to the total levels of PERK was significantly increased in the tumor-bearing vehicle-treated group compared to the tumor-free groups, suggesting that the xenografted ovarian cancer results in activation of PERK signaling (**Figure 5B**). This increase in PERK activation was reversed upon treatment with WFA (4 mg/kg) and did not differ from the levels of PERK activation in the tumor-free vehicle-treated group (**Figure 5B**). To further assess PERK activation, western blotting against the protein CHOP was performed; however, markedly variable results were obtained in all of the groups assessed (Data not shown). The ratio of phosphorylated IRE1α to the total levels of IRE1α was significantly increased in both the tumor-free and tumor-bearing WFA 4 mg/kg groups compared to their vehicle-treated counterparts, suggesting that WFA leads to the activation of the IRE1α arm of the UPR (**Figure 5B**). Limitations of this experiment include the necessity to stratify macromolecular extraction to different muscles of the lower extremity due to the atrophying effects of the cancer on skeletal muscle.

In response to ER stress, IRE1α catalyzes the splicing of *XBP-1* mRNA (Bohnert et al., 2018). To further assess activation of the IRE1α arm of the UPR, we evaluated the splicing of *XBP-1* by performing semi-quantitative RT-PCR using a set of primers that detects both the unspliced (*uXBP-1*) and spliced *XBP-1* (*sXBP-1*) mRNA variants (**Figure 5C**). We also assessed total levels of *XBP-1* using a primer sequence that detects a conserved region shared between the spliced and unspliced variants of *XBP-1*, as well as the unrelated gene β-Actin to use as a control. Representative

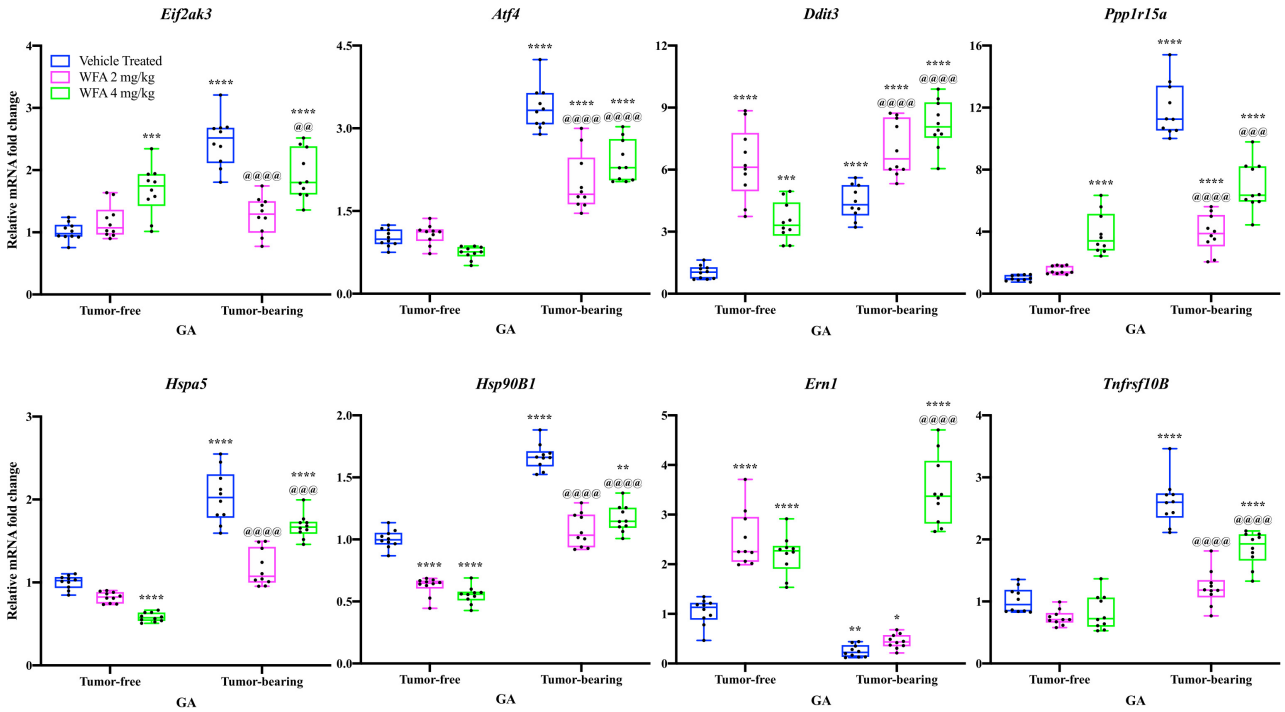

FIGURE 4 | Withaferin A and ovarian cancer differentially transcriptionally regulate the UPR. Relative mRNA levels of select markers of the unfolded protein response (UPR) in the GA muscle of tumor-free and tumor-bearing groups. $N = 10$ in all groups. $^{*}p < 0.05$; $^{**}p < 0.01$; $^{***}p < 0.001$; $^{****}p < 0.0001$, value significantly different from corresponding value of tumor-free vehicle-treated group by two-way ANOVA followed by Tukey's multiple comparison test *post hoc* analysis. $^{@}p < 0.05$, value significantly different from corresponding value of tumor-bearing vehicle-treated group.

images for these experiments are presented in **Figure 5C**. The ratio of *sXBP-1* to *uXBP-1* was significantly increased in all of the WFA-treated groups, and a trend toward increase in the tumor-bearing vehicle-treated group ($p = 0.06$) was observed compared to the tumor-free vehicle-treated group (**Figure 5D**). After normalization by β-Actin, no significant differences in the total amount of *XBP-1* was observed between any of the groups (**Figure 5D**). Based upon the qPCR data and the western blotting results, it appears that WFA and our model of ovarian cancer are antagonistically acting upon the UPR to induce an adaptive or maladaptive response, respectively.

Withaferin A Downregulates Activation of the Ubiquitin Proteasome System

Downstream of the UPR, the UPS is one of the two major proteolytic systems that degrades muscle proteins in oncological settings (Sandri, 2016). As an initial experiment to assess for changes in the UPS, we performed immunoblotting against ubiquitin to detect pan-levels of ubiquitination (**Figure 6A**). As expected, there was a significant increase in the amount of proteins in the QF muscle conjugated to ubiquitin in the tumor-bearing vehicle-treated compared to the tumor-free vehicle-treated group (**Figure 6B**). WFA treatment (4 mg/kg) significantly reduced the levels of ubiquitinated proteins in the tumor-free and tumor-bearing groups compared to their respective vehicle-treated control group.

We next investigated relative transcript levels of muscle-specific E3 ubiquitin ligases, as well as an E3 ubiquitin ligase that is not specific to muscle [*Traf6*, encoding the protein TRAF6 (Cao et al., 1996)] (Bodine and Baehr, 2014; Paul et al., 2012). *Fbxo30* [encoding the protein MUSA1 (Hahn et al., 2020)], *Fbxo32* [encoding the protein MAFbx (Hahn et al., 2020)], and *Trim63* [encoding the protein MuRF1 (Hahn et al., 2020)] are muscle-specific E3 ubiquitin ligases that have been shown to be involved in protein degradation under catabolic settings (Bodine and Baehr, 2014; Foletta et al., 2011). Within the tumor-free groups, there was a significant reduction in the relative transcriptional expression of *Traf6* and *Fbxo30* in the WFA 2 mg/kg group compared to the vehicle-treated group ($p < 0.05$ for both comparisons) (**Figures 6C,D**). The WFA 4 mg/kg group exhibited a significant reduction in relative gene expression of *Fbxo30*, *Fbxo32*, *Trim63*, and *Traf6* compared to the tumor-free vehicle-treated group ($p < 0.0001$, $p = 0.04$, $p = 0.02$, $p < 0.0001$, respectively) (**Figures 6C,D**). The tumor-bearing vehicle-treated group exhibited a significant upregulation in relative transcript levels of all markers of the UPS assessed compared to all tumor-free groups ($p < 0.0001$ for all comparisons) (**Figures 6C,D**). In the tumor-bearing animals, treatment with WFA led to a statistically significant dose-dependent transcriptional downregulation of *Fbxo30*, *Fbxo32*, *Trim63*, and *Traf6* compared to the tumor-bearing vehicle-treated group ($p < 0.0001$ for all comparisons) (**Figures 6C,D**). The results of these experiments suggest that modulation of the

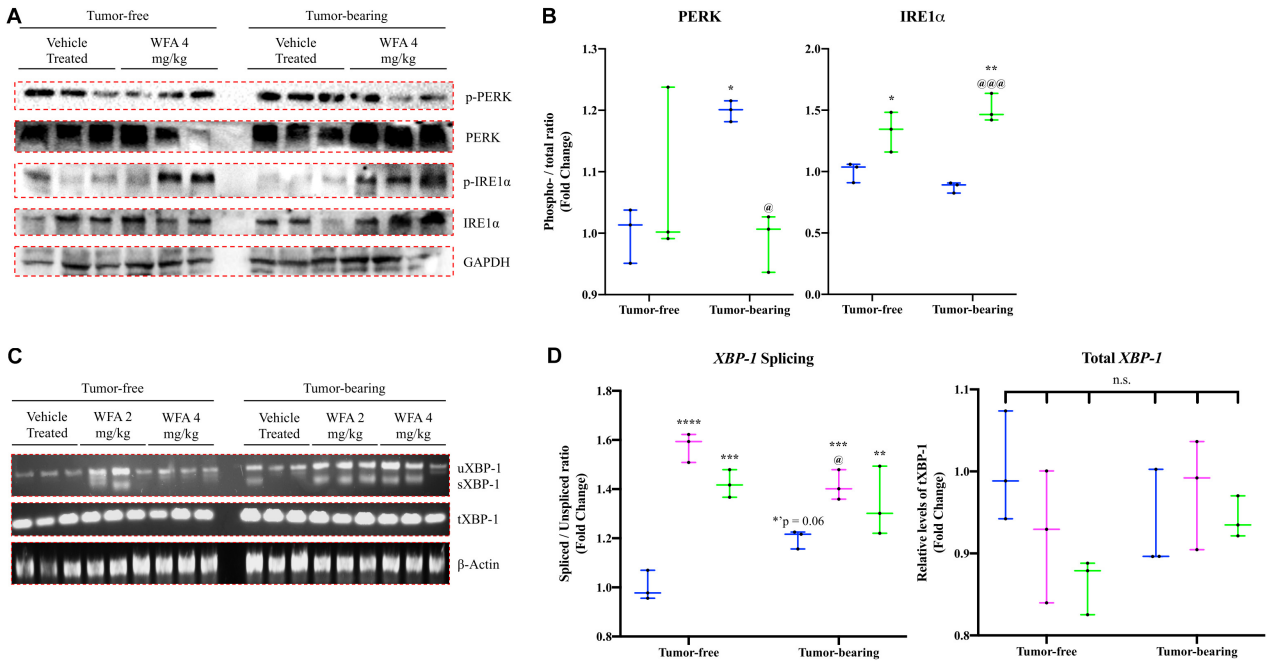

FIGURE 5 | Withaferin A and ovarian cancer's effect on the UPR at the protein level. **(A)** Representative immunoblots for components of the PERK and IRE1α arms of the UPR in QF muscle samples in the tumor-free and tumor-bearing vehicle-treated and WFA 4 mg/kg groups. $N = 3$ in all groups. **(B)** Densitometric quantification of western blot results. **(C)** Representative images of spliced (*sXBP-1*), unspliced (*uXBP-1*) and total *XBP-1* levels in GA muscle samples from tumor-free and tumor-bearing animals. Unrelated gene (β-Actin) was used as a load control for normalization. $N = 3$ per group. **(D)** Densitometric quantification of transcript levels of *XBP-1* and β-Actin. $N = 3$ per group. "n.s." = no significant differences. $^{*}p < 0.05$; $^{**}p < 0.01$; $^{***}p < 0.001$; $^{****}p < 0.0001$, value significantly different from corresponding value of tumor-free vehicle-treated group by two-way ANOVA followed by Tukey's multiple comparison test *post hoc* analysis. $^{@}p < 0.05$, value significantly different from corresponding value of tumor-bearing vehicle-treated group.

UPS could be one of the signaling pathways responsible for WFA's positive effect on skeletal muscle mass.

Withaferin A Transcriptionally Downregulates the Autophagy-Lysosomal System

In addition to the UPS, cancer-induced cachexia has been shown to activate the ALS to facilitate an atrophying effect on skeletal muscle (Sandri, 2010). During autophagy, LC3B-I is converted to LC3B-II to allow interaction with autophagic vesicles (Tanida et al., 2004). p62 is a substrate of autophagy that recognizes and binds to ubiquitinated proteins (Lamark et al., 2017). As such, p62 protein levels decrease with the activation of autophagy and it becomes transcriptionally upregulated to replenish the depleting protein (Lamark et al., 2017). Beclin1 is another autophagy-related protein that is critical for the initiation of the autophagosome (Sun et al., 2009).

To examine the effect of WFA and our xenograft model on the ALS, we measured relative mRNA levels of common autophagy markers: *Sqstm1* [encoding the protein p62 (Sánchez-Martín and Komatsu, 2018)], *Map1lc3b* [encoding the protein LC3B (Kang et al., 2019)], and *Becn1* [encoding the protein Beclin1 (Zheng et al., 2020)] (**Figure 7A**). A significant reduction in relative gene expression of the aforementioned markers of the ALS was observed in the tumor-free WFA 4 mg/kg group compared to the tumor-free vehicle-treated group ($p = 0.04$, $p = 0.013$, $p < 0.0001$, respectively) (**Figure 7A**). In the tumor-bearing vehicle-treated group, we observed a significant increase in relative transcript levels of *Sqstm1*, *Map1lc3b*, and *Becn1* compared to all tumor-free groups ($p < 0.0001$ for all comparisons) (**Figure 7A**). Similar to the results for the UPS, WFA treatment led to a significant dose-dependent reduction in relative mRNA expression of the select ALS markers compared to the tumor-bearing vehicle-treated group ($p < 0.0001$ for all comparisons) (**Figure 7A**).

Subsequently, we performed immunoblotting against LC3B, p62, and Beclin1 to determine whether WFA or ovarian cancer augmented signaling to the ALS at a protein level (**Figures 7B,C**). The ratio of LC3B-II to LC3B-I was significantly increased in the tumor-bearing groups compared to the tumor-free groups. However, WFA treatment did not affect LC3B lipidation under tumor-free or tumor-bearing conditions. Interestingly, protein levels of p62 were significantly increased in the tumor-free WFA 4 mg/kg compared to the tumor-free vehicle-treated group, suggesting a reduction in basal levels of autophagy (**Figure 7C**). A significant reduction in the levels of p62 in the tumor-bearing vehicle-treated and WFA 4 mg/kg groups was observed compared to the tumor-free vehicle-treated group, suggesting an active autophagy process was occurring (**Figure 7C**). Further, we observed a significant increase in Beclin1 only in the tumor-bearing vehicle-treated group compared to the tumor-free vehicle-treated group (**Figure 7C**). The tumor-bearing

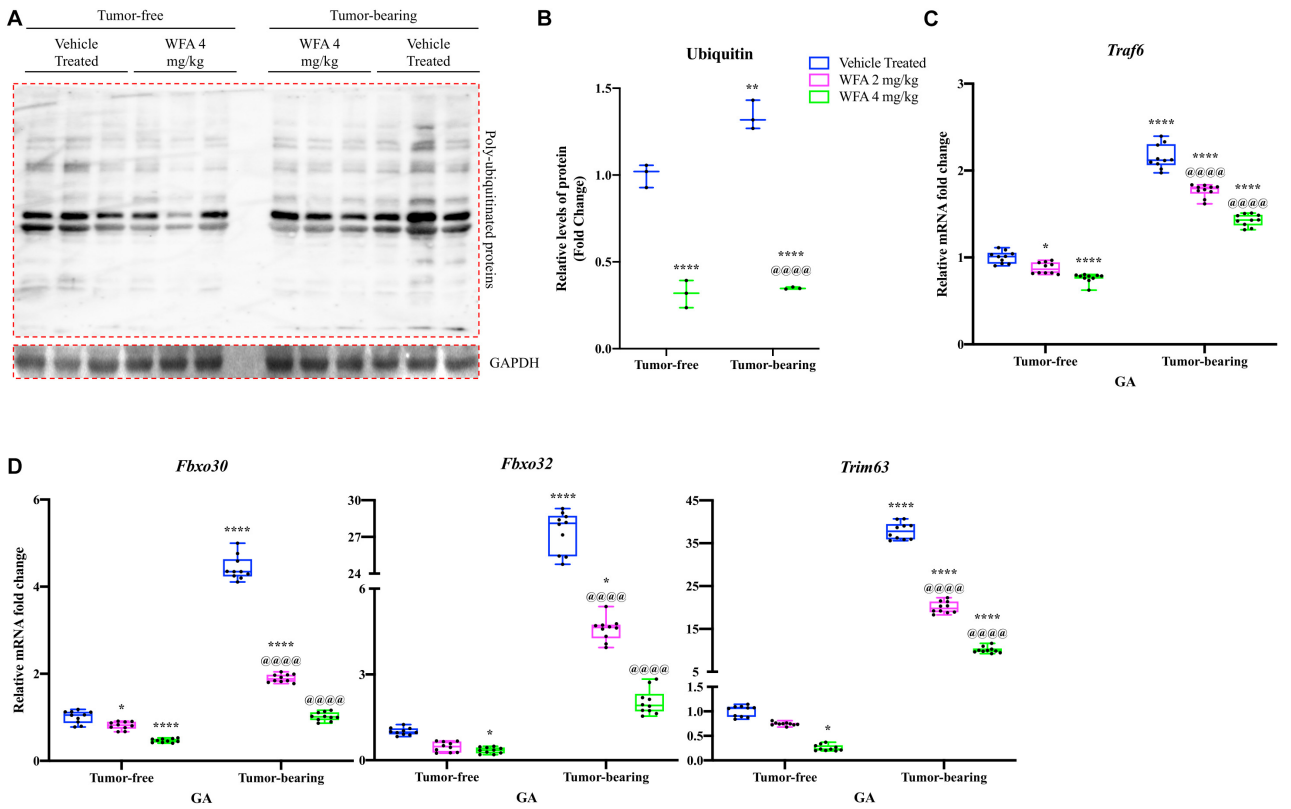

FIGURE 6 | Withaferin A reduces activation of the UPS. **(A)** Representative immunoblots for poly ubiquitinated proteins and unrelated protein GAPDH in tumor-free and tumor-bearing vehicle-treated or WFA 4 mg/kg QF muscle samples. $N = 3$ per group. **(B)** Densitometric quantification of poly ubiquitinated proteins in QF muscle samples. Relative mRNA levels of **(C)** *Traf6* and **(D)** select muscle-specific E3 ubiquitin ligases in GA muscle samples. $N = 10$ in all groups. $^{*}p < 0.05$; $^{**}p < 0.01$; $^{***}p < 0.001$; $^{****}p < 0.0001$, value significantly different from corresponding value of tumor-free vehicle-treated group by two-way ANOVA followed by Tukey's multiple comparison test *post hoc* analysis. $^{@}p < 0.05$, value significantly different from corresponding value of tumor-bearing vehicle-treated group.

WFA 4 mg/kg group had a significant reduction in Beclin1 protein levels compared to the tumor-bearing vehicle-treated group (**Figure 7C**). Similar to the UPS, the results from these experiments suggest that ovarian cancer results in a hyper-catabolic state. However, WFA appears to only regulate the ALS at a transcriptional level.

DISCUSSION

Despite the breadth of preclinical studies investigating cancer-induced cachexia, no pharmacological intervention has been found to be efficacious, with respect to skeletal muscle preservation/recovery, when employed in clinical trials (Naito, 2019). Several pharmacological interventions or targets for therapy are under investigation, with megestrol acetate perhaps being the most well-known (Gullett et al., 2011; Zhang et al., 2018). While megestrol acetate is used clinically to improve appetite and increase total body weight in cancer cachexia patients, its effect on skeletal muscle mass is minimal at best (Gullett et al., 2011). In order to improve the survival rates of cancer patients and preserve quality of life, it is critical that muscle mass be preserved. Prospective interventions could achieve this through regulation of tumor burden or by acting on skeletal muscle itself.

It was previously thought that tumor burden correlated with the induction and severity of cachexia, and that reducing gross tumor burden could rescue muscle mass (De Lerma Barbaro, 2015). Some studies continue to support this hypothesis (Wang et al., 2011; Wyke et al., 2004; Yang et al., 2013), but there are also reports that demonstrate the induction or severity of cachexia is independent of tumor burden (Goncalves et al., 2018; Williams et al., 2012). However, with respect to ovarian cancer, there is scant information available regarding the relationship between tumor burden and the induction of cachexia. Ovarian cancer is one of the most lethal gynecological malignancies and is primarily treated with an initial debulking surgery, followed by an adjuvant platinum-based chemotherapy agent, such as cisplatin (Cannistra, 2004; Ozols et al., 2003; Siegel et al., 2019). The deleterious effects of cisplatin on skeletal muscle are well documented (Conte et al., 2020; Damrauer et al., 2018; Sakai et al., 2014), and a recent report from Huang et al. has demonstrated that surgical debulking of advanced-stage ovarian cancer can lead to a reduction in skeletal muscle mass (Huang et al., 2020).

Recent work from our lab and the present study examined cachexia in response to the xenografting of ovarian cancer in a

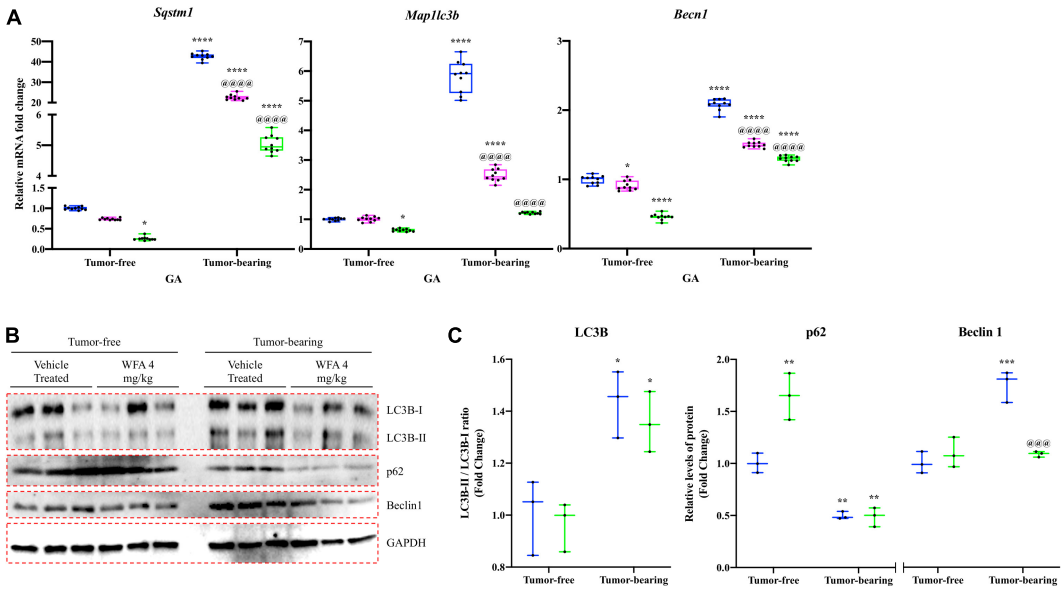

FIGURE 7 | Withaferin A downregulates activation of the ALS. **(A)** Relative mRNA levels of select markers of autophagy in GA muscle samples from tumor-free and tumor-bearing mice. $N = 10$ in all groups. **(B)** Western blot analysis of common markers of autophagy in QF muscle samples. $N = 3$ per group. **(C)** Densitometric quantification of western blot images. $^{*}p < 0.05$; $^{**}p < 0.01$; $^{***}p < 0.001$; $^{****}p < 0.0001$, value significantly different from corresponding value of tumor-free vehicle-treated group by two-way ANOVA followed by Tukey's multiple comparison test *post hoc* analysis. $^{@}p < 0.05$, value significantly different from corresponding value of tumor-bearing vehicle-treated group.

preclinical mouse model and employed WFA as an experimental therapeutic agent to attenuate cachexia. However, it was not determined in our initial study whether WFA's positive effect on skeletal muscle occurred through a reduction in tumor burden or if WFA acted directly upon skeletal muscle (Straughn and Kakar, 2019). The results from this study clearly demonstrate that WFA treatment is capable of increasing functional muscle strength and muscle mass in both tumor-bearing and tumor-free mice, suggesting that the beneficial effect of WFA is not purely as a byproduct of its anti-tumorigenic properties (**Figures 1**, **2**). Yet, this begs the question: how does WFA induce a hypertrophying or anti-cachectic effect on skeletal muscle? Generally, muscle mass is regulated by the pool of myogenic progenitors and the rates of protein degradation and synthesis (Schiaffino et al., 2013).

Satellite cells are the myogenic progenitor type primarily responsible for regenerative myogenesis (He et al., 2013; Relaix and Zammit, 2012). Further, multiple reports have demonstrated that tumor-bearing humans and animals exhibit destructive alterations to the sarcolemma of skeletal muscle fibers (Acharyya et al., 2005; He et al., 2013; Talbert et al., 2014). Indeed, disruption of the sarcolemma is known to activate satellite cells in an effort to repair damage to skeletal muscle (Charge, 2004). Disruption of the sarcolemma within skeletal muscle is thought to occur in response to tumor factors in circulation, as opposed to direct infiltration of the muscle by metastatic cancer cells (He et al., 2013). As such, satellite cells were high on our list of possible targets being augmented by WFA and/or the xenografted ovarian cancer cells. Both inoculation with A2780 ovarian cancer cells and treatment with WFA led to a robust increase in the total amount of satellite cells (**Figure 3**). While the exact signaling mechanism responsible for the dysregulation of muscle repair is not presently known, several prevailing theories exist.

Perhaps the most well-known, dysregulation of NF-κB signaling has been shown to impair regenerative myogenesis in the settings of cancer-induced cachexia (He et al., 2013). It was demonstrated that cancer leads to an overactivation of NF-κB signaling, leading to a Pax7-dependent down-regulation of MyoD (He et al., 2013). In our experiment, when satellite cells were stratified based upon their expression of MyoD, we observed markedly dichotomous results. WFA treatment in tumor-bearing and naïve mice led to a robust increase in the proportion of differentiating satellite cells (i.e., $Pax7^{+}/MyoD^{+}$), whereas the vehicle-treated groups had an overwhelming majority of satellite cells that were quiescent or returning to quiescence (i.e., $Pax7^{+}/MyoD^{-}$). Downstream of NF-κB signaling, proinflammatory cytokines (such as TNFα) and Angiotensin II (Ang-II) were found to prevent the expression of MyoD and myogenin, and thus impairs regenerative myogenesis (Szalay et al., 1997; Langen et al., 2001; Johnston et al., 2010; Yoshida et al., 2013). Indeed, reports from our lab demonstrated that xenografting of the ovarian cancer cell line A2780 results in a similar increase in several NF-κB-dependent proinflammatory cytokines and circulating levels of Ang-II (Kelm et al., 2020; Straughn and Kakar, 2019), perhaps indicating the mechanism through which satellite cells are dysregulated in response to ovarian cancer.

Our data suggests that WFA treatment leads to the functional activation of satellite cells and subsequent fusion of myogenic progenitors through an increase in the proportion of differentiating satellite cells and concomitant increase in

myofibrillar CSA. However, the reported results (**Figures 1**, **2**) are indirect measures that fusion is occurring. Future work from our lab will specifically address whether or not myogenic fusion is occurring in response to WFA treatment to discern if myogenic progenitors are indeed responsible for the beneficial effect on skeletal muscle. Aside from myogenic progenitors, changes in signaling to the UPR have been exhibited in several models of cancer-induced cachexia (Bohnert et al., 2016; Isaac et al., 2016; Roy and Kumar, 2019).

The UPR acts to resolve ER stress and to facilitate the proper folding of proteins by limiting the rate of protein synthesis and upregulating the production of chaperone proteins (Tirasophon et al., 1998; Wang and Kaufman, 2014). In circumstances where ER stress is insurmountable, the UPR will signal proteolytic pathways culminating in cellular death (Hetz, 2012). In our study, we observed that both WFA and ovarian cancer globally regulate various components of the UPR, albeit with a few critical distinctions (**Figures 4**, **5**). WFA treatment led to a transcriptional upregulation of the IRE1α arm of the UPR, and a reduction in Death Receptor 5 expression. Further, WFA treatment resulted in a significant increase in the protein levels of phosphorylated IRE1α. Conversely, xenografting of ovarian cancer cells resulted in an increase in the PERK arm of the UPR and a concomitant increase in Death Receptor 5 expression. A significant increase in the protein levels of phosphorylated PERK was shown in response to the xenografted ovarian cancer cells, but not WFA treatment. However, discrepant results were observed when interrogating the UPR distal to PERK and IRE1α activation.

The protein CHOP is normally associated with activation of autophagy mediated through the PERK arm of the UPR, although both the IRE1α and ATF6 arms of the UPR are capable of augmenting CHOP expression (Hu et al., 2018; Nishitoh, 2012). Conflicting reports exist regarding the effect of CHOP signaling in skeletal muscle. One study found that depletion of CHOP accentuates skeletal muscle atrophy (Yu et al., 2011), whereas a different study reported no significant changes in CHOP in a model of disuse muscle atrophy (Hunter et al., 2001). Thus, it would seem that the effects of CHOP signaling appear to be context-specific. In our study, no consistent changes in the protein levels of CHOP were observed in response to WFA treatment or xenografting of the A2780 ovarian cancer cell line, although we did observe a significant increase in transcript levels of the gene encoding CHOP in response to both WFA treatment and the ovarian cancer cell xenografts. Activation of IRE1α arm of the UPR results in the alternative splicing of *XBP-1* transcripts. WFA treatment under tumor-free and tumor-bearing conditions resulted in a significant increase in activation of IRE1α, as well as in a significant increase in the ratio of *sXBP-1* to *uXBP-1*. Interestingly, xenografting of the ovarian cancer cells into NSG mice did not lead to a significant increase in IRE1α activation or splicing of *XBP-1*. These results suggest that, although WFA and ovarian cancer both generally activate the UPR, a differential pattern of UPR activation is exhibited in response to WFA treatment and the xenografted cancer cells within skeletal muscle.

While we corroborated immediately distal changes in signaling through the IRE1α arm of the UPR, but not the PERK arm, it was unknown whether these changes were of any consequence with respect to muscle atrophy. Thus, we examined the ubiquitin proteasome and ALSs to determine if ovarian cancer produced a hyper-catabolic state. At the protein level, both pan-ubiquitination of proteins and activation of autophagy were exhibited in skeletal muscle in response to ovarian cancer (**Figures 6**, **7**). Transcript levels of select E3 ubiquitin ligases and markers of the ALS were similarly increased in response to the ovarian cancer cell xenografts. Interestingly, WFA treatment produced a robust transcriptional downregulation of several components of the UPS and ALS. However, WFA treatment led to a significant reduction in polyubiquitinated proteins, but only downregulated select ALS proteins. Thus, it is possible that WFA's effect on augmenting protein degradation primarily occurs through changes in the UPS. Skeletal muscle atrophy is known to have various sex-specific effects (Rosa-Caldwell and Greene, 2019; Zhong and Zimmers, 2020). One notable example is that skeletal muscle in males tends to exhibit greater activation of the UPS, whereas skeletal muscle in females preferentially activates the ALS (Ogawa et al., 2017; Oliván et al., 2014; Piekarski et al., 2014; Shu et al., 2018). As a result of this, WFA treatment may show an even greater effect in rescuing skeletal muscle in males.

In this study, we sought to corroborate prior reports from our lab regarding the induction of cachexia by ovarian cancer and investigate signaling pathways distal to those previously reported (Kelm et al., 2020; Straughn and Kakar, 2019). Similar to other models of cancer-induced cachexia, we report that ovarian cancer induces an atrophying effect on skeletal muscle by inhibiting myogenic progenitors and activating proteolytic degradation pathways (**Figure 8**). Based upon current literature and our experimental results, we believe that WFA is targeting the NF-κB signaling axis, the UPS, and the ALS in an attempt to mitigate the effects of ovarian cancer in skeletal muscle. Cumulatively, our results demonstrate for the first time that WFA not only has anti-tumorigenic properties, but also directly targets skeletal muscle resulting in a hypertrophying/anti-cachectic effect. While our study omitted the inclusion of male subjects due to the anatomic origin of the cancer, it would be interesting to observe whether WFA treatment has similar effects on male subjects and whether the anti-tumorigenic and/or anti-cachectic properties carried over into a more traditional model of cachexia.

LIMITATIONS OF THE STUDY

For studies examining changes in skeletal muscle, it is generally preferable to utilize mice that are sexually mature to exclude the potentially confounding effect of stunted growth. However, most xenograft studies employing ovarian cancer use mice between the ages of 4–8 weeks, as older mice have higher rates of xenograft rejection (Helland et al., 2014; Guo et al., 2017; De Haven Brandon et al., 2020; Shaw et al., 2004). Despite this, at least one group of investigators has compared the effects of cancer-induced cachexia in young mice vs. old mice, albeit in a different model of cancer cachexia (Talbert et al., 2014). The authors report that both young and old mice exhibit similar responses to the tumor, with respect to changes in skeletal muscle, and concluded

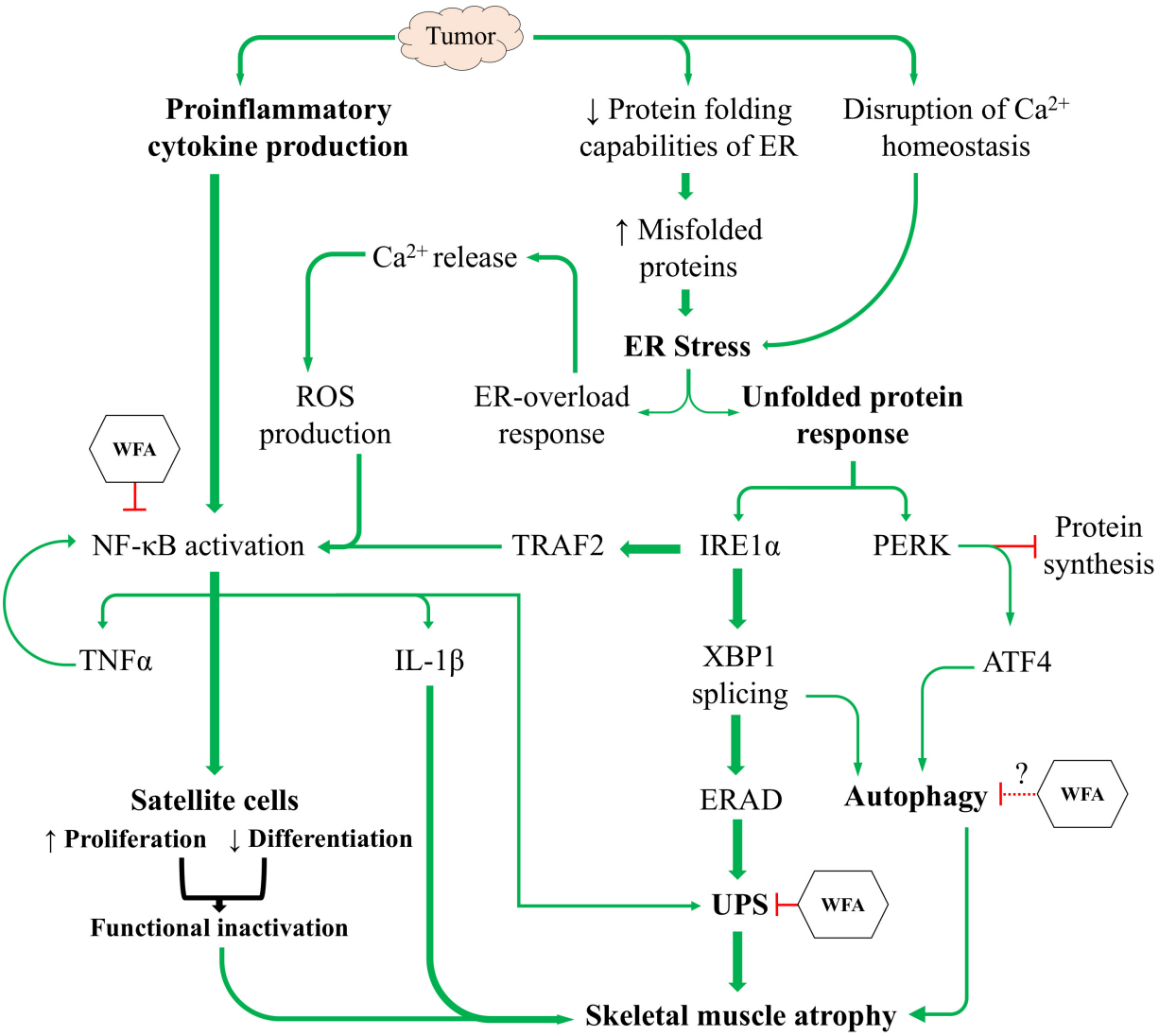

FIGURE 8 | The induction of cachexia by ovarian cancer. Proposed mechanistic model showing ovarian cancer's effect on satellite cell homeostasis and the UPR to facilitate skeletal muscle atrophy, and the proposed mechanism(s) through which WFA interferes with the induction of cachexia.

that, "...there does not seem to be an overwhelming reason to adapt tumor models to older animals..." (Talbert et al., 2014). Second, due to the atrophying effects of the cancer upon skeletal muscle, macromolecular extractions for RNA and protein were stratified to different muscles. As such, it is currently unknown if muscle-specific effects of ovarian cancer and WFA exist, which could augment the results gathered. Third, although a tumor-free control was employed in the study to aide in examining the skeletal muscle effect of WFA, the global nature of the treatment makes it impossible to differentiate between WFA's effect on muscle, the tumor, and global levels of inflammation within the tumor-bearing groups.

Last, a separate limitation of the study involves the mouse strain employed. Most cachexia studies utilize immune-competent mice and a mouse-derived cancer. In our study, we utilized immune-deficient mice, such that we could xenograft ovarian cancer cells of human origin. However, the immune system is well-known to be involved in muscle damage and repair (Tidball and Villalta, 2010). While the immune system is certainly involved in the progression of cachexia, it is primarily centered around the induction of systemic inflammation (Argilés et al., 2009) and tumor surveillance (Miller et al., 2019). Ovarian cancer is considered to be an immunologically "cold" tumor, as they are scarcely immunogenic and have a low number of tumor-infiltrating lymphocytes (Galon and Bruni, 2019; Ghisoni et al., 2019). Due to a loss-of-function mutation of the *Prkdc* gene, NSG mice are deficient in T-cells (Shultz et al., 1995) and can thus provide a suitable environment to produce "cold" tumors upon xenografting of ovarian cancer cells. The pro-inflammatory cytokines TNFα, IL-1β, IL-6, and IFNγ are considered to be some of the critical mediators orchestrating a cachectic phenotype (Argilés et al., 2009; Fearon et al., 2012). Despite

NSG mice lacking a competent immune system, the ovarian cancer cells in our study produces all four of these critical pro-inflammatory cytokines (Straughn and Kakar, 2019; Watanabe et al., 2012). For these reasons, we believe that the phenotype exhibited in our study is fairly faithful to the cachectic phenotype exhibited in humans. However, it is equally plausible that, had immune-competent animals and a suitable mouse-derived ovarian cancer cell line been employed, the cachectic phenotype exhibited could be altered.

DATA AVAILABILITY STATEMENT

The original contributions presented in the study are included in the article/**Supplementary Material**, further inquiries can be directed to the corresponding author/s.

ETHICS STATEMENT

The animal study was reviewed and approved by the University of Louisville's Institutional Animal Care and Use Committee (IACUC).

AUTHOR CONTRIBUTIONS

AS conceived and designed the work, wrote the manuscript, and performed statistical analyses. AS and NK performed the experiments and data acquisition and quantified the data. NK and SK reviewed the statistical analyses. All authors edited the manuscript and read and approved the final manuscript.

FUNDING

This work was supported by NIH grant T32 HL134644 to SK.

ACKNOWLEDGMENTS

We thank Prof. Ashok Kumar (University of Houston, Houston, TX, United States) for the use of his Columbus Instruments grip strength meter. We also thank Jelani Regan for his help in collection of tissues from animals.

SUPPLEMENTARY MATERIAL

The Supplementary Material for this article can be found online at: https://www.frontiersin.org/articles/10.3389/fcell.2021.636498/full#supplementary-material

Supplementary Figure 1 | Basal and intermediate grip strength analyses. Quantification of mean basal **(A)** forelimb and **(B)** total limb grip strength normalized to body weight before xenografting of A2780 cells. Quantification of mean **(C)** forelimb and **(D)** total limb grip strength normalized to body weight at week one post-xenografting of A2780 cells. $N = 30$ in all groups. Quantification of mean **(E)** forelimb and **(F)** total limb grip strength normalized to body weight at week two post-xenografting of A2780 cells. Quantification of mean **(G)** forelimb and **(H)** total limb grip strength normalized to body weight at week three post-xenografting of A2780 cells. $N = 10$ in all groups. $^{*}p < 0.05$; $^{**}p < 0.01$; $^{***}p < 0.001$; $^{****}p < 0.0001$, value significantly different from corresponding value of tumor-free vehicle-treated group by two-way ANOVA followed by Tukey's multiple comparison test *post hoc* analysis. $^{@}p < 0.05$, value significantly different from corresponding value of tumor-bearing vehicle-treated group.

Supplementary Figure 2 | Withaferin A inhibits activation of canonical NF-κB signaling in skeletal muscle. **(A)** Representative immunoblots for phospho- and total p65, as well as unrelated protein GAPDH in QF muscle samples in the tumor-free and tumor-bearing vehicle-treated and WFA 4 mg/kg groups. $N = 3$ in all groups. **(B)** Densitometric quantification of western blotting results. **(C)** Relative mRNA levels of RelA and IKKβ in GA muscle samples from all tumor-free and tumor-bearing groups. $N = 10$ in all groups. $^{*}p < 0.05$; $^{**}p < 0.01$; $^{***}p < 0.001$; $^{****}p < 0.0001$, value significantly different from corresponding value of tumor-free vehicle-treated group by two-way ANOVA followed by Tukey's multiple comparison test *post hoc* analysis. $^{@}p < 0.05$, value significantly different from corresponding value of tumor-bearing vehicle-treated group.

REFERENCES

Acharyya, S., Butchbach, M. E., Sahenk, Z., Wang, H., Saji, M., Carathers, M., et al. (2005). Dystrophin glycoprotein complex dysfunction: a regulatory link between muscular dystrophy and cancer cachexia. *Cancer Cell.* 8, 421–432. doi: 10.1016/j.ccr.2005.10.004

Afroze, D., and Kumar, E. R. (2019). A stress in skeletal muscle remodeling and myopathies. *FEBS J.* 286, 379–398. doi: 10.1111/febs.14358

Argilés, J. M., Busquets, S., Toledo, M., and López-Soriano, F. J. (2009). The role of cytokines in cancer cachexia. *Curr. Opin. Support Palliat. Care.* 3, 263–268.

Barreto, R., Waning, D. L., Gao, H., Liu, Y., Zimmers, T. A., and Bonetto, A. (2016). Chemotherapy-related cachexia is associated with mitochondrial depletion and the activation of ERK1/2 and p38 MAPKs. *Oncotarget* 7, 43442–43460. doi: 10.18632/oncotarget.9779

Bodine, S. C., and Baehr, L. M. (2014). Skeletal muscle atrophy and the E3 ubiquitin ligases MuRF1 and MAFbx/atrogin-1. *Am. J. Physiol. Endocrinol. Metab.* 307, E469–E484.

Bohnert, K. R., Gallot, Y. S., Sato, S., Xiong, G., Hindi, S. M., and Kumar, A. (2016). Inhibition of ER stress and unfolding protein response pathways causes skeletal muscle wasting during cancer cachexia. *FASEB J.* 30, 3053–3068. doi: 10.1096/fj.201600250rr

Bohnert, K. R., McMillan, J. D., and Kumar, A. (2018). Emerging roles of ER stress and unfolded protein response pathways in skeletal muscle health and disease. *J. Cell Physiol.* 233, 67–78. doi: 10.1002/jcp.25852

Bonetto, A., Aydogdu, T., Jin, X., Zhang, Z., Zhan, R., Puzis, L., et al. (2012). JAK/STAT3 pathway inhibition blocks skeletal muscle wasting downstream of IL-6 and in experimental cancer cachexia. *Am. J. Physiol. Endocrinol. Metab.* 303, E410–E421.

Cannistra, S. A. (2004). Cancer of the ovary. *N. Engl. J. Med.* 351, 2519–2529.

Cao, Z., Xiong, J., Takeuchi, M., Kurama, T., and Goeddel, D. V. (1996). TRAF6 is a signal transducer for interleukin-1. *Nature* 383, 443–446. doi: 10.1038/383443a0

Chandrasekaran, B., Pal, D., Kolluru, V., Tyagi, A., Baby, B., Dahiya, N. R., et al. (2018). The chemopreventive effect of withaferin A on spontaneous and inflammation-associated colon carcinogenesis models. *Carcinogenesis.* 39, 1537–1547. doi: 10.1093/carcin/bgy109

Chang, H. W., Li, R. N., Wang, H. R., Liu, J. R., Tang, J. Y., Huang, H. W., et al. (2017). Withaferin A Induces Oxidative Stress-Mediated Apoptosis and DNA Damage in Oral Cancer Cells. *Front Physiol.* 8:634. doi: 10.3389/fphys.2017.00634

Charge, S. B. P. (2004). Cellular and Molecular Regulation of Muscle Regeneration. *Physiol. Rev.* 84, 209–238. doi: 10.1152/physrev.00019.2003

Chen, B., Piel, W. H., Gui, L., Bruford, E., and Monteiro, A. (2005). The HSP90 family of genes in the human genome: insights into their divergence and evolution. *Genomics* 86, 627–637. doi: 10.1016/j.ygeno.2005.08.012

Chen, R., Alvero, A. B., Silasi, D. A., Kelly, M. G., Fest, S., Visintin, I., et al. (2008). Regulation of IKKbeta by miR-199a affects NF-kappaB activity in ovarian cancer cells. *Oncogene* 27, 4712–4723. doi: 10.1038/onc.2008.112

Clavarino, G., Cláudio, N., Dalet, A., Terawaki, S., Couderc, T., Chasson, L., et al. (2012). Protein phosphatase 1 subunit Ppp1r15a/GADD34 regulates cytokine production in polyinosinic:polycytidylic acid-stimulated dendritic cells. *Proc. Natl. Acad. Sci. U S A.* 109, 3006–3011. doi: 10.1073/pnas.1104491109

Conte, E., Bresciani, E., Rizzi, L., Cappellari, O., De Luca, A., Torsello, A., et al. (2020). Cisplatin-Induced Skeletal Muscle Dysfunction: Mechanisms and Counteracting Therapeutic Strategies. *Int. J. Mol. Sci.* 2020:21.

Damrauer, J. S., Stadler, M. E., Acharyya, S., Baldwin, A. S., Couch, M. E., and Guttridge, D. C. (2018). Chemotherapy-induced muscle wasting: association with NF-κB and cancer cachexia. *Eur. J. Transl. Myol.* 28:7590.

De Haven Brandon, A., Box, G., Hallsworth, A., Court, W., Matthews, N., Herodek, B., et al. (2020). Identification of ovarian high-grade serous carcinoma cell lines that show estrogen-sensitive growth as xenografts in immunocompromised mice. *Sci. Rep.* 10:10799.

De Lerma Barbaro, A. (2015). The complex liaison between cachexia and tumor burden (Review). *Oncol. Rep.* 34, 1635–1649. doi: 10.3892/or.2015.4164

Didier, N., Hourdé, C., Amthor, H., Marazzi, G., and Sassoon, D. (2012). Loss of a single allele for Ku80 leads to progenitor dysfunction and accelerated aging in skeletal muscle. *EMBO Mol. Med.* 4, 910–923. doi: 10.1002/emmm.201101075

Dijkgraaf, E. M., Welters, M. J., Nortier, J. W., van der Burg, S. H., and Kroep, J. R. (2012). Interleukin-6/interleukin-6 receptor pathway as a new therapy target in epithelial ovarian cancer. *Curr. Pharm. Des.* 18, 3816–3827. doi: 10.2174/138161212802002797

Dittmann, J., Haydn, T., Metzger, P., Ward, G. A., Boerries, M., Vogler, M., et al. (2020). Next-generation hypomethylating agent SGI-110 primes acute myeloid leukemia cells to IAP antagonist by activating extrinsic and intrinsic apoptosis pathways. *Cell Death Differ.* 27, 1878–1895. doi: 10.1038/s41418-019-0465-8

Domcke, S., Sinha, R., Levine, D. A., Sander, C., and Schultz, N. (2013). Evaluating cell lines as tumour models by comparison of genomic profiles. *Nat. Commun.* 4:2126.

Elfiky, A. A., Baghdady, A. M., Ali, S. A., and Ahmed, M. I. (2020). GRP78 targeting: Hitting two birds with a stone. *Life Sci.* 260:118317. doi: 10.1016/j.lfs.2020.118317

Fearon, K. C., Glass, D. J., and Guttridge, D. C. (2012). Cancer cachexia: mediators, signaling, and metabolic pathways. *Cell Metab.* 16, 153–166. doi: 10.1016/j.cmet.2012.06.011

Fearon, K., Strasser, F., Anker, S. D., Bosaeus, I., Bruera, E., Fainsinger, R. L., et al. (2011). Definition and classification of cancer cachexia: an international consensus. *Lancet Oncol.* 12, 489–495. doi: 10.1016/s1470-2045(10)70218-7

Feng, X., Naz, F., Juan, A. H., Dell'Orso, S., and Sartorelli, V. (2018). Identification of Skeletal Muscle Satellite Cells by Immunofluorescence with Pax7 and Laminin Antibodies. *J. Vis. Exp.* 2018, 134.

Foletta, V. C., White, L. J., Larsen, A. E., Leger, B., and Russell, A. P. (2011). The role and regulation of MAFbx/atrogin-1 and MuRF1 in skeletal muscle atrophy. *Pflugers Arch.* 461, 325–335. doi: 10.1007/s00424-010-0919-9

Fong, M. Y., Jin, S., Rane, M., Singh, R. K., Gupta, R., and Kakar, S. S. (2012). Withaferin A synergizes the therapeutic effect of doxorubicin through ROS-mediated autophagy in ovarian cancer. *PLoS One* 7:e42265. doi: 10.1371/journal.pone.0042265

Gadducci, A., Cosio, S., Fanucchi, A., and Genazzani, A. R. (2001). Malnutrition and cachexia in ovarian cancer patients: pathophysiology and management. *Anticancer Res.* 21, 2941–2947.

Gallot, Y. S., Bohnert, K. R., Straughn, A. R., Xiong, G., Hindi, S. M., and Kumar, A. (2018). PERK regulates skeletal muscle mass and contractile function in adult mice. *FASEB J.* 2018:fj201800683RR.

Galon, J., and Bruni, D. (2019). Approaches to treat immune hot, altered and cold tumours with combination immunotherapies. *Nat. Rev. Drug Discov.* 18, 197–218. doi: 10.1038/s41573-018-0007-y

Ghisoni, E., Imbimbo, M., Zimmermann, S., and Valabrega, G. (2019). Ovarian Cancer Immunotherapy: Turning up the Heat. *Int. J. Mole. Sci.* 2019:20.

Ghosh, K., De, S., Mukherjee, S., Das, S., Ghosh, A. N., and Sengupta, S. B. (2017). Withaferin A induced impaired autophagy and unfolded protein response in human breast cancer cell-lines MCF-7 and MDA-MB-231. *Toxicol In Vitro.* 44, 330–338. doi: 10.1016/j.tiv.2017.07.025

Goncalves, M. D., Hwang, S. K., Pauli, C., Murphy, C. J., Cheng, Z., Hopkins, B. D., et al. (2018). Fenofibrate prevents skeletal muscle loss in mice with lung cancer. *Proc. Natl. Acad. Sci. U S A.* 115, E743–E752.

Gullett, N. P., Mazurak, V. C., Hebbar, G., and Ziegler, T. R. (2011). Nutritional interventions for cancer-induced cachexia. *Curr. Probl. Cancer.* 35, 58–90. doi: 10.1016/j.currproblcancer.2011.01.001

Guo, J., Cai, J., Zhang, Y., Zhu, Y., Yang, P., and Wang, Z. (2017). Establishment of two ovarian cancer orthotopic xenograft mouse models for in vivo imaging: A comparative study. *Int. J. Oncol.* 51, 1199–1208. doi: 10.3892/ijo.2017.4115

Hahn, A., Kny, M., Pablo-Tortola, C., Todiras, M., Willenbrock, M., Schmidt, S., et al. (2020). Serum amyloid A1 mediates myotube atrophy via Toll-like receptors. *J. Cachexia Sarcopenia Muscle.* 11, 103–119. doi: 10.1002/jcsm.12491

Hayes, S. E., Conner, L. J., Stramm, L. E., and Shi, Y. (1999). Assignment of pancreatic eIF-2alpha kinase (EIF2AK3) to human chromosome band 2p12 by radiation hybrid mapping and in situ hybridization. *Cytogenet Cell Genet.* 86, 327–328. doi: 10.1159/000015328

He, W. A., Berardi, E., Cardillo, V. M., Acharyya, S., Aulino, P., Thomas-Ahner, J., et al. (2013). NF-kappaB-mediated Pax7 dysregulation in the muscle microenvironment promotes cancer cachexia. *J. Clin. Invest.* 123, 4821–4835. doi: 10.1172/jci68523

Helland, O., Popa, M., Vintermyr, O. K., Molven, A., Gjertsen, B. T., Bjørge, L., et al. (2014). First in-mouse development and application of a surgically relevant xenograft model of ovarian carcinoma. *PLoS One.* 9:e89527. doi: 10.1371/journal.pone.0089527

Hernandez, L., Kim, M. K., Lyle, L. T., Bunch, K. P., House, C. D., Ning, F., et al. (2016). Characterization of ovarian cancer cell lines as in vivo models for preclinical studies. *Gynecol. Oncol.* 142, 332–340. doi: 10.1016/j.ygyno.2016.05.028

Hetz, C. (2012). The unfolded protein response: controlling cell fate decisions under ER stress and beyond. *Nat. Rev. Mol. Cell Biol.* 13, 89–102. doi: 10.1038/nrm3270

Heyninck, K., Lahtela-Kakkonen, M., Van der Veken, P., Haegeman, G., and Vanden Berghe, W. (2014). Withaferin A inhibits NF-kappaB activation by targeting cysteine 179 in IKKbeta. *Biochem. Pharmacol.* 91, 501–509. doi: 10.1016/j.bcp.2014.08.004

Hindi, S. M., and Kumar, A. (2016). TRAF6 regulates satellite stem cell self-renewal and function during regenerative myogenesis. *J. Clin. Invest.* 126, 151–168. doi: 10.1172/jci81655

Hu, H., Tian, M., Ding, C., and Yu, S. (2018). The C/EBP Homologous Protein (CHOP) Transcription Factor Functions in Endoplasmic Reticulum Stress-Induced Apoptosis and Microbial Infection. *Front. Immunol.* 9:3083. doi: 10.3389/fimmu.2018.03083

Huang, C. Y., Yang, Y. C., Chen, T. C., Chen, J. R., Chen, Y. J., Wu, M. H., et al. (2020). Muscle loss during primary debulking surgery and chemotherapy predicts poor survival in advanced-stage ovarian cancer. *J. Cachexia Sarcopenia Muscle.* 11, 534–546. doi: 10.1002/jcsm.12524

Hunter, R. B., Mitchell-Felton, H., Essig, D. A., and Kandarian, S. C. (2001). Expression of endoplasmic reticulum stress proteins during skeletal muscle disuse atrophy. *Am. J. Physiol. Cell Physiol.* 281, C1285–C1290.

Isaac, S. T., Tan, T. C., and Polly, P. (2016). Endoplasmic Reticulum Stress, Calcium Dysregulation and Altered Protein Translation: Intersection of Processes That Contribute to Cancer Cachexia Induced Skeletal Muscle Wasting. *Curr. Drug Targets* 17, 1140–1146. doi: 10.2174/1389450116666150416115721

Johns, N., Stephens, N. A., and Fearon, K. C. (2013). Muscle wasting in cancer. *Int. J. Biochem. Cell Biol.* 45, 2215–2229.

Johnston, A. P., Baker, J., Bellamy, L. M., McKay, B. R., De Lisio, M., and Parise, G. (2010). Regulation of muscle satellite cell activation and chemotaxis by angiotensin II. *PLoS One.* 5:e15212. doi: 10.1371/journal.pone.0015212

Kaileh, M., Vanden Berghe, W., Heyerick, A., Horion, J., Piette, J., Libert, C., et al. (2007). Withaferin a strongly elicits IkappaB kinase beta hyperphosphorylation concomitant with potent inhibition of its kinase activity. *J. Biol. Chem.* 282, 4253–4264. doi: 10.1074/jbc.m606728200

Kakar, S. S., Jala, V. R., and Fong, M. Y. (2012). Synergistic cytotoxic action of cisplatin and withaferin A on ovarian cancer cell lines. *Biochem. Biophys. Res. Commun.* 423, 819–825. doi: 10.1016/j.bbrc.2012.06.047

Kakar, S. S., Parte, S., Carter, K., Joshua, I. G., Worth, C., Rameshwar, P., et al. (2017). Withaferin A (WFA) inhibits tumor growth and metastasis by targeting ovarian cancer stem cells. *Oncotarget* 8, 74494–74505. doi: 10.18632/oncotarget.20170

Kakar, S. S., Ratajczak, M. Z., Powell, K. S., Moghadamfalahi, M., Miller, D. M., Batra, S. K., et al. (2014). Withaferin a alone and in combination with cisplatin suppresses growth and metastasis of ovarian cancer by targeting putative cancer stem cells. *PLoS One* 9:e107596. doi: 10.1371/journal.pone.0107596

Kakar, S. S., Worth, C. A., Wang, Z., Carter, K., Ratajczak, M., and Gunjal, P. (2016). DOXIL when combined with Withaferin A (WFA) targets ALDH1 positive cancer stem cells in ovarian cancer. *J Cancer Stem Cell Res.* 2016:4.

Kang, H. M., Noh, K. H., Chang, T. K., Park, D., Cho, H. S., Lim, J. H., et al. (2019). Ubiquitination of MAP1LC3B by pVHL is associated with autophagy and cell death in renal cell carcinoma. *Cell Death Dis.* 10:279.

Karpinski, B. A., Morle, G. D., Huggenvik, J., Uhler, M. D., and Leiden, J. M. (1992). Molecular cloning of human CREB-2: an ATF/CREB transcription factor that can negatively regulate transcription from the cAMP response element. *Proc. Natl. Acad. Sci. U S A.* 89, 4820–4824. doi: 10.1073/pnas.89.11.4820

Kelm, N. Q., Straughn, A. R., and Kakar, S. S. (2020). Withaferin A attenuates ovarian cancer-induced cardiac cachexia. *PLoS One* 15:e0236680. doi: 10.1371/journal.pone.0236680

Kuang, S., and Rudnicki, M. A. (2008). The emerging biology of satellite cells and their therapeutic potential. *Trends Mol. Med.* 14, 82–91. doi: 10.1016/j.molmed.2007.12.004

Kuang, S., Kuroda, K., Le Grand, F., and Rudnicki, M. A. (2007). Asymmetric Self-Renewal and Commitment of Satellite Stem Cells in Muscle. *Cell* 129, 999–1010. doi: 10.1016/j.cell.2007.03.044

Kyakulaga, A. H., Aqil, F., Munagala, R., and Gupta, R. C. (2018). Withaferin A inhibits Epithelial to Mesenchymal Transition in Non-Small Cell Lung Cancer Cells. *Sci. Rep.* 8:15737.

Lamark, T., Svenning, S., and Johansen, T. (2017). Regulation of selective autophagy: the p62/SQSTM1 paradigm. *Essays Biochem.* 61, 609–624. doi: 10.1042/ebc20170035

Langen, R. C., Schols, A. M., Kelders, M. C., Wouters, E. F., and Janssen-Heininger, Y. M. (2001). Inflammatory cytokines inhibit myogenic differentiation through activation of nuclear factor-kappaB. *FASEB J.* 15, 1169–1180. doi: 10.1096/fj.00-0463

Loenneke, J. P., Buckner, S. L., Dankel, S. J., and Abe, T. (2019). Exercise-Induced Changes in Muscle Size do not Contribute to Exercise-Induced Changes in Muscle Strength. *Sports Med.* 49, 987–991. doi: 10.1007/s40279-019-01106-9

Marola, O. J., Syc-Mazurek, S. B., and Libby, R. T. (2019). DDIT3 (CHOP) contributes to retinal ganglion cell somal loss but not axonal degeneration in DBA/2J mice. *Cell Death Discov.* 5:140.

Miller, J., Laird, B., and Skipworth, R. (2019). The immunological regulation of cancer cachexia and its therapeutic implications. *J. Cancer Metastasis Treat* 2019:5.

Naito, T. (2019). Emerging Treatment Options For Cancer-Associated Cachexia: A Literature Review. *Ther. Clin. Risk Manag.* 15, 1253–1266. doi: 10.2147/tcrm.s196802

Nishitoh, H. (2012). CHOP is a multifunctional transcription factor in the ER stress response. *J. Biochem.* 151, 217–219. doi: 10.1093/jb/mvr143

Ogawa, M., Kitano, T., Kawata, N., Sugihira, T., Kitakaze, T., Harada, N., et al. (2017). Daidzein down-regulates ubiquitin-specific protease 19 expression through estrogen receptor β and increases skeletal muscle mass in young female mice. *J. Nutr. Biochem.* 49, 63–70. doi: 10.1016/j.jnutbio.2017.07.017

Oliván, S., Calvo, A. C., Manzano, R., Zaragoza, P., and Osta, R. (2014). Sex differences in constitutive autophagy. *Biomed. Res. Int.* 2014:652817.

Ozols, R. F., Bundy, B. N., Greer, B. E., Fowler, J. M., Clarke-Pearson, D., Burger, R. A., et al. (2003). Phase III trial of carboplatin and paclitaxel compared with cisplatin and paclitaxel in patients with optimally resected stage III ovarian cancer: A Gynecologic Oncology Group study. *J. Clin. Oncol.* 21, 3194–3200. doi: 10.1200/jco.2003.02.153

Paul, P. K., Bhatnagar, S., Mishra, V., Srivastava, S., Darnay, B. G., Choi, Y., et al. (2012). The E3 ubiquitin ligase TRAF6 intercedes in starvation-induced skeletal muscle atrophy through multiple mechanisms. *Mole. Cell. Biol.* 32, 1248–1259. doi: 10.1128/mcb.06351-11

Pettersen, K., Andersen, S., van der Veen, A., Nonstad, U., Hatakeyama, S., Lambert, C., et al. (2020). Autocrine activin A signalling in ovarian cancer cells regulates secretion of interleukin 6, autophagy, and cachexia. *J. Cachexia Sarcopenia Muscle.* 11, 195–207. doi: 10.1002/jcsm.12489

Piekarski, A., Khaldi, S., Greene, E., Lassiter, K., Mason, J. G., Anthony, N., et al. (2014). Tissue distribution, gender- and genotype-dependent expression of autophagy-related genes in avian species. *PLoS One.* 9:e112449. doi: 10.1371/journal.pone.0112449

Pin, F., Barreto, R., Kitase, Y., Mitra, S., Erne, C. E., Novinger, L. J., et al. (2018). Growth of ovarian cancer xenografts causes loss of muscle and bone mass: a new model for the study of cancer cachexia. *J. Cachexia Sarcopenia Muscle.* 9, 685–700. doi: 10.1002/jcsm.12311

Qin, L., Wang, Z., Tao, L., and Wang, Y. E. R. (2010). stress negatively regulates AKT/TSC/mTOR pathway to enhance autophagy. *Autophagy.* 6, 239–247. doi: 10.4161/auto.6.2.11062

Relaix, F., and Zammit, P. S. (2012). Satellite cells are essential for skeletal muscle regeneration: the cell on the edge returns centre stage. *Development* 139, 2845–2856. doi: 10.1242/dev.069088

Rosa-Caldwell, M. E., and Greene, N. P. (2019). Muscle metabolism and atrophy: let's talk about sex. *Biol. Sex. Differ.* 10:43.

Roy, A., and Kumar, A. (2019). ER Stress and Unfolded Protein Response in Cancer Cachexia. *Cancers* 11:1929. doi: 10.3390/cancers11121929

Royston, K. J., Paul, B., Nozell, S., Rajbhandari, R., and Tollefsbol, T. O. (2018). Withaferin A and sulforaphane regulate breast cancer cell cycle progression through epigenetic mechanisms. *Exp. Cell Res.* 368, 67–74. doi: 10.1016/j.yexcr.2018.04.015

Sakai, H., Sagara, A., Arakawa, K., Sugiyama, R., Hirosaki, A., Takase, K., et al. (2014). Mechanisms of cisplatin-induced muscle atrophy. *Toxicol. Appl. Pharmacol.* 278, 190–199.

Sánchez-Martín, P., and Komatsu, M. (2018). p62/SQSTM1 - steering the cell through health and disease. *J. Cell Sci.* 2018:131.

Sandri, M. (2010). Autophagy in skeletal muscle. *FEBS Lett.* 584, 1411–1416. doi: 10.1016/j.febslet.2010.01.056

Sandri, M. (2016). Protein breakdown in cancer cachexia. *Semin. Cell Dev Biol.* 54, 11–19. doi: 10.1016/j.semcdb.2015.11.002

Schiaffino, S., Dyar, K. A., Ciciliot, S., Blaauw, B., and Sandri, M. (2013). Mechanisms regulating skeletal muscle growth and atrophy. *FEBS J.* 280, 4294–4314. doi: 10.1111/febs.12253

Shaw, T. J., Senterman, M. K., Dawson, K., Crane, C. A., and Vanderhyden, B. C. (2004). Characterization of intraperitoneal, orthotopic, and metastatic xenograft models of human ovarian cancer. *Mol. Ther.* 10, 1032–1042. doi: 10.1016/j.ymthe.2004.08.013

Shu, Y., Xia, J., Yu, Q., Wang, G., Zhang, J., He, J., et al. (2018). Integrated analysis of mRNA and miRNA expression profiles reveals muscle growth differences between adult female and male Chinese concave-eared frogs (Odorrana tormota). *Gene.* 678, 241–251. doi: 10.1016/j.gene.2018.08.007

Shultz, L. D., Schweitzer, P. A., Christianson, S. W., Gott, B., Schweitzer, I. B., Tennent, B., et al. (1995). Multiple defects in innate and adaptive immunologic function in NOD/LtSz-scid mice. *J. Immunol.* 154, 180–191.

Siegel, R. L., Miller, K. D., and Jemal, A. (2019). Cancer statistics, 2019. *CA Cancer J. Clin.* 69, 7–34.

Straughn, A. R., and Kakar, S. S. (2019). Withaferin A ameliorates ovarian cancer-induced cachexia and proinflammatory signaling. *J. ovarian Res.* 12, 115.

Straughn, A. R., Hindi, S. M., Xiong, G., and Kumar, A. (2019). Canonical NF-kappaB signaling regulates satellite stem cell homeostasis and function during regenerative myogenesis. *J. Mol. Cell. Biol.* 11, 53–66. doi: 10.1093/jmcb/mjy053

Sun, Q., Fan, W., and Zhong, Q. (2009). Regulation of Beclin 1 in autophagy. *Autophagy* 5, 713–716. doi: 10.4161/auto.5.5.8524

Szalay, K., Rázga, Z., and Duda, E. (1997). TNF inhibits myogenesis and downregulates the expression of myogenic regulatory factors myoD and myogenin. *Eur. J. Cell Biol.* 74, 391–398.

Taber, C. B., Vigotsky, A., Nuckols, G., and Haun, C. T. (2019). Exercise-Induced Myofibrillar Hypertrophy is a Contributory Cause of Gains in Muscle Strength. *Sports Med.* 49, 993–997. doi: 10.1007/s40279-019-01107-8

Talbert, E. E., Metzger, G. A., He, W. A., and Guttridge, D. C. (2014). Modeling human cancer cachexia in colon 26 tumor-bearing adult mice. *J. Cachexia Sarcopenia Muscle* 5, 321–328. doi: 10.1007/s13539-014-0141-2

Tanida, I., Ueno, T., and Kominami, E. (2004). LC3 conjugation system in mammalian autophagy. *Int. J. Biochem. Cell Biol.* 36, 2503–2518. doi: 10.1016/j.biocel.2004.05.009

Tidball, J. G., and Villalta, S. A. (2010). Regulatory interactions between muscle and the immune system during muscle regeneration. *Am. J. Physiol. Regul. Integr. Comp. Physiol.* 298, R1173–R1187.

Tirasophon, W., Welihinda, A. A., and Kaufman, R. J. (1998). A stress response pathway from the endoplasmic reticulum to the nucleus requires a novel bifunctional protein kinase/endoribonuclease (Ire1p) in mammalian cells. *Genes Dev.* 12, 1812–1824. doi: 10.1101/gad.12.12.1812

Ubachs, J., Ziemons, J., Minis-Rutten, I. J. G., Kruitwagen, R., Kleijnen, J., Lambrechts, S., et al. (2019). Sarcopenia and ovarian cancer survival: a systematic review and meta-analysis. *J. Cachexia Sarcopenia Muscle.* 10, 1165–1174. doi: 10.1002/jcsm.12468

Wang, H., Lai, Y. J., Chan, Y. L., Li, T. L., and Wu, C. J. (2011). Epigallocatechin-3-gallate effectively attenuates skeletal muscle atrophy caused by cancer cachexia. *Cancer Lett.* 305, 40–49. doi: 10.1016/j.canlet.2011.02.023

Wang, M., and Kaufman, R. J. (2014). The impact of the endoplasmic reticulum protein-folding environment on cancer development. *Nat. Rev. Cancer* 14, 581–597. doi: 10.1038/nrc3800

Watanabe, T., Hashimoto, T., Sugino, T., Soeda, S., Nishiyama, H., Morimura, Y., et al. (2012). Production of IL1-beta by ovarian cancer cells induces mesothelial cell beta1-integrin expression facilitating peritoneal dissemination. *J. Ovarian Res.* 5:7.112.

Williams, J. P., Phillips, B. E., Smith, K., Atherton, P. J., Rankin, D., Selby, A. L., et al. (2012). Effect of tumor burden and subsequent surgical resection on skeletal muscle mass and protein turnover in colorectal cancer patients. *Am. J. Clin. Nutr.* 96, 1064–1070. doi: 10.3945/ajcn.112.045708

Wyke, S. M., Russell, S. T., and Tisdale, M. J. (2004). Induction of proteasome expression in skeletal muscle is attenuated by inhibitors of NF-kappaB activation. *Br. J. Cancer* 91, 1742–1750. doi: 10.1038/sj.bjc.6602165

Xia, S., Miao, Y., and Liu, S. (2018). Withaferin A induces apoptosis by ROS-dependent mitochondrial dysfunction in human colorectal cancer cells. *Biochem. Biophys. Res. Commun.* 503, 2363–2369. doi: 10.1016/j.bbrc.2018.06.162

Xiong, G., Hindi, S. M., Mann, A. K., Gallot, Y. S., Bohnert, K. R., Cavener, D. R., et al. (2017). The PERK arm of the unfolded protein response regulates satellite cell-mediated skeletal muscle regeneration. *Elife* 2017:6.

Yang, Q., Wan, L., Zhou, Z., Li, Y., Yu, Q., Liu, L., et al. (2013). Parthenolide from Parthenium integrifolium reduces tumor burden and alleviate cachexia symptoms in the murine CT-26 model of colorectal carcinoma. *Phytomedicine* 20, 992–998. doi: 10.1016/j.phymed.2013.04.020

Yoshida, N., Yoshida, S., Koishi, K., Masuda, K., and Nabeshima, Y. (1998). Cell heterogeneity upon myogenic differentiation: down-regulation of MyoD and Myf-5 generates 'reserve cells'. *J. Cell Sci.* 111(Pt 6), 769–779.

Yoshida, T., Galvez, S., Tiwari, S., Rezk, B. M., Semprun-Prieto, L., Higashi, Y., et al. (2013). Angiotensin II inhibits satellite cell proliferation and prevents skeletal muscle regeneration. *J. Biol. Chem.* 288, 23823–23832. doi: 10.1074/jbc.m112.449074

Yu, Z., Wang, A. M., Adachi, H., Katsuno, M., Sobue, G., Yue, Z., et al. (2011). Macroautophagy is regulated by the UPR-mediator CHOP and accentuates the phenotype of SBMA mice. *PLoS Genet.* 7:e1002321. doi: 10.1371/journal.pgen.1002321

Zhang, F., Shen, A., Jin, Y., and Qiang, W. (2018). The management strategies of cancer-associated anorexia: a critical appraisal of systematic reviews. *BMC Complement Altern Med.* 18:236. doi: 10.1186/s12906-018-2304-8

Zhang, H. L., and Zhang, H. (2017). Withaferin-A Induces Apoptosis in Osteosarcoma U2OS Cell Line via Generation of ROS and Disruption of Mitochondrial Membrane Potential. *Pharmacogn. Mag.* 13, 523–527. doi: 10.4103/0973-1296.211042

Zheng, H. C., Zhao, S., Xue, H., Zhao, E. H., Jiang, H. M., and Hao, C. L. (2020). The Roles of Beclin 1 Expression in Gastric Cancer: A Marker for Carcinogenesis, Aggressive Behaviors and Favorable Prognosis, and a Target of Gene Therapy. *Front. Oncol.* 10:613679. doi: 10.3389/fonc.2020.613679

Zhong, X., and Zimmers, T. A. (2020). Sex Differences in Cancer Cachexia. *Curr. Osteoporos. Rep.* 18, 646–654. doi: 10.1007/s11914-020-00628-w

Conflict of Interest: The authors declare that the research was conducted in the absence of any commercial or financial relationships that could be construed as a potential conflict of interest.

The handling editor declared a past collaboration with one of the authors AS.

frontiers in Cell and Developmental Biology

ORIGINAL RESEARCH
published: 28 May 2021
doi: 10.3389/fcell.2021.670435

PERK Signaling Controls Myoblast Differentiation by Regulating MicroRNA Networks

Ye-Ya Tan[1†], Yin Zhang[1,2†], Bin Li[1], Yang-Wen Ou[3], Shu-Juan Xie[1], Pei-Pei Chen[4], Shi-Qiang Mei[1], Qiao-Juan Huang[1], Ling-Ling Zheng[1] and Liang-Hu Qu[1]**

[1] MOE Key Laboratory of Gene Function and Regulation, State Key Laboratory of Biocontrol, School of Life Sciences, Sun Yat-sen University, Guangzhou, China, [2] Guangdong Provincial Key Laboratory of Malignant Tumor Epigenetics and Gene Regulation, Research Center of Medicine, Sun Yat-sen Memorial Hospital, Sun Yat-sen University, Guangzhou, China, [3] Department of Cardiovascular Medicine, Second Affiliated Hospital of Guangzhou, University of Chinese Medicine, Guangzhou, China, [4] AMI Key Laboratory of Chinese Medicine in Guangzhou, Guangdong Province Hospital of Chinese Medicine, The Second Affiliated Hospital of Guangzhou University of Chinese Medicine, Guangdong Provincial Academy of Chinese Medical Science, Guangzhou, China

OPEN ACCESS

Edited by:
Yann Simon Gallot, University of Évry Val d'Essonne, France

Reviewed by:
Kyle Bohnert, St. Ambrose University, United States
Alex Ryan Straughn, James Graham Brown Cancer Center, United States

***Correspondence:**
Liang-Hu Qu
lssqlh@mail.sysu.edu.cn
Ling-Ling Zheng
zhengll33@mail.sysu.edu.cn

† These authors have contributed equally to this work and share first authorship

Specialty section:
This article was submitted to Signaling, a section of the journal Frontiers in Cell and Developmental Biology

Received: *21 February 2021*
Accepted: *31 March 2021*
Published: *28 May 2021*

Citation:
Tan Y-Y, Zhang Y, Li B, Ou Y-W, Xie S-J, Chen P-P, Mei S-Q, Huang Q-J, Zheng L-L and Qu L-H (2021) PERK Signaling Controls Myoblast Differentiation by Regulating MicroRNA Networks. Front. Cell Dev. Biol. 9:670435. doi: 10.3389/fcell.2021.670435

The unfolded protein response (UPR) plays important roles in various cells that have a high demand for protein folding, which are involved in the process of cell differentiation and development. Here, we separately knocked down the three sensors of the UPR in myoblasts and found that PERK knockdown led to a marked transformation in myoblasts from a fusiform to a rounded morphology, which suggests that PERK is required for early myoblast differentiation. Interestingly, knocking down PERK induced reprogramming of C2C12 myoblasts into stem-like cells by altering the miRNA networks associated with differentiation and stemness maintenance, and the PERK-ATF4 signaling pathway transactivated muscle differentiation-associated miRNAs in the early stage of myoblast differentiation. Furthermore, we identified Ppp1cc as a direct target gene of miR-128 regulated by the PERK signaling pathway and showed that its repression is critical for a feedback loop that regulates the activity of UPR-associated signaling pathways, leading to cell migration, cell fusion, endoplasmic reticulum expansion, and myotube formation during myoblast differentiation. Subsequently, we found that the RNA-binding protein ARPP21, encoded by the host gene of miR-128-2, antagonized miR-128 activity by competing with it to bind to the 3′ untranslated region (UTR) of Ppp1cc to maintain the balance of the differentiation state. Together, these results reveal the crucial role of PERK signaling in myoblast maintenance and differentiation and identify the mechanism underlying the role of UPR signaling as a major regulator of miRNA networks during early differentiation of myoblasts.

Keywords: myoblasts, differentiation, PERK signaling, microRNA network, C2C12 (mouse skeletal myoblasts)

INTRODUCTION

The unfolded protein response (UPR) is an evolutionarily conserved signaling pathway that responds to perturbations in endoplasmic reticulum (ER) homeostasis. The UPR plays crucial roles in physiological and pathological processes that have high requirements for protein folding when certain cell types are subjected to internal or external stress or even under normal development

conditions (Hetz et al., 2020). The UPR is known to be mediated by three ER transmembrane sensors, each of which plays an important role in normal development: the RNA-dependent protein kinase-like ER eukaryotic translation initiation factor 2 alpha kinase (PERK), inositol-requiring enzyme 1 (IRE1), and activating transcription factor 6 (ATF6) (Godin et al., 2016; Mitra and Ryoo, 2019). The IRE1 and ATF6 signaling pathways mainly activate UPR downstream genes through the downstream effectors X-box-binding protein 1 (XBP1) and 50-kDa nuclear ATF6 (p50ATF6) to alleviate the ER stress response, but the PERK signaling pathway is dependent on eukaryotic translation initiation factor 2α (eIF2α) phosphorylation, which causes a reduction in global protein synthesis while selectively allowing the translation of mRNAs with specific upstream open reading frames (uORFs) in their 5′ untranslated regions (UTRs) (Haze et al., 1999; Calfon et al., 2002; Pakos-Zebrucka et al., 2016). The IRE1 branch is the primary UPR signaling pathway in mammals and has been previously recognized for its essential requirement in the developing liver and in the B cell lineage (Reimold et al., 2000; Reimold et al., 2001). Vertebrate species encode two isoforms of ATF6 (ATF6α and ATF6β), and experiments in mice with single- or double-gene knockout have demonstrated that ATF6α and ATF6β have a necessary but overlapping function in the early embryonic stage (Yamamoto et al., 2007). It has been recently found that dysfunction of ATF6 impedes mesodermal fate specification during development (Kroeger et al., 2018). The extraordinary role of the PERK branch of the UPR in secretory cells with a high protein load has been widely investigated by making use of gene targeting: PERK-knockout mice show dysfunction of islet β cells, pancreatic acinar cells, and cells within the skeletal system (Harding et al., 2001; Zhang et al., 2002; Iida et al., 2007; Gallot et al., 2019). Aside from the function of PERK in secretory cells, inhibition of PERK signaling results in stem cell accumulation in organoid cultures of the primary intestinal epithelium, which disrupts the differentiation of intestinal epithelial stem cells (Heijmans et al., 2013). More importantly, the regulatory effects of PERK also rely on activating transcription factor 4 (ATF4), which is the main downstream transcription factor of PERK-eIF2α-dependent translation in response to various physiological requirements. Notably, ATF4-knockout mice show developmental defects, including pancreatic hypertrophy and severe skeletal defects (Iida et al., 2007; Wang et al., 2009). The physiological activity of the PERK signaling pathway has been found to be tightly associated with the differentiation of some stem cells and embryonal organs; however, the general mechanism underlying this branch of the UPR in developmental processes remains to be elucidated.

Myogenesis is an elaborate process that involves the maintenance of stem and progenitor cells, lineage specification, and terminal differentiation (Bentzinger et al., 2012). During the early phase of embryonic development, progenitors are specified and determined to be myoblasts, and the first muscle fibers are established with differentiated mononucleated myocytes. Myocytes fuse to form multinucleated myofibers that reach a steady state, and progenitors will enter quiescence and henceforth reside within the matured muscle as satellite cells during the late phase of embryonic development (Tajbakhsh, 2009). Satellite cells have the potential to expand mitotically and differentiate to repair the muscle tissue and reestablish homeostasis, when mature muscle is damaged (Rudnicki et al., 2008). Many underlying signaling mechanisms control the genetic networks that promote myogenesis. Myogenic regulatory factors (MRFs), collectively expressed in the skeletal muscle lineage, are required for the terminal differentiation of myoblasts and the expression of myotube-specific genes. Myocyte enhancer factor 2 (MEF2) is a lynchpin for potentiating the function of MRFs through transcriptional cooperation. Satellite cells, the major mediators of myofiber regeneration in adults, are dominated genetically by transcription factor paired box 7 (PAX7), which further regulates downstream myogenic factors, such as myoblast determination protein 1 (MyoD) (Seale et al., 2000; Punch et al., 2009). *In vitro*, myoblast differentiation serves as a powerful model system for studying key signaling mechanisms that control genetic networks during myogenesis (Braun and Gautel, 2011). Intriguingly, the morphological hallmark of the myotube is a highly developed ER network, suggesting that the myogenic process is accompanied by ER membrane expansion, a physiological process facilitated by the UPR (Pedersen and Febbraio, 2012; Afroze and Kumar, 2019).

MicroRNAs (miRNAs), a new class of cell lineage regulators, are also involved throughout the process of embryonic development and cellular differentiation (Ivey and Srivastava, 2010; Vidigal and Ventura, 2015; Singh et al., 2020). Most importantly, many miRNAs, especially muscle-specific clusters, such as the miR-1a and miR-133 families, are required for muscle development and must be subject to strict dynamic regulation during rapid developmental transitions or changes in the cellular environment (Rao et al., 2006; Liu et al., 2007; Braun and Gautel, 2011). The well-established miR-206 is capable of regulating myogenesis by a negative-feedback mechanism, in which miR-206 is upregulated by MyoD and targets *Pax7* mRNA (Chen et al., 2010). Additionally, the highly coordinated and time-dependent UPR can be reciprocally regulated by flexible miRNA networks, which activate the adaptation program without triggering cell death pathways and induce gene transcription tailored to the cellular demand (Behrman et al., 2011; Amodio et al., 2016; Xu et al., 2016). PERK has been shown to contribute to the regulation of regenerative myogenesis, which is essential for the satellite cell homeostasis and differentiation of activated satellite cells into the myogenic lineage (Zismanov et al., 2016; Xiong et al., 2017). By using a myoblast differentiation system *in vitro*, we attempted to explore the functional requirements of the UPR branches during myogenesis and decipher the mechanism underlying the role of PERK signaling in controlling muscle differentiation by regulating miRNA networks.

In our study, knocking down PERK in C2C12 myoblasts resulted in a significantly changed expression of miRNAs related to pluripotency and differentiation. Then, we found that ATF4 directly mediated the transcription of some myomiRs during the early stage of myoblast differentiation. In addition, we found that PERK-regulated miR-128 targeted protein phosphatase 1 catalytic subunit gamma (*Ppp1cc*) mRNA, which is a key regulator of the UPR signaling pathway. We also found that cyclic AMP-regulated phosphoprotein 21 (ARPP21), the host gene

of miR-128-2 encoding an RNA-binding protein, antagonized miR-128 activity during late myogenesis. Based on these data, we propose a model in which a feedback loop between PERK signaling and miR-128 promotes myoblast differentiation.

MATERIALS AND METHODS

Animal

C57/BL6 mice were purchased from the Guangdong Medical Laboratory Animal Center, Guangdong, China. Mice were housed in the animal facility and had free access to water and standard rodent chow. Fetal (E12.5, E15.5, and E18.5) and postnatal (2 and 8 weeks) hind limb muscles were isolated for RNA and protein extraction.

Cell Cultures and Treatments

The mouse skeletal myoblast cell line C2C12 was obtained from the Shanghai Institute of Cell Biology, Chinese Academy of Science. Cells were cultured in a growth medium (GM), which consists of high-glucose Dulbecco's modified Eagle's medium (DMEM, Thermo Fisher) supplemented with 10% FBS (Thermo Fisher) and 1% penicillin/streptomycin (Thermo Fisher), at 37°C in 5% CO_2. Cells were plated and cultured to 100% confluence and were then transferred to a differentiation medium consisting of DMEM containing 2% horse serum (Thermo Fisher) and 1% penicillin/streptomycin for further culture. To inhibit the activity of the PERK signaling pathway, C2C12 cells were incubated with GSK2606414 (Selleck), and PBS was used as the negative control. Transfection of plasmid DNA was performed using ViaFect^{TM} Transfection Reagent (Promega), and all RNA transfections were performed at a final concentration of 50 nM using Lipofectamine 2000 (Thermo Fisher) according to the manufacturer's instructions.

RNA Extraction and qPCR Assays

Total RNA was extracted from mouse muscles or C2C12 cells with TRIzol reagent (Invitrogen) according to the manufacturer's instructions. First-strand cDNA for PCR analyses was synthesized with a PrimeScript^{TM} RT reagent kit (Takara). Real-time PCR was performed using SYBR Premix ExTaq^{TM} (Takara) in a sequence detection system (Thermo Fisher). The *C*t values were first normalized to those of the endogenous control (GAPDH or U6) and then normalized to those of the control group ($\Delta\Delta$CT method) to calculate the fold change between the control and experimental groups. All primer sets were synthesized by Synbio Technologies, and all primer sequences are listed in **Supplementary Tables 5–7**.

Protein Isolation and Western Blot Analysis

Tissue was homogenized and then lysed in ice-cold RIPA buffer (50mM of Tris–HCl (pH 7.4), 150mM of NaCl, 0.1% SDS, 1% sodium deoxycholate, 1% Triton X-100, 2 mM of EDTA, and 1× protease inhibitor cocktail). Samples were then centrifuged for 20 min at 4°C. Total protein extracts were loaded and separated by SDS-polyacrylamide gel electrophoresis (SDS-PAGE) and were then transferred to nitrocellulose membranes (Whatman). Membranes were then blocked with 5% milk for 1 h. Membranes were incubated with primary antibodies against MYOD (Proteintech Cat# 18943-1-AP), MEF2C (Proteintech Cat# 10056-1-AP), MyHC (R&D Cat# MAB4470), PERK (CST Cat# 3192), p-PERK (CST Cat# 3179), phospho-eIF2α (1:1000, CST Cat# 3398), eIF2α (CST Cat# 9722), ATF4 (CST Cat# 11815), p-ATF4(Ser219) (Thermo Fisher Cat# PA5-105835), ATF6 (CST Cat# 65880), IRE1α(CST Cat# 3294), PPP1CC (Proteintech Cat# 55150-1-AP), ARPP21 (Proteintech Cat# 55150-1-AP), c-Myc (CST Cat# 5605), KLF4 (CST Cat# 4038), Nanog (CST Cat# 8822), SOX2 (CST Cat# 4962), OCT4 (CST Cat# 2840), PAX7 (Proteintech Cat# 20570-1-AP), and GAPDH (Proteintech Cat# 55150-1-AP) overnight at 4°C. Horseradish peroxidase-conjugated secondary antibodies were used to detect the primary antibodies and protein signals were then visualized using Chemiluminescent HRP Substrate (Millipore, WBKLS0500).

Vector Construction

3′UTRs containing the putative binding site for miR-128 were cloned into the psiCHECK2 vector (Promega) backbone using the Xho I/Not I restriction enzymes. Genomic fragments of the miRNA precursors were cloned into pcDNA6.2 (Invitrogen). The shRNA oligonucleotides were annealed and cloned into the pLKO.1-TRC plasmid with Age I/EcoR I sites. Cignal 45-pathway reporter arrays, the ATF4 pathway reporter, the ATF6 pathway reporter, and the IRE1 pathway reporter, which measure the activity of the corresponding pathways were purchased from Qiagen. The ATF4 and PPP1CC coding sequence (CDS) was cloned in-frame into a reconstructive TRE3G vector with promoter EF1α for stable expression. The ARPP21-coding sequence (CDS) was cloned in-frame into the p3XFLAG-pCGH vector for stable expression. The primers used for vector construction are listed in **Supplementary Table 4**.

Lentiviral Transduction for the Establishment of Stable Cell Lines

The lentiviral vectors were co-transfected with the packaging vectors psPAX2 and pMD2.G (Addgene) into 293T cells. Supernatants containing viral particles were harvested and were then filtered through a 0.45-μM filter. To establish stable cell lines, C2C12 cells were infected with lentiviral particles, and polybrene (6 μg/mL, Sigma) was added to facilitate infection. After 48 h, the infected cells were subjected to selection in medium containing puromycin (3 μg/mL, Sigma) for 5 days.

Small RNA Sequencing and Analysis

Small RNA sequencing was performed by RiboBio Co., Ltd. Briefly, total RNA or purified sRNA fragments of the samples were extracted and were first ligated to the 3′-terminal and 5′-terminal linkers and then reverse-transcribed into cDNA. PCR amplification was carried out, and the gel was then cut to recover the target fragment library. *In silico* sequencing was performed on libraries that passed the quality inspection. Small RNAs were annotated by direct alignment to the genome and to various

known RNAs using bowtie. All miRNA target sites were further annotated using a mouse genome assembly (mm10). Functional enrichment analysis was performed using the DAVID functional annotation tools (Huang da et al., 2009).

Chromatin Immunoprecipitation (ChIP)

Chromatin immunoprecipitation (ChIP) was performed as described previously (Dong et al., 2014). Briefly, cross-linking was performed with C2C12 cells with 1% formaldehyde (Sigma), and nuclei were extracted using cell lysis buffer (20 mM of Tris–HCl (pH 8.0), 85mM of KCl, and 0.5% NP-40). Nuclei were lysed with nuclear lysis buffer [10 mM of Tris–HCl (pH 7.5), 1% NP40, 0.5% deoxycholate, and 0.1% SDS]. Chromatin/DNA complexes were sheared in a sonicator. Sonicated lysates were cleared and incubated overnight at 4°C with magnetic beads coupled to an anti-ATF4 antibody. The precipitated chromatin was eluted and reverse cross-linked in ChIP Elution Buffer (1% SDS and 0.1 M of NaHCO3) containing proteinase K and RNase A for 2 h at 65°C. The DNA was recovered and purified using a Qiagen PCR purification kit. Semiquantitative PCR or qPCR was performed to analyze the immunoprecipitated DNA. Primers are listed in **Supplementary Table 8**.

Luciferase Reporter Assays

C2C12 cells were transfected with different kinds of reporter plasmids for 48 h. Cells were then lysed in passive lysis buffer, and luciferase activities were measured with a Dual Luciferase Assay Kit (Promega) according to the manufacturer's instructions.

Migration Assays

For the migration assay, C2C12 cells transfected with miR-128 were suspended in 200 μL of FBS-free medium and were then seeded into the upper chamber of transwell inserts (8 μM pore size, Costar). The lower chamber of the transwell inserts was filled with 750 μL of medium supplemented with 10% FBS, which functioned as a chemoattractant. After 24 h of incubation at 37°C, cells that migrated to the lower surface of the insert membrane were fixed with methanol and stained with 0.1% crystal violet.

Cell Counting Kit-8 (CCK-8) Assays

For CCK-8 assays, cells were seeded at a concentration of 1×10^3 cells/well in 96-well plates. Cell numbers were quantified using CCK-8 reagent (Cat# CK04, DOJinDO) at the indicated time according to the manufacturer's instructions.

Colony Formation Assays

For colony formation assays, 1×10^3 cells were seeded into six-well plates. Colonies, which were allowed to form for 5 days after plating, were stained with a crystal violet solution and counted. Assays were done in triplicate.

Fluorescence Microscopy

C2C12 cells grown on glass coverslips were stained according to the manufacturer's instructions. The endoplasmic reticulum was stained using l g/mL of Alexa Fluor® 647 Concanavalin A Conjugates (Thermo Fisher Cat# A12379) for 1 h. The cytoskeleton was stained using l g/mL of Alexa Fluor™ 488 Phalloidin (Thermo Fisher Cat# C21421) for 30 min. Nuclei were labeled using DAPI for 15 min. Images were acquired on a ZEISS fluorescence microscope using a 20× or 40× objective.

Statistical Analysis

Quantitative data are presented as the mean ± the standard deviation (SD) from a minimum of three independent experiments. Comparisons between two groups were analyzed using Student's *t*-test, unless otherwise indicated. Statistical analyses were performed with GraphPad Prism 6 (GraphPad Software Inc.). $p < 0.05$ was considered to be statistically significant.

RESULTS

PERK Is Required for Myoblast Differentiation

To establish a system for studying myoblast differentiation, we utilized C2C12 mouse skeletal myoblasts obtained from the skeletal muscles of myodystrophic mice, which are often used for studying myogenesis *in vitro* (Yaffe and Saxel, 1977). When C2C12 myoblasts proliferated to a high confluence in growth medium, we replaced the medium with the differentiation medium. In the early differentiation stage, C2C12 myoblasts proliferated to myocytes and gradually fused. During differentiation, myocytes fused to form multinucleated myofibers (**Figure 1A**). The protein expression levels of differentiation markers, such as MyoD, MEF2C, and Myosin heavy chain (MyHC) protein, showed signature profiles during C2C12 myoblast differentiation (**Figure 1B**), indicating a consistent trend of skeletal muscle differentiation during embryonic development (**Figure 1C**).

The three sensors of UPR are involved in the differentiation of C2C12 myoblasts, as detected by western blot and reverse transcription quantitative PCR (RT–qPCR) and shown in **Figure 1D** and **Supplementary Figure 1A**. Note that the expression of *Perk* was upregulated on the first day of differentiation and then decreased gradually. Changes in the expression of *Ire1*α were not evident, while the expression of *Atf6* was strongly upregulated on day three of differentiation. Western blot and RT-qPCR showed that the three UPR sensors were highly expressed during the embryonic stage and that their expression then declined (**Figure 1E** and **Supplementary Figure 1B**).

To investigate the important roles of the three UPR sensors in myoblast differentiation, we knocked down their expression separately by constructing three stable lentivirus-mediated C2C12 cell lines expressing a small hairpin RNA (shRNA) against *Perk* (shPerk), *Atf6* (shAtf6), or *Ire1*α (shIre1α) (**Figure 1F** and **Supplementary Table 4**). We compared these knockdown C2C12 myoblasts with wild-type myoblasts 3 days after induction and differentiation and found that each UPR protein is important for myoblast differentiation. As shown in **Figures 1G,H**, disruption of *Ire1*α or *Atf6* expression markedly reduced the expression of MyHC and myotube formation. More

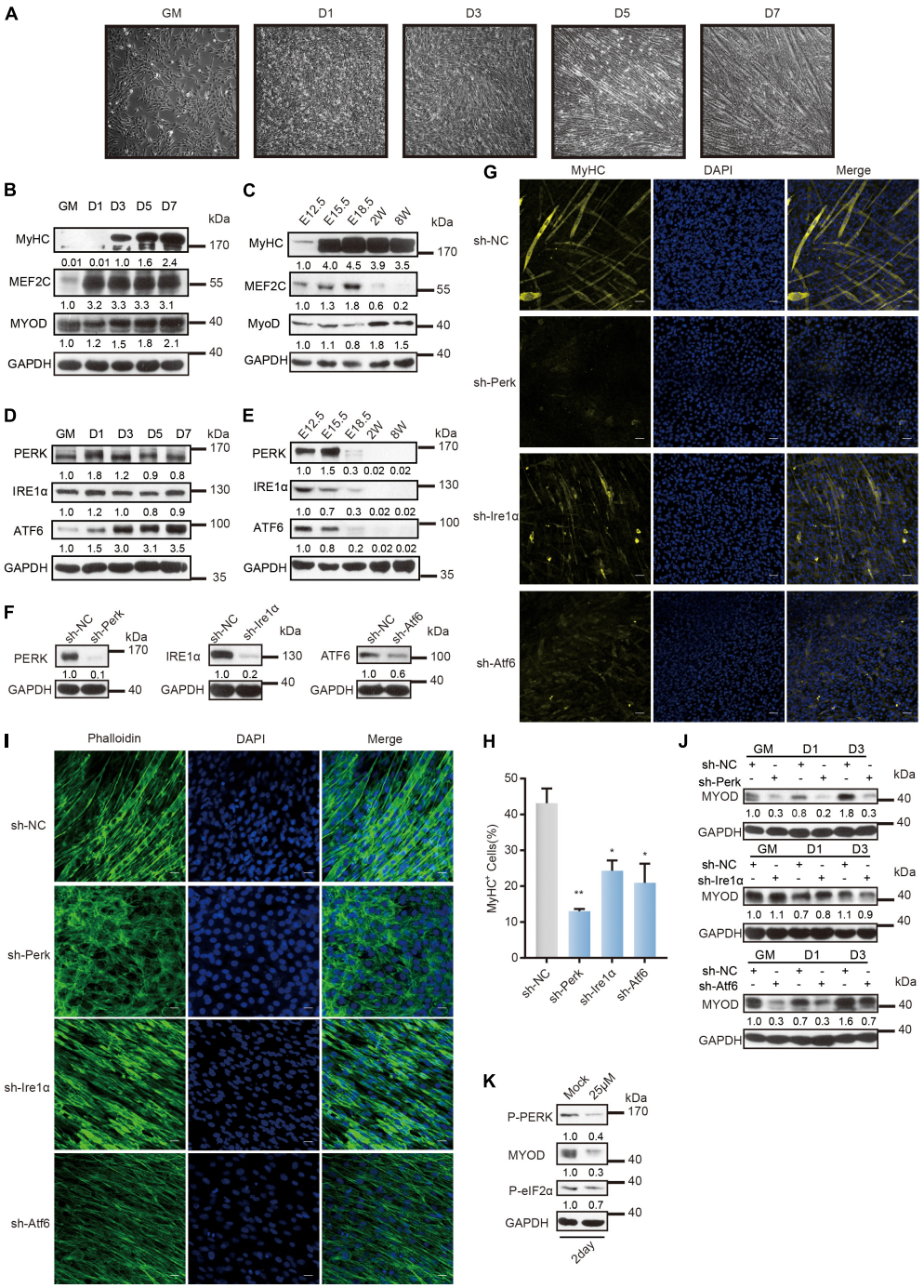

FIGURE 1 | Distinct role of UPR sensors during myoblast differentiation. **(A)** Phase-contrast microscopy of differentiating C2C12 myoblasts in growth medium (GM) or 1, 3, 5, or 7 days in the differentiation medium. **(B)** Western blot analysis of skeletal muscle differentiation markers in whole-cell lysates from differentiating C2C12 myoblasts. **(C)** Western blot analysis of skeletal muscle differentiation markers in tissue lysates from developing mouse embryo muscle. Mouse hind limb muscles were isolated at five time points: E12.5, E15.5, E18.5, postnatal week 2, and postnatal week 8 (adult). Skeletal muscle development in mice consists of embryonic development (E8.5/9-E14.5), fetal development (E14.5-E19), perinatal development (P0–3/4 weeks), and adult development (3/4 week-aging). **(D)** Western blot analysis of the three UPR sensors in whole-cell lysates from differentiating C2C12 myoblasts. **(E)** Western blot analysis of the three UPR sensors in tissue lysates from developing mouse embryo muscle. **(F)** Western blot analysis of whole-cell lysates from PERK-, IRE1α-, or ATF6-knockdown cells and negative control cells to determine the knockdown efficiency. **(G)** Effects of PERK, IRE1α, or ATF6 knockdown on MyHC expression and myotube formation. PERK-, IRE1α-, or ATF6-knockdown cells and negative control cells were incubated in differentiation medium for 3 days and were then stained with an anti-myosin antibody and DAPI (nuclei). Scale bar: 50 μm. **(H)** Quantification of percentage of $MyHC^{+}$ myotubes in wild-type and knockdown cells incubated in differentiation medium for 3 days.

(Continued)

FIGURE 1 | Continued
(I) Effects of PERK, IRE1α, or ATF6 knockdown on cell morphology changes. PERK-, IRE1α-, or ATF6-knockdown cells and negative control cells were incubated in differentiation medium for 3 days and were then fixed, permeabilized, and stained with phalloidin (F-actin) and DAPI (nuclei). Scale bar: 25 μm. **(J)** Western blots showing the effects of PERK, IRE1α, or ATF6 knockdown on the MyoD protein level. **(K)** Western blot analysis of MyoD in whole-cell lysates from C2C12 myoblasts under the optimal treatment time and PERK inhibitor (GSK2606414) concentration conditions. GAPDH was used as the internal control (A representative western blot is shown, $n = 3$.) The error bars indicate the mean ± standard deviation (SD) ($^*p < 0.05$, $^{**}p < 0.01$) from three independent experiments.

critically, disruption of *Perk* expression not only prevented the expression of MyHC and myotube formation but also affected cell morphology. We acquired images of cell morphology after phalloidin immunostaining for the cytoskeletal protein F-actin and found that PERK knockdown cells remained undifferentiated or even exhibited a rounded morphology, indicating that the PERK arm is a critical factor for myogenesis (**Figure 1I**).

Consistent with these results, western blot and RT-qPCR analyses revealed that knocking down each UPR sensor reduced the transcription and translation levels of *Myod* (**Figure 1J** and **Supplementary Figure 1C**). We found that knocking down IRE1α distinctly affected the MyoD protein level in C2C12 myoblasts only after differentiation was induced. Knocking down ATF6 immediately affected the MyoD protein level in C2C12 myoblasts before differentiation was induced, but the MyoD protein level in ATF6 knockdown cells recovered with differentiation. Importantly, knocking down PERK affected the MyoD protein level throughout the change in C2C12 myoblast fate. To further demonstrate the regulatory role of the PERK arm in *Myod* expression during myoblast differentiation, we treated C2C12 myoblasts with the PERK signaling pathway inhibitor GSK2606414, which inhibits the activation of the downstream pathway of PERK by inhibiting the autophosphorylation of PERK, at a concentration of 25 μM for 2 days (**Supplementary Figure 1D**). It was found that this high concentration of the PERK pathway inhibitor significantly inhibited the MyoD protein level (**Figure 1K**).

Taken together, these data indicated that the UPR has a crucial function in myogenesis, where PERK governs the initiation of myoblast differentiation and is required for the differentiation of myoblasts.

Knocking Down PERK Induces Dedifferentiation of C2C12 Myoblasts by Altering the miRNA Network

As PERK knockdown cells remained undifferentiated but the change in cell morphology implied their altered status, we characterized the PERK knockdown cells by their molecular signature. miRNAs are a class of cell lineage determinants, which can also be regarded as molecular indicators of cell type or functional states (Xie et al., 2013). We first profiled miRNA expression by performing small RNA sequencing (RNA-seq) and analysis of PERK knockdown and negative control cells after 3 days of induction of differentiation. Knocking down PERK globally affected miRNA expression in myoblasts; more than 200 miRNAs were changed, among which 112 were significantly upregulated and 117 were significantly downregulated (**Figure 2A** and **Supplementary Table 1**). The most significantly changed miRNAs were verified by RT-qPCR, and the results were consistent with the sequencing results (**Supplementary Figure 2A**). Interestingly, compared with the differentially expressed miRNAs in C2C12 cells differentiated for 3 days, some upregulated miRNAs involved in skeletal muscle differentiation, including many myogenesis-associated miRNAs, such as miR-133a, miR-133b, miR-206, miR-1a, and miR-128, were downregulated in PERK knockdown cells (**Figure 2A** and **Supplementary Table 2**). In contrast, many stemness-related miRNAs were upregulated in PERK knockdown cells (**Figure 2A** and **Supplementary Table 2**). Surprisingly, a class of X-linked miRNAs exist in the fragile X region of the X chromosome of placental mammals and perform an important regulatory function in the transition from proliferation to maturity during spermatogenesis; for example, miR-881, miR-871, miR-741, miR-465, miR-470, and miR-743b were significantly upregulated in PERK knockdown cells (**Figure 2A** and **Supplementary Table 2**) (Ramaiah et al., 2019). Among these miRNAs, miR-470 has been identified as a miRNA that is highly expressed in mouse embryonic stem cells (Tay et al., 2008). Comparison of the differential miRNA expression between PERK knockdown cells and differentiated C2C12 cells indicated that knocking down PERK impacts the state of myoblast differentiation by changing miRNA expression.

KEGG pathway analysis of the targets of the changed miRNAs further showed that the functions of the upregulated miRNAs (e.g., signaling pathway regulating pluripotency of stem cells) were related to the pluripotent state (**Figure 2B**). We further analyzed the activity of the signaling pathways associated with stemness in PERK knockdown cells by using the Qiagen's Cignal pathway reporter vector and dual fluorescence reporter system. Knocking down PERK markedly upregulated the activity of stemness-related signaling pathways, such as the Nanog, Wnt, Myc, Sox2, and Oct4 signaling pathways; in contrast, the TGFβ pathway, which promotes cell transdifferentiation, had no significant change (**Figure 2C** and **Supplementary Figure 2B**) (Cartwright et al., 2005). Meanwhile, knocking down PERK enhanced the expression of the two reprogramming factors *Myc* and *Klf4* (**Figures 2D,E**). The transcription level of the pluripotent stem cell marker *Nanog* was also significantly upregulated by more than 20-fold (**Figure 2D**). We further confirmed that PERK knockdown significantly promoted the stemness of cells by detecting the transcriptional level of lymphocyte antigen 6a/e (*Ly6a/e*), which is highly expressed in various progenitor cells during the differentiation and development of mesoderm cells (**Figure 2F**) (van de Rijn et al., 1989; Van Vlasselaer et al., 1994; Welm et al., 2002; van Bragt et al., 2005). Additionally, knocking down PERK dramatically enhanced the transcriptional level of C–X–C

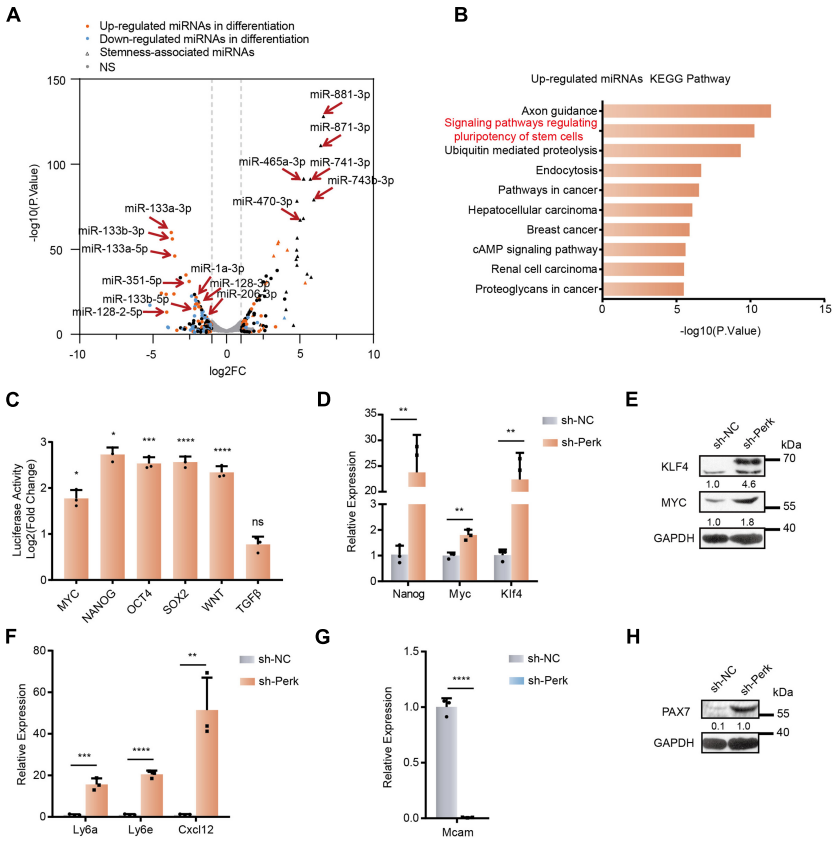

FIGURE 2 | MicroRNA profiles and stemness changes in C2C12 myoblasts upon PERK knockdown. **(A)** A volcano plot of differentially expressed miRNAs in PERK knockdown cells. PERK knockdown cells and negative control cells were differentiated for 3 days. **(B)** KEGG analysis of upregulated miRNAs in PERK-knockdown cells. **(C)** Luciferase reporter assay showing the effects of PERK knockdown on the activity of stemness or differentiation pathways. The exponential calculation on the ratio was employed between each individual experimental value and the control value in their calculations of the luciferase data. **(D)** RT-qPCR was used to detect the effects of PERK knockdown on reprogramming factors. **(E)** Western blots showing the effects of PERK knockdown on the expression of reprogramming factors. **(F)** The relative mRNA expression levels of the stem cell markers *Ly6a*, *Ly6e*, and *Cxcl12* in PERK knockdown cells and negative control cells. **(G)** The relative mRNA expression levels of the myoblast marker *Mcam* in PERK knockdown cells and negative control cells. **(H)** Western blots showing the effects of PERK knockdown on the expression of the satellite cells marker PAX7. GAPDH was used as the internal control (A representative western blot is shown, $n = 3$.) The error bars indicate the mean ± standard deviation (SD) (*$p < 0.05$, **$p < 0.01$, ***$p < 0.001$, ****$p < 0.0001$) from three independent experiments.

motif chemokine ligand 12 (*Cxcl12*), which maintains the stem cell characteristics of bone marrow mesenchymal stem cells (**Figure 2F**) (Peled et al., 1999; Janssens et al., 2018; Matsushita et al., 2020). Notably, PERK suppression also significantly impaired the characteristics of C2C12 myoblast, as we determined by assessing the transcriptional level of melanoma cell adhesion molecule (*Mcam*), which is highly expressed in proliferating myoblasts and significantly downregulated during fusion (**Figure 2G**) (Lapan and Gussoni, 2012; Alexander et al., 2016). PAX7, a marker of satellite cells, was obviously upregulated in PERK knockdown cells, which further demonstrated that dedifferentiation of myoblasts into satellite cells is truly occurring (**Figure 2H** and **Supplementary Figure 2C**). In order to further verify the effects of PERK knockdown on the characteristics of cells, we used cloning and CCK-8 to detect the proliferation rate of PERK knockdown cells and found that the proliferation rate of PERK knockdown cells was reduced (**Supplementary Figures 2D,E**).

Together, these findings indicated that knocking down PERK induced dedifferentiation of myoblasts into stem-like cells by effectively altering key miRNAs and their networks in cell fate determination. These results demonstrated that PERK plays an important role in the formation, maintenance, and differentiation of myoblasts.

The PERK-ATF4 Signaling Pathway Transactivates Differentiation-Associated miRNAs in the Early Stage of Myoblast Differentiation

It is well known that activation of PERK can reduce general translational initiation through eIF2α phosphorylation, which can specifically activate the translation of *Atf4*. ATF4 is the major downstream transcriptional activator of the PERK-eIF2α pathway and may direct the induction of specialized transcriptomes including both coding and non-coding RNAs in response to various physiological stresses (Hinnebusch and Natarajan, 2002; Ron and Walter, 2007; Wang et al., 2009). To investigate whether PERK regulates miRNA expression by activating ATF4 in myoblasts, we first examined the

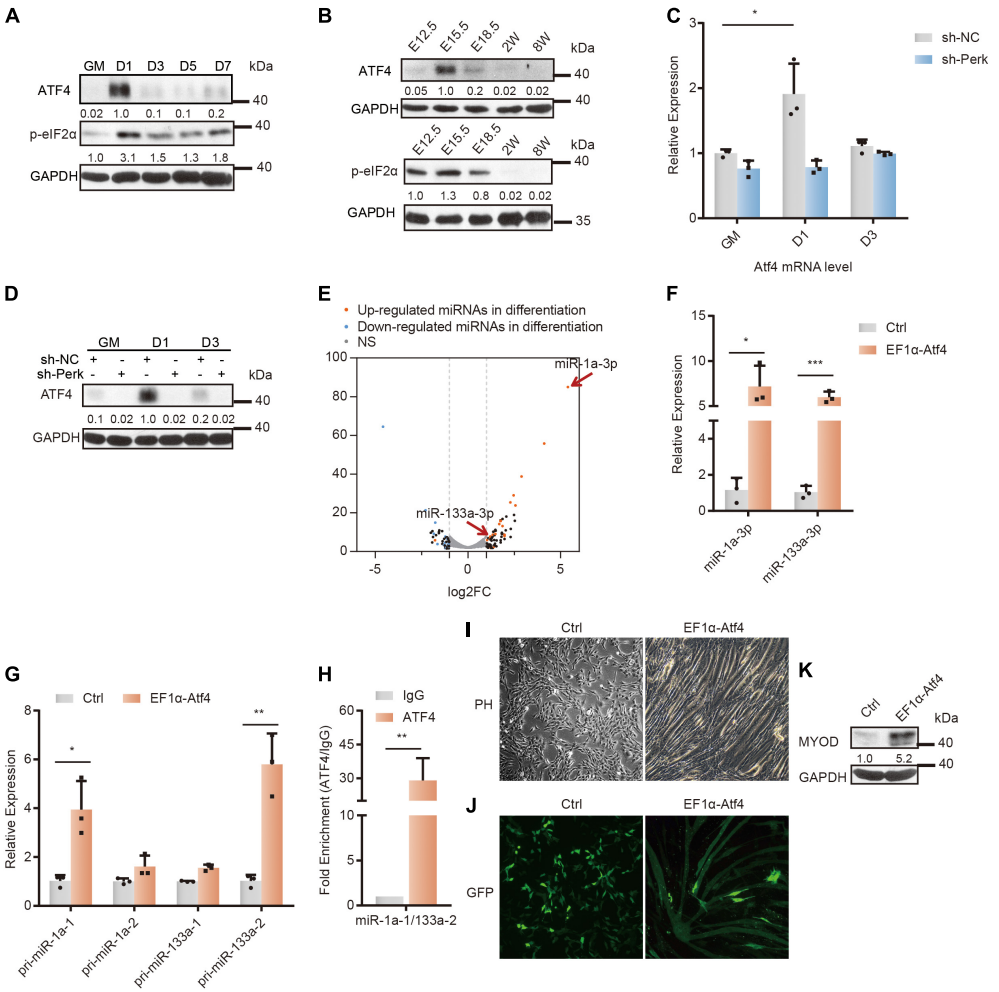

FIGURE 3 | Changes in the microRNA profile and differentiation of C2C12 myoblasts upon ATF4 overexpression. **(A)** Western blot analysis of p-eif2α and ATF4 in whole-cell lysates from differentiating C2C12 myoblasts. **(B)** Western blot analysis of p-eif2α and ATF4 in tissue lysates from developing mouse embryo muscle. **(C)** RT-qPCR was used to detect the effects of PERK knockdown on the transcription level of *Atf4*. **(D)** Western blots showing the effects of PERK knockdown on the ATF4 protein level. **(E)** A volcano plot of differentially expressed miRNAs in ATF4-overexpressing cells. ATF4-overexpressing cells and negative control cells were incubated in growth medium and allowed to proliferate to 80% confluence. **(F)** The relative expression levels of miR-1a-3p and miR-133a-3p in ATF4-overexpressing cells and negative control cells. **(G)** The relative expression levels of primary transcripts of miR-1a and miR-133a in ATF4-overexpressing cells and negative control cells. **(H)** ChIP-qPCR for validation of the ATF4 binding sites in the common promoter region of miR-1a-1 and miR-133a-2. **(I)** Phase-contrast microscopy of ATF4-overexpressing cells or negative control cells in growth medium showing the effects of ATF4 overexpression on myoblast differentiation and myotube formation. **(J)** Fluorescence microscopy of ATF4-overexpressing cells or negative control cells transiently transfected with the same amount of monomeric green fluorescent protein (mGFP) in growth medium showing the effects of ATF4 overexpression on myoblast differentiation and myotube formation. Normal myoblasts do not have enough space to continue to grow after the confluence of the culture reaches 100%, so they must be passaged. **(K)** Western blots showing the effects of ATF4 overexpression on the expression of Myod. GAPDH was used as the internal control (A representative western blot is shown, $n = 3$). The error bars indicate the mean ± standard deviation (SD) (*$p < 0.05$, **$p < 0.01$, ***$p < 0.001$) from three independent experiments.

expression of *Atf4* during myoblast differentiation and compared it with the expression pattern of its upstream PERK-eIF2α signaling mediator phosphorylated eIF2α. Immediately after the differentiation of C2C12 myoblasts was induced, ATF4 was markedly upregulated and then rapidly downregulated, consistent with the activation of eIF2α phosphorylation both *in vitro* and *in vivo* (**Figures 3A,B** and **Supplementary Figures 3A,B**), indicating that ATF4 plays an important role in the early stage of myoblast differentiation. We further confirmed that PERK knockdown inhibited the transcriptional activity of ATF4 by ATF4 signaling pathway reporter vector and dual fluorescence reporter assays (**Supplementary Figure 3C**). The western blot and RT-qPCR results further verified that PERK knockdown suppressed the ATF4 protein level but only slightly affected its transcription (**Figures 3C,D**).

To study the relationship between the ATF4 activation and miRNA expression, we constructed an ATF4 overexpression

vector and introduced it into C2C12 cells (**Supplementary Figures 3D,E**, and **Supplementary Table 4**). Small RNA-seq and analysis showed that ATF4 overexpression partially regulated the differentiation-related miRNA expression profile in myoblasts under undifferentiation conditions (**Figure 3E**). Evidently, miR-133a and miR-1a, specific miRNAs for skeletal muscle differentiation, were upregulated in ATF4-overexpressing cells (**Figures 3E,F** and **Supplementary Table 3**). This typical change in the miRNA profile strongly suggests that ATF4, the PERK-activating transcription factor, can promote myoblast differentiation by regulating miRNA networks.

Furthermore, the primary transcripts of miR-133a-2 and miR-1a-1 were verified to be upregulated by ATF4 overexpression (**Figure 3G**). Subsequently, as miR-133a-2 and miR-1a-1 are derived from the same polycistronic miRNA and co-transcribed, we performed ChIP with an anti-ATF4 antibody in ATF4-overexpressing cells to further determine that ATF4 can regulate the transcription of miR-133a-2 and miR-1a-1 (Chen et al., 2006). By searching for potential ATF4-binding sites in the promoter region of these specific miRNA genes and designing qPCR primers for ChIP-qPCR, we found substantial binding of ATF4 in the promoter region of miR-1a-1 and miR-133a-2, indicating that ATF4 directly bound to the promoter region of these specific miRNA genes to promote their expression (**Figure 3H**).

As a result of differentiation initiation, ATF4 overexpression obviously impaired the proliferation of C2C12 myoblasts (**Supplementary Figure 3F**). Moreover, ATF4-overexpressing cells fused with each other in the growth medium not supplemented with any pro-differentiation factors (**Figure 3I**). In the growth medium, the fluorescent protein GFP was clearly expressed in myotube-like fused ATF4-overexpressing cells, illustrating that ATF4 can facilitate cell fusion and myoblast differentiation (**Figure 3J**). The RT-qPCR results further verified that ATF4 overexpression significantly increased the transcriptional level of myoblast fusion factors myomaker (*Mymk*) and myomixer (*Mymx*) (**Supplementary Figure 3G**) (Millay et al., 2013; Leikina et al., 2018). Importantly, overexpression of only ATF4 increased the MyoD protein level, which demonstrated that ATF4 can activate the differentiation program in myoblasts (**Figure 3K**).

Taken together, these results indicated that ATF4 facilitated the expression of a set of differentiation-associated miRNAs. This finding suggests that the PERK-ATF4 pathway is the major signaling pathway for miRNA regulation during myoblast differentiation and that ATF4, as a PERK-activating transcription factor, plays a key role in cell differentiation and fate determination.

A Positive Feedback Loop Is Formed Between PERK-Regulated miR-128 and UPR by Regulating Ppp1cc in Myoblast Differentiation

To further identify the miRNAs affected by the PERK signaling pathway during myoblast differentiation, we first identified significantly downregulated miRNAs in PERK knockdown cells by using small RNA-seq data. Unsurprisingly, myogenesis-associated miRNAs (mamiRs) that play important roles in signaling pathways were identified (**Figure 4A**) (Xie et al., 2018). As miR-128 was one of the most markedly downregulated mamiRs in PERK knockdown myoblasts (**Figures 4A,B**), we next investigated whether miR-128 is deeply implicated in myoblast differentiation. Immunofluorescence staining for MyHC showed that miR-128 promoted myoblast differentiation and myotube formation (**Figures 4C,D**). In addition, the larger size of the ER in the miR-128-overexpressing cells was corroborated by labeling the differentiated C2C12 myoblasts with the endoplasmic reticulum-specific probe concanavalin A (**Figures 4E,F**), implying a potential functional mechanism of miR-128 in the UPR. Furthermore, miR-128 promoted cell migration, a necessary step in the early differentiation of myoblasts, which requires greatly increased cell surface protein synthesis in the endoplasmic reticulum (**Figure 4G**). The transcriptional level of the myoblast fusion factors *Mymk* and *Mymx* was also significantly upregulated in miR-128-overexpressing cells (**Supplementary Figures 4A,B**). In addition, miR-128 overexpression immediately increased the expression of *Myod* after the differentiation of C2C12 myoblasts was induced (**Supplementary Figures 4C,D**). These observations indicated that miR-128 is involved in the early phase of myoblast differentiation by regulating UPR-associated physiological functions.

To further investigate the potential targets of miR-128 related to the UPR, we combined UPR-associated genes with predicted miR-128 targets from our previous Ago2-PAR-CLIP data and TargetScan database analysis and found that the mRNAs of multiple factors related to the UPR may be regulated by miR-128 (**Figure 4H**) (Xie et al., 2018). We introduced these potential targets and important regulators of the UPR pathway into String online software to explore their functional relationships and found that *Ppp1cc*, *Nfe2l2*, and *Map2k7* are closely related to the UPR pathway (**Supplementary Figure 4E**). To verify the interactions between miR-128 and its potential targets, we constructed Renilla luciferase reporter vectors containing either a wild-type or mutant binding site for the potential target and transfected them into C2C12 cells. Among the potential targets we selected, miR-128 had a relatively high ability for direct binding to the target sites in *Ckap4*, *Ppp1cc*, *Map2k7*, *Nfe2l2*, *Eif2s2*, and *Ngly1* (**Figure 4I**). miR-128 significantly decreased the mRNA level of *Ppp1cc* in this group of potential targets (**Figure 4J**). The PPP1CC protein level was also markedly inhibited by miR-128, further verifying that miR-128 can potently block endogenous translation of *Ppp1cc* (**Figure 4K**).

Of note, the primary regulatory mechanism for the ATF4 protein level depends on the p-eIF2α-mediated translational mechanism, which is destabilized by a catalytic subunit (PP1) and a regulatory subunit, either GADD34 induced by ATF4 or the constitutively expressed paralogue CReP (Novoa et al., 2001). To study the relationship between PPP1CC and myoblast differentiation, we further generated stable PPP1CC overexpression and PPP1CC knockdown C2C12 cells (**Supplementary Figures 5A,B** and **Supplementary Table 4**). PPP1CC overexpression inhibited the phosphorylation

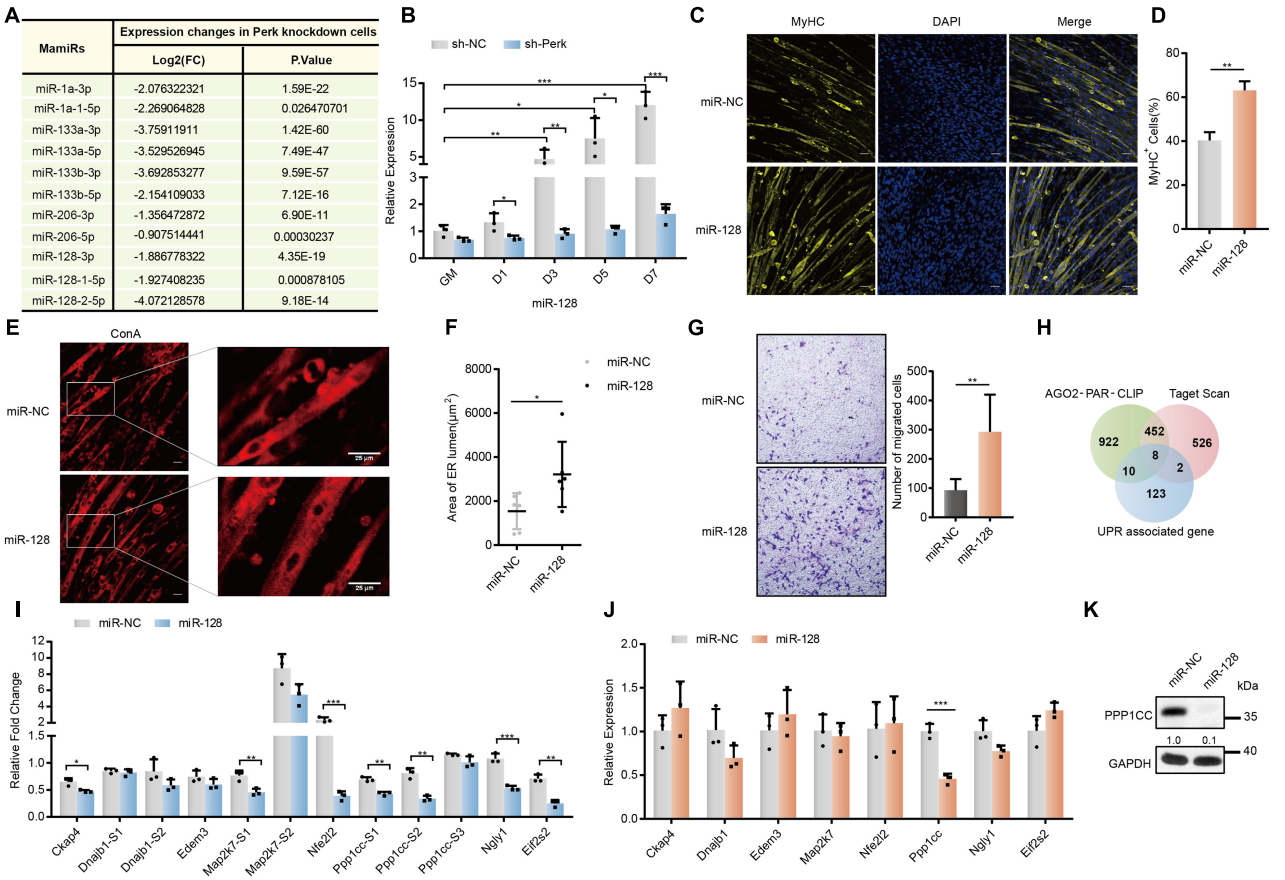

MamiRs	Expression changes in Perk knockdown cells	
	Log2(FC)	P.Value
miR-1a-3p	-2.076322321	1.59E-22
miR-1a-1-5p	-2.269064828	0.026470701
miR-133a-3p	-3.75911911	1.42E-60
miR-133a-5p	-3.529526945	7.49E-47
miR-133b-3p	-3.692853277	9.59E-57
miR-133b-5p	-2.154109033	7.12E-16
miR-206-3p	-1.356472872	6.90E-11
miR-206-5p	-0.907514441	0.00030237
miR-128-3p	-1.886778322	4.35E-19
miR-128-1-5p	-1.927408235	0.000878105
miR-128-2-5p	-4.072128578	9.18E-14

FIGURE 4 | Screening of potential targets for miR-128 regulated by PERK. **(A)** Changes in the expression of mamiRs in PERK knockdown cells. **(B)** The relative expression levels of miR-128 in PERK knockdown cells and negative control cells. **(C)** Effects of miR-128 overexpression on MyHC expression and myotube formation. miR-128-overexpressing cells and negative control cells were incubated in differentiation medium for 3 days and were then stained with an anti-myosin antibody and DAPI (nuclei). Scale bar: 50 μm. **(D)** Quantification of percentage of $MyHC^{+}$ myotubes in wild-type and miR-128-overexpressing cells incubated in differentiation medium for 3 days. **(E)** Effects of miR-128 overexpression on endoplasmic reticulum expansion. miR-128-overexpressing cells and negative control cells were incubated in differentiation medium for 3 days and were then fixed, permeabilized, and stained with Concanavalin A (endoplasmic reticulum). Scale bar: 25 μm. **(F)** The area of ER lumen was quantified by measuring the area of the ER lumen stained with Concanavalin A in the photographs. Values for the area of ER lumen from chosen two multinucleated myofibers of each photograph. **(G)** Cell migration assay showing the effects of miR-128 overexpression on myoblast migration. **(H)** Venn diagram showing the proportion of UPR-associated genes targeted by miR-128 as indicated by AGO2-PAR-CLIP or potentially targeted by miR-128 as indicated by TargetScan database analysis. **(I)** Luciferase reporter assay showing the effects of miR-128 on the wild-type (WT) or mutant (MT) reporter constructs. All luciferase activity levels were normalized to those of firefly luciferase driven by a single promoter in the reporter vector. **(J)** qRT-PCR assays showing the effects of miR-128 overexpression on potential targets. **(K)** Western blots showing the effects of miR-128 overexpression on the potential target *Ppp1cc*. GAPDH was used as the internal control (A representative western blot is shown, $n = 3$). The error bars indicate the mean ± standard deviation (SD) (*$p < 0.05$, **$p < 0.01$, ***$p < 0.001$) from three independent experiments.

of eIF2α and reduced the expression of total ATF4, but PPP1CC knockdown promoted the phosphorylation of eIF2α without the increase in the total ATF4 protein level resulting from the increased phosphorylation level of ATF4 (**Figures 5A,B**), indicating that PPP1CC can regulate the activity of the p-eIF2α-dependent signaling pathway. Unexpectedly, PPP1CC overexpression strikingly prevented the expression of MyHC and myotube formation (**Figures 5C,D**). Meanwhile, we photographed their cell morphology and found that PPP1CC-overexpressing cells remained undifferentiated, with a morphology similar to the rounded morphology of PERK knockdown cells (**Figure 5E**). Western blot analysis further verified that PPP1CC overexpression led to a decrease in protein levels of MyHC and MyoD (**Figure 5F**). However, knocking down PPP1CC could promote levels of MyoD in C2C12 myoblasts that were incubated in the growth medium (**Figure 5G**). Considering this result, we determined that inhibition of Ppp1cc by miR-128 is crucial for myoblast differentiation.

To further verify the mechanism by which miR-128 regulates the UPR signaling pathway, we used the Cignal 45 signaling pathway reporting system to analyze the function of miR-128 in myoblasts. Importantly, the signaling pathway most significantly upregulated by miR-128 was the ATF6 pathway, while the pathway most obviously downregulated by miR-128 was the ATF4 pathway (**Figure 5H**). We found miR-128 promoted

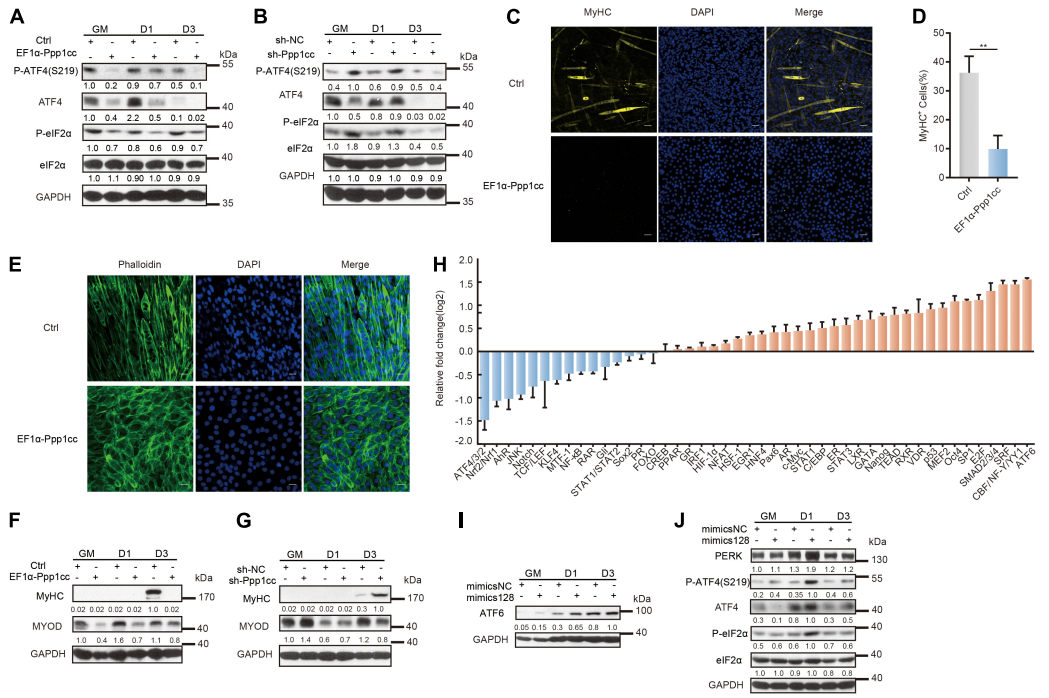

FIGURE 5 | Ppp1cc is the target of miR-128 in a positive feedback loop regulating the UPR during C2C12 myoblast differentiation. **(A)** Western blots showing the effects of PPP1CC overexpression on the p-eIF2α-ATF4 signaling pathway during C2C12 myoblast differentiation. **(B)** Western blots showing the effects of PPP1CC knockdown on p-eIF2α-ATF4 signaling pathway during C2C12 myoblast differentiation. **(C)** Effects of PPP1CC overexpression on MyHC expression and myotube formation. PPP1CC-overexpressing cells and negative control cells were incubated in differentiation medium for 3 days and were then stained with an anti-myosin antibody and DAPI (nuclei). Scale bar: 50 μm. **(D)** Quantification of percentage of MyHC^{+} myotubes in wild-type and PPP1CC-overexpressing cells incubated in differentiation medium for 3 days. **(E)** Effects of PPP1CC overexpression on the morphology of myoblasts. PPP1CC-overexpressing cells and negative control cells were incubated in differentiation medium for 3 days and were then fixed, permeabilized, and stained with Phalloidin (F-actin) and DAPI (nuclei). Scale bar: 25 μm. **(F)** Western blots showing the effects of PPP1CC overexpression on the protein level of MyHC and MyoD during C2C12 myoblast differentiation. **(G)** Western blots showing the effects of PPP1CC knockdown on the protein level of MyHC and MyoD during C2C12 myoblast differentiation. **(H)** Luciferase reporter assay showing the effects of miR-128 overexpression on the activity of signaling pathways. The exponential calculation on the ratio was employed between each individual experimental value and the control value in their calculations of the luciferase data. **(I)** Western blots showing the effects of miR-128 overexpression on the ATF6 protein level during C2C12 myoblast differentiation. **(J)** Western blots showing the effects of miR-128 overexpression on the p-eIF2α-ATF4 signaling pathway during C2C12 myoblast differentiation. GAPDH was used as the internal control (A representative western blot is shown, $n = 3$). The error bars indicate the mean ± standard deviation (SD) (**$p < 0.01$) from three independent experiments.

the ATF6 protein level in C2C12 myoblasts on the first day of induced differentiation (**Figure 5I**). Intriguingly, miR-128 immediately suppressed the total ATF4 protein level in the growth medium, but this effect was impaired when myoblasts were induced to differentiate (**Figure 5J**). Once myoblasts were induced to differentiate, miR-128 promoted the phosphorylation of eIF2α and further enhanced the translation of *Atf4*, but the phosphorylation of ATF4 on S219 was simultaneously promoted (**Figure 5J**). It has been reported that the f-box protein bTrCP, the receptor component of the E3 ubiquitin ligase SCF, can co-localize with ATF4 in the nucleus and bTrCP can control its stability by identifying the phosphorylated S219 site on ATF4 to promote the degradation of ATF4 (Lassot et al., 2001). The phosphatase PP1 is implicated in promoting the translation of *Atf4* and dephosphorylating ATF4 on S219, which is in turn implicated in regulating ATF4 to control the total ATF4 protein level in a time- and dose-dependent manner (Frank et al., 2010). The above experimental results indicate that miR-128 can regulate the activity of the PERK-eIF2α pathway by a positive feedback regulation of eIF2α phosphorylation and further promote the degradation of its downstream effector ATF4 by its phosphorylation on S219 to maintain the ATF4 protein level within a certain range and allow it to perform its functions within this range (**Supplementary Figure 5C**).

Together, our results suggest that PERK-regulated miR-128 is important for myoblast differentiation and that a positive feedback loop is formed between miR-128 and the UPR via the phosphatase subunit PPP1CC during myogenesis.

ARPP21 Antagonizes miR-128 Activity by Co-regulating the Phosphatase Subunit PPP1CC During Myoblast Differentiation

ARPP21, encoding by the host gene of miR-128-2, has been implicated in different aspects of posttranscriptional regulation by binding mRNAs and interacting with the translation initiation complex eIF4F to prevent its association with uridine-rich elements in the 3′UTRs of miR-128 target genes during neural

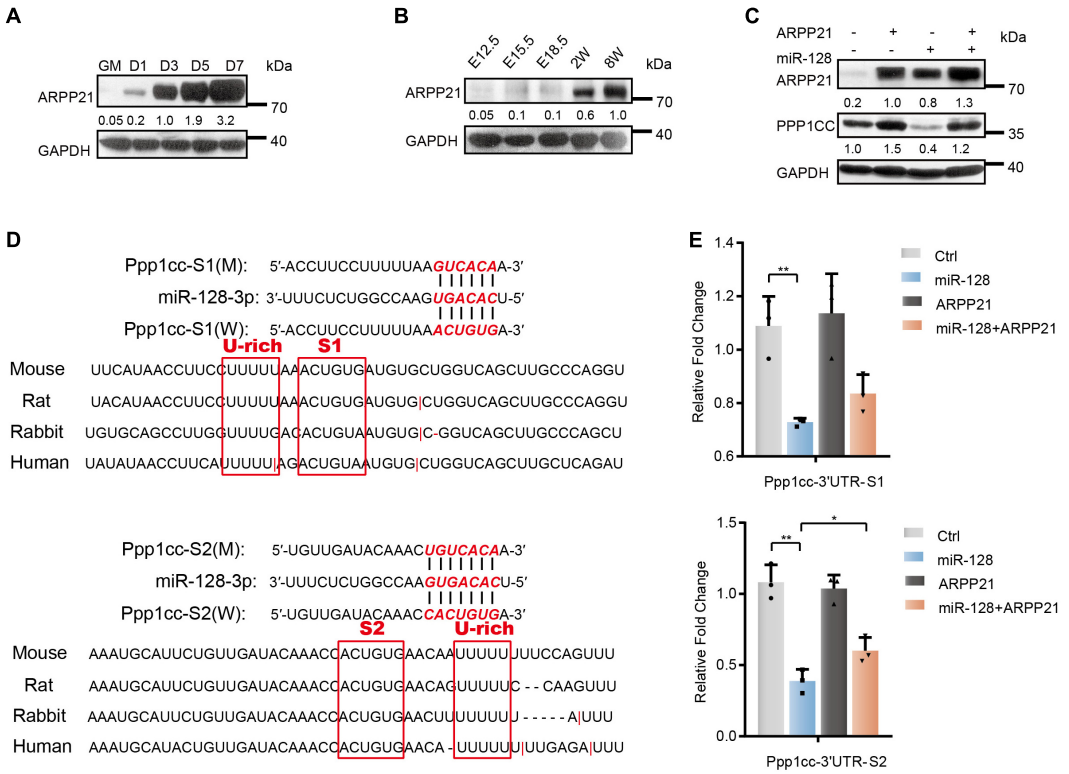

FIGURE 6 | Antagonistic effect of ARPP21 and miR-128 on Ppp1cc mRNA. **(A)** Western blot analysis of ARPP21 in whole-cell lysates from differentiating C2C12 myoblasts. **(B)** Western blot analysis of ARPP21 in tissue lysates from developing mouse embryo muscle for ARPP21. **(C)** Western blots showing PPP1CC protein levels. ARPP21 leads to increased protein expression of PPP1CC. miR-128 leads to reduced expression of PPP1CC. ARPP21 rescued the inhibitory effects of miR-128 on *Ppp1cc*. **(D)** Sequence analysis of the *Ppp1cc* 3′UTR. **(E)** Luciferase reporter assay results showing the effects of miR-128 and ARPP21 on the 3′UTR reporter constructs. GAPDH was used as the internal control (A representative western blot is shown, $n = 3$). The error bars indicate the mean ± standard deviation (SD) (*$p < 0.05$, **$p < 0.01$) from three independent experiments.

development (Rehfeld et al., 2018). To study the endogenous function of ARPP21 during myoblast differentiation, we first evaluated the expression of *Arpp21*. As shown, the ARPP21 protein level was markedly upregulated during the differentiation of C2C12 myoblasts (**Figure 6A**). We also examined levels of ARPP21 in skeletal muscle tissue samples from mouse embryos to determine whether the expression pattern described above is related to the *in vivo* function of ARPP21 in the context of organism development (**Figure 6B**). To further demonstrate whether the miR-128-mediated repression of *Ppp1cc* mRNA can be alleviated by ARPP21, we first detected the PPP1CC protein level in stable ARPP21-overexpressing cells (**Figure 6C**). We found that ARPP21 overexpression increased the PPP1CC protein level. Importantly, this effect was reversed by exogenous expression of miR-128 mimics, which led to a marked reduction in the PPP1CC protein level. As shown in **Figure 6D**, the uridine-rich element was adjacent to the miR-128 seed sequence in the 3′UTR of *Ppp1cc*. To further investigate the role of the *Ppp1cc* 3′UTR in ARPP21-mediated regulation, we constructed a Renilla luciferase (RL) reporter vector containing segments of the *Ppp1cc* 3′UTR. The reporter activity was normalized to the activity of co-expressed firefly luciferase (FL). We found that treatment of ARPP21-overexpressing cells with miR-128 mimics, preventing the repression of RL-Ppp1cc-S2 mRNA by miR-128, abolished the effects of ARPP21 on the activity of this reporter (**Figure 6E**).

Together, the above experiments indicate that the progressive ARPP21 during myoblast differentiation can reduce the inhibitory effects of miR-128 on *Ppp1cc*, negatively regulate miR-128, and avoid the constitutive UPR activity mediated by miR-128. This mechanism is consistent with the inactivation of stress responses, including the UPR, when myoblasts enter homeostasis at a later stage of differentiation.

DISCUSSION

Our study reveals the mechanism of PERK signaling in regulating miRNA networks during myoblast differentiation. A schematic of the molecular regulatory mechanism is shown in **Figure 7**. In the early stage of myoblast differentiation, stress responses, including the UPR, are activated in myoblasts. Once the PERK signaling pathway, one arm of the UPR, is activated, the downstream effector-phosphorylated eIF2α immediately promotes the translation of mRNAs with uORF structures, producing a large number of specific proteins, including ATF4. ATF4 can enter the nucleus, further activating

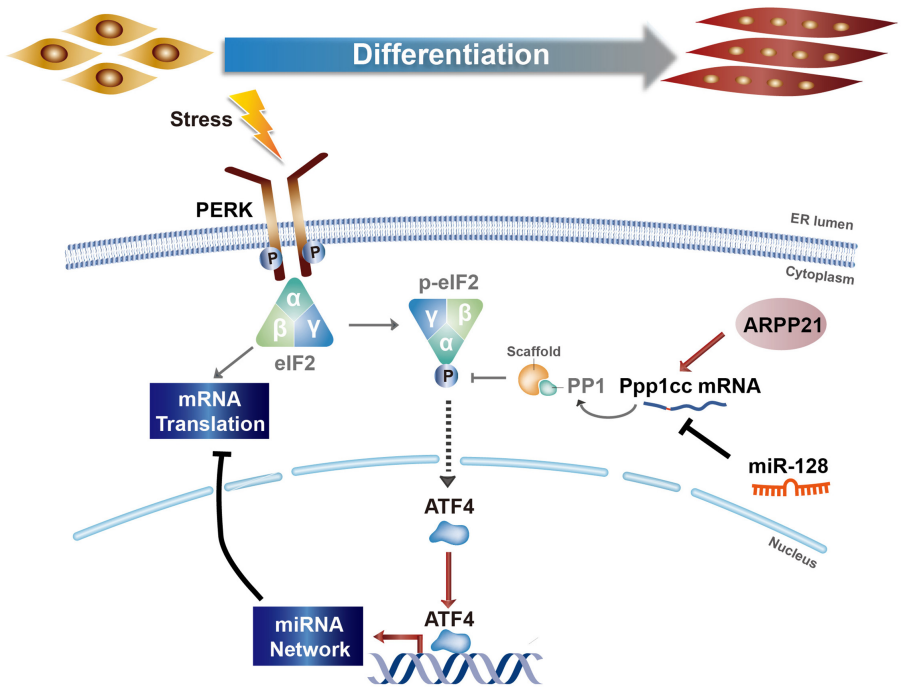

FIGURE 7 | Model of the regulatory relationship between PERK and miRNA networks during myoblast differentiation.

the downstream transcription of specific genes, including many miRNA genes. Our study verified that ATF4, as a downstream effector of PERK signaling, can directly promote the expression of myomiRs, such as miR-1a and miR-133a, in myoblasts. Subsequently, miRNAs activated by the PERK signaling pathway can regulate the posttranscriptional level of a large number of mRNAs in the cytoplasm and inhibit their translation, resulting in dynamic changes in the proteome during myoblast differentiation. In addition, PP1 phosphatase catalytic subunit PPP1CC, the main regulatory protein of p-eIF2α dephosphorylation, was inhibited by PERK-regulated miR-128 during myoblast differentiation, demonstrating that a novel mechanism involving a positive feedback loop between miRNAs and the UPR is active in promoting myoblast differentiation in the early stage. Intriguingly, this mechanism not only positively regulates the functional activity of phosphorylated eIF2α but also promotes the phosphorylation and degradation of ATF4 so that the ATF4 protein level is maintained within a certain range. Along with the process of differentiation, the RNA-binding protein ARPP21, the product of the miR-128-2 host gene *Arpp21*, can antagonize the function of miR-128, thus promoting the expression of *Ppp1cc*, weakening the activity of the PERK-eIF2α signaling pathway and maintaining the homeostasis of myoblast differentiation.

PERK can affect miRNA networks associated with stemness and differentiation to determine the fate of myoblast differentiation, and it is interesting to determine whether this is a common mechanism in the process of cell differentiation. We therefore selected P19 mouse embryonic carcinoma cells for further research. We profiled miRNA expression in PERK knockdown P19 cells and negative control cells and found that knocking down PERK significantly affected the expression of a set of miRNAs, including 103 significantly upregulated miRNAs and 113 significantly downregulated miRNAs (**Supplementary Figures 6A,B** and **Supplementary Table 9**). The miRNA expression profile of PERK knockdown P19 cells was compared with those of undifferentiated P19 cells and P19 cells induced to differentiate into neurons for 4 days (**Supplementary Table 10**) (Huang et al., 2009). As expected, many miRNAs upregulated in P19 cell differentiation were downregulated in PERK knockdown P19 cells. KEGG pathway analysis of the targets of these differentially expressed miRNAs showed that the upregulated miRNAs were related to the pluripotent state (e.g., signaling pathway regulating pluripotency of stem cells) (**Supplementary Figure 6D**). We further determined that PERK suppression significantly upregulated the activity of stemness-related signaling pathways, such as the Nanog signaling pathway (**Supplementary Figure 6F**). Western blot analysis also showed that PERK knockdown significantly enhanced the NANOG protein level (**Supplementary Figure 6E**). These observations and analysis indicated that PERK regulates cell differentiation and fate determination through miRNA networks in different kinds of cells.

The UPR is a highly conserved signaling pathway that maintains endoplasmic reticulum homeostasis during the developmental process. Many studies have shown that the downstream effectors regulated by the three UPR sensors (PERK, IRE1, and ATF6) can affect the transcription and translation of a series of genes and participate in the regulation of cell growth, differentiation, and stemness maintenance.

Our study reveals that PERK signaling acts as the main regulatory factor in the fate determination of myoblasts through regulating miRNA networks, further expanding our understanding of PERK signaling pathways in cell differentiation and biological development.

DATA AVAILABILITY STATEMENT

Small RNA sequencing data that support the findings of this study have been deposited in the Gene Expression Omnibus (GEO) under accession codes GSE167878.

ETHICS STATEMENT

The animal study was reviewed and approved by Institutional Animal Care and Use Committee of Sun Yat-sen University.

AUTHOR CONTRIBUTIONS

L-HQ supervised the project. L-HQ, Y-YT, and YZ designed the experiments. Y-YT, YZ, S-JX, and P-PC performed the experiments. Y-YT, YZ, BL, L-LZ, S-QM, and Q-JH analyzed the data. L-HQ, Y-YT, YZ, and Y-WO wrote the manuscript. All authors contributed to the article and approved the submitted version.

FUNDING

This work was supported by the National Natural Science Foundation of China (31970604, 31801075, 31900903, 31771459, and 31701116); the Major Research plan of the National Natural Science Foundation of China (91940000); the Fundamental Research Funds for the Central Universities (20lgpy112); and the Science and Technology New Star in ZhuJiang Guangzhou city [201806010151]. This research was supported in part by the Guangdong Province Key Laboratory of Computational Science (13lgjc05) and the Guangdong Province Computational Science Innovative Research Team (14lgjc18).

ACKNOWLEDGMENTS

We thank Xiao-Hong Cheng for help with the technique and Hui Xu, Bing Deng, and Wenli Xu for their useful suggestions.

SUPPLEMENTARY MATERIAL

The Supplementary Material for this article can be found online at: https://www.frontiersin.org/articles/10.3389/fcell.2021.670435/full#supplementary-material

REFERENCES

Afroze, D., and Kumar, A. (2019). ER stress in skeletal muscle remodeling and myopathies. *FEBS J.* 286, 379–398. doi: 10.1111/febs.14358

Alexander, M. S., Rozkalne, A., Colletta, A., Spinazzola, J. M., Johnson, S., Rahimov, F., et al. (2016). CD82 is a marker for prospective isolation of human muscle satellite cells and is linked to muscular dystrophies. *Cell Stem Cell* 19, 800–807. doi: 10.1016/j.stem.2016.08.006

Amodio, G., Sasso, E., D'Ambrosio, C., Scaloni, A., Moltedo, O., Franceschelli, S., et al. (2016). Identification of a microRNA (miR-663a) induced by ER stress and its target gene PLOD3 by a combined microRNome and proteome approach. *Cell Biol. Toxicol.* 32, 285–303. doi: 10.1007/s10565-016-9335-z

Behrman, S., Acosta-Alvear, D., and Walter, P. (2011). A CHOP-regulated microRNA controls rhodopsin expression. *J. Cell Biol.* 192, 919–927. doi: 10.1083/jcb.201010055

Bentzinger, C. F., Wang, Y. X., and Rudnicki, M. A. (2012). Building muscle: molecular regulation of myogenesis. *Cold Spring Harb. Perspect. Biol.* 4:a008342. doi: 10.1101/cshperspect.a008342

Braun, T., and Gautel, M. (2011). Transcriptional mechanisms regulating skeletal muscle differentiation, growth and homeostasis. *Nat. Rev. Mol. Cell Biol.* 12, 349–361. doi: 10.1038/nrm3118

Calfon, M., Zeng, H., Urano, F., Till, J. H., Hubbard, S. R., Harding, H. P., et al. (2002). IRE1 couples endoplasmic reticulum load to secretory capacity by processing the XBP-1 mRNA. *Nature* 415, 92–96. doi: 10.1038/415092a

Cartwright, P., McLean, C., Sheppard, A., Rivett, D., Jones, K., and Dalton, S. (2005). LIF/STAT3 controls ES cell self-renewal and pluripotency by a Myc-dependent mechanism. *Development* 132, 885–896. doi: 10.1242/dev.01670

Chen, J. F., Mandel, E. M., Thomson, J. M., Wu, Q., Callis, T. E., Hammond, S. M., et al. (2006). The role of microRNA-1 and microRNA-133 in skeletal muscle proliferation and differentiation. *Nat. Genet.* 38, 228–233. doi: 10.1038/ng1725

Chen, J. F., Tao, Y., Li, J., Deng, Z., Yan, Z., Xiao, X., et al. (2010). microRNA-1 and microRNA-206 regulate skeletal muscle satellite cell proliferation and differentiation by repressing Pax7. *J. Cell Biol.* 190, 867–879. doi: 10.1083/jcb.200911036

Dong, S., Han, J., Chen, H., Liu, T., Huen, M. S. Y., Yang, Y., et al. (2014). The human SRCAP chromatin remodeling complex promotes DNA-end resection. *Curr. Biol.* 24, 2097–2110. doi: 10.1016/j.cub.2014.07.081

Frank, C. L., Ge, X., Xie, Z., Zhou, Y., and Tsai, L.-H. (2010). Control of activating transcription factor 4 (ATF4) persistence by multisite phosphorylation impacts cell cycle progression and neurogenesis. *J. Biol. Chem.* 285, 33324–33337. doi: 10.1074/jbc.M110.140699

Gallot, Y. S., Bohnert, K. R., Straughn, A. R., Xiong, G., Hindi, S. M., and Kumar, A. (2019). PERK regulates skeletal muscle mass and contractile function in adult mice. *FASEB J.* 33, 1946–1962. doi: 10.1096/fj.201800683RR

Godin, J. D., Creppe, C., Laguesse, S., and Nguyen, L. (2016). Emerging roles for the unfolded protein response in the developing nervous system. *Trends Neurosci.* 39, 394–404. doi: 10.1016/j.tins.2016.04.002

Harding, H. P., Zeng, H., Zhang, Y., Jungries, R., Chung, P., Plesken, H., et al. (2001). Diabetes mellitus and exocrine pancreatic dysfunction in perk-/- mice reveals a role for translational control in secretory cell survival. *Mol. Cell* 7, 1153–1163. doi: 10.1016/s1097-2765(01)00264-7

Haze, K., Yoshida, H., Yanagi, H., Yura, T., and Mori, K. (1999). Mammalian transcription factor ATF6 is synthesized as a transmembrane protein and activated by proteolysis in response to endoplasmic reticulum stress. *Mol. Biol. Cell* 10, 3787–3799. doi: 10.1091/mbc.10.11.3787

Heijmans, J., van Lidth, de Jeude, J. F., Koo, B. K., Rosekrans, S. L., Wielenga, M. C., et al. (2013). ER stress causes rapid loss of intestinal epithelial stemness through activation of the unfolded protein response. *Cell Rep.* 3, 1128–1139. doi: 10.1016/j.celrep.2013.02.031

Hetz, C., Zhang, K., and Kaufman, R. J. (2020). Mechanisms, regulation and functions of the unfolded protein response. *Nat. Rev. Mol. Cell Biol.* 21, 421–438. doi: 10.1038/s41580-020-0250-z

Hinnebusch, A. G., and Natarajan, K. (2002). Gcn4p, a master regulator of gene expression, is controlled at multiple levels by diverse signals of starvation and stress. *Eukaryot. Cell* 1, 22–32. doi: 10.1128/ec.01.1.22-32.2002

Huang, B., Li, W., Zhao, B., Xia, C., Liang, R., Ruan, K., et al. (2009). MicroRNA expression profiling during neural differentiation of mouse embryonic carcinoma P19 cells. *Acta Biochim. Biophys. Sin.* 41, 231–236. doi: 10.1093/abbs/gmp006

Huang, da, W., Sherman, B. T., and Lempicki, R. A. (2009). Systematic and integrative analysis of large gene lists using DAVID bioinformatics resources. *Nat. Protoc.* 4, 44–57. doi: 10.1038/nprot.2008.211

Iida, K., Li, Y., McGrath, B. C., Frank, A., and Cavener, D. R. (2007). PERK eIF2 alpha kinase is required to regulate the viability of the exocrine pancreas in mice. *BMC Cell Biol.* 8:38. doi: 10.1186/1471-2121-8-38

Ivey, K. N., and Srivastava, D. (2010). MicroRNAs as regulators of differentiation and cell fate decisions. *Cell Stem Cell* 7, 36–41. doi: 10.1016/j.stem.2010.06.012

Janssens, R., Struyf, S., and Proost, P. (2018). The unique structural and functional features of CXCL12. *Cell. Mol. Immunol.* 15, 299–311. doi: 10.1038/cmi.2017.107

Kroeger, H., Grimsey, N., Paxman, R., Chiang, W. C., Plate, L., Jones, Y., et al. (2018). The unfolded protein response regulator ATF6 promotes mesodermal differentiation. *Sci. Signal.* 11:eaan5785. doi: 10.1126/scisignal.aan5785

Lapan, A. D., and Gussoni, E. (2012). Isolation and characterization of human fetal myoblasts. *Methods Mol. Biol.* 798, 3–19. doi: 10.1007/978-1-61779-343-1_1

Lassot, I., Segeral, E., Berlioz-Torrent, C., Durand, H., Groussin, L., Hai, T., et al. (2001). ATF4 degradation relies on a phosphorylation-dependent interaction with the SCF(betaTrCP) ubiquitin ligase. *Mol. Cell Biol.* 21, 2192–2202. doi: 10.1128/MCB.21.6.2192-2202.2001

Leikina, E., Gamage, D. G., Prasad, V., Goykhberg, J., Crowe, M., Diao, J., et al. (2018). Myomaker and myomerger work independently to control distinct steps of membrane remodeling during myoblast fusion. *Dev. Cell* 76:e767. doi: 10.1016/j.devcel.2018.08.006

Liu, N., Williams, A. H., Kim, Y., McAnally, J., Bezprozvannaya, S., Sutherland, L. B., et al. (2007). An intragenic MEF2-dependent enhancer directs muscle-specific expression of microRNAs 1 and 133. *Proc. Natl. Acad. Sci. U.S.A.* 104, 20844–20849. doi: 10.1073/pnas.0710558105

Matsushita, Y., Nagata, M., Kozloff, K. M., Welch, J. D., Mizuhashi, K., Tokavanich, N., et al. (2020). A Wnt-mediated transformation of the bone marrow stromal cell identity orchestrates skeletal regeneration. *Nat. Commun.* 11:332. doi: 10.1038/s41467-019-14029-w

Millay, D. P., O'Rourke, J. R., Sutherland, L. B., Bezprozvannaya, S., Shelton, J. M., Bassel-Duby, R., et al. (2013). Myomaker is a membrane activator of myoblast fusion and muscle formation. *Nature* 499, 301–305. doi: 10.1038/nature12343

Mitra, S., and Ryoo, H. D. (2019). The unfolded protein response in metazoan development. *J. Cell Sci.* 132:jcs217216. doi: 10.1242/jcs.217216

Novoa, I., Zeng, H., Harding, H. P., and Ron, D. (2001). Feedback inhibition of the unfolded protein response by GADD34-mediated dephosphorylation of eIF2alpha. *J. Cell Biol.* 153, 1011–1022. doi: 10.1083/jcb.153.5.1011

Pakos-Zebrucka, K., Koryga, I., Mnich, K., Ljujic, M., Samali, A., and Gorman, A. M. (2016). The integrated stress response. *EMBO Rep.* 17, 1374–1395. doi: 10.15252/embr.201642195

Pedersen, B. K., and Febbraio, M. A. (2012). Muscles, exercise and obesity: skeletal muscle as a secretory organ. *Nat. Rev. Endocrinol.* 8, 457–465. doi: 10.1038/nrendo.2012.49

Peled, A., Petit, I., Kollet, O., Magid, M., Ponomaryov, T., Byk, T., et al. (1999). Dependence of human stem cell engraftment and repopulation of NOD/SCID mice on CXCR4. *Science* 283, 845–848. doi: 10.1126/science.283.5403.845

Punch, V. G., Jones, A. E., and Rudnicki, M. A. (2009). Transcriptional networks that regulate muscle stem cell function. *Wiley Interdiscip. Rev. Syst. Biol. Med.* 1, 128–140. doi: 10.1002/wsbm.11

Ramaiah, M., Tan, K., Plank, T. M., Song, H. W., Dumdie, J. N., Jones, S., et al. (2019). A microRNA cluster in the Fragile-X region expressed during spermatogenesis targets FMR1. *EMBO Rep.* 20:e46566. doi: 10.15252/embr.201846566

Rao, P. K., Kumar, R. M., Farkhondeh, M., Baskerville, S., and Lodish, H. F. (2006). Myogenic factors that regulate expression of muscle-specific microRNAs. *Proc. Natl. Acad. Sci. U.S.A.* 103, 8721–8726. doi: 10.1073/pnas.0602831103

Rehfeld, F., Maticzka, D., Grosser, S., Knauff, P., Eravci, M., Vida, I., et al. (2018). The RNA-binding protein ARPP21 controls dendritic branching by functionally opposing the miRNA it hosts. *Nat. Commun.* 9:1235. doi: 10.1038/s41467-018-03681-3

Reimold, A. M., Etkin, A., Clauss, I., Perkins, A., Friend, D. S., Zhang, J., et al. (2000). An essential role in liver development for transcription factor XBP-1. *Genes Dev.* 14, 152–157.

Reimold, A. M., Iwakoshi, N. N., Manis, J., Vallabhajosyula, P., Szomolanyi-Tsuda, E., Gravallese, E. M., et al. (2001). Plasma cell differentiation requires the transcription factor XBP-1. *Nature* 412, 300–307. doi: 10.1038/35085509

Ron, D., and Walter, P. (2007). Signal integration in the endoplasmic reticulum unfolded protein response. *Nat. Rev. Mol. Cell Biol.* 8, 519–529. doi: 10.1038/nrm2199

Rudnicki, M. A., Le Grand, F., McKinnell, I., and Kuang, S. (2008). The molecular regulation of muscle stem cell function. *Cold Spring Harb. Symp. Quant. Biol.* 73, 323–331. doi: 10.1101/sqb.2008.73.064

Seale, P., Sabourin, L. A., Girgis-Gabardo, A., Mansouri, A., Gruss, P., and Rudnicki, M. A. (2000). Pax7 is required for the specification of myogenic satellite cells. *Cell* 102, 777–786. doi: 10.1016/s0092-8674(00)00066-0

Singh, G. B., Cowan, D. B., and Wang, D. Z. (2020). Tiny Regulators of massive tissue: microRNAs in skeletal muscle development, myopathies, and cancer cachexia. *Front. Oncol.* 10:598964. doi: 10.3389/fonc.2020.598964

Tajbakhsh, S. (2009). Skeletal muscle stem cells in developmental versus regenerative myogenesis. *J. Intern. Med.* 266, 372–389. doi: 10.1111/j.1365-2796.2009.02158.x

Tay, Y., Zhang, J., Thomson, A. M., Lim, B., and Rigoutsos, I. (2008). MicroRNAs to Nanog, Oct4 and Sox2 coding regions modulate embryonic stem cell differentiation. *Nature* 455, 1124–1128. doi: 10.1038/nature07299

van Bragt, M. P., Ciliberti, N., Stanford, W. L., de Rooij, D. G., and van Pelt, A. M. (2005). LY6A/E (SCA-1) expression in the mouse testis. *Biol. Reprod.* 73, 634–638. doi: 10.1095/biolreprod.105.040303

van de Rijn, M., Heimfeld, S., Spangrude, G. J., and Weissman, I. L. (1989). Mouse hematopoietic stem-cell antigen Sca-1 is a member of the Ly-6 antigen family. *Proc. Natl. Acad. Sci. U.S.A.* 86, 4634–4638. doi: 10.1073/pnas.86.12.4634

Van Vlasselaer, P., Falla, N., Snoeck, H., and Mathieu, E. (1994). Characterization and purification of osteogenic cells from murine bone marrow by two-color cell sorting using anti-Sca-1 monoclonal antibody and wheat germ agglutinin. *Blood* 84, 753–763. doi: 10.1182/blood.v84.3.753.753

Vidigal, J. A., and Ventura, A. (2015). The biological functions of miRNAs: lessons from in vivo studies. *Trends Cell Biol.* 25, 137–147. doi: 10.1016/j.tcb.2014.11.004

Wang, W., Lian, N., Li, L., Moss, H. E., Wang, W., Perrien, D. S., et al. (2009). Atf4 regulates chondrocyte proliferation and differentiation during endochondral ossification by activating Ihh transcription. *Development* 136, 4143–4153. doi: 10.1242/dev.043281

Welm, B. E., Tepera, S. B., Venezia, T., Graubert, T. A., Rosen, J. M., and Goodell, M. A. (2002). Sca-1(pos) cells in the mouse mammary gland represent an enriched progenitor cell population. *Dev. Biol.* 245, 42–56. doi: 10.1006/dbio.2002.0625

Xie, S., Zhang, Y., Qu, L., and Xu, H. (2013). A Helm model for microRNA regulation in cell fate decision and conversion. *Sci. China Life Sci.* 56, 897–906. doi: 10.1007/s11427-013-4547-4

Xie, S. J., Li, J. H., Chen, H. F., Tan, Y. Y., Liu, S. R., Zhang, Y., et al. (2018). Inhibition of the JNK/MAPK signaling pathway by myogenesis-associated miRNAs is required for skeletal muscle development. *Cell Death Differ.* 25, 1581–1597. doi: 10.1038/s41418-018-0063-1

Xiong, G., Hindi, S. M., Mann, A. K., Gallot, Y. S., Bohnert, K. R., Cavener, D. R., et al. (2017). The PERK arm of the unfolded protein response regulates satellite cell-mediated skeletal muscle regeneration. *eLife* 6:e22871. doi: 10.7554/eLife.22871

Xu, G., Chen, J., Jing, G., Grayson, T. B., and Shalev, A. (2016). miR-204 targets PERK and regulates UPR signaling and beta-cell apoptosis. *Mol. Endocrinol.* 30, 917–924. doi: 10.1210/me.2016-1056

Yaffe, D., and Saxel, O. (1977). Serial passaging and differentiation of myogenic cells isolated from dystrophic mouse muscle. *Nature* 270, 725–727. doi: 10.1038/270725a0

Yamamoto, K., Sato, T., Matsui, T., Sato, M., Okada, T., Yoshida, H., et al. (2007). Transcriptional induction of mammalian ER quality control proteins

is mediated by single or combined action of ATF6alpha and XBP1. *Dev. Cell* 13, 365–376. doi: 10.1016/j.devcel.2007.07.018

Zhang, P., McGrath, B., Li, S., Frank, A., Zambito, F., Reinert, J., et al. (2002). The PERK eukaryotic initiation factor 2 alpha kinase is required for the development of the skeletal system, postnatal growth, and the function and viability of the pancreas. *Mol. Cell Biol.* 22, 3864–3874. doi: 10.1128/mcb.22.11.3864-3874.2002

Zismanov, V., Chichkov, V., Colangelo, V., Jamet, S., Wang, S., Syme, A., et al. (2016). Phosphorylation of eIF2alpha is a translational control mechanism regulating muscle stem cell quiescence and self-renewal. *Cell Stem Cell* 18, 79–90. doi: 10.1016/j.stem.2015.09.020

Conflict of Interest: The authors declare that the research was conducted in the absence of any commercial or financial relationships that could be construed as a potential conflict of interest.

frontiers in Cell and Developmental Biology

REVIEW
published: 31 May 2021
doi: 10.3389/fcell.2021.656604

Amino Acid Trafficking and Skeletal Muscle Protein Synthesis: A Case of Supply and Demand

James P. White[1,2,3]*

[1] Department of Medicine, Duke University School of Medicine, Durham, NC, United States, [2] Duke Molecular Physiology Institute, Duke University School of Medicine, Durham, NC, United States, [3] Duke Center for the Study of Aging and Human Development, Duke University School of Medicine, Durham, NC, United States

Skeletal muscle protein synthesis is a highly complex process, influenced by nutritional status, mechanical stimuli, repair programs, hormones, and growth factors. The molecular aspects of protein synthesis are centered around the mTORC1 complex. However, the intricacies of mTORC1 regulation, both up and downstream, have expanded overtime. Moreover, the plastic nature of skeletal muscle makes it a unique tissue, having to coordinate between temporal changes in myofiber metabolism and hypertrophy/atrophy stimuli within a tissue with considerable protein content. Skeletal muscle manages the push and pull between anabolic and catabolic pathways through key regulatory proteins to promote energy production in times of nutrient deprivation or activate anabolic pathways in times of nutrient availability and anabolic stimuli. Branched-chain amino acids (BCAAs) can be used for both energy production and signaling to induce protein synthesis. The metabolism of BCAAs occur in tandem with energetic and anabolic processes, converging at several points along their respective pathways. The fate of intramuscular BCAAs adds another layer of regulation, which has consequences to promote or inhibit muscle fiber protein anabolism. This review will outline the general mechanisms of muscle protein synthesis and describe how metabolic pathways can regulate this process. Lastly, we will discuss how BCAA availability and demand coordinate with synthesis mechanisms and identify key factors involved in intramuscular BCAA trafficking.

Keywords: skeletal muscle, branch chain amino acids, protein synthesis, BCKD, branched-chain α-ketoacid dehydrogenase, AMPK (5′-AMP activated kinase), mammalian target of rapamycin

OPEN ACCESS

Edited by:
Shuichi Sato,
University of Louisiana at Lafayette, United States

Reviewed by:
Olasunkanmi Adegoke,
York University, Canada
Vihang Narkar,
University of Texas Health Science Center at Houston, United States

***Correspondence:**
James P. White
James.white@duke.edu

Specialty section:
This article was submitted to Signaling, a section of the journal Frontiers in Cell and Developmental Biology

Received: *21 January 2021*
Accepted: *28 April 2021*
Published: *31 May 2021*

Citation:
White JP (2021) Amino Acid Trafficking and Skeletal Muscle Protein Synthesis: A Case of Supply and Demand. Front. Cell Dev. Biol. 9:656604. doi: 10.3389/fcell.2021.656604

BRIEF OVERVIEW OF PROTEIN TRANSLATION

Protein synthesis is regulated primarily at the initiation phase of protein translation. A series of signaling proteins, referred to as eukaryotic initiation factors (eIFs), ultimately control this process and depend on upstream signals to modulate their activity. The pathways involved in protein synthesis are extensive, however, two different events govern the translation process, described in **Figure 1**. The binding of the methionyl tRNA (met-tRNA) to the 40S ribosomal subunit is regulated by the eukaryotic initiation factor 2 eIF2 (Price and Proud, 1994). eIF2 binds GTP and the eIF2-GTP-met-tRNA binds to the 40S ribosomal complex forming the 43S preinitiation complex. Once the start codon of an mRNA binds to the complex, GTP is hydrolyzed back to

GDP. The complex cannot form the 43S preinitiation complex until GTP is reformed (Panniers and Henshaw, 1983; Price and Proud, 1994). The enzyme guanine nucleotide exchange factor eIF-2B will return GDP back to GTP and allow the complex to be active again. The regulation of this process is at the phosphorylation state of the α subunit of eIF2. When eIF2 is phosphorylated, eIF2B is inhibited from recycling GDP back to GTP and translation is stopped (Rowlands et al., 1988). eIF2 is phosphorylated by several kinases including double stranded RNA-dependent protein kinase (PKR), heme-regulated inhibitor kinase (HRI), eukaryotic translation initiation factor 2-alpha kinase 3 (PERK), the yeast general control non-derepressible 2 (GCN2) (Proud, 2005), and more recently, glycogen synthase kinase-3 beta (GSK3β) (Welsh et al., 1998). Each kinase appears to target eIF2 under different cellular stresses. PKR is activated in the presence of double stranded RNA (dsRNA) commonly found from viral infections (Meurs et al., 1990). PKR inactivates eIF2 as a protective mechanism to shut down protein synthesis and stop viral replication. HRI was discovered in reticulocytes (Crosby et al., 2000). When heme is deprived from reticulocytes protein synthesis is shut off. This process is associated with the inactivation and subsequent phosphorylation of eIF2. Of these regulators, only GCN2, GSK3β, and PERK regulate eIF2 based on amino acid availability. Their respective actions are illustrated in **Figure 1**. GCN2 is extensively studied in yeast during inhibition of protein synthesis by amino acid deprivation (Marton et al., 1993). It inactivates eIF2 by phosphorylation at serine 51. GSK3β has been shown to be a key regulator in insulin-dependent protein synthesis in skeletal muscle by inactivating eIF2 through phosphorylation at serine 540 (Jefferson et al., 1999). GSK3β and its role in muscle protein synthesis will be discussed in more detail later in the review. PERK has been found to target and inhibit eIF2 by phosphorylation at serine 51 under various conditions, including iron or heme-deficiency, amino acid starvation, viral infection, and accumulation of unfolded proteins (Dever, 2002).

The remaining regulatory mechanisms of protein translation are downstream of the mammalian target of rapamycin complex 1 (mTORC1). mTOR is a Ser/Thr kinase involved in a variety of processes including cell growth and differentiation, protein synthesis, and actin cytoskeletal organization. The mTORC1 complex can phosphorylate both 4E-BP1 and p70S6K to activate two downstream translation pathways, seen in **Figure 1**. Upon phosphorylation, the 4E-BP1 detaches from eIF4E and binds the eIF4F complex (Mader et al., 1995). The eIF4F complex recruits the 40S ribosomal subunit to mRNA through the 5′-cap structure (Proud, 2007). The eIF4F complex consists of three subunits each with distinct functions. eIF4E binds the 5′mRNA, eIF4A is an ATP-dependent RNA helicase and eIF4G serves as structural support for both eIF4E and 4A to form the eIF4F complex. eIF4E has been identified as a main regulatory protein for translation initiation through the eIF4F pathway. During instances of hypophosphorylation, 4E-BP1 remains bound to eIF4E and translation is turned off (Mader et al., 1995).

THE CANONICAL IGF/Akt/mTORC1 PATHWAY

The upstream pathways controlling mRNA translation are, in part, through the IGF-1/mTORC1 pathway (Glass, 2010), illustrated in **Figure 2**. The IGF-Akt (PKB) signaling pathway is well established for its role in regulation of skeletal muscle mass controlling both protein synthesis, degradation, and apoptotic pathways (Frost and Lang, 2007). The binding of IGF-1 activates the receptor tyrosine kinase IGF-1 receptor and recruits insulin receptor substrate (IRS), in particular IRS-1 (Sun et al., 1991; Yamauchi et al., 1998). This leads to the activation of phosphatidylinositol 3′-kinase (PI3K) and the eventual activation of the serine-threonine kinase Akt (PKB) via phosphorylation at serine 473 (Alessi et al., 1997; Andjelkovic et al., 1997; Moelling et al., 2002). Akt is a focal point in insulin and IGF-1 signaling in a variety of tissues. Akt is also phosphorylated by mTORC2 (Sarbassov et al., 2005), which will be discussed later in the review. Upon activation, Akt is involved in a multitude of downstream pathways that will promote muscle growth. During skeletal muscle hypertrophy, Akt activation is increased when examined *in vivo* (Bodine et al., 2001) and in cultured myotubes (Rommel et al., 2001). In addition, a genetically altered, constitutively active Akt was able to induce muscle hypertrophy independent of additional treatments (Bodine et al., 2001; Lai et al., 2004). Akt acts through mTORC1 pathways to initiate and enhance protein synthesis. In addition, Akt can enhance protein synthesis through inhibition of proteins that impede protein synthesis such as GSK-3β and PRAS40. As mentioned previously, GSK3β is an inhibitor of protein synthesis through phosphorylation and inhibition of eIF2. Akt phosphorylates GSK3β at Ser9 and inactivates its kinase activity, thus allowing the initiation of protein synthesis. Activation of the Akt/GSK3β pathway is observed in muscle *in vitro*, using anabolic stimulus on C2C12 myotubes. Administration of IGF-1 resulted in myotube

Abbreviations: 4E-BP1, the eukaryotic initiation factor 4E binding protein 1; ADP, Adenine diphosphate; AICAR, 5-Aminoimidazole-4-carboxamide ribonucleotide; Akt, AKR thymoma; AMP, Adenine monophosphate; AMPK, AMP-activated kinase; ATP, Adenine triphosphate; BCAAs, Branched-chain amino acids; BCAT, Branched-chain amino acid aminotransferase; BCKDH, branched-chain α-keto acid dehydrogenase; BDK, BCKDH kinase; BKAs, branched-chain keto acids; DEPTOR, DEP domain-containing mTOR-interacting protein; eEF, Eukaryotic elongation factor; eIF, eukaryotic initiation factor; GAP, GTPase-activating protein; GCN2, general control non-derepressible 2; GDP, Guanosine diphosphate; GEF, guanine nucleotide exchange factor; GSK3β, glycogen synthase kinase-3; GTP, Guanosine-5′-triphosphate; HRI, heme-regulated inhibitor kinase; IGF-1, Insulin-like growth factor; IRS, insulin receptor substrate; mLst8, mammalian LST8 homolog; mSin1, the mammalian stress-activated protein kinase-interacting 1; mTOR, mechanistic Target of Rapamycin; mTORC1, mammalian/mechanistic Target of Rapamycin Complex 1; mTORC2, mammalian/mechanistic Target of Rapamycin Complex 2; P70S6K, P70 Ribosomal protein S6 kinase; PDK-1, phosphoinositide-dependent kinase 1; PERK, eukaryotic translation initiation factor 2-alpha kinase 3; PGC-1α, Peroxisome proliferator-activated receptor gamma coactivator 1-alpha; PI3K, phosphatidylinositol 3-kinase; PI3P, phosphatidylinositol 3-phosphate; PIP3, phosphatidylinositol (3,4,5)-trisphosphate; PKB, Protein kinase B; PKR, double stranded RNA-dependent protein kinase; PPM1K, protein phosphatase 1K; PRAS40, proline-rich Akt substrate, 40 kDa; Rag, Ras related GTP binding; Raptor, the regulatory-associated protein of mTOR (Raptor); REDD1, protein regulated in DNA damage and development 1; Rheb, Ras homolog enriched in brain; Rictor, the rapamycin-insensitive companion of mTOR; RTK, receptor tyrosine kinase; TCA, tricarboxylic acid; TOR, Target of Rapamycin; TSC, Tuberous sclerosis complex.

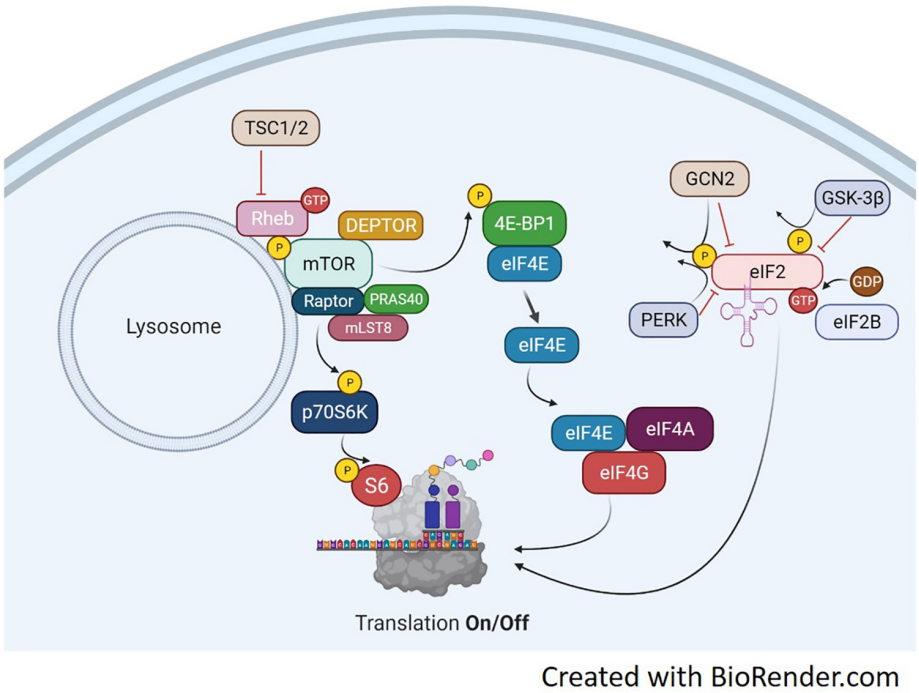

FIGURE 1 | Translation Overview. Protein translation occurs, in part, by mTORC1-dependent regulation of p70S6K and the 4E-BP1/eIF4E complex and the mTORC1-independent eIF2 complex. mTORC1 activation is achieved through several points of regulation including, but not limited to phosphorylation at ser2448, inactivation of the TSC1/2 complex, binding of GTP-bound RHEB and translocation to the lysosome. Upon activation, mTORC1 will phosphorylate p70S6K at Thr389. This activates p70S6K to phosphorylate ribosomal protein S6 at ser236/236 and initiate RNA translation. mTORC1 can also regulate the eIF4E complex by phosphorylating 4E-BP1 which results in detachment of 4E-BP1 from eIF4E. This frees eIF4E to bind with eIF4A and eIF4G which will initiate binding of mRNA to the ribosome. A third point of translation initiation is the eIF2 complex. eIF2 forms a ternary complex with GTP and the Met-rRNA binds to the 40S ribosomal subunit to start the translation process. Its regulation is mediated through phosphorylation by various kinases including GSK-3β, PERK, and GCN2. Phosphorylation of eIF2 inhibits the guanine nucleotide exchange function of eIF2B and prevents translation.

hypertrophy, associated with hyperphosphorylation of both Akt and GSK3β (Rommel et al., 2001).

There are several regulatory points throughout the IGF-1/Akt/mTORC1 pathway, yet mTORC1 appears to be the gateway to downstream anabolic signaling. mTOR assembles into two distinct complexes, mTORC1 and mTORC2. mTORC1 consists of raptor (regulated associated protein of mTOR), mLST8, DEPTOR, PRAS40, and mTOR. mTORC2 consists of rictor (rapamycin insensitive companion of mTOR), mSIN1, mLST8, DEPTOR, and mTOR. mTORC1 activation is well described through PI3K/Akt signaling. Akt can phosphorylate several proteins that regulate mTORC1 activity including mTORC1 itself, PRAS40 and tuberous sclerosis complex 2 (TSC2) (Sancak et al., 2007; Vander Haar et al., 2007). Currently, the signaling mechanism for Akt through TSC2 is the most well described pathway. Akt phosphorylates TSC2 on multiple residues leading to its inactivation. TSC2 is a GTPase activating protein for Rheb. Therefore, inactivation of TSC2 by Akt increases the amount of GTP:Rheb complex bound to mTOR and leads to its activation. The second mechanism by which Akt can activate mTORC1 is through phosphorylation of the mTORC1 inhibitor PRAS40. Phosphorylated PRAS40 will disassociate from mTORC1, release its inhibition and increase mTOR kinase activity (Wang et al., 2012). In relation to mTORC1, there is a limited understanding of the role of mTORC2 in muscle protein synthesis and growth (Bentzinger et al., 2008). Initial studies have shown mTORC2 to be involved in organization of actin cytoskeleton and possibly phosphorylate Akt at Ser473 (Jacinto et al., 2004). In addition, there may be a coordinated effort for both mTOR complexes to work together for maximizing muscle protein synthesis under anabolic conditions (Ogasawara et al., 2020).

THE mTORC1 COMPLEX

The mTORC1 complex has several related protein-protein complexes which regulate signaling activity. Each protein has a unique function in the complex. Raptor acts as a scaffolding protein to recruit downstream targets of mTOR, p70S6K, and 4E-BP1 (Hara et al., 2002; Kim et al., 2002). It is also the anchoring protein used by the Rag GTPases to recruit mTORC1 to the lysosome (Sancak et al., 2008). In skeletal muscle, raptor KO mice have a marked reduction in phosphorylation of both p70S6K and 4E-BP1 (Bentzinger et al., 2008). In addition, p70S6K and 4E-BP1 proteins have common mTORC1 signaling (TOS) motifs, which are essential for mTORC1-targeted phosphorylation (Dunlop et al., 2009). The raptor protein can also be modified at multiple phosphorylation sites. Phosphorylation of raptor appears to

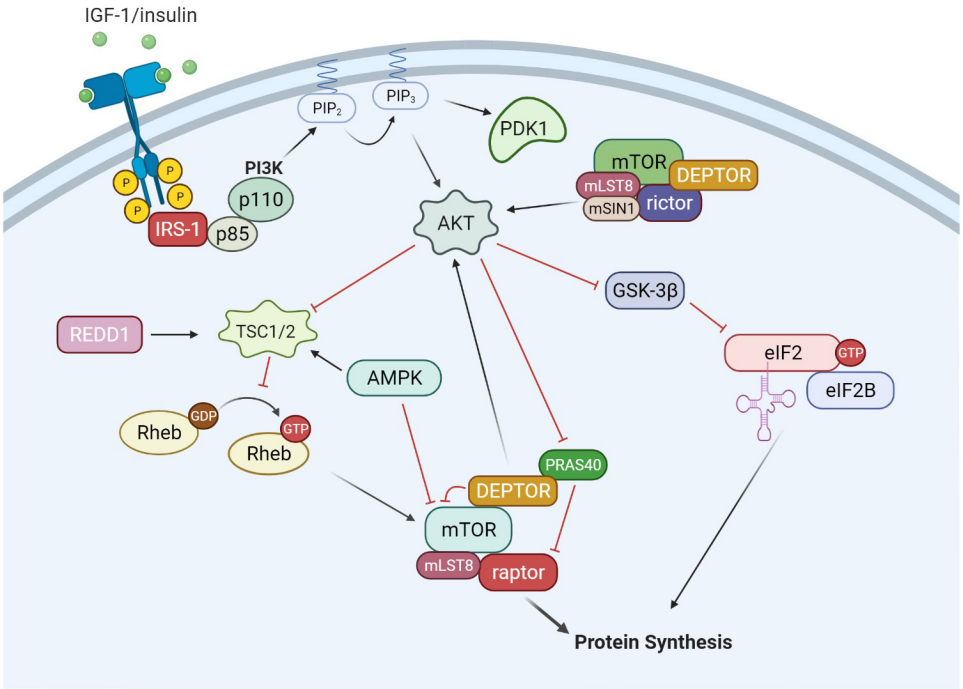

FIGURE 2 | IGF-1/Akt signaling. The binding of growth factors such as IGF-1 and insulin activates receptor tyrosine kinases (RTKs), which recruits and activates IRS-1. IRS-1 then activates phosphatidylinositol-4,5-bisphosphate 3-kinase (PI3K), which consists of a regulator subunit (p85) and a catalytic subunit (p110). PI3K generates phosphoinositide 3,4, 5-phosphate (PIP_3). PIP3 recruits and activates PDK1 and Akt. In addition to PIP3 signaling, mTORC2 can also phosphorylate and activate Akt. From there, Akt can signal through both mTORC1 and eIF2 pathways to increase protein synthesis. Akt can phosphorylate and inactivate GSK-3β, which is an inhibitor of the eIF2 complex. Akt can also activate the mTORC1 complex through inactivation of TSC1/2 and PRAS40. AMPK is a negative regulator of the IGF-1/Akt pathway, inhibiting mTORC1 activity through activation of the TSC1/2 complex and direct inhibition of mTORC1.

happen in a sequential manner (Foster et al., 2010). Once activated, mTOR will phosphorylate raptor at Ser^{863}, which primes raptor for phosphorylation at several other sites including $Ser^{859/855}$ (Foster et al., 2010). The phosphorylation events must be in the presence of adequate amino acid concentrations. In HEK293 cells, insulin-stimulated phosphorylation of raptor was not evident in amino acid depleted serum showing amino acid availability is critical for mTORC1 activity despite the availability of other growth factors (Foster et al., 2010). Raptor can also be phosphorylated by the 5′-adenosine monophosphate-activated protein kinase (AMPK) at Ser792, which inhibits raptor function and related mTORC1 activity (Gwinn et al., 2008). Skeletal muscle raptor phosphorylation at the AMPK targeted Ser792 is associated with body weight loss during cancer-associated muscle wasting (White et al., 2011).

The protein PRAS40 is another member of the TORC1 complex. PRAS40 has been shown to be an inhibitor of mTOR activity (Sancak et al., 2007; Wang et al., 2007). PRAS40 is bound to the inactive mTORC1 complex and directly inhibits substrate binding to raptor preventing downstream phosphorylation (Wang et al., 2007). Akt has been shown to phosphorylate and inhibit PRAS40 binding to raptor (Vander Haar et al., 2007), however, mTOR can phosphorylate PRAS40 as well (Foster et al., 2010). Upon activation from insulin or amino acids, activated mTOR can phosphorylate PRAS40 which facilitated its disassociation from the complex (Foster et al., 2010). Once PRAS40 is off the complex, raptor can bind p70S6K and 4E-BP1 for eventual phosphorylation. In male mice, muscle PRAS40 phosphorylation is responsive to circulating testosterone and muscle mass (White et al., 2012). Castration decreases phospho PRAS40, which is rescued with androgen add-back (White et al., 2012).

DEP domain-containing mTOR-interacting protein is a relatively recent addition to the mTORC1 complex, having an inhibitory function on mTORC1 activity (Peterson et al., 2009). mTORC1 and DEPTOR negatively regulate each other, depending on nutrient availability. In a low nutrient state, the PZD domain of DEPTOR binds to the C-terminal portion of mTOR and inhibits downstream signaling to p70S6K and 4E-BP1. In addition, it also activates mTORC2/Akt signaling by relieving the mTORC1 negative feedback inhibition of PI3K (Peterson et al., 2009). During nutrient availably and subsequent mTORC1 activity, DEPTOR is phosphorylated and released from the mTORC1 complex. The reduction in protein expression is also accompanied with a suppression of DEPTOR mRNA expression (Peterson et al., 2009). In C2C12 myotubes, the knockdown of DEPTOR increased protein synthesis and associated mTORC1 signaling (Kazi et al., 2011). DEPTOR knockdown, *in vivo*, resulted in an attenuation of immobilization-induced muscle atrophy associated with

increased muscle protein synthesis (Kazi et al., 2011). The sensitivity of DEPTOR to atrophy conditions has been replicated by others showing DEPTOR expression increases with limb immobilization (Shimkus et al., 2018) and hind limb unloading (Roberson et al., 2020). The regulation of DEPTOR from nutrient availability does not appear as strong as mechanical loading, as fasting/refeeding did not alter DEPTOR protein expression (Shimkus et al., 2018). However, further investigation is needed to determine how DEPTOR is regulated under different nutrients and availability of amino acids.

NEGATIVE REGULATORS OF mTORC1

There are several negative regulators of mTORC1 activity existing outside the mTORC1 complex. Two well documented inhibitors are AMPK and the protein regulated in DNA damage and development 1 (REDD1, also referred to as Rtp801 and DDIT4). Their respective interactions with the Akt/mTOR pathways are shown in **Figures 2**, **3**. AMPK and mTOR are key energy sensors in the cell, and function to regulate processes to either inhibit or enhance ATP production depending on nutrient availability. AMPK will be discussed in more detail later in this review. REDD1 is thought to inhibit mTORC1 signaling through activation of upstream TSC2 (Brugarolas et al., 2004; Reiling and Hafen, 2004; Sofer et al., 2005). In addition, REDD1 protein and mRNA expression are increased with cellular stress events including ATP depletion (Sofer et al., 2005), DNA damage (Lin et al., 2005), endoplasmic reticulum stress (Wang et al., 2003; Protiva et al., 2008), and hypoxia (Shoshani et al., 2002; Brugarolas et al., 2004; Reiling and Hafen, 2004; Schwarzer et al., 2005). Furthermore, treatment with the synthetic glucocorticoid dexamethasone has shown to increase REDD1 mRNA and protein in skeletal muscle as well as L6 myotubes (Wang et al., 2006). Glucocorticoids such as cortisone are elevated during fasting states which, in part through REDD1, may play a role in the inhibition of mTORC1 signaling and the subsequent reduction in protein synthesis. REDD1 protein and mRNA expression was increased with 18 h of starvation in rats which coincided with a reduction in mTORC1 signaling (McGhee et al., 2009). Upon refeeding, REDD1 protein and mRNA expression was returned to baseline and mTORC1 signaling was increased. Interestingly, fasting-induced glucocorticoid concentrations directly correlated with REDD1 expression showing evidence of cross talk between energy-sensitive hormones and energy-sensitive signaling within muscle (McGhee et al., 2009). Finally, the loss of REDD1 during a mechanical-overload hypertrophy stimuli enhanced the rate of muscle protein synthesis (Gordon et al., 2016), again, suggesting its role as a negative regulator of muscle protein anabolism.

AMPK PROMOTES CATABOLISM OVER ANABOLISM

AMPK is activated through the buildup of low energy phosphate group, AMP or by phosphorylation by one or more upstream kinases at a threonine residue within the activation loop of the α subunit (Hawley et al., 1996; Stein et al., 2000). The multiple targets that AMP can activate will induce a large activation in the activity of AMPK with relatively small changes in AMP. The energy state of the cell is not solely monitored by AMP concentrations. High ATP concentrations will oppose activation of AMP-induced pathways. Thus, the AMP:ATP ratio appears to the critical readout of cellular energy status and regulator of AMPK activity.

During physiological conditions, AMPK can be regulated by chemical mediators of metabolism in addition to ATP:AMP levels. Cellular levels of phosphocreatine can allosterically inhibit AMPK activity (Ponticos et al., 1998). In addition, glycogen content of the cell can affect AMPK activity (Hudson et al., 2003; Polekhina et al., 2003). The β-subunits of AMPK contain a glycogen binding domain. Reports in human and rodent muscle show high glycogen stores can inhibit AMPK activation (Wojtaszewski et al., 2002, 2003). Over expression of AMPK in culture has shown AMPK to localize in large glycogen granules (Hudson et al., 2003). Glycogen will not only bind AMPK, but also contain in close proximity glycogen synthase, a substrate of AMPK. Considering AMPK is allosterically regulated by phosphocreatine and glycogen stores, it has been speculated that AMPK is regulated by both short and long term energy stores (Hardie, 2003).

AMPK TARGETS mTORC1 TO SUPPRESS PROTEIN SYNTHESIS

AMPK has been shown to inhibit protein synthesis in skeletal muscle (Rolfe and Brown, 1997; Bolster et al., 2002; Deshmukh et al., 2008; Thomson et al., 2008; Mounier et al., 2009), liver (Reiter et al., 2005), and cultured myotubes (Williamson et al., 2006; Tong et al., 2009). The potency of AMPK signaling was described by Pruznak et al. (2008), showing AMPK activation can override the stimulatory effects of leucine on muscle protein synthesis (Pruznak et al., 2008). In contrast, deletion of the AMPKα1 gene in primary myotubes resulted in cell hypertrophy (Mounier et al., 2009). The mechanism by which AMPK inhibits muscle protein synthesis is through the inhibition of the mTORC1 complex (Bolster et al., 2002; Horman et al., 2002; Chan et al., 2004; Gwinn et al., 2008). There are currently three proposed mechanisms by which AMPK can inhibit mTORC1 signaling. The first is through phosphorylation of mTOR on Thr2446 (Cheng et al., 2004). This process does not directly inhibit mTOR activity, however, phosphorylation at Ser2446 prevents phosphorylation of Ser2448 which has been shown to increase mTOR activity (Bolster et al., 2002; Chiang and Abraham, 2005). The second method, and perhaps the best described mechanism, is through AMPK-mediated phosphorylation of the tuberous sclerosis complex 2 (TSC2) gene product Tuberin on Thr1227 and Ser1345 (Inoki et al., 2003). TSC2 combines with TSC1 to form a GTPase activator protein (GAP) for the Ras homolog enriched in brain (Rheb), causing an increase in GDP bound to Rheb (Zhang et al., 2003; Long et al., 2005a). The binding of the GDP:Rheb complex to mTORC1

inhibitors mTOR. The third mechanism, as discussed earlier in the review, is the phosphorylation of raptor (Gwinn et al., 2008). This promotes binding of the 14-3-3 protein and inhibition of raptor to signal downstream to p70S6K and 4E-BP1.

The AMPK pathways has been heavily investigated in muscle in regards to other aspects of mTORC1 signaling. In C2C12 cells, AICAR-induced AMPK activation showed a reduction in protein synthesis, polysome aggregation and downstream mTORC1 signaling proteins 4E-BP1, p70S6K and eEF2 (Williamson et al., 2006). Although Akt, upstream of mTORC1, remained unaffected with AICAR treatment, downstream AMPK targets raptor and TSC2 were effected with AMPK activation. In addition, AICAR increased the amount of TSC1 bound to TSC2 (Williamson et al., 2006), suggesting increased GTPase activity and inhibition of Rheb. A study by Du et al. (Tong et al., 2009) treated C2C12 cells with both AICAR and IGF-1 to determine if AMPK signaling can inhibit IGF-1 signaling, with the hypothesis that IGF-1 signaling originates upstream of mTORC1. AICAR treatment without IGF-1 resulted in cell atrophy caused by a reduction in signaling related to protein synthesis and an increase in markers of protein degradation. The addition of IGF-1 did not rescue the inhibition of AICAR treatment despite a significant increase in Akt, supporting the proposed mechanism of potent mTORC1 inhibition by AMPK.

AMPK has been examined in rodent models of muscle hypertrophy to determine its role in growth suppression. Overload-induced hypertrophy of the plantaris muscle was enhanced in AMPKα1−/− mice. This occurred in conjunction with an increase in phosphorylation of downstream targets of mTORC1 signaling p70S6K and 4E-BP1 (Mounier et al., 2009). In contrast, AICAR treatment resulted in a reduction in the percentage of plantaris muscle mass gained after 1 week of over load (Gordon et al., 2008). In the same study, there was a significant negative correlation between the percentage of plantaris hypertrophy and AMPK phosphorylation status in the plantaris muscle. In addition, there were also negative correlations between phosphorylation status of AMPK and p70S6K, eEF2 and 4E-BP1.

Catabolic signaling through AMPK can override amino acid-induced mTORC1 activation. AICAR treatment prevented leucine-stimulated protein synthesis in the mouse gastrocnemius muscle (Pruznak et al., 2008). The prevention of synthesis was accompanied with the prevention of mTOR activation. AMPK can phosphorylate and activate TSC-2, which subsequently inactivates mTOR. AICAR treatment did not increase the phosphorylation of TSC-2 or alter TSC-1/TSC-2 binding. However, AICAR treatment did increase phosphorylation of raptor independent of leucine treatment. The activation of downstream signaling proteins p70S6K1, 4E-BP1, and eIF4F were increased with leucine administration and prevented when leucine was given with AICAR treatment. This data is in agreement with the results from Du et al. (Du et al., 2007) who showed AICAR treatment prevents a leucine-induced increase in protein synthesis in C2C12 myoblasts. In support of these data, myoblasts expressing a dominant negative AMPKα subunit were administered AICAR. Without AMPK activation, leucine was able to increase protein synthesis even with AICAR treatment. Once again, suggesting AMPK-induced inhibition of protein synthesis was through the reduction in mTORC1. These results support the hypothesis that cellular energy demands can supersede the anabolic potential of amino acid availability.

AMINO ACID AVAILABILITY AND mTORC1 ACTIVITY

Although mTORC1 is a key component of the IGF-1/insulin signaling pathway, mTORC1 can be activated independent of upstream signaling by amino acids (Potier et al., 2009). Branched-chain amino acids (BCAAs), especially leucine, are potent regulators of mTORC1 activity and increase rates of protein synthesis (Goberdhan et al., 2009). Infusion of an amino acid mixture into resting human subjects increased protein synthesis as early as 30 min after infusion and remained elevated for 90 min (Bohe et al., 2001). Amino acid infusion has been shown to increase phosphorylation of downstream targets of mTORC1, p70S6K, and 4E-BP1 (Greiwe et al., 2001; Liu et al., 2001) without effecting Akt (Greiwe et al., 2001) or its downstream target GSK3β (Liu et al., 2004). In the rodent, mTORC1 activity is necessary for BCAAs to induce anabolic signaling, as rapamycin prevented leucine-induced increased phosphorylation of p70S6K and 4E-BP1 (Anthony et al., 2000).

Despite strong evidence suggesting BCAAs activate mTORC1 signaling, the direct mechanism for mTORC1 activation remains unclear, especially in skeletal muscle. It has been proposed that BCAAs work through both a TSC1/2 dependent (Gao et al., 2002) and independent (Smith et al., 2005) manner to activate mTORC1 activity. The TSC1/2 complex can mediate amino acid signaling to mTORC1 (Gao et al., 2002), which could be regulated through relative localization of TSC1/2 and mTOR on the lysosome (Demetriades et al., 2014; Menon et al., 2014). Other reports have shown evidence for TSC1/2 independent activation of mTORC1 signaling through RAG and Rheb. In mammals, there are four RAG GTPases (A-D) shown to have a role in amino acid signaling to mTORC1 (Schurmann et al., 1995; Kim et al., 2008; Sancak et al., 2008). Amino acids can convert RAG to an active formation including Rag A/B loaded with GTP and Rag C/D loaded with a GDP. The active Rag A/B recruits the mTORC1 complex to the lysosome through raptor where it is activated by Rheb (Sancak et al., 2008). Rheb activates mTORC1 by direct associated and activation of the mTOR catalytic domain (Long et al., 2005a,b). The regulation of mTORC1 activation with and without amino acid availability is illustrated in **Figure 3**.

REGULATION OF AMINO ACID METABOLISM

Amino acid metabolism has been well described, especially in the context of insulin resistant and obesity (White and Newgard, 2019). In skeletal muscle, the balance between amino acid catabolism and anabolism is complex, due to both metabolic and anabolic flux of the myofiber. BCAAs, in particular, are a widely used source to generate TCA/Krebs cycle intermediates

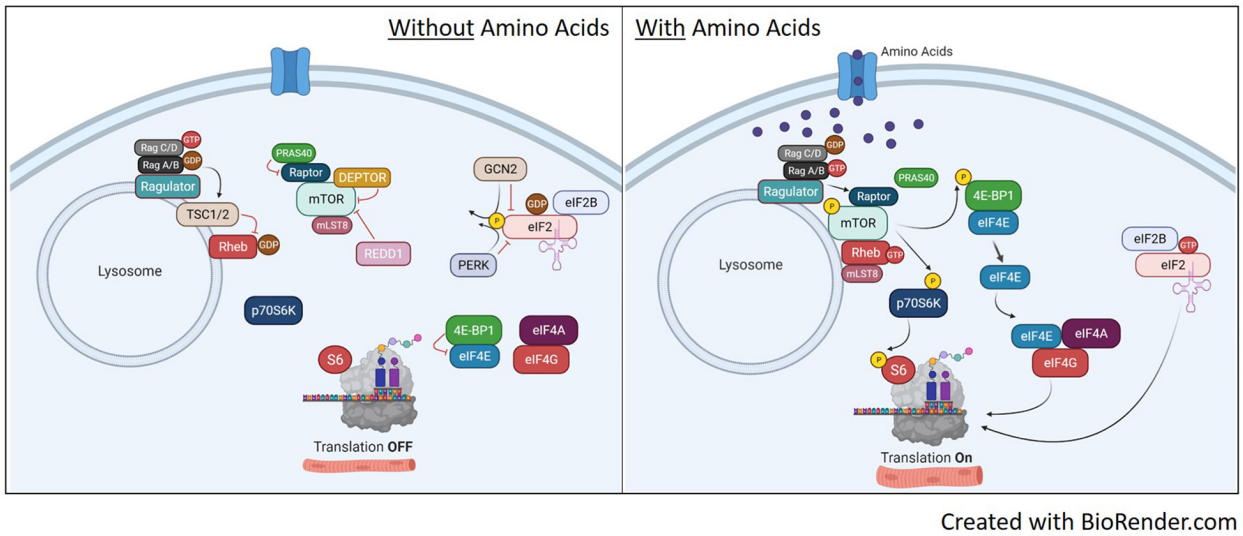

FIGURE 3 | Translation pathways with or without amino acid availability. Without amino acid availability (left image), the heterodimeric Rag protein is loaded with GTP on Rag C/D while Rag A/B has the GDP. This conformation localizes the TSC1/2 complex to the lysosome to prevent GDP-Rheb conversion to GTP and prevents the recruitment of mTORC1 to the lysosome. This renders both S6 and 4E-BP1 unphosphorylated, shutting off translation. In addition, the inactive mTORC1 with be further suppressed by inhibitors DEPTOR, REDD1 and PRAS. On the eIF2 pathway, the absence of amino acids maintains GCN2 and PERK activity, which phosphorylates eIF2, inhibiting guanine nucleotide exchange of eIF2 by eIF2B. With eIF2 bound to GDP, it will release from the ribosome and stop translation. Upon availability of amino acids (right image), RagA/B is now loaded with GTP as it maintains binding to ragulator. This initiates removal of TSC1/2 from the lysosome and Rag-induced recruitment of mTORC1 to the lysosome via raptor. Once at the lysosome, mTOR kinase activity is activated by GTP-bound Rheb and will phosphorylate p70S6K and 4E-BP1 to initiate translation. mTORC1 activation will also disassociate inhibitors DEPTOR and PRAS40. Once dissociated, DEPTROR is quickly degraded. In relation to eIF2, the availability of amino acids will inhibit GCN2 and PERK, reversing phosphorylation on eIF2 and allowing guanine nucleotide exchange of eIF2 back to GTP. This will bind the eIF2 complex to the 40S ribosomal subunit and initiate protein translation.

for energy production. Although the majority of amino acid metabolism occurs in the liver, skeletal muscle has high expression of the branched-chain aminotransferase (BCAT). Interestingly, despite its metabolic nature, the liver does not express BCAT, rendering a unique pathway of BCAA metabolism to skeletal muscle (Hutson, 1989; White et al., 2020). BCAT-mediated transamination of leucine generates α-ketoisocaproate, the first step of BCAA catabolism in muscle. The second step of leucine catabolism is an irreversible oxidative decarboxylation of α-ketoisocaproate, which is catalyzed by the branched-chain α-keto acid dehydrogenase (BCKDH). This reaction is a rate-limiting step in leucine metabolism (Harris et al., 1990, 1994).

Branched-chain α-keto acid dehydrogenase is a highly regulated dehydrogenase enzyme responsible for metabolizing branched-chain keto acids (BCKA) into branched-chain acyl CoAs. The branched-chain CoAs are further metabolized into acetyl CoA or Succinyl CoA and used as TCA intermediates for energy (Walejko et al., 2021). The multi-subunit BCKDH complex consists of three components including the e1, e2, and e3 subunits. Each subunit carries out different reactions to convert BCKAs into branched-chain acyl CoAs. There are two opposing regulators of BCKDH activity, the BCKDH kinase (BDK) and the PPM1K phosphatase (also referred to as PP2Cm) (White et al., 2018). Both enzymes perform phosphorylation and dephosphorylation, respectively, of serine 293 of the e1a subunit. In the liver, increased phosphorylation of BCKDH on serine 293 occurs secondary to elevated expression of BDK, and decreased expression of PPM1K (She et al., 2007; Lian et al., 2015). Murine knockout models of either BDK or PPM1K (Joshi et al., 2006; Lu et al., 2009) show the significance of their respective role in BCAA metabolism, as each manipulation effects circulating BCAAs accordingly. Currently, there is limited understanding of this pathway in skeletal muscle, especially in regards to anabolic and catabolic conditions. BCAA fate and the antagonist relationship between BCKDH and PPM1K is shown in **Figure 4**.

As AMPK is a potent inhibitor of mTORC1 activity, it would also make sense that AMPK would regulate muscle amino acid metabolism. AICAR-induced AMPK activation can increase BCKDH activity in skeletal muscle through a reduction in BDK protein (Lian et al., 2015). Although AICAR increased PPM1K in liver and adipose tissue, muscle PPM1K was not effected by AICAR treatment (Lian et al., 2015). Skeletal muscle PGC-1α over-expression increases gene expression of branched-chain amino transferase (BCAT) 2 and BCKDH, while BDK was not changed. BCAAs levels in the PGC-1α mice were decreased in both muscle and blood (Hatazawa et al., 2014). These outcomes show the coupled relationship between two potent metabolic regulators, i.e., AMPK and PGC-1α, and the shift from anabolism to BCAA catabolism.

The extent of BCAA metabolism can have an impact on global muscle metabolism, as excess BCAAs or branched-chain ketoacids can inhibit insulin signaling in muscle *in vitro* (Moghei et al., 2016; Biswas et al., 2020) and *in vivo* (White et al., 2016, 2018; Wang et al., 2019). Interestingly, this

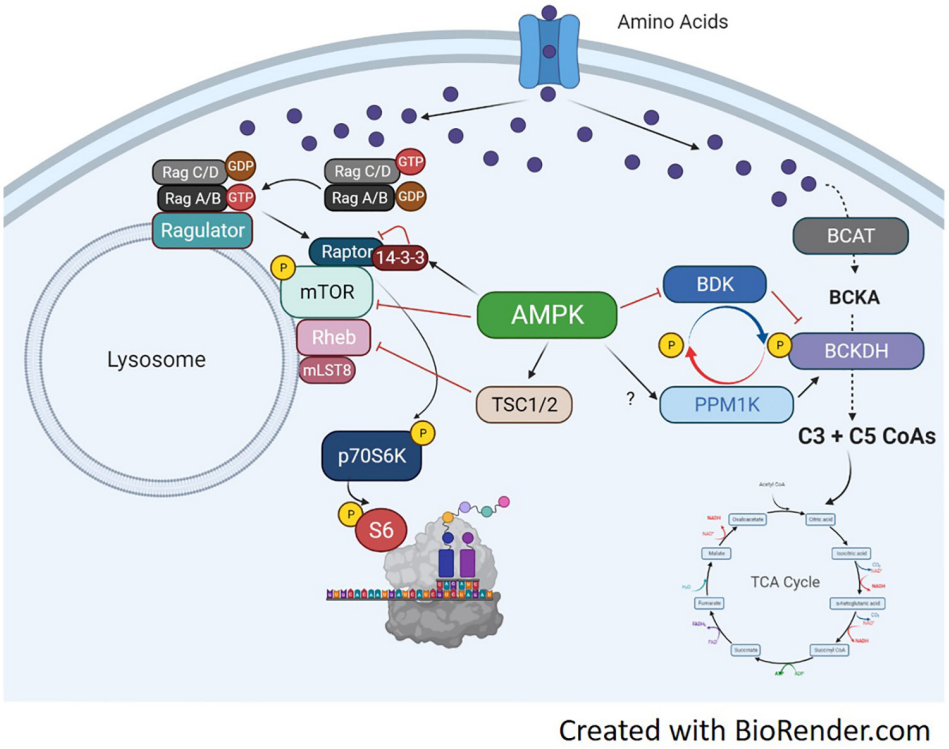

FIGURE 4 | Molecular mechanisms of amino acid trafficking. Amino acids, especially BCAAs, enter the cell via their respective transporters. Once in the cell, depending on metabolic need, they can be metabolized for energy or used for other biochemical processes like protein synthesis. If needed for energy, the enzyme BCAT metabolizes the BCAA into branched-chain keto acids, which undergo a series of catabolic reactions to produce C3 and C5 CoAs by BCKDH. The C3/5 CoAs are then converted to either acetyl CoA or Succinyl CoA and can enter the TCA cycle. BCKDH is regulated by phosphorylation/dephosphorylation by the kinase BDK and the phosphatase PPM1K, respectively. Phosphorylation of BCKDH by BDK inhibits BCKDH activity while dephosphorylation by PPM1K activates BCKDH and increases generation of BCAA-derived CoAs for energy production. The activation of the BCAT/BCKDH pathway pulls amino acids away from the associated mTORC1 complexes and inhibits protein synthesis. If BDK is able to phosphorylate BCKDH, or PPM1K is inhibited, amino acids would be available to active mTORC1 and initiate protein translation. AMPK can regulate BCAA metabolism by increasing PPM1K and lowering BDK expression, which will activate BCKDH and increase BCAA flux to the TCA cycle. AMPK can simultaneously block mTORC1 signaling through activation of TSC1/2 or direct inhibition of mTOR and raptor.

result is dependent on certain BCAAs or a mixture of BCAAs as valine does seem to interfere with myotube insulin signaling *in vitro* (Rivera et al., 2020). Nutrient availability may also regulate metabolic fate of leucine. In C2C12 myotubes, leucine is used preferentially for protein synthesis rather than oxidation for energy production (Estrada-Alcalde et al., 2017). However, in the setting of high palmate, leucine oxidation increases and its incorporation into proteins decreases (Estrada-Alcalde et al., 2017). Moreover, high fat feeding increase BCKDH activity in muscle promoting amino acid catabolism (White et al., 2016). This again, points to the complexity of muscle metabolism and substrate availability altering BCAA trafficking. The proposed BCAA trafficking and related AMPK signaling pathways are shown in **Figure 4**.

In the context of muscle mass regulation, muscle BDK knockout mice have no overt muscle mass phenotype under a typical chow diet, despite a lower BCAA concentration in blood and muscle (Ishikawa et al., 2017). However, under a low protein diet, the lack of BDK magnifies myofibrillar protein loss associated with a reduction in mTORC1 signaling activity. Of note, protein restriction resulted in a reduction of myofibrillar protein synthesis, but not total (soluble) protein, indicating a preferential degradation of myofibrillar proteins to compensate for the low protein diet. A natural hypothesis would point to autophagy as a mechanism to provide amino acids during the restricted feeding. However, this study showed no difference in LC3I/II protein expression, and so the authors concluded autophagy was not playing a role and contributing to the myofibrillar degradation during the low protein diet (Ishikawa et al., 2017). This study highlights the interaction between BCAA metabolism and protein synthesis pathways, supporting an interactive crosstalk between the two processes. More work is needed to gain a better understanding of the molecular network between BCAA trafficking and mTORC1 signaling.

CONCLUSION AND PERSPECTIVE

Together, muscle protein synthesis is an interactive process, taking input from numerous anabolic and catabolic pathways. The unique plasticity of skeletal muscle adds more layers

of regulation, incorporating both metabolic demands and mechanical stimuli into these already intricate pathways. Moreover, there must be an adequate combination of mechanical stimuli and nutritional availability to maintain or hypertrophy myofiber size. In relation to other tissues, especially tumor biology, the molecular mechanisms involved in skeletal muscle protein synthesis are less developed. This concept is supported by the fact that the majority of citations in this review investigating amino acid metabolism and regulation of mTORC1 are not in muscle tissue. This is interesting, considering the extensive protein content of skeletal muscle and the potential utility of skeletal muscle as a model to investigate the complexities of protein synthesis. In regards to muscle signaling pathways, the IGF-1/insulin pathway dominates the literature since muscle is a major therapeutic target for diabetes drugs. However, the anabolic pathways in muscle have been relatively neglected since muscle atrophy/wasting is still considered a secondary symptom among various diseases and not targeted as commonly for pharmaceutical intervention.

A better understanding of the interface between muscle amino acid metabolism and synthesis pathways could uncover additional regulators of muscle protein synthesis. The high expression of BCAT in skeletal muscle supports the preference of branched-chain amino acids as a bioenergetic substrate. There is a gap in our understanding of fate decisions of BCAAs and anabolic signaling in muscle. This could be a result of the temporal nature of muscle energetics, having diverse metabolism with changes in nutrient availability and contractile activity. AMPK is an obvious regulator of BCAA fate, effecting both catabolic and anabolic signaling pathways, including direct/indirect effects on mTORC1 and BCKDH. However, it would not be surprising to identify additional regulators of BCAA metabolism having an impact on both catabolic and anabolic processes.

As for translational potential of these pathways to offset muscle atrophy/wasting, identification of anabolic pathways, unique to skeletal muscle, could open up therapeutic targets. The potency of these pathways to regulate muscle mass is supported by strong *in vivo* studies using preclinical models discussed throughout his review. Manipulation of key regulatory proteins within the mTORC1 signaling pathway can accelerate (Ishikawa et al., 2017) or preserve (Kazi et al., 2011) the loss in muscle mass and/or protein synthesis under atrophy-promoting conditions. Since we now have a general understanding of these pathways, why are there no available drugs to offset muscle wasting? The challenge is to identify key targets within these complex pathways and manipulate them in a muscle-specific manner. The mTORC1 pathway is tightly controlled and ubiquitous across many cell types. Promoting muscle anabolism by manipulating global mTORC1 activity will most likely alter the delicate balance of non-muscle cells and promote unchecked growth and malignancies. Finding key regulators within the mTORC1 pathway, specific to muscle would be ideal for drug development. This warrants continued investigation of anabolic pathways, especially within skeletal muscle.

AUTHOR CONTRIBUTIONS

The author confirms being the sole contributor of this work and has approved it for publication.

FUNDING

This work was supported by grants from the National Institutes of Health (grants K01AG056664 and R21AG065943).

ACKNOWLEDGMENTS

The author would like to thank Phillip White for his valuable discussion and insight pertaining to this review.

REFERENCES

Alessi, D. R., James, S. R., Downes, C. P., Holmes, A. B., Gaffney, P. R., Reese, C. B., et al. (1997). Characterization of a 3-phosphoinositide-dependent protein kinase which phosphorylates and activates protein kinase Balpha. *Curr. Biol.* 7, 261–269. doi: 10.1016/s0960-9822(06)00122-9

Andjelkovic, M., Alessi, D. R., Meier, R., Fernandez, A., Lamb, N. J., Frech, M., et al. (1997). Role of translocation in the activation and function of protein kinase B. *J. Biol. Chem.* 272, 31515–31524.

Anthony, J. C., Yoshizawa, F., Anthony, T. G., Vary, T. C., Jefferson, L. S., and Kimball, S. R. (2000). Leucine stimulates translation initiation in skeletal muscle of postabsorptive rats via a rapamycin-sensitive pathway. *J. Nutr.* 130, 2413–2419. doi: 10.1093/jn/130.10.2413

Bentzinger, C. F., Romanino, K., Cloetta, D., Lin, S., Mascarenhas, J. B., Oliveri, F., et al. (2008). Skeletal muscle-specific ablation of raptor, but not of rictor, causes metabolic changes and results in muscle dystrophy. *Cell Metab.* 8, 411–424. doi: 10.1016/j.cmet.2008.10.002

Biswas, D., Dao, K. T., Mercer, A., Cowie, A. M., Duffley, L., El Hiani, Y., et al. (2020). Branched-chain ketoacid overload inhibits insulin action in the muscle. *J. Biol. Chem.* 295, 15597–15621. doi: 10.1074/jbc.ra120.013121

Bodine, S. C., Stitt, T. N., Gonzalez, M., Kline, W. O., Stover, G. L., Bauerlein, R., et al. (2001). Akt/mTOR pathway is a crucial regulator of skeletal muscle hypertrophy and can prevent muscle atrophy in vivo. *Nat. Cell Biol.* 3, 1014–1019. doi: 10.1038/ncb1101-1014

Bohe, J., Low, J. F., Wolfe, R. R., and Rennie, M. J. (2001). Latency and duration of stimulation of human muscle protein synthesis during continuous infusion of amino acids. *J. Physiol.* 532, 575–579. doi: 10.1111/j.1469-7793.2001.0575f.x

Bolster, D. R., Crozier, S. J., Kimball, S. R., and Jefferson, L. S. (2002). AMP-activated protein kinase suppresses protein synthesis in rat skeletal muscle through down-regulated mammalian target of rapamycin (mTOR) signaling. *J. Biol. Chem.* 277, 23977–23980. doi: 10.1074/jbc.c200171200

Brugarolas, J., Lei, K., Hurley, R. L., Manning, B. D., Reiling, J. H., Hafen, E., et al. (2004). Regulation of mTOR function in response to hypoxia by REDD1 and the TSC1/TSC2 tumor suppressor complex. *Genes Dev.* 18, 2893–2904. doi: 10.1101/gad.1256804

Chan, A. Y., Soltys, C. L., Young, M. E., Proud, C. G., and Dyck, J. R. (2004). Activation of AMP-activated protein kinase inhibits protein synthesis associated with hypertrophy in the cardiac myocyte. *J. Biol. Chem.* 279, 32771–32779. doi: 10.1074/jbc.m403528200

Cheng, S. W., Fryer, L. G., Carling, D., and Shepherd, P. R. (2004). Thr2446 is a novel mammalian target of rapamycin (mTOR) phosphorylation site regulated by nutrient status. *J. Biol. Chem.* 279, 15719–15722. doi: 10.1074/jbc.c300534200

Chiang, G. G., and Abraham, R. T. (2005). Phosphorylation of mammalian target of rapamycin (mTOR) at Ser-2448 is mediated by p70S6 kinase. *J. Biol. Chem.* 280, 25485–25490. doi: 10.1074/jbc.m501707200

Crosby, J. S., Chefalo, P. J., Yeh, I., Ying, S., London, I. M., Leboulch, P., et al. (2000). Regulation of hemoglobin synthesis and proliferation of differentiating erythroid cells by heme-regulated eIF-2alpha kinase. *Blood* 96, 3241–3248. doi: 10.1182/blood.v96.9.3241.h8003241_3241_3248

Demetriades, C., Doumpas, N., and Teleman, A. A. (2014). Regulation of TORC1 in response to amino acid starvation via lysosomal recruitment of TSC2. *Cell* 156, 786–799. doi: 10.1016/j.cell.2014.01.024

Deshmukh, A. S., Treebak, J. T., Long, Y. C., Viollet, B., Wojtaszewski, J. F., and Zierath, J. R. (2008). Role of adenosine 5'-monophosphate-activated protein kinase subunits in skeletal muscle mammalian target of rapamycin signaling. *Mol. Endocrinol.* 22, 1105–1112. doi: 10.1210/me.2007-0448

Dever, T. E. (2002). Gene-specific regulation by general translation factors. *Cell* 108, 545–556. doi: 10.1016/s0092-8674(02)00642-6

Du, M., Shen, Q. W., Zhu, M. J., and Ford, S. P. (2007). Leucine stimulates mammalian target of rapamycin signaling in C2C12 myoblasts in part through inhibition of adenosine monophosphate-activated protein kinase. *J. Anim. Sci.* 85, 919–927. doi: 10.2527/jas.2006-342

Dunlop, E. A., Dodd, K. M., Seymour, L. A., and Tee, A. R. (2009). Mammalian target of rapamycin complex 1-mediated phosphorylation of eukaryotic initiation factor 4E-binding protein 1 requires multiple protein-protein interactions for substrate recognition. *Cell Signal.* 21, 1073–1084. doi: 10.1016/j.cellsig.2009.02.024

Estrada-Alcalde, I., Tenorio-Guzman, M. R., Tovar, A. R., Salinas-Rubio, D., Torre-Villalvazo, I., Torres, N., et al. (2017). Metabolic fate of branched-chain amino acids during adipogenesis, in adipocytes from obese mice and C2C12 Myotubes. *J. Cell Biochem.* 118, 808–818. doi: 10.1002/jcb.25755

Foster, K. G., Acosta-Jaquez, H. A., Romeo, Y., Ekim, B., Soliman, G. A., Carriere, A., et al. (2010). Regulation of mTOR complex 1 (mTORC1) by raptor Ser863 and multisite phosphorylation. *J. Biol. Chem.* 285, 80–94. doi: 10.1074/jbc.m109.029637

Frost, R. A., and Lang, C. H. (2007). Protein Kinase B/Akt: a nexus of growth factor and cytokine signaling in determining muscle mass. *J. Appl. Physiol.* 103, 378–387. doi: 10.1152/japplphysiol.00089.2007

Gao, X., Zhang, Y., Arrazola, P., Hino, O., Kobayashi, T., Yeung, R. S., et al. (2002). Tsc tumour suppressor proteins antagonize amino-acid-TOR signalling. *Nat. Cell Biol.* 4, 699–704. doi: 10.1038/ncb847

Glass, D. J. (2010). PI3 kinase regulation of skeletal muscle hypertrophy and atrophy. *Curr. Top. Microbiol. Immunol.* 346, 267–278. doi: 10.1007/82_2010_78

Goberdhan, D. C., Ogmundsdottir, M. H., Kazi, S., Reynolds, B., Visvalingam, S. M., Wilson, C., et al. (2009). Amino acid sensing and mTOR regulation: inside or out? *Biochem. Soc. Trans.* 37, 248–252. doi: 10.1042/bst0370248

Gordon, B. S., Liu, C., Steiner, J. L., Nader, G. A., Jefferson, L. S., and Kimball, S. R. (2016). Loss of REDD1 augments the rate of the overload-induced increase in muscle mass. *Am. J. Physiol. Regul. Integr. Comp. Physiol.* 311, R545–R557.

Gordon, S. E., Lake, J. A., Westerkamp, C. M., and Thomson, D. M. (2008). Does AMP-activated protein kinase negatively mediate aged fast-twitch skeletal muscle mass? *Exerc. Sport Sci. Rev.* 36, 179–186. doi: 10.1097/jes.0b013e3181877e13

Greiwe, J. S., Kwon, G., McDaniel, M. L., and Semenkovich, C. F. (2001). Leucine and insulin activate p70 S6 kinase through different pathways in human skeletal muscle. *Am. J. Physiol. Endocrinol. Metab.* 281, E466–E471.

Gwinn, D. M., Shackelford, D. B., Egan, D. F., Mihaylova, M. M., Mery, A., Vasquez, D. S., et al. (2008). AMPK phosphorylation of raptor mediates a metabolic checkpoint. *Mol. Cell.* 30, 214–226. doi: 10.1016/j.molcel.2008.03.003

Hara, K., Maruki, Y., Long, X., Yoshino, K., Oshiro, N., Hidayat, S., et al. (2002). Raptor, a binding partner of target of rapamycin (TOR), mediates TOR action. *Cell* 110, 177–189. doi: 10.1016/s0092-8674(02)00833-4

Hardie, D. G. (2003). Minireview: the AMP-activated protein kinase cascade: the key sensor of cellular energy status. *Endocrinology* 144, 5179–5183. doi: 10.1210/en.2003-0982

Harris, R. A., Popov, K. M., Zhao, Y., and Shimomura, Y. (1994). Regulation of branched-chain amino acid catabolism. *J. Nutr.* 124, 1499S–1502S.

Harris, R. A., Zhang, B., Goodwin, G. W., Kuntz, M. J., Shimomura, Y., Rougraff, P., et al. (1990). Regulation of the branched-chain alpha-ketoacid dehydrogenase and elucidation of a molecular basis for maple syrup urine disease. *Adv. Enzyme Regul.* 30, 245–263. doi: 10.1016/0065-2571(90)90021-s

Hatazawa, Y., Tadaishi, M., Nagaike, Y., Morita, A., Ogawa, Y., Ezaki, O., et al. (2014). PGC-1alpha-mediated branched-chain amino acid metabolism in the skeletal muscle. *PLoS One* 9:e91006. doi: 10.1371/journal.pone.0091006

Hawley, S. A., Davison, M., Woods, A., Davies, S. P., Beri, R. K., Carling, D., et al. (1996). Characterization of the AMP-activated protein kinase kinase from rat liver and identification of threonine 172 as the major site at which it phosphorylates AMP-activated protein kinase. *J. Biol. Chem.* 271, 27879–27887. doi: 10.1074/jbc.271.44.27879

Horman, S., Browne, G., Krause, U., Patel, J., Vertommen, D., Bertrand, L., et al. (2002). Activation of AMP-activated protein kinase leads to the phosphorylation of elongation factor 2 and an inhibition of protein synthesis. *Curr. Biol.* 12, 1419–1423. doi: 10.1016/s0960-9822(02)01077-1

Hudson, E. R., Pan, D. A., James, J., Lucocq, J. M., Hawley, S. A., Green, K. A., et al. (2003). A novel domain in AMP-activated protein kinase causes glycogen storage bodies similar to those seen in hereditary cardiac arrhythmias. *Curr. Biol.* 13, 861–866. doi: 10.1016/s0960-9822(03)00249-5

Hutson, S. M. (1989). Regulation of substrate availability for the branched-chain alpha-keto acid dehydrogenase enzyme complex. *Ann. N. Y. Acad. Sci.* 573, 230–239. doi: 10.1111/j.1749-6632.1989.tb15000.x

Inoki, K., Zhu, T., and Guan, K. L. (2003). TSC2 mediates cellular energy response to control cell growth and survival. *Cell* 115, 577–590. doi: 10.1016/s0092-8674(03)00929-2

Ishikawa, T., Kitaura, Y., Kadota, Y., Morishita, Y., Ota, M., Yamanaka, F., et al. (2017). Muscle-specific deletion of BDK amplifies loss of myofibrillar protein during protein undernutrition. *Sci. Rep.* 7:39825.

Jacinto, E., Loewith, R., Schmidt, A., Lin, S., Ruegg, M. A., Hall, A., et al. (2004). Mammalian TOR complex 2 controls the actin cytoskeleton and is rapamycin insensitive. *Nat. Cell Biol.* 6, 1122–1128. doi: 10.1038/ncb1183

Jefferson, L. S., Fabian, J. R., and Kimball, S. R. (1999). Glycogen synthase kinase-3 is the predominant insulin-regulated eukaryotic initiation factor 2B kinase in skeletal muscle. *Int. J. Biochem. Cell Biol.* 31, 191–200. doi: 10.1016/s1357-2725(98)00141-1

Joshi, M. A., Jeoung, N. H., Obayashi, M., Hattab, E. M., Brocken, E. G., Liechty, E. A., et al. (2006). Impaired growth and neurological abnormalities in branched-chain alpha-keto acid dehydrogenase kinase-deficient mice. *Biochem. J.* 400, 153–162. doi: 10.1042/bj20060869

Kazi, A. A., Hong-Brown, L., Lang, S. M., and Lang, C. H. (2011). Deptor knockdown enhances mTOR Activity and protein synthesis in myocytes and ameliorates disuse muscle atrophy. *Mol. Med.* 17, 925–936. doi: 10.2119/molmed.2011.00070

Kim, D. H., Sarbassov, D. D., Ali, S. M., King, J. E., Latek, R. R., Erdjument-Bromage, H., et al. (2002). mTOR interacts with raptor to form a nutrient-sensitive complex that signals to the cell growth machinery. *Cell* 110, 163–175. doi: 10.1016/s0092-8674(02)00808-5

Kim, E., Goraksha-Hicks, P., Li, L., Neufeld, T. P., and Guan, K. L. (2008). Regulation of TORC1 by Rag GTPases in nutrient response. *Nat. Cell Biol.* 10, 935–945. doi: 10.1038/ncb1753

Lai, K. M., Gonzalez, M., Poueymirou, W. T., Kline, W. O., Na, E., Zlotchenko, E., et al. (2004). Conditional activation of akt in adult skeletal muscle induces rapid hypertrophy. *Mol. Cell. Biol.* 24, 9295–9304. doi: 10.1128/mcb.24.21.9295-9304.2004

Lian, K., Du, C., Liu, Y., Zhu, D., Yan, W., Zhang, H., et al. (2015). Impaired adiponectin signaling contributes to disturbed catabolism of branched-chain amino acids in diabetic mice. *Diabetes* 64, 49–59. doi: 10.2337/db14-0312

Lin, L., Qian, Y., Shi, X., and Chen, Y. (2005). Induction of a cell stress response gene RTP801 by DNA damaging agent methyl methanesulfonate through CCAAT/enhancer binding protein. *Biochemistry* 44, 3909–3914. doi: 10.1021/bi047574r

Liu, Z., Jahn, L. A., Long, W., Fryburg, D. A., Wei, L., and Barrett, E. J. (2001). Branched chain amino acids activate messenger ribonucleic acid translation regulatory proteins in human skeletal muscle, and glucocorticoids blunt this action. *J. Clin. Endocrinol. Metab.* 86, 2136–2143. doi: 10.1210/jc.86.5.2136

Liu, Z., Wu, Y., Nicklas, E. W., Jahn, L. A., Price, W. J., and Barrett, E. J. (2004). Unlike insulin, amino acids stimulate p70S6K but not GSK-3 or glycogen synthase in human skeletal muscle. *Am. J. Physiol. Endocrinol. Metab.* 286, E523–E528.

Long, X., Lin, Y., Ortiz-Vega, S., Yonezawa, K., and Avruch, J. (2005a). Rheb binds and regulates the mTOR kinase. *Curr. Biol.* 15, 702–713. doi: 10.1016/j.cub.2005.02.053

Long, X., Ortiz-Vega, S., Lin, Y., and Avruch, J. (2005b). Rheb binding to mammalian target of rapamycin (mTOR) is regulated by amino acid sufficiency. *J. Biol. Chem.* 280, 23433–23436. doi: 10.1074/jbc.c500169200

Lu, G., Sun, H., She, P., Youn, J. Y., Warburton, S., Ping, P., et al. (2009). Protein phosphatase 2Cm is a critical regulator of branched-chain amino acid catabolism in mice and cultured cells. *J. Clin. Invest.* 119, 1678–1687. doi: 10.1172/jci38151

Mader, S., Lee, H., Pause, A., and Sonenberg, N. (1995). The translation initiation factor eIF-4E binds to a common motif shared by the translation factor eIF-4 gamma and the translational repressors 4E-binding proteins. *Mol. Cell Biol.* 15, 4990–4997. doi: 10.1128/mcb.15.9.4990

Marton, M. J., Crouch, D., and Hinnebusch, A. G. (1993). GCN1, a translational activator of GCN4 in Saccharomyces cerevisiae, is required for phosphorylation of eukaryotic translation initiation factor 2 by protein kinase GCN2. *Mol. Cell Biol.* 13, 3541–3556. doi: 10.1128/mcb.13.6.3541

McGhee, N. K., Jefferson, L. S., and Kimball, S. R. (2009). Elevated corticosterone associated with food deprivation upregulates expression in rat skeletal muscle of the mTORC1 repressor. REDD1. *J Nutr.* 139, 828–834. doi: 10.3945/jn.108.099846

Menon, S., Dibble, C. C., Talbott, G., Hoxhaj, G., Valvezan, A. J., Takahashi, H., et al. (2014). Spatial control of the TSC complex integrates insulin and nutrient regulation of mTORC1 at the lysosome. *Cell* 156, 771–785. doi: 10.1016/j.cell.2013.11.049

Meurs, E., Chong, K., Galabru, J., Thomas, N. S., Kerr, I. M., Williams, B. R., et al. (1990). Molecular cloning and characterization of the human double-stranded RNA-activated protein kinase induced by interferon. *Cell* 62, 379–390. doi: 10.1016/0092-8674(90)90374-n

Moelling, K., Schad, K., Bosse, M., Zimmermann, S., and Schweneker, M. (2002). Regulation of Raf-Akt Cross-talk. *J. Biol. Chem.* 277, 31099–31106. doi: 10.1074/jbc.m111974200

Moghei, M., Tavajohi-Fini, P., Beatty, B., and Adegoke, O. A. (2016). Ketoisocaproic acid, a metabolite of leucine, suppresses insulin-stimulated glucose transport in skeletal muscle cells in a BCAT2-dependent manner. *Am. J. Physiol. Cell Physiol.* 311, C518–C527.

Mounier, R., Lantier, L., Leclerc, J., Sotiropoulos, A., Pende, M., Daegelen, D., et al. (2009). Important role for AMPKalpha1 in limiting skeletal muscle cell hypertrophy. *FASEB J.* 23, 2264–2273. doi: 10.1096/fj.08-119057

Ogasawara, R., Knudsen, J. R., Li, J., Ato, S., and Jensen, T. E. (2020). Rapamycin and mTORC2 inhibition synergistically reduce contraction-stimulated muscle protein synthesis. *J Physiol.* 598, 5453–5466. doi: 10.1113/jp280528

Panniers, R., and Henshaw, E. C. (1983). A GDP/GTP exchange factor essential for eukaryotic initiation factor 2 cycling in Ehrlich ascites tumor cells and its regulation by eukaryotic initiation factor 2 phosphorylation. *J. Biol. Chem.* 258, 7928–7934. doi: 10.1016/s0021-9258(20)82007-9

Peterson, T. R., Laplante, M., Thoreen, C. C., Sancak, Y., Kang, S. A., Kuehl, W. M., et al. (2009). DEPTOR is an mTOR inhibitor frequently overexpressed in multiple myeloma cells and required for their survival. *Cell* 137, 873–886. doi: 10.1016/j.cell.2009.03.046

Polekhina, G., Gupta, A., Michell, B. J., van Denderen, B., Murthy, S., Feil, S. C., et al. (2003). AMPK beta subunit targets metabolic stress sensing to glycogen. *Curr. Biol.* 13, 867–871. doi: 10.1016/s0960-9822(03)00292-6

Ponticos, M., Lu, Q. L., Morgan, J. E., Hardie, D. G., Partridge, T. A., and Carling, D. (1998). Dual regulation of the AMP-activated protein kinase provides a novel mechanism for the control of creatine kinase in skeletal muscle. *Embo J.* 17, 1688–1699. doi: 10.1093/emboj/17.6.1688

Potier, M., Darcel, N., and Tome, D. (2009). Protein, amino acids and the control of food intake. *Curr. Opin. Clin. Nutr. Metab. Care* 12, 54–58. doi: 10.1097/mco.0b013e32831b9e01

Price, N., and Proud, C. (1994). The guanine nucleotide-exchange factor, eIF-2B. *Biochimie* 76, 748–760. doi: 10.1016/0300-9084(94)90079-5

Protiva, P., Hopkins, M. E., Baggett, S., Yang, H., Lipkin, M., Holt, P. R., et al. (2008). Growth inhibition of colon cancer cells by polyisoprenylated benzophenones is associated with induction of the endoplasmic reticulum response. *Int. J. Cancer* 123, 687–694. doi: 10.1002/ijc.23515

Proud, C. G. (2005). eIF2 and the control of cell physiology. *Semin. Cell Dev. Biol.* 16, 3–12. doi: 10.1016/j.semcdb.2004.11.004

Proud, C. G. (2007). Signalling to translation: how signal transduction pathways control the protein synthetic machinery. *Biochem. J.* 403, 217–234. doi: 10.1042/bj20070024

Pruznak, A. M., Kazi, A. A., Frost, R. A., Vary, T. C., and Lang, C. H. (2008). Activation of AMP-activated protein kinase by 5-aminoimidazole-4-carboxamide-1-beta-D-ribonucleoside prevents leucine-stimulated protein synthesis in rat skeletal muscle. *J. Nutr.* 138, 1887–1894. doi: 10.1093/jn/138.10.1887

Reiling, J. H., and Hafen, E. (2004). The hypoxia-induced paralogs Scylla and Charybdis inhibit growth by down-regulating S6K activity upstream of TSC in *Drosophila*. *Genes Dev.* 18, 2879–2892. doi: 10.1101/gad.322704

Reiter, A. K., Bolster, D. R., Crozier, S. J., Kimball, S. R., and Jefferson, L. S. (2005). Repression of protein synthesis and mTOR signaling in rat liver mediated by the AMPK activator aminoimidazole carboxamide ribonucleoside. *Am. J. Physiol. Endocrinol. Metab.* 288, E980–E988.

Rivera, M. E., Lyon, E. S., Johnson, M. A., Sunderland, K. L., and Vaughan, R. A. (2020). Effect of valine on myotube insulin sensitivity and metabolism with and without insulin resistance. *Mol. Cell Biochem.* 468, 169–183. doi: 10.1007/s11010-020-03720-y

Roberson, P. A., Shimkus, K. L., Welles, J. E., Xu, D., Whitsell, A. L., Kimball, E. M., et al. (2020). A time course for markers of protein synthesis and degradation with hindlimb unloading and the accompanying anabolic resistance to refeeding. *J. Appl. Physiol.* 129, 36–46. doi: 10.1152/japplphysiol.00155.2020

Rolfe, D. F., and Brown, G. C. (1997). Cellular energy utilization and molecular origin of standard metabolic rate in mammals. *Physiol. Rev.* 77, 731–758. doi: 10.1152/physrev.1997.77.3.731

Rommel, C., Bodine, S. C., Clarke, B. A., Rossman, R., Nunez, L., Stitt, T. N., et al. (2001). Mediation of IGF-1-induced skeletal myotube hypertrophy by PI(3)K/Akt/mTOR and PI(3)K/Akt/GSK3 pathways. *Nat. Cell Biol.* 3, 1009–1013. doi: 10.1038/ncb1101-1009

Rowlands, A. G., Panniers, R., and Henshaw, E. C. (1988). The catalytic mechanism of guanine nucleotide exchange factor action and competitive inhibition by phosphorylated eukaryotic initiation factor 2. *J. Biol. Chem.* 263, 5526–5533. doi: 10.1016/s0021-9258(18)60596-4

Sancak, Y., Peterson, T. R., Shaul, Y. D., Lindquist, R. A., Thoreen, C. C., Bar-Peled, L., et al. (2008). The Rag GTPases bind raptor and mediate amino acid signaling to mTORC1. *Science* 320, 1496–1501. doi: 10.1126/science.1157535

Sancak, Y., Thoreen, C. C., Peterson, T. R., Lindquist, R. A., Kang, S. A., Spooner, E., et al. (2007). PRAS40 is an insulin-regulated inhibitor of the mTORC1 protein kinase. *Mol. Cell* 25, 903–915. doi: 10.1016/j.molcel.2007.03.003

Sarbassov, D. D., Guertin, D. A., Ali, S. M., and Sabatini, D. M. (2005). Phosphorylation and regulation of Akt/PKB by the rictor-mTOR complex. *Science* 307, 1098–1101. doi: 10.1126/science.1106148

Schurmann, A., Brauers, A., Massmann, S., Becker, W., and Joost, H. G. (1995). Cloning of a novel family of mammalian GTP-binding proteins (RagA, RagBs, RagB1) with remote similarity to the Ras-related GTPases. *J. Biol. Chem.* 270, 28982–28988. doi: 10.1074/jbc.270.48.28982

Schwarzer, R., Tondera, D., Arnold, W., Giese, K., Klippel, A., and Kaufmann, J. (2005). REDD1 integrates hypoxia-mediated survival signaling downstream of phosphatidylinositol 3-kinase. *Oncogene* 24, 1138–1149. doi: 10.1038/sj.onc.1208236

She, P., Van Horn, C., Reid, T., Hutson, S. M., Cooney, R. N., and Lynch, C. J. (2007). Obesity-related elevations in plasma leucine are associated with alterations in enzymes involved in branched-chain amino acid metabolism. *Am. J. Physiol. Endocrinol. Metab.* 293, E1552–E1563.

Shimkus, K. L., Jefferson, L. S., Gordon, B. S., and Kimball, S. R. (2018). Repressors of mTORC1 act to blunt the anabolic response to feeding in the soleus muscle of a cast-immobilized mouse hindlimb. *Physiol. Rep.* 6:e13891. doi: 10.14814/phy2.13891

Shoshani, T., Faerman, A., Mett, I., Zelin, E., Tenne, T., Gorodin, S., et al. (2002). Identification of a novel hypoxia-inducible factor 1-responsive gene, RTP801, involved in apoptosis. *Mol. Cell Biol.* 22, 2283–2293. doi: 10.1128/mcb.22.7.2283-2293.2002

Smith, E. M., Finn, S. G., Tee, A. R., Browne, G. J., and Proud, C. G. (2005). The tuberous sclerosis protein TSC2 is not required for the regulation of the

mammalian target of rapamycin by amino acids and certain cellular stresses. *J. Biol. Chem.* 280, 18717–18727. doi: 10.1074/jbc.m414499200

Sofer, A., Lei, K., Johannessen, C. M., and Ellisen, L. W. (2005). Regulation of mTOR and cell growth in response to energy stress by REDD1. *Mol. Cell Biol.* 25, 5834–5845. doi: 10.1128/mcb.25.14.5834-5845.2005

Stein, S. C., Woods, A., Jones, N. A., Davison, M. D., and Carling, D. (2000). The regulation of AMP-activated protein kinase by phosphorylation. *Biochem. J.* 345(Pt 3), 437–443.

Sun, X. J., Rothenberg, P., Kahn, C. R., Backer, J. M., Araki, E., Wilden, P. A., et al. (1991). Structure of the insulin receptor substrate IRS-1 defines a unique signal transduction protein. *Nature* 352, 73–77. doi: 10.1038/352073a0

Thomson, D. M., Fick, C. A., and Gordon, S. E. (2008). AMPK activation attenuates S6K1, 4E-BP1, and eEF2 signaling responses to high-frequency electrically stimulated skeletal muscle contractions. *J. Appl. Physiol.* 104, 625–632. doi: 10.1152/japplphysiol.00915.2007

Tong, J. F., Yan, X., Zhu, M. J., and Du, M. (2009). AMP-activated protein kinase enhances the expression of muscle-specific ubiquitin ligases despite its activation of IGF-1/Akt signaling in C2C12 myotubes. *J. Cell Biochem.* 108, 458–468. doi: 10.1002/jcb.22272

Vander Haar, E., Lee, S. I., Bandhakavi, S., Griffin, T. J., and Kim, D. H. (2007). Insulin signalling to mTOR mediated by the Akt/PKB substrate PRAS40. *Nat. Cell Biol.* 9, 316–323. doi: 10.1038/ncb1547

Walejko, J. M., Christopher, B. A., Crown, S. B., Zhang, G. F., Pickar-Oliver, A., Yoneshiro, T., et al. (2021). Branched-chain alpha-ketoacids are preferentially reaminated and activate protein synthesis in the heart. *Nat. Commun.* 12:1680.

Wang, H., Kubica, N., Ellisen, L. W., Jefferson, L. S., and Kimball, S. R. (2006). Dexamethasone represses signaling through the mammalian target of rapamycin in muscle cells by enhancing expression of REDD1. *J. Biol. Chem.* 281, 39128–39134. doi: 10.1074/jbc.m610023200

Wang, H., Zhang, Q., Wen, Q., Zheng, Y., Lazarovici, P., Jiang, H., et al. (2012). Proline-rich Akt substrate of 40kDa (PRAS40): a novel downstream target of PI3k/Akt signaling pathway. *Cell Signal.* 24, 17–24. doi: 10.1016/j.cellsig.2011.08.010

Wang, J., Liu, Y., Lian, K., Shentu, X., Fang, J., Shao, J., et al. (2019). BCAA catabolic defect alters glucose metabolism in lean mice. *Front. Physiol.* 10:1140. doi: 10.3389/fphys.2019.01140

Wang, L., Harris, T. E., Roth, R. A., and Lawrence, J. C. Jr. (2007). PRAS40 regulates mTORC1 kinase activity by functioning as a direct inhibitor of substrate binding. *J. Biol. Chem.* 282, 20036–20044. doi: 10.1074/jbc.m702376200

Wang, Z., Malone, M. H., Thomenius, M. J., Zhong, F., Xu, F., and Distelhorst, C. W. (2003). Dexamethasone-induced gene 2 (dig2) is a novel pro-survival stress gene induced rapidly by diverse apoptotic signals. *J. Biol. Chem.* 278, 27053–27058. doi: 10.1074/jbc.m303723200

Welsh, G. I., Miller, C. M., Loughlin, A. J., Price, N. T., and Proud, C. G. (1998). Regulation of eukaryotic initiation factor eIF2B: glycogen synthase kinase-3 phosphorylates a conserved serine which undergoes dephosphorylation in response to insulin. *FEBS Lett.* 421, 125–130. doi: 10.1016/s0014-5793(97)01548-2

White, J. P., Baynes, J. W., Welle, S. L., Kostek, M. C., Matesic, L. E., Sato, S., et al. (2011). The regulation of skeletal muscle protein turnover during the progression of cancer cachexia in the Apc(Min/+) mouse. *PLoS One* 6:e24650. doi: 10.1371/journal.pone.0024650

White, J. P., Gao, S., Puppa, M. J., Sato, S., Welle, S. L., and Carson, J. A. (2012). Testosterone regulation of Akt/mTORC1/FoxO3a signaling in skeletal muscle. *Mol. Cell Endocrinol.* 365, 174–186. doi: 10.1016/j.mce.2012.10.019

White, P. J., Lapworth, A. L., An, J., Wang, L., McGarrah, R. W., Stevens, R. D., et al. (2016). Branched-chain amino acid restriction in Zucker-fatty rats improves muscle insulin sensitivity by enhancing efficiency of fatty acid oxidation and acyl-glycine export. *Mol. Metab.* 5, 538–551. doi: 10.1016/j.molmet.2016.04.006

White, P. J., Lapworth, A. L., McGarrah, R. W., Kwee, L. C., Crown, S. B., Ilkayeva, O., et al. (2020). Muscle-liver trafficking of BCAA-derived nitrogen underlies obesity-related glycine depletion. *Cell Rep.* 33:108375. doi: 10.1016/j.celrep.2020.108375

White, P. J., McGarrah, R. W., Grimsrud, P. A., Tso, S. C., Yang, W. H., Haldeman, J. M., et al. (2018). The BCKDH kinase and phosphatase integrate BCAA and lipid metabolism via regulation of ATP-citrate lyase. *Cell Metab.* 27, 1281.e7–1293.e7.

White, P. J., and Newgard, C. B. (2019). Branched-chain amino acids in disease. *Science* 363, 582–583.

Williamson, D. L., Bolster, D. R., Kimball, S. R., and Jefferson, L. S. (2006). Time course changes in signaling pathways and protein synthesis in C2C12 myotubes following AMPK activation by AICAR. *Am. J. Physiol. Endocrinol. Metab.* 291, E80–E89.

Wojtaszewski, J. F., Jorgensen, S. B., Hellsten, Y., Hardie, D. G., and Richter, E. A. (2002). Glycogen-dependent effects of 5-aminoimidazole-4-carboxamide (AICA)-riboside on AMP-activated protein kinase and glycogen synthase activities in rat skeletal muscle. *Diabetes* 51, 284–292. doi: 10.2337/diabetes.51.2.284

Wojtaszewski, J. F., MacDonald, C., Nielsen, J. N., Hellsten, Y., Hardie, D. G., Kemp, B. E., et al. (2003). Regulation of 5'AMP-activated protein kinase activity and substrate utilization in exercising human skeletal muscle. *Am. J. Physiol. Endocrinol. Metab.* 284, E813–E822.

Yamauchi, T., Kaburagi, Y., Ueki, K., Tsuji, Y., Stark, G. R., Kerr, I. M., et al. (1998). Growth hormone and prolactin stimulate tyrosine phosphorylation of insulin receptor substrate-1, -2, and -3, their association with p85 phosphatidylinositol 3-kinase (PI3-kinase), and concomitantly PI3-kinase activation via JAK2 kinase. *J. Biol. Chem.* 273, 15719–15726. doi: 10.1074/jbc.273.25.15719

Zhang, Y., Gao, X., Saucedo, L. J., Ru, B., Edgar, B. A., and Pan, D. (2003). Rheb is a direct target of the tuberous sclerosis tumour suppressor proteins. *Nat. Cell Biol.* 5, 578–581. doi: 10.1038/ncb999

Conflict of Interest: The author declares that the research was conducted in the absence of any commercial or financial relationships that could be construed as a potential conflict of interest.

frontiers in Cell and Developmental Biology

ORIGINAL RESEARCH
published: 15 July 2021
doi: 10.3389/fcell.2021.662133

Absence of Desmin Results in Impaired Adaptive Response to Mechanical Overloading of Skeletal Muscle

*Pierre Joanne[1], Yeranuhi Hovhannisyan[1], Maximilien Bencze[2], Marie-Thérèse Daher[1], Ara Parlakian[1], Geraldine Toutirais[3], Jacqueline Gao-Li[1], Alain Lilienbaum[4], Zhenlin Li[1], Ekaterini Kordeli[1], Arnaud Ferry[5,6] and Onnik Agbulut[1]**

[1] Sorbonne Université, Institut de Biologie Paris-Seine (IBPS), CNRS UMR 8256, Inserm ERL U1164, Biological Adaptation and Ageing, Paris, France, [2] U955-IMRB, Team 10, Biology of the Neuromuscular System, Inserm, UPEC, ENVA, EFS, Créteil, France, [3] Muséum National d'Histoire Naturelle (MNHN), Unité Molécules de Communication et Adaptation des Micro-organismes (MCAM), CNRS UMR 7245, Plateau technique de Microscopie Electronique (PtME), Paris, France, [4] Unité de Biologie Fonctionnelle et Adaptative, CNRS UMR 8251, Université de Paris, Paris, France, [5] Institut de Myologie, INSERM U974, Centre de Recherche en Myologie, Sorbonne Université, Paris, France, [6] Université de Paris, Paris, France

OPEN ACCESS

Edited by:
Shuichi Sato,
University of Louisiana at Lafayette, United States

Reviewed by:
Toshinori Yoshihara,
Juntendo University, Japan
Viviana Moresi,
National Research Council (CNR), Italy

***Correspondence:**
Onnik Agbulut
onnik.agbulut@sorbonne-universite.fr

Specialty section:
This article was submitted to Signaling, a section of the journal Frontiers in Cell and Developmental Biology

Received: *31 January 2021*
Accepted: *23 June 2021*
Published: *15 July 2021*

Citation:
Joanne P, Hovhannisyan Y, Bencze M, Daher M-T, Parlakian A, Toutirais G, Gao-Li J, Lilienbaum A, Li Z, Kordeli E, Ferry A and Agbulut O (2021) Absence of Desmin Results in Impaired Adaptive Response to Mechanical Overloading of Skeletal Muscle. Front. Cell Dev. Biol. 9:662133. doi: 10.3389/fcell.2021.662133

Background: Desmin is a muscle-specific protein belonging to the intermediate filament family. Desmin mutations are linked to skeletal muscle defects, including inherited myopathies with severe clinical manifestations. The aim of this study was to examine the role of desmin in skeletal muscle remodeling and performance gain induced by muscle mechanical overloading which mimics resistance training.

Methods: Plantaris muscles were overloaded by surgical ablation of gastrocnemius and soleus muscles. The functional response of plantaris muscle to mechanical overloading in desmin-deficient mice (*Des*KO, n = 32) was compared to that of control mice (n = 36) after 7-days or 1-month overloading. To elucidate the molecular mechanisms implicated in the observed partial adaptive response of *Des*KO muscle, we examined the expression levels of genes involved in muscle growth, myogenesis, inflammation and oxidative energetic metabolism. Moreover, ultrastructure and the proteolysis pathway were explored.

Results: Contrary to control, absolute maximal force did not increase in *Des*KO muscle following 1-month mechanical overloading. Fatigue resistance was also less increased in *Des*KO as compared to control muscle. Despite impaired functional adaptive response of *Des*KO mice to mechanical overloading, muscle weight and the number of oxidative MHC2a-positive fibers per cross-section similarly increased in both genotypes after 1-month overloading. However, mechanical overloading-elicited remodeling failed to activate a normal myogenic program after 7-days overloading, resulting in proportionally reduced activation and differentiation of muscle stem cells. Ultrastructural analysis of the plantaris muscle after 1-month overloading revealed muscle fiber damage in *Des*KO, as indicated by the loss of sarcomere integrity and mitochondrial abnormalities. Moreover, the observed accumulation of autophagosomes and lysosomes in *Des*KO muscle fibers

could indicate a blockage of autophagy. To address this issue, two main proteolysis pathways, the ubiquitin-proteasome system and autophagy, were explored in *Des*KO and control muscle. Our results suggested an alteration of proteolysis pathways in *Des*KO muscle in response to mechanical overloading.

Conclusion: Taken together, our results show that mechanical overloading increases the negative impact of the lack of desmin on myofibril organization and mitochondria. Furthermore, our results suggest that under these conditions, the repairing activity of autophagy is disturbed. Consequently, force generation is not improved despite muscle growth, suggesting that desmin is required for a complete response to resistance training in skeletal muscle.

Keywords: intermediate filament, cytoskeleton, muscle hypertrophy, autophagy, exercice

INTRODUCTION

Desmin belongs to the family of intermediate filaments and is specifically expressed in skeletal, smooth and cardiac muscle cells. In absence of desmin, or due to mutations in the encoding gene, several defects have been described in all three muscle types, and particularly in cardiac (Brodehl et al., 2018) and skeletal muscle (Goldfarb and Dalakas, 2009; van Spaendonck-Zwarts et al., 2010). In skeletal muscle cells, desmin forms filaments that connect different organelles between them, to the cytoskeleton, and to the plasma membrane. Desmin filaments are linked to the costameres and Z-discs through interactions with synemin (Granger and Lazarides, 1980; Bellin et al., 2001), plectin (Konieczny et al., 2008), nebulette and indirectly to actin filaments (Hernandez et al., 2016), contributing to its role in the maintenance of the structural and mechanical integrity of the contractile apparatus in muscle tissues.

Since their generation (Li et al., 1996; Milner et al., 1996), the desmin knock-out mice (*Des*KO) were used to assess the role of this intermediate filament in skeletal muscles. Under resting conditions, desmin-deficient soleus muscle shows an increase in the number of slow/oxidative fibers, but also a decrease in force and fatigue resistance, as compared to control (Li et al., 1997). However, the role of desmin in the long-term adaptation process following extreme muscle mechanical stimulation is not clear. It has been suggested that desmin is protective in the case of remodeling induced by endurance exercice and, on the contrary, deleterious when the muscle is submitted to eccentric exercise (Sam et al., 2000).

Mechanical overloading (OVL) of plantaris muscle mimics resistance training and powerfully induces muscle remodeling and hypertrophy as well as increase in muscle function. In response to OVL, the weight of plantaris muscle almost doubles, absolute maximal force and fatigue resistance increase, and muscle fibers exhibit a fast/glycolytic to slow/oxidative type transition (Ianuzzo et al., 1976; Roy and Edgerton, 1995; Parsons et al., 2004; Joanne et al., 2012). Since desmin expression can be increased in response to resistance training (Woolstenhulme et al., 2006; Parcell et al., 2009), in this study, we addressed the putative role of desmin on muscle remodeling and performance gain induced by OVL in mice.

Herein, we compared the effects of 1 month-OVL on absolute maximal force, specific maximal force, fatigue resistance, muscle growth, and fiber type transition of the plantaris muscle of adult desmin-deficient mice (*Des*KO) and of age- and sex-matched control mice. We collected evidence of a dichotomy between the OVL- induced muscle gain of mass, and the effects on muscle function in *DesKO* muscles compared to controls. Our data suggest that the down regulation of the myostatin pathway efficiently promotes muscle hypertrophy in *DesKO* muscles. However, OVL-elicited remodeling failed to activate normal myogenic program, resulting in proportionally less muscle stem cell (MuSC) activation and differentiation. Furthermore, desmin absence prevented the upregulation of LC3, suggesting that there is a link between desmin and the autophagic process that accompanies muscle remodeling following mechanical overloading.

MATERIALS AND METHODS

Animals and Treatments

All procedures were performed in accordance with national and European legislations, in conformity with the Public Health Service Policy on Human Care and Use of Laboratory Animals under the license 75-1102. 32 2-months-old *Des*KO female mice were used in this study. Age-matched wild-type (n = 24) or $Des^{+/-}$ heterezygous (n = 12) female mice were used as controls. Mice were randomly divided into different control and experimental groups. All animal studies were approved by our institutional Ethics Committee (Charles Darwin, projet number: 01362.02) and conducted according to the French and European laws, directives, and regulations on animal care (European Commission Directive 86/609/EEC). Our animal facility is fully licensed by the French competent authorities and has animal welfare insurance. For OVL, the mice were anesthetized with

Abbreviations: *Des*KO, desmin knock-out mice; GAPDH, glyceraldehyde 3-phosphate dehydrogenase; Hmbs, hydroxymethylbilane synthase; Igf1, insulin growth factor 1; i.p., intraperitoneal; MHC, myosin heavy chain; Mstn, Myostatin; MuSCs, Muscle stem cells; OVL, mechanical overloading; Perlecan, heparan sulfate proteoglycan; PKARIIα, protein kinase A regulatory subunit IIα; P0, maximal force; SDH, succinate deshydrogenease; Sdha, succinate dehydrogenase complex flavoprotein subunit A; sP0, specific maximal force.

pentobarbital (50 mg/kg body weight, i.p.). The plantaris muscles of both legs were mechanically overloaded for 7 days or 1 month by the surgical removal of soleus muscles and a major portion of the gastrocnemius muscles as described (Joanne et al., 2012; Ferry et al., 2015).

Muscle Force Measurements

Plantaris muscle function was evaluated by measuring *in situ* isometric force, as described (Vignaud et al., 2007; Hourdé et al., 2013a). Briefly, mice were anesthetized (pentobarbital sodium, 50 mg/kg, i.p.). During physiological experiments, supplemental doses were given as required, to maintain deep anesthesia. The knee and foot were fixed with clamps and stainless-steel pins. The plantaris muscle was exposed (and the distal tendon of the gastrocnemius and soleus muscle complex was cut in non-overloaded muscles). The distal tendon of the plantaris muscle was attached to an isometric transducer (Harvard Apparatus) with a silk ligature. The sciatic nerves were proximally crushed and distally stimulated by a bipolar silver electrode using supramaximal square wave pulses of 0.1 ms duration. Responses to tetanic stimulation (pulse frequency 75–143 Hz) were successively recorded. At least 1 min was allowed between contractions. Absolute maximal forces were determined at optimal length (length at which maximal tension was obtained during the tetanus). Force was normalized to the muscle mass (m) as an estimate of specific maximal force. Fatigue resistance was then determined after a 5-min rest period. The muscle was continuously stimulated at 50 Hz for 2 min (submaximal continuous tetanus). The duration corresponding to a 50% decrease in force was noted. Body temperature was maintained at 37°C using radiant heat. After the measurements, mice were euthanized with an overdose of pentobarbital.

Histology and Immunohistochemistry

Transverse 10 μm-thick frozen sections were prepared from the mid-belly region of plantaris muscles using a cryostat (Leica Microsystems, Nanterre, France). Some sections were processed for histological analysis (Hematoxylin-eosin, Sirius red stainings) according to standard protocols. Other sections were processed for immunohistochemistry as described previously (Joanne et al., 2012; Hourdé et al., 2013b). Briefly, the sections were incubated with primary antibodies against heparan sulfate proteoglycan (Perlecan) (1:400, rat monoclonal, Millipore), myosin heavy chain (MHC)-2a (1:50, mouse monoclonal, clone SC-71, Developmental Studies Hybridoma Bank, University of Iowa) or MHC-2b (1:5, mouse monoclonal, clone BF-F3, Developmental Studies Hybridoma Bank, University of Iowa). After washing in PBS, sections were incubated 1 h with secondary antibodies (Alexa Fluor®, Life Technologies). After washing in PBS, slides were finally mounted using mowiol containing 5 μg/ml Hoescht 33342 (Life Technologies). Images were captured using a motorized fluorescent microscope (Dmi8, Leica Microsystems). Morphometric analyses were made using the ImageJ software and a custom macro as described previously (Joanne et al., 2012; Hourdé et al., 2013a). The percentage of fiber type and smallest diameter (min-Ferret) of all muscle fibers of the whole muscle section were measured.

Electron Microscopy

Electron microscopy was carried out as described previously (Agbulut et al., 2001; Joanne et al., 2013). Briefly, the calf muscles of mice were fixed in 2% glutaraldehyde and 2% paraformaldéhyde in 0.2 M phosphate buffer at pH 7.4 for 1 h at room temperature. After 1 h, the plantaris muscle was dissected and separated in three by a short-axis section, then fixed overnight at 4°C in the same fixative. After washing, specimens were post-fixed for 1 h with 1% osmium tetroxide solution, dehydrated in increasing concentrations of ethanol and finally in acetone, and embedded in epoxy resin. The resin was polymerized for 48 h at 60°C. Ultrathin sections (70 nm) were cut with an ultramicrotome (Leica UC6, Leica Microsystems), picked-up on copper rhodium-coated grids and stained for 2 min with Uranyl-Less solution (Delta Microscopies, France) and 2 min with 0.2% lead citrate before observation at 80 kV with an electron microscope (912 Omega, Zeiss) equipped with a digital camera (Veleta 2kx2k, Emsis, Germany).

Western-Blotting

Immunoblotting was carried out as described previously (Joanne et al., 2012; Li et al., 2014). Muscle tissues were snap-frozen in liquid nitrogen immediately after dissection. Frozen muscles were placed into an ice-cold homogenization buffer containing: 50 mM Tris (pH 7.6), 250 mM NaCl, 3 mM EDTA, 3 mM EGTA, 0.5% NP40, 2 mM dithiothreitol, 10 mM sodium orthovanadate, 10 mM NaF, 10 mM glycerophosphate and 2% of protease inhibitor cocktail (Sigma-Aldrich). Samples were minced with scissors and homogenized using plastic pestles, incubated 30 min on ice, sonicated 3 times for 5 s with 30-s intervals on ice, then centrifuged at 12,000 g for 30 min at 4°C. Protein concentration was measured using the Bradford method with bovine serum albumin as a standard. Equal amounts of protein extracts (25 μg) were separated by SDS-PAGE before electrophoretic transfer onto a nitrocellulose membrane (GE Healthcare). Western-blot analysis was carried out using anti-total-protein kinase A regulatory subunit IIα (PKARIIα) (1:1,00, rabbit polyclonal, Millipore), anti-phospho-PKARIIα (Ser96) (1:1,000, rabbit polyclonal, Millipore), anti-LC3-II (1:1,000, rabbit polyclonal, Sigma-Aldrich), anti-β-tubulin (1:1,000, mouse monoclonal, Sigma-Aldrich) and anti-Glyceraldehyde 3-phosphate dehydrogenase (GAPDH) antibody (1:5,000, mouse monoclonal, Santa Cruz Biotechnology). Proteins bound to primary antibodies were visualized with peroxidase-conjugated secondary antibodies (Thermo Fisher Scientific) and a chemiluminescent detection system (ECL-Plus, GE Healthcare). Bands were quantified by densitometric software (Multi Gauge, Fujifilm). At least three animals were used for each experimental point. The levels of activation of autophagy were calculated by quantification of the LC3-II (anti-LC3 antibody, Sigma-Aldrich) band normalized to β-tubulin (anti-β-tubulin antibody) (Sarkar et al., 2009).

Proteasome Activity Measurement

Tissue homogenates containing proteasome were prepared just after dissection using ice-cold homogenization buffer containing:

20 mM Tris-HCl (pH 7.6), 250 mM NaCl, 3 mM EDTA, 3 mM EGTA and 2 mM DTT (Hovhannisyan et al., 2019). Samples were minced with scissors and homogenized using plastic pestles, incubated 30 min on ice, then centrifuged at 12,000 g for 15 min at 4°C. Protein concentration was measured using the Bradford method with bovine serum albumin as a standard. The proteasomal chymotrypsin-like, trypsin-like and caspase-like activities of the 20S catalytic core were assayed using the fluorogenic substrates *N*-Succinyl-Leu-Leu-Val-Tyr-7-amino-4-methylcoumarin (Suc-LLVY-AMC, Enzo Life Sciences), Bz-Val-Gly-7-amino-4-methylcoumarin (Bz-VGR-AMC, Enzo Life Sciences) and Z-Leu-Leu-Glu-7-amino-4-methylcoumarin (Z-LLE-AMC, Enzo Life Sciences), respectively. The mixture, containing 10 μg of total protein in 20 mM Tris (pH 8) and 10% gylcerol, was incubated at 37°C with 20 μM peptide substrates in a final volume of 100 μl. Enzymatic kinetics were monitored in a temperature-controlled microplate fluorimetric reader (FLUOstar Galaxy, BMG labtech). Excitation/emission wavelengths were 350/440 nm. The difference between assays with or without MG-132, a proteasome inhibitor, represented the proteasome-specific activity.

Relative Quantification of Gene Expression by qPCR

Total RNA was extracted from the plantaris muscle using QIAzol® lysis reagent, TissueLyser II system, and Rneasy minikit (Qiagen France SAS) following the manufacturer's instructions. Extracted RNA was spectrophotometrically quantified using NanoDrop 2000 (Thermo Fisher Scientific). From 500 ng of extracted RNA, the first-strand cDNA was then synthesized using the Transcriptor First Strand cDNA Synthesis Kit (Roche Diagnostics) with anchored-oligo(dT)18 primer and according to the manufacturer's instructions. Using a Light Cycler® 480 system (Roche Diagnostics), the reaction was carried out in duplicate for each sample in a 6 μl reaction volume containing 3 μl of SYBR Green Master Mix, 500 nM of the forward and reverse primers each and 3 μl of diluted (1:25) cDNA. The thermal profile for SYBR Green qPCR was 95°C for 8 min, followed by 40 cycles at 95°C for 15 s, 60°C for 15 s and 72°C for 30 s. To exclude PCR products amplified from genomic DNA, primers were designed, when possible, to span one exon-exon junction. Primers sequences used in this study are available on request. The expression of hydroxymethylbilane synthase (Hmbs) and succinate dehydrogenase complex flavoprotein subunit A (Sdha) was used as a reference transcript. At least five animals were used for each experimental point.

Statistical Analysis

Groups were statistically compared with GraphPad Prism 7 using ordinary two-way analysis of variance. Multiple comparisons were performed to compare means of Basal groups to OVL-treated groups (see **Supplementary Table 1**). Multiple comparisons were corrected by the Tukey statistical hypothesis testing. Gain between WT and KO groups were statistically compared using unpaired two-tailed *T*-test. If normal distribution (verified using Shapiro-Wilk's test) and/or equal variance (verified using Bartlett's test) are not assumed, groups were statistically compared using the test of Wilcoxon-Mann-Whitney. A $p < 0.05$ was considered significant. Values are given as means ± SEM.

RESULTS

Reduced Gain of Muscle Performance in Response to Mechanical Overload (OVL) in Desmin Knock-Out Mice

To analyze the role of desmin during adaptation to resistance training, we examined the gains in muscle weight, muscle force generation capacity and fatigue resistance in response to overload (OVL) in *DesKO* and control mice. Plantaris muscles were overloaded by surgical ablation of gastrocnemius and soleus muscles. One month following OVL, muscle weight was markedly upregulated in both genotypes (**Figure 1A**). The percentage of muscle weight gain compared to the unchallenged muscle was calculated and was not different in both groups (**Figure 1B**), suggesting that desmin depletion does not prevent muscle mass regulation following resistance training. It should be noted that body weight in *DesKO* mice in basal state was lower compared to control mice (16.80 g ± 0.60 g in *DesKO* vs. 21.24 g ± 0.50 g in Ctr, $p = 0.0001$) and OVL did not modify this difference (18.40 ± 0.15 for *DesKO* + OVL vs. 20.27 ± 0.27 for Ctr + OVL, $p = 0{,}0258$). *In situ* force production in response to nerve stimulation was analyzed. In contrast to control mice, OVL did not increase absolute maximal force of plantaris muscle in *Des*KO mice (**Figures 1C,D**). The specific maximal force, which represents the normalization of absolute maximal force by muscle weight, was decreased in response to OVL in both genotypes (**Figure 1E**) ($p < 0.05$). Notably, this decrease was higher in *Des*KO mice as compared to control mice (**Figure 1F**) ($p < 0.05$). Fatigue resistance was also analyzed by continuously stimulating plantaris muscle and measuring the time corresponding to a decrease of 50% of initial force. Our results showed that fatigue resistance increased in response to OVL only in control mice (**Figures 1G,H**) ($p < 0.05$). Taken together, our results indicate that desmin plays an important role in the gain of muscle performance, but not in the gain of muscle weight in response to OVL.

Muscle Remodeling in Response to Mechanical Overload (OVL) in Desmin Knock-Out Mice

Since the changes in muscle force generation capacity and fatigue resistance can be related to myosin heavy chain (MHC) composition of muscle fibers, we used immunohistochemistry to compare MHC composition of *Des*KO and control plantaris muscles after 1 month of OVL (**Figures 2A–D**). The proportion of fibers expressing two major MHC isoforms, MHC-2a (oxidative fiber) and MHC-2b (glycolytic fiber), was analyzed using a custom macro (ImageJ software) to count MHC-positive cells. The proportion of MHC-2a-expressing fibers increased and the proportion of MHC-2b-expressing fibers decreased in

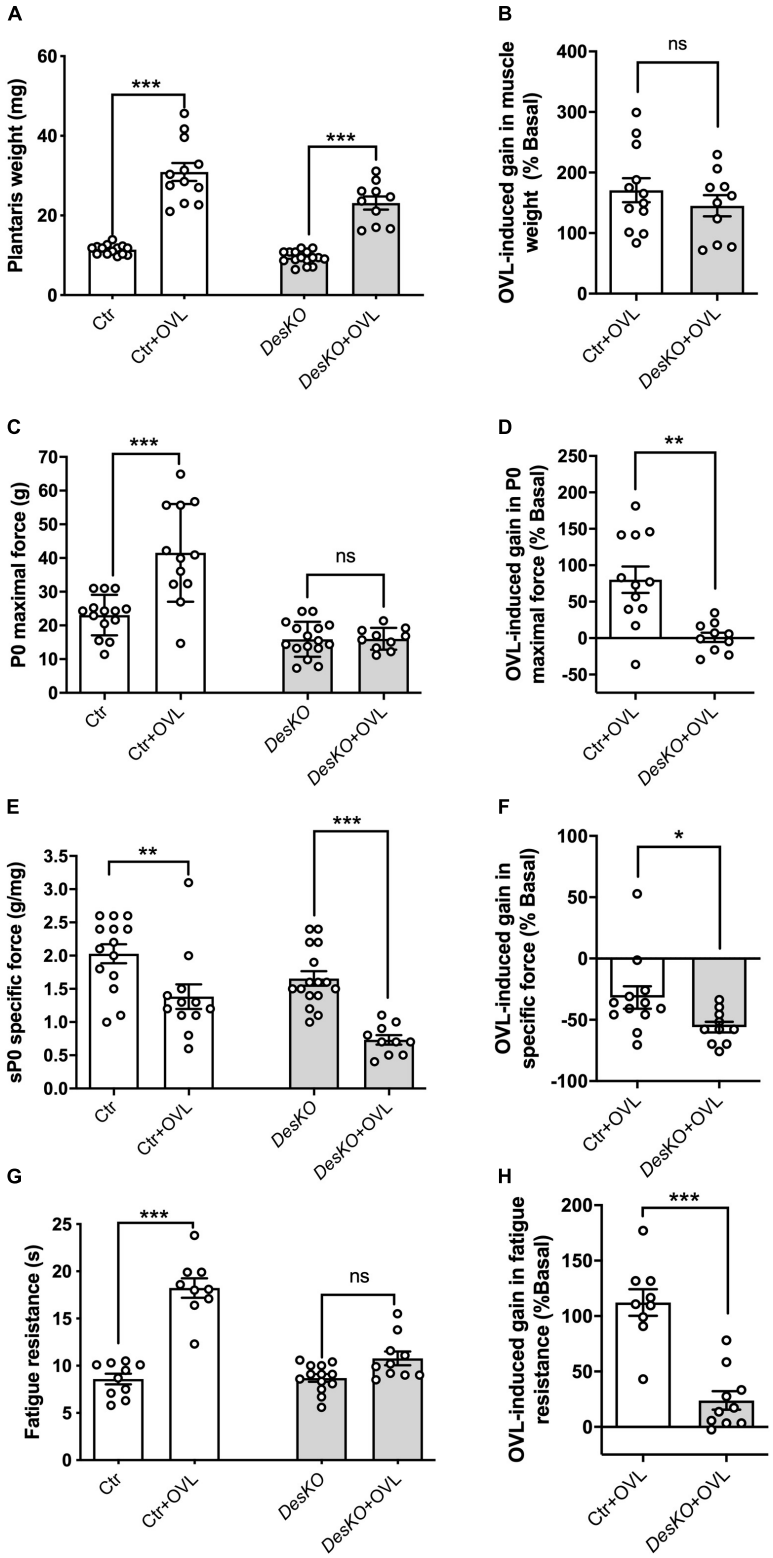

FIGURE 1 | Maximal force of plantaris is not increased in response to OVL in DesKO mice. Muscle weight **(A)**, maximal force (P0, **C**), specific force (sP0, **E**) and fatigue resistance **(G)** were evaluated in both genotypes (Ctr and *Des*KO) in basal condition or after 1 month of OVL. The gain or loss in these parameters was calculated compared to the corresponding basal condition for the Ctr + OVL and *Des*KO + OVL groups **(B,D,F,H)**. Data are given as means ± SEM. *Des*KO, Desmin knock-out mice; Ctr, Control mice; OVL, mechanical overloading. *ns*: non-significant, $^{*}p < 0.05$, $^{**}p < 0.01$, $^{***}p < 0.001$.

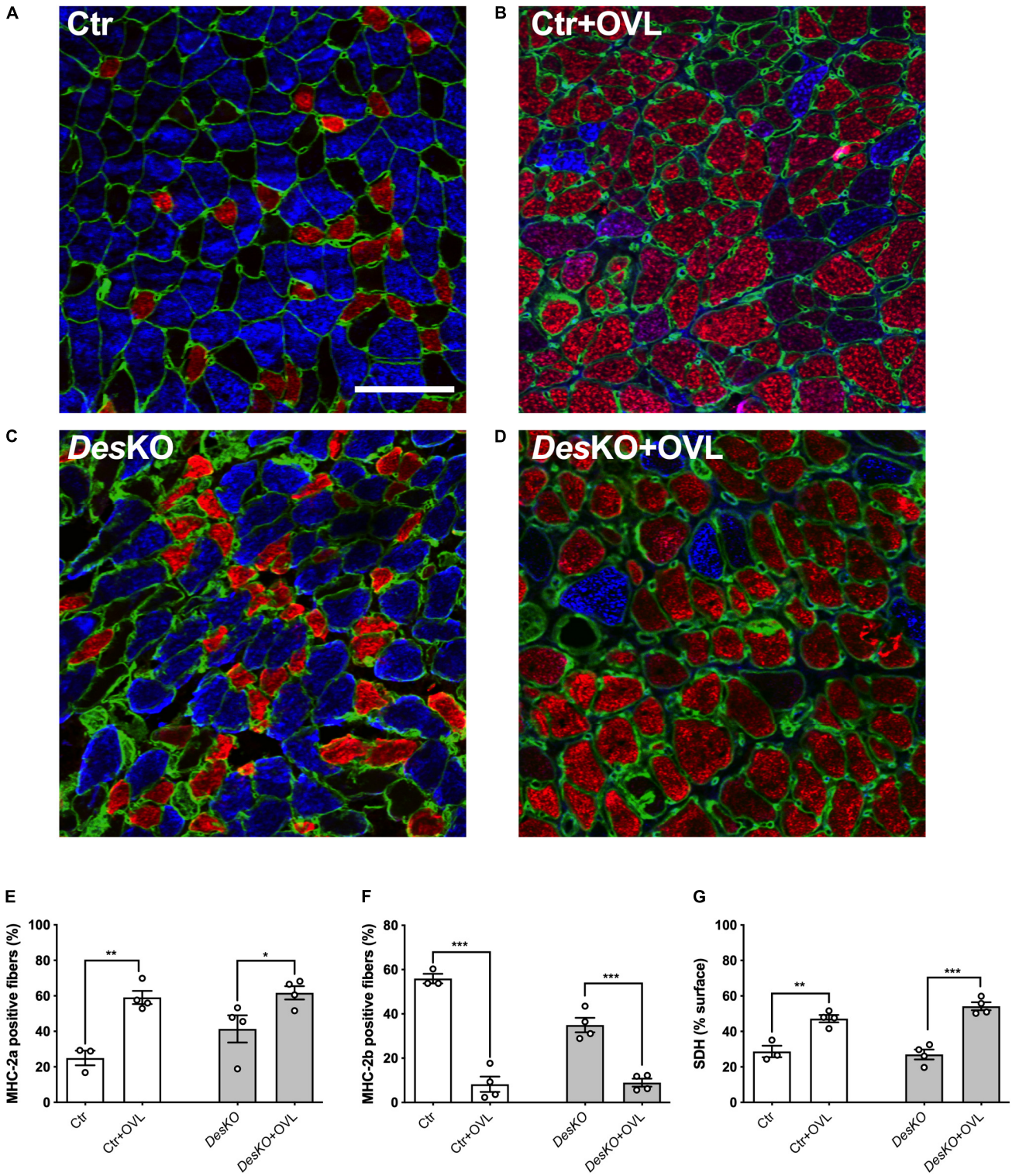

FIGURE 2 | Transition toward oxidative fibers is not impaired in DesKO plantaris in response to OVL. Representative images **(A–D)** of plantaris section immunostained for MHC-2a (red), MHC-2b (blue) and perlecan (green) from both genotype (Ctr and *Des*KO) in basal condition or after 1 month of OVL. Percentage of MHC-2a positive fibers **(E)** or MHC-2b positive fibers **(F)**. Percentage of the surface of muscle section demonstrating succinate dehydrogenase activity **(G)**. Scale bar = 100 μm. Data are given as means ± SEM. *Des*KO, Desmin knock-out mice; Ctr, Control mice; OVL, mechanical overloading; MHC, myosin heavy chain; SDH, succinate dehydrogenase. *ns*: non-significant, $^{*}p < 0.05$, $^{**}p < 0.01$, $^{***}p < 0.001$.

response to OVL in both genotypes (**Figures 2E,F**). Despite the fact that the change in MHC composition of plantaris muscle was found similar between *Des*KO and control mice, the increase rate of the percentage of MHC-2a fiber in response to OVL in *Des*KO mice was lower by more than 2.5-fold compared to control mice (+ 49% ± 9% in *Des*KO vs. + 136% ± 15% in control, $p = 0.002$). However, it should be noted that the percentage of oxidative MHC-2a fibers in *DesKO* mice was already increased before OVL (**Figure 2E**) ($p < 0.05$), presumably as a consequence of the lack of desmin as previously demonstrated (Agbulut et al., 1996). We also examined the oxidative energetic metabolism of plantaris muscle after 1 month of OVL using succinate dehydrogenase (SDH) staining. Our results indicated higher SDH activity in response to OVL in both genotypes (**Figure 2G**) ($p < 0.05$). Taken together, our results indicate that the glycolytic to oxidative metabolism transition pattern in response to OVL did not markedly differ between *Des*KO and control mice.

Myostatin Pathway Mediates Muscle Mass Plasticity in Desmin Knock-Out Mice

OVL is known to induce muscle hypertrophy and hyperplasia. As several players can be involved in the control of the muscle mass, we examined the mRNA levels of intracellular signaling molecules involved in hypertrophy. Semi-quantitative PCR analysis was performed on muscle samples after 7 days of OVL during the early phase of muscle remodeling (**Figures 3A–J**). Myostatin (Mstn or Gdf8), an mTOR deactivator, mRNA levels decreased with OVL (**Figure 3A**), to a lower extent in *DesKO* mice (**Figure 3B**). In the same line, the transcript of follistatin (**Figures 3C,D**), an antagonist of myostatin, and insulin growth factor 1 (Igf1) (**Figures 3E,F**) increased in all genotypes but these increases were lower in *DesKO* compared to control mice muscles. In addition, two other markers MuRF1 and atrogin, which are important markers for skeletal muscle atrophy by promoting protein catabolism and contribute to the decline of muscle mass and strength in sarcopenia, were examined. Our results demonstrated that OVL did not modify MuRF1 expression in control, but strongly reduced it in DesKO mice, suggesting that desmin presence reduces protein degradation upon OVL stimulation (**Figures 3G,H**). Regarding atrogin expression, no stricking difference was observed after OVL between the two genotypes (**Figures 3I,J**). Taken together, our data suggest that conventional muscle mass regulation pathways are activated in *DesKO* mice and contribute to the plasticity of muscle mass in OVL-elicited remodeling.

To complete these results, we analyzed the number and the size distribution of the MHC-2a and the MHC-2b muscle fibers on cross sections of plantaris muscle in basal condition and 1 month after OVL. As demonstrated in **Figure 4**, the number of MHC-2a fibers was increased in both genotypes. Interstingly, in control mice the size distribution of MHC-2a fibers was not modified by OVL. On the other hand, in *DesKO* mice, the size distribution was slightly shifted toward the higher values indicating an asymmetrical increase in the number of MHC-2a fibers with high diameter (**Figures 4A,B**). Thus, the mean diameter of MHC-2a fibers was increased in response to OVL in *DesKO* mice but not in control mice (+ 31.91% ± 11.32% in *DesKO* vs. + 2.93% ± 3.18% in control, $p = 0.048$) (**Figure 4C**). As expected, after 1 month of OVL, the number of MHC-2b fibers was decreased in both genotypes (**Figures 4D,E**). However, it seems that the decrease in the mean size of MHC-2b fibers in response to OVL was more important in control mice compared to *DesKO* mice although the difference did not reach statistical significance (–15.79% ± 7.09% in *DesKO* vs. –27.11% ± 5.87% in control, $p = 0.264$) (**Figure 4F**).

Mechanisms Responsible for the Reduced Gain of Performance in Desmin Knock-Out Mice

To determine the mechanisms involved in the deficit of muscle function observed in *DesKO* muscles challenged with OVL, myofiber number were quantified in plantaris muscles. Myofiber number was increased by OVL in control muscle, but not in *DesKO* (**Figure 5A**). A defect in myogenesis affecting *DesKO* muscles could lead to less myofiber formation following OVL, and could participate in the observed deficit in muscle function. Thus, Pax7 transcripts were quantified (**Figure 5B**). Pax7 expression increased in response to OVL both in control and *DesKO* mice while there was no statistically significant difference observed between the two genotypes (**Figures 5B,C**). To support this result, we also quantified Pax7 positive cells in *DesKO* and control mice after OVL (**Figure 5D**). Our results show no difference in the ratio of Pax7 positive cells between control and *Des*KO mice in response to OVL, suggesting that MuSC are not depleted in absence of desmin. However, we found that the induction of MyoD expression due to OVL was repressed in *DesKO* muscle, suggesting that MuSC activation is repressed (**Figures 5E,F**). Consistent with this observation, myogenin, neonatal and embryonic MHC were less induced by OVL in *DesKO* mice compared to control mice muscles (**Figures 5G–L**). Unchanged Pax7 expression associated with decreased markers for regeneration in response to OVL in *DesKO* compared to control muscles, pleads for a reduction in the myogenic program affecting *DesKO* MuSCs in response to OVL. In order to explore the consequences of this reduced myogenic program on the capacity of *DesKO* muscle to repair muscle damage due to the mechanical overloading, we evaluated the extent of fibrosis and inflammatory response in *DesKO* and control mice. Fibrosis was first assessed by Sirius red staining after 1 month of OVL (**Supplementary Figure 1A**). No difference was found between the two genotypes. Moreover, qPCR analyses were performed on muscle samples 7 days after OVL during the early phase of muscle remodeling (**Supplementary Figure 1B**). The mRNA levels of the fibrosis and inflammation markers Il1b, Tgfβ1, Col3a1, Col1a1 and Timp1 increased strongly in response to OVL in a similar manner in both genotypes ($p < 0.05$). We also studied protein kinase PKA since it contributes to muscle regeneration (Stewart et al., 2011). We found that the levels of the phosphorylated forms of PKA regulatory subunit IIα (PKA RIIα) protein increased in control mice in response to OVL but not in *Des*KO mice (**Supplementary Figures 1C,D**). Taken together, despite minor

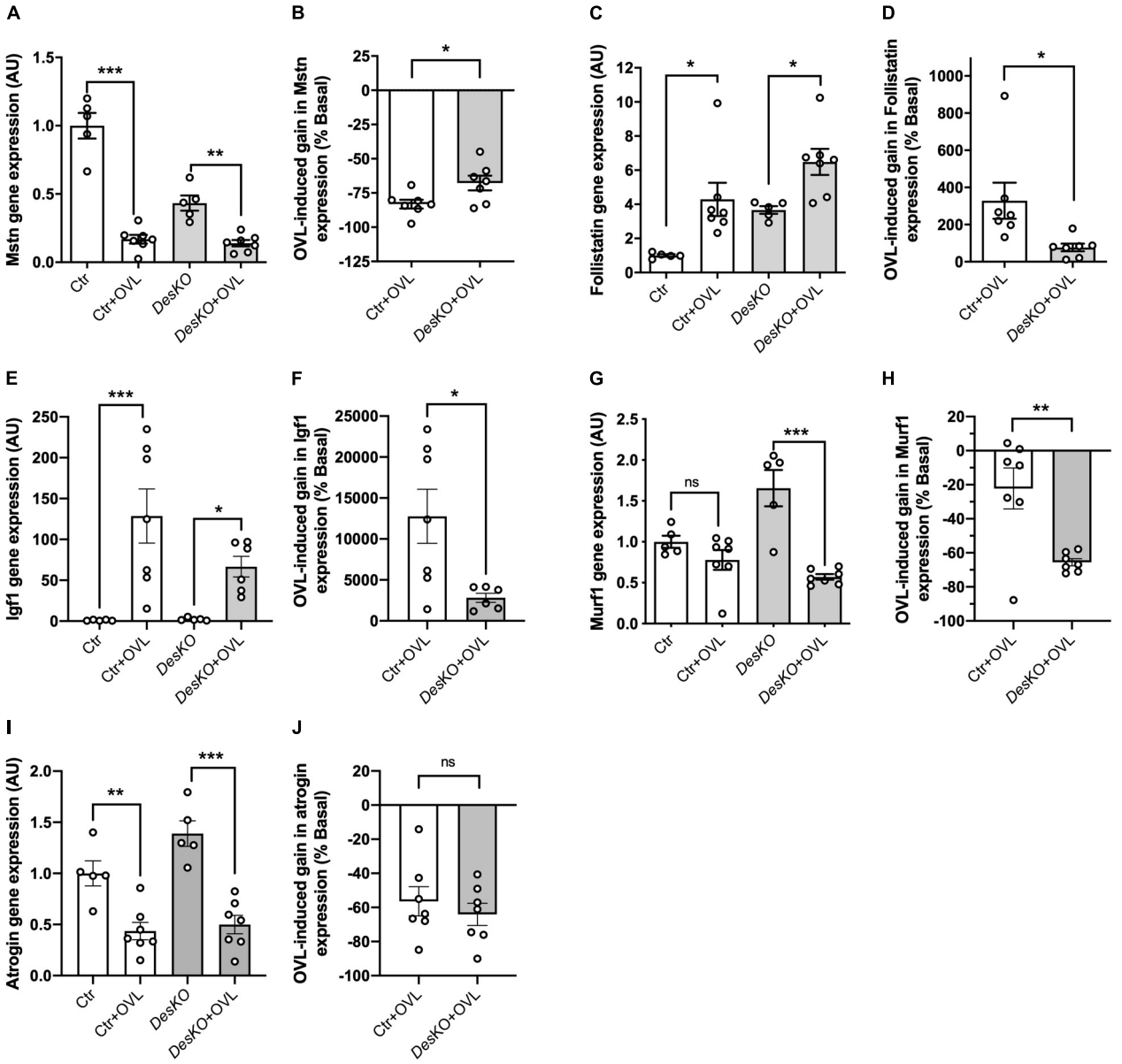

FIGURE 3 | Expression of genes involved in the regulation of muscle mass pathways regulation is modified in DesKO mice after OVL. Gene expression of the hypertrophic markers myostatin **(A,B)**, Follistatin **(C,D)**, Igf1 **(E,F)** and of the anti-hypertrophic markers Murf1 **(G,H)** and Atrogin **(I,J)** were evaluated in both genotype (Ctr and *Des*KO) in basal condition or after 7 days of OVL. The gain or loss of expression of these genes was calculated compared to the corresponding basal condition for the Ctr + OVL and *Des*KO + OVL groups **(B,D,F,H,J)**. Data are given as means ± SEM. *Des*KO, Desmin knock-out mice; Ctr, Control mice; OVL, mechanical overloading. *ns,* non-significant, $^{*}p < 0.05$, $^{**}p < 0.01$, $^{***}p < 0.001$.

modifications observed in *Des*KO mice compared to control, the absence of desmin does not impair muscle fiber regeneration.

To better understand the morphological perturbations affecting *DesKO* muscles, we also examined the ultrastructure of the plantaris muscle fibers using transmission electron microscopy (**Figure 6**). In comparison to control muscles, *Des*KO myofibers present increased number of mitochondria and irregularities in the organization of the myofibrils, with misalignment of Z-lines (**Figures 6A,B**). One month after OVL, control mice present only minor modifications, i.e., increase of the number and the size of mitochondria (**Figure 6C**, see asterisk). In contrast, *Des*KO mice presented serious muscle damages as indicated by the loss of sarcomere integrity, alignment and orientation, and abnormalities in size, number and distribution of mitochondria (**Figures 6D,E**). Moreover, mitochondria appeared swollen and accumulated in the muscle fibers. As presented in **Figure 6F**, an accumulation of autophagosomes was spotted under the sarcolemma (white arrowheads) and lysosomes (white empty arrowheads) in *Des*KO mice after 1 month of OVL. These observations could

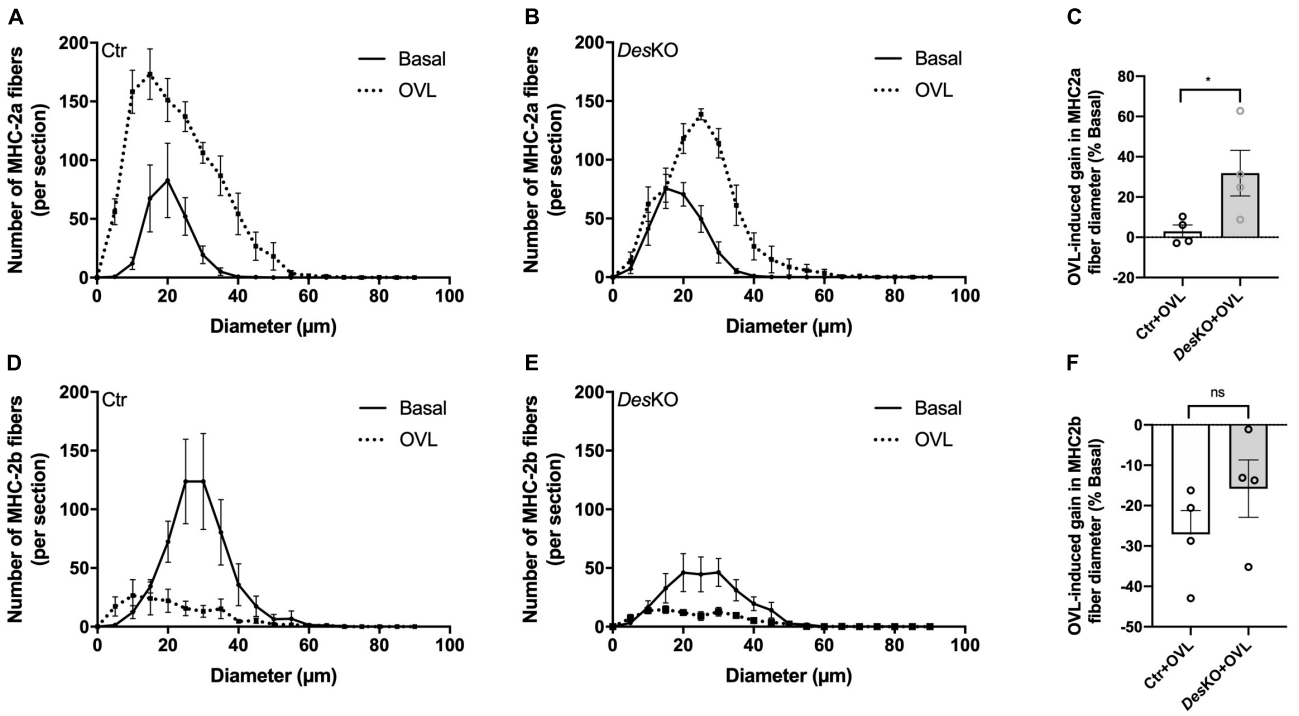

FIGURE 4 | Size distribution of plantaris muscle fibers is modified in DesKO mice after OVL. Size distribution of plantaris muscle fibers expressing only MHC-2a **(A,B)** or MHC-2b **(D,E)** for both genotypes (Ctr and *Des*KO) in basal condition (black line) or after 1 month of OVL (black dotted line). The gain or loss in these parameters was calculated compared to the corresponding basal condition for the Ctr + OVL and *Des*KO + OVL groups **(C,F)**. Data are given as means ± SEM. For the size distribution, $n = 4$ for all conditions ($n = 3$ for Ctr + Basal group). *Des*KO, Desmin knock-out mice; Ctr, Control mice; OVL, mechanical overloading; MHC, myosin heavy chain. *ns*, non-significant, $^*p < 0.05$.

indicate a perturbation of autophagy. Indeed, an impairment of proteolysis mechanisms leading to the accumulation of unfunctional proteins, such as proteins contributing to muscle contraction, could participate in the reduced gain of performance in *Des*KO mice. To address this possibility, we explored two main proteolysis pathways, the ubiquitin-proteasome system and the autophagy, in *Des*KO and control mice and in response to OVL. Regarding the ubiquitin-proteasome system, we measured chymotrypsin-like, trypsin-like and caspase-like activities of the proteasome 20S catalytic core using the fluorogenic substrates Suc-LLVY-AMC in *Des*KO and control muscle homogenates after 1 month of OVL. Chemotrypsin-like and caspase-like activities show no difference between *Des*KO and control mice (**Figures 7B,C**). However, the proteasome trypsin-like activity was increased in response to OVL in *Des*KO mice but not in control mice (**Figure 7A**) ($p < 0.05$). Concerning autophagy, we examined LC3-II protein level by western-blotting in *Des*KO and control plantaris muscle 1-month after OVL (**Figure 7D**). Our results show that both mRNA and protein levels of LC3-II did not change in *Des*KO mice, while they increased in control mice, in response to OVL (**Figures 7D–H**) ($p < 0.05$). It should be noted that the mRNA levels of LC3 were higher in DesKO mice at the baseline compared to the control. Together, these results underline alteration of proteolysis pathways in *Des*KO mice in response to OVL.

DISCUSSION

Skeletal muscle responds to resistance training by activating adaptation mechanisms at the cellular level, which result in muscle fiber growth and regeneration, increase in fatigue resistance, and gain of force (Joanne et al., 2012). In this study, we used the desmin-deficient (*Des*KO) female mouse to address the role of desmin in the response of skeletal muscle to mechanical overload (OVL), a well-studied experimental model which mimics resistance training. We found that, in response to OVL, gain in performance is not fully achieved in the absence of desmin, despite notable muscle remodeling and in relation with impaired proteolysis.

Muscle Remodeling Is Affected by Desmin Depletion in Response to OVL

One month after surgical ablation of gastrocnemius and soleus muscles, the plantaris muscle of both *Des*KO and control mice responded by an important increase in weight (**Figure 1**), suggesting resistance training-induced muscle growth (Joanne et al., 2012). Both genotypes also displayed a fiber type switch toward a more oxidative phenotype, which is consistent with increased fatigue resistance. In particular, MHC2b-positive, glycolytic fibers are partially replaced by MHC2a-positive and more oxidative fibers. Also, mitochondrial activity, as detected

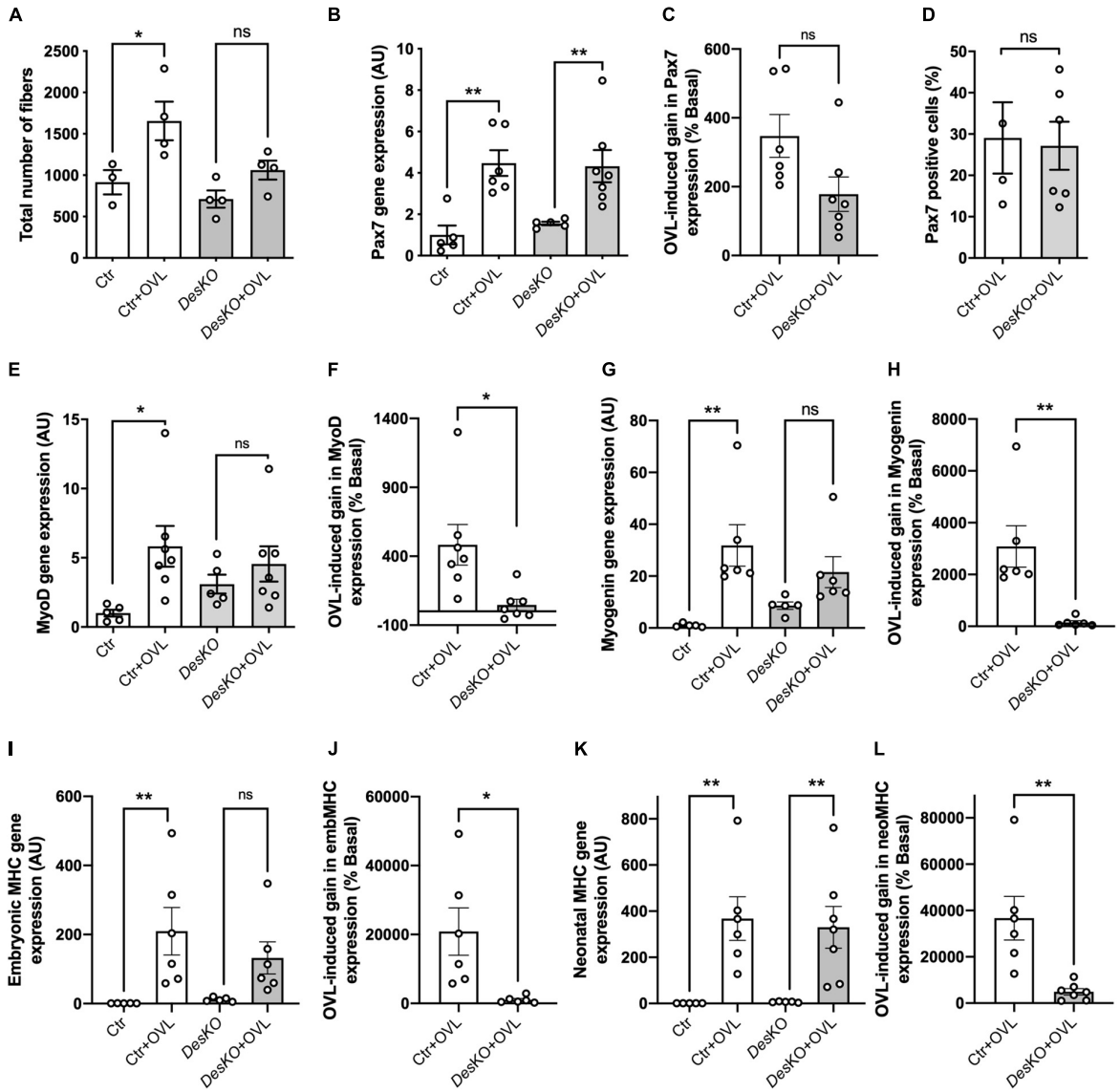

FIGURE 5 | The myogenic program is disturbed in DesKO after OVL. Total number of fibers of plantaris muscle were evaluated after 1 month of OVL **(A)**. Gene expression analysis for Pax7 **(B,C)**, MyoD **(E,F)**, Myogenin **(G,H)**, embryonic MHC **(I,J)** and neonatal MHC **(K,L)** were evaluated in both genotype (Ctr and *Des*KO) in basal condition or after 7 days of OVL. The gain or loss of expression of these genes was calculated compared to the corresponding basal condition for the Ctr + OVL and *Des*KO + OVL groups **(C,F,H,J,L)**. Moreover, Pax7 positive cells were counted after 7 days of OVL **(D)**. Data are given as means ± SEM. *Des*KO, Desmin knock-out mice; Ctr, Control mice; OVL, mechanical overloading; MHC, myosin heavy chain. *ns*: non-significant, $^{*}p < 0.05$, $^{**}p < 0.01$.

by SDH staining, appeared increased by twofold (**Figure 2**). Gene expression levels of mTOR deactivator myostatin decreased whereas follistatin, an antagonist of myostatin, and the positive regulator of muscle growth Igf1 transcripts increased in both genotypes, also suggesting that the hypertrophy process is activated (**Figure 3**). Igf1 is also implicated in muscle regeneration by promoting both proliferation and differentiation of MuSCs (Jang et al., 2011). However, desmin-deficiency toned down both OVL-elicited myostatin reduction and stimulated follistatin expression (**Figures 3A–D**). This suggests that the regulation of muscle mass is not affected by desmin deficiency. Overloaded *Des*KO and control muscles showed increase in gene expression of Pax7, embryonic MHC and neonatal MHC (**Figure 5**). These results suggest that hyperplasia and regeneration also occur in both genotypes. Interestingly, OVL does not increase myofiber number in *DesKO* muscles, although it does in control mice (**Figure 5A**). While Pax7-positive cells, and OVL-induced gain of Pax7 expression was identical in control and *DesKO* muscles. However, OVL-induced upregulation of MyoD, Myogenin, neonatal, and embryonic MHC were dampened in *DesKO* muscles (**Figure 5**). Our data suggest that the myogenic program triggered by OVL stimulation is only partially supported in absence of desmin. We also examined differences in phosphorylation of PKARIIα which leads

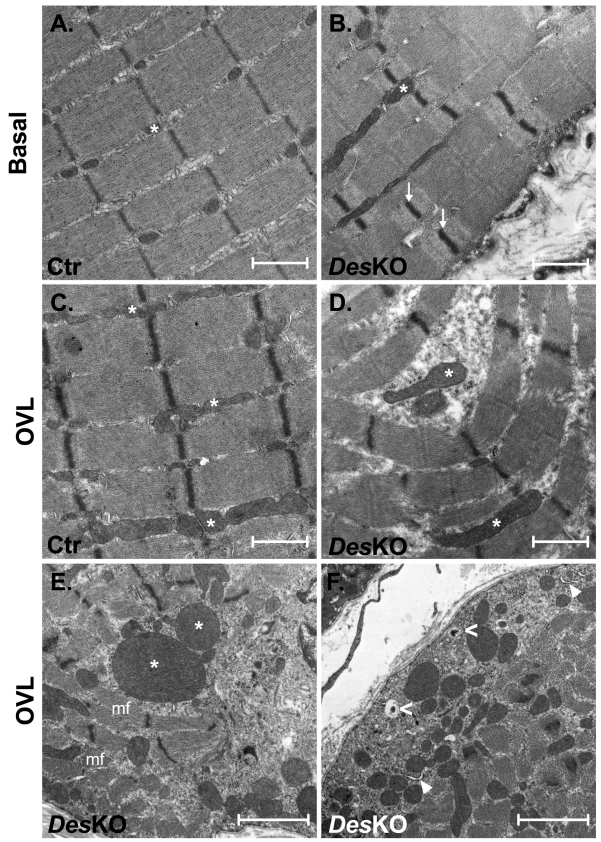

FIGURE 6 | Myofibrils organization of plantaris is highly disturbed in DesKO after OVL. Transmission electron microscopy images of ultrathin sections of plantaris of both genotype (Ctr and *Des*KO) in basal condition or after 1 month of OVL. Asterisks (*) indicate mitochondria; white arrows indicate Z-lines; mf indicates myofibrils; white arrowheads indicate autophagosome; white empty arrowheads indicate autolysosome. *Des*KO, Desmin knock-out mice; Ctr, Control mice; OVL, mechanical overloading. **(A–D)** Scale bar = 1 μm. **(E,F)** Scale bar = 2 μm.

to an increase in protein synthesis, in favor of hypertrophy and muscle growth. Although the levels of phosphorylated PKARIIα increased only in the control muscle after OVL, these levels were already elevated in the *Des*KO in the basal condition. A possible explanation may be related to another intermediate filament, synemin. Synemin is involved in the control of hypertrophy by modulating the subcellular localization of PKA. We have previously reported higher phosphorylated levels of PKA and increased hypertrophy in the synemin-deficient skeletal muscle as compared to control mice and in response to OVL (Li et al., 2014). Formation of synemin filaments in muscle requires copolymerization with desmin. Consequently, synemin appears unstable and delocalized in *Des*KO muscle fibers (Carlsson et al., 2000), providing one possible explanation for the higher levels of phosphorylated PKARII in *Des*KO under basal conditions. Taken together, these results suggested that the process of muscle fiber remodeling was activated. Muscle fiber type switch as well as hypertrophy and regeneration appear to occur in both genotypes as a response to OVL. These processes are not impaired by the lack of desmin; however, our data suggest that muscle remodeling is moderated in response to OVL.

Impaired Gain in Performance in the Absence of Desmin

Interestingly, here we show that, despite muscle hypertrophy, maximal force production is not improved in *Des*KO plantaris muscle in response to OVL. It was known that muscle hypertrophy does not necessarily increase maximal force production as shown in the case of myostatin inhibition (Stantzou et al., 2017). Increased fibrosis and inflammation as compared to control could be a possible partial explanation for the fact that maximal force was not proportional to muscle weight in *Des*KO (Costamagna et al., 2015). However, although gene expression of proteins involved in inflammation and fibrosis greatly increased after 7 days of OVL, this increase was similar for both genotypes and no statistically significant increase in fibrosis was measured *in situ* on muscle sections, at least after 1 month of OVL (**Supplementary Figure 1**). Efficient muscle fiber contraction can be impaired by structural disorganization of sarcomeres, and in particular by misalignment, disintegration, and loss of myofibrils (Li et al., 1997). Electron microscopy analysis (**Figure 6**) showed that OVL did not destabilize the contractile apparatus in control muscle fibers. The main effect was the increased number of mitochondria, as expected by the switch toward a more oxidative metabolism. On the contrary, OVL had major structural consequences in *Des*KO muscle. Under basal conditions, *Des*KO muscle fibers displayed intermyofibrillar accumulation of mitochondria as well as misaligned Z-lines. However, the contractile apparatus was not disintegrated. After OVL, *Des*KO muscle fibers appeared damaged, with abnormally accumulated and often swollen mitochondria as well as misaligned, disintegrated and disoriented myofibrils, as shown by the coexistence of longitudinal and cross-sectioned myofibrils within the same muscle fiber (**Figure 6E**). A similar cellular phenotype has been previously described for *Des*KO muscle fibers in basal condition (Milner et al., 1996; Li et al., 1997), although only for slow-twitch muscles and in older mice (≥5 months-old). Therefore, we conclude that in the absence of desmin, muscle fiber growth cannot compensate the increased structural damage of the contractile apparatus, and is not sufficient to improve force production.

It is known that accumulation of damaged mitochondria leads to increased reactive oxygen species generation, decreased ATP production, cellular dysfunction, and finally cell death (Bloemberg and Quadrilatero, 2019). Intense muscle effort under OVL conditions results in production of damaged proteins and organelles which need to be effectively cleared. We examined the two major proteolytic pathways, the ubiquitin-proteasome system and autophagy, in *Des*KO and control muscles. Proteasomal activity was reported in OVL experiments (Baehr et al., 2014), and the role of autophagy in muscle adaptation to exercise has been extensively studied and established (Lira et al., 2013; Luo et al., 2013). In our experiments, in response to OVL, the proteasome activity appeared partially

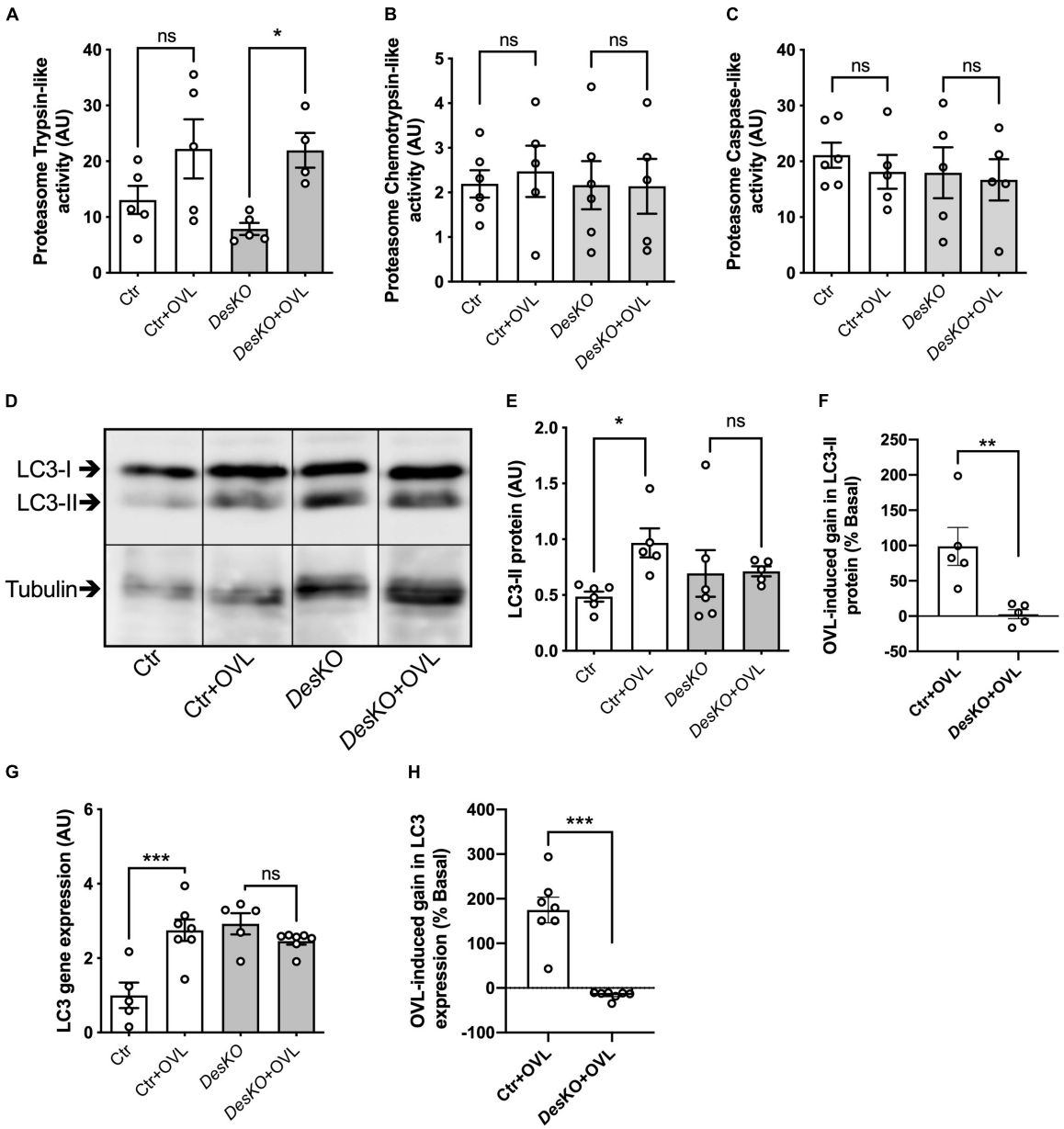

FIGURE 7 | Proteostasis pathways are disturbed in DesKO after OVL. The trypsin-like activity **(A)**, chymotrypsin-like activity **(B)** and caspase-like activity **(C)** of proteasome were measured in both genotype (Ctr and *Des*KO) in basal condition or after 1 month of OVL. LC3-II protein **(D–F)** and LC3 gene expression **(G,H)** were quantified in both genotype (Ctr and *Des*KO) in basal condition or after 1 month of OVL. Data are given as means ± SEM. *Des*KO, Desmin knock-out mice; Ctr, Control mice; OVL, mechanical overloading. *ns*: non-significant, $^{*}p < 0.05$, $^{**}p < 0.01$, $^{***}p < 0.001$.

activated (trypsin-like activity), whereas the levels of LC3-II, the activated (lipidated) form of autophagy marker LC3 protein, did not increase in *Des*KO muscle fibers. On the contrary, both LC3 gene expression and LC3-II protein levels increased in control muscle fibers after OVL. Interestingly, LC3 gene expression was already increased in *Des*KO muscle fibers under basal conditions. Moreover, electron microscopy reveals the presence of autophagosomes and autolysosomes in the cytoplasm of *Des*KO muscle fibers after OVL (**Figure 6F**). One possible explanation could be that although the process is activated, the autophagy machinery (autophagosome production, fusion to lysosomes and clearance) in *Des*KO is already at maximum capacity in basal state because of high production of damaged cell material due to the lack of desmin, and is getting inefficient under OVL conditions. This hypothesis is supported by the accumulation of damaged mitochondria under OVL conditions (**Figure 6**). Interestingly, it has been previously shown that blockage of autophagy in muscle-specific *Atg7*-null mice resulted in impairment of force transmission and in accumulation of dysfunctional mitochondria (Masiero et al., 2009). We therefore

propose that, after OVL and in the absence of desmin, the repairing activity of autophagy could be disturbed and this may at least partially explain the accumulation of damaged mitochondria and dysfunctional contractile proteins which leads to compromised integrity of muscle and reduced production of specific maximal force, as was shown in other cases (Wohlgemuth et al., 2010). Further studies are required to elucidate the role of autophagy in our model system by generating functional data of autophagy inhibition/promotion *in vivo*.

CONCLUSION

In conclusion, here we show that during muscle remodeling in response to OVL, muscle growth and increase in force production can be dissociated in *Des*KO mice. It has been proposed that, during resistance exercise, force transmission at the myofibril level must be supported by the cytoskeleton, as suggested by increased expression of desmin (Parcell et al., 2009). We propose that mechanical OVL increases the negative impact of the lack of desmin on myofibril organization and mitochondria. Furthermore, our results suggest that under these conditions, the repairing activity of autophagy is impaired. Consequently, force generation is not improved despite muscle growth, suggesting that desmin is required for a complete response to resistance training in skeletal muscle.

DATA AVAILABILITY STATEMENT

The original contributions presented in the study are included in the article/**Supplementary Material**, further inquiries can be directed to the corresponding author/s.

ETHICS STATEMENT

All animal studies were approved by our institutional Ethics Committee (Charles Darwin, project number: 01362.02) and conducted according to the French and European laws, directives, and regulations on animal care (European Commission Directive 86/609/EEC).

AUTHOR CONTRIBUTIONS

PJ, MB, OA, AF, and EK contributed to the data collection, the statistical analysis, the interpretation, and the manuscript writing. PJ, YH, MB, and JG-L carried out the histological and immunostainig and molecular analysis. AL, YH, M-TD, AP, and ZL carried out the western blot experiments and proteasome activity measurement and analysis. GT and OA carried out the electron microscopy experiments. AF carried out the muscle force measurements. OA and AF designed and supervised the research. All authors read and approved the final manuscript.

FUNDING

This work was supported by funds from CNRS, Sorbonne Université, Université de Paris, the "Association Française contre les Myopathies" (AFM) (contracts numbers: 16605, 19353, and 20479). YH and M-TD were supported by fellowships from the "Association Française contre les Myopathies."

ACKNOWLEDGMENTS

We would like to thank Nathalie Vadrot and Pauline Roy for technical assistance, Dr. Philippe Noirez for developing ImageJ software macros, and Sorbonne Université for animal facilities. Experiences in electron microscopy have been realized in the electron microscopy service in IBPS/FR3631-Sorbonne Université. We also thank all of the personnel of the Animal Facility of the Sorbonne Université (UMS28, Paris-France); the Microscopy Platform (IBPS, Paris-France) for helpful advice and technical assistance during microscopy image acquisition and analysis.

SUPPLEMENTARY MATERIAL

The Supplementary Material for this article can be found online at: https://www.frontiersin.org/articles/10.3389/fcell.2021.662133/full#supplementary-material

Supplementary Figure 1 | Fibrosis and inflammation are not impaired in DesK0 after OVL. Quantification of fibrosis **(A)** and relative gene expression of inflammation and fibrosis markers **(B)**. Quantification of the phosphorylation of PKA (pPKA, **C,D**). Parameters were measured in both genotypes (Ctr and *Des*KO) in basal condition or after one month of OVL. For gene expression analysis, $n = 5$ for Ctr groups and $n = 7$ for OVL groups. Data are given as means±SEM. *Des*KO, Desmin knock-out mice; Ctr, Control mice; OVL, mechanical overloading. *ns*: non significant, $^{*}p < 0.05$, $^{**}p < 0.01$.

Supplementary Table 1 | Number of samples for each evaluated parameter and *p*-values following two-way ANOVA analysis. DesKO, Desmin knock-out mice; Ctr, Control mice; OVL, mechanical overloading; ns, non-significant.

REFERENCES

Agbulut, O., Li, Z., Mouly, V., and Butler-Browne, G. S. (1996). Analysis of skeletal and cardiac muscle from desmin knock-out and normal mice by high resolution separation of myosin heavy-chain isoforms. *Biol. Cell* 88, 131–135.

Agbulut, O., Li, Z., Périé, S., Ludosky, M. A., Paulin, D., Cartaud, J., et al. (2001). Lack of desmin results in abortive muscle regeneration and modifications in synaptic structure. *Cell Motil. Cytoskeleton* 49, 51–66. doi: 10.1002/cm.1020

Baehr, L. M., Tunzi, M., and Bodine, S. C. (2014). Muscle hypertrophy is associated with increases in proteasome activity that is independent of MuRF1 and MAFbx expression. *Front. Physiol.* 5:69. doi: 10.3389/fphys.2014.00069

Bellin, R. M., Huiatt, T. W., Critchley, D. R., and Robson, R. M. (2001). Synemin may function to directly link muscle cell intermediate filaments to both myofibrillar Z-lines and costameres. *J. Biol. Chem.* 276, 32330–32337. doi: 10.1074/jbc.M104005200

Bloemberg, D., and Quadrilatero, J. (2019). Autophagy, apoptosis, and mitochondria: molecular integration and physiological relevance in skeletal

muscle. *Am. J. Physiol. Physiol.* 317, C111–C130. doi: 10.1152/ajpcell.00261.2018

Brodehl, A., Gaertner-Rommel, A., and Milting, H. (2018). Molecular insights into cardiomyopathies associated with desmin (DES) mutations. *Biophys. Rev.* 10, 983–1006. doi: 10.1007/s12551-018-0429-420

Carlsson, L., Li, Z. L., Paulin, D., Price, M. G., Breckler, J., Robson, R. M., et al. (2000). Differences in the distribution of synemin, paranemin, and plectin in skeletal muscles of wild-type and desmin knock-out mice. *Histochem. Cell Biol.* 114, 39–47.

Costamagna, D., Costelli, P., Sampaolesi, M., and Penna, F. (2015). Role of inflammation in muscle homeostasis and myogenesis. *Mediators Inflamm.* 2015, 1–14. doi: 10.1155/2015/805172

Ferry, A., Benchaouir, R., Joanne, P., Peat, R. A., Mougenot, N., Agbulut, O., et al. (2015). Effect of voluntary physical activity initiated at age 7 months on skeletal hindlimb and cardiac muscle function in mdx mice of both sexes. *Muscle Nerve* 52, 788–794. doi: 10.1002/mus.24604

Goldfarb, L. G., and Dalakas, M. C. (2009). Tragedy in a heartbeat: malfunctioning desmin causes skeletal and cardiac muscle disease. *J. Clin. Invest.* 119, 1806–1813. doi: 10.1172/JCI38027

Granger, B. L., and Lazarides, E. (1980). Synemin: a new high molecular weight protein associated with desmin and vimentin filaments in muscle. *Cell* 22, 727–738.

Hernandez, D. A., Bennett, C. M., Dunina-Barkovskaya, L., Wedig, T., Capetanaki, Y., Herrmann, H., et al. (2016). Nebulette is a powerful cytolinker organizing desmin and actin in mouse hearts. *Mol. Biol. Cell* 27, 3869–3882. doi: 10.1091/mbc.E16-04-0237

Hourdé, C., Joanne, P., Medja, F., Mougenot, N., Jacquet, A., Mouisel, E., et al. (2013a). Voluntary physical activity protects from susceptibility to skeletal muscle contraction-induced injury but worsens heart function in mdx mice. *Am. J. Pathol.* 182, 1509–1518. doi: 10.1016/j.ajpath.2013.01.020

Hourdé, C., Joanne, P., Noirez, P., Agbulut, O., Butler-Browne, G., and Ferry, A. (2013b). Protective effect of female gender-related factors on muscle force-generating capacity and fragility in the dystrophic mdx mouse. *Muscle Nerve* 48, 68–75. doi: 10.1002/mus.23700

Hovhannisyan, Y., Melikyan, G., Mougenot, N., Gao-Li, J., Friguet, B., Paulin, D., et al. (2019). Effects of the selective inhibition of proteasome caspase-like activity by CLi a derivative of nor-cerpegin in dystrophic mdx mice. *PLoS One* 14:e0215821. doi: 10.1371/journal.pone.0215821

Ianuzzo, C. D., Gollnick, P. D., and Armstrong, R. B. (1976). Compensatory adaptations of skeletal muscle fiber types to a long-term functional overload. *Life Sci.* 19, 1517–1523.

Jang, Y. C., Sinha, M., Cerletti, M., Dall'Osso, C., and Wagers, A. J. (2011). Skeletal muscle stem cells: effects of aging and metabolism on muscle regenerative function. *Cold Spring Harb. Symp. Quant. Biol.* 76, 101–111. doi: 10.1101/sqb.2011.76.010652

Joanne, P., Chourbagi, O., Hourdé, C., Ferry, A., Butler-Browne, G., Vicart, P., et al. (2013). Viral-mediated expression of desmin mutants to create mouse models of myofibrillar myopathy. *Skelet. Muscle* 3:4. doi: 10.1186/2044-5040-3-4

Joanne, P., Hourdé, C., Ochala, J., Caudéran, Y., Medja, F., Vignaud, A., et al. (2012). Impaired adaptive response to mechanical overloading in dystrophic skeletal muscle. *PLoS One* 7:e35346. doi: 10.1371/journal.pone.0035346

Konieczny, P., Fuchs, P., Reipert, S., Kunz, W. S., Zeöld, A., Fischer, I., et al. (2008). Myofiber integrity depends on desmin network targeting to Z-disks and costameres via distinct plectin isoforms. *J. Cell Biol.* 181, 667–681. doi: 10.1083/jcb.200711058

Li, Z., Colucci-Guyon, E., Pinçon-Raymond, M., Mericskay, M., Pournin, S., Paulin, D., et al. (1996). Cardiovascular lesions and skeletal myopathy in mice lacking desmin. *Dev. Biol.* 175, 362–366. doi: 10.1006/dbio.1996.0122

Li, Z., Mericskay, M., Agbulut, O., Butler-Browne, G., Carlsson, L., Thornell, L. E., et al. (1997). Desmin is essential for the tensile strength and integrity of myofibrils but not for myogenic commitment, differentiation, and fusion of skeletal muscle. *J. Cell Biol.* 139, 129–144.

Li, Z., Parlakian, A., Coletti, D., Alonso-Martin, S., Hourdé, C., Joanne, P., et al. (2014). Synemin acts as a regulator of signalling molecules during skeletal muscle hypertrophy. *J. Cell Sci.* 127, 4589–4601. doi: 10.1242/jcs.143164

Lira, V. A., Okutsu, M., Zhang, M., Greene, N. P., Laker, R. C., Breen, D. S., et al. (2013). Autophagy is required for exercise training-induced skeletal muscle adaptation and improvement of physical performance. *FASEB J.* 27, 4184–4193.

Luo, L., Lu, A.-M., Wang, Y., Hong, A., Chen, Y., Hu, J., et al. (2013). Chronic resistance training activates autophagy and reduces apoptosis of muscle cells by modulating IGF-1 and its receptors, Akt/mTOR and Akt/FOXO3a signaling in aged rats. *Exp. Gerontol.* 48, 427–436. doi: 10.1016/J.EXGER.2013.02.009

Masiero, E., Agatea, L., Mammucari, C., Blaauw, B., Loro, E., Komatsu, M., et al. (2009). Autophagy is required to maintain muscle mass. *Cell Metab.* 10, 507–515. doi: 10.1016/J.CMET.2009.10.008

Milner, D. J., Weitzer, G., Tran, D., Bradley, A., and Capetanaki, Y. (1996). Disruption of muscle architecture and myocardial degeneration in mice lacking desmin. *J. Cell Biol.* 134, 1255–1270.

Parcell, A. C., Woolstenhulme, M. T., and Sawyer, R. D. (2009). Structural protein alterations to resistance and endurance cycling exercise training. *J. Strength Cond. Res.* 23, 359–365. doi: 10.1519/JSC.0b013e318198fd62

Parsons, S. A., Millay, D. P., Wilkins, B. J., Bueno, O. F., Tsika, G. L., Neilson, J. R., et al. (2004). Genetic loss of calcineurin blocks mechanical overload-induced skeletal muscle fiber type switching but not hypertrophy. *J. Biol. Chem.* 279, 26192–26200. doi: 10.1074/jbc.M313800200

Roy, R. R., and Edgerton, V. R. (1995). Response of mouse plantaris muscle to functional overload: comparison with rat and cat. *Comp. Biochem. Physiol. A Physiol.* 111, 569–575.

Sam, M., Shah, S., Fridén, J., Milner, D. J., Capetanaki, Y., and Lieber, R. L. (2000). Desmin knockout muscles generate lower stress and are less vulnerable to injury compared with wild-type muscles. *Am. J. Physiol. Physiol.* 279, C1116–C1122. doi: 10.1152/ajpcell.2000.279.4.C1116

Sarkar, S., Korolchuk, V. I., Renna, M., Winslow, A. R., and Rubinsztein, D. C. (2009). Methodological considerations for assessing autophagy modulators: a study with calcium phosphate precipitates. *Autophagy* 5, 307–313. doi: 10.4161/auto.5.3.7664

Stantzou, A., Ueberschlag-Pitiot, V., Thomasson, R., Furling, D., Bonnieu, A., Amthor, H., et al. (2017). Effect of constitutive inactivation of the myostatin gene on the gain in muscle strength during postnatal growth in two murine models. *Muscle Nerve* 55, 254–261. doi: 10.1002/mus.25220

Stewart, R., Flechner, L., Montminy, M., and Berdeaux, R. (2011). CREB is activated by muscle injury and promotes muscle regeneration. *PLoS One* 6:e24714. doi: 10.1371/journal.pone.0024714

van Spaendonck-Zwarts, K., van Hessem, L., Jongbloed, J. D. H., de Walle, H. E. K., Capetanaki, Y., van der Kooi, A. J., et al. (2010). Desmin-related myopathy: a review and meta-analysis. *Clin. Genet.* 80, 354–366. doi: 10.1111/j.1399-0004.2010.01512.x

Vignaud, A., Hourdé, C., Butler-Browne, G., and Ferry, A. (2007). Differential recovery of neuromuscular function after nerve/muscle injury induced by crude venom from Notechis scutatus, cardiotoxin from Naja atra and bupivacaine treatments in mice. *Neurosci. Res.* 58, 317–323. doi: 10.1016/J.NEURES.2007.04.001

Wohlgemuth, S. E., Seo, A. Y., Marzetti, E., Lees, H. A., and Leeuwenburgh, C. (2010). Skeletal muscle autophagy and apoptosis during aging: effects of calorie restriction and life-long exercise. *Exp. Gerontol.* 45, 138–148. doi: 10.1016/J.EXGER.2009.11.002

Woolstenhulme, M. T., Conlee, R. K., Drummond, M. J., Stites, A. W., and Parcell, A. C. (2006). Temporal response of desmin and dystrophin proteins to progressive resistance exercise in human skeletal muscle. *J. Appl. Physiol.* 100, 1876–1882. doi: 10.1152/japplphysiol.01592.2005

Conflict of Interest: The authors declare that the research was conducted in the absence of any commercial or financial relationships that could be construed as a potential conflict of interest.

The reviewer VM declared a past co- authorship with the authors ZL, OA to the handling editor.

frontiers in Cell and Developmental Biology

MINI REVIEW
published: 21 July 2021
doi: 10.3389/fcell.2021.690577

LINCing Nuclear Mechanobiology With Skeletal Muscle Mass and Function

Maria J. A. van Ingen[1] *and Tyler J. Kirby*[2]*

[1] *Biomolecular Sciences, Faculty of Science, Vrije Universiteit Amsterdam, Amsterdam, Netherlands,* [2] *Department of Physiology, Amsterdam Cardiovascular Sciences, Amsterdam Movement Sciences, Amsterdam UMC, Amsterdam, Netherlands*

Skeletal muscle demonstrates a high degree of adaptability in response to changes in mechanical input. The phenotypic transformation in response to mechanical cues includes changes in muscle mass and force generating capabilities, yet the molecular pathways that govern skeletal muscle adaptation are still incompletely understood. While there is strong evidence that mechanotransduction pathways that stimulate protein synthesis play a key role in regulation of muscle mass, there are likely additional mechano-sensitive mechanisms important for controlling functional muscle adaptation. There is emerging evidence that the cell nucleus can directly respond to mechanical signals (i.e., nuclear mechanotransduction), providing a potential additional level of cellular regulation for controlling skeletal muscle mass. The importance of nuclear mechanotransduction in cellular function is evident by the various genetic diseases that arise from mutations in proteins crucial to the transmission of force between the cytoskeleton and the nucleus. Intriguingly, these diseases preferentially affect cardiac and skeletal muscle, suggesting that nuclear mechanotransduction is critically important for striated muscle homeostasis. Here we discuss our current understanding for how the nucleus acts as a mechanosensor, describe the main cytoskeletal and nuclear proteins involved in the process, and propose how similar mechanoresponsive mechanisms could occur in the unique cellular environment of a myofiber. In addition, we examine how nuclear mechanotransduction fits into our current framework for how mechanical stimuli regulates skeletal muscle mass.

Keywords: mechanotransduction, nucleus, LINC complex, muscle mass, muscle adaptation, nuclear lamina, nesprins

OPEN ACCESS

Edited by:
Yuji Ogura,
St. Marianna University School of Medicine, Japan

Reviewed by:
Jung Yul Lim,
University of Nebraska-Lincoln, United States
G. W. Luxton,
University of Minnesota, United States

***Correspondence:**
Tyler J. Kirby
t.kirby@amsterdamumc.nl

Specialty section:
This article was submitted to Signaling, a section of the journal Frontiers in Cell and Developmental Biology

Received: *03 April 2021*
Accepted: *25 June 2021*
Published: *21 July 2021*

Citation:
van Ingen MJA and Kirby TJ (2021) LINCing Nuclear Mechanobiology With Skeletal Muscle Mass and Function. Front. Cell Dev. Biol. 9:690577. doi: 10.3389/fcell.2021.690577

INTRODUCTION

Skeletal muscle cells have the remarkable ability to adapt their size and force-generating capacity in response to changes in mechanical load. As a response to mechanical stimuli, skeletal muscle cells alter their protein metabolism primarily by modulating protein synthesis rates, with the importance of protein synthesis in determining muscle mass being well documented

Abbreviations: BAF, barrier-to-autointegration factor; CIP, cardiac Islet-1 interaction protein; CH, calponin homology domain; cPLA2, phospholipase A2; ECM, extracellular matrix; ER, endoplasmic reticulum; INM, inner nuclear membrane; KASH, Klarsicht, ANC-1, Syne homology; LAD, lamina-associated domain; LEM, LAP2-emerin-MAN1 domain; LINC, linkers of nucleoskeleton and cytoskeleton; NE, nuclear envelope; nesprin, nuclear envelope spectrin repeat protein; NPC, nuclear pore complex; ONM, outer nuclear membrane; PCM1, pericentriolar material 1; PNS, perinuclear space; Pol-II, RNA-polymerase II; PPARγ, peroxisome proliferators-activated receptors γ; SUN1/2, Sad1p-UNC-84 domain 1 and 2 proteins; TAZ, transcriptional coactivator with PDZ-binding motif; YAP, Yes-associated protein.

(Bodine et al., 2001; Marcotte et al., 2015; You et al., 2019). The mechanosensitive biochemical signaling pathways that regulate protein synthesis, such as mTORC1, MAPK, WNT/β-catenin, and YAP/TAZ, have been studied intensively over the past years and have been summarized in several excellent reviews (Bamman et al., 2018; Watt et al., 2018; Sartori et al., 2021). Our framework for how mechanotransduction, the conversion of mechanical forces into a cellular response, controls skeletal muscle mass is primarily through these biochemical signaling events. Traditionally the cell nucleus has been viewed as a passive organelle, simply serving as a reservoir for DNA and requiring cytosolic events to dictate nuclear responses. However, recent evidence has emerged showing that the nucleus itself can act as a mechanosensitive element, directly translating mechanical forces into a cellular response (Kirby and Lammerding, 2018; Aureille et al., 2019; Stephens et al., 2019) in a process termed "nuclear mechanotransduction." The mechanisms by which nuclear mechanotransduction impacts cellular processes include nuclear envelope stretching (Enyedi et al., 2016; Lomakin et al., 2020; Venturini et al., 2020), modification of nuclear envelope proteins (Guilluy et al., 2014), histone modifications and chromatin architecture (Le et al., 2016; Nava et al., 2020), transcription factor localization (Elosegui-Artola et al., 2017; Cosgrove et al., 2021), and gene expression (Tajik et al., 2016). Limited evidence exists for a putative role of nuclear mechanotransduction in regulating muscle homeostasis and adaptation (Piccus and Brayson, 2020; Jabre et al., 2021), despite the clear link between mechanical loading and skeletal muscle mass. Much of the evidence linking nuclear mechanotransduction to skeletal muscle function comes from the study of genetic diseases, where mutations in key proteins involved in nuclear mechanotransduction result in severe dystrophic phenotypes primarily affecting skeletal and cardiac muscle (Puckelwartz et al., 2010; McGlory and Phillips, 2015; Zhou et al., 2017; Piekarowicz et al., 2019; Heller et al., 2020). While these tissue-specific disease phenotypes suggest that nuclear mechanotransduction may be important in the context of normal muscle physiology, we still have limited knowledge regarding if and how myonuclei respond to the various mechanical forces present in skeletal muscle, and how this might integrate with other well-characterized mechanosensitive signaling cascades to ultimately control muscle mass and function. In this review, we will highlight the complexes involved in nuclear mechanotransduction, examine the latest evidence for nuclear mechanotransduction in cellular adaptation, and propose mechanisms for how nuclear mechanotransduction could play a role in the regulation of muscle mass.

COMPLEXES INVOLVED IN NUCLEAR MECHANOTRANSDUCTION

Recent evidence demonstrates that a nucleus is able to "sense" mechanical forces and elicit various biological responses (Kirby and Lammerding, 2018; Janota et al., 2020; Lomakin et al., 2020; Venturini et al., 2020). Mechanical forces can be transmitted to the nucleus from the exterior environment through cellular adhesion complexes (Maniotis et al., 1997; Tajik et al., 2016), intracellular generated forces (Earle et al., 2020), physical compression (Lomakin et al., 2020; Venturini et al., 2020), or osmotic changes (Enyedi et al., 2016; Petridou et al., 2017). Thus, one important consideration is that differences in force application may dictate the specificity of the response. The cytoskeleton is made up out of three main polymers; actin filaments, microtubules and intermediate filaments. Together, they organize the contents of the cell, enable organelle movement, dictate the cells' motility and shape, and connect the cell physically and biochemically to the external environment. One mechanism by which mechanical forces are transduced to the nucleus is through an intercellular network that physically connects the cytoskeleton to the nucleoskeleton via the LInker of Nucleoskeleton and Cytoskeleton (LINC) complex (Guilluy et al., 2014; Hao and Starr, 2019; Janota et al., 2020; Wong et al., 2021). The significance of this physical connection is that mechanical signals can propagate at speeds 12.5–25 times faster than passive diffusion or molecular motor-based signaling (Maurer and Lammerding, 2019), facilitating an extremely rapid cellular response. The LINC complex is a group of proteins that transverse through the nuclear envelope (NE), forming a bridge between the cytoskeleton and the nucleoskeleton (Lombardi et al., 2011; Hao and Starr, 2019). The LINC complex consists of two classes of proteins; the Klarsicht/ANC-1/SYNE homology (KASH) domain-containing proteins and the Sad-1 and UNC-84 (SUN) domain-containing proteins. The KASH family of proteins is composed of six members: nesprin-1 (encoded by *SYNE1*), nesprin-2 (encoded by *SYNE2*), nesprin-3 (encoded by *SYNE3*), nesprin-4 (encoded by *SYNE4*), Jaw1/LRMP (encoded by *JAW1*), and KASH5 (encoded by *KASH5*) (Horn et al., 2013b; Rajgor and Shanahan, 2013; Kozono et al., 2018; Janin and Gache, 2018; Zhou et al., 2018). Nesprins localize to the outer nuclear membrane (ONM) and interact with SUN proteins in the perinuclear space (PNS). Multiple nesprin-1 and -2 isoforms can be generated through alternative transcription and splicing, with the so-called giant isoforms interacting with actin via their calponin homology (CH) domain and/or microtubules via a LEWD motif-kinesin-1 interaction (Wilson and Holzbaur, 2015). In addition, smaller isoforms can interact with microtubules via various interacting partners, including AKAP450 (aka AKAP9) (Gimpel et al., 2017; Janin and Gache, 2018). Nesprin-3 interacts with intermediate filaments via the cytoskeletal linker protein plectin (Wilhelmsen et al., 2005; Wiche et al., 2015). In the case of striated muscle, the major intermediate filament protein is desmin (Heffler et al., 2020) and the major nuclear-associated plectin isoform is plectin-1 (Staszewska et al., 2015). Nesprin-4 interacts with microtubules via kinesin-1; however, its expression is restricted mainly to secretory epithelia (Roux et al., 2009) and outer hair cells of the inner ear (Horn et al., 2013a). The SUN family of proteins comprise five family members; of these, SUN1 and SUN2 are the most widely expressed (Malone et al., 1999; Crisp et al., 2005). SUN proteins form a trimeric complex that span the inner nuclear membrane (INM) and into the PNS, where their SUN domain interacts with the C-terminal KASH domain of the nesprins (Jahed et al., 2019). The N-terminus of the SUN proteins associates with nucleoplasmic structures, including the nuclear

lamina (Crisp et al., 2005; Haque et al., 2006) and chromatin (Horn et al., 2013b).

Within the INM reside members of the LAP2-emerin-MAN1 (LEM) domain family of proteins (Barton et al., 2015). Of these, emerin is the most studied in the context of skeletal muscle biology, due to mutations in emerin giving rise to Emery Dreifuss muscular dystrophy (Heller et al., 2020). Emerin can bind a chromatin-interacting protein named barrier-to-autointegration factor (BAF) (Samson et al., 2018), small isoforms of nesprin-1 and nesprin-2 (Mislow et al., 2002; Zhang et al., 2005; Wheeler et al., 2007), and SUN proteins (Haque et al., 2010). Additionally, emerin binds to the nuclear lamina, enabling it to retain chromatin close to the NE during cell interphase (Berk et al., 2013; Samson et al., 2018). Furthermore, due to the physical connection to the LINC complex (Haque et al., 2006) and LEM domain proteins (Barton et al., 2015), the nuclear lamina serves as one of the major integration sites for nuclear mechanotransduction. The nuclear lamina is a filamentous meshwork of A-type lamins (lamins A and C) and B-type lamins (lamins B1 and B2). The lamina lies just underneath the INM and interacts with LEM domain proteins (Gesson et al., 2014), nuclear pore complexes (NPCs) (Xie et al., 2016), transcription factors (Ivorra et al., 2006), and chromatin through lamina-associated domains (LADs) present in the genome (van Steensel and Belmont, 2017). The nuclear lamina, along with heterochromatin, provides mechanical stability to the nucleus (Lammerding et al., 2006; Stephens et al., 2017), and the expression of lamin A scales with tissue stiffness (Swift et al., 2013). Collectively, the cytoskeleton - LINC complex - lamina - chromatin interaction network can serve as a powerful mechanism to convert mechanical signals into a cellular response.

The composition and function of the LINC complex have been studied extensively in mononucleated adherent cells, including fibroblasts, endothelial cells, and enucleated mammalian cells (cytoplasts) (Lombardi et al., 2011; Anno et al., 2012; Graham et al., 2018; Bouzid et al., 2019). Skeletal muscle cells have a unique, highly structured cytoskeletal organization, specifically designed for high force generation. Thus, the nucleo-cytoskeletal interactions in myofibers need to be arranged to accommodate this specialized cellular function (**Figure 1**). Moreover, myofibers are multinucleated syncytial cells with an ordered arrangement of hundreds of myonuclei located on the periphery of the myofiber, with additional myonuclei being added during muscle growth via the fusion of satellite cells (Snijders et al., 2015; Murach et al., 2017). The importance of the LINC complex in skeletal muscle has been primarily examined for its role in nuclear movement and organization during myogenesis (Zhang et al., 2010; Gimpel et al., 2017; Stroud et al., 2017); however, it may have different functions in fully mature myofibers. For example, Nesprin-1α2 associates with kinesin-1 at myotube outer nuclear membranes (Gimpel et al., 2017), but is restricted to neuromuscular junction nuclei in adult muscle (Holt et al., 2019). The current body of research about the organization and importance of the LINC complex in adult striated muscle cells comes from recent studies in cardiomyocytes (Heffler et al., 2020); however, cardiomyocytes are either mono- or bi-nucleated, with the nucleus located in the center of the cell (Janin and Gache, 2018). In cardiac cells, microtubules interact with the nucleus via AKAP6 and AKAP9 (Vergarajauregui et al., 2020); AKAP9 serves an additional function in skeletal muscle cells, where it is required for microtubule-mediated nuclear migration (Gimpel et al., 2017). Interestingly, another microtubule-organizing protein, pericentriolar material 1 (PCM1), is enriched on myonuclei in adult muscle (Winje et al., 2018). Recently, Liu et al. (2020) discovered that an alternatively spliced version of Cardiac Islet-1 Interaction Protein (CIP) interacts with several LINC complex proteins and plays a role in microtubule-mediated nuclear movement during differentiation. However, the functional role of PCM1 and CIP in myonuclear force transmission in adult muscle is still not known.

Microtubules play an important role in mechanotransduction in cardiac cells (Kerr et al., 2015; Vergarajauregui et al., 2020), where they form a cage-like structure around the nucleus. Similar cage-like structures are observed in skeletal muscle cells (Becker et al., 2020; Earle et al., 2020), although the significance of these microtubule-myonuclear interactions on nuclear morphology and mechanotransduction requires additional investigation. Similarly, the desmin - plectin - nesprin-3 interlinkage (Wilhelmsen et al., 2005; Ketema et al., 2007; Wiche et al., 2015) appears to play a role in maintaining nuclear morphology (Heffler et al., 2020) and mechanotransduction (Palmisano et al., 2015; Staszewska et al., 2015), making this complex an intriguing candidate in the context of skeletal muscle adaptation. An important consideration is that the arrangement of the LINC complex, nuclear lamina, and NE could deviate between cardiac and skeletal muscle – and even more distinctively compared to previously studied non-muscle cell-lines. We suggest that this warrants additional investigations into how the nucleus interacts with cytoskeleton and other organelles (ER, golgi, etc.) in skeletal muscle cells. Moreover, it is still not clear how newly acquired myonuclei integrate into the highly complex and ordered cytoskeletal network and what LINC complex reorganization must occur to facilitate this process. Finally, the contribution of specific proteins in nucleo-cytoskeletal coupling will have to be considered when determining what forces may be transmitted to myonuclei during passive (stretch) and active (contractile) force generation.

EVIDENCE FOR NUCLEAR MECHANOTRANSDUCTION IN NON-SKELETAL MUSCLE CELLS

The first evidence of nuclear mechanotransduction came in the 1990s, when pioneering work by the Ingber laboratory showed that nuclei are "hard-wired" to their surrounding cytoplasm and that forces applied to either integrins or the cytoskeleton could elicit a physical response from the nucleus (Maniotis et al., 1997). Since those seminal studies, significant work has gone into trying to dissect which cellular responses to mechanical signals can be attributed to direct responses by nuclei themselves. Supporting evidence for the importance of nuclear mechanics come from disease-causing mutations in proteins involved in nuclear mechanotransduction

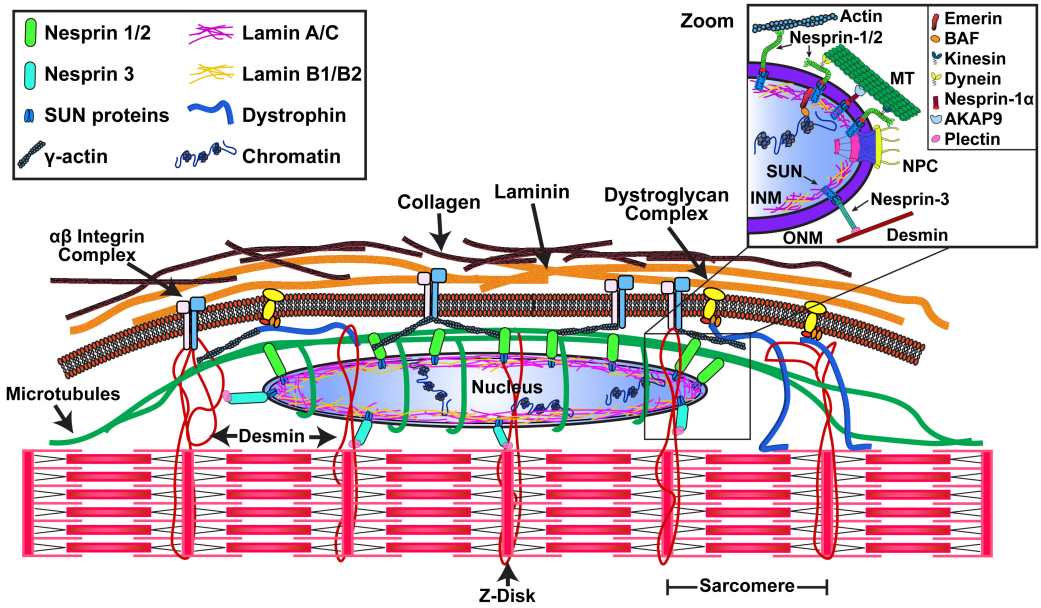

FIGURE 1 | Cytoskeletal organization around myonuclei provides a mechanism for nuclear mechanotransduction. Cytoskeletal proteins (microtubules, desmin, and γ-actin) are directly connected to myonuclei via the LINC (Linker of Nucleus and Cytoskeleton) complex. The LINC complex is composed of nesprin and SUN proteins, with SUN proteins interacting with the nuclear lamina (composed of A- and B-type lamins). Chromatin is tethered to the periphery of the nucleus via the nuclear lamina, providing a mechanism for cytoskeletal mechanical signals to be transmitted directly to the nuclear interior and chromatin. Inset: The SUN components of the LINC complex interact with NPCs. Emerin binds to the nuclear lamina and the chromatin-interacting protein BAF. The giant isoforms of Nesprin-1/2 interact with actin through their CH domain and microtubules via kinesin-1 and dynein (Zhu et al., 2017), while Nesprin-1α uses AKAP9. Nesprin-3 binds to desmin via plectin. Modified from Kirby (2019).

(Piekarowicz et al., 2019; Donnaloja et al., 2020; Heller et al., 2020). Though the underlying molecular mechanisms by which these proteins regulate tissue homeostasis have not yet been fully elucidated, nuclear mechanotransduction has been shown to induce chromatin rearrangement (Le et al., 2016; Nava et al., 2020), NE-unfolding (Enyedi et al., 2016; Lomakin et al., 2020; Venturini et al., 2020), the post-translational modification of nuclear proteins (Guilluy et al., 2014), transcription factor translocation (Elosegui-Artola et al., 2017), and gene expression (Tajik et al., 2016).

Chromatin Stretching/Modifications

One proposed mechanism for how mechanical forces transmitted to the nucleus can lead directly to a cellular response is through changes in chromatin organization or accessibility to transcription factors. Condensed chromatin, or heterochromatin, that is localized to the nuclear periphery is often adjacent to and makes contact with the nuclear lamina at LADs (van Steensel and Belmont, 2017). DNA is wrapped around histones, forming tightly compacted heterochromatin, inaccessible for transcription, along with less condensed euchromatin (Janssen et al., 2018). Moreover, A-type lamins, in cooperation with LEM-domain proteins, are critical for tethering heterochromatin to the NE (Solovei et al., 2013); thus, these physical interactions between chromatin and the nuclear lamina can allow forces to be transmitted to chromatin. To this end, Tajik et al. (2016) showed that local surface force at the plasma membrane, acting through the LINC complex, can directly stretch the chromatin and induce a rapid increase in transcription. This force-induced chromatin stretching and transcriptional upregulation is sensitive to both levels of H3K9me3 and force application frequency, where low H3K9me3 levels and low frequency are required for sufficient chromatin stretching and subsequent recruitment of RNA-polymerase II (Pol II) (Sun et al., 2020). Thus, epigenetic alterations to chromatin may serve as a mechanism for determining the specificity of the transcriptional response to nuclear force transmission. Recently, Nava et al. (2020) found that stretching of the nuclear membrane results in the rapid loss of histone methylation at H3K9 and H3K27, producing a more deformable nucleus that is protected from force-induced damage. Intriguingly, prolonged mechanical strain leads to large-scale chromatin rearrangements and the replacement of H3K9me2,3 with H3K27me3, leading to global transcriptional silencing during stem cell commitment (Le et al., 2016); however, it is unclear if a similar mechanism would occur in a terminally differentiated cell. The frequency and duration of force application on the nucleus appear to be important for determining the change in chromatin organization.

Transcription Factor Localization/Nuclear Pores

It is suggested that transmission of mechanical forces between the cytoskeleton and nucleoskeleton could directly influence the transport of proteins across the NE through NPCs

(Donnaloja et al., 2019). NPCs have been shown to interact with both the nuclear lamina (Al-Haboubi et al., 2011; Xie et al., 2016; Kittisopikul et al., 2021) and SUN1 (Liu et al., 2007), providing a mechanism for nuclear force transmission to alter NPC conformation. Work from the Roca-Cusachs laboratory demonstrated that direct application of force to the nucleus causes nuclear deformation, thereby stretching the NPC and allowing for increased import of YAP into the nucleus (Elosegui-Artola et al., 2017). Similarly, YAP nuclear entry in response to cyclic strain is impaired when the LINC complex is disrupted in mesenchymal stem cells, (Driscoll et al., 2015), indicating that nuclear mechanotransduction can regulate YAP localization in response to mechanical cues. In addition to altering the permeability of NPCs, mechanical signals can alter NPC localization through the redistribution of LINC complex proteins (Hoffman et al., 2020). The dogma of the NPC being a highly rigid structure has been challenged in recent years (Knockenhauer and Schwartz, 2016; Pulupa et al., 2020). One intriguing hypothesis is that repeated mechanical signals result in the clustering of NPCs at the site of force transmission and physically influence NPC conformation to affect nuclear transport.

Additionally, it has become evident that INM proteins influence the nucleo-cytoplasmic flux of transcription factors. The transcription factor β-catenin has been shown to be associated with nuclear envelope proteins such as emerin, lamins A/C and the LINC complex (Markiewicz et al., 2006; Tilgner et al., 2009; Neumann et al., 2010; Uzer et al., 2018). Uzer and colleagues found that disabling the LINC complex via co-depletion of SUN1/2 impedes the nuclear entry of β-catenin by limiting its nesprin-mediated interaction with the NE (Uzer et al., 2018). Since the LINC complex plays a critical part in the transmission of applied mechanical force from the cellular surface to the nucleus, Uzer et al., propose a new pathway by which LINC complex-mediated connectivity may play a role in signaling pathways that depend on the nuclear entry of β-catenin. In addition to the LINC complex, emerin contributes to the regulation of the β-catenin nuclear flux by binding to cytoplasmic β-catenin to restrict it from the nucleus (Markiewicz et al., 2006). To further investigate the relationship between β-catenin and nuclear β-catenin-binding partners, Tilgner et al. (2009) performed a study focusing on the expression of emerin, A-type lamins, and peroxisome proliferators-activated receptors γ (PPARγ) in preadipocytes and dermal fibroblasts. The authors found that the expression of NE proteins, A-type lamins, and emerin is directly linked to the balance between β-catenin and the PPARγ signaling to control the adipogenic capacity of the cell. Collectively, nuclear mechanotransduction can influence transcription factor localization to the nucleus, either through direct interactions or by modulating transport across the NPC.

NE and ER Unfolding

Another mechanism through which the nucleus responds to external forces is via the unfolding and stretching of the NE. Recently, Lomakin et al. (2020) found that migrating immune cells unfold and stretch their NE to adapt to environmental confinement and that enucleated cells show less motility in similar circumstances. Venturini et al. (2020) support these findings, with the demonstration of nuclear deformation due to confinement of primary progenitor stem cells, which leads to INM unfolding and intracellular spatial positioning of the nucleus. Mechanistically, NE stretching leads to the release of calcium; this activates calcium-dependent cytosolic phospholipase A2 (cPLA2), which catalyzes the formation of arachidonic acid to ultimately regulate myosin-II activity (Lomakin et al., 2020; Venturini et al., 2020). This mechanism of nuclear stretch-activation of cPLA2 was first identified by the Niethammer group in response to tissue damage (Enyedi et al., 2016). Similarly, deformation of nuclei with high membrane tension triggers Ca^{2+} release from the ER to modulate chromatin methylation levels (Nava et al., 2020). Collectively, NE stretch-dependent Ca^{2+} release is emerging as a powerful intermediary between mechanical inputs and cellular responses. In addition to the effect on calcium release, the amount of NE folding or "wrinkling" is associated with the translocation of mechanosensitive transcription factors, including YAP/TAZ (Cosgrove et al., 2021). One explanation for this altered transcription factor localization could be the accumulation of NPCs in NE invaginations, as has been shown in progeroid cells (Goldman et al., 2004; Röhrl et al., 2021), leading to a physical barrier affecting NPC transport. Lastly, nuclear force transmission has been shown to alter the assembly of the network of A-type lamins, exposing epitopes that are involved in chromatin interactions (Ihalainen et al., 2015). Thus, the extent of NE stretching will be highly dependent on the ability of forces to deform the nucleus, a process determined by the mechanical properties of the nucleus (Lammerding et al., 2006; Stephens et al., 2017).

Biochemical

Finally, mechanical signals lead to post-translational modifications of INM proteins and A-type lamins resulting in changes to the mechanical properties of the nucleus (Swift et al., 2013; Buxboim et al., 2014; Guilluy et al., 2014; Guilluy and Burridge, 2015; Graham et al., 2018; Gilbert et al., 2019; Ikegami et al., 2020). In isolated mammalian nuclei, pulses of force applied to nesprin 1 result in a decrease in nuclear strain, indicating local nuclear stiffening (Guilluy et al., 2014). The authors found that neither chromatin nor nuclear actin were involved in force response; however, emerin becomes tyrosine phosphorylated by tyrosine kinase Src as a reaction to applied force, strengthening the connection between A-type lamins and the LINC complex. In addition to phosphorylation of emerin, phosphorylation of lamins is a well-known mechanism involved in nuclear lamina assembly and disassembly in cell division. During interphase, A-type lamins phosphorylation is low, allowing for network assembly beneath the INM, whereas phosphorylation results in a shift toward nucleoplasmic localization (Buxboim et al., 2014; Kochin et al., 2014; Ikegami et al., 2020). Studies show that phosphorylation of A-type lamins on Ser22 is associated with soft matrix (Swift et al., 2013), and that their dephosphorylation is caused by myosin-II activity and matrix stiffness (Buxboim et al., 2014). Further experimentation revealed that the phosphodynamics of Ser22 are critical in determining the structural organization and mechanics of nuclei during

cell spreading (Buxboim et al., 2014). The precise mechanism by which mechanical forces can modulate phosphorylation of nuclear envelope proteins remains under investigation, including whether this process is regulated by altering kinase activities or accessibility of the kinase to cryptic phosphorylation sites within their protein substrates. Nevertheless, the observed mechanically induced phosphorylation implicates a structural role for phosphorylation in mechanotransduction through control of nuclear stiffening and nucleo-cytoskeletal coupling (Maurer and Lammerding, 2019).

POTENTIAL MECHANISMS FOR NUCLEAR MECHANOTRANSDUCTION IN REGULATING MUSCLE MASS AND FUNCTION

Many structural adaptations occur in skeletal muscle that give rise to changes in muscle mass (Jorgenson et al., 2020), with mechanical loading being a primary driver. Despite this clear association, further work is necessary to determine how structural changes in the muscle may provide feedback to alter the mechanosensitivity of the tissue. Muscle mass is largely governed by protein synthesis rates (Joanisse et al., 2020). However, studies using genetic approaches to manipulate protein turnover and increase muscle mass have failed to demonstrate a concomitant change in force output (Graber et al., 2019; Hunt et al., 2021), suggesting that mechanical input is critical for functional adaptations. To this end, mechanical signals may be important for creating a transcriptional profile that is permissive for changes in muscle mass and function (Phillips et al., 2013; Stokes et al., 2020). Therefore, force transmission to the nucleus could serve as an important regulatory mechanism for altering chromatin organization and transcription factor localization/activity in skeletal muscle cells.

Mislocalization of myonuclei is associated with cellular dysfunction and a range of muscle diseases. An intact LINC-complex is critical for the localization of the nuclei in skeletal muscle development (Gundersen and Worman, 2013; Janota et al., 2020). For example, nesprin-1 is required for myonuclear anchoring in skeletal muscle (Zhang et al., 2010; Stroud et al., 2017). Double knock-out mouse models of nesprin-1 and nesprin-2 show a cardiomyopathy phenotype alongside changes in nuclear deformation and chromatin decondensation (Banerjee et al., 2014). Moreover, the loss of SUN1 and SUN2 in knockout mouse models demonstrated that nuclear positioning in skeletal muscle cells is disrupted (Lei et al., 2009). Conditional deletion of LAP1, an emerin-interacting protein, causes muscular dystrophy in mice, suggesting that this emerin binding partner is essential for skeletal muscle maintenance and postnatal skeletal muscle growth (Shin et al., 2013, 2014, 2017). In addition to genetically induced disruption of nuclear position, changes in myonuclear morphology have been observed following chronic resistance exercise followed by detraining (Murach et al., 2020) and physiological aging (Brack et al., 2005; Bruusgaard et al., 2006; Cristea et al., 2010), suggesting that nuclear stability and/or nucleo-cytoskeletal coupling may adapt to changes in mechanical signals. It remains unclear whether this change in morphology is the result of intrinsic myonuclear adaptations or altered LINC complex connections and cytoskeletal forces (**Figure 2**). Moreover, how this change affects the mechanoresponsiveness of the myonucleus is unknown, as are the potential implications for myofiber homeostasis and adaptation, including nuclear mechanotransduction potentially coordinating a transcriptional profile that complements proteins synthesis changes to influence myofiber structure and function.

It remains to be determined whether mechanoresponsive protein synthetic pathways such as mTORC1, YAP/TAZ, and β-catenin are influenced by nuclear mechanotransduction in mature muscle cells, and if so, how these processes might synergize to affect muscle function. YAP/TAZ signaling has emerged as a potent regulator of skeletal muscle mass and function (Watt et al., 2015, 2018) and adaptation (Goodman et al., 2015), and has been suggested to be involved in age-related muscle atrophy (Setiawan et al., 2021). A proteomics study revealed that the expression of YAP is ∼two fold higher in slow-twitch muscle fibers than in fast-twitch muscle fibers from young subjects; in aged subjects, the YAP expression was ∼50% lower in both muscle fiber types compared to younger controls (Murgia et al., 2017). However, YAP/TAZ signaling may be elevated in aged skeletal muscle and associated with changes in the nuclear lamina (Iyer et al., 2021).Together, these results suggest that altered YAP expression and localization via changes in nuclear architecture (Cosgrove et al., 2021) or nuclear mechanotransduction (Driscoll et al., 2015) could play a role in muscle adaptation and age-dependent loss of skeletal muscle mass. Wnt/β-catenin signaling has been suggested to be involved in augmenting myofiber hypertrophy in response to increased mechanical load (Armstrong and Esser, 2005; Armstrong et al., 2006) and may be modulated by nuclear access to β-catenin via the LINC complex (Uzer et al., 2018). The well-characterized mechanosensitive MRTF/SRF pathway was recently shown to be activated in response to muscle contractions and associated with increased protein synthesis (Solagna et al., 2020), with the nuclear retention of MRTF-A being regulated by A-type lamins and emerin (Ho et al., 2013). Lastly, the transcription factor JunB is important for maintaining skeletal muscle mass and can promote hypertrophy (Raffaello et al., 2010). JunB is a member of the AP-1 family of proteins, of which c-Jun and c-Fos have been shown to interact with A-type lamins (Ivorra et al., 2006; Ikegami et al., 2020). Thus, it would be interesting to determine whether similar interactions occur between A-type lamins and JunB in skeletal muscle, and if so, whether the interaction is modulated by mechanical inputs. Collectively, changes in transcription factor localization or activity in response to alterations in nuclear morphology or mechanics may have important implications for regulating the skeletal muscle transcriptome.

Recently, mechanical loading has been shown to induce both DNA and histone modifications in skeletal muscle (McGee and Walder, 2017; Jacques et al., 2019; Solagna et al., 2020; Walden et al., 2020). Specifically, acute mechanical overload in mice results in hypomethylation of genes known to be involved in

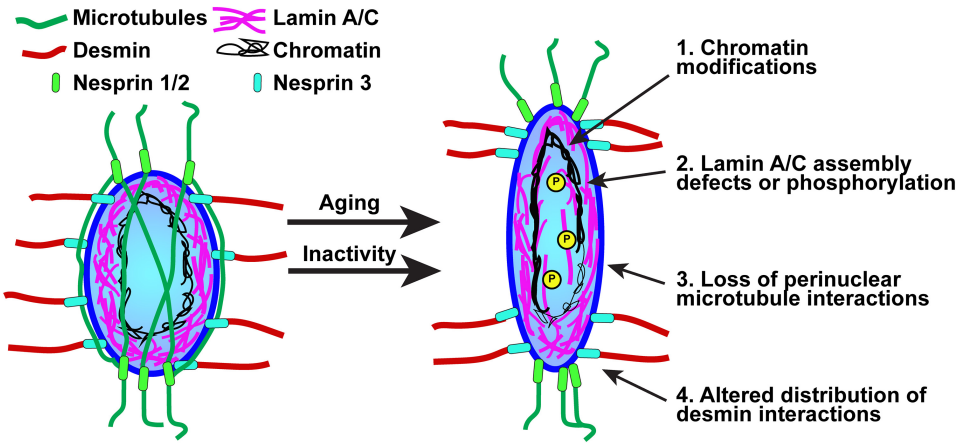

FIGURE 2 | Proposed mechanisms for nuclear-intrinsic and -extrinsic changes that could alter nuclear morphology in response to inactivity or aging. Nuclear stiffness is determined by both A-type lamins expression/assembly and chromatin modifications, specifically the amount of heterochromatin. Phosphorylation of A-type lamins leads to a nucleoplasmic localization and a decrease in nuclear stiffness. Nuclear morphology is also influenced by cytoskeletal forces acting through the LINC complex. Microtubules form a cage-like structure around the nucleus and provide compressive force; thus, elongation could be driven by a decrease in microtubule-nuclear interactions. Loss of desmin or plectin-1 results in more rounded nuclei, suggesting that changes in either the number or arrangement of desmin-nuclear interactions could elicit a change in nuclear morphology.

muscle maintenance, including known regulators of mTORC1 signaling (Walden et al., 2020). Similarly, an acute bout of resistance exercise in humans increases H3K27me3 distribution at 16 loci while total H3K27me3 levels were unaffected (Lim et al., 2020). Eccentric contraction induces phosphorylation of serine 10 on histone 3 (H3S10ph) in mice, with no changes in levels of H3-K9K14ac and H3K4me3 (Solagna et al., 2020). Collectively, these results suggest that changes in mechanical load alter DNA methylation and histone modifications to facilitate a mechanosensitive transcriptional response. During physiological aging there are global changes in histone modifications, including loss of H3K9me3 (Yoshihara et al., 2019) and increased H3K27ac (Zhou et al., 2019), it is possible that age-related alterations in nuclear morphology (Brack et al., 2005; Bruusgaard et al., 2006; Cristea et al., 2010) could promote changes in global chromatin organization. Further investigations are warranted to investigate how these modifications alter the chromatin accessibility in skeletal muscle and whether nuclear mechanotransduction plays a regulatory role in the response to mechanical loading or aging.

IMPORTANT CONSIDERATIONS AND FUTURE DIRECTIONS

The importance of protein metabolism in establishing a given level of muscle mass is clear; however, changes in protein synthesis do not always correspond to a change in muscle function, suggesting that the effect is dependent on the specific proteins being synthesized. We propose that the impact of nuclear morphology and nuclear mechanotransduction in skeletal muscle homeostasis and adaptation is an area worthy of further investigation. To date, most of the work in skeletal muscle has focused on nuclear abundance as an important determinant of myofiber size and adaptation (McCarthy et al., 2011; Murach et al., 2017; Psilander et al., 2019; Cramer et al., 2020; Hansson et al., 2020), with almost no focus on the nucleus as being a central player in the mechanotransduction response to mechanical load. The importance of nuclear mechanotransduction and the LINC complex in nuclear migration during myogenesis is well established (Zhang et al., 2010; Gimpel et al., 2017; Stroud et al., 2017), yet whether this importance persists for tissue maintenance is unclear. We still have a limited understanding of how myonuclei are integrated into the cytoskeleton in muscle fibers, how this is accomplished during the unique phenomenon of myonuclear addition, and finally, how this integration may change during adaptation, disease, or aging.

One of the primary challenges in studying the role of nuclear mechanotransduction in a specific cellular response is decoupling the mechanoresponse of the nucleus from cell surface/cytoplasmic signaling events. This can be accomplished by either performing assays on isolated nuclei (Guilluy and Burridge, 2015; Stephens et al., 2019), or via the more biologically relevant technique of restricting mechanical signals from reaching the nucleus. In practice, this can be done by expressing dominant-negative nesprin or SUN constructs (Lombardi et al., 2011; Uzer et al., 2018), which globally disrupt all LINC complexes, or via targeting of specific LINC complex or LINC-complex associated proteins (Staszewska et al., 2015; Tajik et al., 2016; Cosgrove et al., 2021).

Another significant challenge will be identifying mechanisms that control the specificity of the response. For example, if chromatin stretching can induce transcriptional activation, how can this be restricted to specific genes or loci? There may need to be additional layers of regulation, such as additional epigenetic modifications that modulate the response (Sun et al., 2020). Integrating genetic and biophysical methods

with either advanced-tissue engineering approaches or novel mouse models will be necessary to study the causative effects of nuclear mechanotransduction on muscle mass and function. For the mouse models, utilizing inducible- and tissue-specific strains (Murach et al., 2020) will allow for separating developmental effects from those necessary for maintenance and adaptation during adulthood. Combining these approaches with recent advances in single-nuclear sequencing (Ding et al., 2020; Dos Santos et al., 2020; Petrany et al., 2020) and chromatin-accessibility technologies (Klein and Hainer, 2020) could allow for discovery of novel transcriptional and/or chromatin organization mechanisms. Moreover, recently developed LINC complex-based tension sensors (Arsenovic et al., 2016; Déjardin et al., 2020) could be implemented to quantify the amount of cytoskeleton-to-nucleus force transmission in muscle fibers. Lastly, as an alternative to experimental-based approaches, computational modeling has potential utility for the prediction of how various mechanical force-generating and -transmitting structures in skeletal muscle contribute to nuclear mechanobiology (Mohammed et al., 2019).

Seminal work over the past 30 years has started to unravel the molecular details for how mechanical forces are transduced in skeletal muscle in order to control tissue mass and function. Nevertheless, the potential influence of nuclear mechanotransduction on directly modulating myonuclear organization and/or activity has been largely overlooked. Additional work is necessary to understand the precise role that cytoskeletal-nuclear force transmission has on the skeletal muscle transcriptome, and if so, how specificity in controlled. Furthermore, decoupling these events from cytoplasmic signaling events remains a challenge, as it is likely that synergy between multiple mechanotransduction pathways is required to produce the appropriate response. We propose that nuclear mechanotransduction may provide an additional "fine-tuning" role for priming the muscle cell for the appropriate transcriptional response to mechanical stimuli (Tajik et al., 2016), or possibly serve to alter the mechanical properties of the nucleus to protect the genome from repeated mechanical stresses (Nava et al., 2020), ultimately serving as an integral link between mechanical loading and muscle mass regulation.

AUTHOR CONTRIBUTIONS

All authors listed have made a substantial, direct and intellectual contribution to the work, and approved it for publication.

FUNDING

This work was supported by funding from the Muscular Dystrophy Association (Career Development Grant; MDA603238) and the Dutch Cardiovascular Alliance (Talent Grant) awarded to TK.

ACKNOWLEDGMENTS

The authors apologize to the many colleagues whose work could not be cited due to space constraints. The authors thank Dr. Coen Ottenheijm and Mary Godec for their helpful discussion and feedback during the drafting of the manuscript.

REFERENCES

Al-Haboubi, T., Shumaker, D. K., Köser, J., Wehnert, M., and Fahrenkrog, B. (2011). Distinct association of the nuclear pore protein Nup153 with A- and B-type lamins. *Nucleus* 2, 500–509. doi: 10.4161/nucl.2.5.17913

Anno, T., Sakamoto, N., and Sato, M. (2012). Role of nesprin-1 in nuclear deformation in endothelial cells under static and uniaxial stretching conditions. *Biochem. Biophys. Res. Commun.* 424, 94–99. doi: 10.1016/j.bbrc.2012.06.073

Armstrong, D. D., and Esser, K. A. (2005). Wnt/β-catenin signaling activates growth-control genes during overload-induced skeletal muscle hypertrophy. *Am. J. Physiol. Cell Physiol.* 289, C853–C859. doi: 10.1152/ajpcell.00093.2005

Armstrong, D. D., Wong, V. L., and Esser, K. A. (2006). Expression of β-catenin is necessary for physiological growth of adult skeletal muscle. *Am. J. Physiol. Cell Physiol.* 291, C185–C188. doi: 10.1152/ajpcell.00644.2005

Arsenovic, P. T., Ramachandran, I., Bathula, K., Zhu, R., Narang, J. D., Noll, N. A., et al. (2016). Nesprin-2G, a Component of the Nuclear LINC complex, is subject to myosin-dependent tension. *Biophys. J.* 110, 34–43. doi: 10.1016/j.bpj.2015.11.014

Aureille, J., Buffière-Ribot, V., Harvey, B. E., Boyault, C., Pernet, L., Andersen, T., et al. (2019). Nuclear envelope deformation controls cell cycle progression in response to mechanical force. *EMBO Rep.* 20:e48084. doi: 10.15252/embr.201948084

Bamman, M. M., Roberts, B. M., and Adams, G. R. (2018). Molecular regulation of exercise-induced muscle fiber hypertrophy. *Cold Spring Harb. Perspect. Med.* 8:a029751. doi: 10.1101/cshperspect.a029751

Banerjee, I., Zhang, J., Moore-Morris, T., Pfeiffer, E., Buchholz, K. S., Liu, A., et al. (2014). Targeted ablation of Nesprin 1 and Nesprin 2 from murine myocardium results in cardiomyopathy, altered nuclear morphology and inhibition of the biomechanical gene response. *PLoS Genet.* 10:e1004114. doi: 10.1371/journal.pgen.1004114

Barton, L. J., Soshnev, A. A., and Geyer, P. K. (2015). Networking in the nucleus: a spotlight on LEM-domain proteins. *Curr. Opin. Cell Biol.* 34, 1–8. doi: 10.1016/j.ceb.2015.03.005

Becker, R., Leone, M., and Engel, F. B. (2020). Microtubule organization in striated muscle cells. *Cells* 9:1395. doi: 10.3390/cells9061395

Berk, J. M., Tifft, K. E., and Wilson, K. L. (2013). The nuclear envelope LEM-domain protein emerin. *Nucleus* 4, 298–314. doi: 10.4161/nucl.25751

Bodine, S. C., Stitt, T. N., Gonzalez, M., Kline, W. O., Stover, G. L., Bauerlein, R., et al. (2001). Akt/mTOR pathway is a crucial regulator of skeletal muscle hypertrophy and can prevent muscle atrophy in vivo. *Nat. Cell Biol.* 3, 1014–1019. doi: 10.1038/ncb1101-1014

Bouzid, T., Kim, E., Riehl, B. D., Esfahani, A. M., Rosenbohm, J., Yang, R., et al. (2019). The LINC complex, mechanotransduction, and mesenchymal stem cell function and fate. *J. Biol. Eng.* 13:68. doi: 10.1186/s13036-019-0197-9

Brack, A. S., Bildsoe, H., and Hughes, S. M. (2005). Evidence that satellite cell decrement contributes to preferential decline in nuclear number from large fibres during murine age-related muscle atrophy. *J. Cell Sci.* 118, 4813–4821. doi: 10.1242/jcs.02602

Bruusgaard, J. C., Liestøl, K., and Gundersen, K. (2006). Distribution of myonuclei and microtubules in live muscle fibers of young, middle-aged, and old mice. *J. Appl. Physiol.* 100, 2024–2030. doi: 10.1152/japplphysiol.00913.2005

Buxboim, A., Swift, J., Irianto, J., Spinler, K. R., Dingal, P. C. D. P., Athirasala, A., et al. (2014). Matrix elasticity regulates lamin-A,C phosphorylation and turnover with feedback to actomyosin. *Curr. Biol.* 24, 1909–1917. doi: 10.1016/j.cub.2014.07.001

Cosgrove, B. D., Loebel, C., Driscoll, T. P., Tsinman, T. K., Dai, E. N., Heo, S.-J., et al. (2021). Nuclear envelope wrinkling predicts mesenchymal progenitor cell mechano-response in 2D and 3D microenvironments. *Biomaterials* 270:120662. doi: 10.1016/j.biomaterials.2021.120662

Cramer, A. A. W., Prasad, V., Eftestøl, E., Song, T., Hansson, K.-A., Dugdale, H. F., et al. (2020). Nuclear numbers in syncytial muscle fibers promote size but limit the development of larger myonuclear domains. *Nat. Commun.* 11:6287. doi: 10.1038/s41467-020-20058-7

Crisp, M., Liu, Q., Roux, K., Rattner, J. B., Shanahan, C., Burke, B., et al. (2005). Coupling of the nucleus and cytoplasm: role of the LINC complex. *J. Cell Biol.* 172, 41–53. doi: 10.1083/jcb.200509124

Cristea, A., Qaisar, R., Edlund, P. K., Lindblad, J., Bengtsson, E., and Larsson, L. (2010). Effects of aging and gender on the spatial organization of nuclei in single human skeletal muscle cells. *Aging Cell* 9, 685–697. doi: 10.1111/j.1474-9726.2010.00594.x

Déjardin, T., Carollo, P. S., Sipieter, F., Davidson, P. M., Seiler, C., Cuvelier, D., et al. (2020). Nesprins are mechanotransducers that discriminate epithelial-mesenchymal transition programs. *J. Cell Biol.* 219:e201908036. doi: 10.1083/jcb.201908036

Ding, J., Adiconis, X., Simmons, S. K., Kowalczyk, M. S., Hession, C. C., Marjanovic, N. D., et al. (2020). Systematic comparison of single-cell and single-nucleus RNA-sequencing methods. *Nat. Biotechnol.* 38, 737–746. doi: 10.1038/s41587-020-0465-8

Donnaloja, F., Carnevali, F., Jacchetti, E., and Raimondi, M. T. (2020). Lamin A/C mechanotransduction in laminopathies. *Cells* 9:1306. doi: 10.3390/cells9051306

Donnaloja, F., Jacchetti, E., Soncini, M., and Raimondi, M. T. (2019). Mechanosensing at the nuclear envelope by nuclear pore complex stretch activation and its effect in physiology and pathology. *Front. Physiol.* 10:896. doi: 10.3389/fphys.2019.00896

Dos Santos, M., Backer, S., Saintpierre, B., Izac, B., Andrieu, M., Letourneur, F., et al. (2020). Single-nucleus RNA-seq and FISH identify coordinated transcriptional activity in mammalian myofibers. *Nat. Commun.* 11:5102. doi: 10.1038/s41467-020-18789-8

Driscoll, T. P., Cosgrove, B. D., Heo, S.-J., Shurden, Z. E., and Mauck, R. L. (2015). Cytoskeletal to nuclear strain transfer regulates YAP signaling in mesenchymal stem cells. *Biophys. J.* 108, 2783–2793. doi: 10.1016/j.bpj.2015.05.010

Earle, A. J., Kirby, T. J., Fedorchak, G. R., Isermann, P., Patel, J., Iruvanti, S., et al. (2020). Mutant lamins cause nuclear envelope rupture and DNA damage in skeletal muscle cells. *Nat. Mater.* 19, 464–473. doi: 10.1038/s41563-019-0563-5

Elosegui-Artola, A., Andreu, I., Beedle, A. E. M., Lezamiz, A., Uroz, M., Kosmalska, A. J., et al. (2017). Force triggers Yap nuclear entry by regulating transport across nuclear pores. *Cell* 171, 1397.e14–1410.e14. doi: 10.1016/j.cell.2017.10.008

Enyedi, B., Jelcic, M., and Niethammer, P. (2016). The cell nucleus serves as a mechanotransducer of tissue damage-induced inflammation. *Cell* 165, 1160–1170. doi: 10.1016/j.cell.2016.04.016

Gesson, K., Vidak, S., and Foisner, R. (2014). Lamina-associated polypeptide (LAP)2α and nucleoplasmic lamins in adult stem cell regulation and disease. *Semin. Cell Dev. Biol.* 29, 116–124. doi: 10.1016/j.semcdb.2013.12.009

Gilbert, H. T. J., Mallikarjun, V., Dobre, O., Jackson, M. R., Pedley, R., Gilmore, A. P., et al. (2019). Nuclear decoupling is part of a rapid protein-level cellular response to high-intensity mechanical loading. *Nat. Commun.* 10:4149. doi: 10.1038/s41467-019-11923-1

Gimpel, P., Lee, Y. L., Sobota, R. M., Calvi, A., Koullourou, V., Patel, R., et al. (2017). Nesprin-1α-dependent microtubule nucleation from the nuclear envelope via Akap450 is necessary for nuclear positioning in muscle cells. *Curr. Biol.* 27, 2999.e9–3009.e9. doi: 10.1016/j.cub.2017.08.031

Goldman, R. D., Shumaker, D. K., Erdos, M. R., Eriksson, M., Goldman, A. E., Gordon, L. B., et al. (2004). Accumulation of mutant lamin A causes progressive changes in nuclear architecture in Hutchinson–Gilford progeria syndrome. *Proc. Natl. Acad. Sci. U.S.A.* 101, 8963–8968. doi: 10.1073/pnas.0402943101

Goodman, C. A., Dietz, J. M., Jacobs, B. L., McNally, R. M., You, J.-S., and Hornberger, T. A. (2015). Yes-Associated Protein is up-regulated by mechanical overload and is sufficient to induce skeletal muscle hypertrophy. *FEBS Lett.* 589, 1491–1497. doi: 10.1016/j.febslet.2015.04.047

Graber, T. G., Fry, C. S., Brightwell, C. R., Moro, T., Maroto, R., Bhattarai, N., et al. (2019). Skeletal muscle–specific knockout of DEP domain containing 5 protein increases mTORC1 signaling, muscle cell hypertrophy, and mitochondrial respiration. *J. Biol. Chem.* 294, 4091–4102. doi: 10.1074/jbc.RA118.005970

Graham, D. M., Andersen, T., Sharek, L., Uzer, G., Rothenberg, K., Hoffman, B. D., et al. (2018). Enucleated cells reveal differential roles of the nucleus in cell migration, polarity, and mechanotransduction. *J. Cell Biol.* 217, 895–914. doi: 10.1083/jcb.201706097

Guilluy, C., and Burridge, K. (2015). Nuclear mechanotransduction: forcing the nucleus to respond. *Nucleus* 6, 19–22. doi: 10.1080/19491034.2014.1001705

Guilluy, C., Osborne, L. D., Van Landeghem, L., Sharek, L., Superfine, R., Garcia-Mata, R., et al. (2014). Isolated nuclei adapt to force and reveal a mechanotransduction pathway within the nucleus. *Nat. Cell Biol.* 16, 376–381. doi: 10.1038/ncb2927

Gundersen, G. G., and Worman, H. J. (2013). Nuclear positioning. *Cell* 152, 1376–1389. doi: 10.1016/j.cell.2013.02.031

Hansson, K.-A., Eftestøl, E., Bruusgaard, J. C., Juvkam, I., Cramer, A. W., Malthe-Sørenssen, A., et al. (2020). Myonuclear content regulates cell size with similar scaling properties in mice and humans. *Nat. Commun.* 11:6288. doi: 10.1038/s41467-020-20057-8

Hao, H., and Starr, D. A. (2019). SUN/KASH interactions facilitate force transmission across the nuclear envelope. *Nucleus* 10, 73–80. doi: 10.1080/19491034.2019.1595313

Haque, F., Lloyd, D. J., Smallwood, D. T., Dent, C. L., Shanahan, C. M., Fry, A. M., et al. (2006). SUN1 interacts with nuclear lamin a and cytoplasmic nesprins to provide a physical connection between the nuclear lamina and the cytoskeleton. *Mol. Cell. Biol.* 26, 3738–3751. doi: 10.1128/MCB.26.10.3738-3751.2006

Haque, F., Mazzeo, D., Patel, J. T., Smallwood, D. T., Ellis, J. A., Shanahan, C. M., et al. (2010). Mammalian SUN protein interaction networks at the inner nuclear membrane and their role in laminopathy disease processes. *J. Biol. Chem.* 285, 3487–3498. doi: 10.1074/jbc.M109.071910

Heffler, J., Shah, P. P., Robison, P., Phyo, S., Veliz, K., Uchida, K., et al. (2020). A Balance between intermediate filaments and microtubules maintains nuclear architecture in the cardiomyocyte. *Circ. Res.* 126, e10–e26. doi: 10.1161/CIRCRESAHA.119.315582

Heller, S. A., Shih, R., Kalra, R., and Kang, P. B. (2020). Emery-Dreifuss muscular dystrophy. *Muscle Nerve* 61, 436–448. doi: 10.1002/mus.26782

Ho, C. Y., Jaalouk, D. E., Vartiainen, M. K., and Lammerding, J. (2013). Lamin A/C and emerin regulate MKL1-SRF activity by modulating actin dynamics. *Nature* 497, 507–511. doi: 10.1038/nature12105

Hoffman, L. M., Smith, M. A., Jensen, C. C., Yoshigi, M., Blankman, E., Ullman, K. S., et al. (2020). Mechanical stress triggers nuclear remodeling and the formation of transmembrane actin nuclear lines with associated nuclear pore complexes. *Mol. Biol. Cell* 31, 1774–1787. doi: 10.1091/mbc.E19-01-0027

Holt, I., Fuller, H. R., Lam, L. T., Sewry, C. A., Shirran, S. L., Zhang, Q., et al. (2019). Nesprin-1-alpha2 associates with kinesin at myotube outer nuclear membranes, but is restricted to neuromuscular junction nuclei in adult muscle. *Sci. Rep.* 9:14202. doi: 10.1038/s41598-019-50728-6

Horn, H. F., Brownstein, Z., Lenz, D. R., Shivatzki, S., Dror, A. A., Dagan-Rosenfeld, O., et al. (2013a). The LINC complex is essential for hearing. *J. Clin. Invest.* 123, 740–750. doi: 10.1172/JCI66911

Horn, H. F., Kim, D. I., Wright, G. D., Wong, E. S. M., Stewart, C. L., Burke, B., et al. (2013b). A mammalian KASH domain protein coupling meiotic chromosomes to the cytoskeleton. *J. Cell Biol.* 202, 1023–1039. doi: 10.1083/jcb.201304004

Hunt, L. C., Schadeberg, B., Stover, J., Haugen, B., Pagala, V., Wang, Y.-D., et al. (2021). Antagonistic control of myofiber size and muscle protein quality control by the ubiquitin ligase UBR4 during aging. *Nat. Commun.* 12:1418. doi: 10.1038/s41467-021-21738-8

Ihalainen, T. O., Aires, L., Herzog, F. A., Schwartlander, R., Moeller, J., and Vogel, V. (2015). Differential basal-to-apical accessibility of lamin A/C epitopes in the nuclear lamina regulated by changes in cytoskeletal tension. *Nat. Mater.* 14, 1252–1261. doi: 10.1038/nmat4389

Ikegami, K., Secchia, S., Almakki, O., Lieb, J. D., and Moskowitz, I. P. (2020). Phosphorylated lamin A/C in the nuclear interior binds active enhancers associated with abnormal transcription in progeria. *Dev. Cell* 52, 699.e11–713.e11. doi: 10.1016/j.devcel.2020.02.011

Ivorra, C., Kubicek, M., González, J. M., Sanz-González, S. M., Álvarez-Barrientos, A., O'Connor, J.-E., et al. (2006). A mechanism of AP-1 suppression through interaction of c-Fos with lamin A/C. *Genes Dev.* 20, 307–320. doi: 10.1101/gad.349506

Iyer, S. R., Hsia, R.-C., Folker, E. S., and Lovering, R. M. (2021). Age-dependent changes in nuclear-cytoplasmic signaling in skeletal muscle. *Exp. Gerontol.* 150, 111338. doi: 10.1016/j.exger.2021.111338

Jabre, S., Hleihel, W., and Coirault, C. (2021). Nuclear mechanotransduction in skeletal muscle. *Cells* 10:318. doi: 10.3390/cells10020318

Jacques, M., Hiam, D., Craig, J., Barrès, R., Eynon, N., and Voisin, S. (2019). Epigenetic changes in healthy human skeletal muscle following exercise–a systematic review. *Epigenetics* 14, 633–648. doi: 10.1080/15592294.2019.1614416

Jahed, Z., Hao, H., Thakkar, V., Vu, U. T., Valdez, V. A., Rathish, A., et al. (2019). Role of KASH domain lengths in the regulation of LINC complexes. *Mol. Biol. Cell* 30, 2076–2086. doi: 10.1091/mbc.E19-02-0079

Janin, A., and Gache, V. (2018). Nesprins and lamins in health and diseases of cardiac and skeletal muscles. *Front. Physiol.* 9:1277. doi: 10.3389/fphys.2018.01277

Janota, C. S., Calero-Cuenca, F. J., and Gomes, E. R. (2020). The role of the cell nucleus in mechanotransduction. *Curr. Opin. Cell Biol.* 63, 204–211. doi: 10.1016/j.ceb.2020.03.001

Janssen, A., Colmenares, S. U., and Karpen, G. H. (2018). Heterochromatin: guardian of the genome. *Annu. Rev. Cell Dev. Biol.* 34, 265–288. doi: 10.1146/annurev-cellbio-100617-062653

Joanisse, S., Lim, C., McKendry, J., Mcleod, J. C., Stokes, T., and Phillips, S. M. (2020). Recent advances in understanding resistance exercise training-induced skeletal muscle hypertrophy in humans. *F1000Research* 9:141. doi: 10.12688/f1000research.21588.1

Jorgenson, K. W., Phillips, S. M., and Hornberger, T. A. (2020). Identifying the structural adaptations that drive the mechanical load-induced growth of skeletal muscle: a scoping review. *Cells* 9:1658. doi: 10.3390/cells9071658

Kerr, J. P., Robison, P., Shi, G., Bogush, A. I., Kempema, A. M., Hexum, J. K., et al. (2015). Detyrosinated microtubules modulate mechanotransduction in heart and skeletal muscle. *Nat. Commun.* 6:8526. doi: 10.1038/ncomms9526

Ketema, M., Wilhelmsen, K., Kuikman, I., Janssen, H., Hodzic, D., and Sonnenberg, A. (2007). Requirements for the localization of nesprin-3 at the nuclear envelope and its interaction with plectin. *J. Cell Sci.* 120, 3384–3394. doi: 10.1242/jcs.014191

Kirby, T. J. (2019). Mechanosensitive pathways controlling translation regulatory processes in skeletal muscle and implications for adaptation. *J. Appl. Physiol.* 127, 608–618. doi: 10.1152/japplphysiol.01031.2018

Kirby, T. J., and Lammerding, J. (2018). Emerging views of the nucleus as a cellular mechanosensor. *Nat. Cell Biol.* 20, 373–381. doi: 10.1038/s41556-018-0038-y

Kittisopikul, M., Shimi, T., Tatli, M., Tran, J. R., Zheng, Y., Medalia, O., et al. (2021). Computational analyses reveal spatial relationships between nuclear pore complexes and specific lamins. *J. Cell Biol.* 220, e202007082. doi: 10.1083/jcb.202007082

Klein, D. C., and Hainer, S. J. (2020). Genomic methods in profiling DNA accessibility and factor localization. *Chromosome Res.* 28, 69–85. doi: 10.1007/s10577-019-09619-9

Knockenhauer, K. E., and Schwartz, T. U. (2016). The nuclear pore complex as a flexible and dynamic gate. *Cell* 164, 1162–1171. doi: 10.1016/j.cell.2016.01.034

Kochin, V., Shimi, T., Torvaldson, E., Adam, S. A., Goldman, A., Pack, C.-G., et al. (2014). Interphase phosphorylation of lamin A. *J. Cell Sci.* 127, 2683–2696. doi: 10.1242/jcs.141820

Kozono, T., Tadahira, K., Okumura, W., Itai, N., Tamura-Nakano, M., Dohi, T., et al. (2018). Jaw1/LRMP has a role in maintaining nuclear shape via interaction with SUN proteins. *J. Biochem.* 164, 303–311. doi: 10.1093/jb/mvy053

Lammerding, J., Fong, L. G., Ji, J. Y., Reue, K., Stewart, C. L., Young, S. G., et al. (2006). Lamins A and C but not lamin B1 regulate nuclear mechanics *. *J. Biol. Chem.* 281, 25768–25780. doi: 10.1074/jbc.M513511200

Le, H. Q., Ghatak, S., Yeung, C.-Y. C., Tellkamp, F., Günschmann, C., Dieterich, C., et al. (2016). Mechanical regulation of transcription controls Polycomb-mediated gene silencing during lineage commitment. *Nat. Cell Biol.* 18, 864–875. doi: 10.1038/ncb3387

Lei, K., Zhang, X., Ding, X., Guo, X., Chen, M., Zhu, B., et al. (2009). SUN1 and SUN2 play critical but partially redundant roles in anchoring nuclei in skeletal muscle cells in mice. *Proc. Natl. Acad. Sci. U.S.A.* 106, 10207–10212. doi: 10.1073/pnas.0812037106

Lim, C., Shimizu, J., Kawano, F., Kim, H. J., and Kim, C. K. (2020). Adaptive responses of histone modifications to resistance exercise in human skeletal muscle. *PLoS One* 15:e0231321. doi: 10.1371/journal.pone.0231321

Liu, J., Huang, Z.-P., Nie, M., Wang, G., Silva, W. J., Yang, Q., et al. (2020). Regulation of myonuclear positioning and muscle function by the skeletal muscle-specific CIP protein. *Proc. Natl. Acad. Sci. U.S.A.* 117, 19254–19265. doi: 10.1073/pnas.1922911117

Liu, Q., Pante, N., Misteli, T., Elsagga, M., Crisp, M., Hodzic, D., et al. (2007). Functional association of Sun1 with nuclear pore complexes. *J. Cell Biol.* 178, 785–798. doi: 10.1083/jcb.200704108

Lomakin, A. J., Cattin, C. J., Cuvelier, D., Alraies, Z., Molina, M., Nader, G. P. F., et al. (2020). The nucleus acts as a ruler tailoring cell responses to spatial constraints. *Science* 370:eaba2894. doi: 10.1126/science.aba2894

Lombardi, M. L., Jaalouk, D. E., Shanahan, C. M., Burke, B., Roux, K. J., and Lammerding, J. (2011). The interaction between nesprins and sun proteins at the nuclear envelope is critical for force transmission between the nucleus and cytoskeleton. *J. Biol. Chem.* 286, 26743–26753. doi: 10.1074/jbc.M111.233700

Malone, C. J., Fixsen, W. D., Horvitz, H. R., and Han, M. (1999). UNC-84 localizes to the nuclear envelope and is required for nuclear migration and anchoring during *C. elegans* development. *Development* 126, 3171–3181. doi: 10.1242/dev.126.14.3171

Maniotis, A. J., Chen, C. S., and Ingber, D. E. (1997). Demonstration of mechanical connections between integrins, cytoskeletal filaments, and nucleoplasm that stabilize nuclear structure. *Proc. Natl. Acad. Sci. U.S.A.* 94, 849–854. doi: 10.1073/pnas.94.3.849

Marcotte, G. R., West, D. W. D., and Baar, K. (2015). The molecular basis for load-induced skeletal muscle hypertrophy. *Calcif. Tissue Int.* 96, 196–210. doi: 10.1007/s00223-014-9925-9

Markiewicz, E., Tilgner, K., Barker, N., van de Wetering, M., Clevers, H., Dorobek, M., et al. (2006). The inner nuclear membrane protein Emerin regulates β-catenin activity by restricting its accumulation in the nucleus. *EMBO J.* 25, 3275–3285. doi: 10.1038/sj.emboj.7601230

Maurer, M., and Lammerding, J. (2019). The driving force: nuclear mechanotransduction in cellular function, fate, and disease. *Annu. Rev. Biomed. Eng.* 21, 443–468. doi: 10.1146/annurev-bioeng-060418-052139

McCarthy, J. J., Mula, J., Miyazaki, M., Erfani, R., Garrison, K., Farooqui, A. B., et al. (2011). Effective fiber hypertrophy in satellite cell-depleted skeletal muscle. *Development* 138, 3657–3666. doi: 10.1242/dev.068858

McGee, S. L., and Walder, K. R. (2017). Exercise and the skeletal muscle epigenome. *Cold Spring Harb. Perspect. Med.* 7:a029876. doi: 10.1101/cshperspect.a029876

McGlory, C., and Phillips, S. M. (2015). "Exercise and the regulation of skeletal muscle hypertrophy," in *Progress in Molecular Biology and Translational Science*, ed. D. B. Teplow (Amsterdam: Elsevier), 153–173. doi: 10.1016/bs.pmbts.2015.06.018

Mislow, J. M. K., Holaska, J. M., Kim, M. S., Lee, K. K., Segura-Totten, M., Wilson, K. L., et al. (2002). Nesprin-1α self-associates and binds directly to emerin and lamin A in vitro. *FEBS Lett.* 525, 135–140. doi: 10.1016/S0014-5793(02)03105-8

Mohammed, D., Versaevel, M., Bruyère, C., Alaimo, L., Luciano, M., Vercruysse, E., et al. (2019). Innovative tools for mechanobiology: unraveling outside-in and inside-out mechanotransduction. *Front. Bioeng. Biotechnol.* 7:162. doi: 10.3389/fbioe.2019.00162

Murach, K. A., Fry, C. S., Kirby, T. J., Jackson, J. R., Lee, J. D., White, S. H., et al. (2017). Starring or supporting role? Satellite cells and skeletal muscle fiber size regulation. *Physiology* 33, 26–38. doi: 10.1152/physiol.00019.2017

Murach, K. A., McCarthy, J. J., Peterson, C. A., and Dungan, C. M. (2020). Making Mice Mighty: recent advances in translational models of load-induced muscle hypertrophy. *J. Appl. Physiol. Bethesda Md* 129, 516–521. doi: 10.1152/japplphysiol.00319.2020

Murgia, M., Toniolo, L., Nagaraj, N., Ciciliot, S., Vindigni, V., Schiaffino, S., et al. (2017). Single muscle fiber proteomics reveals fiber-type-specific features of human muscle aging. *Cell Rep.* 19, 2396–2409. doi: 10.1016/j.celrep.2017.05.054

Nava, M. M., Miroshnikova, Y. A., Biggs, L. C., Whitefield, D. B., Metge, F., Boucas, J., et al. (2020). Heterochromatin-driven nuclear softening protects the genome against mechanical stress-induced damage. *Cell* 181, 800.e22–817.e22. doi: 10.1016/j.cell.2020.03.052

Neumann, S., Schneider, M., Daugherty, R. L., Gottardi, C. J., Eming, S. A., Beijer, A., et al. (2010). Nesprin-2 interacts with α-catenin and regulates Wnt signaling at the nuclear envelope. *J. Biol. Chem.* 285, 34932–34938. doi: 10.1074/jbc.M110.119651

Palmisano, M. G., Bremner, S. N., Hornberger, T. A., Meyer, G. A., Domenighetti, A. A., Shah, S. B., et al. (2015). Skeletal muscle intermediate filaments form a stress-transmitting and stress-signaling network. *J. Cell Sci.* 128, 219–224. doi: 10.1242/jcs.142463

Petrany, M. J., Swoboda, C. O., Sun, C., Chetal, K., Chen, X., Weirauch, M. T., et al. (2020). Single-nucleus RNA-seq identifies transcriptional heterogeneity in multinucleated skeletal myofibers. *Nat. Commun.* 11:6374. doi: 10.1038/s41467-020-20063-w

Petridou, N. I., Spiró, Z., and Heisenberg, C.-P. (2017). Multiscale force sensing in development. *Nat. Cell Biol.* 19, 581–588. doi: 10.1038/ncb3524

Phillips, B. E., Williams, J. P., Gustafsson, T., Bouchard, C., Rankinen, T., Knudsen, S., et al. (2013). Molecular Networks of Human Muscle Adaptation to Exercise and Age. *PLoS Genet.* 9:e1003389. doi: 10.1371/journal.pgen.1003389

Piccus, R., and Brayson, D. (2020). The nuclear envelope: LINCing tissue mechanics to genome regulation in cardiac and skeletal muscle. *Biol. Lett.* 16:20200302. doi: 10.1098/rsbl.2020.0302

Piekarowicz, K., Machowska, M., Dzianisava, V., and Rzepecki, R. (2019). Hutchinson-gilford progeria syndrome—current status and prospects for gene therapy treatment. *Cells* 8:88. doi: 10.3390/cells8020088

Psilander, N., Eftestøl, E., Cumming, K. T., Juvkam, I., Ekblom, M. M., Sunding, K., et al. (2019). Effects of training, detraining, and retraining on strength, hypertrophy, and myonuclear number in human skeletal muscle. *J. Appl. Physiol.* 126, 1636–1645. doi: 10.1152/japplphysiol.00917.2018

Puckelwartz, M. J., Kessler, E. J., Kim, G., DeWitt, M. M., Zhang, Y., Earley, J. U., et al. (2010). Nesprin-1 mutations in human and murine cardiomyopathy. *J. Mol. Cell. Cardiol.* 48, 600–608. doi: 10.1016/j.yjmcc.2009.11.006

Pulupa, J., Prior, H., Johnson, D. S., and Simon, S. M. (2020). Conformation of the nuclear pore in living cells is modulated by transport state. *eLife* 9:e60654. doi: 10.7554/eLife.60654

Raffaello, A., Milan, G., Masiero, E., Carnio, S., Lee, D., Lanfranchi, G., et al. (2010). JunB transcription factor maintains skeletal muscle mass and promotes hypertrophy. *J. Cell Biol.* 191, 101–113. doi: 10.1083/jcb.201001136

Rajgor, D., and Shanahan, C. M. (2013). Nesprins: from the nuclear envelope and beyond. *Expert Rev. Mol. Med.* 15:e5. doi: 10.1017/erm.2013.6

Röhrl, J. M., Arnold, R., and Djabali, K. (2021). Nuclear pore complexes cluster in dysmorphic nuclei of normal and progeria cells during replicative senescence. *Cells* 10:153. doi: 10.3390/cells10010153

Roux, K. J., Crisp, M. L., Liu, Q., Kim, D., Kozlov, S., Stewart, C. L., et al. (2009). Nesprin 4 is an outer nuclear membrane protein that can induce kinesin-mediated cell polarization. *Proc. Natl. Acad. Sci. U.S.A.* 106, 2194–2199. doi: 10.1073/pnas.0808602106

Samson, C., Petitalot, A., Celli, F., Herrada, I., Ropars, V., Le Du, M.-H., et al. (2018). Structural analysis of the ternary complex between lamin A/C, BAF and emerin identifies an interface disrupted in autosomal recessive progeroid diseases. *Nucleic Acids Res.* 46, 10460–10473. doi: 10.1093/nar/gky736

Sartori, R., Romanello, V., and Sandri, M. (2021). Mechanisms of muscle atrophy and hypertrophy: implications in health and disease. *Nat. Commun.* 12:330. doi: 10.1038/s41467-020-20123-1

Setiawan, I., Sanjaya, A., Lesmana, R., Yen, P. M., and Goenawan, H. (2021). Hippo pathway effectors YAP and TAZ and their association with skeletal muscle ageing. *J. Physiol. Biochem.* 77, 63–73. doi: 10.1007/s13105-021-00787-z

Shin, J.-Y., Dour, C. L., Sera, F., Iwata, S., Homma, S., Joseph, L. C., et al. (2014). Depletion of lamina-associated polypeptide 1 from cardiomyocytes causes cardiac dysfunction in mice. *Nucleus* 5, 260–268. doi: 10.4161/nucl.29227

Shin, J.-Y., Méndez-López, I., Hong, M., Wang, Y., Tanji, K., Wu, W., et al. (2017). Lamina-associated polypeptide 1 is dispensable for embryonic myogenesis but required for postnatal skeletal muscle growth. *Hum. Mol. Genet.* 26, 65–78. doi: 10.1093/hmg/ddw368

Shin, J.-Y., Méndez-López, I., Wang, Y., Hays, A. P., Tanji, K., Lefkowitch, J. H., et al. (2013). Lamina-associated polypeptide-1 interacts with the muscular dystrophy protein emerin and is essential for skeletal muscle maintenance. *Dev. Cell* 26, 591–603. doi: 10.1016/j.devcel.2013.08.012

Snijders, T., Nederveen, J. P., McKay, B. R., Joanisse, S., Verdijk, L. B., van Loon, L. J. C., et al. (2015). Satellite cells in human skeletal muscle plasticity. *Front. Physiol.* 6:283. doi: 10.3389/fphys.2015.00283

Solagna, F., Nogara, L., Dyar, K. A., Greulich, F., Mir, A. A., Türk, C., et al. (2020). Exercise-dependent increases in protein synthesis are accompanied by chromatin modifications and increased MRTF-SRF signalling. *Acta Physiol.* 230, e13496. doi: 10.1111/apha.13496

Solovei, I., Wang, A. S., Thanisch, K., Schmidt, C. S., Krebs, S., Zwerger, M., et al. (2013). LBR and lamin A/C sequentially tether peripheral heterochromatin and inversely regulate differentiation. *Cell* 152, 584–598. doi: 10.1016/j.cell.2013.01.009

Staszewska, I., Fischer, I., and Wiche, G. (2015). Plectin isoform 1-dependent nuclear docking of desmin networks affects myonuclear architecture and expression of mechanotransducers. *Hum. Mol. Genet.* 24, 7373–7389. doi: 10.1093/hmg/ddv438

Stephens, A. D., Banigan, E. J., Adam, S. A., Goldman, R. D., and Marko, J. F. (2017). Chromatin and lamin A determine two different mechanical response regimes of the cell nucleus. *Mol. Biol. Cell* 28, 1984–1996. doi: 10.1091/mbc.e16-09-0653

Stephens, A. D., Liu, P. Z., Kandula, V., Chen, H., Almassalha, L. M., Herman, C., et al. (2019). Physicochemical mechanotransduction alters nuclear shape and mechanics via heterochromatin formation. *Mol. Biol. Cell* 30, 2320–2330. doi: 10.1091/mbc.E19-05-0286

Stokes, T., Timmons, J. A., Crossland, H., Tripp, T. R., Murphy, K., McGlory, C., et al. (2020). Molecular transducers of human skeletal muscle remodeling under different loading states. *Cell Rep.* 32:7980. doi: 10.1016/j.celrep.2020.107980

Stroud, M. J., Feng, W., Zhang, J., Veevers, J., Fang, X., Gerace, L., et al. (2017). Nesprin 1α2 is essential for mouse postnatal viability and nuclear positioning in skeletal muscle. *J. Cell Biol.* 216, 1915–1924. doi: 10.1083/jcb.201612128

Sun, J., Chen, J., Mohagheghian, E., and Wang, N. (2020). Force-induced gene up-regulation does not follow the weak power law but depends on H3K9 demethylation. *Sci. Adv.* 6:eaay9095. doi: 10.1126/sciadv.aay9095

Swift, J., Ivanovska, I. L., Buxboim, A., Harada, T., Dingal, P. C. D. P., Pinter, J., et al. (2013). Nuclear Lamin-A scales with tissue stiffness and enhances matrix-directed differentiation. *Science* 341:1240104. doi: 10.1126/science.1240104

Tajik, A., Zhang, Y., Wei, F., Sun, J., Jia, Q., Zhou, W., et al. (2016). Transcription upregulation via force-induced direct stretching of chromatin. *Nat. Mater.* 15, 1287–1296. doi: 10.1038/nmat4729

Tilgner, K., Wojciechowicz, K., Jahoda, C., Hutchison, C., and Markiewicz, E. (2009). Dynamic complexes of A-type lamins and emerin influence adipogenic capacity of the cell via nucleocytoplasmic distribution of β-catenin. *J. Cell Sci.* 122, 401–413. doi: 10.1242/jcs.026179

Uzer, G., Bas, G., Sen, B., Xie, Z., Birks, S., Olcum, M., et al. (2018). Sun-mediated mechanical LINC between nucleus and cytoskeleton regulates βcatenin nuclear access. *J. Biomech.* 74, 32–40. doi: 10.1016/j.jbiomech.2018.04.013

van Steensel, B., and Belmont, A. S. (2017). Lamina-associated domains: links with chromosome architecture, heterochromatin, and gene repression. *Cell* 169, 780–791. doi: 10.1016/j.cell.2017.04.022

Venturini, V., Pezzano, F., Castro, F. C., Häkkinen, H.-M., Jiménez-Delgado, S., Colomer-Rosell, M., et al. (2020). The nucleus measures shape changes for cellular proprioception to control dynamic cell behavior. *Science* 370:eaba2644. doi: 10.1126/science.aba2644

Vergarajauregui, S., Becker, R., Steffen, U., Sharkova, M., Esser, T., Petzold, J., et al. (2020). AKAP6 orchestrates the nuclear envelope microtubule-organizing center by linking golgi and nucleus via AKAP9. *eLife* 9:e61669. doi: 10.7554/eLife.61669

Walden, F. V., Rea, M., Mobley, C. B., Fondufe-Mittendorf, Y., McCarthy, J. J., Peterson, C. A., et al. (2020). The myonuclear DNA methylome in response to an acute hypertrophic stimulus. *Epigenetics* 15, 1151–1162. doi: 10.1080/15592294.2020.1755581

Watt, K. I., Goodman, C. A., Hornberger, T. A., and Gregorevic, P. (2018). The hippo signaling pathway in the regulation of skeletal muscle mass and function. *Exerc. Sport Sci. Rev.* 46, 92–96. doi: 10.1249/JES.0000000000000142

Watt, K. I., Turner, B. J., Hagg, A., Zhang, X., Davey, J. R., Qian, H., et al. (2015). The Hippo pathway effector YAP is a critical regulator of skeletal muscle fibre size. *Nat. Commun.* 6:6048. doi: 10.1038/ncomms7048

Wheeler, M. A., Davies, J. D., Zhang, Q., Emerson, L. J., Hunt, J., Shanahan, C. M., et al. (2007). Distinct functional domains in nesprin-1alpha and nesprin-2beta bind directly to emerin and both interactions are disrupted in X-linked Emery-Dreifuss muscular dystrophy. *Exp. Cell Res.* 313, 2845–2857. doi: 10.1016/j.yexcr.2007.03.025

Wiche, G., Osmanagic-Myers, S., and Castañón, M. J. (2015). Networking and anchoring through plectin: a key to IF functionality and mechanotransduction. *Curr. Opin. Cell Biol.* 32, 21–29. doi: 10.1016/j.ceb.2014.10.002

Wilhelmsen, K., Litjens, S. H. M., Kuikman, I., Tshimbalanga, N., Janssen, H., van den Bout, I., et al. (2005). Nesprin-3, a novel outer nuclear membrane protein,

associates with the cytoskeletal linker protein plectin. *J. Cell Biol.* 171, 799–810. doi: 10.1083/jcb.200506083

Wilson, M. H., and Holzbaur, E. L. F. (2015). Nesprins anchor kinesin-1 motors to the nucleus to drive nuclear distribution in muscle cells. *Development* 142, 218–228. doi: 10.1242/dev.114769

Winje, I. M., Bengtsen, M., Eftestøl, E., Juvkam, I., Bruusgaard, J. C., and Gundersen, K. (2018). Specific labelling of myonuclei by an antibody against pericentriolar material 1 on skeletal muscle tissue sections. *Acta Physiol.* 223:e13034. doi: 10.1111/apha.13034

Wong, X., Loo, T.-H., and Stewart, C. L. (2021). LINC complex regulation of genome organization and function. *Curr. Opin. Genet. Dev.* 67, 130–141. doi: 10.1016/j.gde.2020.12.007

Xie, W., Chojnowski, A., Boudier, T., Lim, J. S. Y., Ahmed, S., Ser, Z., et al. (2016). A-type lamins form distinct filamentous networks with differential nuclear pore complex associations. *Curr. Biol.* 26, 2651–2658. doi: 10.1016/j.cub.2016.07.049

Yoshihara, T., Machida, S., Tsuzuki, T., Kakigi, R., Chang, S., Sugiura, T., et al. (2019). Age-related changes in histone modification in rat gastrocnemius muscle. *Exp. Gerontol.* 125, 110658. doi: 10.1016/j.exger.2019.110658

You, J.-S., Mcnally, R. M., Jacobs, B. L., Privett, R. E., Gundermann, D. M., Lin, K.-H., et al. (2019). The role of raptor in the mechanical load-induced regulation of mTOR signaling, protein synthesis, and skeletal muscle hypertrophy. *FASEB J.* 33, 4021–4034. doi: 10.1096/fj.201801653RR

Zhang, J., Felder, A., Liu, Y., Guo, L. T., Lange, S., Dalton, N. D., et al. (2010). Nesprin 1 is critical for nuclear positioning and anchorage. *Hum. Mol. Genet.* 19, 329–341. doi: 10.1093/hmg/ddp499

Zhang, Q., Ragnauth, C. D., Skepper, J. N., Worth, N. F., Warren, D. T., Roberts, R. G., et al. (2005). Nesprin-2 is a multi-isomeric protein that binds lamin and emerin at the nuclear envelope and forms a subcellular network in skeletal muscle. *J. Cell Sci.* 118, 673–687. doi: 10.1242/jcs.01642

Zhou, C., Li, C., Zhou, B., Sun, H., Koullourou, V., Holt, I., et al. (2017). Novel nesprin-1 mutations associated with dilated cardiomyopathy cause nuclear envelope disruption and defects in myogenesis. *Hum. Mol. Genet.* 26, 2258–2276. doi: 10.1093/hmg/ddx116

Zhou, C., Rao, L., Shanahan, C. M., and Zhang, Q. (2018). Nesprin-1/2: roles in nuclear envelope organisation, myogenesis and muscle disease. *Biochem. Soc. Trans.* 46, 311–320. doi: 10.1042/BST20170149

Zhou, J., So, K. K., Li, Y., Li, Y., Yuan, J., Ding, Y., et al. (2019). Elevated H3K27ac in aged skeletal muscle leads to increase in extracellular matrix and fibrogenic conversion of muscle satellite cells. *Aging Cell* 18:e12996. doi: 10.1111/acel.12996

Zhu, R., Antoku, S., and Gundersen, G. G. (2017). Centrifugal displacement of nuclei reveals multiple LINC complex mechanisms for homeostatic nuclear positioning. *Curr. Biol. CB* 27, 3097.e5–3110.e5. doi: 10.1016/j.cub.2017.08.073

Conflict of Interest: The authors declare that the research was conducted in the absence of any commercial or financial relationships that could be construed as a potential conflict of interest.

frontiers in Cell and Developmental Biology

ORIGINAL RESEARCH
published: 30 July 2021
doi: 10.3389/fcell.2021.690452

The Effect of Mechanical Stretch on Myotube Growth Suppression by Colon-26 Tumor-Derived Factors

*Jessica L. Halle, Brittany R. Counts-Franch, Rose M. Prince and James A. Carson**

Integrative Muscle Biology Laboratory, Division of Rehabilitation Sciences, College of Health Professions, University of Tennessee Health Science Center, Memphis, TN, United States

Preclinical models and *in vitro* experiments have provided valuable insight into the regulation of cancer-induced muscle wasting. Colon-26 (C26) tumor cells induce cachexia in mice, and conditioned media (CM) from these cells promotes myotube atrophy and catabolic signaling. While mechanical stimuli can prevent some effects of tumor-derived factors on myotubes, the impact of mechanical signaling on tumor-derived factor regulation of myosin heavy chain (MyHC) expression is not well understood. Therefore, we examined the effects of stretch-induced mechanical signaling on C2C12 myotube growth and MyHC expression after C26 CM exposure. C26 CM was administered to myotubes on day 5 of differentiation for 48 h. During the last 4 or 24 h of C26 CM exposure, 5% static uniaxial stretch was administered. C26 CM suppressed myotube growth and MyHC protein and mRNA expression. Stretch for 24 h increased myotube size and prevented the C26 CM suppression of MyHC-Fast protein expression. Stretch did not change suppressed MyHC mRNA expression. Stretch for 24 h reduced Atrogin-1/MAFbx, MuRF-1, and LC3B II/I ratio and increased integrin β1D protein expression and the myogenin-to-MyoD protein ratio. Stretch in the last 4 h of CM increased ERK1/2 phosphorylation but did not alter the CM induction of STAT3 or p38 phosphorylation. These results provide evidence that in myotubes pre-incubated with CM, the induction of mechanical signaling can still provide a growth stimulus and preserve MyHC-Fast protein expression independent of changes in mRNA expression.

Keywords: cancer cachexia, skeletal muscle (myotubes), myosin heavy chain, myogenic differentiation, passive stretch

OPEN ACCESS

Edited by:
Yuji Ogura,
St. Marianna University School of Medicine, Japan

Reviewed by:
Wataru Aoi,
Kyoto Prefectural University, Japan
Dario Coletti,
Sapienza University of Rome, Italy

****Correspondence:***
James A. Carson
jcarso16@uthsc.edu

Specialty section:
This article was submitted to Signaling, a section of the journal Frontiers in Cell and Developmental Biology

Received: *02 April 2021*
Accepted: *08 July 2021*
Published: *30 July 2021*

Citation:
Halle JL, Counts-Franch BR, Prince RM and Carson JA (2021) The Effect of Mechanical Stretch on Myotube Growth Suppression by Colon-26 Tumor-Derived Factors. Front. Cell Dev. Biol. 9:690452. doi: 10.3389/fcell.2021.690452

INTRODUCTION

Cancer-induced skeletal muscle wasting, or cancer cachexia, is multifactorial and involves a complex interplay between host- and tumor-derived factors resulting in disrupted skeletal muscle function and metabolism (Jackman et al., 2017; Argiles et al., 2019). Posture, breathing, and daily activities require functional skeletal muscle. While dynamic exercise promotes metabolic and functional adaptations, mechanical stimulation of muscle involving passive movement (i.e., stretch) can produce important functional adaptations (Carson et al., 1995; Carson, 1997; De Deyne, 2001; Zöllner et al., 2012; Schiaffino et al., 2013; Hardee et al., 2016). Critical gaps remain in our knowledge of how tumor-derived cachectic factors influence mechanotransduction in cachectic muscle. Furthermore, it is not well understood if mechanical stimulation can induce

growth or prevent further atrophy in muscle that has been exposed to cachectic tumor-derived factors. While our mechanistic understanding of the drivers of cancer cachexia has advanced significantly, it is also critical to investigate the constraints that cachexia places on intrinsic muscle properties, such as mechanical regulation. Furthermore, a better understanding of how increased mechanotransduction may elicit beneficial effects on cancer-induced muscle wasting is necessary.

Stretching cultured myotubes can increase the protein synthesis rate and size. Furthermore, stretch activates mechanical sensitive signaling involving ERK1/2, p38 MAPK, and JNK signaling while decreasing muscle-specific proteolytic factors (Kumar et al., 2002; Pereira et al., 2011; Moustogiannis et al., 2020). Lewis lung carcinoma (LLC) cachectic factors can impair stretch-induced protein synthesis (Gao and Carson, 2016). However, the effects of stretch on markers of autophagy flux and protein degradation such as the E3 ubiquitin ligases Atrogin-1/MAFbx and MuRF-1 in myotubes exposed to cachectic factors is less understood. Different tumor types can differentially release factors that can target myotube and skeletal muscle dysfunction and wasting (Freire et al., 2020). While LLC factors can disrupt myotube stretch-induced signaling (Gao and Carson, 2016), it is not well established if cachectic colon-26 (C26) tumor-derived factors can inhibit mechanical signaling in myotubes. Transmembrane integrin proteins can transmit mechanical signaling into the cell. Skeletal muscle β1D integrin isoform has an established role in myoblast differentiation and muscle fiber growth (van der Flier et al., 1995; Carson and Wei, 2000). The activation of myogenic transcription factors, including myogenin and MyoD, contributes to stretch-induced hypertrophy (Carson and Booth, 1998). Dynamic stretch of myotubes during treatment with C26 tumor-derived factors can increase myotube size, promote myoblast differentiation, and improve myogenesis markers (i.e., myogenin and MyoD) related to myotube fusion (Baccam et al., 2019). Stretch of myotubes is also associated with myokine release and an improved follistatin/activin ratio (Baccam et al., 2019). The role of myosin heavy chain (MyHC) as a contractile protein is fundamental for cross-bridge formation and skeletal muscle function (Schiaffino and Reggiani, 1994; Toth et al., 2013). MyHC loss occurs with C26 cachexia (Diffee et al., 2002; Yamada et al., 2020). Although myotube size measured by diameter is often increased with stretch (Vandenburgh and Karlisch, 1989; Gao and Carson, 2016), conflicting results have been reported relating to stretch and MyHC expression. Studies often examine MyHC as a marker of myotube differentiation in stretched myoblasts (Wang et al., 2020). The interaction of passive stretch and C26 cachectic factors on myogenesis and MyHC at late stages of differentiation could offer valuable insight into mechanisms mediating skeletal muscle repair and regeneration.

Colon-26 carcinoma *in vivo* is associated with a progressive loss of skeletal muscle mass and function mediated by increased circulating pro-inflammatory cytokines and the activation of muscle-specific E3 ligases (Aulino et al., 2010; Bonetto et al., 2011, 2016; Halle et al., 2019). Preclinical cachexia models have provided valuable insight into how host- and tumor-derived factors regulate muscle mass. *In vitro* culture models have provided a further mechanistic understanding of tumor-derived factors' potential direct effects on myotubes using tumor cell conditioned media (CM) (Jackman et al., 2017). C26 CM induces myotube atrophy and intrinsic signaling involving JAK/STAT, p38 MAPK, ERK1/2 activation, and muscle-specific E3 ubiquitin ligase expression (Seto et al., 2015; Jackman et al., 2017; Liu et al., 2019). While exercise can prevent skeletal muscle atrophy and dysfunction in C26 tumor-bearing mice (Pigna et al., 2016; Ballaro et al., 2019), it is not fully established if exercise-induced systemic alterations or intrinsic muscle signaling involving contraction or stretch are responsible for these effects. Dynamic stretch occurring with the administration of C26-derived catabolic factors for 48 h maintains the ability to promote increased myotube diameter (Baccam et al., 2019). However, the stretch response after the initiation of C26-induced myotube catabolism and whether mechanical signaling can generate a growth stimulus in an already catabolic state warrants further investigation. Furthermore, the interaction of mechanical signaling and C26 CM in a high serum, growth-promoting state is also less understood. While MyHC expression is critical for myotube differentiation and growth, there is a limited understanding of how stretch-induced mechanical signaling impacts the regulation of myotube MyHC expression by tumor-derived factors. Therefore, we examined the effects of mechanical signaling induced by both acute and chronic passive stretch on C2C12 myotube growth and MyHC expression when previously exposed to C26 CM. C26 CM was administered to C2C12 myotubes at day 5 of differentiation for 48 h. During the last 4 or 24 h of C26 CM exposure, a subset of samples were administered 5% static uniaxial stretch.

MATERIALS AND METHODS

Cell Culture

All cells were purchased through ATCC (Manassas, VA, United States) and used within the first 15 passages. Murine C2C12 myoblasts (CRL-1772), C26 adenocarcinoma (CRL-2638), or EL4 lymphoma (TIB-39) cells were maintained at 37°C, 5% CO_2 in growth media (GM): Dulbecco's Modified Eagle Media (DMEM; #11995-065; Gibco, Grand Island, NY, United States) supplemented with 10% fetal bovine serum (FBS), 50 U/ml of penicillin, and 50 μg/ml of streptomycin.

C2C12 Myotube Differentiation

C2C12 myoblasts were seeded on type I collagen-coated polystyrene plastic or flexible silastic Uniflex® membranes (Flexcell International, Burlington, NC, United States) at a density of 8.0×10^4 cells per well (six-well plate) in GM: DMEM (#11995-065; Gibco) supplemented with 10% FBS, 50 U/ml of penicillin, and 50 μg/ml of streptomycin. To induce myoblast differentiation, cells were rinsed with phosphate-buffered saline (PBS) and switched to differentiation media (DM): DMEM supplemented with 2% heat-inactivated horse serum, 50 U/ml of penicillin, and 50 μg/ml of streptomycin to form myotubes. Media was replenished every 48 h, and

experiments were performed starting at day 5 of differentiation when multinucleated contractile myotubes are present.

Conditioned Media Collection

Colon-26 cells, a murine colon adenocarcinoma that promotes cachexia in mice, or EL4 lymphoma cells that do not promote cachexia in mice (Bonetto et al., 2016; Zhang et al., 2017), were cultured as described above. Conditioned media (CM) consists of consists of secreted factors from tumor cells and has been described previously (Kandarian et al., 2018). Briefly, 2×10^6 cells were seeded in 100-mm tissue culture-treated plates in GM. Tumor cell CM was collected at ∼90% confluence 48 h post cell seeding and spun down at 3,000 rpm for 5 min to remove cell debris. Cells on the plate were pelleted and counted via trypan blue exclusion test to ensure an equivalent number of cells on the plate, with a final density averaging $7.0–9.0 \times 10^6$ cells per culture dish. CM was stored for one-time use in aliquots at −20°C, used within 2 months, and then thawed in a warm water bath at the time of the experiment. GM with no cells was used as a media control.

Treatment of Myotubes With Conditioned Media

At the time of the experiment, GM control or C26 CM is diluted with 50% serum-free DMEM for a final serum concentration of 5% FBS; 50% CM was chosen, as it has been shown to produce significant myotube atrophy (Pin et al., 2018; Zhong et al., 2019). It should be noted that myotubes were differentiated up to day 5 in 2% horse serum; thus upon CM addition, myotubes were switched to a higher serum environment, which can induce myotube hypertrophy (von Walden et al., 2016). Therefore, in the figures and results, EL4 and C26 CM are referred to as EL4 + GM or C26 + GM. A mixture of myoblasts and myotubes at day 5 of differentiation was rinsed with PBS and then switched to GM media control or C26 CM (C26 + GM) for 48 h (days 5–7 of differentiation). CM was replenished after 24 h. In a separate experiment, C2C12 myoblasts were grown and differentiated on type I collagen-coated rigid polystyrene plates to examine the effects of the cachectic tumor cell CM on a commonly utilized substratum. Briefly, differentiated myotubes at day 5 were treated with 50% GM, C26, or EL4 CM (EL4 + GM) for 48 h. EL4 CM was used to determine if effects on myotube growth are specific to cachectic tumor-derived factor media.

Myotube Uniaxial Stretch With Conditioned Media

Static stretch was administered (FX-6000 Tension System, Flexcell International Corporation) as previously described (Hornberger et al., 2005; Baccam et al., 2019) with the following modifications. Cells were subjected to a static 5% uniaxial stretch in the last 4 or 24 h of CM treatment (as described above). Control cells (0% stretch) were grown under identical conditions but left unstretched and placed beside the incubator's baseplate. For administration of stretch, culture plates were removed from the incubator, rapidly placed onto the stretch device's baseplate, and then placed back in the incubator. The Flexcell Arctangle® loading station was used for all experiments, which consists of six rigid posts covered in a thin layer of silicone lubricant, centered beneath the six-well Uniflex plate. Applied vacuum pressure deforms the membrane across the loading post in a single direction (e.g., north and south poles), creating a uniaxial stretch (**Figure 3B**). A custom ramp protocol, described here, was designed to ensure cell adherence to the membrane while vacuum pressure is applied: the Flexcell tension system was set to increase vacuum pressure gradually, and thus % elongation in increments of 1% every 2 s, up to 5%, which is then maintained for the duration of the experiment (e.g., 24 h), followed by a ramp-down to 0% at the conclusion of the experiment.

Protein Synthesis Measurement

Protein synthesis was measured in myotubes treated with CM grown on type I collagen-coated polystyrene plates using the surface sensing of translation (SUnSET) method as previously described (Goodman et al., 2011). Puromycin (#540411; Sigma-Aldrich, St. Louis, MO, United States) was added to culture media 30 min prior to protein harvest at a final concentration of 1 μM per well. The amount of puromycin incorporated into newly synthesized protein was determined by Western blotting.

Myotube Diameter

Myotube diameter was quantified as previously described (Gao and Carson, 2016) with the following modifications. C2C12 myotube diameter was quantified using ImageJ software (National Institutes of Health, Bethesda, MD, United States). Digital images were captured at ×20 objective brightfield. Five non-overlapping images were captured within each well, and three images were randomly chosen for the analysis. The analysis used unmodified tiff images accessed in NIH ImageJ software. A blinded investigator randomly took diameter measurements of six myotubes per image based on preset inclusion/exclusion criteria: elongated structure with distinct membrane outlines, little to no cellular debris, and no branching points. The average diameter per myotube was calculated as the mean of eight measurements taken along the myotube length. For each condition, $n = 162–378$ myotubes were analyzed.

Western Blotting

Western blotting analysis was performed as previously described (Gao and Carson, 2016). Briefly, cells were scraped into ice-cold radioimmunoprecipitation assay (RIPA) buffer [25 nM of Tris HCl at pH 7.6, 150 nM of NaCl, 1% NP-40, 1% sodium deoxycholate, and 0.1% sodium dodecyl sulfate (SDS)] (#89900; Thermo Fisher Scientific, Waltham, MA, United States) and 1% Halt protease and phosphatase inhibitor cocktail [1 mM of EDTA, 5 mM of NaF, 1 nM of $NaVO_4$, and 1 mM of glycerophosphate] (#78440; Thermo Fisher Scientific). Cell lysates were centrifuged at 14,000 rpm for 15 min at 4°C, and supernatants were collected. Protein concentrations were determined using the Bradford method. Homogenates were fractionated on SDS–polyacrylamide gels and transferred to polyvinylidene difluoride (PVDF) membrane. Membranes were blocked for 1 h in 5% non-fat milk–TBST. After blocking, primary antibodies for phosphorylated STAT3 (Y705) 1:1,000,

total STAT3 1:2,000, phosphorylated p38 (T180/Y182) 1:1,000, total p38 1:2,000, phosphorylated ERK1/2 (T202/Y204) 1:1,000, total ERK1/2 1:2,000, phosphorylated rpS6 (S240/244) 1:1,000, and total rpS6 1:2,000, phosphorylated Akt (S473) 1:1,000, total Akt 1:2,000, phosphorylated 4E-BP1 (T37/46) 1:1,000, total 4E-BP1 1:2,000, phosphorylated SAPK/JNK (T183/Y185) 1:1,000, total SAPK/JNK 1:2,000 (Cell Signaling Technology, Danvers, MA, United States), Atrogin-1/MAFbx, MuRF-1 1:1,000 (ECM Biosciences, Versailles, KY, United States), and MyHC-Fast (protein stain for fast type II fibers; corresponding genes: MyH1 and MyH2) and MyHC-Slow 1:4,000 (protein stain for slow type I fibers; corresponding gene MyH7), serum response factor (SRF) 1:500, myogenin 1:500, and MyoD 1:500 (Santa Cruz Biotechnology, Dallas, TX, United States), integrin β1D 1:1,000, and puromycin 1:2,000 (Millipore, Billerica, MA, United States) were incubated overnight at 4°C in 5% non-fat milk–TBST. Secondary anti-rabbit or anti-mouse IgG horseradish peroxidase (HRP)-linked (Cell Signaling Technology) antibodies were incubated at 1:4,000 dilution for 1 h at room temperature in 5% non-fat milk–TBST. Enhanced chemiluminescence (Prometheus Pro-Signal Femto, #20-302; Genesee Scientific, San Diego, CA, United States) was used to visualize the antibody–antigen interactions, and membranes were digitally imaged using the iBright 1500 system (Invitrogen, Carlsbad, CA, United States). Immunoblots were analyzed by measuring each band's integrated optical density (IOD) with ImageJ software (National Institutes of Health, Bethesda, MD, United States).

RNA Isolation, cDNA Synthesis, and Real-Time PCR

Total RNA was isolated from C2C12 myotubes using TRIzol reagent (Invitrogen, Carlsbad, CA, United States) per manufacturer's guidelines and as previously described (White et al., 2009). After phenol–chloroform extraction, RNA was purified using the PureLink® RNA Mini Kit (Invitrogen, Carlsbad, CA, United States) and eluted in RNAase-free water. Total RNA concentration (260 nm) and purity (260/280 ratio) were measured using UV spectrophotometry, and total RNA was stored at −80°C. cDNA was reverse transcribed from 1 μg of total RNA using Superscript IV Reverse Transcriptase and random hexamers according to manufacturer guidelines (#18090200; Invitrogen) in a final volume of 20 μl at 23°C for 10 min, 50°C for 10 min, and 80°C for 10 min. cDNA was stored at −80°C. Real-time PCR was performed using reagents from Applied Biosystems (Foster City, CA, United States). Gene expression was carried out in 20-μl reactions using 2 × PowerTrack SYBR Green master mix, 2 μl of cDNA, 1 μl of forward and reverse primers (500 nM), and nuclease-free H_2O. The sequences of the primers were verified using NIH Primer Blast software, as follows: MyHC-Slow Type I (Myh7) [NM_080728.3]: Fw 5′-CCAAGGGCCTGAATGAGGAG-3′, Rv 5′-GCAAAGGCTCCAGGTCTGAG-3′; MyHC-Fast type IIA (Myh2) [NM_001039545.2]: Fw 5′-AGGCGGCTGAGGAGC ACGTA-3′, Rv 5′-GCGGCACAAGCAGCGTTGG-3′; MyHC-Fast type IIB (Myh4) [NM_010855.3]: Fw 5′-CACCTGG ACGATGCTCTCAGA-3′, Rv 5′-GCTCTTGCTCGGCCACTCC -3′; MyHC-Fast type IIX (Myh1) [NM_030679.2]: Fw 5′-GAGG GACAGTTCATCGATAGCAA-3′, Rv 5′-GGGCCAACTTGTCA TCTCTCAT-3′; skeletal muscle alpha actin (Acta1) [NM_00127 2041.1]: Fw 5′-CTCCTACGTGGGTGATGAGG-3′, Rv 5′-AGGTGTGGTGCCAGATCTTC-3′; myogenin (Myog) [NM _031189.2]: Fw 5′-GCACTGGAGTTCGGTCCCAA-3′, Rv 5′-TA TCCTCCACCGTGATGCTG-3′; MyoD (Myod1) [NM_010866. 2]: Fw 5′-GAGATGCGCTCCACTATGCT-3′, Rv 5′-TGGCAT GATGGATTACAGCG-3′; Myocyte Enhancer Factor 2C (MEF 2C) [NM_001170537.1]: Fw 5′-GAGCCGGACAAACTCAGA CA-3′ Rv 5′-GGCTGTGACCTACTGAATCGT-3′; and GAPDH [NM_001289726]: Fw 5′-ACCACAGTCCATGCCATCAC-3′ Rv 5′-TCCACCACCCTGTTGCTGTA-3′. Primer sequences were synthesized by Integrated DNA Technologies (IDT, Coralville, IA, United States) and validated via agarose gel electrophoresis. RT-PCR was carried out on the Applied Biosystems QuantStudio3 system. Reactions were incubated for 2 min at 50°C, 10 min at 95°C, followed by 40 cycles of a 15-s denaturation step at 95°C, and 1-min annealing/extension at 60°C. The $2^{-\Delta\Delta Ct}$ method (Livak and Schmittgen, 2001) was used to determine gene expression changes between treatment groups with the GAPDH Ct as the correction factor.

Statistical Analysis

All experiments included a minimum of three replicates from at least two independent experiments. Results are expressed as mean ± SEM. Student's unpaired *t*-test, one-way ANOVA, and two-way ANOVA (indicated in the figure legends) were used to examine the effects of stretch and culture conditions. Tukey's *post hoc* multiple comparisons test was used when a significant interaction was present. *p*-Values ≤0.05 were considered significant.

RESULTS

Effects of Colon-26 Tumor Cell Conditioned Media in C2C12 Myotubes Grown on Rigid Polystyrene Substratum

We examined the effects of tumor cell CM under standard culture conditions. GM, C26 CM (C26 + GM), or EL4 CM (EL4 + GM) was administered to 5-day differentiated myotubes grown on type I collagen-coated polystyrene plates for 48 h (**Figure 1A**). EL4 lymphoma cells that do not induce cachexia (Zhang et al., 2017) were used as a tumor cell CM control. Myotubes were imaged for diameter Pre (day 5) and Post (day 7) CM exposure (**Figure 1B**). Myotubes maintained in DM were imaged and used as a control for myotube growth. Under standard DM culture conditions, myotubes increased diameter from day 5 to day 7 (24%; $p < 0.0001$) (**Figure 1C**). EL4 + GM-treated myotubes significantly increased diameter compared to Pre ($p < 0.0001$), and this increase was equivalent to GM treatment (42%) (**Figure 1C**). C26 + GM-treated myotubes significantly increased diameter compared to Pre (15%). However, they were significantly smaller in size than both GM and EL4 + GM-treated myotubes (**Figure 1C**). Along with decreased myotube size, C26 + GM-treated myotubes had significantly lower protein

expression of both MyHC-Fast ($p < 0.001$, −50%) and MyHC-Slow ($p = 0.007$, −60%) isoforms compared with the GM and EL4 + GM conditions (**Figure 1D**). These results demonstrate that C26 tumor-derived factors can suppress myotube growth and MyHC protein expression and that these effects are specific to cachectic tumor-derived factors.

Altered muscle protein turnover regulation contributes to cachexia development (Baracos, 2000), and tumor-derived factors can disrupt this regulation in cultured myotubes (Gao and Carson, 2016; Gao et al., 2017; Chiappalupi et al., 2020). Both EL4 and C26 tumor-derived factors displayed significant reductions in protein synthesis rate measured by puromycin incorporation (EL4 + GM: −29%, C26 + GM: −46%) (**Figures 1E,I**). Compared with EL4 + GM, C26 + GM-treated myotubes displayed a significant reduction in the phosphorylation of Akt (S473) ($p = 0.025$) and rpS6 (S240/244) ($p < 0.001$); both EL4 + GM ($p = 0.047$) and C26 + GM ($p < 0.001$) tumor-derived factors significantly reduced the phosphorylation of 4E-BP1 (T37/46) (**Figures 1F,J**). C26 + GM induced STAT3 phosphorylation (Y705) 138% compared with controls ($p < 0.001$), and ERK1/2 phosphorylation was unchanged across all conditions (**Figures 1G,J**). Under standard culture conditions, 48 h incubation with C26 + GM significantly induced Atrogin-1 ($p = 0.009$, 111%) and MuRF-1 ($p < 0.001$, 85%) as compared with GM and EL4 + GM (**Figures 1H,J**). These data suggest that C26 tumor-derived factors can alter protein turnover signaling involving Akt/mTORC1 signaling (i.e., 4E-BP1 and rpS6) and ubiquitin–proteasome-mediated breakdown.

Myotube Growth Suppression by Colon-26 Tumor-Derived Factors on Flexible Silastic Membranes

Growth media or C26 tumor cell CM (C26 + GM) was administered to myotubes at day 5 of differentiation for 48 h on type I collagen-coated silastic membranes (**Figure 2A**). Myotubes were imaged for diameter at day 5 (Pre) and day 7 (Post) (**Figure 2B**). Switching C2C12 myotubes from DM (2% horse serum) to GM (5% FBS) has been shown to induce myotube growth (von Walden et al., 2016). GM significantly increased myotube diameter compared with DM ($p < 0.001$) (**Figure 2C**). Compared with Pre, GM treatment increased myotube diameter 29% ($p < 0.001$), and C26 + GM-treated myotubes did not change ($p = 0.618$) myotube diameter (**Figure 2C**). These results demonstrate that C26 tumor-derived factors can suppress myotube growth measured by diameter despite a high growth factor environment.

Myosin heavy chain isoform protein expression was quantified on day 7 after 48 h of GM or C26 + GM exposure. Increased MyHC isoform expression is critical for myotube differentiation and growth (Brown et al., 2012). We report that C26 CM can decrease myotube MyHC protein concentration in myotubes grown on flexible silastic membranes. C26 + GM-treated myotubes decreased MyHC-Fast protein expression −17% ($p = 0.002$) and MyHC-Slow protein expression −47% ($p < 0.0001$) (**Figure 2D**). We next examined if C26 tumor-derived factors regulate changes in myotube MyHC expression at the mRNA level. mRNA expression was quantified at day 7 after 48 h of GM or C26 + GM exposure. C26 CM induced isoform-specific shifts in MyHC mRNA expression (**Figure 2E**). The expression of MyHC-Fast type IIA (Myh2) mRNA was reduced by −78% ($p < 0.0001$), type IIB (Myh4) mRNA was increased by 133%, type IIX (Myh1) did not significantly change, and MyHC-Slow type I (Myh7) was reduced by -59% ($p = 0.003$) by the C26 + GM treatment (**Figure 2E**). Skeletal α-actin is a principle component of muscle thin filaments and interacts with the MyHC proteins for contraction (Sparrow et al., 2003). Forty-eight hours of C26 + GM incubation did not alter skeletal α-actin mRNA expression (**Figure 2E**). Therefore, C26-derived factors reduce the concentration of both MyHC protein and mRNA in myotubes, and this preferential loss of MyHC has potential implications for both size and contractile function.

C26 CM can activate multiple signaling pathways associated with myotube catabolic signaling (Seto et al., 2015). We examined several proteins that can regulate muscle growth and are implicated in cancer cachexia, including STAT3 (Puppa et al., 2014), p38 MAPK (Ding et al., 2017; Brown et al., 2018), and ERK1/2 (Gao and Carson, 2016; VanderVeen et al., 2018). Despite incubation in a high serum growth-promoting environment, C26 + GM induced a 57% increase in the phosphorylation of STAT3 (Y705) ($p < 0.001$), an 89% increase ($p = 0.011$) in p38 (T180/Y182) phosphorylation, and a 34% increase ($p = 0.033$) in ERK1/2 (T202/Y204) phosphorylation (**Figures 2F,G**).

Mechanical Stretch Effects on Growth and Myosin Protein Expression in Colon-26 Treated Myotubes

Mechanical signaling induced by chronic passive stretch is a potent inducer of myotube growth and anabolic signaling (Vandenburgh and Kaufman, 1979; Gao and Carson, 2016). Additionally, dynamic stretch occurring with the administration of C26-derived catabolic factors can promote increased myotube diameter (Baccam et al., 2019). Our study extends this understanding by examining chronic stretch application after the initiation of catabolism inducing C26 CM. We assessed if stretch could induce a growth stimulus in myotubes already exposed to C26 cachectic factors. Furthermore, we examined the effects of stretch in a high serum growth-promoting state. Myotubes were uniaxially stretched 5% after 24 h of exposure to C26 + GM and then maintained in the stretched state in C26 + GM for 24 h (**Figure 3A**). There was a main effect for myotubes treated with C26 + GM for 48 h to decrease ($p < 0.0001$) myotube diameter (**Figure 3C**). However, there was a main effect for the 24-h stretch treatment to increase ($p = 0.003$) myotube diameter in both GM and C26 + GM conditions (**Figure 3C**). These results provide evidence that stretch can induce a growth stimulus in myotubes that are in a catabolic state and in a growth factor-rich environment (5% FBS) that generated growth in the absence of tumor-derived factors.

We next examined if 24 h of stretch could rescue suppressed MyHC-Fast and MyHC-Slow protein expression in myotubes incubated with C26 CM. We report that stretch has different effects on fast and slow MyHC protein expression. Stretch

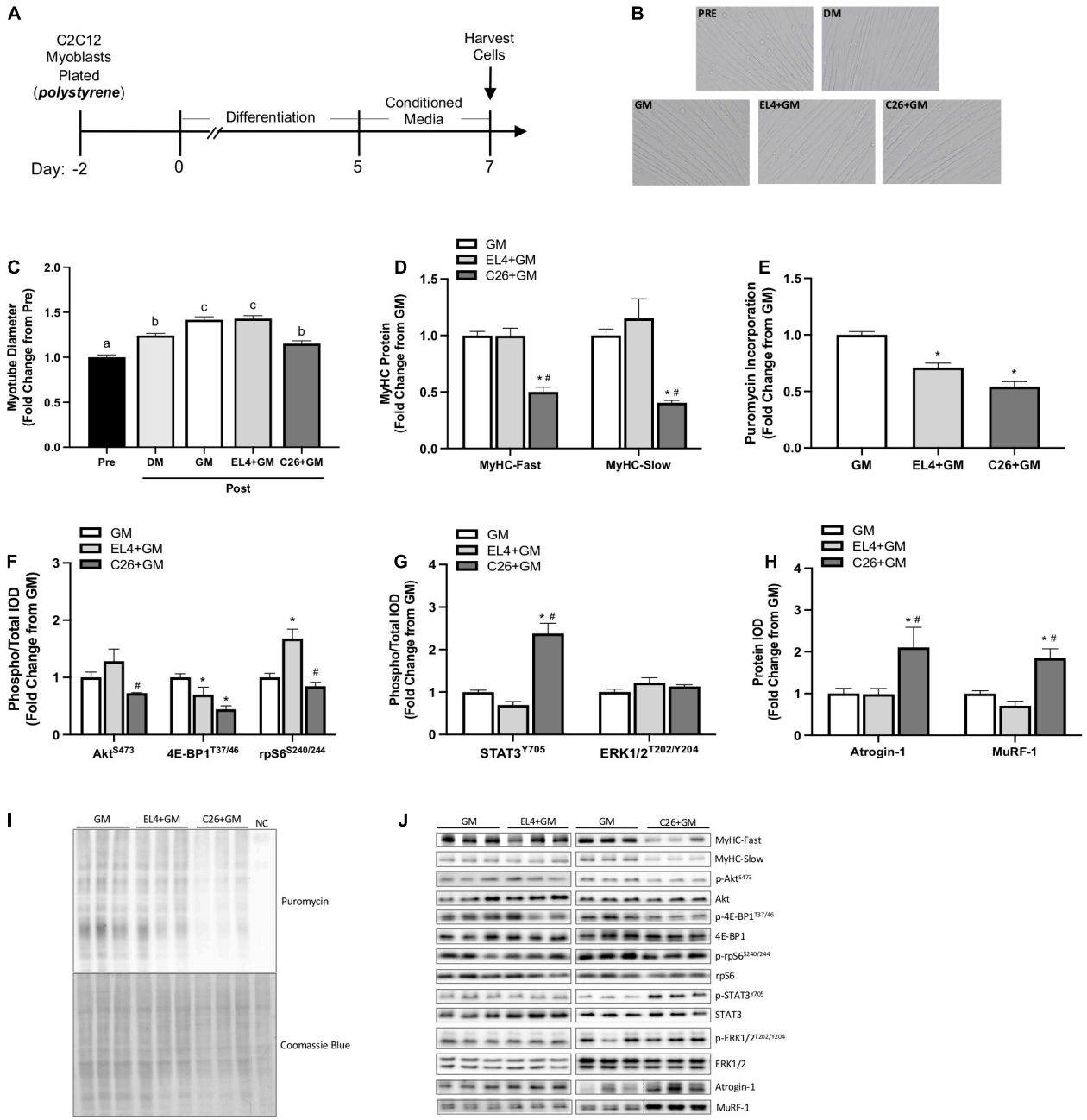

FIGURE 1 | Effects of tumor cell conditioned media on C2C12 myotube size and protein turnover signaling on type I collagen-coated polystyrene plates. **(A)** Experiment overview: C2C12 myoblasts are plated on type I collagen-coated rigid polystyrene plates in growth media (GM); after 48 h at ∼85% confluence, differentiation media (DM) is added, which corresponds to day 0 of differentiation. At 5 days post-differentiation, myotubes are imaged (Pre) and then 50% tumor cell conditioned media (CM) is diluted with serum-free DMEM and added to wells for 48 h. Conditioned media is collected from cachectic colon-26 (C26 + GM), non-cachectic EL4 lymphoma (EL4 + GM), or growth media with no cells, which is used as a media control (GM). Myotubes maintained in DM for 48 h are used as a control for myotube growth. Cells are harvested at day 7 post-differentiation for protein. **(B)** Representative × 20 brightfield myotube images. **(C)** Myotube diameter Pre (day 5; n = 216 myotubes) and Post (day 7; n = 162–216 myotubes/group) 48 h DM, GM, or CM incubation. **(D)** Myosin heavy chain (MyHC)-Fast (type II fibers) and MyHC-Slow (type I fibers) protein expression measured by Western blotting. **(E)** Quantified protein synthesis rate measured by Western blotting against puromycin (n = 6–12/group). Western blotting analyses of panel **(F)** ratio of phosphorylated (p-) to total protein expression of Akt^{S473} (n = 6/group), $4E\text{-}BP1^{T37/46}$ (n = 6/group), and $rpS6^{S240/244}$ (n = 6/group). **(G)** Ratio of phosphorylated (p-) to total protein expression of $STAT3^{Y705}$ (n = 6–12/group) and $ERK1/2^{T202/Y204}$ (n = 6/group) and **(H)** Atrogin-1/MAFbx and MuRF-1 (n = 6/group). **(I)** Representative Western blotting image displaying puromycin incorporation and corresponding Coomassie blue stain; NC is the negative control protein sample from C2C12 myotubes without puromycin treatment. **(J)** Representative Western blotting images, separate panels are from separate blots each ran with GM control, and dashed lines represent different areas of the same gel. Data are presented as means ± SEM as a fold change from GM. One-way ANOVA was performed to determine differences. Lowercase letters (a, b, and c) denote significant difference between groups; *significant from GM control; #significant from EL4 + GM. Statistical significance set at $p \leq 0.05$.

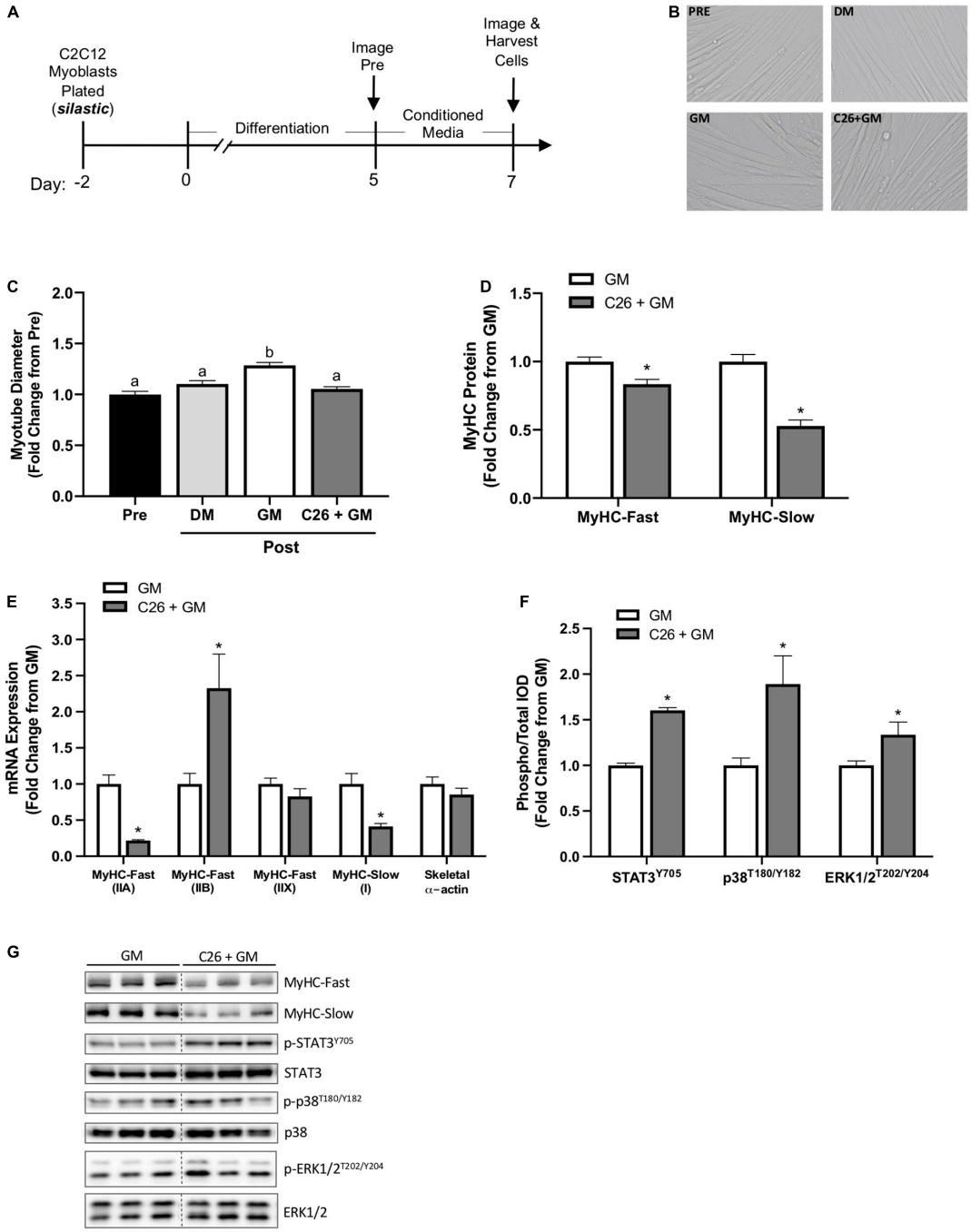

FIGURE 2 | C2C12 myotube growth suppression by colon-26 (C26) tumor-derived factors on type I collagen-coated silastic membranes. **(A)** Experiment overview: C2C12 myoblasts are plated on type I collagen-coated silastic Uniflex membranes in growth media (GM). After 48 h at ∼85% confluence, differentiation media (DM) is added, which corresponds to day 0 of differentiation. On day 5 of differentiation, myotubes are fully formed, and conditioned media (CM: GM, C26 + GM) diluted with 50% serum-free DMEM is added to wells for 48 h. Myotubes are imaged Pre and Post 48-h incubation with DM, GM, or C26 + GM for diameter measurements. Cells are harvested for protein and RNA on day 7 of differentiation. **(B)** Representative × 20 brightfield images. **(C)** Myotube diameter quantification Pre (day 5; n = 162 myotubes) and Post 48 h DM, GM, or C26 + GM incubation (n = 162–378 myotubes/group). **(D)** Myosin heavy chain (MyHC)-Fast (type II fibers) and MyHC-Slow (type I fibers) protein expression measured by Western blotting (Fast: n = 18–21/group; Slow: n = 9/group). **(E)** MyHC-Fast type IIA (Myh2), type IIB (Myh4), type IIX (Myh1), MyHC-Slow type I (Myh7), and skeletal muscle α-actin (Acta1) mRNA expression (n = 6/group) calculated using the $2^{-\Delta\Delta Ct}$ method with GAPDH as a housekeeping gene. **(F)** Ratio of phosphorylated (p-) to total protein expression of signal transducer and activator of transcription 3 ($STAT3^{Y705}$) (n = 12–15/group); $p38^{T180/Y182}$ mitogen-activated protein kinase (MAPK) (n = 6/group), and extracellular signal-regulated kinase 1/2 ($ERK1/2^{T202/Y204}$) (n = 6/group) measured by Western blotting. **(G)** Representative Western blotting images: dashed line represents different areas of the same gel. Data are presented as means ± SEM as a fold change from GM. One-way ANOVA **(C)** or Student's unpaired t-test was performed to determine differences. Lowercase letters (a, b, and c) denote significant difference between groups; *significant from GM control. Statistical significance set at $p \leq 0.05$.

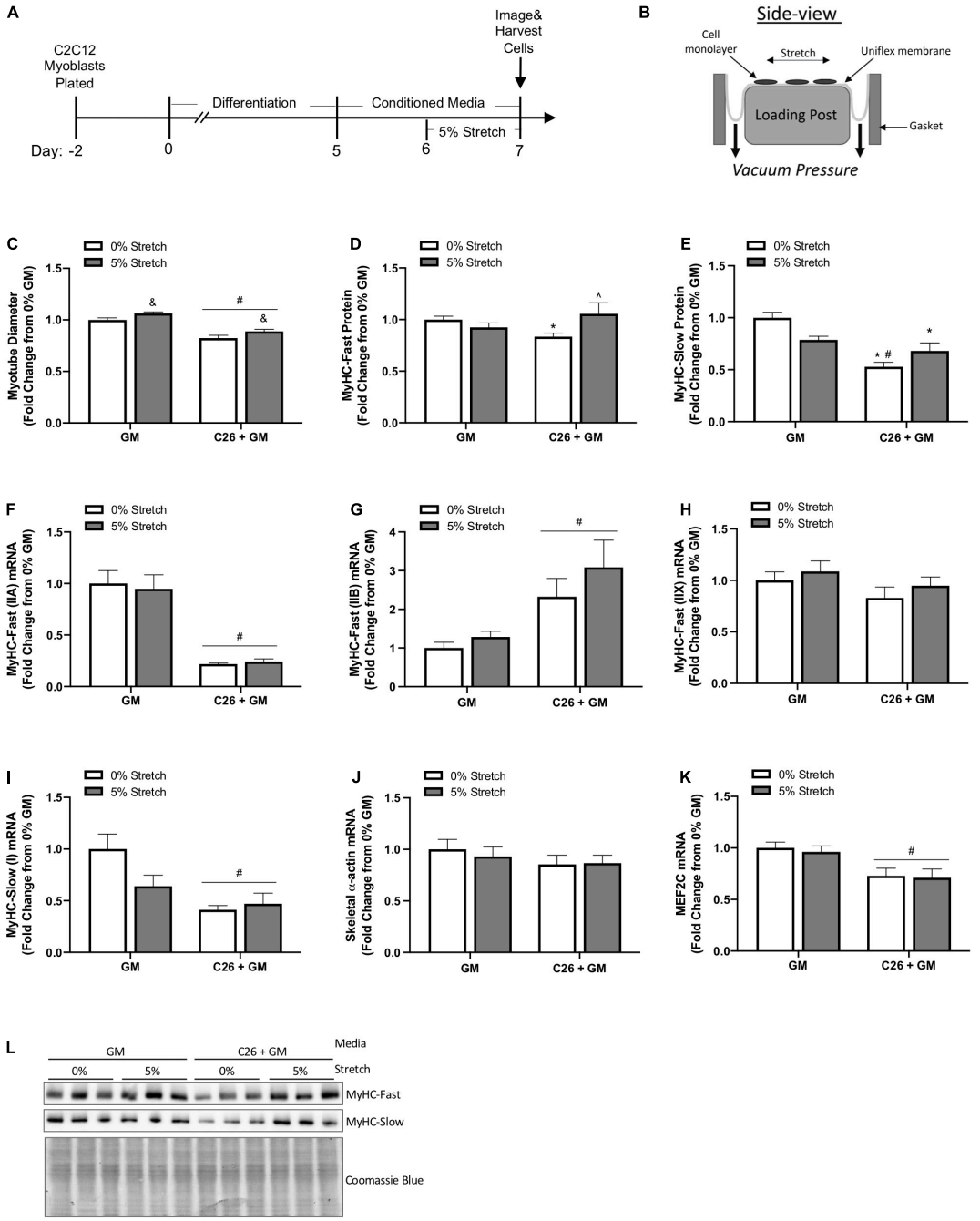

FIGURE 3 | Effects of mechanical stretch on growth and myosin expression in colon-26 (C26)-treated myotubes. **(A)** Experiment overview: C2C12 myoblasts are plated on in growth media (GM); after 48 h at ∼85% confluence, differentiation media is added, which corresponds to day 0. At day 5 of differentiation, fully formed contractile myotubes are present, and conditioned media (CM; GM or C26 + GM) is diluted with 50% serum-free DMEM and added to wells for 48 h. Myotubes are either left unstretched (0%) or stretched 5% in the last 24 h of CM incubation. **(B)** The side view of the stretching device; cells adhere to the type I collagen coated Uniflex membrane, and a rubber gasket is placed around each six-well plate to create a tight seal; vacuum pressure is applied to deform the membrane around the loading post, which creates a uniaxial stretch (image adapted from Flexcell International). **(C)** Myotube diameter of unstretched (0%) and stretched (5%) myotubes treated with GM control or C26 + GM (n = 216 myotubes/group). **(D)** Myosin heavy chain (MyHC)-Fast (0% n = 18–21/group; 5% n = 9/group) and **(E)** MyHC-Slow (n = 9–11/group) protein expression measured by Western blotting. **(F)** MyHC-Fast (type IIA, Myh2) (n = 6/group), **(G)** MyHC-Fast (type IIB, Myh4) (n = 6/group), **(H)** MyHC-Fast (type IIX, Myh1) (n = 6/group), **(I)** MyHC-Slow (type I, Myh7) (n = 6/group), **(J)** skeletal α-actin (Acta1) (n = 6/group), and **(K)** Myocyte Enhancer Factor 2C (MEF2C) (n = 6/group) mRNA expression calculated using $2^{-\Delta\Delta Ct}$ method with GAPDH as a housekeeping gene. **(L)** Representative Western blotting images with Coomassie blue stain as a protein loading control. Data are presented as means ± SEM as a fold change from GM 0% stretch. Two-way ANOVAs were performed to determine differences. $^{\&}$Main effect of stretch; $^{\#}$main effect of C26 + GM; *significant from GM 0% stretch; $^{\#}$significant from GM 5% stretch; ^significant from C26 + GM 0% stretch. Statistical significance set at $p \leq 0.05$.

increased MyHC-Fast protein expression (26%, $p = 0.023$) in C26 + GM myotubes compared with unstretched C26 + GM myotubes (**Figures 3D,L**). Furthermore, MyHC-Fast protein expression in stretched C26 + GM myotubes was not different than GM levels, indicating that stretch had rescued MyHC-Fast protein expression. Interestingly, stretch did not change ($p = 0.251$) MyHC-Slow protein expression in C26 + GM incubated myotubes, and unstretched (0%) C26 + GM-treated myotubes had significantly lower MyHC-Slow protein expression than both unstretched ($p < 0.001$) and stretched ($p = 0.021$) GM-treated myotubes (**Figures 3E,L**). We also examined the effect of stretch on MyHC mRNA expression. We measured MyHC-Fast type IIA, IIB, IIX, and MyHC-Slow type I mRNA expression after 24 h of stretch. Stretch did not change the C26 + GM suppression MyHC-Fast type IIA (**Figure 3F**) or MyHC-Slow type I (**Figure 3I**) mRNA expression. Likewise, in both GM and C26 conditions, passive stretch did not alter mRNA expression of MyHC-Fast type IIB (**Figure 3G**), type IIX (**Figure 3H**), and skeletal muscle α-actin (**Figure 3J**). There were main effects for C26 + GM to decrease MyHC-Fast type IIA ($p < 0.001$) (**Figure 3F**), increase type IIB ($p = 0.002$) (**Figure 3G**), and decrease MyHC-Slow type I ($p = 0.002$) (**Figure 3I**) mRNA expression. MEF2C is an important transcriptional regulator of MyHC genes and can regulate thick filament assembly in myotubes (Hinits and Hughes, 2007; Piasecka et al., 2021). There was a main effect for C26 + GM to decrease (27%; $p = 0.001$) MEF2C mRNA expression (**Figure 3K**). Stretch did not change MEF2C mRNA expression ($p = 0.687$). These data suggest that stretch-induced mechanical signaling can rescue suppressed MyHC-Fast protein expression in myotubes undergoing catabolism initiated by C26 tumor-derived factors. Interestingly, this effect was independent of changes in MyHC mRNA expression and specific to MyHC-Fast protein. Suppressed MyHC-Slow protein expression by C26 CM was not responsive to stretch-induced mechanical signaling.

Chronic Mechanical Stretch Effects on Protein Turnover Signaling in Colon-26 Treated Myotubes

Skeletal muscle atrophy is associated with suppressed mTORC1 signaling, disrupted autophagy flux, and decreased RNA content, diminishing ribosomal capacity for protein synthesis (Bhogal et al., 2006). E3 ligases Atrogin-1/MAFbx and MuRF-1 are involved in ubiquitin–proteasome degradation and have an established role in muscle atrophy (Lecker et al., 1999; Bodine et al., 2001; Kandarian and Stevenson, 2002). Therefore, we assessed these factors to gain insight into the stretch regulation of myotube growth and protein turnover after exposure to C26 tumor-derived factors (**Figure 4A**). We first measured the phosphorylation of ribosomal protein S6 (rpS6), one downstream marker of the mammalian target of rapamycin (mTOR) pathway (Mieulet et al., 2007). rpS6 phosphorylation (S240/244) was unchanged by C26 + GM and stretch (**Figures 4B,I**). Skeletal muscle-specific E3 ubiquitin ligases Atrogin-1/MAFbx and MuRF-1 can degrade myosin (Clarke et al., 2007; Cohen et al., 2009; Bodine and Baehr, 2014). Interestingly, we observed a main effect for 24 h of stretch to decrease Atrogin-1 and MuRF-1 protein expression in both GM and C26 + GM-treated myotubes (**Figures 4C,D,I**). We next examined established markers of autophagy flux, including microtubule-associated protein light chain 3 (LC3B) I and II, Beclin-1, and p62/SQSTM1 (Mizushima and Yoshimori, 2007; Penna et al., 2013). We observed a main effect for chronic stretch to decrease the LC3B II/I ratio ($p < 0.001$) (**Figures 4E,I**) with no changes in Beclin-1 or p62 protein expression (**Figures 4F,G,I**). Total RNA content in myotubes remained unchanged across all conditions (**Figure 4H**). These data suggest that chronic stretch may protect myosin content by decreasing the expression of Atrogin-1 and MuRF-1 and reduced autophagy flux, rather than the induction of anabolic signaling involving total RNA and mTOR signaling relating to rpS6.

Stretch Effect on Mechanical and Growth-Related Factors After Colon-26 Conditioned Media Exposure

We investigated the effects of 24 h stretch on various regulators of muscle growth during C26 CM incubation (**Figure 5A**). We observed a main effect for mechanical stretch to increase integrin β1D protein expression ($p < 0.001$) (**Figure 5B**). SRF is a member of the MADS-box family of transcription factors important for growth and myogenic processes (Li et al., 2005). Moreover, mechanical stretch can induce SRF mRNA expression (Carson and Booth, 1999). Surprisingly, there was a main effect for both stretch ($p = 0.035$) and C26 tumor-derived factors ($p < 0.001$) to decrease SRF protein expression (**Figures 5C,G**). We further examined the role of stretch and C26 + GM on myogenesis by measuring the ratio of myogenin, which is expressed in late stages of differentiation, to MyoD, a marker of myoblast proliferation and initiation of differentiation. The relative mRNA expression of myogenin (GM 0%, 1.00 ± 0.03; GM 5%, 1.03 ± 0.09; C26 + GM 0%, 0.809 ± 0.08; and C26 + GM 5%, 1.01 ± 0.08) and MyoD (GM 0%, 1.02 ± 0.10; GM 5%, 0.905 ± 0.12; C26 + GM 0%, 0.752 ± 0.07; and C26 + GM 5%, 0.842 ± 0.10) was unchanged. Due to variability in protein expression, myogenin (**Figure 5D**) and MyoD (**Figure 5E**) individual protein expression was similar across groups. To account for variability between samples, we calculated the ratio of myogenin-to-MyoD protein expression in each sample. There was a main effect for stretch to increase the myogenin-to-MyoD ratio ($p = 0.027$) (**Figure 5F**). These results provide evidence that regardless of C26 tumor-derived factor incubation, stretch can increase integrin β1D protein expression to modulate intrinsic mechanical signaling. These changes are independent of stretch-induced increases in SRF protein expression and associated with an effect for stretch to increase the myogenin-to-MyoD protein ratio.

Acute Stretch Effects on Mechanical and Colon-26-Induced C2C12 Myotube Signaling

In a separate experiment, we examined the effects of acute 4-h stretch on cachectic and growth-related signaling in C26 + GM-treated myotubes. Several cytokines associated with cancer-induced wasting can stimulate muscle STAT3

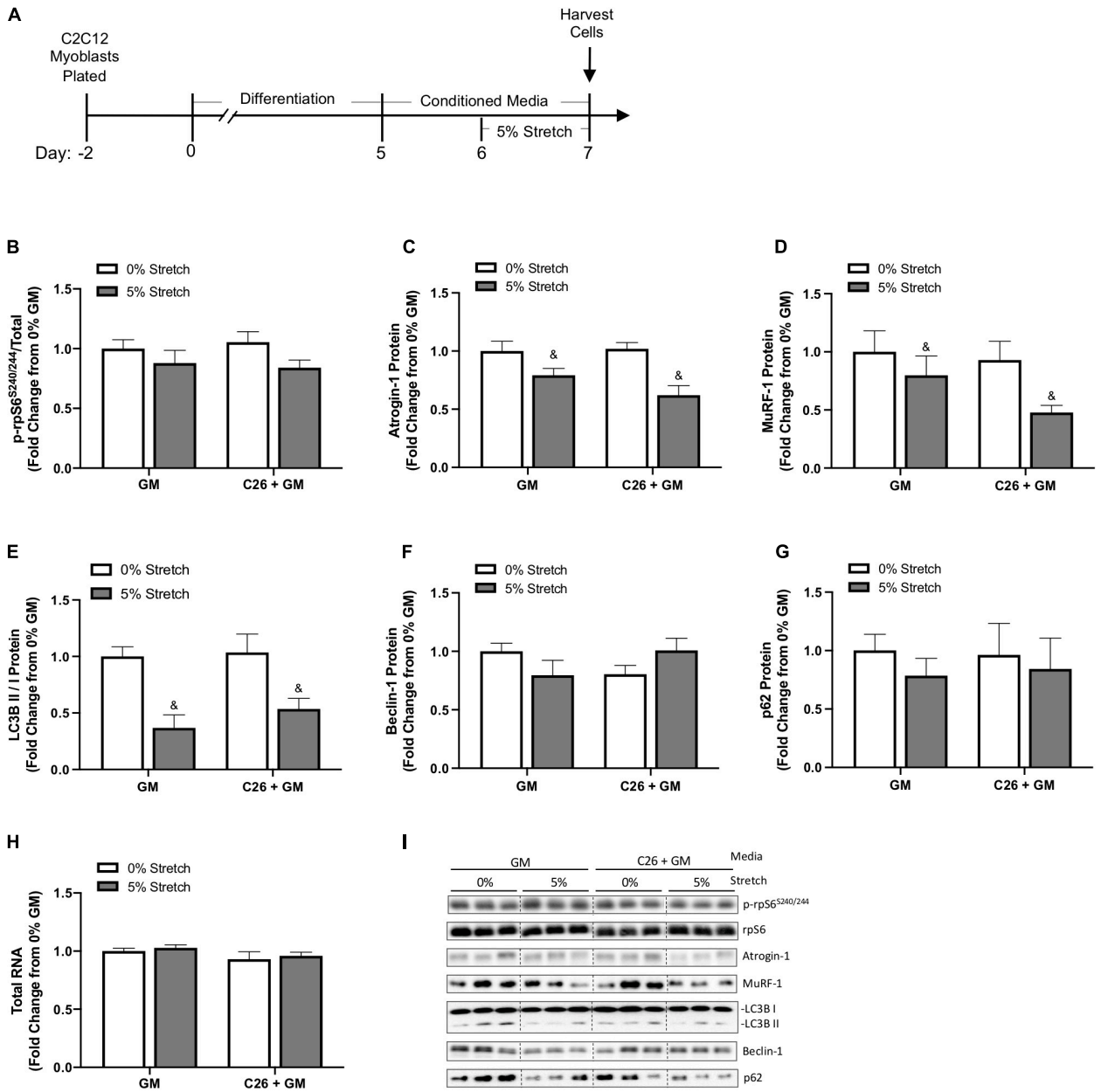

FIGURE 4 | Effects of 24-h stretch on growth related signaling in myotubes treated with colon-26 (C26) tumor-derived factors. **(A)** Experiment overview: C2C12 myoblasts are plated on Uniflex membranes in growth media (GM); after 48 h at ∼85% confluence, differentiation media is added, which corresponds to day 0. Myotubes are differentiated for 5 days upon which 50% conditioned media (CM; GM or C26 + GM) is diluted with serum-free DMEM and added to wells for 48 h; myotubes are either left unstretched (0%) or stretched 5% in the last 24 h of CM incubation. Western blotting analyses of **(B)** ratio of phosphorylated (p-) to total protein expression of ribosomal protein S6 ($rpS6^{S240/244}$) (n = 6/group), **(C)** Atrogin-1/muscle atrophy F-box (MAFbx) (n = 6/group), **(D)** Muscle RING finger 1 (MuRF-1) (n = 6/group), **(E)** microtubule-associated protein light chain 3B (LC3B) II/I ratio (n = 6–12/group), **(F)** Beclin-1 (n = 6/group), and **(G)** p62/SQSTM1 (n = 6/group) protein expression. **(H)** Total RNA content (n = 6/group). **(I)** Representative Western blotting images; dashed line represents different areas of the same gel. Data are presented as means ± SEM as a fold change from GM 0% stretch. Two-way ANOVAs were performed to determine differences. $^{\&}$Main effect of stretch. Statistical significance set at $p \leq 0.05$.

phosphorylation (Bonetto et al., 2011; Puppa et al., 2014; Zimmers et al., 2016). Cancer cachexia can induce muscle p38 MAPK, ERK1/2, and JNK signaling (Brown et al., 2018; Mulder et al., 2020). Interestingly, mechanical signaling can also activate these pathways (Kumar et al., 2002; Martineau and Gardiner, 2002; Gao and Carson, 2016). Several well-characterized stretch-activated signaling pathways increase at the onset of chronic stretch and then return to baseline (Zhan et al., 2007). Therefore, we examined 4 h of stretch to determine acute activation of these signaling pathways.

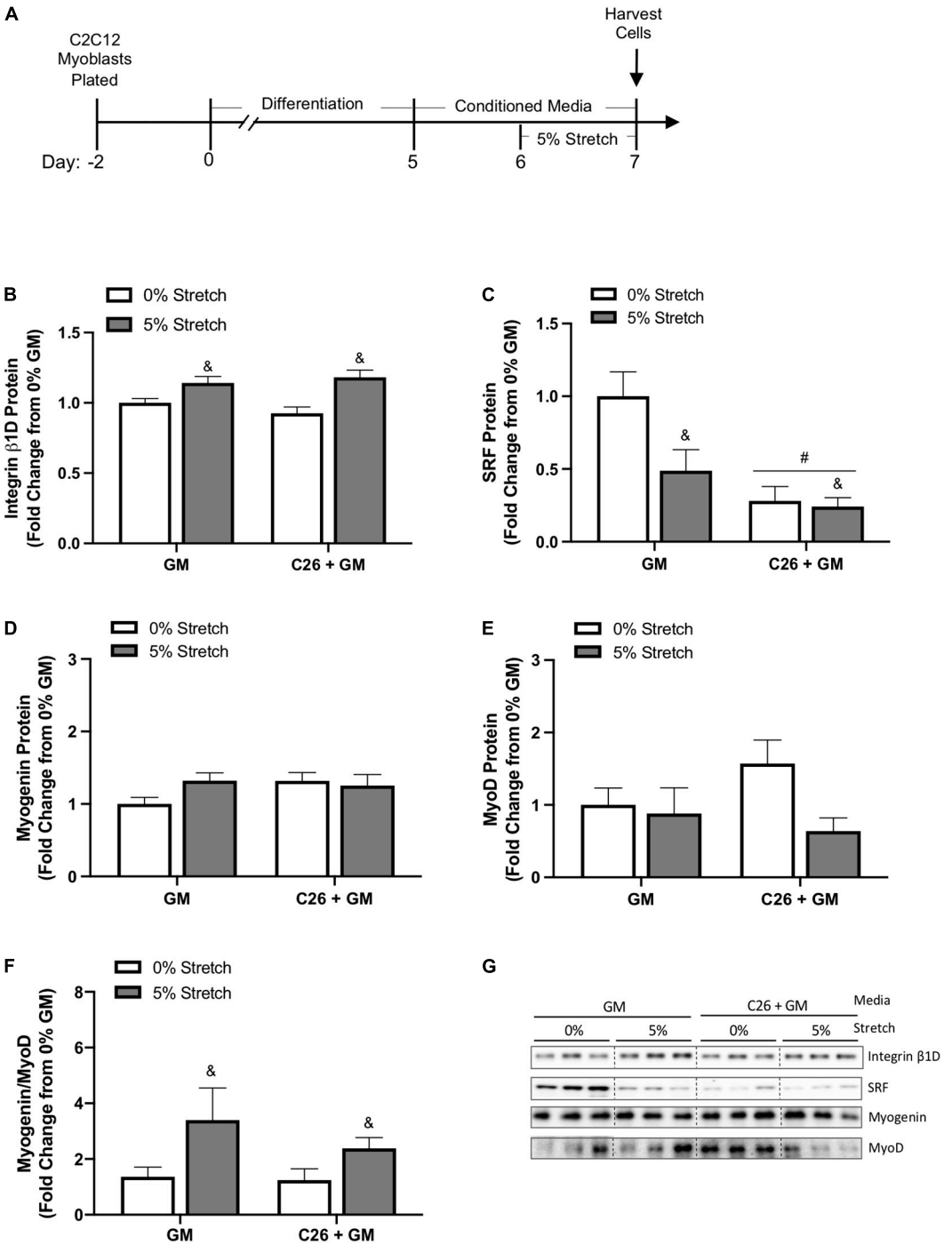

FIGURE 5 | Effects of 24-h stretch mechanical and growth-related signaling in colon-26 (C26)-treated myotubes. **(A)** Experiment overview: C2C12 myoblasts are plated on Uniflex membranes in growth media (GM); after 48 h at ∼85% confluence, differentiation media is added corresponding to day 0. Myotubes are differentiated for 5 days upon which 50% conditioned media (CM; GM or C26 + GM) is diluted with serum-free DMEM and added to wells for 48 h; myotubes are either left unstretched (0%) or stretched 5% in the last 24 h of CM incubation. Immediately after stretch, cells are harvested for protein. Western blotting analyses of **(B)** integrin β1D (n = 9/group), **(C)** serum response factor (SRF) (n = 9/group), **(D)** myogenin (n = 6/group), and **(E)** MyoD (n = 6/group) protein expression. **(F)** Ratio individual protein expression of myogenin, a marker of terminal myoblast differentiation, to MyoD, a marker of myoblast proliferation and initiation of differentiation (n = 6/group). **(G)** Representative Western blotting images; dashed line represents different areas of the same gel. Data are presented as means ± SEM as a fold change from GM 0% stretch. Two-way ANOVAs were performed to determine differences. $^{\&}$Main effect of stretch, $^{\#}$main effect of C26 + GM. Statistical significance set at $p \leq 0.05$.

Myotubes were stretched 5% for the last 4 h of either the GM or C26 + GM treatment (**Figure 6A**). There was no effect for stretch to change STAT3 (Y705) phosphorylation (p = 0.865) (**Figure 6B**), p38 (T180/Y182) phosphorylation (p = 0.809) (**Figure 6C**), or JNK (T183/Y185) phosphorylation (p = 0.067) (**Figures 6E,F**). A preplanned analysis determined the effect of stretch in the GM condition; stretch induced a 42% increase in p38 (T180/Y182) (p = 0.014) phosphorylation and a 25% increase in ERK1/2 (T202/Y204) (p = 0.015) phosphorylation. Interestingly, this signaling activation occurred within the high serum environment. Stretch-induced ERK1/2 phosphorylation was further induced 54% in C26 + GM-treated stretched cells ($p < 0.001$) (**Figures 6D,F**). These data suggest that C26 + GM does not blunt the stretch response of p-p38 and p-ERK1/2 and that acute static stretch had no effect on the C26 CM induction of STAT3 phosphorylation, which was similarly elevated with 4 h of stretch.

DISCUSSION

Colon-26 carcinoma represents a well-characterized and extensively used preclinical cancer cachexia model (Bonetto et al., 2016). *In vitro*, C26 CM produces myotube atrophy, and tumor-derived factors in the CM can disrupt the regulation of myotube protein turnover (Jackman et al., 2017; Kandarian et al., 2018; Liu et al., 2019; Chiappalupi et al., 2020; Schmidt et al., 2020; Wang et al., 2021). Dynamic exercise can prevent metabolic and functional disruptions and suppress signaling associated with cachexia (Halle et al., 2020). Mechanical stimulation of muscle via passive stretch can promote muscle growth and functional adaptations (Carson et al., 1995; De Deyne, 2001; Zöllner et al., 2012). Skeletal muscle MyHC is a critical protein involved in skeletal muscle force generation and function (Weiss et al., 1999). Cancer can cause MyHC loss in muscle and myotubes (Acharyya et al., 2004; Guigni et al., 2018; Liu et al., 2019; Yamada et al., 2020). While our mechanistic understanding of cancer cachexia has advanced significantly, critical gaps remain in our knowledge of constraints that cachectic factors place on intrinsic muscle properties such as mechanotransduction. How stretch-induced mechanical signaling impacts the regulation of MyHC expression after exposure to cachectic tumor-derived factors is uncertain. Therefore, we sought to examine whether mechanical signaling induced by both chronic and acute passive stretch can impact C2C12 myotube growth and MyHC expression after incubation with C26 CM. Our data provide intriguing evidence that myotubes pretreated with C26 CM can still respond to mechanical stimuli associated with passive stretch. The induction of mechanical signaling provides a growth stimulus and maintains MyHC-Fast protein expression, independent of changes in MyHC mRNA expression changes. These benefits correspond to increased integrinβ1D expression, a stretch activation of ERK1/2, increased myogenin/MyoD ratio, and the suppression of Atrogin-1/MAFbx, MuRF-1, and LC3B II/I ratio.

In vitro studies have consistently reported that tumor-derived factors can reduce myotube size. Higher tumor-CM concentrations can decrease diameter in a dose-dependent manner (Pin et al., 2018; Zhong et al., 2019). As in the present study, myotube atrophy mechanisms have been investigated with 50% CM. However, this dilution of tumor-derived media can provide a serum-rich growth environment of myotubes consisting of 5% FBS. Tumor cells, such as C26 and EL4 cells, are cultured in serum-rich media (10% FBS). Therefore, increasing the percentage of CM also increases the serum concentration and modifies C2C12 myotube culture conditions compared with standard differentiation conditions (e.g., 2% horse serum). Mature myotubes exposed to high serum elicit a robust growth response (von Walden et al., 2016), which aligns with our results of significant growth of myotubes treated with 50% GM. These results held under two different culture conditions, including myotubes plated on rigid polystyrene collagen coated plates and flexible silastic membranes coated with collagen. Interestingly, despite a high growth factor environment, myotubes exposed to C26 CM exhibit suppressed growth, which was not observed with EL4 CM, suggesting that this response is specific to factors implicated in cachexia. Inflammatory factors such as interleukin-6 (IL-6), tumor necrosis factor (TNF)-α, and leukemia inhibitory factor (LIF) are commonly examined for their roles in cancer-induced muscle wasting (Carson and Baltgalvis, 2010; Patel and Patel, 2017). It has been previously described that C26 media contains low levels of IL-6 and TNF-α and high levels of LIF, which are thought to be a key factor for C26 atrophy *in vivo* and *in vitro* (Seto et al., 2015; Kandarian et al., 2018). In line with previously published data, C26 secreted factors induced STAT3 phosphorylation under both plating conditions, indicating an important role for STAT signaling in C26 cachexia. CM experiments are regularly utilized to examine the effects of tumor-derived factors on skeletal muscle myotubes. However, it is important to note that this *in vitro* model is a biological assay and does not precisely mimic preclinical and patient serum concentrations of secreted factors. Mechanical stimulation of myotubes via dynamic and static stretch can increase myotube diameter even in the presence of tumor-derived factors (Gao and Carson, 2016; Baccam et al., 2019). While myotubes incubated with C26 CM suppressed growth over the 48 h period, stretch in the last 24 h promoted growth, although to a lesser extent than 5% FBS GM. Further research is warranted to examine this differential growth response to anabolic stimuli in myotubes treated with tumor-derived factors and the potential effects that high serum with tumor-derived factors may have on muscle signaling.

Cachectic tumor-derived factors can produce atrophy by altering protein turnover signaling. We observed suppression of protein synthesis, Akt/mTORC1 signaling, and induction of E3 ubiquitin ligases under standard culture conditions in response to tumor-derived factors. C26 CM induces the phosphorylation of p38 MAPK and ERK1/2, which are well-characterized signaling molecules implicated in cancer cachexia (Seto et al., 2015; Gao and Carson, 2016). Interestingly, mechanical stimulation via stretch also activates these signaling pathways in myotubes and are linked to skeletal muscle growth (Kumar et al., 2002; You et al., 2012; Goodman, 2019; Lin and Liu, 2019; Moustogiannis et al., 2020). Stretched myotubes treated with LLC CM

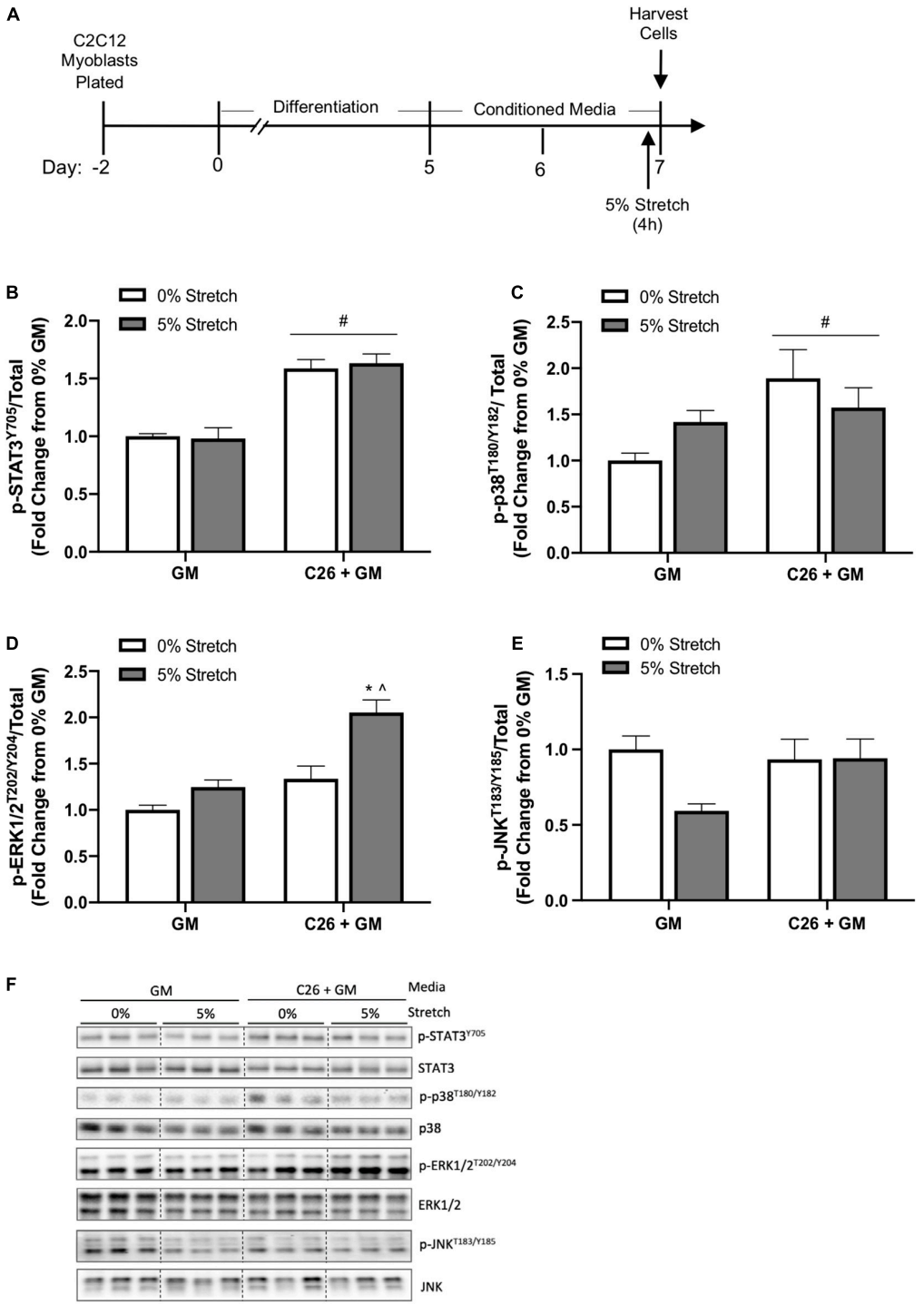

FIGURE 6 | Effects of 4-h stretch on colon-26 (C26) conditioned media-induced myotube signaling pathways. **(A)** Experiment overview: C2C12 myoblasts are plated on in growth media (GM); after 48 h at ∼85% confluence, differentiation media is added, which corresponds to day 0. At day 5 of differentiation, conditioned media (CM; GM or C26 + GM) is diluted with 50% serum-free DMEM and added to wells for 48 h. Myotubes are either left unstretched (0%) or stretched 5% in the last 4 h of CM incubation. Immediately after stretch, cells are harvested for protein. Western blotting analyses of the ratio of phosphorylated (p-) to total protein expression of **(B)** signal transducer and activator of transcription 3 (STAT3^{Y705}) (n = 9–12/group), **(C)** p38$^{T180/Y182}$ MAPK (n = 6/group), **(D)** extracellular signal-regulated kinase 1/2 (ERK1/2$^{T202/Y204}$) (n = 6/group), and **(E)** c-Jun N-terminal kinase (JNK$^{T183/Y185}$) (n = 9/group) protein expression. **(F)** Representative Western blotting images; dashed line represents different areas of the same gel. Data are presented as means ± SEM as a fold change from GM 0% stretch. Two-way ANOVAs were performed to determine differences. #Main effect of C26 + GM; *significant from GM 0% stretch, ^significant from C26 + GM 0% stretch. Statistical significance set at $p \leq 0.05$.

exhibit blunted protein synthesis signaling and responsiveness to mechanical stimuli (Gao and Carson, 2016). Intracellular mechanical signaling can be initiated from the extracellular environment via transmembrane proteins such as integrins (Carson and Wei, 2000). Specifically, the muscle-specific integrin β1D isoform is essential for myoblast differentiation and, upon activation, initiates intracellular signaling to regulate muscle growth (Boppart and Mahmassani, 2019). Chronic stretch for 24 h increased integrin β1D protein expression in both GM and C26 conditions, which may have important implications for the transduction of mechanical and growth-related signals during cachexia. In addition to p38 MAPK and ERK1/2, mechanical stimuli can modulate the JNK pathway (Pereira et al., 2011). Acute stretch did not significantly alter JNK phosphorylation. However, studies often report rapid increases within 5–10 min, compared with the 4-h stretch used in our study (Martineau and Gardiner, 2002; Lessard et al., 2018). C26 CM did not suppress the stretch activation of p38 and ERK1/2 phosphorylation, and there was an additive effect of stretched and C26 CM on ERK1/2 phosphorylation. Therefore, it is interesting to speculate that different tumor types (i.e., LLC versus C26) may differentially alter the responsiveness to mechanical signaling. C26 CM and stretch did not alter rpS6 phosphorylation, a downstream target of mTORC1. However, the lack of observed changes could be in part due to a high growth factor environment. The induction of E3 ligases Atrogin-1/MAFbx and MuRF-1 is often associated with cancer-induced muscle wasting *in vitro* and preclinical models (Bodine and Baehr, 2014; Rom and Reznick, 2016). Studies report phenotypic differences in myotube growth when plated on various substrates (Cittadella Vigodarzere and Mantero, 2014; Ostrovidov et al., 2014; Denes et al., 2019). We sought to expand on these ideas and examined myotube growth and signaling in response to tumor-derived factors on both polystyrene and silastic membranes. In both culture conditions, C26 factors suppressed myotube growth and MyHC isoform protein expression. In myotubes differentiated on a rigid polystyrene substratum, C26 media reduced protein synthesis and increased Atrogin-1 and MuRF-1 protein expression. Surprisingly, C26 tumor-derived factors did not induce either Atrogin-1 or MuRF-1 protein expression in myotubes grown on silastic membranes. However, other signaling pathways and proteins may be involved in the growth suppression by C26 tumor-derived factors. These pathways include calpain and caspase activation, impaired protein synthesis, inflammatory cytokine-induced glucocorticoid release, and forkhead transcription factor activation (Fearon et al., 2012; Silva et al., 2015; Yamada et al., 2020). Notably, C26 CM induction of p38 MAPK and CCAAT/enhancer binding protein beta (C/EBPβ) signaling pathway can induce muscle atrophy (Sin et al., 2019). We observed a stretch suppression of E3 ligase expression, which has been previously reported (Moustogiannis et al., 2020), along with suppressing the LC3B II/I ratio. LC3B II protein levels are increased with cancer, and reduced levels suggest either reduced autophagosome formation or increased autophagosome turnover (Mizushima and Yoshimori, 2007; Aversa et al., 2016; Pettersen et al., 2017). These reductions could, in part, be mediating the protective effects of stretch on MyHC-Fast protein expression. However, mechanical stimulation can activate other pathways such as myokine release to counteract the adverse impact on myotubes treated with tumor-derived media (Baccam et al., 2019).

Skeletal muscle MyHC is a motor protein of thick filaments and the most abundant protein in skeletal muscle, and its expression is crucial in cross-bridge formation and force generation (Weiss et al., 1999; Deshmukh et al., 2015). MyHC expression is also an indicator of C2C12 myotube terminal differentiation (Silberstein et al., 1986; Brown et al., 2012), and stretch effects on the regulation of MyHC expression have been limited to this differentiation role (Wang et al., 2020). Our results suggest that stretch can rescue C26 suppression of MyHC-Fast protein expression independent of changes in MyHC isoform mRNA expression. Stretch did not alter MyHC-Slow protein expression compared with unstretched C26 + GM-treated myotubes. This isoform-specific response has implications for adult skeletal muscle since muscle fibers are heterogeneous, including MyHC fast (type IIA), intermediate/mixed (type IIX or IIB), and slow (type I) fibers (Miller and Stockdale, 1986; Ostrovidov et al., 2014). Over the course of differentiation, C2C12 myotubes display a shift in MyHC mRNA isoform expression. Specifically, type I is predominant early but declines between days 4 and 6 of differentiation, while type II isoforms (IIA, IIX, and IIB) significantly increase starting at 4 days post-differentiation (Brown et al., 2012). In the current study, myotubes were analyzed 7 days post-differentiation. Therefore, it is interesting to speculate that the temporal pattern of MyHC mRNA expression may factor into observed responses relating to the stretch rescue of MyHC-Fast and not slow isoforms. The specific phenotypic composition of fast and slow muscle MyHC isoforms determines fatigue resistance and contraction velocity (Ostrovidov et al., 2014). MyHC isoform expression is regulated at several levels, including the calcineurin/NFAT signaling pathway, MEF2C, and various microRNAs (Swoap et al., 2000; Cheng et al., 2018; Xu et al., 2018). How stretch impacts these potential control mechanisms for fast and slow isoform protein expression warrants further investigation. MEF2 transcription factors have critical roles in muscle cell differentiation and myofibers' structural integrity. Specifically, MEF2C can control MyHC IIA expression (Allen and Leinwand, 2002; Potthoff et al., 2007), and cachexia decreases muscle MEF2C expression in C26 tumor-bearing mice (Shum et al., 2012). We provide evidence that C26-derived factors can directly suppress myotube MEF2C and MyHC IIA mRNA expression. Interestingly, in line with published *in vivo* reports (Diffee et al., 2002; Roberts et al., 2013), C26 cachexia resulted in a shift in myosin mRNA expression to have greater type IIB, while types IIA and I were reduced. Reductions in myotube contractile elements after C26 exposure seem to be specific to myosin, as skeletal α-actin mRNA is unchanged. Myoblast proliferation and fusion contribute to stretch-induced *de novo* synthesis of myofibers, which also involves inducing myogenic transcription factors (e.g., myogenin and MyoD) (Carson and Booth, 1998). Dynamic stretch in the presence of tumor-derived factors can promote myoblast fusion into nascent myotubes (Baccam et al., 2019). High growth factor serum can activate myogenic transcription factors and

promote myoblast proliferation (Lawson and Purslow, 2000). While we report no effect of CM or stretch on myogenin and MyoD protein expression, stretch increased the myogenin-to-MyoD protein expression ratio. These results suggest that stretch-related growth effects can involve increased myogenic differentiation. To this end, a dynamic myotube stretch does increase the fusion index in hypertrophying myotubes (Baccam et al., 2019). Further research is warranted to examine the interaction of mechanical signaling and myogenic regulator factors to rescue tumor-derived atrophy.

In summary, we examined the effects of mechanical signaling induced by a chronic passive stretch on growth and MyHC expression in C2C12 myotubes after incubation with C26 CM. Chronic stretch administered after 24 h of C26 CM exposure provided a growth stimulus and rescued MyHC-Fast protein expression independent of mRNA expression changes. These benefits were associated with the stretch activation of ERK1/2 phosphorylation, muscle-specific E3 ubiquitin ligase suppression, LC3B II/I ratio suppression, increased integrin β1D protein expression, and increased myogenin-to-MyoD ratio. However, we must consider that mechanical signaling can activate other signaling pathways, which could also impact tumor-derived factors' suppression of myotube growth. The impact of mechanical signaling on MyHC-Fast expression may significantly preserve or restore muscle function and mass during cancer. Investigations to define how mechanical signaling can produce this effect are highly justified. Preclinical and clinical examinations of muscle stimulation via passive movement (e.g., stretch) are well tolerated, can promote muscle growth and functional adaptations, and have clear potential to improve patient health (Carson et al., 1995; De Deyne, 2001; Deng and Cassileth, 2014; Berrueta et al., 2018). Our results suggest that mechanical stimuli can positively impact myotube growth in the presence of cachectic tumor-derived factors and a high serum environment. Understanding how mechanical signaling pathways can be successfully harnessed to benefit skeletal muscle in a catabolic cancer environment has a high potential for future cachexia therapy.

DATA AVAILABILITY STATEMENT

The original contributions presented in the study are included in the article/supplementary material, further inquiries can be directed to the corresponding author/s.

AUTHOR CONTRIBUTIONS

JC conceived and designed the study. JH performed the experiments. JH, BC-F, RP, and JC contributed to the statistical analysis, figure set preparation, and interpretation of the data. JH, BC-F, and JC contributed to the writing and editing of the manuscript. All authors reviewed the results and approved the final version of the manuscript.

FUNDING

This work was supported by the National Institutes of Health Grants R01 CA-121249 (National Cancer Institute) and R21 CA-231131 to JC.

REFERENCES

Acharyya, S., Ladner, K. J., Nelsen, L. L., Damrauer, J., Reiser, P. J., Swoap, S., et al. (2004). Cancer cachexia is regulated by selective targeting of skeletal muscle gene products. *J. Clin. Invest.* 114, 370–378. doi: 10.1172/JCI20174

Allen, D. L., and Leinwand, L. A. (2002). Intracellular calcium and myosin isoform transitions: calcineurin and calcium-calmodulin kinase pathways regulate preferential activation of the IIa myosin heavy chain promoter. *J. Biol. Chem.* 277, 45323–45330. doi: 10.1074/jbc.m208302200

Argiles, J. M., Lopez-Soriano, F. J., and Busquets, S. (2019). Mediators of cachexia in cancer patients. *Nutrition* 66, 11–15. doi: 10.1016/j.nut.2019.03.012

Aulino, P., Berardi, E., Cardillo, V. M., Rizzuto, E., Perniconi, B., Ramina, C., et al. (2010). Molecular, cellular and physiological characterization of the cancer cachexia-inducing C26 colon carcinoma in mouse. *BMC Cancer* 10:363. doi: 10.1186/1471-2407-10-363

Aversa, Z., Pin, F., Lucia, S., Penna, F., Verzaro, R., Fazi, M., et al. (2016). Autophagy is induced in the skeletal muscle of cachectic cancer patients. *Sci. Rep.* 6:30340.

Baccam, A., Benoni-Sviercovich, A., Rocchi, M., Moresi, V., Seelaender, M., Li, Z., et al. (2019). The mechanical stimulation of myotubes counteracts the effects of tumor-derived factors through the modulation of the activin/follistatin ratio. *Front. Physiol.* 10:401. doi: 10.3389/fphys.2019.00401

Ballaro, R., Penna, F., Pin, F., Gomez-Cabrera, M. C., Vina, J., and Costelli, P. (2019). Moderate exercise improves experimental cancer cachexia by modulating the redox homeostasis. *Cancers (Basel)* 11:285. doi: 10.3390/cancers11030285

Baracos, V. E. (2000). Regulation of skeletal-muscle-protein turnover in cancer-associated cachexia. *Nutrition* 16, 1015–1018. doi: 10.1016/s0899-9007(00)00407-x

Berrueta, L., Bergholz, J., Munoz, D., Muskaj, I., Badger, G., Shukla, A., et al. (2018). Stretching reduces tumor growth in a mouse breast cancer model. *Sci. Rep.* 8:7864.

Bhogal, A. S., Lorite, M. L., and Tisdale, M. J. (2006). Changes in nucleic acid and protein levels in atrophying skeletal muscle in cancer cachexia. *Anticancer Res.* 26, 4149–4154.

Bodine, S. C., and Baehr, L. M. (2014). Skeletal muscle atrophy and the E3 ubiquitin ligases MuRF1 and MAFbx/atrogin-1. *Am. J. Physiol. Endocrinol. Metab.* 307, E469–E484. doi: 10.1152/ajpendo.00204.2014

Bodine, S. C., Latres, E., Baumhueter, S., Lai, V. K., Nunez, L., Clarke, B. A., et al. (2001). Identification of ubiquitin ligases required for skeletal muscle atrophy. *Science* 294, 1704–1708. doi: 10.1126/science.1065874

Bonetto, A., Aydogdu, T., Kunzevitzky, N., Guttridge, D. C., Khuri, S., Koniaris, L. G., et al. (2011). STAT3 activation in skeletal muscle links muscle wasting and the acute phase response in cancer cachexia. *PLoS One* 6:e22538. doi: 10.1371/journal.pone.0022538

Bonetto, A., Rupert, J. E., Barreto, R., and Zimmers, T. A. (2016). The colon-26 carcinoma tumor-bearing mouse as a model for the study of cancer cachexia. *JoVE J. Vis. Exp.* 117:e54893. doi: 10.3791/54893

Boppart, M. D., and Mahmassani, Z. S. (2019). Integrin signaling: linking mechanical stimulation to skeletal muscle hypertrophy. *Am. J. Physiol. Cell Physiol.* 317, C629–C641.

Brown, D. M., Parr, T., and Brameld, J. M. (2012). Myosin heavy chain mRNA isoforms are expressed in two distinct cohorts during C2C12 myogenesis. *J. Muscle Res. Cell Motil.* 32, 383–390. doi: 10.1007/s10974-011-9267-4

Brown, J. L., Lee, D. E., Rosa-Caldwell, M. E., Brown, L. A., Perry, R. A., Haynie, W. S., et al. (2018). Protein imbalance in the development of skeletal muscle wasting in tumour-bearing mice. *J. Cachexia Sarcopenia Muscle* 9, 987–1002. doi: 10.1002/jcsm.12354

Carson, J. A. (1997). 11 The regulation of gene expression in hypertrophying skeletal muscle. *Exerc. Sport Sci. Rev.* 25, 301–320.

Carson, J. A., and Baltgalvis, K. A. (2010). Interleukin 6 as a key regulator of muscle mass during Cachexia. *Exerc. Sport Sci. Rev.* 38, 168–176. doi: 10.1097/JES.0b013e3181f44f11

Carson, J. A., and Booth, F. (1998). Myogenin mRNA is elevated during rapid, slow, and maintenance phases of stretch-induced hypertrophy in chicken slow-tonic muscle. *Pflügers Arch.* 435, 850–858. doi: 10.1007/s004240050593

Carson, J. A., and Booth, F. W. (1999). Serum response factor mRNA induction in the hypertrophying chicken patagialis muscle. *J. Appl. Physiol.* 86, 377–382. doi: 10.1152/jappl.1999.86.1.377

Carson, J. A., and Wei, L. (2000). Integrin signaling's potential for mediating gene expression in hypertrophying skeletal muscle. *J. Appl. Physiol.* 88, 337–343. doi: 10.1152/jappl.2000.88.1.337

Carson, J. A., Yamaguchi, M., and Alway, S. E. (1995). Hypertrophy and proliferation of skeletal muscle fibers from aged quail. *J. Appl. Physiol.* 78, 293–299. doi: 10.1152/jappl.1995.78.1.293

Cheng, X., Du, J., Shen, L., Tan, Z., Jiang, D., Jiang, A., et al. (2018). MiR-204-5p regulates C2C12 myoblast differentiation by targeting MEF2C and ERRgamma. *Biomed. Pharmacother.* 101, 528–535. doi: 10.1016/j.biopha.2018.02.096

Chiappalupi, S., Sorci, G., Vukasinovic, A., Salvadori, L., Sagheddu, R., Coletti, D., et al. (2020). Targeting RAGE prevents muscle wasting and prolongs survival in cancer cachexia. *J. Cachexia Sarcopenia Muscle* 11, 929–946. doi: 10.1002/jcsm.12561

Cittadella Vigodarzere, G., and Mantero, S. (2014). Skeletal muscle tissue engineering: strategies for volumetric constructs. *Front. Physiol.* 5:362. doi: 10.3389/fphys.2014.00362

Clarke, B. A., Drujan, D., Willis, M. S., Murphy, L. O., Corpina, R. A., Burova, E., et al. (2007). The E3 Ligase MuRF1 degrades myosin heavy chain protein in dexamethasone-treated skeletal muscle. *Cell Metab.* 6, 376–385. doi: 10.1016/j.cmet.2007.09.009

Cohen, S., Brault, J. J., Gygi, S. P., Glass, D. J., Valenzuela, D. M., Gartner, C., et al. (2009). During muscle atrophy, thick, but not thin, filament components are degraded by MuRF1-dependent ubiquitylation. *J. Cell Biol.* 185, 1083–1095. doi: 10.1083/jcb.200901052

De Deyne, P. G. (2001). Application of passive stretch and its implications for muscle fibers. *Phys. Ther.* 81, 819–827. doi: 10.1093/ptj/81.2.819

Denes, L. T., Riley, L. A., Mijares, J. R., Arboleda, J. D., McKee, K., Esser, K. A., et al. (2019). Culturing C2C12 myotubes on micromolded gelatin hydrogels accelerates myotube maturation. *Skeletal muscle* 9, 1–10.

Deng, G., and Cassileth, B. (2014). Integrative oncology: an overview. *Am. Soc. Clin. Oncol. Educ. Book* 34, 233–242. doi: 10.14694/edbook_am.2014.34.233

Deshmukh, A. S., Murgia, M., Nagaraj, N., Treebak, J. T., Cox, J., and Mann, M. (2015). Deep proteomics of mouse skeletal muscle enables quantitation of protein isoforms, metabolic pathways, and transcription factors. *Mol. Cell. Proteomics* 14, 841–853. doi: 10.1074/mcp.M114.044222

Diffee, G. M., Kalfas, K., Al-Majid, S., and McCarthy, D. O. (2002). Altered expression of skeletal muscle myosin isoforms in cancer cachexia. *Am. J. Physiol. Cell Physiol.* 283, C1376–C1382. doi: 10.1152/ajpcell.00154.2002

Ding, H., Zhang, G., Sin, K. W., Liu, Z., Lin, R. K., Li, M., et al. (2017). Activin A induces skeletal muscle catabolism via p38beta mitogen-activated protein kinase. *J. Cachexia Sarcopenia Muscle* 8, 202–212. doi: 10.1002/jcsm.12145

Fearon, K. C., Glass, D. J., and Guttridge, D. C. (2012). Cancer cachexia: mediators, signaling, and metabolic pathways. *Cell Metab.* 16, 153–166. doi: 10.1016/j.cmet.2012.06.011

Freire, P. P., Fernandez, G. J., de Moraes, D., Cury, S. S., Dal Pai-Silva, M., Dos Reis, P. P., et al. (2020). The expression landscape of cachexia-inducing factors in human cancers. *J. Cachexia Sarcopenia Muscle* 11, 947–961. doi: 10.1002/jcsm.12565

Gao, S., and Carson, J. A. (2016). Lewis lung carcinoma regulation of mechanical stretch-induced protein synthesis in cultured myotubes. *Am. J. Physiol. Cell Physiol.* 310, C66–C79. doi: 10.1152/ajpcell.00052.2015

Gao, S., Durstine, J. L., Koh, H.-J., Carver, W. E., Frizzell, N., and Carson, J. A. (2017). Acute myotube protein synthesis regulation by IL-6-related cytokines. *Am. J. Physiol. Cell Physiol.* 313, C487–C500.

Goodman, C. A. (2019). Role of mTORC1 in mechanically induced increases in translation and skeletal muscle mass. *J. Appl. Physiol.* 127, 581–590. doi: 10.1152/japplphysiol.01011.2018

Goodman, C. A., Mabrey, D. M., Frey, J. W., Miu, M. H., Schmidt, E. K., Pierre, P., et al. (2011). Novel insights into the regulation of skeletal muscle protein synthesis as revealed by a new nonradioactive in vivo technique. *FASEB J.* 25, 1028–1039. doi: 10.1096/fj.10-168799

Guigni, B. A., Callahan, D. M., Tourville, T. W., Miller, M. S., Fiske, B., Voigt, T., et al. (2018). Skeletal muscle atrophy and dysfunction in breast cancer patients: role for chemotherapy-derived oxidant stress. *Am. J. Physiol. Cell Physiol.* 315, C744–C756. doi: 10.1152/ajpcell.00002.2018

Halle, J. L., Counts, B. R., and Carson, J. A. (2020). Exercise as a therapy for cancer-induced muscle wasting. *Sports Med. Health Sci.* 2, 186–194. doi: 10.1016/j.smhs.2020.11.004

Halle, J. L., Pena, G. S., Paez, H. G., Castro, A. J., Rossiter, H. B., Visavadiya, N. P., et al. (2019). Tissue-specific dysregulation of mitochondrial respiratory capacity and coupling control in colon-26 tumor-induced cachexia. *Am. J. Physiol. Regul. Integr. Comp. Physiol.* 317, R68–R82. doi: 10.1152/ajpregu.00028.2019

Hardee, J. P., Mangum, J. E., Gao, S., Sato, S., Hetzler, K. L., Puppa, M. J., et al. (2016). Eccentric contraction-induced myofiber growth in tumor-bearing mice. *J. Appl. Physiol.* 120, 29–37. doi: 10.1152/japplphysiol.00416.2015

Hinits, Y., and Hughes, S. M. (2007). Mef2s are required for thick filament formation in nascent muscle fibres. *Development* 134, 2511–2519. doi: 10.1242/dev.007088

Hornberger, T. A., Armstrong, D. D., Koh, T. J., Burkholder, T. J., and Esser, K. A. (2005). Intracellular signaling specificity in response to uniaxial vs. multiaxial stretch: implications for mechanotransduction. *Am. J. Physiol. Cell Physiol.* 288, C185–C194. doi: 10.1152/ajpcell.00207.2004

Jackman, R. W., Floro, J., Yoshimine, R., Zitin, B., Eiampikul, M., El-Jack, K., et al. (2017). Continuous release of tumor-derived factors improves the modeling of cachexia in muscle cell culture. *Front. Physiol.* 8:738. doi: 10.3389/fphys.2017.00738

Kandarian, S. C., and Stevenson, E. J. (2002). Molecular events in skeletal muscle during disuse atrophy. *Exerc. Sport Sci. Rev.* 30, 111–116. doi: 10.1097/00003677-200207000-00004

Kandarian, S. C., Nosacka, R. L., Delitto, A. E., Judge, A. R., Judge, S. M., Ganey, J. D., et al. (2018). Tumour-derived leukaemia inhibitory factor is a major driver of cancer cachexia and morbidity in C26 tumour-bearing mice. *J. Cachexia Sarcopenia Muscle* 9, 1109–1120. doi: 10.1002/jcsm.12346

Kumar, A., Chaudhry, I., Reid, M. B., and Boriek, A. M. (2002). Distinct signaling pathways are activated in response to mechanical stress applied axially and transversely to skeletal muscle fibers. *J. Biol. Chem.* 277, 46493–46503. doi: 10.1074/jbc.M203654200

Lawson, M. A., and Purslow, P. P. (2000). Differentiation of myoblasts in serum-free media: effects of modified media are cell line-specific. *Cells Tissues Organs* 167, 130–137. doi: 10.1159/000016776

Lecker, S. H., Solomon, V., Mitch, W. E., and Goldberg, A. L. (1999). Muscle protein breakdown and the critical role of the ubiquitin-proteasome pathway in normal and disease states. *J. Nutr.* 129(Suppl. 1), 227S–237S. doi: 10.1093/jn/129.1.227S

Lessard, S. J., MacDonald, T. L., Pathak, P., Han, M. S., Coffey, V. G., Edge, J., et al. (2018). JNK regulates muscle remodeling via myostatin/SMAD inhibition. *Nat. Commun.* 9:3030.

Li, S., Czubryt, M. P., McAnally, J., Bassel-Duby, R., Richardson, J. A., Wiebel, F. F., et al. (2005). Requirement for serum response factor for skeletal muscle growth and maturation revealed by tissue-specific gene deletion in mice. *Proc. Natl. Acad. Sci. U.S.A.* 102, 1082–1087. doi: 10.1073/pnas.0409103102

Lin, S. S., and Liu, Y. W. (2019). Mechanical stretch induces mTOR recruitment and activation at the phosphatidic acid-enriched macropinosome in muscle cell. *Front. Cell Dev. Biol.* 7:78. doi: 10.3389/fcell.2019.00078

Liu, D., Qiao, X., Ge, Z., Shang, Y., Li, Y., Wang, W., et al. (2019). IMB0901 inhibits muscle atrophy induced by cancer cachexia through MSTN signaling pathway. *Skeletal Muscle* 9:8. doi: 10.1186/s13395-019-0193-2

Livak, K. J., and Schmittgen, T. D. (2001). Analysis of relative gene expression data using real-time quantitative PCR and the 2− ΔΔCT method. *Methods* 25, 402–408. doi: 10.1006/meth.2001.1262

Martineau, L. C., and Gardiner, P. F. (2002). Skeletal muscle is sensitive to the tension–time integral but not to the rate of change of tension, as assessed by mechanically induced signaling. *J. Biomech.* 35, 657–663. doi: 10.1016/s0021-9290(01)00249-4

Mieulet, V., Roceri, M., Espeillac, C., Sotiropoulos, A., Ohanna, M., Oorschot, V., et al. (2007). S6 kinase inactivation impairs growth and translational target phosphorylation in muscle cells maintaining proper regulation of protein turnover. *Am. J. Physiol. Cell Physiol.* 293, C712–C722. doi: 10.1152/ajpcell.00499.2006

Miller, J. B., and Stockdale, F. E. (1986). Developmental origins of skeletal muscle fibers: clonal analysis of myogenic cell lineages based on expression of fast and slow myosin heavy chains. *Proc. Natl. Acad. Sci. U.S.A.* 83, 3860–3864. doi: 10.1073/pnas.83.11.3860

Mizushima, N., and Yoshimori, T. (2007). How to interpret LC3 immunoblotting. *Autophagy* 3, 542–545. doi: 10.4161/auto.4600

Moustogiannis, A., Philippou, A., Zevolis, E., Taso, O., Chatzigeorgiou, A., and Koutsilieris, M. (2020). Characterization of optimal strain, frequency and duration of mechanical loading on skeletal myotubes' Biological Responses. *In Vivo* 34, 1779–1788. doi: 10.21873/invivo.11972

Mulder, S. E., Dasgupta, A., King, R. J., Abrego, J., Attri, K. S., Murthy, D., et al. (2020). JNK signaling contributes to skeletal muscle wasting and protein turnover in pancreatic cancer cachexia. *Cancer Lett.* 491, 70–77. doi: 10.1016/j.canlet.2020.07.025

Ostrovidov, S., Hosseini, V., Ahadian, S., Fujie, T., Parthiban, S. P., Ramalingam, M., et al. (2014). Skeletal muscle tissue engineering: methods to form skeletal myotubes and their applications. *Tissue Eng. Part B Rev.* 20, 403–436. doi: 10.1089/ten.teb.2013.0534

Patel, H. J., and Patel, B. M. (2017). TNF-alpha and cancer cachexia: molecular insights and clinical implications. *Life Sci.* 170, 56–63. doi: 10.1016/j.lfs.2016.11.033

Penna, F., Costamagna, D., Pin, F., Camperi, A., Fanzani, A., Chiarpotto, E. M., et al. (2013). Autophagic degradation contributes to muscle wasting in cancer cachexia. *Am. J. Pathol.* 182, 1367–1378. doi: 10.1016/j.ajpath.2012.12.023

Pereira, A. M., Tudor, C., Kanger, J. S., Subramaniam, V., and Martin-Blanco, E. (2011). Integrin-dependent activation of the JNK signaling pathway by mechanical stress. *PLoS One* 6:e26182. doi: 10.1371/journal.pone.0026182

Pettersen, K., Andersen, S., Degen, S., Tadini, V., Grosjean, J., Hatakeyama, S., et al. (2017). Cancer cachexia associates with a systemic autophagy-inducing activity mimicked by cancer cell-derived IL-6 trans-signaling. *Sci. Rep.* 7:2046.

Piasecka, A., Sekrecki, M., Szczesniak, M. W., and Sobczak, K. (2021). MEF2C shapes the microtranscriptome during differentiation of skeletal muscles. *Sci. Rep.* 11:3476. doi: 10.1038/s41598-021-82706-2

Pigna, E., Berardi, E., Aulino, P., Rizzuto, E., Zampieri, S., Carraro, U., et al. (2016). Aerobic exercise and pharmacological treatments counteract cachexia by modulating autophagy in colon cancer. *Sci. Rep.* 6:26991. doi: 10.1038/srep26991

Pin, F., Barreto, R., Kitase, Y., Mitra, S., Erne, C. E., Novinger, L. J., et al. (2018). Growth of ovarian cancer xenografts causes loss of muscle and bone mass: a new model for the study of cancer cachexia. *J. Cachexia Sarcopenia Muscle* 9, 685–700. doi: 10.1002/jcsm.12311

Potthoff, M. J., Arnold, M. A., McAnally, J., Richardson, J. A., Bassel-Duby, R., and Olson, E. N. (2007). Regulation of skeletal muscle sarcomere integrity and postnatal muscle function by Mef2c. *Mol. Cell. Biol.* 27, 8143–8151. doi: 10.1128/MCB.01187-07

Puppa, M. J., Gao, S., Narsale, A. A., and Carson, J. A. (2014). Skeletal muscle glycoprotein 130's role in Lewis lung carcinoma-induced cachexia. *FASEB J.* 28, 998–1009. doi: 10.1096/fj.13-240580

Roberts, B., Frye, G., Ahn, B., Ferreira, L., and Judge, A. (2013). Cancer cachexia decreases specific force and accelerates fatigue in limb muscle. *Biochem. Biophys. Res. Commun.* 435, 488–492. doi: 10.1016/j.bbrc.2013.05.018

Rom, O., and Reznick, A. Z. (2016). The role of E3 ubiquitin-ligases MuRF-1 and MAFbx in loss of skeletal muscle mass. *Free Radic. Biol. Med.* 98, 218–230. doi: 10.1016/j.freeradbiomed.2015.12.031

Schiaffino, S., and Reggiani, C. (1994). Myosin isoforms in mammalian skeletal muscle. *J. Appl. Physiol. (1985)* 77, 493–501. doi: 10.1152/jappl.1994.77.2.493

Schiaffino, S., Dyar, K. A., Ciciliot, S., Blaauw, B., and Sandri, M. (2013). Mechanisms regulating skeletal muscle growth and atrophy. *FEBS J.* 280, 4294–4314. doi: 10.1111/febs.12253

Schmidt, M., Poser, C., and von Maltzahn, J. (2020). Wnt7a counteracts cancer cachexia. *Mol. Ther. Oncolytics* 16, 134–146. doi: 10.1016/j.omto.2019.12.011

Seto, D. N., Kandarian, S. C., and Jackman, R. W. (2015). A key role for leukemia inhibitory factor in C26 cancer cachexia. *J. Biol. Chem.* 290, 19976–19986. doi: 10.1074/jbc.m115.638411

Shum, A. M., Mahendradatta, T., Taylor, R. J., Painter, A. B., Moore, M. M., Tsoli, M., et al. (2012). Disruption of MEF2C signaling and loss of sarcomeric and mitochondrial integrity in cancer-induced skeletal muscle wasting. *Aging (Albany NY)* 4, 133–143. doi: 10.18632/aging.100436

Silberstein, L., Webster, S. G., Travis, M., and Blau, H. M. (1986). Developmental progression of myosin gene expression in cultured muscle cells. *Cell* 46, 1075–1081. doi: 10.1016/0092-8674(86)90707-5

Silva, K. A., Dong, J., Dong, Y., Dong, Y., Schor, N., Tweardy, D. J., et al. (2015). Inhibition of Stat3 activation suppresses caspase-3 and the ubiquitin-proteasome system, leading to preservation of muscle mass in cancer cachexia. *J. Biol. Chem.* 290, 11177–11187. doi: 10.1074/jbc.M115.641514

Sin, T. K., Zhang, G., Zhang, Z., Gao, S., Li, M., and Li, Y. P. (2019). Cancer takes a toll on skeletal muscle by releasing heat shock proteins-an emerging mechanism of cancer-induced cachexia. *Cancers (Basel)* 11:1272. doi: 10.3390/cancers11091272

Sparrow, J. C., Nowak, K. J., Durling, H. J., Beggs, A. H., Wallgren-Pettersson, C., Romero, N., et al. (2003). Muscle disease caused by mutations in the skeletal muscle alpha-actin gene (ACTA1). *Neuromuscul. Disord.* 13, 519–531. doi: 10.1016/s0960-8966(03)00101-9

Swoap, S. J., Hunter, R. B., Stevenson, E. J., Felton, H. M., Kansagra, N. V., Lang, J. M., et al. (2000). The calcineurin-NFAT pathway and muscle fiber-type gene expression. *Am. J. Physiol. Cell Physiol.* 279, C915–C924. doi: 10.1152/ajpcell.2000.279.4.C915

Toth, M. J., Miller, M. S., Callahan, D. M., Sweeny, A. P., Nunez, I., Grunberg, S. M., et al. (2013). Molecular mechanisms underlying skeletal muscle weakness in human cancer: reduced myosin-actin cross-bridge formation and kinetics. *J. Appl. Physiol. (1985)* 114, 858–868. doi: 10.1152/japplphysiol.01474.2012

van der Flier, A., Kuikman, I., Baudoin, C., van der Neut, R., and Sonnenberg, A. (1995). A novel β1 integrin isoform produced by alternative splicing: unique expression in cardiac and skeletal muscle. *FEBS Lett.* 369, 340–344. doi: 10.1016/0014-5793(95)00814-p

Vandenburgh, H. H., and Karlisch, P. (1989). Longitudinal growth of skeletal myotubes in vitro in a new horizontal mechanical cell stimulator. *In Vitro Cell. Dev. Biol.* 25, 607–616. doi: 10.1007/BF02623630

Vandenburgh, H., and Kaufman, S. (1979). In vitro model for stretch-induced hypertrophy of skeletal muscle. *Science* 203, 265–268. doi: 10.1126/science.569901

VanderVeen, B. N., Hardee, J. P., Fix, D. K., and Carson, J. A. (2018). Skeletal muscle function during the progression of cancer cachexia in the male ApcMin/+ mouse. *J. Appl. Physiol.* 124, 684–695. doi: 10.1152/japplphysiol.00897.2017

von Walden, F., Liu, C., Aurigemma, N., and Nader, G. A. (2016). mTOR signaling regulates myotube hypertrophy by modulating protein synthesis, rDNA transcription, and chromatin remodeling. *Am. J. Physiol. Cell Physiol.* 311, C663–C672. doi: 10.1152/ajpcell.00144.2016

Wang, H., Niu, M., Song, S., Su, Z., Wei, L., Li, L., et al. (2021). Inhibition of HSP90 reversed STAT3 mediated muscle wasting induced by cancer cachexia. *BioRxiv* [preprint] doi: 10.1101/2021.01.27.428420

Wang, Y., Song, J., Liu, X., Liu, J., Zhang, Q., Yan, X., et al. (2020). Multiple effects of mechanical stretch on myogenic progenitor cells. *Stem Cells Dev.* 29, 336–352. doi: 10.1089/scd.2019.0286

Weiss, A., McDonough, D., Wertman, B., Acakpo-Satchivi, L., Montgomery, K., Kucherlapati, R., et al. (1999). Organization of human and mouse skeletal myosin heavy chain gene clusters is highly conserved. *Proc. Natl. Acad. Sci. U.S.A.* 96, 2958–2963. doi: 10.1073/pnas.96.6.2958

White, J. P., Baltgalvis, K. A., Sato, S., Wilson, L. B., and Carson, J. A. (2009). Effect of nandrolone decanoate administration on recovery from bupivacaine-induced muscle injury. *J. Appl. Physiol. (1985)* 107, 1420–1430. doi: 10.1152/japplphysiol.00668.2009

Xu, M., Chen, X., Huang, Z., Chen, D., Yu, B., Chen, H., et al. (2018). MicroRNA-139-5p suppresses myosin heavy chain I and IIa expression via inhibition of the calcineurin/NFAT signaling pathway. *Biochem. Biophys. Res. Commun.* 500, 930–936. doi: 10.1016/j.bbrc.2018.04.202

Yamada, T., Ashida, Y., Tatebayashi, D., Abe, M., and Himori, K. (2020). Cancer cachexia induces preferential skeletal muscle myosin loss when combined with denervation. *Front. Physiol.* 11:445.

You, J. S., Frey, J. W., and Hornberger, T. A. (2012). Mechanical stimulation induces mTOR signaling via an ERK-independent mechanism: implications for a direct activation of mTOR by phosphatidic acid. *PLoS One* 7:e47258. doi: 10.1371/journal.pone.0047258

Zhan, M., Jin, B., Chen, S. E., Reecy, J. M., and Li, Y. P. (2007). TACE release of TNF-alpha mediates mechanotransduction-induced activation of p38 MAPK and myogenesis. *J. Cell Sci.* 120(Pt 4), 692–701. doi: 10.1242/jcs.03372

Zhang, G., Liu, Z., Ding, H., Zhou, Y., Doan, H. A., Sin, K. W. T., et al. (2017). Tumor induces muscle wasting in mice through releasing extracellular Hsp70 and Hsp90. *Nat. Commun.* 8:589. doi: 10.1038/s41467-017-00726-x

Zhong, X., Pons, M., Poirier, C., Jiang, Y., Liu, J., Sandusky, G. E., et al. (2019). The systemic activin response to pancreatic cancer: implications for effective cancer cachexia therapy. *J. Cachexia Sarcopenia Muscle* 10, 1083–1101. doi: 10.1002/jcsm.12461

Zimmers, T. A., Fishel, M. L., and Bonetto, A. (2016). STAT3 in the systemic inflammation of cancer cachexia. *Semin. Cell Dev. Biol.* 54, 28–41. doi: 10.1016/j.semcdb.2016.02.009

Zöllner, A. M., Abilez, O. J., Böl, M., and Kuhl, E. (2012). Stretching skeletal muscle: chronic muscle lengthening through sarcomerogenesis. *PLoS One* 7:e45661. doi: 10.1371/journal.pone.0045661

Conflict of Interest: The authors declare that the research was conducted in the absence of any commercial or financial relationships that could be construed as a potential conflict of interest.

Publisher's Note: All claims expressed in this article are solely those of the authors and do not necessarily represent those of their affiliated organizations, or those of the publisher, the editors and the reviewers. Any product that may be evaluated in this article, or claim that may be made by its manufacturer, is not guaranteed or endorsed by the publisher.

frontiers in Cell and Developmental Biology

REVIEW
published: 14 September 2021
doi: 10.3389/fcell.2021.719643

Skeletal Muscle Deconditioning in Breast Cancer Patients Undergoing Chemotherapy: Current Knowledge and Insights From Other Cancers

Joris Mallard[1,2,3], *Elyse Hucteau*[1,2,3], *Thomas J. Hureau*[2,3] *and Allan F. Pagano*[2,3]*

[1] *Institut de Cancérologie Strasbourg Europe (ICANS), Strasbourg, France,* [2] *Centre de Recherche en Biomédecine de Strasbourg (CRBS), Fédération de Médecine Translationnelle, UR 3072, Université de Strasbourg, Strasbourg, France,* [3] *Faculté des Sciences du Sport, Centre Européen d'Enseignement de Recherche et d'Innovation en Physiologie de l'Exercice (CEERIPE), Université de Strasbourg, Strasbourg, France*

OPEN ACCESS

Edited by:
Yann Simon Gallot, University of Évry Val d'Essonne, France

Reviewed by:
Paola Costelli, University of Turin, Italy
Bert Blaauw, University of Padua, Italy
Amélie Rébillard, Laboratoire des Sciences du Mouvement, du Sport et de la Santé (M2S), France

***Correspondence:**
Allan F. Pagano
allan.pagano@unistra.fr; pagano.allan@gmail.com

Specialty section:
This article was submitted to Signaling, a section of the journal Frontiers in Cell and Developmental Biology

Received: *02 June 2021*
Accepted: *10 August 2021*
Published: *14 September 2021*

Citation:
Mallard J, Hucteau E, Hureau TJ and Pagano AF (2021) Skeletal Muscle Deconditioning in Breast Cancer Patients Undergoing Chemotherapy: Current Knowledge and Insights From Other Cancers. Front. Cell Dev. Biol. 9:719643. doi: 10.3389/fcell.2021.719643

Breast cancer represents the most commonly diagnosed cancer while neoadjuvant and adjuvant chemotherapies are extensively used in order to reduce tumor development and improve disease-free survival. However, chemotherapy also leads to severe off-target side-effects resulting, together with the tumor itself, in major skeletal muscle deconditioning. This review first focuses on recent advances in both macroscopic changes and cellular mechanisms implicated in skeletal muscle deconditioning of breast cancer patients, particularly as a consequence of the chemotherapy treatment. To date, only six clinical studies used muscle biopsies in breast cancer patients and highlighted several important aspects of muscle deconditioning such as a decrease in muscle fibers cross-sectional area, a dysregulation of protein turnover balance and mitochondrial alterations. However, in comparison with the knowledge accumulated through decades of intensive research with many different animal and human models of muscle atrophy, more studies are necessary to obtain a comprehensive understanding of the cellular processes implicated in breast cancer-mediated muscle deconditioning. This understanding is indeed essential to ultimately lead to the implementation of efficient preventive strategies such as exercise, nutrition or pharmacological treatments. We therefore also discuss potential mechanisms implicated in muscle deconditioning by drawing a parallel with other cancer cachexia models of muscle wasting, both at the pre-clinical and clinical levels.

Keywords: cancer cachexia, muscle atrophy, protein turnover, intermuscular adipose tissue, inflammatory cytokines, mitochondria, oxidative stress, satellite cells

INTRODUCTION

Cancer represents the leading cause of death worldwide and a substantial barrier to increasing life expectancy. Among the different cancer sites, breast cancer is the most commonly diagnosed cancer, with 11.7% of total cases and 6.9% of cancer deaths (Sung et al., 2021). Effective therapy of breast cancer requires a multidisciplinary approach including surgery, radiotherapy, neoadjuvant and/or adjuvant therapies. Currently, neoadjuvant and adjuvant chemotherapies are extensively

used in breast cancer patients to reduce tumor development and improve disease-free survival, but also leads to severe off-target side-effects (Maughan et al., 2010; Redden and Fuhrman, 2013; Fisusi and Akala, 2019; Schirrmacher, 2019). Among these treatment-related side effects, both pre-clinical and clinical studies highlighted that chemotherapeutic agents result in major skeletal muscle deconditioning and, together with exacerbated fatigue, are part of a vicious cycle which negatively impacts their quality of life (Berger et al., 2015; Caan et al., 2018; Aleixo et al., 2019; Cespedes Feliciano et al., 2019; Hiensch et al., 2019; Mallard et al., 2020). Although breast cancer represents the most deadly female cancer, 5-year survival rate is over 90% (National Cancer Institute, Surveillance, Epidemiology, and End Result program, 2019) emphasizing the critical need to fight long-lasting effects observed in survivors such as skeletal muscle deconditioning.

Skeletal muscle deconditioning is a direct consequence of global muscle homeostasis perturbation, leading to both structural and functional alterations that will translate into a decrease in muscle mass and/or force as well as an increase in fatigability (Chopard et al., 2009; Baldwin et al., 2013; Brioche et al., 2016; Cruz-Jentoft et al., 2019; Arc-Chagnaud et al., 2020). In the context of cancer patients, skeletal muscle atrophy represents a major characteristic of cachexia, which can be defined as an ongoing loss of skeletal muscle mass that cannot be fully reversed with nutrition and leading to functional alterations (Fearon et al., 2011). It is now well admitted that cancer cachexia is one of the most life-threatening aspects of cancer. Indeed, it has been shown that cachexia substantially increases sedentary behavior, functional impairment, loss of autonomy, quality of life degradation, surgical risks and overall adverse effects of chemotherapy (Fouladiun et al., 2007; Fearon et al., 2011; Roberts et al., 2013; Wallengren et al., 2013; Mason et al., 2016; Rutten et al., 2016; Schwarz et al., 2017; Baracos et al., 2018; Daly et al., 2018). Importantly, cachexia is also strongly correlated with a decrease in cancer patients survival and is actually the leading cause of death in cancer (Warren, 1932; Martin et al., 2015; Deluche et al., 2018; Huh et al., 2020). Thus, the management of skeletal muscle deconditioning during cancer and its treatment represents a major challenge for healthcare, particularly in breast cancer patients, considering both the high incidence of new cases (Sung et al., 2021) and the prevalence of cancer cachexia (∼25%) in breast cancer patients (Baracos et al., 2018). Even if, compared to other cancers, breast cancer does not display the highest prevalence of cachexia, it is important to note that cachexia diagnosis is based on global weight loss (Fearon et al., 2011), and not only muscle mass loss, which likely led to an underestimation of cachexia prevalence in clinical practice (Roeland et al., 2017).

To date, the cellular mechanisms of skeletal muscle deconditioning are of great importance and have been extensively reviewed in healthy people, elderly as well as in relation with many chronic diseases (Sandri, 2008; Chopard et al., 2009; Bodine, 2013; Bonaldo and Sandri, 2013; Schiaffino et al., 2013; Argilés et al., 2014; Bowen et al., 2015; Brioche et al., 2016; Petruzzelli and Wagner, 2016; Baracos et al., 2018; Larsson et al., 2019; Dolly et al., 2020; Silva et al., 2020; Vainshtein and Sandri, 2020; Sartori et al., 2021). However, in comparison with the knowledge accumulated through decades of intensive research with many different animal and human models, a comprehensive understanding of the cellular processes implicated in breast cancer-mediated muscle deconditioning is still needed in order to develop efficient strategies to counteract it.

This review focuses on recent advances in both macroscopic changes and cellular mechanisms implicated in skeletal muscle deconditioning of breast cancer patients, specifically as a consequence of chemotherapy treatment. This review also aims to highlight other potential mechanisms by drawing a parallel with cancer cachexia models of muscle wasting, both at the pre-clinical and clinical levels.

CHEMOTHERAPY-INDUCED SKELETAL MUSCLE MACROSCOPIC ALTERATIONS IN BREAST CANCER PATIENTS

Two families of chemotherapeutic agents are commonly used in clinical practice for breast cancer patients: anthracyclines (i.e., doxorubicin or epirubicin) leading to DNA damage, and taxanes (i.e., docetaxel or paclitaxel) acting as cytoskeletal disruptors (Shah and Gradishar, 2018; Willson et al., 2019). Importantly, non-hormone-dependent (i.e., triple-negative or HER2-positive) breast cancer treatment also includes immunotherapy, a promising new field in breast cancer therapy (Emens, 2018; Keenan and Tolaney, 2020). If immunotherapy has been identified to induce severe cardiotoxicity (Behr et al., 2001; Rochette et al., 2015; Bregni et al., 2016; Varricchi et al., 2018), there is no study to date with a focus on skeletal muscle. On the other hand, chemotherapeutic agents are recognized to contribute to skeletal muscle deconditioning, resulting in an altered quality of life, increased treatment-related toxicity, and to an increased mortality risk (Rier et al., 2016; Shachar et al., 2017; Deluche et al., 2018; Trestini et al., 2018; Cespedes Feliciano et al., 2019; Huh et al., 2020). To date, several skeletal muscle structural and functional alterations were identified (loss of muscle mass and force, altered quality) with severe consequences on exercise tolerance.

Muscle Mass

Although it is widely accepted that chemotherapy induces skeletal muscle loss in breast cancer patients, very few studies clearly demonstrated it. Indeed, by excluding all non-longitudinal studies (i.e., with no pre *vs*. post-chemotherapy assessments) and lean body mass measurements (i.e., with no assessment of muscle mass in isolation), only two studies emerged (Rossi et al., 2020; Wiederin et al., 2020). Both studies demonstrated a decrease in pectoralis muscle area after chemotherapy. Wiederin et al. (2020) found a 10% reduction in muscle mass using magnetic resonance imaging in a cohort of breast cancer (N = 221), sarcoma (N = 115) and lymphoma (N = 216) female patients. In breast cancer only, Rossi et al. (2020) found a 15% reduction in muscle mass by using CT Scan. Surprisingly, we were unable to find any other longitudinal study on whole-body or locomotor muscle mass for breast-cancer patients undergoing chemotherapy. As a loss of skeletal muscle mass is strongly

associated with poor functional outcomes (Fearon et al., 2011; Baracos et al., 2018; Cruz-Jentoft et al., 2019; Aleixo et al., 2020a) and chemotherapy efficacy (Caan et al., 2018; Lee et al., 2021) in breast cancer patients, further studies are needed to better characterize the loss of muscle mass in order to counteract it effectively thereafter.

Muscle Force

On the other hand, the impact of chemotherapy treatment on muscle force is more documented. Numerous studies, with various protocols of force evaluation (handgrip, isometric knee extension, mid-thigh pull, and shoulder strength, etc.), found inconsistent results on chemotherapy-treated breast cancer patients. Indeed, some longitudinal studies (Schmidt et al., 2015; Ramos da Silva et al., 2021) documented no change in isometric muscle force in both lower limbs (quadriceps femoris muscle) and upper limbs (latissimus dorsi, pectoralis, and handgrip muscles), while others found a significant reduction from −4 to −17% in handgrip or knee extensors muscle force (van Waart et al., 2015; Gadéa et al., 2018; Mijwel et al., 2018a; CeŠeiko et al., 2020; Toth et al., 2020). Discrepancies in study protocols (study duration, measurements timepoints, and treatments administered) and in the methods of force evaluation (isometric *vs.* isokinetic contractions, different muscle groups investigated) may explain these contrasting results. Other studies also highlighted a decrease in muscle force of breast cancer patients undergoing chemotherapy in comparison with healthy women (Klassen et al., 2017; Marques et al., 2020), supporting the fact that chemotherapeutic agents may affect skeletal muscle force production.

Muscle Quality

There is a growing body of evidence that the loss of muscle strength and power mostly exceeds the loss of muscle mass observed in many diseases or inactivity experiments, emphasizing that a deterioration in muscle quality could explain the loss in force and lead to functional impairments (di Prampero and Narici, 2003; Brioche et al., 2016; Pagano et al., 2018; CeŠeiko et al., 2020; Toth et al., 2020). Muscle quality can be assessed through different techniques, including magnetic resonance imaging, computed tomography or ultrasound echography (Karampinos et al., 2012; Addison et al., 2014; Aubrey et al., 2014; Khan et al., 2019; Stock and Thompson, 2021), that allows the detection and quantification of abnormalities in skeletal muscle composition. Among these abnormalities, intermuscular adipose tissue (IMAT) accumulation is particularly of interest. Indeed, these muscle fatty infiltrations (i.e., adipocytes located between muscle fibers and muscle groups), also referred as myosteatosis, are known to be associated with inactivity (Manini et al., 2007; Leskinen et al., 2009; Tuttle et al., 2011; Pagano et al., 2018), pathologies (Gorgey and Dudley, 2007; Wren et al., 2008; Karampinos et al., 2012; Gallagher et al., 2014; Uezumi et al., 2014b) and have been particularly investigated in sarcopenia (Goodpaster et al., 2000, 2001; Song et al., 2004; Marcus et al., 2010; Brioche et al., 2016). An accumulation of IMAT is closely linked to poor muscle quality and therefore muscle dysfunction (Jubrias et al., 1997; Visser et al., 2002, 2005; Delmonico et al., 2009; Marcus et al., 2010; Murphy et al., 2011; Tuttle et al., 2011; Beavers et al., 2013). In the specific context of cachexia, a reduction in muscle quality has been observed in breast cancer patients treated with chemotherapeutic agents. In a longitudinal study, metastatic breast cancer patients showed an altered muscle attenuation after taxane-based chemotherapy, indicating a decrease in muscle quality (Rier et al., 2018). In a cross-sectional study, breast cancer survivors who received anthracyclines were compared to control subjects and a clear increase in thigh IMAT content (∼30%) have been found and was interestingly correlated with an impaired cardiorespiratory fitness (Beaudry et al., 2020). Another cross sectional study highlighted an increased IMAT content in cancer patients (including breast-cancer patients) when compared to non-cancer individuals (Reding et al., 2019) and also showed a good correlation with the development of exercise intolerance.

Exercise Tolerance

As a consequence of the abovementioned skeletal muscle alterations, combined with a well-known cardiotoxicity (Bird and Swain, 2008; Kazemi-Bajestani et al., 2014; Nicolazzi et al., 2018; Varricchi et al., 2018; Jerusalem et al., 2019), chemotherapy is strongly impacting exercise tolerance. In clinical setting, the six-minute walk test (6MWT) represents a reference test reflecting exercise tolerance and is widely used in various pathologic populations (Enright, 2003; Agarwala and Salzman, 2020), including cancer patients (Galiano-Castillo et al., 2016; Wesolowski et al., 2020). A recent systematic-review reported, through the analysis of 21 original studies using the 6MWT, that 1,084 breast cancer patients (including both patients under treatment and survivors) showed a 24% reduction in performance compared to 878 healthy people (But-Hadzic et al., 2021). Aside the 6MWT, widely used as an indirect measurement of cardiorespiratory fitness, the assessment of the maximal oxygen consumption ($\dot{V}O_{2max}$) represents the gold standard measurement of exercise tolerance (Astrand and Saltin, 1961; Schumacher et al., 2019). Interestingly, consistent results between the 6MWT and $\dot{V}O_{2max}$ were found in breast cancer patients. Indeed, another systematic review reported, from the analysis of 27 clinical trials, a significant 25% reduction in $\dot{V}O_{2max}$ after chemotherapy treatment compared to healthy sedentary women (Peel et al., 2014). This cardiorespiratory deconditioning seems to strengthen the development of cancer-related fatigue and particularly physical fatigue (Neil et al., 2013), with consequences on exercise intolerance. Indeed, physical fatigue, assessed by the reduction in force during the repetition of maximal voluntary contractions, has been found to be exacerbated in breast cancer patients undergoing chemotherapy treatment compared to healthy individuals (Klassen et al., 2017), negatively impacting their exercise tolerance. Together with the decrease of skeletal muscle mass, a reduction in exercise capacity is also strongly associated with higher risk of adverse outcomes such as treatment-induced toxicity, mortality or functional impairment (Jones et al., 2012; Peel et al., 2014; Foulkes et al., 2019; Yu et al., 2020).

CELLULAR MECHANISMS OF SKELETAL MUSCLE DECONDITIONING IN BREAST CANCER PATIENTS: WHAT DO WE KNOW?

Skeletal muscle biopsy (e.g., using Bergström needle) is the only technique allowing full investigation of the cellular mechanisms of muscle deconditioning (Bergstrom, 1975; Tarnopolsky et al., 2011). To date, only six clinical studies, published in seven different publications, used muscle biopsies in early breast cancer patients (stage I–III) to decipher mechanisms of muscle deconditioning (Lønbro et al., 2017; Bohlen et al., 2018; Guigni et al., 2018; Mijwel et al., 2018b; Møller et al., 2019; Toth et al., 2020; Wilson et al., 2020). Altogether, these studies highlighted several important aspects of muscle deconditioning detailed below and outlined in **Figure 1**.

Decrease in Skeletal Muscle Fibers Cross-Sectional Area and Phenotypic Shift

Muscle fibers CSA is one of the most substantial measurement of muscle deconditioning at the cellular level. Recently, Mijwel et al. (2018b) and Guigni et al. (2018) showed a clear decrease in both type I and type II vastus lateralis muscle fibers CSA after anthracycline-cyclophosphamide and taxane-based chemotherapy treatment. Interestingly, Mijwel et al. (2018b) demonstrated it through a longitudinal study while Guigni et al. (2018) have done it with a cross-sectional study design, by comparing breast cancer patients to healthy individuals. To highlight the substantial magnitude of the decrease in overall muscle fibers CSA during chemotherapy in breast cancer patients, it should be noted that this decrease was comparable to the considerable effect of 60 years of healthy aging (Lexell et al., 1988). If comparing muscle CSA of breast cancer patients under chemotherapy for 4 months with 60 years of aging is insightful to emphasize the profound impact of chemotherapy on the skeletal muscle apparatus, it is not fully accurate as other mechanisms are involved and interact with CSA differently in cancer *vs.* aging. Two other longitudinal studies found no reduction in muscle fibers vastus lateralis CSA during chemotherapy including taxanes, cyclophosphamide, doxorubicin, and carboplatin (Lønbro et al., 2017; Toth et al., 2020). However, in these studies, the second muscle biopsy was performed after ∼5 weeks and might explain the lack of atrophy as the effects of chemotherapeutic agents on skeletal muscle are strongly suggested to be cumulative. It is important to note that *in vitro* and *in vivo* studies also demonstrated the negative impact of both chemotherapeutic agents (McLoon et al., 1998; Gouspillou et al., 2015; Min et al., 2015; Barreto et al., 2016; Guigni et al., 2018) and breast cancer-bearing mice models (Hesse et al., 2019; Wang et al., 2021) on skeletal muscle structure, strengthening the results obtained in clinical studies.

Concerning fiber type distribution, only Mijwel et al. (2018b) reported significant changes, with a reduced proportion of type I muscle fibers after chemotherapy treatment. This potential type I to type II phenotypic shift is classically found in muscle disuse models (Baldwin et al., 2013) while the opposite is observed with aging (Larsson et al., 2019). This suggests that muscle deconditioning in breast cancer patients might also be driven by a decrease in overall physical activity during their treatment (De Groef et al., 2018; Gadéa et al., 2018; Yildiz Kabak et al., 2020), a well-known trigger of protein turnover dysregulation.

Protein Turnover

If a large number of excellent reviews have already documented the critical role of protein turnover homeostasis in the mechanisms related to skeletal muscle atrophy (Sandri, 2008; Chopard et al., 2009; Bodine, 2013; Bonaldo and Sandri, 2013; Schiaffino et al., 2013; Brioche et al., 2016; Larsson et al., 2019; Vainshtein and Sandri, 2020; Sartori et al., 2021) including in cancer cachexia (Argilés et al., 2014; Bowen et al., 2015; Petruzzelli and Wagner, 2016; Baracos et al., 2018; Dolly et al., 2020; Silva et al., 2020), little is known in the unique context of breast cancer. Indeed, only four studies investigated the mechanisms related to protein turnover homeostasis in breast cancer patients (Bohlen et al., 2018; Mijwel et al., 2018b; Møller et al., 2019; Wilson et al., 2020). Two publications from the same research team showed, through RNAseq analysis on pectoralis muscle, an increased expression of genes related to ubiquitin-mediated proteolysis and a decreased expression of genes related to ribosomes (Bohlen et al., 2018; Wilson et al., 2020). These results potentially indicate an altered protein turnover balance, with a reduced protein synthesis and an increased protein breakdown. Mijwel et al. (2018b) did not find any changes in MuRF1 protein expression (a key E3 ligase implicated in the ubiquitin-proteasome system) after chemotherapy in breast cancer patients, nor concerning the autophagy pathway, with no changes in the protein expression of different key markers implicated in this pathway (i.e., p-Ulk1, LC3B-II/I ratio, beclin-1, all reflecting autophagosome formation). These results could be explained by the "late" time-point of biopsy collection in this study as cellular processes triggering muscle atrophy, particularly those related to protein breakdown, tend to go back to "normal" expression profiles when the muscle atrophy is well established (Ferreira et al., 2008; Hanson et al., 2013; Atherton et al., 2016; Kawanishi et al., 2018). Finally, the study conducted by Møller et al. (2019) also investigated proteins involved in signaling pathways implicated in protein turnover from vastus lateralis muscle. Very surprisingly, they found a decreased protein expression of the E3 Ligases MAFbx and MuRF1 as well as an increase in p62 and phosphorylated-Ulk1 expression (Ser757), suggesting a decreased activity of the ubiquitin proteasome and autophagy systems, respectively. However, it is important to highlight that 9 out of 10 patients included in this study performed the baseline biopsy after at least one cycle of chemotherapy with epirubicin and doxorubicin (Lønbro et al., 2017). Given the aggressiveness of chemotherapy treatments, this is a serious methodological bias that likely altered "baseline" measures, and therefore, conclusions. Another limitation lays in the heterogeneous population of cancer patients investigated (i.e., seven patients with breast-cancer, one patient with head and neck cancer, one patient with rectal cancer,

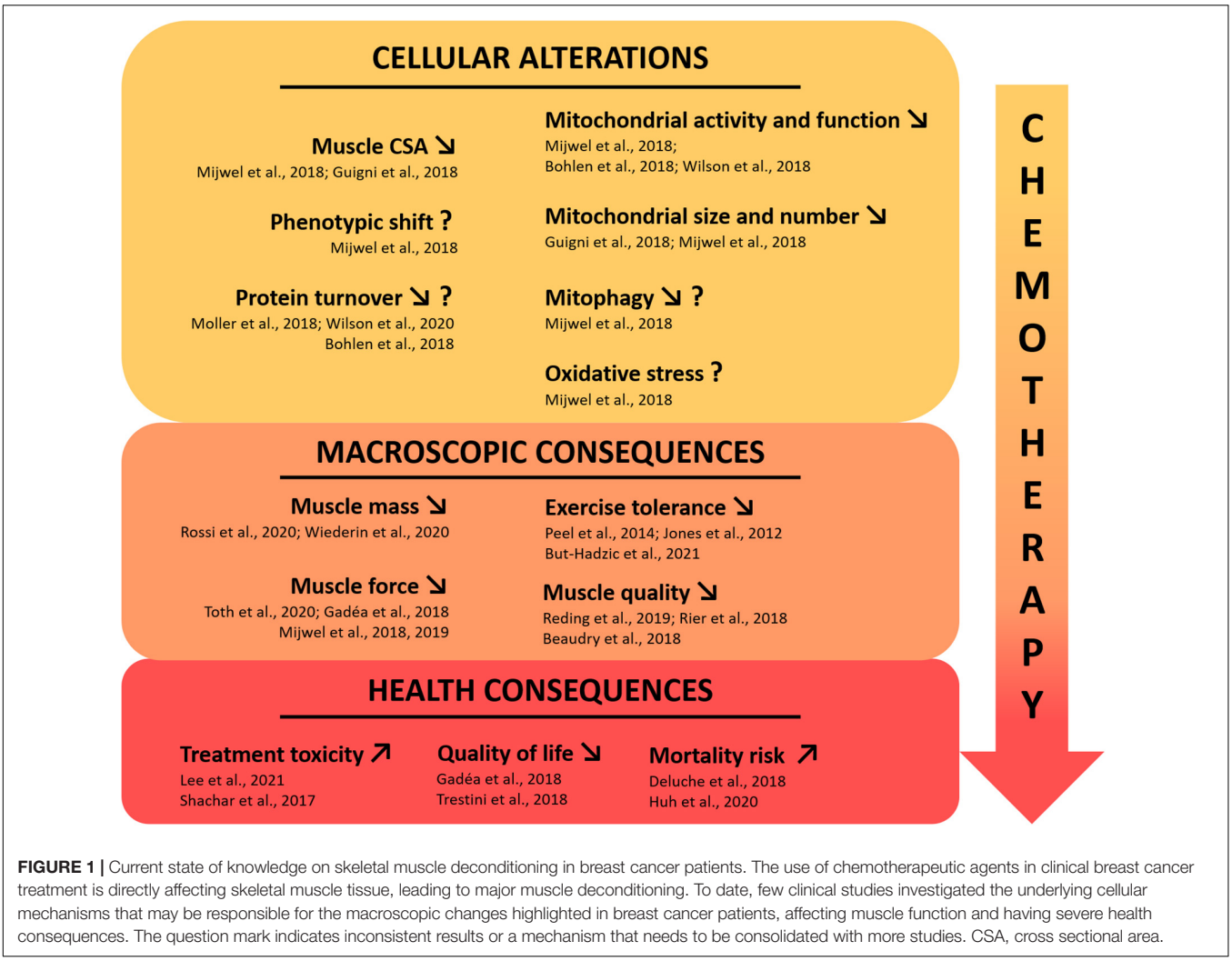

FIGURE 1 | Current state of knowledge on skeletal muscle deconditioning in breast cancer patients. The use of chemotherapeutic agents in clinical breast cancer treatment is directly affecting skeletal muscle tissue, leading to major muscle deconditioning. To date, few clinical studies investigated the underlying cellular mechanisms that may be responsible for the macroscopic changes highlighted in breast cancer patients, affecting muscle function and having severe health consequences. The question mark indicates inconsistent results or a mechanism that needs to be consolidated with more studies. CSA, cross sectional area.

and one patient with sarcoma). To sum up, there are strong discrepancies between studies that investigated pathways of protein synthesis and breakdown in breast cancer patients undergoing chemotherapy. Further studies are needed as the understanding of these processes is critical to counteract the skeletal muscle atrophy outlined above.

Mitochondrial Alterations

Mitochondrial alterations represent, to date, one of the most investigated aspect of muscle deconditioning in breast cancer, especially in response to chemotherapeutic agents. In clinical studies, the RNAseq analysis used by both Bohlen et al. (2018) and Wilson et al. (2020) showed a clear dysregulation of genes implicated in mitochondrial function and oxidative phosphorylation. Interestingly, the authors showed a decrease in multiple genes implicated in the electron transport chain, antioxidant capacity, and altered PPAR signaling (including PGC-1α), emphasizing that mitochondria and overall energy homeostasis may be perturbed in breast cancer patients treated with chemotherapeutic agents. Guigni et al. (2018) confirmed a clear decrease in mitochondrial content and size for breast cancer patients compared to healthy matched controls, in both the intermyofibrillar and subsarcolemmal compartments. The authors concluded that these alterations, due to the mitotoxic effects of antineoplastic drugs, may constitute a possible explanation to the high prevalence of exercise intolerance and fatigue in all cancer's types, including those not typically prone to cachexia such as breast cancer patients. Finally, the longitudinal study of Mijwel et al. (2018b) highlighted a decrease in citrate synthase activity with chemotherapy. The decrease in citrate synthase activity, a marker for mitochondrial quantity (Larsen et al., 2012), is in line with the results of Guigni et al. (2018) and confirms the likely lower mitochondria quantity in breast cancer patients. This study also reports a decreased protein expression of PINK1, an essential protein implicated in the final stages of mitophagy, therefore suggesting a lower mitophagy process in breast cancer patients. In addition, no variation in protein levels of Parkin has been detected in this study, nor those of the autophagy pathway, clearly indicating that mitophagy is not upregulated and that future studies should investigate this mitochondrial quality control pathway. Finally, an increased protein expression of SOD2, an essential antioxidant

enzyme and redox signaling trigger through H_2O_2 production (Zou et al., 2017), was also found. Alone, this result does not permit to raise any conclusion whether it reflects an increase in antioxidant defenses or, at the opposite, a compensation for an increase in oxidative stress (i.e., superoxide anion) linked to the chemotherapeutic treatment. Clearly, future studies with protein expression analysis of oxidative stress and antioxidant pathways as well as enzymes activities are still necessary to understand the potential implication of redox balance in skeletal muscle deconditioning of breast cancer patients.

POTENTIAL OTHER CELLULAR MECHANISMS OF MUSCLE DECONDITIONING IN BREAST CANCER PATIENTS: WHAT CAN WE LEARN FROM OTHER CANCERS?

Based on the knowledge accumulated through decades of intensive research, this part of the review aims to identify potential cellular mechanisms responsible for skeletal muscle deconditioning in breast cancer patients by drawing a parallel with pre-clinical studies and other cancers models of muscle wasting. As summarized in **Figure 2**, we have limited our review to the main and well admitted mechanisms of muscle wasting in cancer; our list is therefore not exhaustive. Among the large variety of studies discussed hereafter, we found few studies related to skeletal muscle plasticity conducted on mouse models of breast cancer while several pre-clinical studies explored the effect of doxorubicin administration, one of the most commonly used chemotherapeutic agents to treat breast cancer patients. This lack of specific investigations indicates a major imbalance in comparison with other cancers and also emphasizes the need to remain cautious with the mechanisms identified thereafter as they mainly stem from the analysis of different cancers and treatments. However, it will provide future directions for researchers willing to investigate specifically the mechanisms of muscle deconditioning in breast cancer.

Protein Turnover

The sensitive balance between protein synthesis and protein breakdown is the major mechanism regulating muscle mass (Chopard et al., 2009; Schiaffino et al., 2013; Bowen et al., 2015; Argilés et al., 2019; Silva et al., 2020; Vainshtein and Sandri, 2020).

Skeletal muscle protein synthesis is mainly promoted by the PI3K-Akt-mTOR pathway and cachexia patients with pancreatic carcinoma or lung cancer demonstrated an altered PI3K-Akt-mTOR signaling (Schmitt et al., 2007; Murton et al., 2017), a result also found in various pre-clinical models (White et al., 2011; Padrão et al., 2013; Gallot et al., 2014; Puppa et al., 2014; Bohnert et al., 2016; Chen M. C. et al., 2016; de Lima Junior et al., 2016; Sun et al., 2016; Chacon-Cabrera et al., 2017; Quan-Jun et al., 2017; Nissinen et al., 2018; Salazar-Degracia et al., 2018). Importantly, both clinical (Bennegård et al., 1984; Emery et al., 1984; Dworzak et al., 1998) and pre-clinical studies (Beck et al., 1991; Smith and Tisdale, 1993; Samuels et al., 2001; Smith et al., 2004; Constantinou et al., 2011; Nissinen et al., 2016, 2018; Toledo et al., 2016; Antoun and Raynard, 2018; Cruz et al., 2019; Costamagna et al., 2020) highlighted a reduction in muscle protein synthesis, emphasizing that a reduction in protein synthesis may explain, at least in part, the muscle deconditioning occurring in cancer patients. Among all these studies, only two worked on rodents treated with doxorubicin and showed a reduced PI3K-Akt-mTOR signaling (de Lima Junior et al., 2016; Nissinen et al., 2016). Moreover, through RNAseq analysis, Wilson et al. (2019) also found an altered skeletal muscle mTOR signaling in breast cancer-bearing mice. These important studies clearly demonstrated that both breast cancer *per se* and the chemotherapeutic agents used in clinical setting to treat it may alter the main protein synthesis pathway in skeletal muscle, possibly leading to altered protein turnover.

On the other hand, protein breakdown includes two major pathways, the ubiquitin-proteasome and autophagy-lysosomal systems (UPS and autophagy, respectively), that are responsible for the degradation of most proteins and organelles in skeletal muscle cells. First, numerous pre-clinical studies observed an increase in skeletal muscle protein breakdown (Beck et al., 1991; Smith and Tisdale, 1993; Temparis et al., 1994; Baracos et al., 1995; Samuels et al., 2001; Smith et al., 2004; Silva et al., 2015; Toledo et al., 2016), demonstrating that a decrease in protein synthesis is not the only mechanism that could explain the loss muscle mass in cancer cachexia. UPS and autophagy pathways have been largely investigated both in clinical and pre-clinical studies. The UPS is almost unanimously found to be increased in cancer patients, particularly the "atrogenes" MAFbx and MuRF1 and the overall ubiquitination profile (Williams et al., 1999; Bossola et al., 2003; DeJong et al., 2005; Khal et al., 2005; Constantinou et al., 2011; Puig-Vilanova et al., 2015; Zhang et al., 2020). Importantly, the increase in UPS activity as well as mRNA/proteins implicated in this pathway is also consistently found in a large number of pre-clinical studies (Baracos et al., 1995; Gomes et al., 2001; Lecker et al., 2004; Acharyya et al., 2005; Khal et al., 2005; Moore-Carrasco et al., 2007; Zhou et al., 2010; Julienne et al., 2012; Padrão et al., 2013; Chacon-Cabrera et al., 2014, 2017; Gallot et al., 2014; Johnston et al., 2015; Silva et al., 2015; Bohnert et al., 2016; Chen M. C. et al., 2016; Hatakeyama et al., 2016; Sun et al., 2016; Toledo et al., 2016; Guo et al., 2017; Damrauer et al., 2018; Pin et al., 2018; Salazar-Degracia et al., 2018; Chen L. et al., 2019; Lee et al., 2019; Liu et al., 2019; Ranjbar et al., 2019; Bae et al., 2020; Huot et al., 2020), strengthening the fact that the UPS plays a major role in the protein breakdown aggravation. Concerning the autophagy system, clinical studies also demonstrated an increase in several important markers such as beclin1, Atg5, or LC3B-II/I ratio (Op den Kamp et al., 2012; Johns et al., 2014; Aversa et al., 2016; Pigna et al., 2016; de Castro et al., 2019; Zhang et al., 2020). Together with pre-clinical studies showing the same results (Penna et al., 2013, 2019a; Chacon-Cabrera et al., 2014; Bohnert et al., 2016; Salazar-Degracia et al., 2016, 2018; Sirago et al., 2017; Ballarò et al., 2019; Ranjbar et al., 2019), autophagy might also play a significant role in the increased protein breakdown of cancer patients. However, it appears of great importance to highlight that the majority of these studies also

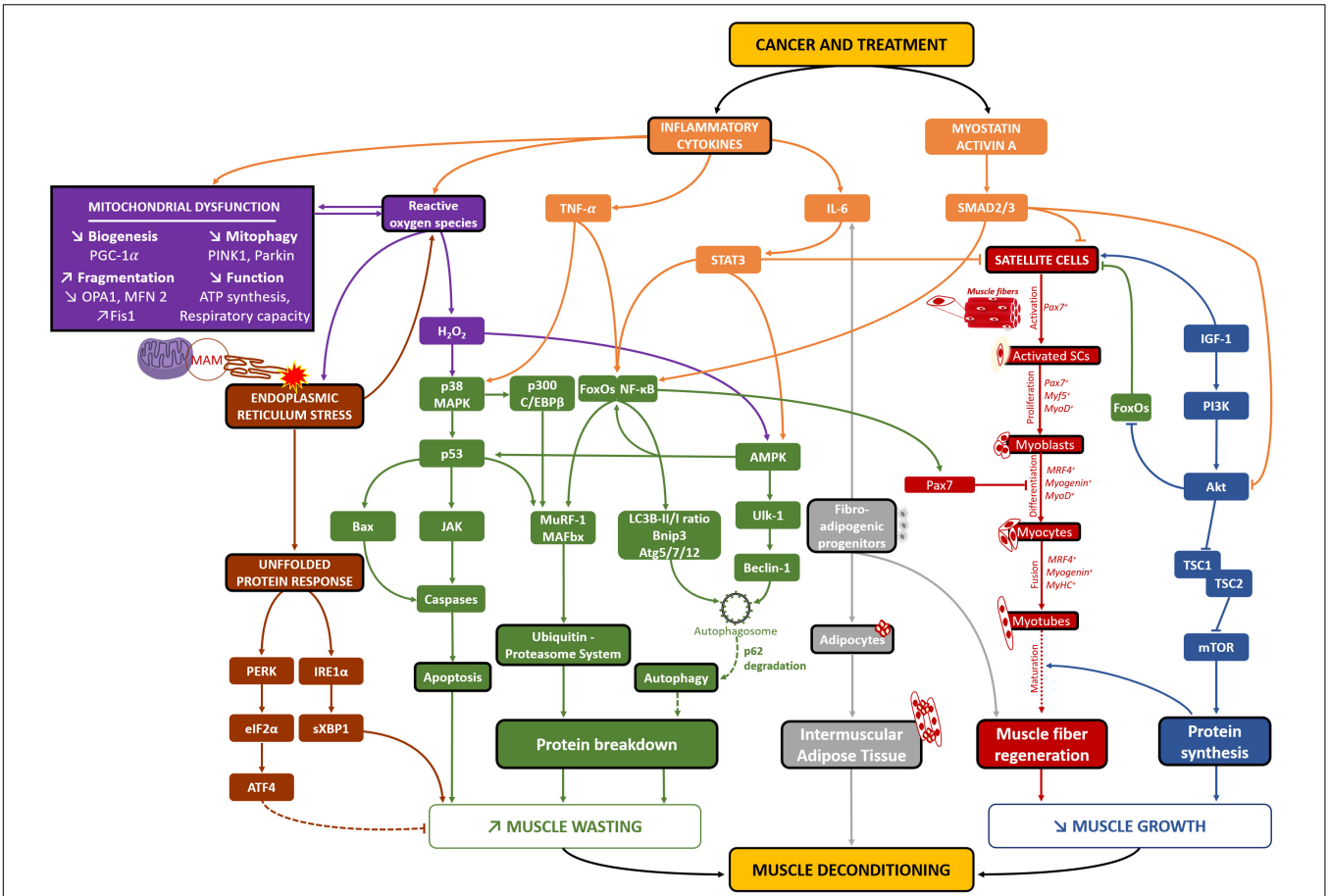

FIGURE 2 | Potential cellular mechanisms of skeletal muscle deconditioning in breast cancer patients. Through the analysis of clinical and pre-clinical studies related to all cancer's types, several different pathways may be implicated in skeletal muscle deconditioning in breast cancer patients. Both the cancer *per se* and its treatment lead to increased levels of inflammatory cytokines and Myostatin/Activin A pathways (in orange), consequently decreasing protein synthesis (in blue) and increasing pathways implicated in protein breakdown (in green). The activation of the autophagy-lysosomal system needs to be elucidated as an increase in autophagosomes formation has been consistently found as well as increased levels of p62, suggesting that lysosome activity might be disrupted in cancer cachexia, leading to no change in autophagy flux (green dotted line). The combination of high levels of inflammatory cytokines, ROS and mitochondrial altered dynamics, biogenesis and function (in purple) would also lead to increased protein breakdown and apoptosis. On the other hand, it would also lead to high levels of endoplasmic reticulum stress, resulting in an increase in the UPR system (in brown) and consequently protein breakdown. The involvement of the PERK/eiF2α/ATF4 pathway, known to be implicated in non-cancer models of muscle atrophy, needs to be clarified, as it might surprisingly be necessary to counteract muscle atrophy in cancer-related models of muscle atrophy (brown dotted line). Moreover, different studies also highlighted a reduction in the number of satellite cells (SCs), their capacity to differentiate and skeletal muscle capacity to regenerate, emphasizing that cancer-related muscle atrophy may also result from muscle altered repair/regrowth (in red). Finally, increased presence of fibro-adipogenic progenitors might also be implicated in muscle deconditioning as they are implicated in both IL-6-mediated muscle atrophy (in non-cancer models of muscle atrophy) and Intermuscular adipose tissue development (in gray). Altogether, these cellular mechanisms might play an important role in breast cancer-related skeletal muscle deconditioning and clearly need to be further investigated through clinical studies using muscle biopsies. MAM, mitochondria-associated ER membranes.

found an increase in p62 mRNA/protein expression, suggesting that if autophagosome formation is certainly increased, lysosome activity might be disrupted in cancer patients, leading to no modifications in autophagy flux (Penna et al., 2014; Klionsky et al., 2021). Furthermore, different studies showed that skeletal muscle protein breakdown is mostly ATP-dependent (i.e., UPS) in pre-clinical models of cancer cachexia (Temparis et al., 1994; Baracos et al., 1995; White et al., 2011), emphasizing again that autophagy might not be implicated or has a minor role in cancer-induced skeletal muscle wasting. As it is well known that the loss of autophagy leads to muscle wasting exacerbation in response to atrophic stimulus (Vainshtein and Sandri, 2020), further studies are needed to elucidate the variations of autophagic flux, whether it is an increase or a decrease, in cancer cachexia.

The FoxO family of transcription factors (FoxO1 and FoxO3 particularly) and NF-κB are known to be essential transcription factors implicated in the regulation of numerous genes of both UPS and autophagy pathways in various models of skeletal muscle atrophy (Vainshtein and Sandri, 2020). These transcription factors have been found to be upregulated in different cancer cachexia models (Cai et al., 2004;

Lecker et al., 2004; White et al., 2011; Op den Kamp et al., 2013; Chacon-Cabrera et al., 2014, 2017; Gallot et al., 2014; Puppa et al., 2014; Chen M. C. et al., 2016; Sun et al., 2016; Sirago et al., 2017; Salazar-Degracia et al., 2018; Lee et al., 2019; Bae et al., 2020) including in cancer patients (Rhoads et al., 2010; Skorokhod et al., 2012; Puig-Vilanova et al., 2015; Johns et al., 2017).

Aside from studies presented in the section of this review dedicated to breast cancer clinical studies (Lønbro et al., 2017; Bohlen et al., 2018; Guigni et al., 2018; Mijwel et al., 2018b; Møller et al., 2019; Wilson et al., 2020), no preclinical study has been done in order to explore protein breakdown in breast cancer models. However, some pre-clinical studies explored the effect of doxorubicin on skeletal muscle and an increase in both UPS and autophagy pathways was suggested as MAFbx, beclin1, Atg12, Atg7, and LC3B-II/I ratio increased with doxorubicin treatment in mice and rats (Smuder et al., 2011; Kavazis et al., 2014; Hulmi et al., 2018; Montalvo et al., 2020). Importantly, only Montalvo et al. (2020) explored p62 protein levels and found no change in its expression, again emphasizing the need to obtain a more precise understanding of the autophagic pathway. Interestingly, Yu et al. (2014) also treated mice with doxorubicin and found no change in numerous autophagy markers. Altogether, pre-clinical studies demonstrated altered protein synthesis and breakdown mainly in response to doxorubicin administration in rodents, again emphasizing that these mechanisms may induce skeletal muscle wasting in breast cancer patients.

Pro-inflammatory and TGF-β Family Cytokines

As a critical upstream of protein turnover alteration, inflammation plays a key role in the development of muscle wasting in cancer patients. Indeed, either released by the tumor or immune cells, pro-inflammatory cytokines like TNF-α, TWEAK, IL-6, IL-1β, IL-8, and INFγ have been found to be upregulated at a systemic level in animals (Costelli et al., 1993; Baltgalvis et al., 2008; Zhou et al., 2010; Toledo et al., 2016; Guo et al., 2017; Chen T. et al., 2018; Bae et al., 2020; Bernardo et al., 2020; Huot et al., 2020) and in cancer patients (Scott et al., 1996; DeJong et al., 2005; Moses et al., 2009; Skipworth et al., 2011; Op den Kamp et al., 2013; Puig-Vilanova et al., 2015; Johns et al., 2017; Riccardi et al., 2020). Importantly, from a study that included 661 breast cancer patients, systemic inflammatory cytokines were associated with a poor survival, reduced disease-specific survival and disease-free survival (Cho et al., 2018). These inflammatory cytokines have been also found to be upregulated within skeletal muscle in pre-clinical studies (Skipworth et al., 2011; Johnston et al., 2015; Chen M. C. et al., 2016; Hatakeyama et al., 2016; Chen L. et al., 2019; Lee et al., 2019; Bae et al., 2020), but none of these has been investigated in breast cancer models.

In addition to pro-inflammatory cytokines, two particular members of the TGF-β family have been particularly explored in cancer cachexia: myostatin (MSTN) and Activin A. MSTN clearly represents one of the most potent negative regulator of muscle growth and is known to act through its receptor ActRIIB and the subsequent activation of the SMAD2/SMAD3 cascade (Rodriguez et al., 2014). MSTN and/or its downstream targets have been found to be upregulated in many experiments on cancer cachexia (Costelli et al., 2008; Bonetto et al., 2009; Zhou et al., 2010; Murphy et al., 2011; Aversa et al., 2012; Padrão et al., 2013; Chacon-Cabrera et al., 2014; Silva et al., 2015; Chen M. C. et al., 2016; Sun et al., 2016; Chen M. C. et al., 2018; Salazar-Degracia et al., 2018; Lee et al., 2019; Huot et al., 2020), as well as in studies exploring the effect of doxorubicin administration (Kavazis et al., 2014; Liu et al., 2019). Acting through the same receptor than MSTN (ActRIIB), Activin A is also found to be increased in cancer cachexia (Leto et al., 2006; Loumaye et al., 2015; Matsuyama et al., 2015; Chen J. L. et al., 2016; Chen M. C. et al., 2016; Barreto et al., 2017; Zhong et al., 2019; Bernardo et al., 2020) and an independent prognosis factor of survival in cancer patients (Loumaye et al., 2017). Several authors conducted experiments with inhibition of the MSTN/Activin A pathway and found a reduction, or even a complete reversal, in the decrease of muscle mass and function in pre-clinical models (Liu et al., 2008; Benny Klimek et al., 2010; Murphy et al., 2011; Busquets et al., 2012a,b; Gallot et al., 2014; Hatakeyama et al., 2016; Levolger et al., 2019; Ojima et al., 2020; Pettersen et al., 2020), leading to the consideration of this pharmacological strategy for human cancer patients.

Mitochondrial Alterations, Oxidative Stress, and Unfolded Protein Response

Mitochondrial alterations represent a major aspect of muscle deconditioning that have been already associated with skeletal muscle atrophy in breast cancer patients (Bohlen et al., 2018; Guigni et al., 2018; Mijwel et al., 2018b; Wilson et al., 2020), and in other cancers such as gastrointestinal and lung cancer patients (Op den Kamp et al., 2015; de Castro et al., 2019). Triggered by both structural and functional mitochondrial impairments, mitochondrial alterations have been particularly studied in pre-clinical studies. First, altered morphology and/or mitochondria loss have been found in different models of cancer in animals and/or with chemotherapeutic agents (Shum et al., 2012; White et al., 2012; Fontes-Oliveira et al., 2013; Barreto et al., 2016; Brown et al., 2017; Sorensen et al., 2017) as well as in gastric cancer patients (Zhang et al., 2020). Taken together, these results showing mitochondrial alterations on other cancer types strengthen the abovementioned results specifically observed in breast cancer (Guigni et al., 2018; Mijwel et al., 2018b) and might be a specific maladaptation between cancers. Concerning mitochondrial function, the overall oxidative pathway is clearly affected by both cancer and chemotherapeutic agents (Ushmorov et al., 1999; Constantinou et al., 2011; Julienne et al., 2012; Fermoselle et al., 2013; Gilliam et al., 2013, 2016; Padrão et al., 2013; Tzika et al., 2013; McLean et al., 2014; Gouspillou et al., 2015; Op den Kamp et al., 2015; Puig-Vilanova et al., 2015; de Lima Junior et al., 2016; Brown et al., 2017; Crouch et al., 2017; Pin et al., 2018; Ryan et al., 2018; Neyroud et al., 2019; Penna et al., 2019b; Hulmi et al., 2020; Kunzke et al., 2020). Among these studies, only two showed the potent negative impact of doxorubicin on complexes respiratory capacity (Gilliam et al., 2013; Gouspillou et al., 2015) while

Crouch et al. (2017) highlighted a decrease in ATP production with cyclophosphamide administration, an immunosuppressor commonly associated with doxorubicin in breast cancer treatment. Interestingly, various authors also found altered mitochondrial dynamics, with a decreased fusion and increased fission, leading to mitochondria fragmentation in cancer cachexia (White et al., 2011, 2012; Barreto et al., 2016; Brown et al., 2017; Marzetti et al., 2017; Pin et al., 2018; de Castro et al., 2019; Huot et al., 2020). Surprisingly, although it was found that breast cancer patients lost mitochondria during their chemotherapeutic treatment (Guigni et al., 2018), mitochondria dynamics has not been investigated to date in specific preclinical models of breast cancer patients. Even if it is well known that mitochondria fission is prerequisite for the activation of the mitophagy process, it seems that mitophagy is also dysfunctional in cancer as several authors showed a decrease in key markers such as PINK1 or Parkin (Aversa et al., 2016; Marzetti et al., 2017). This statement has been also confirmed in the study of Gouspillou et al. (2015) with mice treated with doxorubicin (reduced Parkin protein levels) as well as in the study of Mijwel et al. (2018b) with breast cancer patients (reduced PINK1 protein levels).

As a consequence of mitochondrial dysfunction and potential reduced mitophagy, fragmented and damaged mitochondria accumulate in skeletal muscle and, in addition to being less bioenergetically efficient, produce excessive amounts of oxidative stress, mediated through increases in reactive oxygen species (ROS). Indeed, many different studies found an increase in ROS (Gilliam et al., 2013, 2016; Gouspillou et al., 2015; Min et al., 2015; Chacon-Cabrera et al., 2017; Pin et al., 2018; Ballarò et al., 2019; Montalvo et al., 2020), more specifically elevated levels of hydrogen peroxide (H_2O_2). Unanimously, several studies reported that doxorubicin administration in rodents led to an increase in H_2O_2 production (Gilliam et al., 2013, 2016; Min et al., 2015; Montalvo et al., 2020), while there is still no clinical study available to confirm this increase in breast cancer patients. One of the consequences of the increase in oxidative stress is the alteration of protein turnover pathways, with a decrease in protein synthesis, supported by an altered PI3k-Akt-mTOR pathway, and an increase in protein breakdown systems (i.e., UPS and autophagy). Aside the protein turnover deregulation, mitochondria-mediated oxidative stress is also a potent initiator of apoptosis [see reviews from Powers et al. (2016),Aggarwal et al. (2019), Sies and Jones (2020), and Hyatt and Powers (2021)]. Many studies showed an increase in key markers of apoptosis in various pre-clinical models (Belizário et al., 2001; Ishiko et al., 2001; Yoshida et al., 2001; Tsang et al., 2003; Figueras et al., 2004; Schwarzkopf et al., 2006; Baltgalvis et al., 2008; Murphy et al., 2011; Smuder et al., 2011; Chacon-Cabrera et al., 2014; Salazar-Degracia et al., 2016, 2018) and in cancer patients (Busquets et al., 2007; de Castro et al., 2019). Three other studies also explored the effect of doxorubicin treatment in rodents and *in vitro* (C2C12) and found increased levels of caspase 3 (both its activity and cleaved form of caspase 3 protein expression) and of Bax (Gilliam et al., 2012; Yu et al., 2014; Min et al., 2015). Finally, the study of Ahmadabadi et al. (2020) also observed a decrease in Bcl-2/Bax ratio in breast cancer-bearing mice, showing once again that apoptosis might be upregulated in breast cancer patients. Intuitively, the loss of muscle cells or myonuclei would appear like one of the causes of muscle atrophy, and studies have already shown associations between loss of muscle mass/CSA and the number of apoptotic cells (Allen et al., 1997; Borisov and Carlson, 2000; Smith et al., 2000; Dupont-Versteegden, 2005; Andrianjafiniony et al., 2010; Guo et al., 2012; Chacon-Cabrera et al., 2014; Cheema et al., 2015; Salazar-Degracia et al., 2016).

Increased levels in unfolded or misfolded proteins and oxidative stress (due to the potential deficit in autophagy/mitophagy and mitochondrial dysfunction) will lead to endoplasmic reticulum stress and trigger the unfolded protein response (UPR) that might represent another major maladaptation taking place during cancer cachexia. Acting through three pathways (PERK-eIf2α-ATF4, IRE1α-sXBP1, and ATF6-ATF6N) the UPR contributes to skeletal muscle atrophy by decreasing protein synthesis, increasing protein breakdown and, ultimately, inducing apoptosis (Urbina-Varela et al., 2020; Vainshtein and Sandri, 2020; Gallot and Bohnert, 2021). The UPR has been shown to be upregulated in several pre-clinical studies of cancer cachexia (Bohnert et al., 2016, 2019; Gallot et al., 2019; Straughn et al., 2021) and in response to doxorubicin treatment (Montalvo et al., 2020) leading to the conclusion that the increased activity of the UPR system would trigger the muscle atrophy program and contribute to muscle wasting. However, as clearly described in the review of Gallot and Bohnert (2021), specific increase in the PERK-eIf2α-ATF4 pathway might also be necessary during skeletal muscle atrophy to counteract it, as both pharmacological (Bohnert et al., 2016) or genetical tools (Gallot et al., 2019) aiming to inhibit this pathway aggravated cancer-related muscle atrophy. On the contrary, muscle-specific deletion of XBP1 in LLC-bearing mice exhibited a reduced muscle atrophy, demonstrating that the IRE1α-sXBP1 axis of the UPR system seems to be implicated in cancer-mediated muscle atrophy.

Satellite Cells

The capacity of skeletal muscle to regenerate is another key parameter of its functionality. After injury, successful skeletal muscle regeneration appears to be driven by complex and precisely orchestrated processes involving multiple cell types. Of these cell types, satellite cells (SCs), localized between the sarcolemma and the basal lamina of myofibers (Mauro, 1961), represents the most studied and essential stem cells in order to support the regeneration process. In the context of cancer cachexia, several studies already showed that skeletal muscle tissue exhibited signs of ongoing degeneration/regeneration cycles, including ultrastructural damage, central nuclei localization, increased macrophages abundance as well as SCs proliferation in patients (Zampieri et al., 2010; He et al., 2013) and in pre-clinical models (Mehl et al., 2005; Chacon-Cabrera et al., 2014, 2017; Salazar-Degracia et al., 2016, 2018; Judge et al., 2018), including in breast cancer-bearing mice (Ahmadabadi et al., 2020). These signs of damage and regeneration might indicate an increased fragility of the skeletal muscle and an environment prone to lead to more degeneration/regeneration cycles. Having in mind that several authors also highlighted a clear decrease in regeneration capacity (He et al., 2013;

Coletti et al., 2016; Inaba et al., 2018; Costamagna et al., 2020), cancer-related muscle atrophy may also result from muscle decreased repair/regrowth after injury and not only from different pathways causing protein turnover dysregulation. More specifically, the excellent study of He et al. (2013) demonstrated that SCs were able to proliferate and commit to the myogenic lineage, but unable to differentiate properly due to an NF-κB dependent increase in Pax7 expression. This increase in Pax7 expression was also found in breast cancer-bearing mice (Hesse et al., 2019) as well as in other cancers pre-clinical studies (Penna et al., 2010; Coletti et al., 2016; Costamagna et al., 2020), ultimately leading to muscle regeneration dysfunction. Importantly, D'Lugos et al. (2019) found that chronic doxorubicin administration drastically reduced SCs content in rats, suggesting that if cancer *per se* would inhibit myogenic differentiation process, the combination of both the disease and chemotherapeutic drugs administration might lead to global SCs dysfunction and loss in breast cancer patients. However, as highlighted in our section dedicated to clinical studies in breast cancer patients, only Mijwel et al. (2018b) investigated $Pax7^{+}$-labeled SCs and found no change in their number. Therefore, more studies are necessary to clarify SCs fate and implication in breast cancer patients and/or pre-clinical models.

Intermuscular Adipose Tissue and Fibro-Adipogenic Progenitors

The abnormal development of fibrotic and/or IMAT deposits within skeletal muscle is a strong marker of regenerative failure. As documented above, breast cancer patients exhibit an increase in IMAT (Rier et al., 2018; Reding et al., 2019; Beaudry et al., 2020), a result also found in other types of cancers [for a systematic review see Aleixo et al. (2020b)]. However, we did not find any study exploring the cellular mechanisms related to IMAT development in preclinical models of breast cancer or with the administration of commonly used chemotherapeutic agents. In muscle disuse or pathological conditions, such as Duchenne muscular dystrophy, FAPs proliferate and differentiate into adipose and/or fibrous tissue (Uezumi et al., 2011, 2014a; Ieronimakis et al., 2016) and are currently accepted to represent the major population that appears to play a role in IMAT development (Brioche et al., 2016; Biferali et al., 2019; Theret et al., 2021). In the context of cancer cachexia, one study found an increased presence of FAPs in the muscle environment of pancreatic cancer patients (Judge et al., 2018) that might explain the development of myosteatosis observed in overall cancer patients. Considering the increase in IMAT development found in breast cancer patients (Rier et al., 2018; Reding et al., 2019; Beaudry et al., 2020), it thus appears essential to explore FAPs fate in this specific context.

Other than their important role in muscle regeneration and abnormal development of IMAT, FAPs have been recently shown to promote skeletal muscle atrophy. Indeed, the study of Madaro et al. (2018) demonstrated that FAPs progressively accumulate and exhibit increased IL-6/STAT3 signaling, promoting muscle atrophy in different mouse models. Interestingly, inactivation of this pathway effectively countered the muscle atrophy and fibrosis observed in these models, emphasizing a potential role of FAPs secretome and paracrine effects on skeletal muscle fibers. Considering the ambivalent role of FAPs in the development of IMAT and muscle atrophy, further studies should focus on these stem cells in order to elucidate their potential role in both pre-clinical and clinical models of cancer-related skeletal muscle wasting.

CONCLUSION

Breast cancer patients undergoing chemotherapy definitively experience skeletal muscle deconditioning, mainly characterized by both a decrease in muscle mass and function. Despite the fact that mechanisms of muscle deconditioning are well known in many other muscle wasting models, including in other pre-clinical or clinical models of cancers, they still remain relatively unknown in breast cancer patients. In fact, some studies using muscle biopsies highlighted protein turnover and mitochondrial alterations in breast cancer patients, but other studies are clearly needed to obtain a more precise understanding of the cellular processes implicated in breast cancer-mediated muscle deconditioning. This lack of knowledge inevitably leads to difficulties for the implementation of efficient preventive strategies such as exercise, nutrition or pharmacological treatments.

AUTHOR CONTRIBUTIONS

JM, EH, TH, and AP contributed to writing or editing the manuscript and approved the final version of the manuscript. All authors contributed to the article and approved the submitted version.

FUNDING

This work was supported by the Institut de Cancérologie Strasbourg Europe. This work has been published under the framework of the IdEx Unistra supported by the investments for the future program of the French Government.

REFERENCES

Acharyya, S., Butchbach, M. E. R., Sahenk, Z., Wang, H., Saji, M., Carathers, M., et al. (2005). Dystrophin glycoprotein complex dysfunction: a regulatory link between muscular dystrophy and cancer cachexia. *Cancer Cell* 8, 421–432. doi: 10.1016/j.ccr.2005.10.004

Addison, O., Marcus, R. L., Lastayo, P. C., and Ryan, A. S. (2014). Intermuscular fat: a review of the consequences and causes. *Int. J. Endocrinol.* 2014:309570. doi: 10.1155/2014/309570

Agarwala, P., and Salzman, S. H. (2020). Six-Minute walk test: clinical role, technique, coding, and reimbursement. *Chest* 157, 603–611. doi: 10.1016/j.chest.2019.10.014

Aggarwal, V., Tuli, H. S., Varol, A., Thakral, F., Yerer, M. B., Sak, K., et al. (2019). Role of reactive oxygen species in cancer progression: molecular mechanisms and recent advancements. *Biomolecules* 9:735. doi: 10.3390/biom9110735

Ahmadabadi, F., Saghebjoo, M., Huang, C.-J., Saffari, I., and Zardast, M. (2020). The effects of high-intensity interval training and saffron aqueous extract supplementation on alterations of body weight and apoptotic indices in skeletal muscle of 4T1 breast cancer-bearing mice with cachexia. *Appl. Physiol. Nutr. Metab. Physiol. Appl. Nutr. Metab.* 45, 555–563. doi: 10.1139/apnm-2019-0352

Aleixo, G. F. P., Deal, A. M., Nyrop, K. A., Muss, H. B., Damone, E. M., Williams, G. R., et al. (2020a). Association of body composition with function in women with early breast cancer. *Breast Cancer Res. Treat.* 181, 411–421. doi: 10.1007/s10549-020-05624-3

Aleixo, G. F. P., Shachar, S. S., Nyrop, K. A., Muss, H. B., Malpica, L., and Williams, G. R. (2020b). Myosteatosis and prognosis in cancer: systematic review and meta-analysis. *Crit. Rev. Oncol. Hematol.* 145:102839. doi: 10.1016/j.critrevonc.2019.102839

Aleixo, G. F. P., Williams, G. R., Nyrop, K. A., Muss, H. B., and Shachar, S. S. (2019). Muscle composition and outcomes in patients with breast cancer: meta-analysis and systematic review. *Breast Cancer Res. Treat.* 177, 569–579. doi: 10.1007/s10549-019-05352-3

Allen, D. L., Linderman, J. K., Roy, R. R., Grindeland, R. E., Mukku, V., and Edgerton, V. R. (1997). Growth hormone/IGF-I and/or resistive exercise maintains myonuclear number in hindlimb unweighted muscles. *J. Appl. Physiol. Bethesda Md 1985* 83, 1857–1861. doi: 10.1152/jappl.1997.83.6.1857

Andrianjafiniony, T., Dupré-Aucouturier, S., Letexier, D., Couchoux, H., and Desplanches, D. (2010). Oxidative stress, apoptosis, and proteolysis in skeletal muscle repair after unloading. *Am. J. Physiol. Cell Physiol.* 299, C307–C315. doi: 10.1152/ajpcell.00069.2010

Antoun, S., and Raynard, B. (2018). Muscle protein anabolism in advanced cancer patients: response to protein and amino acids support, and to physical activity. *Ann. Oncol. Off. J. Eur. Soc. Med. Oncol.* 29, ii10–ii17. doi: 10.1093/annonc/mdx809

Arc-Chagnaud, C., Py, G., Fovet, T., Roumanille, R., Demangel, R., Pagano, A. F., et al. (2020). Evaluation of an antioxidant and anti-inflammatory cocktail against human hypoactivity-induced skeletal muscle deconditioning. *Front. Physiol.* 11:71. doi: 10.3389/fphys.2020.00071

Argilés, J. M., Busquets, S., Stemmler, B., and López-Soriano, F. J. (2014). Cancer cachexia: understanding the molecular basis. *Nat. Rev. Cancer* 14, 754–762. doi: 10.1038/nrc3829

Argilés, J. M., López-Soriano, F. J., and Busquets, S. (2019). Mediators of cachexia in cancer patients. *Nutrition* 66, 11–15. doi: 10.1016/j.nut.2019.03.012

Astrand, P. O., and Saltin, B. (1961). Maximal oxygen uptake and heart rate in various types of muscular activity. *J. Appl. Physiol.* 16, 977–981. doi: 10.1152/jappl.1961.16.6.977

Atherton, P. J., Greenhaff, P. L., Phillips, S. M., Bodine, S. C., Adams, C. M., and Lang, C. H. (2016). Control of skeletal muscle atrophy in response to disuse: clinical/preclinical contentions and fallacies of evidence. *Am. J. Physiol. Endocrinol. Metab.* 311, E594–E604. doi: 10.1152/ajpendo.00257.2016

Aubrey, J., Esfandiari, N., Baracos, V. E., Buteau, F. A., Frenette, J., Putman, C. T., et al. (2014). Measurement of skeletal muscle radiation attenuation and basis of its biological variation. *Acta Physiol. Oxf. Engl.* 210, 489–497. doi: 10.1111/apha.12224

Aversa, Z., Bonetto, A., Penna, F., Costelli, P., Di Rienzo, G., Lacitignola, A., et al. (2012). Changes in myostatin signaling in non-weight-losing cancer patients. *Ann. Surg. Oncol.* 19, 1350–1356. doi: 10.1245/s10434-011-1720-5

Aversa, Z., Pin, F., Lucia, S., Penna, F., Verzaro, R., Fazi, M., et al. (2016). Autophagy is induced in the skeletal muscle of cachectic cancer patients. *Sci. Rep.* 6:30340. doi: 10.1038/srep30340

Bae, T., Jang, J., Lee, H., Song, J., Chae, S., Park, M., et al. (2020). *Paeonia lactiflora* root extract suppresses cancer cachexia by down-regulating muscular NF-κB signalling and muscle-specific E3 ubiquitin ligases in cancer-bearing mice. *J. Ethnopharmacol.* 246:112222. doi: 10.1016/j.jep.2019.112222

Baldwin, K. M., Haddad, F., Pandorf, C. E., Roy, R. R., and Edgerton, V. R. (2013). Alterations in muscle mass and contractile phenotype in response to unloading models: role of transcriptional/pretranslational mechanisms. *Front. Physiol.* 4:284. doi: 10.3389/fphys.2013.00284

Ballarò, R., Beltrà, M., De Lucia, S., Pin, F., Ranjbar, K., Hulmi, J. J., et al. (2019). Moderate exercise in mice improves cancer plus chemotherapy-induced muscle wasting and mitochondrial alterations. *FASEB J.* 33, 5482–5494. doi: 10.1096/fj.201801862R

Baltgalvis, K. A., Berger, F. G., Pena, M. M. O., Davis, J. M., Muga, S. J., and Carson, J. A. (2008). Interleukin-6 and cachexia in ApcMin/+ mice. *Am. J. Physiol. Regul. Integr. Comp. Physiol.* 294, R393–R401. doi: 10.1152/ajpregu.00716.2007

Baracos, V. E., DeVivo, C., Hoyle, D. H., and Goldberg, A. L. (1995). Activation of the ATP-ubiquitin-proteasome pathway in skeletal muscle of cachectic rats bearing a hepatoma. *Am. J. Physiol.* 268, E996–E1006. doi: 10.1152/ajpendo.1995.268.5.E996

Baracos, V. E., Martin, L., Korc, M., Guttridge, D. C., and Fearon, K. C. H. (2018). Cancer-associated cachexia. *Nat. Rev. Dis. Primers* 4:17105. doi: 10.1038/nrdp.2017.105

Barreto, R., Kitase, Y., Matsumoto, T., Pin, F., Colston, K. C., Couch, K. E., et al. (2017). ACVR2B/Fc counteracts chemotherapy-induced loss of muscle and bone mass. *Sci. Rep.* 7:14470. doi: 10.1038/s41598-017-15040-1

Barreto, R., Waning, D. L., Gao, H., Liu, Y., Zimmers, T. A., and Bonetto, A. (2016). Chemotherapy-related cachexia is associated with mitochondrial depletion and the activation of ERK1/2 and p38 MAPKs. *Oncotarget* 7, 43442–43460. doi: 10.18632/oncotarget.9779

Beaudry, R. I., Kirkham, A. A., Thompson, R. B., Grenier, J. G., Mackey, J. R., and Haykowsky, M. J. (2020). Exercise intolerance in anthracycline-treated breast cancer survivors: the role of skeletal muscle bioenergetics, oxygenation, and composition. *The Oncologist* 25, e852–e860. doi: 10.1634/theoncologist.2019-0777

Beavers, K. M., Beavers, D. P., Houston, D. K., Harris, T. B., Hue, T. F., Koster, A., et al. (2013). Associations between body composition and gait-speed decline: results from the Health, Aging, and Body Composition study. *Am. J. Clin. Nutr.* 97, 552–560. doi: 10.3945/ajcn.112.047860

Beck, S. A., Smith, K. L., and Tisdale, M. J. (1991). Anticachectic and antitumor effect of eicosapentaenoic acid and its effect on protein turnover. *Cancer Res.* 51, 6089–6093.

Behr, T. M., Béhé, M., and Wörmann, B. (2001). Trastuzumab and breast cancer. *N. Engl. J. Med.* 345, 995–996. doi: 10.1056/NEJM200109273451312

Belizário, J. E., Lorite, M. J., and Tisdale, M. J. (2001). Cleavage of caspases-1, -3, -6, -8 and -9 substrates by proteases in skeletal muscles from mice undergoing cancer cachexia. *Br. J. Cancer* 84, 1135–1140. doi: 10.1054/bjoc.2001.1700

Bennegård, K., Lindmark, L., Edén, E., Svaninger, G., and Lundholm, K. (1984). Flux of amino acids across the leg in weight-losing cancer patients. *Cancer Res.* 44, 386–393.

Benny Klimek, M. E., Aydogdu, T., Link, M. J., Pons, M., Koniaris, L. G., and Zimmers, T. A. (2010). Acute inhibition of myostatin-family proteins preserves skeletal muscle in mouse models of cancer cachexia. *Biochem. Biophys. Res. Commun.* 391, 1548–1554. doi: 10.1016/j.bbrc.2009.12.123

Berger, A. M., Mitchell, S. A., Jacobsen, P. B., and Pirl, W. F. (2015). Screening, evaluation, and management of cancer-related fatigue: ready for implementation to practice? *CA Cancer J. Clin.* 65, 190–211. doi: 10.3322/caac.21268

Bergstrom, J. (1975). Percutaneous needle biopsy of skeletal muscle in physiological and clinical research. *Scand. J. Clin. Lab. Invest.* 35, 609–616.

Bernardo, B., Joaquim, S., Garren, J., Boucher, M., Houle, C., LaCarubba, B., et al. (2020). Characterization of cachexia in the human fibrosarcoma HT-1080 mouse tumour model. *J. Cachexia Sarcopenia Muscle* 11, 1813–1829. doi: 10.1002/jcsm.12618

Biferali, B., Proietti, D., Mozzetta, C., and Madaro, L. (2019). Fibro-Adipogenic progenitors cross-talk in skeletal muscle: the social network. *Front. Physiol.* 10:1074. doi: 10.3389/fphys.2019.01074

Bird, B. R. J. H., and Swain, S. M. (2008). Cardiac toxicity in breast cancer survivors: review of potential cardiac problems. *Clin. Cancer Res.* 14, 14–24. doi: 10.1158/1078-0432.CCR-07-1033

Bodine, S. C. (2013). Disuse-induced muscle wasting. *Int. J. Biochem. Cell Biol.* 45, 2200–2208. doi: 10.1016/j.biocel.2013.06.011

Bohlen, J., McLaughlin, S. L., Hazard-Jenkins, H., Infante, A. M., Montgomery, C., Davis, M., et al. (2018). Dysregulation of metabolic-associated pathways in muscle of breast cancer patients: preclinical evaluation of interleukin-15

targeting fatigue. *J. Cachexia Sarcopenia Muscle* 9, 701–714. doi: 10.1002/jcsm.12294

Bohnert, K. R., Gallot, Y. S., Sato, S., Xiong, G., Hindi, S. M., and Kumar, A. (2016). Inhibition of ER stress and unfolding protein response pathways causes skeletal muscle wasting during cancer cachexia. *FASEB J. Off. Publ. Fed. Am. Soc. Exp. Biol.* 30, 3053–3068. doi: 10.1096/fj.201600250RR

Bohnert, K. R., Goli, P., Roy, A., Sharma, A. K., Xiong, G., Gallot, Y. S., et al. (2019). The toll-like receptor/MyD88/XBP1 signaling axis mediates skeletal muscle wasting during cancer cachexia. *Mol. Cell. Biol.* 39:e00184-19. doi: 10.1128/MCB.00184-19

Bonaldo, P., and Sandri, M. (2013). Cellular and molecular mechanisms of muscle atrophy. *Dis. Model. Mech.* 6, 25–39. doi: 10.1242/dmm.010389

Bonetto, A., Penna, F., Minero, V. G., Reffo, P., Bonelli, G., Baccino, F. M., et al. (2009). Deacetylase inhibitors modulate the myostatin/follistatin axis without improving cachexia in tumor-bearing mice. *Curr. Cancer Drug Targets* 9, 608–616. doi: 10.2174/156800909789057015

Borisov, A. B., and Carlson, B. M. (2000). Cell death in denervated skeletal muscle is distinct from classical apoptosis. *Anat. Rec.* 258, 305–318.

Bossola, M., Muscaritoli, M., Costelli, P., Grieco, G., Bonelli, G., Pacelli, F., et al. (2003). Increased muscle proteasome activity correlates with disease severity in gastric cancer patients. *Ann. Surg.* 237, 384–389. doi: 10.1097/01.SLA.0000055225.96357.71

Bowen, T. S., Schuler, G., and Adams, V. (2015). Skeletal muscle wasting in cachexia and sarcopenia: molecular pathophysiology and impact of exercise training. *J. Cachexia Sarcopenia Muscle* 6, 197–207. doi: 10.1002/jcsm.12043

Bregni, G., Galli, G., Gevorgyan, A., de Braud, F., and Di Cosimo, S. (2016). Trastuzumab cardiac toxicity: a problem we put our heart into. *Tumori* 102, 1–5. doi: 10.5301/tj.5000393

Brioche, T., Pagano, A. F., Py, G., and Chopard, A. (2016). Muscle wasting and aging: experimental models, fatty infiltrations, and prevention. *Mol. Aspects Med.* 50, 56–87. doi: 10.1016/j.mam.2016.04.006

Brown, J. L., Rosa-Caldwell, M. E., Lee, D. E., Blackwell, T. A., Brown, L. A., Perry, R. A., et al. (2017). Mitochondrial degeneration precedes the development of muscle atrophy in progression of cancer cachexia in tumour-bearing mice. *J. Cachexia Sarcopenia Muscle* 8, 926–938. doi: 10.1002/jcsm.12232

Busquets, S., Deans, C., Figueras, M., Moore-Carrasco, R., López-Soriano, F. J., Fearon, K. C. H., et al. (2007). Apoptosis is present in skeletal muscle of cachectic gastro-intestinal cancer patients. *Clin. Nutr. Edinb. Scotl.* 26, 614–618. doi: 10.1016/j.clnu.2007.06.005

Busquets, S., Toledo, M., Marmonti, E., Orpí, M., Capdevila, E., Betancourt, A., et al. (2012a). Formoterol treatment downregulates the myostatin system in skeletal muscle of cachectic tumour-bearing rats. *Oncol. Lett.* 3, 185–189. doi: 10.3892/ol.2011.442

Busquets, S., Toledo, M., Orpí, M., Massa, D., Porta, M., Capdevila, E., et al. (2012b). Myostatin blockage using actRIIB antagonism in mice bearing the Lewis lung carcinoma results in the improvement of muscle wasting and physical performance. *J. Cachexia Sarcopenia Muscle* 3, 37–43. doi: 10.1007/s13539-011-0049-z

But-Hadzic, J., Dervisevic, M., Karpljuk, D., Videmsek, M., Dervisevic, E., Paravlic, A., et al. (2021). Six-Minute walk distance in breast cancer survivors-a systematic review with meta-analysis. *Int. J. Environ. Res. Public. Health* 18:2591. doi: 10.3390/ijerph18052591

Caan, B. J., Feliciano, E. M. C., Prado, C. M., Alexeeff, S., Kroenke, C. H., Bradshaw, P., et al. (2018). Association of muscle and adiposity measured by computed tomography with survival in patients with nonmetastatic breast cancer. *JAMA Oncol.* 4, 798–804. doi: 10.1001/jamaoncol.2018.0137

Cai, D., Frantz, J. D., Tawa, N. E., Melendez, P. A., Oh, B.-C., Lidov, H. G. W., et al. (2004). IKKbeta/NF-kappaB activation causes severe muscle wasting in mice. *Cell* 119, 285–298. doi: 10.1016/j.cell.2004.09.027

CeŠeiko, R., Thomsen, S. N., Tomsone, S., EglĪtis, J., Vçtra, A., Srebnijs, A., et al. (2020). Heavy resistance training in breast cancer patients undergoing adjuvant therapy. *Med. Sci. Sports Exerc.* 52, 1239–1247. doi: 10.1249/MSS.0000000000002260

Cespedes Feliciano, E. M., Chen, W. Y., Lee, V., Albers, K. B., Prado, C. M., Alexeeff, S., et al. (2019). Body composition, adherence to anthracycline and taxane-based chemotherapy, and survival after nonmetastatic breast cancer. *JAMA Oncol.* 6, 264-270. doi: 10.1001/jamaoncol.2019.4668

Chacon-Cabrera, A., Fermoselle, C., Urtreger, A. J., Mateu-Jimenez, M., Diament, M. J., de Kier Joffé, E. D. B., et al. (2014). Pharmacological strategies in lung cancer-induced cachexia: effects on muscle proteolysis, autophagy, structure, and weakness. *J. Cell. Physiol.* 229, 1660–1672. doi: 10.1002/jcp.24611

Chacon-Cabrera, A., Mateu-Jimenez, M., Langohr, K., Fermoselle, C., García-Arumí, E., Andreu, A. L., et al. (2017). Role of PARP activity in lung cancer-induced cachexia: effects on muscle oxidative stress, proteolysis, anabolic markers, and phenotype. *J. Cell. Physiol.* 232, 3744–3761. doi: 10.1002/jcp.25851

Cheema, N., Herbst, A., McKenzie, D., and Aiken, J. M. (2015). Apoptosis and necrosis mediate skeletal muscle fiber loss in age-induced mitochondrial enzymatic abnormalities. *Aging Cell* 14, 1085–1093. doi: 10.1111/acel.12399

Chen, J. L., Walton, K. L., Qian, H., Colgan, T. D., Hagg, A., Watt, M. J., et al. (2016). Differential effects of IL6 and activin a in the development of cancer-associated cachexia. *Cancer Res.* 76, 5372–5382. doi: 10.1158/0008-5472.CAN-15-3152

Chen, L., Chen, L., Wan, L., Huo, Y., Huang, J., Li, J., et al. (2019). Matrine improves skeletal muscle atrophy by inhibiting E3 ubiquitin ligases and activating the Akt/mTOR/FoxO3α signaling pathway in C2C12 myotubes and mice. *Oncol. Rep.* 42, 479–494. doi: 10.3892/or.2019.7205

Chen, M. C., Hsu, W.-L., and Chou, T.-C. (2018). Anti-cachectic effect of Antrodia cinnamomea extract in lung tumor-bearing mice under chemotherapy. *Oncotarget* 9, 19584–19596. doi: 10.18632/oncotarget.24680

Chen, M. C., Hsu, W.-L., Hwang, P.-A., Chen, Y.-L., and Chou, T.-C. (2016). Combined administration of fucoidan ameliorates tumor and chemotherapy-induced skeletal muscle atrophy in bladder cancer-bearing mice. *Oncotarget* 7, 51608–51618. doi: 10.18632/oncotarget.9958

Chen, T., Li, B., Xu, Y., Meng, S., Wang, Y., and Jiang, Y. (2018). Luteolin reduces cancer-induced skeletal and cardiac muscle atrophy in a Lewis lung cancer mouse model. *Oncol. Rep.* 40, 1129–1137. doi: 10.3892/or.2018.6453

Cho, U., Park, H. S., Im, S. Y., Yoo, C. Y., Jung, J. H., Suh, Y. J., et al. (2018). Prognostic value of systemic inflammatory markers and development of a nomogram in breast cancer. *PLoS One* 13:e0200936. doi: 10.1371/journal.pone.0200936

Chopard, A., Hillock, S., and Jasmin, B. J. (2009). Molecular events and signalling pathways involved in skeletal muscle disuse-induced atrophy and the impact of countermeasures. *J. Cell. Mol. Med.* 13, 3032–3050. doi: 10.1111/j.1582-4934.2009.00864.x

Coletti, D., Aulino, P., Pigna, E., Barteri, F., Moresi, V., Annibali, D., et al. (2016). Spontaneous physical activity downregulates Pax7 in cancer cachexia. *Stem Cells Int.* 2016:6729268. doi: 10.1155/2016/6729268

Constantinou, C., Fontes de Oliveira, C. C., Mintzopoulos, D., Busquets, S., He, J., Kesarwani, M., et al. (2011). Nuclear magnetic resonance in conjunction with functional genomics suggests mitochondrial dysfunction in a murine model of cancer cachexia. *Int. J. Mol. Med.* 27, 15–24. doi: 10.3892/ijmm.2010.557

Costamagna, D., Duelen, R., Penna, F., Neumann, D., Costelli, P., and Sampaolesi, M. (2020). Interleukin-4 administration improves muscle function, adult myogenesis, and lifespan of colon carcinoma-bearing mice. *J. Cachexia Sarcopenia Muscle* 11, 783–801. doi: 10.1002/jcsm.12539

Costelli, P., Carbó, N., Tessitore, L., Bagby, G. J., Lopez-Soriano, F. J., Argilés, J. M., et al. (1993). Tumor necrosis factor-alpha mediates changes in tissue protein turnover in a rat cancer cachexia model. *J. Clin. Invest.* 92, 2783–2789. doi: 10.1172/JCI116897

Costelli, P., Muscaritoli, M., Bonetto, A., Penna, F., Reffo, P., Bossola, M., et al. (2008). Muscle myostatin signalling is enhanced in experimental cancer cachexia. *Eur. J. Clin. Invest.* 38, 531–538. doi: 10.1111/j.1365-2362.2008.01970.x

Crouch, M.-L., Knowels, G., Stuppard, R., Ericson, N. G., Bielas, J. H., Marcinek, D. J., et al. (2017). Cyclophosphamide leads to persistent deficits in physical performance and in vivo mitochondria function in a mouse model of chemotherapy late effects. *PLoS One* 12:e0181086. doi: 10.1371/journal.pone.0181086

Cruz, B., Oliveira, A., Ventrucci, G., and Gomes-Marcondes, M. C. C. (2019). A leucine-rich diet modulates the mTOR cell signalling pathway in the gastrocnemius muscle under different Walker-256 tumour growth conditions. *BMC Cancer* 19:349. doi: 10.1186/s12885-019-5448-0

Cruz-Jentoft, A. J., Bahat, G., Bauer, J., Boirie, Y., Bruyère, O., Cederholm, T., et al. (2019). Sarcopenia: revised European consensus on definition and diagnosis. *Age Ageing* 48, 16–31. doi: 10.1093/ageing/afy169

D'Lugos, A. C., Fry, C. S., Ormsby, J. C., Sweeney, K. R., Brightwell, C. R., Hale, T. M., et al. (2019). Chronic doxorubicin administration impacts satellite cell and capillary abundance in a muscle-specific manner. *Physiol. Rep.* 7:e14052. doi: 10.14814/phy2.14052

Daly, L. E., Bhuachalla, N., Ní Bhuachalla, ÉB., Power, D. G., Cushen, S. J., James, K., et al. (2018). Loss of skeletal muscle during systemic chemotherapy is prognostic of poor survival in patients with foregut cancer. *J. Cachexia Sarcopenia Muscle* 9, 315–325. doi: 10.1002/jcsm.12267

Damrauer, J. S., Stadler, M. E., Acharyya, S., Baldwin, A. S., Couch, M. E., and Guttridge, D. C. (2018). Chemotherapy-induced muscle wasting: association with NF-κB and cancer cachexia. *Eur. J. Transl. Myol.* 28:7590. doi: 10.4081/ejtm.2018.7590

de Castro, G. S., Simoes, E., Lima, J. D. C. C., Ortiz-Silva, M., Festuccia, W. T., Tokeshi, F., et al. (2019). Human cachexia induces changes in mitochondria, autophagy and apoptosis in the skeletal muscle. *Cancers* 11:1264. doi: 10.3390/cancers11091264

De Groef, A., Geraerts, I., Demeyer, H., Van der Gucht, E., Dams, L., de Kinkelder, C., et al. (2018). Physical activity levels after treatment for breast cancer: two-year follow-up. *Breast Edinb. Scotl.* 40, 23–28. doi: 10.1016/j.breast.2018.04.009

de Lima Junior, E. A., Yamashita, A. S., Pimentel, G. D., De Sousa, L. G. O., Santos, R. V. T., Gonçalves, C. L., et al. (2016). Doxorubicin caused severe hyperglycaemia and insulin resistance, mediated by inhibition in AMPk signalling in skeletal muscle. *J. Cachexia Sarcopenia Muscle* 7, 615–625. doi: 10.1002/jcsm.12104

DeJong, C. H. C., Busquets, S., Moses, A. G. W., Schrauwen, P., Ross, J. A., Argiles, J. M., et al. (2005). Systemic inflammation correlates with increased expression of skeletal muscle ubiquitin but not uncoupling proteins in cancer cachexia. *Oncol. Rep.* 14, 257–263.

Delmonico, M. J., Harris, T. B., Visser, M., Park, S. W., Conroy, M. B., Velasquez-Mieyer, P., et al. (2009). Longitudinal study of muscle strength, quality, and adipose tissue infiltration. *Am. J. Clin. Nutr.* 90, 1579–1585. doi: 10.3945/ajcn.2009.28047

Deluche, E., Leobon, S., Desport, J. C., Venat-Bouvet, L., Usseglio, J., and Tubiana-Mathieu, N. (2018). Impact of body composition on outcome in patients with early breast cancer. *Support. Care Cancer* 26, 861–868. doi: 10.1007/s00520-017-3902-6

di Prampero, P. E., and Narici, M. V. (2003). Muscles in microgravity: from fibres to human motion. *J. Biomech.* 36, 403–412. doi: 10.1016/s0021-9290(02)00418-9

Dolly, A., Dumas, J.-F., and Servais, S. (2020). Cancer cachexia and skeletal muscle atrophy in clinical studies: what do we really know? *J. Cachexia Sarcopenia Muscle* 11, 1413–1428. doi: 10.1002/jcsm.12633

Dupont-Versteegden, E. E. (2005). Apoptosis in muscle atrophy: relevance to sarcopenia. *Exp. Gerontol.* 40, 473–481. doi: 10.1016/j.exger.2005.04.003

Dworzak, F., Ferrari, P., Gavazzi, C., Maiorana, C., and Bozzetti, F. (1998). Effects of cachexia due to cancer on whole body and skeletal muscle protein turnover. *Cancer* 82, 42–48.

Emens, L. A. (2018). Breast cancer immunotherapy: facts and hopes. *Clin. Cancer Res. Off. J. Am. Assoc. Cancer Res.* 24, 511–520. doi: 10.1158/1078-0432.CCR-16-3001

Emery, P. W., Edwards, R. H., Rennie, M. J., Souhami, R. L., and Halliday, D. (1984). Protein synthesis in muscle measured in vivo in cachectic patients with cancer. *Br. Med. J. Clin. Res. Ed* 289, 584–586. doi: 10.1136/bmj.289.6445.584

Enright, P. L. (2003). The six-minute walk test. *Respir. Care* 48, 783–785.

Fearon, K., Strasser, F., Anker, S. D., Bosaeus, I., Bruera, E., Fainsinger, R. L., et al. (2011). Definition and classification of cancer cachexia: an international consensus. *Lancet Oncol.* 12, 489–495. doi: 10.1016/S1470-2045(10)70218-7

Fermoselle, C., García-Arumí, E., Puig-Vilanova, E., Andreu, A. L., Urtreger, A. J., de Kier Joffé, E. D. B., et al. (2013). Mitochondrial dysfunction and therapeutic approaches in respiratory and limb muscles of cancer cachectic mice. *Exp. Physiol.* 98, 1349–1365. doi: 10.1113/expphysiol.2013.072496

Ferreira, R., Neuparth, M. J., Vitorino, R., Appell, H. J., Amado, F., and Duarte, J. A. (2008). Evidences of apoptosis during the early phases of soleus muscle atrophy in hindlimb suspended mice. *Physiol. Res.* 57, 601–611. doi: 10.33549/physiolres.931272

Figueras, M., Busquets, S., Carbó, N., Barreiro, E., Almendro, V., Argilés, J. M., et al. (2004). Interleukin-15 is able to suppress the increased DNA fragmentation associated with muscle wasting in tumour-bearing rats. *FEBS Lett.* 569, 201–206. doi: 10.1016/j.febslet.2004.05.066

Fisusi, F. A., and Akala, E. O. (2019). Drug combinations in breast cancer therapy. *Pharm. Nanotechnol.* 7, 3–23. doi: 10.2174/2211738507666190122111224

Fontes-Oliveira, C. C., Busquets, S., Toledo, M., Penna, F., Paz Aylwin, M., Sirisi, S., et al. (2013). Mitochondrial and sarcoplasmic reticulum abnormalities in cancer cachexia: altered energetic efficiency? *Biochim. Biophys. Acta* 1830, 2770–2778. doi: 10.1016/j.bbagen.2012.11.009

Fouladiun, M., Körner, U., Gunnebo, L., Sixt-Ammilon, P., Bosaeus, I., and Lundholm, K. (2007). Daily physical-rest activities in relation to nutritional state, metabolism, and quality of life in cancer patients with progressive cachexia. *Clin. Cancer Res. Off. J. Am. Assoc. Cancer Res.* 13, 6379–6385. doi: 10.1158/1078-0432.CCR-07-1147

Foulkes, S. J., Howden, E. J., Bigaran, A., Janssens, K., Antill, Y., Loi, S., et al. (2019). Persistent impairment in cardiopulmonary fitness after breast cancer chemotherapy. *Med. Sci. Sports Exerc.* 51, 1573–1581. doi: 10.1249/MSS.0000000000001970

Gadéa, E., Thivat, E., Dubray-Longeras, P., Arbre, M., Van-praagh, I., Mouret-Reynier, M.-A., et al. (2018). Prospective study on body composition, energy balance and biological factors changes in post-menopausal women with breast cancer receiving adjuvant chemotherapy including taxanes. *Nutr. Cancer* 70, 997–1006. doi: 10.1080/01635581.2018.1502330

Galiano-Castillo, N., Arroyo-Morales, M., Ariza-Garcia, A., Sánchez-Salado, C., Fernández-Lao, C., Cantarero-Villanueva, I., et al. (2016). The six-minute walk test as a measure of health in breast cancer patients. *J. Aging Phys. Act.* 24, 508–515. doi: 10.1123/japa.2015-0056

Gallagher, D., Heshka, S., Kelley, D. E., Thornton, J., Boxt, L., Pi-Sunyer, F. X., et al. (2014). Changes in adipose tissue depots and metabolic markers following a 1-year diet and exercise intervention in overweight and obese patients with type 2 diabetes. *Diabetes Care* 37, 3325–3332. doi: 10.2337/dc14-1585

Gallot, Y. S., and Bohnert, K. R. (2021). Confounding roles of ER stress and the unfolded protein response in skeletal muscle atrophy. *Int. J. Mol. Sci.* 22:2567. doi: 10.3390/ijms22052567

Gallot, Y. S., Bohnert, K. R., Straughn, A. R., Xiong, G., Hindi, S. M., and Kumar, A. (2019). PERK regulates skeletal muscle mass and contractile function in adult mice. *FASEB J. Off. Publ. Fed. Am. Soc. Exp. Biol.* 33, 1946–1962. doi: 10.1096/fj.201800683RR

Gallot, Y. S., Durieux, A.-C., Castells, J., Desgeorges, M. M., Vernus, B., Plantureux, L., et al. (2014). Myostatin gene inactivation prevents skeletal muscle wasting in cancer. *Cancer Res.* 74, 7344–7356. doi: 10.1158/0008-5472.CAN-14-0057

Gilliam, L. A. A., Fisher-Wellman, K. H., Lin, C.-T., Maples, J. M., Cathey, B. L., and Neufer, P. D. (2013). The anticancer agent doxorubicin disrupts mitochondrial energy metabolism and redox balance in skeletal muscle. *Free Radic. Biol. Med.* 65, 988–996. doi: 10.1016/j.freeradbiomed.2013.08.191

Gilliam, L. A. A., Lark, D. S., Reese, L. R., Torres, M. J., Ryan, T. E., Lin, C.-T., et al. (2016). Targeted overexpression of mitochondrial catalase protects against cancer chemotherapy-induced skeletal muscle dysfunction. *Am. J. Physiol. Endocrinol. Metab.* 311, E293–E301. doi: 10.1152/ajpendo.00540.2015

Gilliam, L. A. A., Moylan, J. S., Patterson, E. W., Smith, J. D., Wilson, A. S., Rabbani, Z., et al. (2012). Doxorubicin acts via mitochondrial ROS to stimulate catabolism in C2C12 myotubes. *Am. J. Physiol. Cell Physiol.* 302, C195–C202. doi: 10.1152/ajpcell.00217.2011

Gomes, M. D., Lecker, S. H., Jagoe, R. T., Navon, A., and Goldberg, A. L. (2001). Atrogin-1, a muscle-specific F-box protein highly expressed during muscle atrophy. *Proc. Natl. Acad. Sci. U.S.A.* 98, 14440–14445. doi: 10.1073/pnas.251541198

Goodpaster, B. H., Carlson, C. L., Visser, M., Kelley, D. E., Scherzinger, A., Harris, T. B., et al. (2001). Attenuation of skeletal muscle and strength in the elderly: the Health ABC Study. *J. Appl. Physiol. Bethesda Md 1985* 90, 2157–2165. doi: 10.1152/jappl.2001.90.6.2157

Goodpaster, B. H., Thaete, F. L., and Kelley, D. E. (2000). Composition of skeletal muscle evaluated with computed tomography. *Ann. N. Y. Acad. Sci.* 904, 18–24. doi: 10.1111/j.1749-6632.2000.tb06416.x

Gorgey, A. S., and Dudley, G. A. (2007). Skeletal muscle atrophy and increased intramuscular fat after incomplete spinal cord injury. *Spinal Cord* 45, 304–309. doi: 10.1038/sj.sc.3101968

Gouspillou, G., Scheede-Bergdahl, C., Spendiff, S., Vuda, M., Meehan, B., Mlynarski, H., et al. (2015). Anthracycline-containing chemotherapy causes long-term impairment of mitochondrial respiration and increased reactive oxygen species release in skeletal muscle. *Sci. Rep.* 5:8717. doi: 10.1038/srep08717

Guigni, B. A., Callahan, D. M., Tourville, T. W., Miller, M. S., Fiske, B., Voigt, T., et al. (2018). Skeletal muscle atrophy and dysfunction in breast cancer patients: role for chemotherapy-derived oxidant stress. *Am. J. Physiol. Cell Physiol.* 315, C744–C756. doi: 10.1152/ajpcell.00002.2018

Guo, B.-S., Cheung, K.-K., Yeung, S. S., Zhang, B.-T., and Yeung, E. W. (2012). Electrical stimulation influences satellite cell proliferation and apoptosis in unloading-induced muscle atrophy in mice. *PLoS One* 7:e30348. doi: 10.1371/journal.pone.0030348

Guo, D., Wang, C., Wang, Q., Qiao, Z., and Tang, H. (2017). Pantoprazole blocks the JAK2/STAT3 pathway to alleviate skeletal muscle wasting in cancer cachexia by inhibiting inflammatory response. *Oncotarget* 8, 39640–39648. doi: 10.18632/oncotarget.17387

Hanson, A. M., Harrison, B. C., Young, M. H., Stodieck, L. S., and Ferguson, V. L. (2013). Longitudinal characterization of functional, morphologic, and biochemical adaptations in mouse skeletal muscle with hindlimb suspension. *Muscle Nerve* 48, 393–402. doi: 10.1002/mus.23753

Hatakeyama, S., Summermatter, S., Jourdain, M., Melly, S., Minetti, G. C., and Lach-Trifilieff, E. (2016). ActRII blockade protects mice from cancer cachexia and prolongs survival in the presence of anti-cancer treatments. *Skelet. Muscle* 6:26. doi: 10.1186/s13395-016-0098-2

He, W. A., Berardi, E., Cardillo, V. M., Acharyya, S., Aulino, P., Thomas-Ahner, J., et al. (2013). NF-κB-mediated Pax7 dysregulation in the muscle microenvironment promotes cancer cachexia. *J. Clin. Invest.* 123, 4821–4835. doi: 10.1172/JCI68523

Hesse, E., Schröder, S., Brandt, D., Pamperin, J., Saito, H., and Taipaleenmäki, H. (2019). Sclerostin inhibition alleviates breast cancer-induced bone metastases and muscle weakness. *JCI Insight* 5:125543. doi: 10.1172/jci.insight.125543

Hiensch, A. E., Bolam, K. A., Mijwel, S., Jeneson, J. A. L., Huitema, A. D. R., Kranenburg, O., et al. (2019). Doxorubicin-induced skeletal muscle atrophy: elucidating the underlying molecular pathways. *Acta Physiol. Oxf. Engl.* 229:e13400. doi: 10.1111/apha.13400

Huh, J., Park, B., Lee, H., An, Y.-S., Jung, Y., Kim, J. Y., et al. (2020). Prognostic value of skeletal muscle depletion measured on computed tomography for overall survival in patients with non-metastatic breast cancer. *J. Breast Cancer* 23, 80–92. doi: 10.4048/jbc.2020.23.e8

Hulmi, J. J., Nissinen, T. A., Räsänen, M., Degerman, J., Lautaoja, J. H., Hemanthakumar, K. A., et al. (2018). Prevention of chemotherapy-induced cachexia by ACVR2B ligand blocking has different effects on heart and skeletal muscle. *J. Cachexia Sarcopenia Muscle* 9, 417–432. doi: 10.1002/jcsm.12265

Hulmi, J. J., Penna, F., Pöllänen, N., Nissinen, T. A., Hentilä, J., Euro, L., et al. (2020). Muscle NAD+ depletion and Serpina3n as molecular determinants of murine cancer cachexia-the effects of blocking myostatin and activins. *Mol. Metab.* 41:101046. doi: 10.1016/j.molmet.2020.101046

Huot, J. R., Pin, F., Narasimhan, A., Novinger, L. J., Keith, A. S., Zimmers, T. A., et al. (2020). ACVR2B antagonism as a countermeasure to multi-organ perturbations in metastatic colorectal cancer cachexia. *J. Cachexia Sarcopenia Muscle* 11, 1779–1798. doi: 10.1002/jcsm.12642

Hyatt, H. W., and Powers, S. K. (2021). Mitochondrial dysfunction is a common denominator linking skeletal muscle wasting due to disease, aging, and prolonged inactivity. *Antioxid. Basel Switz.* 10:588. doi: 10.3390/antiox10040588

Ieronimakis, N., Hays, A., Prasad, A., Janebodin, K., Duffield, J. S., and Reyes, M. (2016). PDGFRα signalling promotes fibrogenic responses in collagen-producing cells in Duchenne muscular dystrophy. *J. Pathol.* 240, 410–424. doi: 10.1002/path.4801

Inaba, S., Hinohara, A., Tachibana, M., Tsujikawa, K., and Fukada, S.-I. (2018). Muscle regeneration is disrupted by cancer cachexia without loss of muscle stem cell potential. *PLoS One* 13:e0205467. doi: 10.1371/journal.pone.0205467

Ishiko, O., Sumi, T., Yoshida, H., Hyun, Y., and Ogita, S. (2001). Expression of apoptosis regulatory proteins in the skeletal muscle of tumor-bearing rabbits compared with diet-restricted rabbits. *Int. J. Mol. Med.* 8, 279–283. doi: 10.3892/ijmm.8.3.279

Jerusalem, G., Lancellotti, P., and Kim, S.-B. (2019). HER2+ breast cancer treatment and cardiotoxicity: monitoring and management. *Breast Cancer Res. Treat.* 177, 237–250. doi: 10.1007/s10549-019-05303-y

Johns, N., Hatakeyama, S., Stephens, N. A., Degen, M., Degen, S., Frieauff, W., et al. (2014). Clinical classification of cancer cachexia: phenotypic correlates in human skeletal muscle. *PLoS One* 9:e83618. doi: 10.1371/journal.pone.0083618

Johns, N., Stretch, C., Tan, B. H. L., Solheim, T. S., Sørhaug, S., Stephens, N. A., et al. (2017). New genetic signatures associated with cancer cachexia as defined by low skeletal muscle index and weight loss. *J. Cachexia Sarcopenia Muscle* 8, 122–130. doi: 10.1002/jcsm.12138

Johnston, A. J., Murphy, K. T., Jenkinson, L., Laine, D., Emmrich, K., Faou, P., et al. (2015). Targeting of Fn14 prevents cancer-induced cachexia and prolongs survival. *Cell* 162, 1365–1378. doi: 10.1016/j.cell.2015.08.031

Jones, L. W., Hornsby, W. E., Goetzinger, A., Forbes, L. M., Sherrard, E. L., Quist, M., et al. (2012). Prognostic significance of functional capacity and exercise behavior in patients with metastatic non-small cell lung cancer. *Lung Cancer* 76, 248–252. doi: 10.1016/j.lungcan.2011.10.009

Jubrias, S. A., Odderson, I. R., Esselman, P. C., and Conley, K. E. (1997). Decline in isokinetic force with age: muscle cross-sectional area and specific force. *Pflugers Arch.* 434, 246–253. doi: 10.1007/s004240050392

Judge, S. M., Nosacka, R. L., Delitto, D., Gerber, M. H., Cameron, M. E., Trevino, J. G., et al. (2018). Skeletal muscle fibrosis in pancreatic cancer patients with respect to survival. *JNCI Cancer Spectr.* 2:ky043. doi: 10.1093/jncics/pky043

Julienne, C. M., Dumas, J.-F., Goupille, C., Pinault, M., Berri, C., Collin, A., et al. (2012). Cancer cachexia is associated with a decrease in skeletal muscle mitochondrial oxidative capacities without alteration of ATP production efficiency. *J. Cachexia Sarcopenia Muscle* 3, 265–275. doi: 10.1007/s13539-012-0071-9

Karampinos, D. C., Baum, T., Nardo, L., Alizai, H., Yu, H., Carballido-Gamio, J., et al. (2012). Characterization of the regional distribution of skeletal muscle adipose tissue in type 2 diabetes using chemical shift-based water/fat separation. *J. Magn. Reson. Imaging JMRI* 35, 899–907. doi: 10.1002/jmri.23512

Kavazis, A. N., Smuder, A. J., and Powers, S. K. (2014). Effects of short-term endurance exercise training on acute doxorubicin-induced FoxO transcription in cardiac and skeletal muscle. *J. Appl. Physiol. Bethesda Md 1985* 117, 223–230. doi: 10.1152/japplphysiol.00210.2014

Kawanishi, N., Funakoshi, T., and Machida, S. (2018). Time-course study of macrophage infiltration and inflammation in cast immobilization-induced atrophied muscle of mice. *Muscle Nerve* 57, 1006–1013. doi: 10.1002/mus.26061

Kazemi-Bajestani, S. M. R., Becher, H., Fassbender, K., Chu, Q., and Baracos, V. E. (2014). Concurrent evolution of cancer cachexia and heart failure: bilateral effects exist. *J. Cachexia Sarcopenia Muscle* 5, 95–104. doi: 10.1007/s13539-014-0137-y

Keenan, T. E., and Tolaney, S. M. (2020). Role of immunotherapy in triple-negative breast cancer. *J. Natl. Compr. Cancer Netw. JNCCN* 18, 479–489. doi: 10.6004/jnccn.2020.7554

Khal, J., Hine, A. V., Fearon, K. C. H., Dejong, C. H. C., and Tisdale, M. J. (2005). Increased expression of proteasome subunits in skeletal muscle of cancer patients with weight loss. *Int. J. Biochem. Cell Biol.* 37, 2196–2206. doi: 10.1016/j.biocel.2004.10.017

Khan, A. I., Reiter, D. A., Sekhar, A., Sharma, P., Safdar, N. M., Patil, D. H., et al. (2019). MRI quantitation of abdominal skeletal muscle correlates with CT-based analysis: implications for sarcopenia measurement. *Appl. Physiol. Nutr. Metab. Physiol. Appl. Nutr. Metab.* 44, 814–819. doi: 10.1139/apnm-2018-0473

Klassen, O., Schmidt, M. E., Ulrich, C. M., Schneeweiss, A., Potthoff, K., Steindorf, K., et al. (2017). Muscle strength in breast cancer patients receiving different treatment regimes. *J. Cachexia Sarcopenia Muscle* 8, 305–316. doi: 10.1002/jcsm.12165

Klionsky, D. J., Abdel-Aziz, A. K., Abdelfatah, S., Abdellatif, M., Abdoli, A., Abel, S., et al. (2021). Guidelines for the use and interpretation of assays for monitoring autophagy (4th edition). *Autophagy* 17, 1–382. doi: 10.1080/15548627.2020.1797280

Kunzke, T., Buck, A., Prade, V. M., Feuchtinger, A., Prokopchuk, O., Martignoni, M. E., et al. (2020). Derangements of amino acids in cachectic skeletal muscle are caused by mitochondrial dysfunction. *J. Cachexia Sarcopenia Muscle* 11, 226–240. doi: 10.1002/jcsm.12498

Larsen, S., Nielsen, J., Hansen, C. N., Nielsen, L. B., Wibrand, F., Stride, N., et al. (2012). Biomarkers of mitochondrial content in skeletal muscle of healthy young human subjects. *J. Physiol.* 590, 3349–3360. doi: 10.1113/jphysiol.2012.230185

Larsson, L., Degens, H., Li, M., Salviati, L., Lee, Y. I., Thompson, W., et al. (2019). Sarcopenia: aging-related loss of muscle mass and function. *Physiol. Rev.* 99, 427–511. doi: 10.1152/physrev.00061.2017

Lecker, S. H., Jagoe, R. T., Gilbert, A., Gomes, M., Baracos, V., Bailey, J., et al. (2004). Multiple types of skeletal muscle atrophy involve a common program of changes in gene expression. *FASEB J. Off. Publ. Fed. Am. Soc. Exp. Biol.* 18, 39–51. doi: 10.1096/fj.03-0610com

Lee, B. M., Cho, Y., Kim, J. W., Ahn, S. G., Kim, J. H., Jeung, H. C., et al. (2021). Association between skeletal muscle loss and the response to neoadjuvant chemotherapy for breast cancer. *Cancers* 13:1806. doi: 10.3390/cancers13081806

Lee, H., Heo, J.-W., Kim, A.-R., Kweon, M., Nam, S., Lim, J.-S., et al. (2019). Z-ajoene from crushed garlic alleviates cancer-induced skeletal muscle atrophy. *Nutrients* 11:2724. doi: 10.3390/nu11112724

Leskinen, T., Sipilä, S., Alen, M., Cheng, S., Pietiläinen, K. H., Usenius, J.-P., et al. (2009). Leisure-time physical activity and high-risk fat: a longitudinal population-based twin study. *Int. J. Obes. 2005* 33, 1211–1218. doi: 10.1038/ijo.2009.170

Leto, G., Incorvaia, L., Badalamenti, G., Tumminello, F. M., Gebbia, N., Flandina, C., et al. (2006). Activin A circulating levels in patients with bone metastasis from breast or prostate cancer. *Clin. Exp. Metastasis* 23, 117–122. doi: 10.1007/s10585-006-9010-5

Levolger, S., Wiemer, E. A. C., van Vugt, J. L. A., Huisman, S. A., van Vledder, M. G., van Damme-van Engel, S., et al. (2019). Inhibition of activin-like kinase 4/5 attenuates cancer cachexia associated muscle wasting. *Sci. Rep.* 9:9826. doi: 10.1038/s41598-019-46178-9

Lexell, J., Taylor, C. C., and Sjöström, M. (1988). What is the cause of the ageing atrophy? Total number, size and proportion of different fiber types studied in whole vastus lateralis muscle from 15- to 83-year-old men. *J. Neurol. Sci.* 84, 275–294. doi: 10.1016/0022-510x(88)90132-3

Liu, C.-M., Yang, Z., Liu, C.-W., Wang, R., Tien, P., Dale, R., et al. (2008). Myostatin antisense RNA-mediated muscle growth in normal and cancer cachexia mice. *Gene Ther.* 15, 155–160. doi: 10.1038/sj.gt.3303016

Liu, D., Qiao, X., Ge, Z., Shang, Y., Li, Y., Wang, W., et al. (2019). IMB0901 inhibits muscle atrophy induced by cancer cachexia through MSTN signaling pathway. *Skelet. Muscle* 9:8. doi: 10.1186/s13395-019-0193-2

Lønbro, S., Farup, J., Bentsen, S., Voss, T., Rittig, N., Wang, J., et al. (2017). Lean body mass, muscle fibre size and muscle function in cancer patients during chemotherapy and 10 weeks exercise. *JCSM Clin. Rep.* 2, 1–15. doi: 10.17987/jcsm-cr.v2i1.26

Loumaye, A., de Barsy, M., Nachit, M., Lause, P., Frateur, L., van Maanen, A., et al. (2015). Role of Activin A and myostatin in human cancer cachexia. *J. Clin. Endocrinol. Metab.* 100, 2030–2038. doi: 10.1210/jc.2014-4318

Loumaye, A., de Barsy, M., Nachit, M., Lause, P., van Maanen, A., Trefois, P., et al. (2017). Circulating Activin A predicts survival in cancer patients. *J. Cachexia Sarcopenia Muscle* 8, 768–777. doi: 10.1002/jcsm.12209

Madaro, L., Passafaro, M., Sala, D., Etxaniz, U., Lugarini, F., Proietti, D., et al. (2018). Denervation-activated STAT3-IL-6 signalling in fibro-adipogenic progenitors promotes myofibres atrophy and fibrosis. *Nat. Cell Biol.* 20, 917–927. doi: 10.1038/s41556-018-0151-y

Mallard, J., Hucteau, E., Schott, R., Petit, T., Demarchi, M., Belletier, C., et al. (2020). Evolution of physical status from diagnosis to the end of first-line treatment in breast, lung, and colorectal cancer patients: the PROTECT-01 cohort study protocol. *Front. Oncol.* 10:1304. doi: 10.3389/fonc.2020.01304

Manini, T. M., Clark, B. C., Nalls, M. A., Goodpaster, B. H., Ploutz-Snyder, L. L., and Harris, T. B. (2007). Reduced physical activity increases intermuscular adipose tissue in healthy young adults. *Am. J. Clin. Nutr.* 85, 377–384. doi: 10.1093/ajcn/85.2.377

Marcus, R. L., Addison, O., Kidde, J. P., Dibble, L. E., and Lastayo, P. C. (2010). Skeletal muscle fat infiltration: impact of age, inactivity, and exercise. *J. Nutr. Health Aging* 14, 362–366. doi: 10.1007/s12603-010-0081-2

Marques, V. A., Ferreira-Junior, J. B., Lemos, T. V., Moraes, R. F., Junior, J. R., de, S., et al. (2020). Effects of chemotherapy treatment on muscle strength, quality of life, fatigue, and anxiety in women with breast cancer. *Int. J. Environ. Res. Public. Health* 17:7289. doi: 10.3390/ijerph17197289

Martin, L., Senesse, P., Gioulbasanis, I., Antoun, S., Bozzetti, F., Deans, C., et al. (2015). Diagnostic criteria for the classification of cancer-associated weight loss. *J. Clin. Oncol. Off. J. Am. Soc. Clin. Oncol.* 33, 90–99. doi: 10.1200/JCO.2014.56.1894

Marzetti, E., Lorenzi, M., Landi, F., Picca, A., Rosa, F., Tanganelli, F., et al. (2017). Altered mitochondrial quality control signaling in muscle of old gastric cancer patients with cachexia. *Exp. Gerontol.* 87, 92–99. doi: 10.1016/j.exger.2016.10.003

Mason, M. C., Garcia, J. M., Sansgiry, S., Walder, A., Berger, D. H., and Anaya, D. A. (2016). Preoperative cancer cachexia and short-term outcomes following surgery. *J. Surg. Res.* 205, 398–406. doi: 10.1016/j.jss.2016.06.076

Matsuyama, T., Ishikawa, T., Okayama, T., Oka, K., Adachi, S., Mizushima, K., et al. (2015). Tumor inoculation site affects the development of cancer cachexia and muscle wasting. *Int. J. Cancer* 137, 2558–2565. doi: 10.1002/ijc.29620

Maughan, K. L., Lutterbie, M. A., and Ham, P. S. (2010). Treatment of breast cancer. *Am. Fam. Physician* 81, 1339–1346.

Mauro, A. (1961). Satellite cell of skeletal muscle fibers. *J. Biophys. Biochem. Cytol.* 9, 493–495. doi: 10.1083/jcb.9.2.493

McLean, J. B., Moylan, J. S., and Andrade, F. H. (2014). Mitochondria dysfunction in lung cancer-induced muscle wasting in C2C12 myotubes. *Front. Physiol.* 5:503. doi: 10.3389/fphys.2014.00503

McLoon, L. K., Falkenberg, J. H., Dykstra, D., and Iaizzo, P. A. (1998). Doxorubicin chemomyectomy as a treatment for cervical dystonia: histological assessment after direct injection into the sternocleidomastoid muscle. *Muscle Nerve* 21, 1457–1464.

Mehl, K. A., Davis, J. M., Berger, F. G., and Carson, J. A. (2005). Myofiber degeneration/regeneration is induced in the cachectic ApcMin/+ mouse. *J. Appl. Physiol. Bethesda Md 1985* 99, 2379–2387. doi: 10.1152/japplphysiol.00778.2005

Mijwel, S., Backman, M., Bolam, K. A., Olofsson, E., Norrbom, J., Bergh, J., et al. (2018a). Highly favorable physiological responses to concurrent resistance and high-intensity interval training during chemotherapy: the OptiTrain breast cancer trial. *Breast Cancer Res. Treat.* 169, 93–103. doi: 10.1007/s10549-018-4663-8

Mijwel, S., Cardinale, D. A., Norrbom, J., Chapman, M., Ivarsson, N., Wengström, Y., et al. (2018b). Exercise training during chemotherapy preserves skeletal muscle fiber area, capillarization, and mitochondrial content in patients with breast cancer. *FASEB J.* 32, 5495–5505. doi: 10.1096/fj.201700968R

Min, K., Kwon, O.-S., Smuder, A. J., Wiggs, M. P., Sollanek, K. J., Christou, D. D., et al. (2015). Increased mitochondrial emission of reactive oxygen species and calpain activation are required for doxorubicin-induced cardiac and skeletal muscle myopathy. *J. Physiol.* 593, 2017–2036. doi: 10.1113/jphysiol.2014.286518

Møller, A. B., Lønbro, S., Farup, J., Voss, T. S., Rittig, N., Wang, J., et al. (2019). Molecular and cellular adaptations to exercise training in skeletal muscle from cancer patients treated with chemotherapy. *J. Cancer Res. Clin. Oncol.* 145, 1449–1460. doi: 10.1007/s00432-019-02911-5

Montalvo, R. N., Doerr, V., Min, K., Szeto, H. H., and Smuder, A. J. (2020). Doxorubicin-induced oxidative stress differentially regulates proteolytic signaling in cardiac and skeletal muscle. *Am. J. Physiol. Regul. Integr. Comp. Physiol.* 318, R227–R233. doi: 10.1152/ajpregu.00299.2019

Moore-Carrasco, R., Busquets, S., Almendro, V., Palanki, M., López-Soriano, F. J., and Argilés, J. M. (2007). The AP-1/NF-kappaB double inhibitor SP100030 can revert muscle wasting during experimental cancer cachexia. *Int. J. Oncol.* 30, 1239–1245.

Moses, A. G. W., Maingay, J., Sangster, K., Fearon, K. C. H., and Ross, J. A. (2009). Pro-inflammatory cytokine release by peripheral blood mononuclear cells from

patients with advanced pancreatic cancer: relationship to acute phase response and survival. *Oncol. Rep.* 21, 1091–1095. doi: 10.3892/or_00000328

Murphy, J. C., McDaniel, J. L., Mora, K., Villareal, D. T., Fontana, L., and Weiss, E. P. (2011). Preferential reductions in intermuscular and visceral adipose tissue with exercise-induced weight loss compared with calorie restriction. *J. Appl. Physiol.* 112, 79–85. doi: 10.1152/japplphysiol.00355.2011

Murton, A. J., Maddocks, M., Stephens, F. B., Marimuthu, K., England, R., and Wilcock, A. (2017). Consequences of late-stage non-small-cell lung cancer cachexia on muscle metabolic processes. *Clin. Lung Cancer* 18, e1–e11. doi: 10.1016/j.cllc.2016.06.003

National Cancer Institute, Surveillance, Epidemiology, and End Result program (2019). *Cancer Stat Facts: Female Breast Cancer*. Bethesda, MD: National Cancer Institute.

Neil, S. E., Klika, R. J., Garland, S. J., McKenzie, D. C., and Campbell, K. L. (2013). Cardiorespiratory and neuromuscular deconditioning in fatigued and non-fatigued breast cancer survivors. *Support. Care Cancer Off. J. Multinatl. Assoc. Support. Care Cancer* 21, 873–881. doi: 10.1007/s00520-012-1600-y

Neyroud, D., Nosacka, R. L., Judge, A. R., and Hepple, R. T. (2019). Colon 26 adenocarcinoma (C26)-induced cancer cachexia impairs skeletal muscle mitochondrial function and content. *J. Muscle Res. Cell Motil.* 40, 59–65. doi: 10.1007/s10974-019-09510-4

Nicolazzi, M. A., Carnicelli, A., Fuorlo, M., Scaldaferri, A., Masetti, R., Landolfi, R., et al. (2018). Anthracycline and trastuzumab-induced cardiotoxicity in breast cancer. *Eur. Rev. Med. Pharmacol. Sci.* 22, 2175–2185. doi: 10.26355/eurrev_201804_14752

Nissinen, T. A., Degerman, J., Räsänen, M., Poikonen, A. R., Koskinen, S., Mervaala, E., et al. (2016). Systemic blockade of ACVR2B ligands prevents chemotherapy-induced muscle wasting by restoring muscle protein synthesis without affecting oxidative capacity or atrogenes. *Sci. Rep.* 6:32695. doi: 10.1038/srep32695

Nissinen, T. A., Hentilä, J., Penna, F., Lampinen, A., Lautaoja, J. H., Fachada, V., et al. (2018). Treating cachexia using soluble ACVR2B improves survival, alters mTOR localization, and attenuates liver and spleen responses. *J. Cachexia Sarcopenia Muscle* 9, 514–529. doi: 10.1002/jcsm.12310

Ojima, C., Noguchi, Y., Miyamoto, T., Saito, Y., Orihashi, H., Yoshimatsu, Y., et al. (2020). Peptide-2 from mouse myostatin precursor protein alleviates muscle wasting in cancer-associated cachexia. *Cancer Sci.* 111, 2954–2964. doi: 10.1111/cas.14520

Op den Kamp, C. M., Gosker, H. R., Lagarde, S., Tan, D. Y., Snepvangers, F. J., Dingemans, A.-M. C., et al. (2015). Preserved muscle oxidative metabolic phenotype in newly diagnosed non-small cell lung cancer cachexia. *J. Cachexia Sarcopenia Muscle* 6, 164–173. doi: 10.1002/jcsm.12007

Op den Kamp, C. M., Langen, R. C., Minnaard, R., Kelders, M. C., Snepvangers, F. J., Hesselink, M. K., et al. (2012). Pre-cachexia in patients with stages I–III non-small cell lung cancer: systemic inflammation and functional impairment without activation of skeletal muscle ubiquitin proteasome system. *Lung Cancer* 76, 112–117. doi: 10.1016/j.lungcan.2011.09.012

Op den Kamp, C. M., Langen, R. C., Snepvangers, F. J., de Theije, C. C., Schellekens, J. M., Laugs, F., et al. (2013). Nuclear transcription factor κ B activation and protein turnover adaptations in skeletal muscle of patients with progressive stages of lung cancer cachexia. *Am. J. Clin. Nutr.* 98, 738–748. doi: 10.3945/ajcn.113.058388

Padrão, A. I., Oliveira, P., Vitorino, R., Colaço, B., Pires, M. J., Márquez, M., et al. (2013). Bladder cancer-induced skeletal muscle wasting: disclosing the role of mitochondria plasticity. *Int. J. Biochem. Cell Biol.* 45, 1399–1409. doi: 10.1016/j.biocel.2013.04.014

Pagano, A. F., Brioche, T., Arc-Chagnaud, C., Demangel, R., Chopard, A., and Py, G. (2018). Short-term disuse promotes fatty acid infiltration into skeletal muscle. *J. Cachexia Sarcopenia Muscle* 9, 335–347. doi: 10.1002/jcsm.12259

Peel, A. B., Thomas, S. M., Dittus, K., Jones, L. W., and Lakoski, S. G. (2014). Cardiorespiratory fitness in breast cancer patients: a call for normative values. *J. Am. Heart Assoc.* 3:e000432. doi: 10.1161/JAHA.113.000432

Penna, F., Baccino, F. M., and Costelli, P. (2014). Coming back: autophagy in cachexia. *Curr. Opin. Clin. Nutr. Metab. Care* 17, 241–246. doi: 10.1097/MCO.0000000000000048

Penna, F., Ballarò, R., Beltrà, M., De Lucia, S., García Castillo, L., and Costelli, P. (2019a). The skeletal muscle as an active player against cancer cachexia. *Front. Physiol.* 10:41. doi: 10.3389/fphys.2019.00041

Penna, F., Ballarò, R., Martinez-Cristobal, P., Sala, D., Sebastian, D., Busquets, S., et al. (2019b). Autophagy exacerbates muscle wasting in cancer cachexia and impairs mitochondrial function. *J. Mol. Biol.* 431, 2674–2686. doi: 10.1016/j.jmb.2019.05.032

Penna, F., Costamagna, D., Fanzani, A., Bonelli, G., Baccino, F. M., and Costelli, P. (2010). Muscle wasting and impaired myogenesis in tumor bearing mice are prevented by ERK inhibition. *PLoS One* 5:e13604. doi: 10.1371/journal.pone.0013604

Penna, F., Costamagna, D., Pin, F., Camperi, A., Fanzani, A., Chiarpotto, E. M., et al. (2013). Autophagic degradation contributes to muscle wasting in cancer cachexia. *Am. J. Pathol.* 182, 1367–1378. doi: 10.1016/j.ajpath.2012.12.023

Petruzzelli, M., and Wagner, E. F. (2016). Mechanisms of metabolic dysfunction in cancer-associated cachexia. *Genes Dev.* 30, 489–501. doi: 10.1101/gad.276733.115

Pettersen, K., Andersen, S., van der Veen, A., Nonstad, U., Hatakeyama, S., Lambert, C., et al. (2020). Autocrine activin A signalling in ovarian cancer cells regulates secretion of interleukin 6, autophagy, and cachexia. *J. Cachexia Sarcopenia Muscle* 11, 195–207. doi: 10.1002/jcsm.12489

Pigna, E., Berardi, E., Aulino, P., Rizzuto, E., Zampieri, S., Carraro, U., et al. (2016). Aerobic exercise and pharmacological treatments counteract cachexia by modulating autophagy in colon cancer. *Sci. Rep.* 6:26991. doi: 10.1038/srep26991

Pin, F., Barreto, R., Kitase, Y., Mitra, S., Erne, C. E., Novinger, L. J., et al. (2018). Growth of ovarian cancer xenografts causes loss of muscle and bone mass: a new model for the study of cancer cachexia. *J. Cachexia Sarcopenia Muscle* 9, 685–700. doi: 10.1002/jcsm.12311

Powers, S. K., Morton, A. B., Ahn, B., and Smuder, A. J. (2016). Redox control of skeletal muscle atrophy. *Free Radic. Biol. Med.* 98, 208–217. doi: 10.1016/j.freeradbiomed.2016.02.021

Puig-Vilanova, E., Rodriguez, D. A., Lloreta, J., Ausin, P., Pascual-Guardia, S., Broquetas, J., et al. (2015). Oxidative stress, redox signaling pathways, and autophagy in cachectic muscles of male patients with advanced COPD and lung cancer. *Free Radic. Biol. Med.* 79, 91–108. doi: 10.1016/j.freeradbiomed.2014.11.006

Puppa, M. J., Gao, S., Narsale, A. A., and Carson, J. A. (2014). Skeletal muscle glycoprotein 130's role in Lewis lung carcinoma-induced cachexia. *FASEB J. Off. Publ. Fed. Am. Soc. Exp. Biol.* 28, 998–1009. doi: 10.1096/fj.13-240580

Quan-Jun, Y., Yan, H., Yong-Long, H., Li-Li, W., Jie, L., Jin-Lu, H., et al. (2017). Selumetinib attenuates skeletal muscle wasting in murine cachexia model through ERK inhibition and AKT activation. *Mol. Cancer Ther.* 16, 334–343. doi: 10.1158/1535-7163.MCT-16-0324

Ramos da Silva, B., Mialich, M. S., Cruz, L. P., Rufato, S., Gozzo, T., and Jordao, A. A. (2021). Performance of functionality measures and phase angle in women exposed to chemotherapy for early breast cancer. *Clin. Nutr. ESPEN* 42, 105–116. doi: 10.1016/j.clnesp.2021.02.007

Ranjbar, K., Ballarò, R., Bover, Q., Pin, F., Beltrà, M., Penna, F., et al. (2019). Combined exercise training positively affects muscle wasting in tumor-bearing mice. *Med. Sci. Sports Exerc.* 51, 1387–1395. doi: 10.1249/MSS.0000000000001916

Redden, M. H., and Fuhrman, G. M. (2013). Neoadjuvant chemotherapy in the treatment of breast cancer. *Surg. Clin. North Am.* 93, 493–499. doi: 10.1016/j.suc.2013.01.006

Reding, K. W., Brubaker, P., D'Agostino, R., Kitzman, D. W., Nicklas, B., Langford, D., et al. (2019). Increased skeletal intermuscular fat is associated with reduced exercise capacity in cancer survivors: a cross-sectional study. *Cardio Oncol.* 5:3. doi: 10.1186/s40959-019-0038-5

Rhoads, M. G., Kandarian, S. C., Pacelli, F., Doglietto, G. B., and Bossola, M. (2010). Expression of NF-kappaB and IkappaB proteins in skeletal muscle of gastric cancer patients. *Eur. J. Cancer Oxf. Engl. 1990* 46, 191–197. doi: 10.1016/j.ejca.2009.10.008

Riccardi, D. M., dos, R., das Neves, R. X., de Matos-Neto, E. M., Camargo, R. G., Lima, J. D. C. C., et al. (2020). Plasma lipid profile and systemic inflammation in patients with cancer cachexia. *Front. Nutr.* 7:4. doi: 10.3389/fnut.2020.00004

Rier, H. N., Jager, A., Sleijfer, S., Maier, A. B., and Levin, M.-D. (2016). The prevalence and prognostic value of low muscle mass in cancer patients: a review of the literature. *The Oncologist* 21, 1396–1409. doi: 10.1634/theoncologist.2016-0066

Rier, H. N., Jager, A., Sleijfer, S., van Rosmalen, J., Kock, M. C. J. M., and Levin, M.-D. (2018). Changes in body composition and muscle attenuation during taxane-based chemotherapy in patients with metastatic breast cancer. *Breast Cancer Res. Treat.* 168, 95–105. doi: 10.1007/s10549-017-4574-0

Roberts, B. M., Frye, G. S., Ahn, B., Ferreira, L. F., and Judge, A. R. (2013). Cancer cachexia decreases specific force and accelerates fatigue in limb muscle. *Biochem. Biophys. Res. Commun.* 435, 488–492. doi: 10.1016/j.bbrc.2013.05.018

Rochette, L., Guenancia, C., Gudjoncik, A., Hachet, O., Zeller, M., Cottin, Y., et al. (2015). Anthracyclines/trastuzumab: new aspects of cardiotoxicity and molecular mechanisms. *Trends Pharmacol. Sci.* 36, 326–348. doi: 10.1016/j.tips.2015.03.005

Rodriguez, J., Vernus, B., Chelh, I., Cassar-Malek, I., Gabillard, J. C., Hadj Sassi, A., et al. (2014). Myostatin and the skeletal muscle atrophy and hypertrophy signaling pathways. *Cell. Mol. Life Sci. CMLS* 71, 4361–4371. doi: 10.1007/s00018-014-1689-x

Roeland, E. J., Ma, J. D., Nelson, S. H., Seibert, T., Heavey, S., Revta, C., et al. (2017). Weight loss versus muscle loss: re-evaluating inclusion criteria for future cancer cachexia interventional trials. *Support. Care Cancer* 25, 365–369. doi: 10.1007/s00520-016-3402-0

Rossi, F., Torri, L., Lambertini, M., De Giorgis, S., Calabrese, M., and Tagliafico, A. S. (2020). Muscle mass loss after neoadjuvant chemotherapy in breast cancer: estimation on breast magnetic resonance imaging using pectoralis muscle area. *Eur. Radiol.* 30, 4234–4241. doi: 10.1007/s00330-020-06799-5

Rutten, I. J. G., van Dijk, D. P. J., Kruitwagen, R. F. P. M., Beets-Tan, R. G. H., Olde Damink, S. W. M., and van Gorp, T. (2016). Loss of skeletal muscle during neoadjuvant chemotherapy is related to decreased survival in ovarian cancer patients. *J. Cachexia Sarcopenia Muscle* 7, 458–466. doi: 10.1002/jcsm.12107

Ryan, Z. C., Craig, T. A., Wang, X., Delmotte, P., Salisbury, J. L., Lanza, I. R., et al. (2018). 1α,25-dihydroxyvitamin D3 mitigates cancer cell mediated mitochondrial dysfunction in human skeletal muscle cells. *Biochem. Biophys. Res. Commun.* 496, 746–752. doi: 10.1016/j.bbrc.2018.01.092

Salazar-Degracia, A., Blanco, D., Vilà-Ubach, M., de Biurrun, G., de Solórzano, C. O., Montuenga, L. M., et al. (2016). Phenotypic and metabolic features of mouse diaphragm and gastrocnemius muscles in chronic lung carcinogenesis: influence of underlying emphysema. *J. Transl. Med.* 14:244. doi: 10.1186/s12967-016-1003-9

Salazar-Degracia, A., Busquets, S., Argilés, J. M., Bargalló-Gispert, N., López-Soriano, F. J., and Barreiro, E. (2018). Effects of the beta2 agonist formoterol on atrophy signaling, autophagy, and muscle phenotype in respiratory and limb muscles of rats with cancer-induced cachexia. *Biochimie* 149, 79–91. doi: 10.1016/j.biochi.2018.04.009

Samuels, S. E., Knowles, A. L., Tilignac, T., Debiton, E., Madelmont, J. C., and Attaix, D. (2001). Higher skeletal muscle protein synthesis and lower breakdown after chemotherapy in cachectic mice. *Am. J. Physiol. Regul. Integr. Comp. Physiol.* 281, R133–R139. doi: 10.1152/ajpregu.2001.281.1.R133

Sandri, M. (2008). Signaling in muscle atrophy and hypertrophy. *Physiol. Bethesda Md* 23, 160–170. doi: 10.1152/physiol.00041.2007

Sartori, R., Romanello, V., and Sandri, M. (2021). Mechanisms of muscle atrophy and hypertrophy: implications in health and disease. *Nat. Commun.* 12:330. doi: 10.1038/s41467-020-20123-1

Schiaffino, S., Dyar, K. A., Ciciliot, S., Blaauw, B., and Sandri, M. (2013). Mechanisms regulating skeletal muscle growth and atrophy. *FEBS J.* 280, 4294–4314. doi: 10.1111/febs.12253

Schirrmacher, V. (2019). From chemotherapy to biological therapy: a review of novel concepts to reduce the side effects of systemic cancer treatment (Review). *Int. J. Oncol.* 54, 407–419. doi: 10.3892/ijo.2018.4661

Schmidt, T., Weisser, B., Dürkop, J., Jonat, W., Van Mackelenbergh, M., Röcken, C., et al. (2015). Comparing endurance and resistance training with standard care during chemotherapy for patients with primary breast cancer. *Anticancer Res.* 35, 5623–5629.

Schmitt, T. L., Martignoni, M. E., Bachmann, J., Fechtner, K., Friess, H., Kinscherf, R., et al. (2007). Activity of the Akt-dependent anabolic and catabolic pathways in muscle and liver samples in cancer-related cachexia. *J. Mol. Med. Berl. Ger.* 85, 647–654. doi: 10.1007/s00109-007-0177-2

Schumacher, A. N., Shackelford, D. Y. K., Brown, J. M., and Hayward, R. (2019). Validation of the 6-min walk test for predicting peak V·O2 in cancer survivors. *Med. Sci. Sports Exerc.* 51, 271–277. doi: 10.1249/MSS.0000000000001790

Schwarz, S., Prokopchuk, O., Esefeld, K., Gröschel, S., Bachmann, J., Lorenzen, S., et al. (2017). The clinical picture of cachexia: a mosaic of different parameters (experience of 503 patients). *BMC Cancer* 17:130. doi: 10.1186/s12885-017-3116-9

Schwarzkopf, M., Coletti, D., Sassoon, D., and Marazzi, G. (2006). Muscle cachexia is regulated by a p53–PW1/Peg3-dependent pathway. *Genes Dev.* 20, 3440–3452. doi: 10.1101/gad.412606

Scott, H. R., McMillan, D. C., Crilly, A., McArdle, C. S., and Milroy, R. (1996). The relationship between weight loss and interleukin 6 in non-small-cell lung cancer. *Br. J. Cancer* 73, 1560–1562. doi: 10.1038/bjc.1996.294

Shachar, S. S., Deal, A. M., Weinberg, M., Williams, G. R., Nyrop, K. A., Popuri, K., et al. (2017). Body composition as a predictor of toxicity in patients receiving anthracycline and taxane–based chemotherapy for early-stage breast cancer. *Clin. Cancer Res.* 23, 3537–3543. doi: 10.1158/1078-0432.CCR-16-2266

Shah, A. N., and Gradishar, W. J. (2018). Adjuvant anthracyclines in breast cancer: what is their role? *The Oncologist* 23, 1153–1161. doi: 10.1634/theoncologist.2017-0672

Shum, A. M. Y., Mahendradatta, T., Taylor, R. J., Painter, A. B., Moore, M. M., Tsoli, M., et al. (2012). Disruption of MEF2C signaling and loss of sarcomeric and mitochondrial integrity in cancer-induced skeletal muscle wasting. *Aging* 4, 133–143. doi: 10.18632/aging.100436

Sies, H., and Jones, D. P. (2020). Reactive oxygen species (ROS) as pleiotropic physiological signalling agents. *Nat. Rev. Mol. Cell Biol.* 21, 363–383. doi: 10.1038/s41580-020-0230-3

Silva, K. A. S., Dong, J., Dong, Y., Dong, Y., Schor, N., Tweardy, D. J., et al. (2015). Inhibition of Stat3 activation suppresses caspase-3 and the ubiquitin-proteasome system, leading to preservation of muscle mass in cancer cachexia. *J. Biol. Chem.* 290, 11177–11187. doi: 10.1074/jbc.M115.641514

Silva, S. P., Santos, J. M., Silva, M. P., Costa, R. M., and Medeiros, R. (2020). Cancer cachexia and its pathophysiology: links with sarcopenia, anorexia and asthenia. *J. Cachexia Sarcopenia Muscle* 11, 619–635. doi: 10.1002/jcsm.12528

Sirago, G., Conte, E., Fracasso, F., Cormio, A., Fehrentz, J.-A., Martinez, J., et al. (2017). Growth hormone secretagogues hexarelin and JMV2894 protect skeletal muscle from mitochondrial damages in a rat model of cisplatin-induced cachexia. *Sci. Rep.* 7:13017. doi: 10.1038/s41598-017-13504-y

Skipworth, R. J. E., Moses, A. G. W., Sangster, K., Sturgeon, C. M., Voss, A. C., Fallon, M. T., et al. (2011). Interaction of gonadal status with systemic inflammation and opioid use in determining nutritional status and prognosis in advanced pancreatic cancer. *Support. Care Cancer Off. J. Multinatl. Assoc. Support. Care Cancer* 19, 391–401. doi: 10.1007/s00520-010-0832-y

Skorokhod, A., Bachmann, J., Giese, N. A., Martignoni, M. E., and Krakowski-Roosen, H. (2012). Real-imaging cDNA-AFLP transcript profiling of pancreatic cancer patients: Egr-1 as a potential key regulator of muscle cachexia. *BMC Cancer* 12:265. doi: 10.1186/1471-2407-12-265

Smith, H. J., Greenberg, N. A., and Tisdale, M. J. (2004). Effect of eicosapentaenoic acid, protein and amino acids on protein synthesis and degradation in skeletal muscle of cachectic mice. *Br. J. Cancer* 91, 408–412. doi: 10.1038/sj.bjc.6601981

Smith, H. K., Maxwell, L., Martyn, J. A., and Bass, J. J. (2000). Nuclear DNA fragmentation and morphological alterations in adult rabbit skeletal muscle after short-term immobilization. *Cell Tissue Res.* 302, 235–241. doi: 10.1007/s004410000280

Smith, K. L., and Tisdale, M. J. (1993). Increased protein degradation and decreased protein synthesis in skeletal muscle during cancer cachexia. *Br. J. Cancer* 67, 680–685. doi: 10.1038/bjc.1993.126

Smuder, A. J., Kavazis, A. N., Min, K., and Powers, S. K. (2011). Exercise protects against doxorubicin-induced markers of autophagy signaling in skeletal muscle. *J. Appl. Physiol. Bethesda Md 1985* 111, 1190–1198. doi: 10.1152/japplphysiol.00429.2011

Song, M.-Y., Ruts, E., Kim, J., Janumala, I., Heymsfield, S., and Gallagher, D. (2004). Sarcopenia and increased adipose tissue infiltration of muscle in elderly African American women. *Am. J. Clin. Nutr.* 79, 874–880. doi: 10.1093/ajcn/79.5.874

Sorensen, J. C., Petersen, A. C., Timpani, C. A., Campelj, D. G., Cook, J., Trewin, A. J., et al. (2017). BGP-15 protects against oxaliplatin-induced skeletal myopathy and mitochondrial reactive oxygen species production in mice. *Front. Pharmacol.* 8:137. doi: 10.3389/fphar.2017.00137

Stock, M. S., and Thompson, B. J. (2021). Echo intensity as an indicator of skeletal muscle quality: applications, methodology, and future directions. *Eur. J. Appl. Physiol.* 121, 369–380. doi: 10.1007/s00421-020-04556-6

Straughn, A. R., Kelm, N. Q., and Kakar, S. S. (2021). Withaferin a and ovarian cancer antagonistically regulate skeletal muscle mass. *Front. Cell Dev. Biol.* 9:636498. doi: 10.3389/fcell.2021.636498

Sun, R., Zhang, S., Hu, W., Lu, X., Lou, N., Yang, Z., et al. (2016). Valproic acid attenuates skeletal muscle wasting by inhibiting C/EBPβ-regulated atrogin1 expression in cancer cachexia. *Am. J. Physiol. Cell Physiol.* 311, C101–C115. doi: 10.1152/ajpcell.00344.2015

Sung, H., Ferlay, J., Siegel, R. L., Laversanne, M., Soerjomataram, I., Jemal, A., et al. (2021). Global cancer statistics 2020: GLOBOCAN estimates of incidence and mortality worldwide for 36 cancers in 185 countries. *CA. Cancer J. Clin.* 71, 209–249. doi: 10.3322/caac.21660

Tarnopolsky, M. A., Pearce, E., Smith, K., and Lach, B. (2011). Suction-modified Bergström muscle biopsy technique: experience with 13,500 procedures. *Muscle Nerve* 43, 717–725. doi: 10.1002/mus.21945

Temparis, S., Asensi, M., Taillandier, D., Aurousseau, E., Larbaud, D., Obled, A., et al. (1994). Increased ATP-ubiquitin-dependent proteolysis in skeletal muscles of tumor-bearing rats. *Cancer Res.* 54, 5568–5573.

Theret, M., Rossi, F. M. V., and Contreras, O. (2021). Evolving roles of muscle-resident fibro-adipogenic progenitors in health, regeneration, neuromuscular disorders, and aging. *Front. Physiol.* 12:673404. doi: 10.3389/fphys.2021.673404

Toledo, M., Busquets, S., Penna, F., Zhou, X., Marmonti, E., Betancourt, A., et al. (2016). Complete reversal of muscle wasting in experimental cancer cachexia: additive effects of activin type II receptor inhibition and β-2 agonist. *Int. J. Cancer* 138, 2021–2029. doi: 10.1002/ijc.29930

Toth, M. J., Voigt, T. B., Tourville, T. W., Prior, S. M., Guigni, B. A., Schlosberg, A. V., et al. (2020). Effect of neuromuscular electrical stimulation on skeletal muscle size and function in patients with breast cancer receiving chemotherapy. *J. Appl. Physiol.* 128, 1654–1665. doi: 10.1152/japplphysiol.00203.2020

Trestini, I., Carbognin, L., Monteverdi, S., Zanelli, S., De Toma, A., Bonaiuto, C., et al. (2018). Clinical implication of changes in body composition and weight in patients with early-stage and metastatic breast cancer. *Crit. Rev. Oncol. Hematol.* 129, 54–66. doi: 10.1016/j.critrevonc.2018.06.011

Tsang, W. P., Chau, S. P. Y., Kong, S. K., Fung, K. P., and Kwok, T. T. (2003). Reactive oxygen species mediate doxorubicin induced p53-independent apoptosis. *Life Sci.* 73, 2047–2058. doi: 10.1016/s0024-3205(03)00566-6

Tuttle, L. J., Sinacore, D. R., Cade, W. T., and Mueller, M. J. (2011). Lower physical activity is associated with higher intermuscular adipose tissue in people with type 2 diabetes and peripheral neuropathy. *Phys. Ther.* 91, 923–930. doi: 10.2522/ptj.20100329

Tzika, A. A., Fontes-Oliveira, C. C., Shestov, A. A., Constantinou, C., Psychogios, N., Righi, V., et al. (2013). Skeletal muscle mitochondrial uncoupling in a murine cancer cachexia model. *Int. J. Oncol.* 43, 886–894. doi: 10.3892/ijo.2013.1998

Uezumi, A., Fukada, S., Yamamoto, N., Ikemoto-Uezumi, M., Nakatani, M., Morita, M., et al. (2014a). Identification and characterization of PDGFRα+ mesenchymal progenitors in human skeletal muscle. *Cell Death Dis.* 5:e1186. doi: 10.1038/cddis.2014.161

Uezumi, A., Ikemoto-Uezumi, M., and Tsuchida, K. (2014b). Roles of nonmyogenic mesenchymal progenitors in pathogenesis and regeneration of skeletal muscle. *Front. Physiol.* 5:68. doi: 10.3389/fphys.2014.00068

Uezumi, A., Ito, T., Morikawa, D., Shimizu, N., Yoneda, T., Segawa, M., et al. (2011). Fibrosis and adipogenesis originate from a common mesenchymal progenitor in skeletal muscle. *J. Cell Sci.* 124, 3654–3664. doi: 10.1242/jcs.086629

Urbina-Varela, R., Castillo, N., Videla, L. A., and Del Campo, A. (2020). Impact of mitophagy and mitochondrial unfolded protein response as new adaptive mechanisms underlying old pathologies: sarcopenia and non-alcoholic fatty liver disease. *Int. J. Mol. Sci.* 21:7704. doi: 10.3390/ijms21207704

Ushmorov, A., Hack, V., and Dröge, W. (1999). Differential reconstitution of mitochondrial respiratory chain activity and plasma redox state by cysteine and ornithine in a model of cancer cachexia. *Cancer Res.* 59, 3527–3534.

Vainshtein, A., and Sandri, M. (2020). Signaling pathways that control muscle mass. *Int. J. Mol. Sci.* 21:4759. doi: 10.3390/ijms21134759

van Waart, H., Stuiver, M. M., van Harten, W. H., Geleijn, E., Kieffer, J. M., Buffart, L. M., et al. (2015). Effect of low-intensity physical activity and moderate- to high-intensity physical exercise during adjuvant chemotherapy on physical fitness, fatigue, and chemotherapy completion rates: results of the PACES randomized clinical trial. *J. Clin. Oncol. Off. J. Am. Soc. Clin. Oncol.* 33, 1918–1927. doi: 10.1200/JCO.2014.59.1081

Varricchi, G., Ameri, P., Cadeddu, C., Ghigo, A., Madonna, R., Marone, G., et al. (2018). Antineoplastic drug-induced cardiotoxicity: a redox perspective. *Front. Physiol.* 9:167. doi: 10.3389/fphys.2018.00167

Visser, M., Goodpaster, B. H., Kritchevsky, S. B., Newman, A. B., Nevitt, M., Rubin, S. M., et al. (2005). Muscle mass, muscle strength, and muscle fat infiltration as predictors of incident mobility limitations in well-functioning older persons. *J. Gerontol. A. Biol. Sci. Med. Sci.* 60, 324–333. doi: 10.1093/gerona/60.3.324

Visser, M., Kritchevsky, S. B., Goodpaster, B. H., Newman, A. B., Nevitt, M., Stamm, E., et al. (2002). Leg muscle mass and composition in relation to lower extremity performance in men and women aged 70 to 79: the health, aging and body composition study. *J. Am. Geriatr. Soc.* 50, 897–904. doi: 10.1046/j.1532-5415.2002.50217.x

Wallengren, O., Lundholm, K., and Bosaeus, I. (2013). Diagnostic criteria of cancer cachexia: relation to quality of life, exercise capacity and survival in unselected palliative care patients. *Support. Care Cancer Off. J. Multinatl. Assoc. Support. Care Cancer* 21, 1569–1577. doi: 10.1007/s00520-012-1697-z

Wang, R., Kumar, B., Bhat-Nakshatri, P., Prasad, M. S., Jacobsen, M. H., Ovalle, G., et al. (2021). Aging-associated skeletal muscle defects in HER2/Neu transgenic mammary tumor model. *JCSM Rapid Commun.* 4, 24–39. doi: 10.1002/rco2.23

Warren, S. (1932). The immediate causes of death in cancer. *Am. J. Med. Sci.* 184, 610–615. doi: 10.1097/00000441-193211000-00002

Wesolowski, S., Orlowski, T. M., and Kram, M. (2020). The 6-min walk test in the functional evaluation of patients with lung cancer qualified for lobectomy. *Interact. Cardiovasc. Thorac. Surg.* 30, 559–564. doi: 10.1093/icvts/ivz313

White, J. P., Baynes, J. W., Welle, S. L., Kostek, M. C., Matesic, L. E., Sato, S., et al. (2011). The regulation of skeletal muscle protein turnover during the progression of cancer cachexia in the Apc(Min/+) mouse. *PLoS One* 6:e24650. doi: 10.1371/journal.pone.0024650

White, J. P., Puppa, M. J., Sato, S., Gao, S., Price, R. L., Baynes, J. W., et al. (2012). IL-6 regulation on skeletal muscle mitochondrial remodeling during cancer cachexia in the ApcMin/+ mouse. *Skelet. Muscle* 2:14. doi: 10.1186/2044-5040-2-14

Wiederin, J., Gu, C., Jewett, P., and Blaes, A. H. (2020). Pectoralis muscle wasting during chemotherapy. *J. Clin. Oncol.* 38:e24069. doi: 10.1200/JCO.2020.38.15_suppl.e24069

Williams, A., Sun, X., Fischer, J. E., and Hasselgren, P. O. (1999). The expression of genes in the ubiquitin-proteasome proteolytic pathway is increased in skeletal muscle from patients with cancer. *Surgery* 126, 744–749; discussion 749-750.

Willson, M. L., Burke, L., Ferguson, T., Ghersi, D., Nowak, A. K., and Wilcken, N. (2019). Taxanes for adjuvant treatment of early breast cancer. *Cochrane Database Syst. Rev.* 9:CD004421. doi: 10.1002/14651858.CD004421.pub3

Wilson, H. E., Rhodes, K. K., Rodriguez, D., Chahal, I., Stanton, D. A., Bohlen, J., et al. (2019). Human breast cancer Xenograft model implicates peroxisome proliferator-activated receptor signaling as driver of cancer-induced muscle fatigue. *Clin. Cancer Res. Off. J. Am. Assoc. Cancer Res.* 25, 2336–2347. doi: 10.1158/1078-0432.CCR-18-1565

Wilson, H. E., Stanton, D. A., and Pistilli, E. E. (2020). Breast cancer-associated skeletal muscle mitochondrial dysfunction and lipid accumulation is reversed by PPARG. *BioRxiv* [preprint]. doi: 10.1101/2020.04.05.026617

Wren, T. A. L., Bluml, S., Tseng-Ong, L., and Gilsanz, V. (2008). Three-point technique of fat quantification of muscle tissue as a marker of disease progression in Duchenne muscular dystrophy: preliminary study. *AJR Am. J. Roentgenol.* 190, W8–W12. doi: 10.2214/AJR.07.2732

Yildiz Kabak, V., Gursen, C., Aytar, A., Akbayrak, T., and Duger, T. (2020). Physical activity level, exercise behavior, barriers, and preferences of patients with breast cancer-related lymphedema. *Support. Care Cancer Off. J. Multinatl. Assoc. Support. Care Cancer* 29, 3593–3602. doi: 10.1007/s00520-020-05858-3

Yoshida, H., Ishiko, O., Sumi, T., Honda, K. I., Hirai, K., and Ogita, S. (2001). Expression of apoptosis regulatory proteins in the skeletal muscle of tumor-bearing rabbits. *Jpn. J. Cancer Res. Gann* 92, 631–637. doi: 10.1111/j.1349-7006.2001.tb01141.x

Yu, A. F., Flynn, J. R., Moskowitz, C. S., Scott, J. M., Oeffinger, K. C., Dang, C. T., et al. (2020). Long-term cardiopulmonary consequences of treatment-induced cardiotoxicity in survivors of ERBB2-positive breast cancer. *JAMA Cardiol.* 5, 309–317. doi: 10.1001/jamacardio.2019.5586

Yu, A. P., Pei, X. M., Sin, T. K., Yip, S. P., Yung, B. Y., Chan, L. W., et al. (2014). Acylated and unacylated ghrelin inhibit doxorubicin-induced apoptosis in skeletal muscle. *Acta Physiol. Oxf. Engl.* 211, 201–213. doi: 10.1111/apha.12263

Zampieri, S., Doria, A., Adami, N., Biral, D., Vecchiato, M., Savastano, S., et al. (2010). Subclinical myopathy in patients affected with newly diagnosed colorectal cancer at clinical onset of disease: evidence from skeletal muscle biopsies. *Neurol. Res.* 32, 20–25. doi: 10.1179/016164110X12556180205997

Zhang, Y., Wang, J., Wang, X., Gao, T., Tian, H., Zhou, D., et al. (2020). The autophagic-lysosomal and ubiquitin proteasome systems are simultaneously activated in the skeletal muscle of gastric cancer patients with cachexia. *Am. J. Clin. Nutr.* 111, 570–579. doi: 10.1093/ajcn/nqz347

Zhong, X., Pons, M., Poirier, C., Jiang, Y., Liu, J., Sandusky, G. E., et al. (2019). The systemic activin response to pancreatic cancer: implications for effective cancer cachexia therapy. *J. Cachexia Sarcopenia Muscle* 10, 1083–1101. doi: 10.1002/jcsm.12461

Zhou, X., Wang, J. L., Lu, J., Song, Y., Kwak, K. S., Jiao, Q., et al. (2010). Reversal of cancer cachexia and muscle wasting by ActRIIB antagonism leads to prolonged survival. *Cell* 142, 531–543. doi: 10.1016/j.cell.2010.07.011

Zou, X., Ratti, B. A., O'Brien, J. G., Lautenschlager, S. O., Gius, D. R., Bonini, M. G., et al. (2017). Manganese superoxide dismutase (SOD2): is there a center in the universe of mitochondrial redox signaling? *J. Bioenerg. Biomembr.* 49, 325–333. doi: 10.1007/s10863-017-9718-8

Conflict of Interest: The authors declare that the research was conducted in the absence of any commercial or financial relationships that could be construed as a potential conflict of interest.

Publisher's Note: All claims expressed in this article are solely those of the authors and do not necessarily represent those of their affiliated organizations, or those of the publisher, the editors and the reviewers. Any product that may be evaluated in this article, or claim that may be made by its manufacturer, is not guaranteed or endorsed by the publisher.

Advantages of publishing in Frontiers

OPEN ACCESS
Articles are free to read for greatest visibility and readership

FAST PUBLICATION
Around 90 days from submission to decision

HIGH QUALITY PEER-REVIEW
Rigorous, collaborative, and constructive peer-review

TRANSPARENT PEER-REVIEW
Editors and reviewers acknowledged by name on published articles

Frontiers
Avenue du Tribunal-Fédéral 34
1005 Lausanne | Switzerland

Visit us: www.frontiersin.org
Contact us: frontiersin.org/about/contact

REPRODUCIBILITY OF RESEARCH
Support open data and methods to enhance research reproducibility

DIGITAL PUBLISHING
Articles designed for optimal readership across devices

FOLLOW US
@frontiersin

IMPACT METRICS
Advanced article metrics track visibility across digital media

EXTENSIVE PROMOTION
Marketing and promotion of impactful research

LOOP RESEARCH NETWORK
Our network increases your article's readership